

This PDF was created from the British Library's microfilm copy of the original thesis. As such the images are greyscale and no colour was captured.

Due to the scanning process, an area greater than the page area is recorded and extraneous details can be captured.

This is the best available copy

DX

175943

THE BRITISH LIBRARY
BRITISH THESIS SERVICE

TITLE. SYNTHESIS, CHARACTERISATION AND STABILITY OF SOME N-DONOR
LIGANDS AND THEIR METAL COMPLEXES

AUTHOR Ian Jonathan Scowen

DEGREE

AWARDING BODY University of North London 1993.
DATE

THESIS
NUMBER

THIS THESIS HAS BEEN MICROFILMED EXACTLY AS RECEIVED

The quality of this reproduction is dependent upon the quality of the original thesis submitted for microfilming. Every effort has been made to ensure the highest quality of reproduction.

Some pages may have indistinct print, especially if the original papers were poorly produced or if the awarding body sent an inferior copy.

If pages are missing, please contact the awarding body which granted the degree.

Previously copyrighted materials (journal articles, published texts, etc.) are not filmed.

This copy of the thesis has been supplied on condition that anyone who consults it is understood to recognise that its copyright rests with its author and that no information derived from it may be published without the author's prior written consent.

Reproduction of this thesis, other than as permitted under the United Kingdom Copyright Designs and Patents Act 1988, or under specific agreement with the copyright holder, is prohibited.

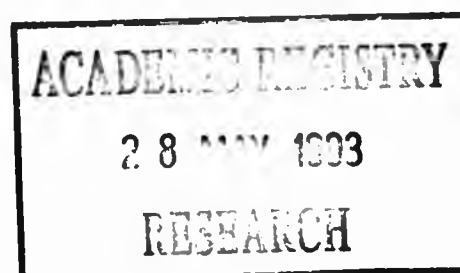
1	2	3	4	5	6	REDUCTION X	12
cms						CAMERA	12.
						No. of pages	

SYNTHESIS, CHARACTERISATION AND STABILITY OF SOME N-DONOR
LIGANDS AND THEIR METAL COMPLEXES

Ian Jonathan Scowen

A thesis submitted in partial fulfilment of the requirements of
the University of North London for the degree of
Doctor of Philosophy

This research programme was carried out in the
School of Applied Chemistry, University of North London



May 1993

**Synthesis, Characterisation and Stability of some N-donor
Ligands and their Metal Complexes**

ABSTRACT

The investigation has consisted of two elements, one concentrating on the stabilities of metal complexes in solution, and the other on the co-ordination chemistry of some new N-donor macrocyclic ligands.

Equilibrium Studies

An automated potentiometric titration system has been developed to provide accurate acid-base data for determination of protonation and metal complexation equilibrium constants in three different solvent systems; aqueous, *aqu.* hydrogen peroxide and *aqu.* methanol. Measurement accuracy has been established with the aqueous nickel(II)-glycine system; results obtained are in excellent agreement with published values.

Protonation constants and stability constants for complexes with Cu(II) and Ni(II) are reported for 1-aminopropylphosphonic acid in aqueous solution ($I = 0.1 \text{ mol dm}^{-3}$, KNO_3 ; 25°C). The tertiary aminomethylenephosphonic acids, diethylaminomethylenephosphonic acid and ethyliminomethylenephosphonic acid, were synthesised and their protonation and Cu(II) and Ni(II) metal complexation behaviour in aqueous solution ($I = 0.1 \text{ mol dm}^{-3}$, KNO_3 ; 25°C) is reported. Additionally, speciation of protonated forms of these ligands in aqueous solution has been achieved using ^{31}P nmr. These investigations have required development of a 'small volume' potentiometric titration system, applied to give *in situ* acid-base titrations in an nmr tube.

Extension of potentiometric techniques to dilute hydrogen peroxide solutions of these ligands was complicated by solution instability and evidence of ligand derivatisation. Two distinct types of derivatisations of ligands are established by ^{13}C and ^{31}P nmr.

Protonation and stability constants for complexes with Zn(II) and Cd(II) are reported for dibenzo-pyrido-pentaaza and dibenzo-triaza-dioxa macrocycles in 95% methanol-water solution ($I = 0.1 \text{ Et}_4\text{NClO}_4$; 25°C). The pentaaza ligand shows an unusual preference for Cd(II) over Zn(II) although it binds relatively strongly to both metals. In contrast, the triaza-dioxa ligands show low affinities for both Zn(II) and Cd(II).

Synthetic and Structural Studies

Isolation and characterisation of metal complexes of a novel hexaaza-tetraoxa [2+2] Schiff-base macrocycle (L^1) have been achieved by metal template condensation of *bis*-(2-aminophenoxy)-*o*-xylene and pyridine-2,6-dicarbaldehyde in the presence of the appropriate metal perchlorate. Complexes of new triaza-dithia and hexaaza-tetrathia macrocycles were obtained by using Ag(I) and Pb(II), respectively, as templating ions. A number of mononuclear first row transition and post-transition metal ion complexes of L^1 have been prepared by transmetallation of the disilver(I) complex.

Single crystal X-ray structures have been determined for mononuclear Zn(II) and Ni(II) diperchlorate complexes of L^1 and each show that the ligand adopts a double-helical configuration resulting from co-ordination *via* the six nitrogen donors of the ligand. The potentially coordinating phenoxy ether donors of the ligand are extruded away from the metal co-ordination sphere. Intramolecular π - π stacking interactions further stabilise the twisted ligand configuration in these complexes. Detailed assignments of ^1H and ^{13}C nmr spectra of diamagnetic complexes of L^1 have been achieved using homo- and hetero-nuclear 2D spectroscopy. The results indicate that the complexes are helical in solution. Two distinct fluxional processes for the co-ordinated ligand are suggested by variable temperature studies of the Pb(II) complex. Somewhat more complicated temperature dependence, presumably involving metal exchange, is noted for the Ag(I) complex.

Acknowledgements

I gratefully acknowledge the advice and expertise of the following during the preparation of this manuscript:

Dr. Ray Matthews, the Director of Studies, for his encouragement, friendship and tireless attention to detail throughout the realisation of this work.

Dr. Brian Murphy, my second supervisor, for advice during the synthetic studies reported herein.

Dr. Gareth Morris and the staff of Interlox Research and Development at Widnes for advice on hydrogen peroxide stabilisation and their hospitality during a safety course for handling hydrogen peroxide solutions. I gratefully acknowledge financial contributions from Peroxid-Chemie GmbH.

Prof. Len Lindoy and Mr. Tony Leong for their patient instruction on experimental procedures for stability constant determinations. I am also very grateful to Prof. Lindoy and his group, especially Mr. Peter Eaglen and his family, for their kind hospitality during a study visit to James Cook University of North Queensland.

Mr. John Crowder for the many excellent high field 1D- and 2D-nmr spectra reported herein.

Prof. Mary McPartlin, Mr. Alan Bashall and Dr. Harry Powell for their invaluable instruction during X-ray crystallographic studies.

Prof. David Fenton and his group at the University of Sheffield for the gifts of some macrocyclic ligands studied herein and access to results prior to their publication.

Mr. Paul Biggins and Mr. Chris Silwood for their invaluable contributions during development of the automated titration systems described herein.

I gratefully acknowledge a studentship (No. 87800151) and financial support for a study trip to Australia from the SERC.

For Kathy

Contents

1. Introduction

1.1 Characterisation of metal complex stability	3
1.1.1 Statistical effects	4
1.1.2 Influence of metal ion	7
1.1.3 Ligand basicity and metal complex stability	10
1.1.4 Complementarity of donor and acceptor atoms; the HSAB principle	12
1.1.5 Multidentate ligands and the 'chelate effect'	16
1.1.6 Influence of topology; the macrocyclic and cryptate effects	19
1.1.7 Ligand preorganisation	23
1.2 Metal ion recognition	28
1.2.1 Size match selectivity	29
1.2.2 Dislocation discrimination	34
References	39

Section A - Equilibrium Studies

2. Introduction

2.1 Stepwise formation of complexes	45
2.2 Mass balance	49
2.3 Thermodynamic and stoichiometric stability constants	50
2.4 Potentiometry in analysis of equilibria	52
2.5 Computational methods for determining equilibrium constants	52
2.5.1 The programs MINQUAD and SUPERQUAD	53

3. Experimental methods

3.1 Aminomethylenephosphonate syntheses.	57
3.1.1 Starting materials	57
3.1.2 Physical measurements	57
3.1.3 Preparation of diethylaminomethylenephosphonic acid	58
3.1.4 Preparation of ethyliminodimethylenephosphonic acid	59
3.2 Determination of protonation and metal complex stability constants by potentiometric titration.	60
3.2.1 Reagents used during potentiometric titrations	60
3.2.2 Solvents	60
3.2.3 Preparation of acid solutions	62

3.2.4 Preparation of base solutions	63
3.2.5 Preparation of metal salt solutions	64
3.2.6 Preparation of calomel reference electrodes	64
3.2.7 Preparation of salt bridge solutions	66
3.2.8 Potentiometric titrations in dilute hydrogen peroxide solutions	66
3.2.9 Preparation of tetraethylammonium salts for titrations in 95 % methanol-water medium.	66
3.2.10 Data acquisition	68
3.2.11 Cell calibration	69
3.2.12 Conditions for ligand and metal-ligand titrations	69
3.2.13 Data Processing	78
3.3 Nmr studies of phosphonic acids in aqu. hydrogen peroxide solutions	80
3.3.1 Interaction of disodium 1-hydroxyethyl-1,1-diphosphate with hydrogen peroxide	81
3.3.2 Interaction of diethylaminomethylenephosphonic acid and hydrogen peroxide	81
3.4 Studies of the pH dependence of phosphorus-31 nmr chemical shifts for alkylaminomethylenephosphonic acids	83
4. A Potentiometric titration system	
4.1 Introduction	86
4.2 Automated titration system	87
4.3 Titration software	90
4.3.1 The menu program - S.SCMMENU	91
4.3.2 The titration program - S.SCMTITR	92
4.3.3 Auxiliary programs	99
4.4 Cell calibration in aqueous solution	100
4.4.1 Theory	101
4.4.2 Calibration of the computer-controlled apparatus	103
4.4.4 A program to calculate cell parameters from strong acid-strong base titration data - S.SCMCAL	103
4.4.5 Correction for liquid-liquid junction potentials	105
4.4.6 Cell calibration for a potentiometric cell ($I = 0.1 \text{ mol dm}^{-3}$, KNO_3)	108
4.5 The aqu. nickel-glycine system - a bench standard	114

4.6 Potentiometric titration in dilute hydrogen peroxide solution	121
4.6.1 Composition of the potentiometric cell	121
4.6.2 Cell calibration	122
4.6.3 Nickel glycinate in 3% and 10% aqu. hydrogen peroxide solution	127
5. Stability and solution speciation of some aminomethylenephosphonic acids and their complexes with metal ions	
5.1 Introduction	132
5.2 Synthesis and characterisation of diethylaminomethylene-phosphonic acid and ethyliminobis(methylenephosphonic acid)	134
5.3 Protonation equilibria for 1-aminopropylphosphonic acid	136
5.3.1 Protonation constants for 1-aminopropylphosphonic acid	136
5.3.2 Phosphorus-31 nmr studies	139
5.4 Stability of copper(II) and nickel(II) complexes of 1-aminopropylphosphonic acid	141
5.4.1 Copper(II) studies	144
5.4.2 Nickel(II) studies	147
5.4.3 Discussion	149
5.5 Protonation equilibria of diethylaminomethylene-phosphonic acid and ethyliminobis(methylenephosphonic acid)	154
5.5.1 Potentiometric studies	154
5.5.2 Phosphorus-31 nmr studies	163
5.6 Stability of transition metal complexes of diethylaminomethylenephosphonic acid and ethyliminobis(methylenephosphonic acid)	170
5.6.1 Copper(II)	172
5.6.2 Nickel(II)	176
5.6.3 Discussion	180
5.7 Studies of simple alkylphosphonic acids in dilute aqu. hydrogen peroxide solution	185
5.7.1 A potentiometric study of 1-aminopropylphosphonic acid in 10% hydrogen peroxide solution	185

5.7.2 Chemical stability of 1-hydroxyethyl-1,1-phosphonic acid in aqu. hydrogen peroxide solution	186
5.7.3 Multinuclear nmr studies of DEAMPH ₂ in aqueous and aqu. hydrogen peroxide	190
6. Potentiometric investigations into functionalised pyridine macrocycles in 95 % methanol-water solution	
6.1 Potentiometric titrations in methanol/water medium	201
6.1.1 Composition of the potentiometric cell	201
6.1.2 Cell calibration	203
6.2 Complexes of a pentaaza macrocycle	206
6.2.1 The protonation constants for NpynNenH ₄	206
6.2.2 NpynNenH ₄ - Copper(II) Titrations	213
6.2.3 Nickel(II)-NpynNenH ₄ titrations	215
6.2.4 Zinc(II)-NpynNenH ₄ titrations	216
6.2.5 Cadmium(II)-NpynNenH ₄ titrations	222
6.2.6 Cadmium vs. zinc selectivity.	227
6.3 Protonation and metal complexation studies of a series of triaza-dioxa macrocycles	229
References	232

Section B - Synthetic and Structural Studies of Semi-rigid Mixed-donor Schiff-base Macrocyclic Complexes

7. Introduction	242
8. Experimental methods	
8.1 List of compounds synthesised	246
8.1.1 Starting materials	246
8.1.2 Organic precursor compounds	247
8.1.3 Template reaction products	247
8.1.4 Transmetalation reaction products	249
8.1.5 Other materials used	249
8.2 Solvents	250
8.3 Synthesis of organic precursor compounds	250
8.3.1 Preparation of α,α' -Bis(2-nitrophenoxy)-o-xylene	250
8.3.2 Attempted synthesis of α,α' -Bis(2-aminophenoxy)-o-xylene	251
8.3.3 Preparation of α,α' -Bis(2-aminophenoxy)-o-xylene	252

8.3.4 Preparation of α, α' -Bis(2-aminothiophenoxy)- o-xylene	254
8.3.5 Preparation of pyridine-2,6-dicarbaldehyde	255
8.4 Metal template syntheses	256
8.4.1 Preparation of $[\text{MnL}^1][\text{ClO}_4]_2 \cdot 2\text{H}_2\text{O}$	256
8.4.2 Preparation of $[\text{Ag}_2\text{L}^1][\text{ClO}_4]_2 \cdot 0.5\text{CH}_3\text{CN}$	257
8.4.3 Preparation of $[\text{PbL}^1][\text{ClO}_4]_2 \cdot \text{H}_2\text{O}$	258
8.4.4 Preparation of $[\text{PbL}^1][\text{NCS}]_2$	258
8.4.5 Preparation of $[\text{PbL}^2][\text{ClO}_4]_2$	259
8.4.6 Preparation of $[\text{AgL}^3][\text{ClO}_4]$	260
8.5 Transmetalation syntheses	261
8.5.1 $[\text{CoL}^1][\text{ClO}_4]_2$	262
8.5.2 $[\text{NiL}^1][\text{ClO}_4]_2 \cdot \text{CH}_3\text{CN}$	262
8.5.3 $[\text{ZnL}^1][\text{ClO}_4]_2 \cdot 2\text{CH}_3\text{CN}$	263
8.5.4 $[\text{CdL}^1][\text{ClO}_4]_2 \cdot \text{CH}_3\text{CN} \cdot \text{H}_2\text{O}$	263
8.6 Instrumental methods	264
8.6.1 ^1H nmr spectra	264
8.6.2 ^{13}C nmr spectra	264
8.6.3 2-D nmr spectra	265
8.6.4 Infrared spectra	265
8.6.5 C, H, and N analysis	266
8.6.6 Mass spectra	266
9. Synthesis and characterisation of mixed donor macrocyclic imine complexes	
9.1 Synthesis of diamine precursors M^3 and 2	267
9.2 Metal template reactions	271
9.2.1 Synthesis of $[\text{MnL}^1][\text{ClO}_4]_2$	271
9.2.2 Synthesis of $[\text{Ag}_2\text{L}^1][\text{ClO}_4]_2$	274
9.2.3 Syntheses of $[\text{PbL}^1][\text{ClO}_4]_2$ and $[\text{PbL}^1][\text{SCN}]_2$	277
9.2.4 Synthesis of $[\text{PbL}^2][\text{ClO}_4]_2$	280
9.2.5 Synthesis of $[\text{AgL}^3][\text{ClO}_4]$	283
9.3 Transmetalation Syntheses	285
9.3.1 Preparation of $[\text{CoL}^1][\text{ClO}_4]_2$	286
9.3.2 Synthesis of $[\text{NiL}^1][\text{ClO}_4]_2$, $[\text{ZnL}^1][\text{ClO}_4]_2$, and $[\text{CdL}^1][\text{ClO}_4]_2$	289

10. X-ray diffraction studies	
10.1 Structure solution and refinement	292
10.1.1 Determination of crystal system and unit cell dimensions	292
10.1.2 Data collection and reduction	293
10.1.3 Identification of space group	294
10.1.4 Structure solution and refinement for $[\text{ZnL}^1][\text{ClO}_4]_2 \cdot 2\text{CH}_3\text{CN}$	296
10.1.5 Structure solution and refinement for $[\text{NiL}^1][\text{ClO}_4]_2 \cdot 2\text{CH}_3\text{CN}$	298
10.1.6 Mean plane calculations	300
10.2 The solid state structures of metal complexes of L^1	301
10.2.1 Description of the structure of $[\text{ZnL}^1][\text{ClO}_4]_2$	301
10.2.2 The structure of $[\text{NiL}^1][\text{ClO}_4]_2 \cdot 2\text{CH}_3\text{CN}$ in the solid state	320
11. Nuclear magnetic resonance studies of the diamagnetic complexes of L^1	
11.1. Assignment of proton nmr spectra	333
11.1.1 General features	333
11.1.2 The ^1H nmr spectrum of $[\text{ZnL}^1][\text{ClO}_4]_2$	340
11.1.3 The ^1H nmr spectrum of $[\text{CdL}^1][\text{ClO}_4]_2$	345
11.1.4 The ^1H nmr spectra of $[\text{PbL}^1][\text{ClO}_4]_2$ and $[\text{PbL}^1][\text{NCS}]_2$	351
11.1.5 The ^1H nmr spectra of Group II metal complexes of L^1	358
11.1.6 ^1H nmr spectra of $[\text{Ag}_2\text{L}^1][\text{ClO}_4]_2$	362
11.2 Carbon-13 nmr spectra of diamagnetic complexes of L^1	368
11.2.1 Spectral assignment	368
11.2.2 Metal-carbon-13 coupling	376
11.3 Discussion	379
11.3.1 Symmetry considerations	379
11.3.2 Metal-ligand spin-spin coupling and dynamic stability of complexes	385
11.3.3 The effects of temperature and enantiomeric interchange	388
11.3.4 Analysis of chemical shifts.	391
References	399

Appendix I Crystal data for $[\text{ZnL}^1][\text{ClO}_4]_2 \cdot 2\text{CH}_3\text{CN}$

Appendix II Crystal data for $[\text{NiL}^1][\text{ClO}_4]_2 \cdot 2\text{CH}_3\text{CN}$

1. INTRODUCTION

The development in the late nineteenth century of Alfred Werner's concept of a primary and an auxiliary valence in a metal-ion signals the origin of metal-ion co-ordination chemistry.^[1] Werner reasoned that there are two spheres for substrate interaction with the metal-ion in a complex;^[2a] the outer or primary sphere, containing ions (usually anions) satisfying the valence of the central ion and, an inner or co-ordination sphere containing atoms, ions or groups held in a firm or relatively non-dissociating combination with the central ion (ions co-ordinated in the inner sphere can also contribute to the fulfillment of the primary valence in the complex). The number of atoms or groups contained in the inner sphere is termed the co-ordination number of the metal (N). Structures of optically active cobalt complexes derived using these concepts established first the correlation between the structure of a metal complex and its physical properties.^[2b]

During the twentieth century metal ion co-ordination chemistry has achieved a pre-eminent position in inorganic chemistry and the study of the interaction of metal ions with organic substrates (usually referred to as ligands) has implications in fields as diverse as medicinal,^[3] biological,^[4] industrial^[5] and environmental chemistry.^[6] Applications of co-ordination chemistry may be classified according to the properties induced as a result of the metal-ligand interaction;^[7] complex formation may generate useful properties by transforming the properties of the metal ion [e.g. enabling its transportation into an organic solvent (exploited in extractive hydrometallurgy)^[8] or suppressing its reactivity in solution (as in the widespread use of metal ion sequestrants in chemical industry)^[9]], by

transforming the properties of the ligand [e.g. metal ion catalysed reactions]^[10] or by generating materials with novel properties [e.g. semiconductors^[11] or supramolecular devices^[12]].

This thesis describes a number of discrete projects encompassing various aspects of metal-ion co-ordination chemistry and for clarity is divided into two sections. Section A describes the development of an experimental methodology for accurate measurement of equilibrium constants for metal complex formation in aqueous solution (Chapter 3) and its application to some simple aminomethylenephosphonic acid systems (Chapter 4). Because of the ability of these latter systems to model more complicated compounds employed to stabilise commercial hydrogen peroxide solutions, the studies also included an investigation of their solution speciation in both aqueous and *aqu.* hydrogen peroxide media. Equilibrium studies were further extended to 95 % *aqu.* methanol media to allow investigation of some novel macrocyclic systems with potential for metal-ion discrimination. These investigations are described in Chapter 5.

Section B describes synthetic and structural studies of some novel macrocyclic ligands. These ligands supplement existing compounds which have been synthesized in order to systematically vary certain structural properties (e.g. number and orientation of donor atoms, structural rigidity of the ligand backbone) and yield a 'matrix' against which metal-ion discrimination may be probed.^[13,14,15]

In order to design ligands to fulfill specific rôles an understanding of the the factors affecting the magnitude of the interaction between the metal-ion and the ligand is required. The following sections introduce the factors

which most commonly appear to influence the stability of metal complexes and illustrate each with specific examples from the chemical literature.

1.1 Characterisation of metal complex stability

The thermodynamic quantity that has the most direct bearing on the course of a chemical reaction is the Gibbs free energy change (ΔG).^[16] For the complexation reaction,



the Gibbs free energy change at temperature T is given by the enthalpy and entropy changes (ΔH and ΔS respectively) that occur in the system as a result of reaction. The relationship

$$\Delta G = \Delta H - T\Delta S \quad 1.1$$

applies and more stable products arise when larger amounts of heat are generated by the reaction (ΔH more negative) and/or the reaction products are less ordered (ΔS more positive). The most direct measure of the Gibbs free energy change is given by the equilibrium constant (K) since these parameters are related by

$$\Delta G = -RT \ln K \quad 1.2$$

where R is the gas constant. Hence comparison of equilibrium constants for complexation reactions (also known as stability or formation constants) gives a quantitative measure of the relative affinities of the reactants and the thermodynamic stabilities of resulting complexes.

Thermodynamic and kinetic stability

The distinction between thermodynamic and kinetic stability of metal complexes is worthy of note. Metal complexes can be classified as kinetically inert, *i.e* those which undergo slow ligand substitution reactions, or kinetically labile, *i.e* those which undergo rapid ligand substitution reactions. Although

the equilibrium constant for formation of a complex is related to the rate of association (k_f) of reactants and dissociation (k_r) of products by^[17]

$$K = k_f/k_r \quad 1.3$$

there is no relationship between the thermodynamic stability of a complex (characterised by a high formation constant) and its kinetic stability (or inertness, characterised by a slow exchange rate of co-ordinated ligands). For example, the tetracyanonickel(II) dianion has a high formation constant ($K \approx 10^{22}$), but studies indicate extremely rapid exchange of the CN^- ligands in the complex with radiolabelled $^{14}\text{CN}^-$ in aqueous solution.^[18a]

[A more detailed description of the terms and conventions employed to describe equilibrium constants in this work is given in Chapter 2.]

1.1.1 Statistical effects

If the constitution of a complex involves the co-ordination of more than one ligand to the central ion, the mononuclear complex ML_N is accompanied by the formation of a number of intermediate species [$\text{ML}_{(N-1)}$, $\text{ML}_{(N-2)}$, ..., etc] in a stepwise process. If it can be assumed that each co-ordination site of the central metal-ion is equivalent and is unaffected by co-ordination at any other site, the ratio of stability constants for each successive complex formed in the series is governed statistically.^[19] For a unidentate ligand L, the tendency of the complex ML_n to add another ligand is proportional to the number of available co-ordination sites ($N-n$), where N is the maximum co-ordination number of the metal ion); similarly the tendency of the complex to eliminate a ligand is proportional to the number of occupied sites (n). The equilibrium constants for successive complexation steps under these conditions are related by^[1,19]

$$K_n : K_{n-1} = \frac{(N-n+1)}{n} : \frac{(N-n)}{(n+1)} \quad 1.4$$

$$K_{N-1} : K_N = \frac{2}{(N-1)} : \frac{1}{N} \quad 1.5$$

and the ratio of successive stability constants is given by,^[1,19]

$$\frac{K_n}{K_{n+1}} = \frac{(n+1)(N-n+1)}{n(N-n)} \quad 1.6$$

Table 1.1.1 The logarithms of ratios of successive stability constants for ammine and monodentate N-donor systems.^a

System	N	K_1/K_2	K_2/K_3	K_3/K_4	K_4/K_5	K_5/K_6	I^b	T^c
Theoretical ^d	2	0.60						
Ag ⁺ -NH ₃	2	0.68					0.5	25.0
Ag ⁺ -MeNH ₂	2	-0.38					0.5	25.0
Ag ⁺ -Et ₃ N	2	0.50					0.4	25.0
Cu ²⁺ -2-picoline	2	0.58					0.6	25.0
Theoretical ^d	3	0.48	0.48					
Zn ²⁺ -pyridine	3	0.62	0.18				0.5	25.0
Cd ²⁺ -pyridine	3	0.55	0.51				0.5	25.0
Theoretical ^d	4	0.43	0.35	0.43				
Pd ²⁺ -NH ₃	4	0.7	1.4	0.7			1.0	25.0
Cu ²⁺ -pyridine	4	0.67	0.64	0.45			0.5	25.0
Cu ²⁺ -pyrrolidine	4	0.4	0.6	0.2			0.2	25.0
Theoretical ^d	6	0.38	0.27	0.25	0.27	0.38		
Ni ²⁺ -NH ₃	6	0.54	0.50	0.50	0.46	0.66	2.0	25.0

^a Data from Ref. [20]. Number of decimal places reflects accuracy for quoted log β. ^b Ionic strength /mol dm⁻³. ^c Temperature /°C. ^d Calculated from Eqn. 1.6.

The ratios of stepwise stability constants^[20] for several monodentate nitrogen donor ligands and those derived from statistical factors^[1,19] alone are compared in Table 1.1.1. Clearly factors other than pure statistical influences are operative in real systems and these will be discussed in the following sections. Additionally, the ratios derived for the monodentate case change when multidentate ligands are involved in binding; e.g. for stepwise binding of bidentate ligands to an octahedral central ion (N = 6) there are twelve edges of the octahedron available for the first ligand bound in the metal co-ordination sphere but only five for the second. The ratio of the three successive constants is,^[1,19]

$$K_1 : K_2 : K_3 = \frac{12}{5} : \frac{5}{2} : \frac{4}{15} \quad 1.7$$

When N = 4 the metal ion may adopt either a tetrahedral or a square planar configuration. However, ratios of successive constants for bidentate ligands derived from statistical considerations alone,

$$K_1 : K_2 = \frac{2}{1} : \frac{1}{4} \quad 1.8$$

are independent of the metal configuration.^[1,19] Although these ratios do not regularly predict stepwise constants accurately in real systems they are an important factor when the stepwise formation of ternary complexes is under consideration^[21] (and can also be useful when deducing initial log β estimates for least squares programs; see Section 2.5).

1.1.2 Influence of metal ion

The strength of the chemical bond between a metal-ion and a ligand and hence the magnitude of the formation constant depends on many physical and chemical characteristics of the metal ion in solution. In the absence of other influences, the bond may be considered to be due to an electrostatic interaction between the centres and the bond strength therefore depends on the respective charges of the metal-ion and the ligand donor atom, and the distance between the two centres (d). Figure 1.1.1 shows the qualitative relationship between the magnitude of the first stepwise formation constant^[20] and the metal ion radius^[22] for Group II metal-ion complexes of the N-donor ligands, glycinate, pyridine and 1,10-phenanthroline.

From an electrostatic model of the metal-ion-ligand interaction, Williams^[23] developed an argument concerning the stability of complexes of Group II cations in terms of the ratio z/r (z is the charge of the metal-ion, r its radius) but found its predictive value was limited unless short range electrostatic repulsions between co-ordinated anions were considered. A number of authors have described similar functions (based on e.g. z^2/r ,^[24] z/d ,^[25] and z^2/r^2 ^[26]) in order to account for the observed trends in the hydrolysis constants of metal-ions, and latterly Huheey^[27] generalised this approach by stating that any function, z^m/r^n , can be used in this context. Recently, Sylva and co-workers have had some success in predicting the magnitudes of the first hydrolysis constants of wide range of metal-ions by using a linear equation based on the effective nuclear charge of the metal ion.^[26] However while functions of this type may be effective when small ligands are under consideration, Williams's observations^[23] about the influence of steric crowding around the central ion are bound to apply for larger organic moieties.

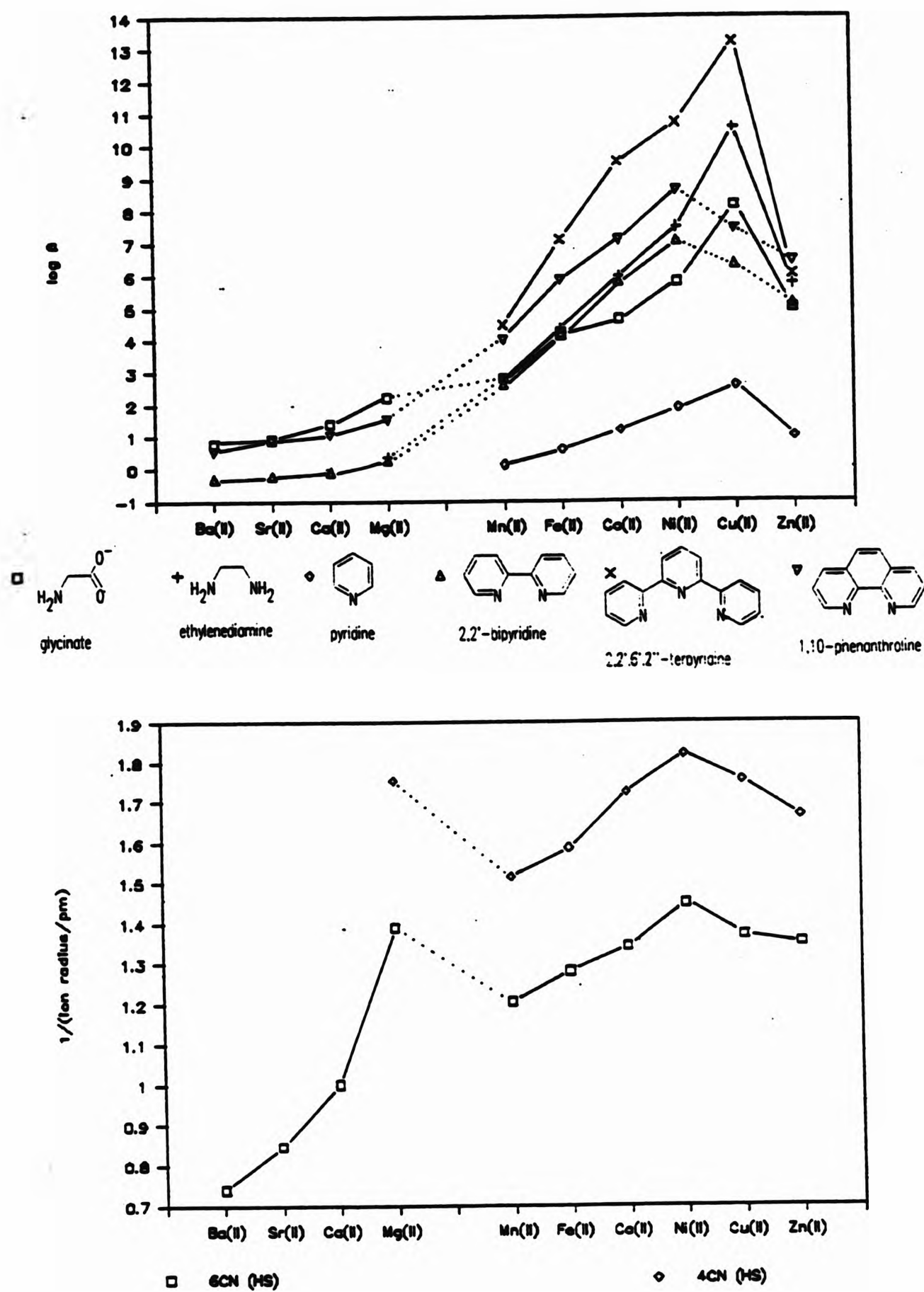


Figure 1.1.1 The qualitative correlation between (a) the reciprocal of metal-ion radius^[22] for Group II and transition metal-ions and (b) the stabilities (log β_{110}) of their complexes^[20] with several N-donor systems.

The complex-forming abilities of the transition metal ions are characterised by the Irving-Williams series.^[28] The stability order first established for complexes of nitrogen and oxygen donor ligands, $\text{Mn}^{2+} < \text{Fe}^{2+} < \text{Co}^{2+} < \text{Ni}^{2+} < \text{Cu}^{2+} > \text{Zn}^{2+}$, remains valid in a large number of high spin complexes (*vide infra*) irrespective of the nature of the ligand. The rationalisation for this order lies in a combination of effects due to ionic radius [Fig. 1.1.1(a)] and the electronic configuration of the d-orbitals in the metal-ion.^[18b]

The effect of electrostatic fields on the relative energies of each of the five metal d-orbitals is obtained from crystal field theory;^[29] e.g. the effect of six point negative charges orientated at the vertices of an octahedron around a metal ion destabilises (by charge repulsion) electrons occupying d-orbitals with lobes that lie on the co-ordinate axes ($d_{x^2-y^2}$ and d_{z^2} combine into the e_g orbital in an octahedral field relative to the free ion. Correspondingly, electrons in lobes between the axes (d_{xy} , d_{xz} and d_{yz} combine into the t_{2g} orbital in an octahedral field) are stabilised relative to the free ion. In such an octahedral field, lowering of the overall energy [the crystal field stabilisation energy (CFSE)] results for configurations other than d^0 , d^5 and d^{10} . In the absence of electron spin pairing (the so-called high spin complexes), the CFSE reaches a maximum value for d^8 ions (e.g. Ni^{2+}) and follows the general trend of the Irving-Williams series. [The higher (apparently anomalous) stability of Cu^{2+} complexes, as described by the series, arises in some part as a result of Jahn-Teller distortions of the regular octahedron leading to further splitting of the octahedral energy levels resulting in lowering of the overall energy.]

When the energy difference between the e_g and t_{2g} orbitals, Δ_o , becomes larger than the pairing energy, electron spin coupling occurs yielding so-called

low-spin complexes. In these cases, the CFSE is maximised for d^6 metal-ions (e.g. Fe^{2+}) and deviations of orders of complex stabilities from the Irving-Williams series often occur.^[30]

In the majority of transition metal-ion complexes a simple electrostatic model is insufficient to accurately describe the metal-ligand interaction. Binding in these cases involves varying degrees of covalency in the co-ordination bond, dependent on both electronic structures of the ligand and the metal-ion. A detailed description of the ligand field theory^[31] governing these influences is beyond the scope of this study.

1.1.3 Ligand basicity and metal complex stability

Linear relationships between protonation constants and complex stability constants of the form,

$$\log \beta_{1m0} = a \log K_{01n} + b \quad 1.9$$

where a and b are constants, m and n are integers, have been established for a number of different ligand classes; e.g. salicylaldehydes,^[32] quinolines,^[33] aminocarboxylic acids,^[32] phosphonic and aminophosphonic acids,^[34] primary amines,^[35] and nitrogen heterocycles.^[35] The relationship between the first protonation constant of seventeen monodentate N-donor ligands and the first stepwise stability constant of their silver(I) complexes, similar to that first observed by Bruehlman and Verhoeck,^[35] is illustrated in Figure 1.1.2. The graph was plotted using equilibrium constants from Martell and Smith's compilations.^[20]

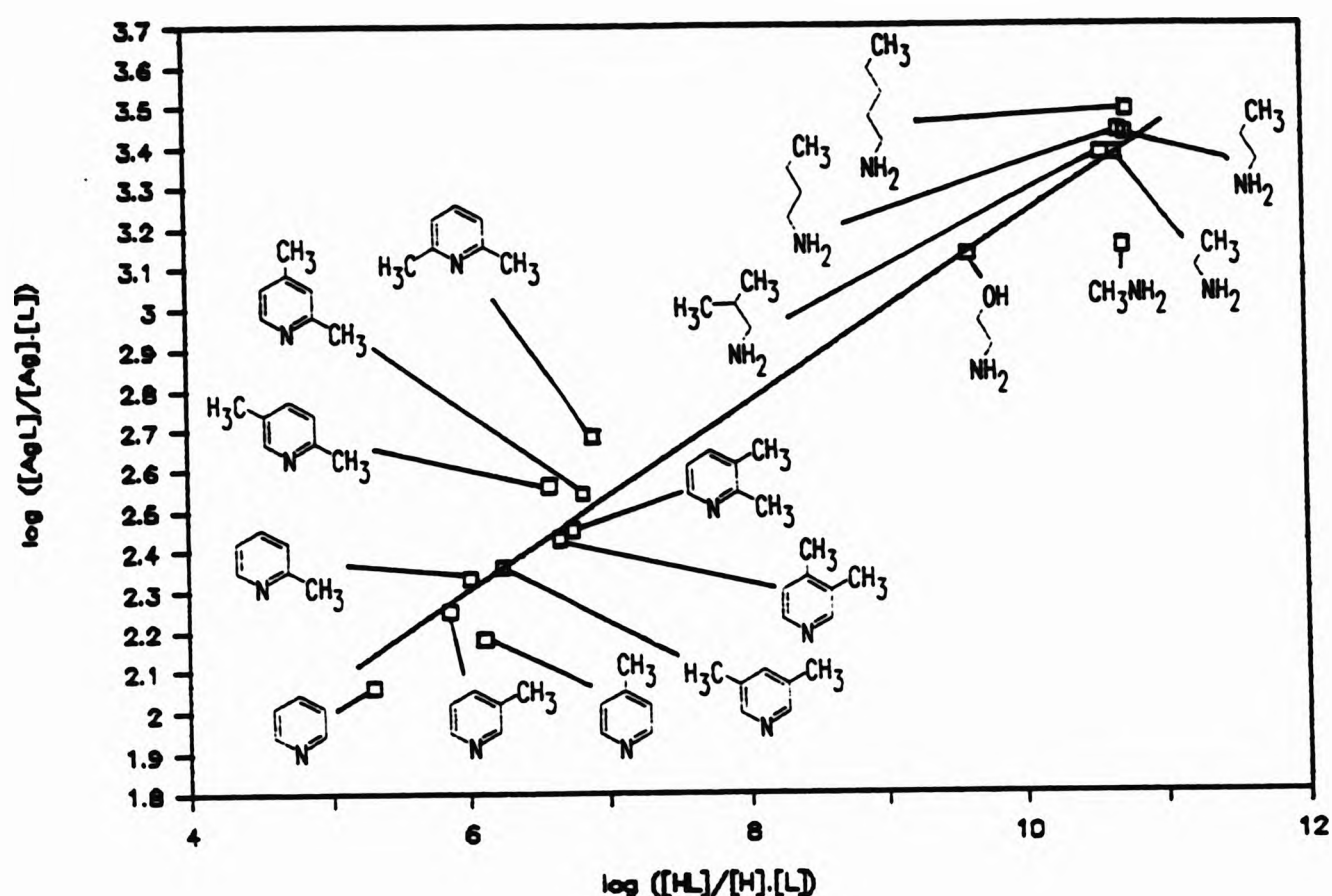


Figure 1.1.2 The linear dependence of $\log \beta_{110}$ on the first ligand protonation constant for silver(I) complexes of some monodentate N-donor ligands (after Ref. [35]). The least squares line for data from Ref. [20] is given by $\log \beta_{110} = 0.23 \log K_{011} + 0.92$ (correlation coefficient = 0.97).

That equations of the type (1.9) hold is perhaps unsurprising given that the proton may be formally regarded as a metal-ion, and its binding to the ligand is controlled by at least one common factor, namely the electrostatic component to the co-ordination bond, with metal-ion complex formation. [32] However, such relationships have no general validity and depend substantially on the particular of ligand group chosen - indeed non-linearity for particular ligand types is well known. [36] Even when linear relationships do hold, factors other than the electrostatic component, such as π -bonding or steric factors, intervene in varying degrees and cause the graphical data to divide into several separate groups. [32] The influence of such factors on the complex stabilities will be described in the following sections.

Competition between metal-ions and protons

As the majority of metal co-ordinating ligands are also proton bases, the degree of complex formation depends not only on the magnitude of the stability constant but also on the pH of the solution. This effect is exploited in acid-base titrimetry for determining metal complex stability constants (see Chapter 2). In addition, the competition for binding sites between metal-ions and protons is an important consideration when complex formation in pH buffered solutions is considered; for example, at physiological pH an imidazole nitrogen is a more effective binding site than an amine nitrogen donor.^[37] In these circumstances, a standardised stability constant (χ_{mlh}), which applies only to the pH for which it is calculated, is sometimes used. For a monobasic ligand the standardised stability constant is related to the 'normal' stoichiometric stability constant (β_{mlh} , see Section 2.3) by Eqn. 1.10.^[37]

$$\chi_{110} = \beta_{110} \frac{1}{1 + [\text{H}^+]/K_{011}} \quad 1.10$$

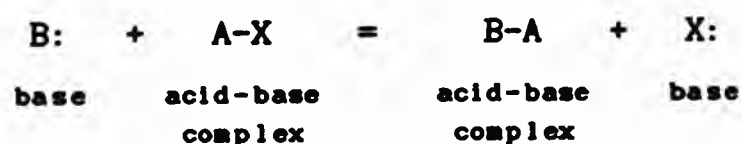
1.1.4 Complementarity of donor and acceptor atoms; the HSAB principle

Schwarzenbach noted that the nature of the atom which binds a ligand to the metal-ion largely determines the ligand behaviour and that certain metal-ions co-ordinate preferentially with specific donor types.^[38] Classifying the metal-ions into two groups, denoted A and B metals, he noted that for the first group - d^0 cations, e.g. the alkaline earth dications, Al^{3+} , Sc^{3+} , lanthanide trications, Ti^{4+} , Nb^{5+} - the stability of complexes increases rapidly with charge and that within isoelectric series, metal-ions with the smallest radius form the most stable complexes. For the B metals - d^{10} cations, e.g. Cu^+ , Ag^+ , Zn^{2+} , Cd^{2+} , Hg^{2+} , Ga^{3+} , In^{3+} , Tl^{3+} - Schwarzenbach

observed that charge does not play a decisive rôle in determining stability and stability sequences in isoelectric series are in reverse order to those expected on the basis of ionic radius.

Using a similar empirical basis for their observations, Ahrland, Chatt and Davies deduced a similar classification for metal-ions based on their Lewis acid (electron pair acceptor) properties.^[39] These authors suggested two classes of acceptor; class (a), metal ions which form their most stable complexes with the first ligand atom of the periodic group (*i.e.* N, O, and F) and class (b), those which form their most stable complexes with the second or subsequent ligand atom in each group (*i.e.* P, S, or Cl). In addition, they identified that several metals (principally the transition metals and some heavier post-transition metals) that could not be classified exclusively in either group. Of these, the transition metals tend to class (a) behaviour in their higher valence states and to class (b) behaviour in their lower valence states, while the post-transition metals (*e.g.* Tl, Pb, Bi) show opposite tendencies *i.e.* their higher valent states show more class (b) characteristics.

Pearson generalised these considerations to the formation of adducts from Lewis acids and Lewis bases, *e.g.*



where B and X are electron donors, A is an electron acceptor (in solution X is the solvent and is absent in the gas phase) and the adduct formed in the forward reaction, B-A, could be any stable organic or inorganic molecule, charge transfer complex or complex ion.^[40] Pearson divided the substrate

acids into two categories; those which bind strongly to highly polarisable (or unsaturated) bases which have negligible proton affinity, and those which bind strongly to predominantly non-polarisable bases which, in turn, bind the proton strongly. The two types were named, respectively, 'soft' and 'hard' acids and similarly, the types of bases to which they bind strongly were also termed 'soft' and 'hard' bases [the terms 'hard' and 'soft' are attributed to a suggestion by D. H. Busch in Ref. 40(a)].

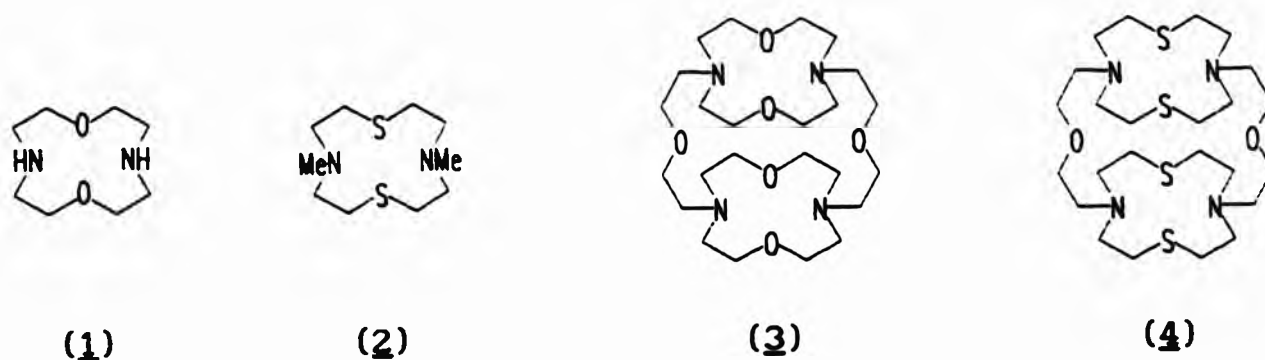
Table 1.1.2 Survey of hard and soft acids and bases. [40]

<u>HARD</u>	<u>SOFT</u>	<u>borderline</u>
ACIDS		
$H^+ Li^+ Na^+ K^+$	$Cu^+ Ag^+ Au^+ Tl^+ Hg^+ Cs^+$	$Fe^{2+} Co^{2+} Ni^{2+} Cu^{2+}$
$Be^{2+} Mg^{2+} Ca^{2+} Sr^{2+} Sn^{2+}$	$Pd^{2+} Cd^{2+} Pt^{2+} Hg^{2+} CH_3Hg^+$	$Zn^{2+} Pb^{2+}$
$Al^{3+} Sc^{3+} Ga^{3+} In^{3+} La^{3+}$	$Tl^{3+} Tl(CH_3)_3 BH_3$	$B(CH_3)_3 SO_2 NO^+$
$Cr^{3+} Co^{3+} Fe^{3+} As^{3+} Ir^{3+}$		
$Si^{4+} Ti^{4+} Zr^{4+} Th^{4+} Pu^{4+}$		
$VO_2^{2+} UO_2^{2+} (CH_3)_2Sn^{2+}$		
BASES		
$H_2O OH^- F^-$	$R_2S RSH RS^-$	$C_6H_5NH_2 C_6H_5N$
$CH_3CO_2^- PO_4^{2-} SO_4^{2-}$	$I^- SCN^- S_2O_3^{2-}$	$N_3^- Br^-$
$Cl^- CO_3^{2-} ClO_4^- NO_3^-$	$R_3P R_3As (RO)_3P$	$NO_2^- SO_3^{2-}$
$ROH RO^- R_2O$	$CN^- RNC CO$	
$NH_3 RNH_2 N_2H_4$	$C_2H_4 C_6H_6$	

In cases where metal-ions are the Lewis acids, Ahrland, Chatt and Davies's

class (a) and (b) classifications^[39] can be used interchangeably with the terms hard and soft. Hard acid-hard base interactions are characterised by components of small size and low polarisability bound by predominantly ionic forces and soft acid-soft base interactions are characterised by large, easily polarised components bound by predominantly covalent bonds. The principle of hard and soft acids and bases (HSAB) can be summarised as *hard acids bind strongly to hard bases and soft acids bind strongly to soft bases*.

Unfortunately, examples of reliable thermodynamic data for complexes derived via systematic substitution of donor atoms in modern metal-ion binding agents illustrating this principle are rare. In many cases HSAB influences are obscured by other factors. However, comparison of binding constants for macrocycles (1) and (2) and the macrotricycles (3) and (4), due to Lehn and co-workers,^[41] reveals that substitution of the 'hard' ether oxygen donors with 'soft' thioether donors causes dramatic increases in the affinity for the 'soft' silver(I) ion. In the macrocycles the affinity is increased by a factor of ca. 10^6 and in the binucleating macrotricycles the Ag^+ affinity is increased by ca. 10^{10} . Similarly, replacement of ether oxygen donors with thioether donors has recently found application as a design strategy for selective complexands of toxic heavy metal ions in these laboratories.^[42]



As ligand design has become more elaborate, Schwarzenbach's maxim that the

donor atom of a ligand largely controls its co-ordination behaviour has been overridden to some extent by the influence of other factors, particularly the steric preferences of ligands. These factors have been comprehensively reviewed by Hancock and Martell in the context of tailored ligand design.^[43]

1.1.5 Multidentate ligands and the 'chelate effect'

Much of the preceding discussion has considered unidentate ligands only and, as might be expected, as the number of points of attachment between the ligand and the metal-ion increases, more stable complexes result. However, it has generally been observed that polydentate ligands form more stable complexes than an equivalent number of monodentate ligands;^[44,45] this 'extra' contribution to stability is termed the chelate effect and is characterised by the competition reaction,



where the chelate ligand (L' with n donor atoms) displaces n comparable unidentate ligands (L) from the metal-ion co-ordination sphere. [Such increases in stability resulting from formation of five-membered chelate rings are illustrated in Figure 1.1.3 for a number of Ni(II) complexes of polyamine and polypyridine ligands]. The equilibrium constant for the displacement reaction,

$$K_{\text{chel}} = \frac{[ML'] [L]^n}{[ML_n] [L']} = \beta_{ML'} / \beta_{ML_n} \quad 1.12$$

can be used to quantify the chelate effect^[46] and corresponds to the ratio of the overall stability constants for the metal chelate ($\beta_{ML'}$) and metal complex of the unidentate ligands (β_{ML_n}).

Considerable discussion has surrounded the origin of the chelate effect.^[44,45,46,47,48,49,50] On the assumption that the affinities of each

donor atom of both types of ligand in the competition reaction are equal, Schwarzenbach's original model attributes the chelate effect to the reduced volume in which the second donor atom of the chelating ligand is confined to move once the first donor atom of the chelating ligand is bound to the metal.^[44,45] Defined in this way, the chelate effect is largely due to the increase in the translational entropy of the system^[44,45] which, in turn depends on the choice of the reference standard state for concentrations (significantly, the formation constants of the chelate and non-chelate complexes have different dimensions).^[47] If a hypothetical standard state of unit mole fraction for the solute (as well as the solvent) is chosen, the translational entropy of the solute and, hence the chelate effect, 'disappears' since the solute fully occupies the volume of the standard state.^[47] As Munro points out, this choice of standard state does not reflect practical situations and, although the numerical value of the chelate effect can even become negative if appropriate standard states are chosen, the experimentally observed phenomenon of ligand competition in solution remains valid.^[46] To overcome these ambiguities Fraústo da Silva has recently proposed a redefinition of the effect.^[48]

The basic assumption of the Schwarzenbach model, namely that the affinities of all donor atoms in the chelate and non-chelate ligands are identical, limits its applicability in practice and much discussion has surrounded appropriate choices of ligands for comparison.^[43,49,50] A number of possible enthalpic contributions to the chelate effect have been identified, of which the intrinsic ability of the chelate ligand to overcome steric and electrostatic repulsions between donor groups was considered as the most important.^[45] Intramolecular steric strain in the ligand backbone was also considered as a factor of some importance and its influence in the polyalkylamines has been

investigated recently with molecular mechanics.^[51] Greater (unfavourable) strain energies diminish the magnitude of the chelate effect in more complex ligands compared to their simpler homologues; force field calculations show that the change in strain energy of tetraethylenediamine is some 18 times that of ethylenediamine on co-ordination of Ni(II).^[51]

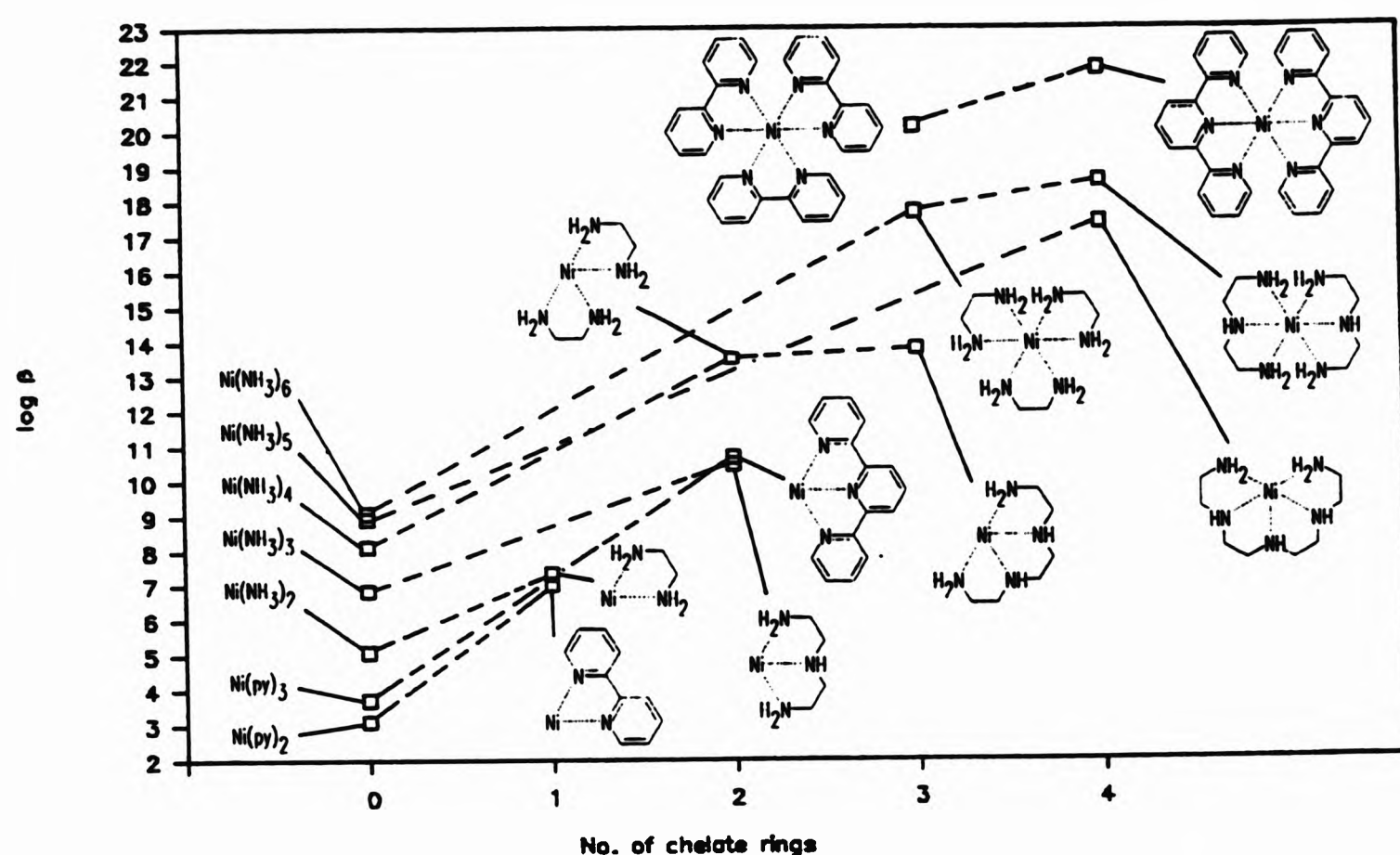


Figure 1.1.3 The increase in overall formation constant ($\log \beta$) with the number of five-membered chelate rings in various Ni(II) polyamine and polypyridine complexes. [Dotted lines relate comparable complexes with equal numbers of donor atoms].

Several important entropic influences to the magnitude of the chelate effect have also been identified;^[45] the size and order of the chelate rings (see Section 1.2.1) and changes in the solvation of species during complex formation. Displacement of solvating molecules of reactants during complexation results in a positive entropic contribution to the free energy change and therefore differences in the extent of solvation of either ligand

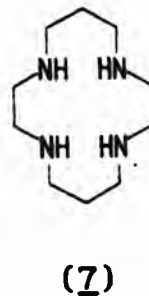
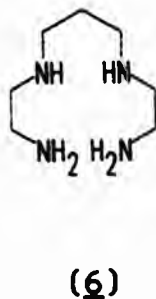
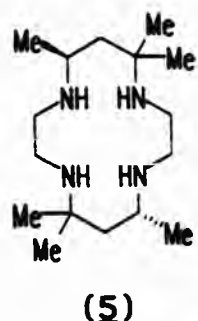
in a competition reaction (Eqn. 1.11) affects the magnitude of the chelate effect. However the entropic contribution is offset to some extent by the enthalpic implications of desolvation; e.g. should the chelate ligand have one less molecule of solvation then the enthalpy of complexation will be more favourable (less energy is required to desolvate the ligand prior to complexation), while the entropy of complexation is less favourable (fewer molecules are released during complex formation). Thus, free energy changes are less affected by solvation effects than entropy or enthalpy changes.^[52]

1.1.6 Influence of topology; the macrocyclic and cryptate effects

Rather in the same way that joining donor groups in chelating ligands increases the stability of their metal complexes over that of their monodentate analogues, cyclisation of polydentate ligands into macrocycles and macrobicycles increases complex stability above that of the corresponding chelate compounds. These influences are termed, respectively, the macrocyclic^[53] and cryptate^[54] effects and may be defined in terms of ligand metathesis reactions similar to the that employed in defining the chelate effect (Eqn. 1.12). However, comparisons for defining the macrocyclic and cryptate effects are more direct since formation constants with the same dimensions are compared.

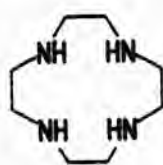
Cabiness and Margerum originally identified the macrocyclic effect in comparing the stabilities of Cu(II) complexes of the reduced Curtis ligand (5) and its acyclic analogue 2,3,2-tet (6).^[53] In the macrocyclic complex, the increase in stability was attributed to the stabilising effects of restricted ligand conformations and diminished ligand solvation as a result of steric hindrance of solvent molecules in the macrocyclic cavity.^[53] The first effect may be considered as a positive entropic contribution to complex

stability since unfavourable entropy changes result from restricting the open chain ligand in the complex. The second effect represents a negative (stabilising) enthalpy contribution to the free energy change on complexation since less energy is required to desolvate the cyclic ligand prior to complexation resulting in a more favourable enthalpy of complexation. In a study of the Ni(II) complex of cyclam (7), a macrocyclic effect of ca. 10^7 with respect to the Ni(II) complex of 2,3,2-tet (6) was identified by the Hinz and Margerum.^[55] Because of the predominance of enthalpic contributions to this increase in stability, the macrocyclic effect in this system was attributed to ligand solvation effects.^[55] These authors obtained similar results with other Ni(II)-tetramine complexes and the macrocyclic effects in these systems were also attributed to ligand solvation effects.^[56] These conclusions were confirmed subsequently in studies identifying that the differences in enthalpy changes on complexation lie in the different hydration energies of the non-coordinated cyclic and acyclic ligands.^[57]

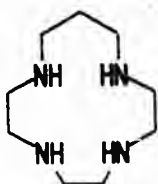


In contrast, Kodama and Kimura reported dominant entropy contributions to the macrocyclic effect for Cu(II) complexes of the smaller tetramine macrocycles (8 and 9) from formation constant determinations over a range of temperatures.^[58] Using similar experiments to determine thermodynamic parameters, these authors also attributed macrocyclic effects observed with d^{10} metal-ion complexes of triamine and pentamine macrocycles (e.g. 10 and 11) to favourable entropy contributions;^[59] although macrocyclic effects for

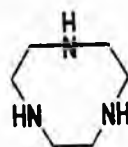
Cu(II) complexes of the same pentamine ligands were assigned to dominant enthalpic contributions.^[60] Interestingly, Paoletti and co-workers re-examined the thermodynamic parameters for Cu(II) and Zn(II)-tetramine systems in the light of ΔH measurements from calorimetry (purported to be more accurate than values derived from the temperature dependence of $\log K$) and concluded that enthalpy makes a significant but not dominant contribution to the macrocyclic effects in these systems.^[61] They also point out the importance of comparability between the macrocyclic complex and its linear counterpart, stating that valid comparisons can only be made if the co-ordination number and geometry of the metal is known to be the same in both complexes.^[62]



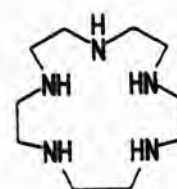
(8)



(9)

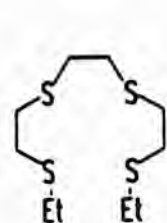


(10)

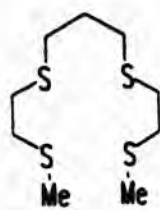


(11)

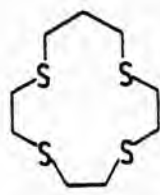
The importance of solvation has been highlighted in studies of macrocyclic effects in polythia ether systems.^[63] In comparing open-chain polythia ethers such as (12) and (13) with their macrocyclic counterparts (14) and (15), Rorabacher and co-workers identified relatively small macrocyclic effects in aqueous and *aqu.* methanol media (respectively 180 and 220).^[63] As these macrocyclic effects are entropy controlled, approximately independent of the medium and relatively small, observations that the polythia systems are not strongly solvated in aqueous and alcoholic media^[63] reiterates the importance of solvation in governing the magnitudes of macrocyclic effects.^[63]



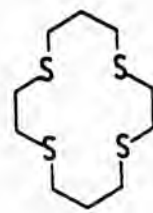
(12)



(13)

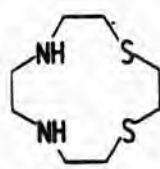


(14)

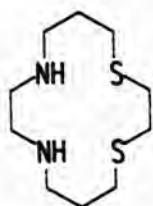


(15)

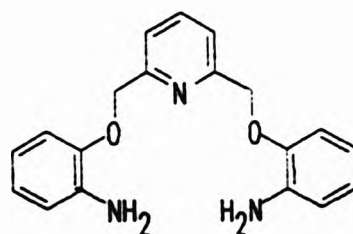
Rather larger macrocyclic effects (ca. 10^4) are observed in the Ni(II) and Cu(II) complexes of the corresponding mixed donor dithia-diaza systems, (16 and 17).^[64] Cyclisation in these ligands mainly influences the entropies of complexation although enthalpy changes also exert a stabilising influence in the complexes of the cyclic ligands.^[64] Of interest to studies in this dissertation, significant macrocyclic effects have recently been identified on comparison of Cu(II) and Zn(II) formation constants of the benzo-functionalised triaza-dioxo ligands (18 and 19).^[14b] To date however, enthalpy and entropy changes on complexation have not been obtained for these systems.



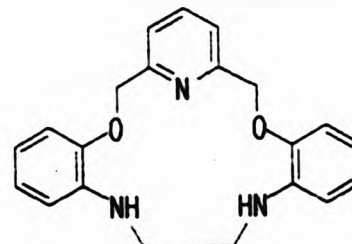
(16)



(17)



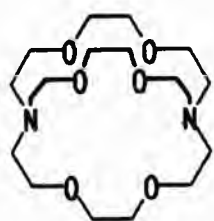
(18)



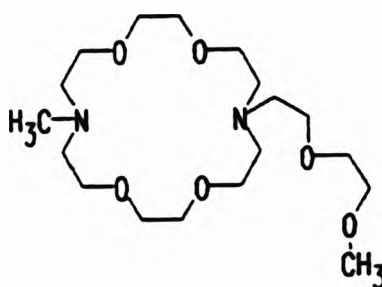
(19)

In conclusion, the important contributions to the macrocyclic effect appear to be;^[50] the enthalpy contributions arising from desolvation of ligand donors in the macrocyclic cavity, smaller losses of configurational entropy of macrocyclic systems on co-ordination compared to their acyclic analogues, increases of intrinsic ligand basicity due to an increased number of substituents at donor atoms, and 'pre-straining' of the donor atoms into a suitable configuration for interaction with the metal-ion. Although this last

point will be covered more generally in the following section it is noteworthy that its importance in determining macrocyclic effects has been highlighted by *ab initio* quantum mechanical calculations on cyclic tetramines.^[65]



(20)



(21)

The macrobicyclic or 'cryptate' effect has received rather less study than the macrocyclic effect although its origins are seen to lie with some common influences.^[66] Adoption of a bicyclic topology leads to a 10^5 increase in stability for K^+ complexes of 2,2,2-cryptand (20) over the complexes of (21), its pendant arm macrocyclic analogue.^[54] The alkali cryptates display large favourable enthalpies of formation due to the strong interaction of the metal cations with the weakly solvated polydentate ligand cavity.^[67] The relatively large negative (unfavourable) entropy changes accompanying complexation for these systems were attributed to outer sphere interaction of the large organic cation complex with solvent molecules in addition to the losses of the configurational entropy of the free ligand on complexation.^[67]

1.1.7 Ligand preorganisation

That stable complexes result from ligands that adopt similar conformations in complexed and uncomplexed states has been proposed under a number of guises; *e.g.* the concepts of pre-straining,^[68] pre-orientating,^[69] and juxtapositional fixedness^[70] have been used to describe contributions of this type to the macrocyclic effect. Cram's general principle of

preorganization for host-guest interactions^[71,72] can be used to group these concepts.^[50] As defined,^[72] hosts are characterised by convergent binding sites (the ligands in metal-ion co-ordination chemistry) and guests (the metal-ions) by divergent orientation of binding sites. Cram asserts^[72] that preorganization is the central determinant of the binding power and that, *the more highly hosts and guests are organized for binding and low solvation prior to their complexation, the more stable will be their complexes.*

While the organization level of a ligand can only be assessed qualitatively the concept can be widely applied to both cyclic and non-cyclic systems. The simplest examples of the rôle preorganization plays in determining metal complex stabilities can be found by comparing the ligands ethylenediamine-N,N'-tetraacetate (EDTA) with cyclohexyl-1,2-diamine-N,N'-tetraacetate (CDTA),^[50,73] and 2,2'-bipyridine with 1,10-phenanthroline^[43,74] (see Fig. 1.1.4). The uncomplexed tetraacetate ligands adopt different configurations; free rotation of the central C-C bond of EDTA allows the ligand to adopt the trans configuration, minimising repulsions between the acetate groups. Rotation of the corresponding bond in CDTA is precluded by the cyclohexane ring and the acetate groups are constrained in a skew arrangement. This latter arrangement corresponds with the configuration of the acetate groups in the complexed ligands and CDTA is thus preorganized for complex formation. Energy is not expended in orientating the acetate groups for complexation and this contributes to the higher stability of CDTA complexes (ca. 10^2 for first row transition metal-ions).^[20a]

		[20] log β_{110}			
		Co ²⁺	Ni ²⁺	Cu ²⁺	Zn ²⁺
'FREE' LIGAND	COMPLEXED LIGAND				
		16.3	18.5	18.7	16.4
		19.6	20.2	21.9	19.4
		5.8	7.0	6.3	5.1
		7.1	8.6	7.4	6.4

Figure 1.1.4 Ligand preorganization in chelating ligands; (i) Newman projections along the central C-C bonds of EDTA and CDTA and (ii) 2,2'-bipyridine vs. 1,10-phenanthroline.

Metal complexes of 1,10-phenanthroline are generally an order of magnitude more stable than those of 2,2'-bipyridine despite the similarities of their proton basicities.^[20] The increase in complex stability can be attributed to the effects of ligand preorganization.^[43,74] The cis-planar conformer of both ligands is required for metal chelation but is disfavoured in the 'free' 2,2'-bipy ligand because of steric clash between the 3- and 3'-hydrogens and

dipole-dipole repulsions between the nitrogen lone pairs. As rotation about the interannular bond is possible a 'skew' arrangement is adopted in the uncomplexed ligand (Fig. 1.1.4). Fusing the two pyridine rings yields 1,10-phen and imposes a cis-planar conformation for the nitrogen donor atoms in the uncomplexed ligand - hence 1,10-phen is preorganized for chelation and forms more stable complexes.

Although macrocycles and cryptands represent higher levels of organization than their chelate counterparts they are not, in the majority of cases, completely preorganized for metal-ion co-ordination. For example, X-ray studies indicate that the preferred ligand conformers for 18-crown-6, a macrocyclic polyether, and [2.2.2]-cryptand, a bicyclic polyether, involve exodentate orientations of some O-donor atoms resulting in methylene groups facing into the macrocyclic cavities.^[75a,76a] Spectroscopic studies indicate that these conformers are retained for the free ligands in solution.^[66,77] Clearly, a rearrangement occurs when spherical metal-ions are encapsulated by the ligands resulting in the 'open' cavities, with all donor atoms orientated in an endodentate configuration, that occur in the complexes (Fig. 1.1.5).^[75b,76b] Even in cases where unco-ordinated macrocyclic ligands adopt an 'open' configurations prior to complexation, solvation of donor atoms in the macrocyclic cavity^[78] precludes their complete preorganization for complexation.

Highly preorganized ligands have been synthesized by Cram and co-workers^[71,79,80] and the spherand (S) shown in Figure 1.1.5 represents one of the most highly preorganized ligands yet prepared.^[72] The ligand organizes six anisole oxygen donors in an octahedral array and completely excludes solvent molecules from its cavity.^[71] This results in some

remarkable binding constants for the smaller alkali metal ions (e.g. the Li^+ complex has a formation constant greater than 10^{16}).^[81] The preorganization of the macrocyclic cavity in this ligand also confers high size-based selectivity in its binding for the alkali metal-ions (see Section 1.2); while Li^+ and Na^+ are strongly bound by the ligand, complexation with the larger alkali metal-ions, which are too large to occupy the rigid ligand cavity, is negligible.^[81] Interestingly, this results in the ability of the spherand to selectively bind lithium and sodium impurities in concentrated KOH solutions.^[72]

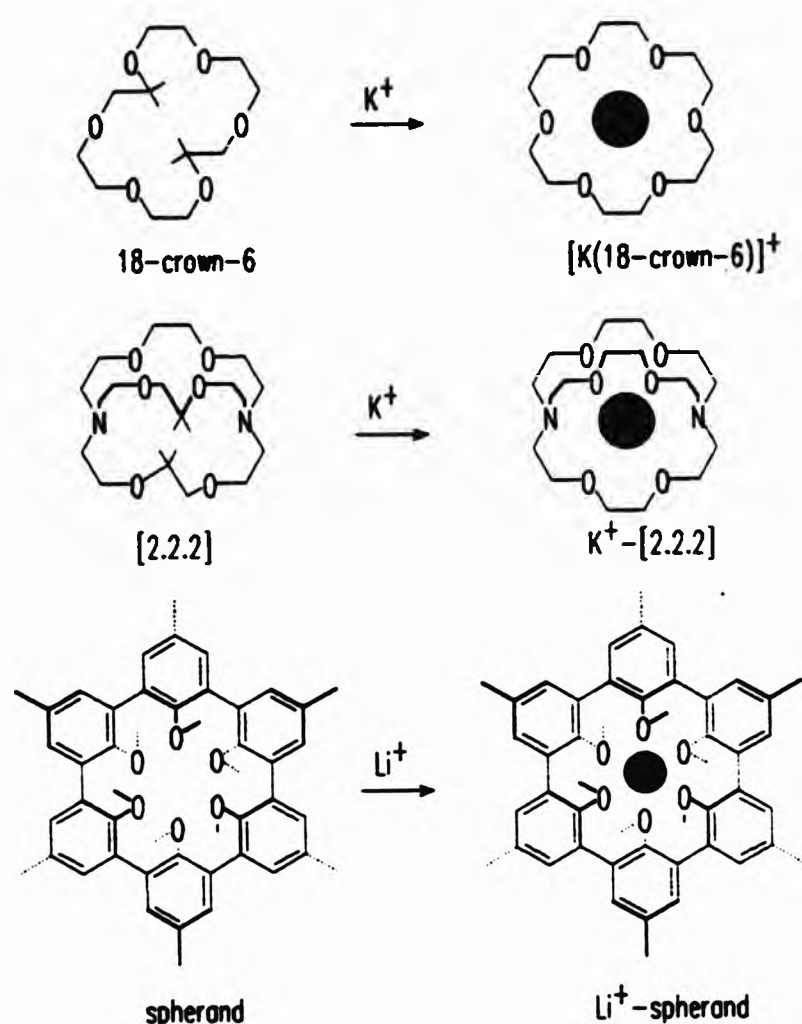


Figure 1.1.5 The incomplete preorganization of the binding cavities of 18-crown-6^[75] and [2.2.2]-cryptand^[76] in contrast to the complete preorganization of the binding cavity of the spherand (S)^[71] (After Ref. [71]).

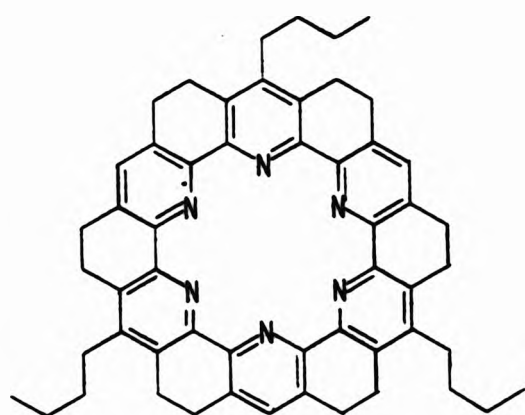
1.2 Metal ion recognition

While absolute binding strength is an important consideration for metal-ion co-ordination compounds, a large number of applications require ligands to bind metals selectively. The selectivity of metal-ion co-ordination^[82] is readily quantified in terms of the metathesis reactions such as,

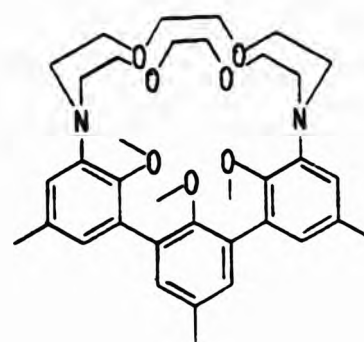


which may be viewed as competition for the ligand by the metal-ions. The equilibrium is therefore similar to the competition reactions used to quantify the chelate and macrocyclic effects (Eqns. 1.11 and 1.12) and its equilibrium constant is thus given by quotient of the respective metal complex formation constants. A parameter describing the preference of a ligand for a particular metal ion, i.e. its metal-ion selectivity, can be defined on this basis.

$$\Delta \log K = \log K_{ML} - \log K_{M'L}$$



(22)



(23)

That strongly binding ligands are not necessarily selective can be illustrated by considering the Na⁺ and K⁺ binding properties of the torand (22)^[83] in contrast to the cryptahemispherand (23)^[80,84] and spherand^[71,81] (S, Fig. 1.1.6). All these ligands show high levels of preorganization but while (23)

favours K^+ over Na^+ ($\Delta \log K = 4$)^[84] and the spherand is highly selective for Na^+ over K^+ ($\Delta \log K > 9$)^[81], the torand (22), despite binding both metals more strongly than the other ligands, shows negligible selectivity ($\Delta \log K = 0.4$).^[83]

As many of the HSAB properties (see Section 1.1.4) of related metals are similar, metal-ion recognition relies on one of two features of the metal-ion; its size and its ability to adopt specific co-ordination geometries. The rôle of each of these factors in determining metal-ion discrimination will be illustrated in the following sections.

1.2.1 Size match selectivity

Discrimination between metal-ions on the basis of size has received much attention in macrocyclic chemistry where 'tuning' of the macrocyclic cavity to the metal-ion size can lead to dramatic increases in selectivity for one metal in an otherwise closely related series of ions.^[82] Such size-match selectivity results from the tenet that ligands have the highest affinities for metal-ions whose diameter most closely matches that of the macrocyclic cavity. In such cases all donor atoms of the ligand fully participate in binding and hence bond energies between the ligand and metal are maximised.^[85]

The classic example of size-match selectivity in macrocyclic ligands is given by the binding of 18-crown-6 with the alkali and alkaline-earth metal-ions (Fig. 1.1.7).^[86] A size-match parameter quantifying the 'goodness-of-fit' of the metal-ion for the macrocyclic cavity can be defined in these systems.^[85] In order to reflect the electrostatic metal-ligand interaction in the complexes, the fit parameter is obtained from the ratio of the metal-ion

diameter to the diameter of the macrocyclic cavity. The latter value is obtained from X-ray structures of the complexed ligand.^[87] A plot of complex formation constant vs. this size-match parameter (Fig. 1.1.7) shows that complex stability is maximised in systems where the metal-ion best fits the macrocyclic cavity, i.e. where the size-match parameter is closest to unity. Calorimetric studies for 18-crown-6 complexes indicate that the trends in complex stability are reflected in the enthalpies of complexation,^[86] confirming the rôle of bond energy maximisation in this mechanism of metal-ion discrimination.

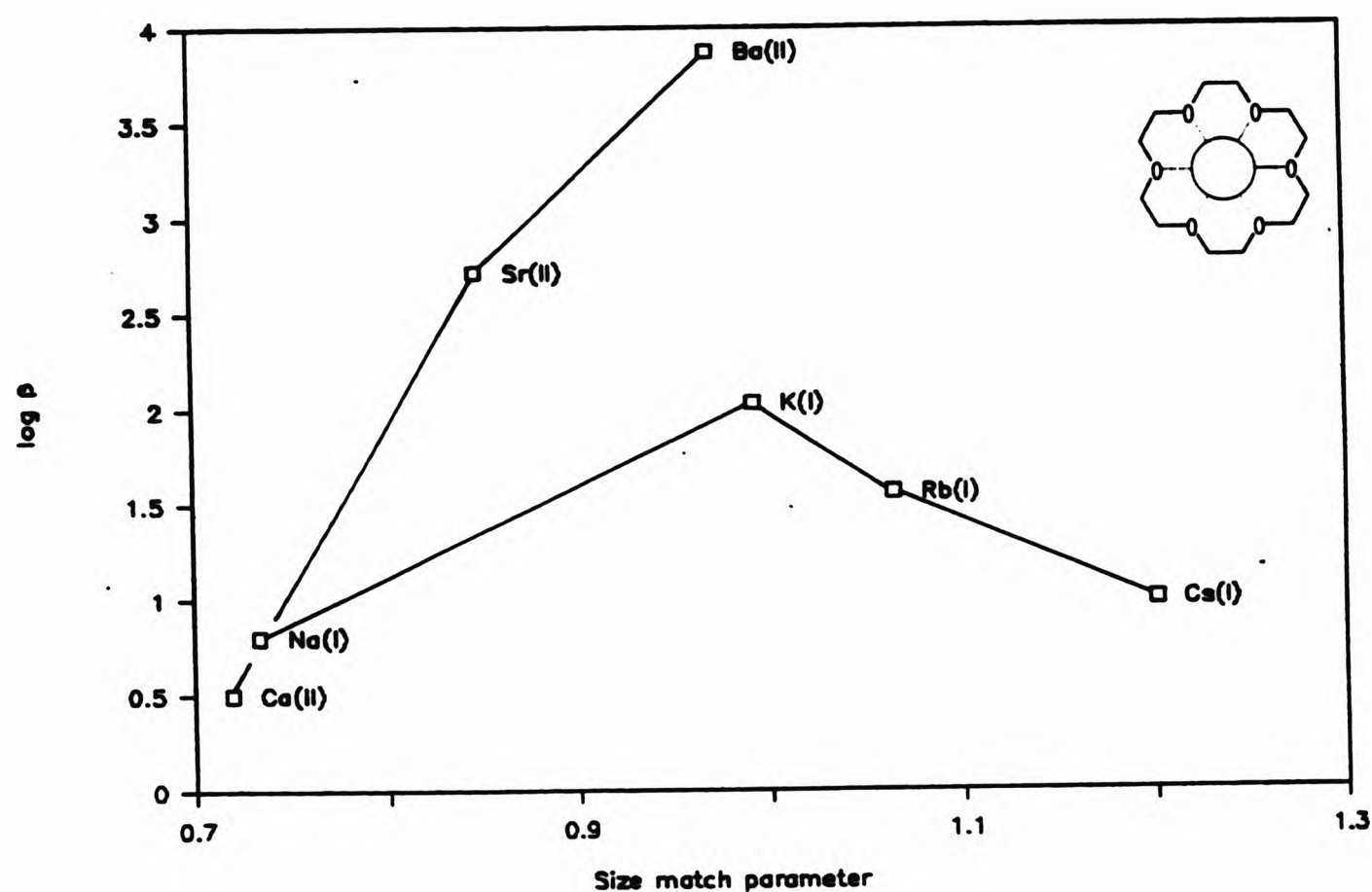


Figure 1.1.7 Formation constants of Group I and Group II metal-ion complexes of 18-crown-6 plotted against the ratio of ionic diameter^[22] to macrocyclic cavity.^[87] (After Ref. [85])

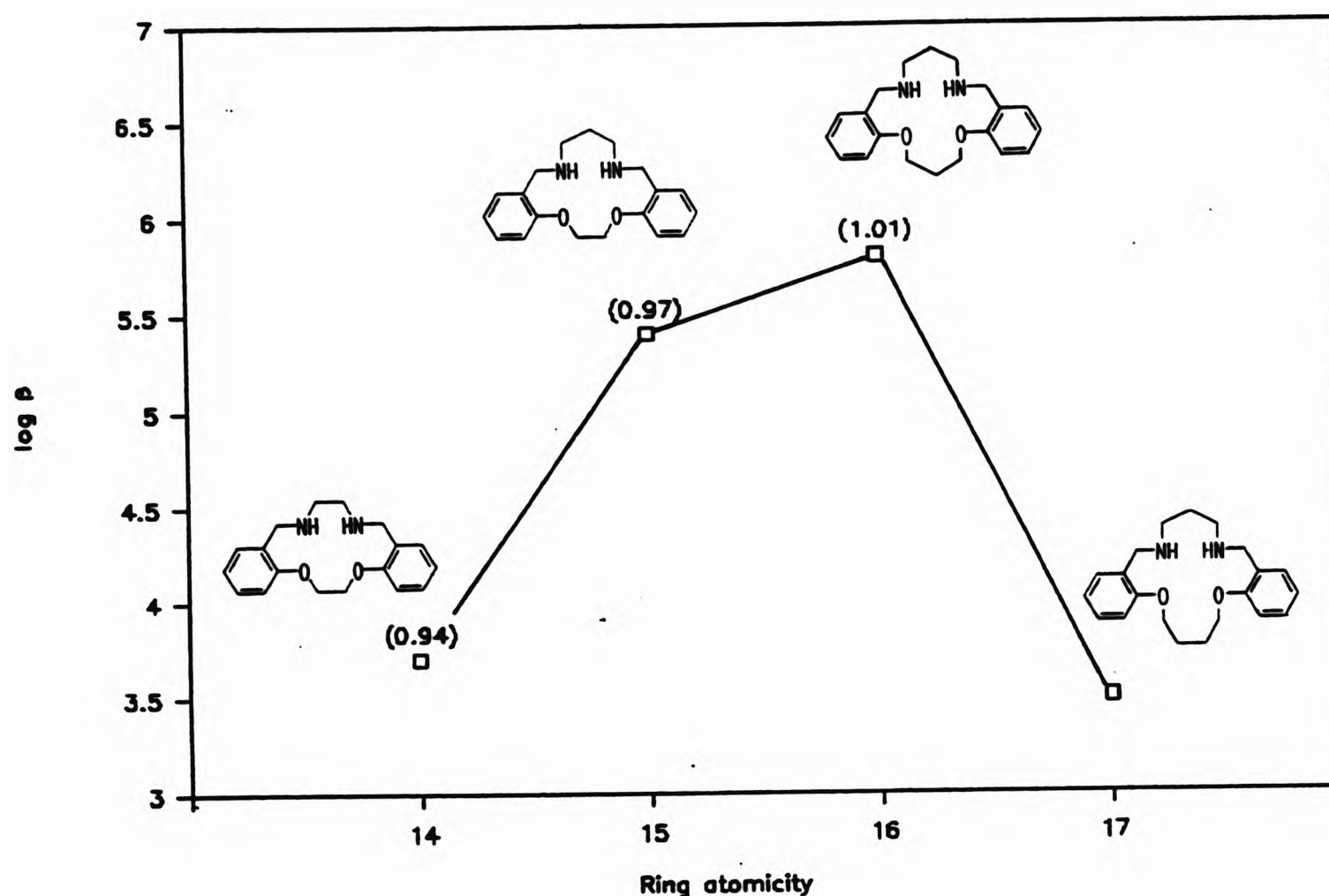
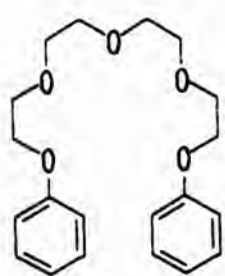


Fig. 1.1.8 Hole size vs. thermodynamic stability for nickel(II) complexes of a homologous series of dibenzo-diazadioxo macrocyclic ligands. 'Goodness of fit' parameters^[88] are shown in parentheses; no structural data exists for the 17-membered macrocycle. (After Ref. [88])

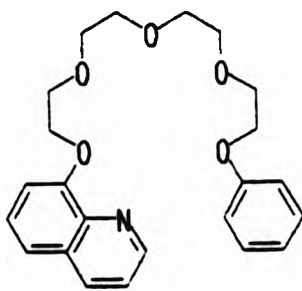
In order to account for non-planarity of donor sets in macrocyclic ligands and covalent components to their interaction with transition metal-ions, Henrick, Tasker and Lindoy have established procedures for specifying bonding cavities including corrections for the effective covalent radii of donor atoms in N-donor macrocyclic systems.^[88] A goodness-of-fit parameter in this context is derived from the ratio of the bonding cavity radius to the Pauling covalent radius^[89] for the metal-ion. A size-based recognition of Ni^{2+} was deduced for a series of N_2O_2 macrocyclic ligands using these considerations (see Fig. 1.1.8).^[88,90] For this series, the largest formation constant of the

nickel(II) complex was observed for the ligand which provides the best fit for the metal-ion, i.e. that with the goodness of fit parameter closest to unity.^[88] It is worth noting however, that the sensitivity of this goodness-of-fit function may limit its predictive powers, e.g. changes of ca. 4 % in the goodness of fit parameter translate into changes of log K between 0.4 and 1.7 (see Fig. 1.1.8).

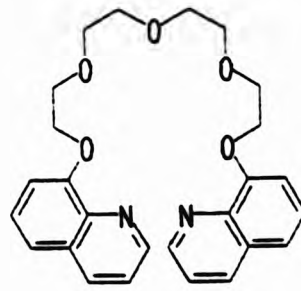
Recognition of metal ions on the basis of size is not limited to cyclic ligands. For example, Maas and co-workers reported potassium-selective open chain glyme ligands [(24), (25) and (26)].^[91] The K⁺-selectivity is greatest in (24) and approaches that of its cyclic analogue, 15-crown-5.^[50] A pseudo-cyclic structure for (24), stabilised to some extent by π -stacking interactions between the aromatic glyme substituents, was proposed as the basis for this selectivity.^[91] In contrast, the lower K⁺-selectivity displayed by (25) and (26) was attributed to the presence of the relatively strong 8-oxyquinoline donors in the ligands, which in providing the centre of nucleation for the complexes, predominate in determining the complexation behaviour. In these cases, the ether chains are thought to adapt to different cation sizes as the gross structure of the complexes is determined by the orientation of the N-donor sites.^[91]



(24)



(25)



(26)

Lindoy states that hole-size effects, including size-match selectivity, are more dominant in rigid macrocyclic systems;^[82] as flexibility in the ligand increases it becomes more able to adapt its configuration to compensate for mismatches between the relative sizes of the metal and its cavity. In such cases, hole-size effects in determining orders of stability can become obscured. Accordingly, in studies of a homologous series of tetraaza macrocycles, Hancock and co-workers observed selectivity patterns that are reversed from those expected on size-match criteria;^[92] larger metal-ions, e.g. Cd^{2+} and Pb^{2+} , form their most stable complexes with the smallest macrocycle (8) in the series while the smaller metal-ions formed progressively more stable complexes with the larger macrocycles in the series, e.g. cyclam (7). Force field calculations revealed that the flexibility of the ligands was crucial in determining their complexation behaviour.^[93] Due to the flexibility of the ligand backbone, out-of-plane modes of metal co-ordination are readily adopted in these systems and, in these cases, the metal binding affinities are controlled by the sizes of the chelate rings formed on co-ordination, not by the relative fit of the metal to the macrocyclic cavity.^[93]

Using molecular mechanics, Hancock and co-workers have investigated the rôle of chelate ring size in determining a size-based selectivity of metal-ions in some detail.^[94] Modelling 5-membered chelate rings with ethylenediamine and 6-membered rings with propylenediamine, minima in strain energies were calculated at a metal-to-nitrogen distance of 2.5 Å with a N-M-N bite angle of 70 ° for 5-membered chelate rings; an M-N distance of 1.6 Å and a bite angle of 100 ° corresponds to a minimum strain energy in 6-membered chelate rings.^[94] Thus smaller ions are expected to bind preferentially within 6-membered chelate rings, and larger ions within 5-membered chelate rings.

These patterns are amplified in polydentate systems, e.g. 2,2,2-tet vs. 2,3,2-tet (6) and also apply in chelate rings rigidified by aromatic substituents.^[94] These patterns have been confirmed by comparing log K data in suitable systems,^[43,94,95] and their implications have been discussed in terms of directed ligand design for selective complexing agents.^[43]

1.2.2 Dislocation discrimination

Lindoy and co-workers have identified a second mechanism for metal-ion discrimination based on the ability of a metal-ion to adopt specific co-ordination geometries.^[13,96] Changes in the metal-ion co-ordination geometry in complex structures of a series of closely related ligands can result from systematic changes to the ligand structure.^[13,96]

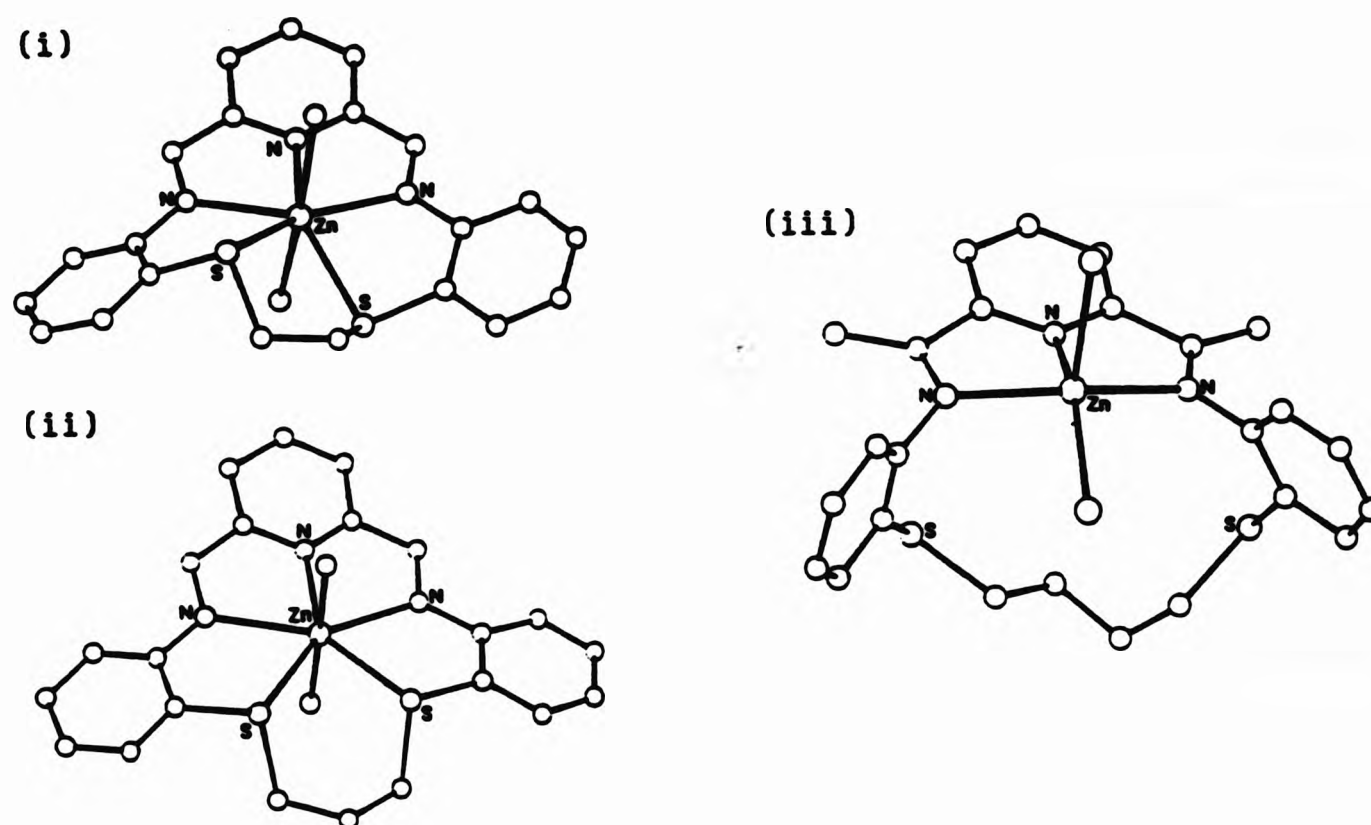


Figure 1.1.9 Structural 'dislocation' of S-donors in zinc(II) complexes of an homologous series of triazadithia macrocyclic ligands.^[97,98] Zinc(II) co-ordination spheres are completed with (i) unidentate ClO_4^- , (ii) H_2O and (iii) I^- ; non-coordinated anion atoms and hydrogen atoms are omitted for clarity.

A structural dislocation is illustrated in Figure 1.1.9 with X-ray structures of zinc(II) complexes of a series of triazadithia ligands.^[97,98] Monotonic increase of the alkyl chain separating the thioether donor atoms causes a structural dislocation; the co-ordination number of the Zn(II) changes as the S-donors atoms become dissociated from the metal co-ordination sphere in the 17-membered macrocycle [Fig. 1.1.9(iii)].

Although in the case of these triazadithia ligands (Figure 1.1.9) stability constant measurements are precluded by the hydrolytic tendencies of the imine functions in the ligands,^[97] such 'dislocations' can induce dramatic changes in complex stabilities and if they occur at different ligands in the series for different metal-ions, metal selectivity is enhanced for closely related metal-ions.^[13,96] The stability patterns for Zn(II) and Cd(II) complexes of the dibenzo-tetraaza macrocycles demonstrate such an enhancement of metal selectivity (Fig. 1.1.10).^[96b,99]

Increasing the ring atomicity from the 14-membered to the 15-membered macrocycle causes a substantial drop (ca. 2.4 log units) in the stability of Cd(II) complex while the stability of the Zn(II) complex remains unaffected. However a corresponding drop in stability (ca. 2.2 log units) in the Zn(II) complexes occurs when a further methylene group is inserted into the macrocyclic ring while the stability of the Cd(II) complex remains largely unchanged. Thus the Zn(II) over Cd(II) discrimination is maximised in the 15-membered ligand ($\Delta \log K = 3.2$).

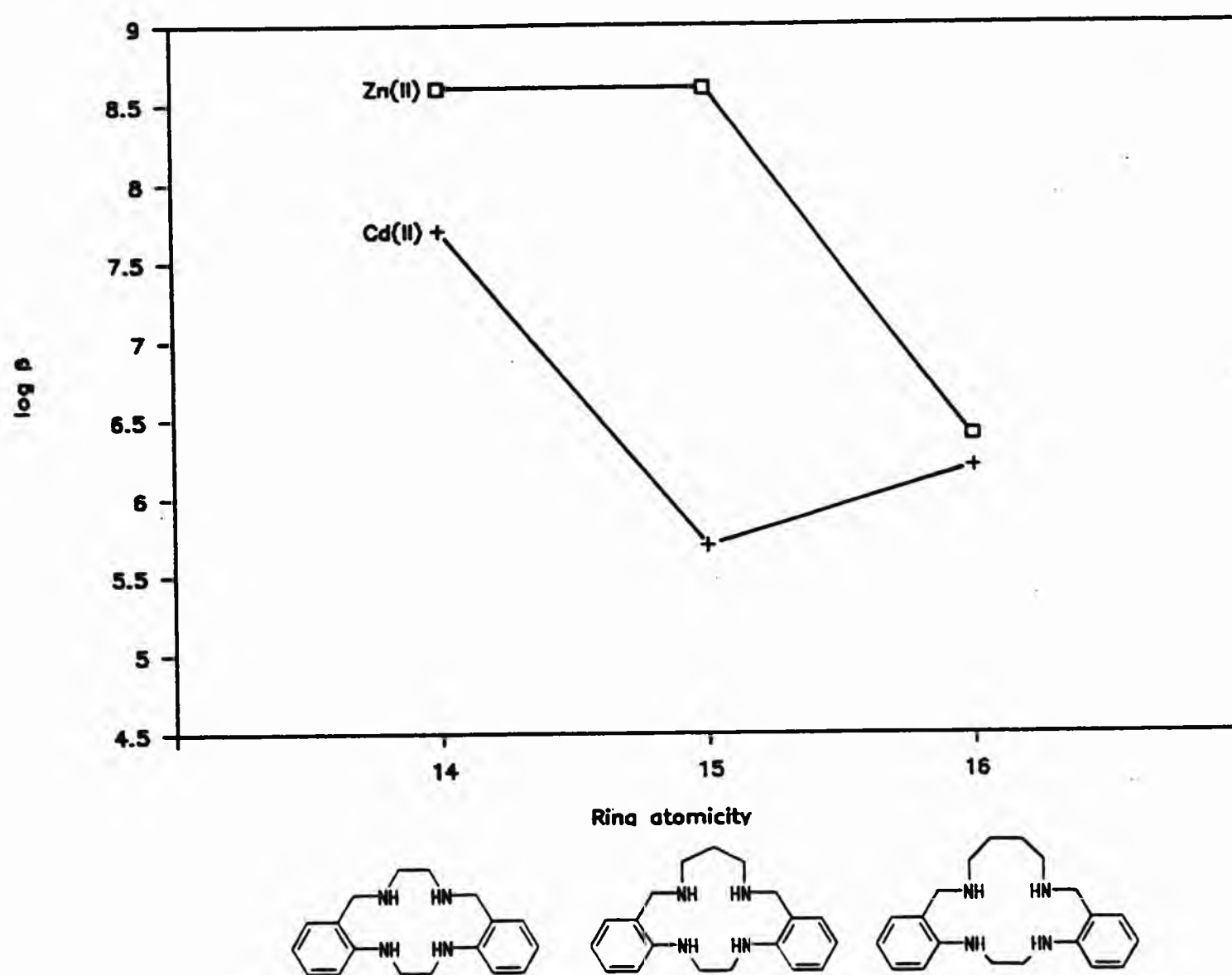
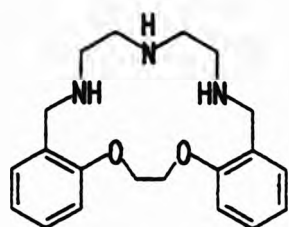


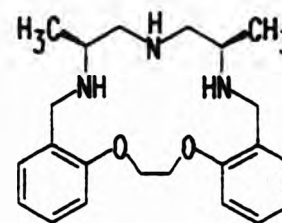
Figure 1.1.10 Stability patterns for Zn(II) and Cd(II) complexes of dibenzo-tetraaza macrocycles. [96b, 99]

X-ray structural evidence does not fully substantiate the occurrence of a structural dislocation in the Cd(II) complex of the 15-membered macrocycle. [99] However, the metal-ion lies substantially out of the N_4 -donor plane and possesses a severely distorted 6-co-ordinate geometry (the remaining co-ordination sites are occupied by a bidentate nitrate anion). In contrast, the Zn(II) complex of the same ligand shows the metal-ion in a pseudo-octahedral co-ordination geometry, lying within the equatorially orientated N_4 -donor plane (remaining co-ordination sites are occupied by a

unidentate nitrate ion and a water molecule). While these differences in structure are likely to stabilise the Zn(II) complex to some extent, the authors recognize that such structures may not be retained in solution and point to the possibility that the relatively weak anilino donors may be involved in structural dislocation, perhaps leading to *exo*-macrocyclic metal co-ordination.^[99]



(27)



(28)

The preceding examples show the rôle of variation of ring size in inducing structural changes, and hence differences in stabilities, for complexes. However, an example of structural dislocation due to differences in macrocyclic substituents has been identified.^[100] Introduction of methyl substituents to the external structure of the triazadioxa macrocycle (27), yielding (28), results in a drop in stability of nickel(II) complexes of ca. 10^3 .^[100] Differences in complex stabilities have been attributed to differences in the structures of the complexes; in the unsubstituted ligand the triazaheptane unit adopts a facial configuration as part of a pseudo-octahedral nickel co-ordination sphere whereas in the dimethyl derivative the triazaheptane unit adopts a meridional configuration as part of a 5-co-ordinate metal geometry. Molecular mechanics calculations^[101] indicate that the *fac*-configuration is destabilised in the dimethyl substituted macrocycle relative to the *mer*-configuration as a result of the steric requirements of the methyl substituents. In this compound a less

stable 5-co-ordinate geometry is therefore imposed on the Ni^{2+} ion which, assuming that these effects are replicated in solution, translates into the lowered stability constant.

References

1. M. T. Beck, *Chemistry of Complex Equilibria*, Van Nostrand Reinhold, London, 1970.
- 2 (a) S. Soloveichik and H. Krakauer, in *Werner Centennial - Advances in Chemistry Series No. 62*, ed. R. F. Gould, ACS Publications, Washington D. C., 1967, ch. 2; P. S. Shea, *ibid*, ch. 3; (b) F. R. Morral, *ibid*, ch. 5.
3. See for example, R. A. Bulman, *Struct. Bonding*, 1987, 67, 91; D. Bryce-Smith, *Chem. Soc. Rev.*, 1986, 15, 93; D. Parker, *Chem. Br.*, 1990, 26, 942; R. A. Bulman, in *Trace Metals and Fluoride in Bones and Teeth*, eds. N. D. Priest and F. L. Van De Vyver, CRC Press, Boca Raton, 1990; R. B. Lauffer, *Chem. Rev.*, 1987, 87, 901.
4. See for example, R. W. Hay, *Bio-inorganic Chemistry*, Ellis Horwood, Chichester, 1987; J. F. Stoddart, in *Progress in Macrocyclic Chemistry*, eds. R. M. Izatt and J. J. Christensen, 1981, vol. 2, ch. 4; S. Silver, in *Membrane and Transport*, ed. A. N. Martibisum, Plenum Press, New York, 1982, vol. 2; L. F. Lindoy, *The Chemistry of Macrocyclic Ligand Complexes*, Cambridge University Press, Cambridge, 1989, ch. 9; J. A. Tainer, E. D. Getzoff, D. C. Richardson and J. S. Richardson, *Nature*, 1983, 306, 284; L. Banci, A. Bencini, I. Bertini, C. Luchinat and M. Piccioli, *Inorg. Chem.*, 1990, 29, 4867.
5. See for example, A. L. McCrary and W. L. Howard, in *Encyclopaedia of Chemical Technology*, ed. Kirk-Othmer, Wiley Interscience, New York, 3rd Edn., vol. 5, pp. 361-367; R. Thompson (ed.), *Trace Metal Removal from Aqueous Solution*, Royal Society of Chemistry (Publ.), London, 1986; F. Habashi, *Chem Eng. News*, 1982, Feb. 8, 46.
6. K. J. Irgolic and A. E. Martell (eds.), *Environmental Inorganic Chemistry*, VCH Publishers, Deerfield Beach, 1985.
7. P. A. Tasker, presented at the 14th International Symposium on Macrocyclic Chemistry, Townsville, Australia, 1989.
8. M. Calvin and A. E. Martell, *Chemistry of Metal Chelate Compounds*, Prentice-Hall, Englewood Cliffs, N. J., 1952, pp. 451-462; B. R. Green and R. D. Hancock, *S. Afr. Inst. Min. Metall.*, 1982, 82, 303.
9. R. L. Smith, *The Sequestration of Metals: Theoretical Considerations and Practical Applications*, Chapman and Hall, London, 1959.
10. D. St.C. Black, in *Comprehensive Coordination Chemistry*, Pergamon Press, Oxford, 1987, vol. 6, pp. 155-227.
11. J. Becher, G. Bojesen, B. Girmay, M. E. Harman, M. B. Hursthouse,

- J. D. Kilburn, A. E. Underhill, K. S. Varma, *J. Chem. Soc., Chem. Commun.*, 1989, 1406.
12. J-M. Lehn, *Angew. Chem. Int. Ed. Engl.*, 1988, 27, 89.
 13. L. F. Lindoy, in *Current Topics in Macrocyclic Chemistry in Japan*, ed. E. Kimura, Hiroshima School of Medicine (Publ.), 1987.
 14. (a) A. Bashall, D. E. Fenton, A. J. Leong, L. F. Lindoy, M. McPartlin and B. P. Murphy, *J. Chem. Soc., Dalton Trans.*, 1987, 2543; (b) K. R. Adam, A. Bashall, M. R. Dent, S. Donnelly, D. E. Fenton, A. J. Leong, L. F. Lindoy, B. J. McCool, M. McPartlin, B. P. Murphy and P. A. Tasker, *J. Chem. Soc., Dalton Trans.*, 1990, 1635.
 15. (a) N. A. Bailey, D. E. Fenton, S. J. Kitchen, A. J. Leong, T. H. Lilley, L. F. Lindoy, P. A. Tasker and M. G. Williams, *J. Chem. Soc., Dalton Trans.*, 1991, 627; (b) H. Adams, N. A. Bailey, D. E. Fenton, I. G. Ford, S. J. Kitchen, A. J. Leong, T. H. Lilley, L. F. Lindoy, P. A. Tasker and M. G. Williams, *J. Chem. Soc., Dalton Trans.*, 1991, 1665; (c) N. A. Bailey, D. E. Fenton, S. J. Kitchen, A. J. Leong, T. H. Lilley, L. F. Lindoy, P. A. Tasker and M. G. Williams, *J. Chem. Soc., Dalton Trans.*, 1991, 2989.
 16. D. Sherwood, *Introductory Thermodynamics*, Longman Group, London, 1971.
 17. P. W. Atkins, *Physical Chemistry*, Oxford University Press, 1982, 2nd Edn., p. 939.
 18. (a) F. A. Cotton and G. Wilkinson, *Advanced Inorganic Chemistry*, Wiley Interscience, 1972, 3rd Edn., p. 652; (b) *ibid*, p. 596.
 19. J. Bjerrum, *Metal Amine Formation in Aqueous Solution*, P. Hasse and Son, Copenhagen, 1957; B. Sen, *Anal. Chim. Acta*, 1962, 27, 515.
 20. (a) A. E. Martell and R. M. Smith, *Critical Stability Constants, Volume 1: Amino Acids*, Plenum Press, 1974; (b) *ibid*, Volume 2: *Amines*, 1975; (c) *ibid*, Volume 3: *Other Organic Ligands*, 1977; (d) Volume 4: *Inorganic Complexes*, 1976; (e) Volume 5: *First Supplement*, 1982; (f) Volume 6: *Second Supplement*, 1989.
 21. H. Sigel, *Angew. Chem. Int. Ed. Engl.*, 1975, 6, 394.
 22. R. D. Shannon, *Acta Cryst.*, 1976, A32, 751.
 23. R. J. P. Williams, *J. Chem. Soc.*, 1952, 3770.
 24. C. W. Davies, *J. Chem. Soc.*, 1951, 1256.
 25. C. F. Baes and R. F. Mesner, *The Hydrolysis of Cations*, Wiley, New York, 1976.
 26. P. L. Brown, J. Ellis and R. N. Sylva, *J. Chem. Soc., Dalton Trans.*, 1985, 723.

27. J. E. Huheey, *Inorganic Chemistry*, Harper and Row, New York, 1978, 2nd Edn., p. 294.
28. H. Irving and R. J. P. Williams, *Nature*, 1948, 162, 746; H. Irving and R. J. P. Williams, *J. Chem. Soc.*, 1953, 3192.
29. See for example; A. G. Sharpe, *Inorganic Chemistry*, Longman, London, 1981, pp. 465-472; D. S. Urch, *Orbitals and Symmetry*, Macmillan, London, 1979, pp. 165-176.
30. J. C. Kotz and K. F. Purcell, *Inorganic Chemistry*, W. B. Saunders Company, Philadelphia, 1977, p. 573.
31. See C. J. Ballhausen, *Introduction to Ligand Field Theory*, McGraw-Hill, New York, 1962; B. N. Figgis, *Introduction to Ligand Fields*, Wiley, New York, 1966.
32. M. Calvin and A. E. Martell, *Chemistry of Metal Chelate Compounds*, Prentice-Hall, Englewood Cliffs, N. J., 1952, pp. 151-159.
33. J. G. Jones, J. B. Poole, J. C. Tomkinson and R. J. P. Williams, *J. Chem. Soc.*, 1958, 2001.
34. E. N. Rizkalla, *Rev. Inorg. Chem.*, 1983, 5, 223.
35. R. J. Bruehlman and F. H. Verhoek, *J. Am. Chem. Soc.*, 1948, 70, 1401.
36. See for example, H. Irving and H. Rossotti, *Acta Chem. Scand.*, 1956, 10, 72; T. Kaden and H. Sigel, *Helv. Chim. Acta*, 1966, 49, 1617.
37. D. B. McCormick and H. Sigel, *Acc. Chem. Res.*, 1970, 3, 201.
38. G. Schwarzenbach, *Experientia Suppl.*, 1956, 5, 162; *Adv. Inorg. Radiochem.*, 1961, 3, 257.
39. S. Ahrland, J. Chatt and N. R. Davies, *Quart. Rev.*, 1958, 12, 265.
40. (a) R. G. Pearson, *J. Am. Chem. Soc.*, 1963, 85, 3533; (b) *Science*, 1966, 151, 172; (c) *Chem. Brit.*, 1967, 3, 103; (d) *J. Chem. Ed.*, 1968, 45, 581, 643.
41. F. Arnaud-Neu, J-M. Lehn, M. Sanchez, M-J. Schwing-Weill and R. Yahaya, *Helv. Chim. Acta*, 1985, 68, 456; M-C. Alamasio, F. Arnaud-Neu, J-M. Lehn, M-J. Schwing-Weill and S. A. Sullivan, *Helv. Chim. Acta*, 1985, 68, 831.
42. S. Waikar, Ph.D. Thesis, University of North London, 1992.
43. A. E. Martell and R. D. Hancock, *Chem. Rev.*, 1989, 89, 1875.
44. G. Schwarzenbach, *Helv. Chim. Acta.*, 1952, 35, 2344.
45. A. E. Martell, in *Werner Centennial - Advances in Chemistry Series No. 62*, ed. R. F. Gould, ACS Publications, Washington D. C., 1967, ch. 19.
46. D. Munro, *Chem. Brit.*, 1977, 13, 100.
47. A. W. Adamson, *J. Am. Chem. Soc.*, 1954, 76, 1578.

48. J. J. R. Fraústo da Silva, *J. Chem. Ed.*, 1983, 60, 390.
49. R. D. Hancock and F. Marsicano, *J. Chem. Soc., Dalton Trans.*, 1976, 1096.
50. R. D. Hancock and A. E. Martell, *Comments Inorg. Chem.*, 1988, 6, 237.
51. R. D. Hancock, G. J. McDougall and F. Marsicano, *Inorg. Chem.*, 1979, 18, 2847.
52. R. D. Hancock, B. S. Nakani and F. Marsicano, *Inorg. Chem.*, 1983, 22, 2531.
53. D. K. Cabbiness and D. W. Margerum, *J. Am. Chem. Soc.*, 1969, 91, 6540.
54. J-M. Lehn and J-P. Sauvage, *J. Am. Chem. Soc.*, 1975, 97, 6700.
55. F. P. Hinz and D. W. Margerum, *J. Am. Chem. Soc.*, 1974, 96, 4993.
56. F. P. Hinz and D. W. Margerum, *Inorg. Chem.*, 1974, 13, 2941.
57. R. M. Clay, S. Corr, G. Keenan and W. V. Steele, *J. Am. Chem. Soc.*, 1983, 105, 2070.
58. E. Kimura and M. Kodama, *J. Chem. Soc., Dalton Trans.*, 1976, 116; *ibid*, 1720.
59. E. Kimura and M. Kodama, *J. Chem. Soc., Dalton Trans.*, 1978, 1081.
60. E. Kimura and M. Kodama, *J. Chem. Soc., Dalton Trans.*, 1978, 104.
61. A. Anchini, R. M. Clay, L. Fabrizzi and P. Paoletti, *Inorg. Chim. Acta*, 1977, 22, L25.
62. M. Micheloni and P. Paoletti, *Inorg. Chim. Acta*, 1980, 43, 109.
63. L. L. Diaddario, T. E. Jones, L. A. Ochrymowycz, D. B. Rorabacher and L. L. Zimmer, *J. Am. Chem. Soc.*, 1975, 97, 7163; R. B. Cruz, L. L. Diaddario, T. E. Jones, L. A. Ochrymowycz, D. B. Rorabacher, L. S. W. L. Sokol, E. L. Yee and L. L. Zimmer, *J. Am. Chem. Soc.*, 1975, 97, 7163; L. A. Ochrymowycz, D. B. Rorabacher and L. S. W. L. Sokol, *Inorg. Chem.*, 1981, 20, 3189.
64. T. A. Kaden, M. Micheloni, P. Paoletti and L. Siegfried-Hertli, *J. Chem. Soc., Dalton Trans.*, 1985, 1169.
65. G. J. Reibnegger and B. M. Rode, *Inorg. Chim. Acta*, 1983, 72, 47.
66. J-M. Lehn, *Acc. Chem. Res.*, 1978, 11, 49.
67. J-M. Lehn, E. Kauffmann and J-P. Sauvage, *Helv. Chim. Acta*, 1976, 59, 1099.
68. J. C. A. Boeyens, R. D. Hancock and G. J. MacDougall, *J. Chem. Soc., Dalton Trans.*, 1978, 1438.
69. A. Anchini, R. M. Clay, L. Fabrizzi and P. Paoletti, *J. Chem. Soc., Dalton Trans.*, 1978, 577; R. M. Clay, L. Fabrizzi and P. Paoletti, *Inorg. Chem.*, 1978, 17, 1043.
70. D. H. Busch, K. Farmery, V. Goedken, V. Katovic, A. C. Melnyk,

- C. R. Sperati and N. Tokel, *Adv. Chem. Ser.*, 1971, 100, 44.
71. S. B. Brown, D. J. Cram, R. C. Helgeson, T. Kaneda, E. Maverick and K. N. Trueblood, *J. Am. Chem. Soc.*, 1985, 107, 3645.
 72. D. J. Cram, *Angew. Chem. Int. Ed. Engl.*, 1986, 25, 1039.
 73. Y. Moriguchi, N. Okatu, K. Toyoda and K. Ueno, *Bull. Chem. Soc. Jpn.*, 1967, 40, 2326.
 74. G. Nord, *Comments Inorg. Chem.*, 1985, 4, 193.
 75. (a) J. D. Dunitz and P. Seiler, *Acta Cryst.*, B30, 2739;
(b) J. D. Dunitz, M. Dobler, R. P. Phizackerly and P. Seiler, *Acta Cryst.*, B30, 2733.
 76. (a) B. Metz, D. Moras and R. Weiss, *Proc. Int. Conf. Coord. Chem.*, 1970, 13, 85; B. Metz, D. Moras and R. Weiss, *J. Chem. Soc., Perkin Trans. 2*, 1976, 423; (b) B. Metz, D. Moras and R. Weiss, *Acta Cryst.*, 1973, B29, 1377.
 77. J. Dale and P. O. Kristiansen, *Acta Chem. Scand.*, 1972, 26, 1471.
 78. See for example, M. Bos, J. van Eerden, P. D. J. Grootenhuys, S. Harkema, W. T. Klooster, L. Kruise, D. N. Reinhoudt, C. J. van Staveren, E. J. R. Sudhölter and J. W. H. M. Uiterwijk, *J. Am. Chem. Soc.*, 1986, 108, 780.
 79. D. J. Cram, I. B. Dicker, M. Lauer, C. B. Knobler and K. N. Trueblood, *J. Am. Chem. Soc.*, 1984, 106, 7150.
 80. D. J. Cram, S. P. Ho, C. B. Knobler, E. Maverick and K. N. Trueblood, *J. Am. Chem. Soc.*, 1986, 108, 2989.
 81. D. J. Cram and G. M. Lein, *J. Am. Chem. Soc.*, 1985, 107, 3657.
 82. L. F. Lindoy, *The Chemistry of Macrocyclic Ligand Complexes*, Cambridge University Press, Cambridge, 1989, pp. 185-191; L. F. Lindoy, in *Synthesis of Macrocycles: The Design of Selective Complexing Agents*, eds. D. Christensen and R. M. Izatt, John Wiley, New York, 1987, ch. 2.
 83. T. W. Bell, A. Firestone and R. Ludwig, *J. Chem. Soc., Chem. Commun.*, 1989, 1902.
 84. D. J. Cram and S. P. Ho, *J. Am. Chem. Soc.*, 1986, 108, 2998.
 85. J. J. Christensen, D. J. Eatough, R. M. Izatt and J. D. Lamb, in *Coordination Chemistry of Macrocyclic Compounds*, ed. G. A. Melson, Plenum Press, New York, 1979.
 86. A. G. Avondet, J. J. Christensen, N. K. Dally, L. D. Hansen, B. L. Haymore, R. M. Izatt and R. M. Terry, *J. Am. Chem. Soc.*, 1976, 98, 7620.
 87. N. K. Dally, in *Synthetic Multidentate Macrocyclic Compounds*, eds.

- J. J. Christensen and R. M. Izatt, Academic Press, New York, 1978.
88. K. Henrick, L. F. Lindoy and P. A. Tasker, *Prog. Inorg. Chem.*, 1985, 33, 1.
89. L. Pauling, *The Nature of the Chemical Bond*, Cornell University Press, New York, 3rd edn., 1960.
90. K. R. Adam, G. Anderegg, A. Ekstrom, K. Henrick, M. McPartlin, L. F. Lindoy, R. J. Smith and P. A. Tasker, *J. Chem. Soc., Chem. Commun.*, 1979, 812; G. Anderegg, A. Ekstrom, L. F. Lindoy and R. J. Smith, *J. Am. Chem. Soc.*, 1980, 102, 2670.
91. U. Heimann, G. Maas, H. Sieger, B. Tümmeler, F. Vögtle and E. Weber, *J. Am. Chem. Soc.*, 1979, 101, 2588.
92. R. D. Hancock, G. D. Hosken and V. J. Thom, *Inorg. Chem.*, 1985, 24, 3378; R. D. Hancock and V. J. Thom, *J. Chem. Soc., Dalton Trans.*, 1985, 1877; R. D. Hancock and M. P. Ngwenya, *J. Chem. Soc., Dalton Trans.*, 1987, 2911. 93. R. D. Hancock, *Pure Appl. Chem.*, 1986, 58, 1445 and refs. therein.
94. K. V. Damu, R. D. Hancock, M. P. Ngwenya, A. S. de Sousa and P. W. Wade, *Inorg. Chem.*, 1990, 29, 1968.
95. R. D. Hancock, *J. Chem. Ed.*, 1992, 69, 615.
96. (a) K. R. Adam, K. P. Dancey, B. A. Harrison, A. J. Leong, L. F. Lindoy, M. McPartlin and P. A. Tasker, *J. Chem. Soc., Chem. Commun.*, 1983, 1351; (b) K. R. Adam, C. W. G. Ansell, K. P. Dancey, L. A. Drummond, A. J. Leong, L. F. Lindoy and P. A. Tasker, *J. Chem. Soc., Chem. Commun.*, 1986, 1011.
97. D. C. Liles, M. McPartlin and P. A. Tasker, *J. Chem. Soc., Dalton Trans.*, 1987, 1631.
98. M. G. B. Drew and S. Hollis, *J. Chem. Soc., Dalton Trans.*, 1978, 511.
99. K. R. Adam, C. W. G. Ansell, P. J. Baillie, K. P. Dancey, L. A. Drummond, K. Henrick, A. J. Leong, L. F. Lindoy, B. J. McCool, M. McPartlin, P. A. Tasker, and D. K. Uppal, *J. Chem. Soc., Dalton Trans.*, 1990, 3435.
100. K. R. Adam, A. J. Leong, L. F. Lindoy, H. C. Lip, B. W. Skelton and A. H. White, *J. Am. Chem. Soc.*, 1983, 105, 4645; P. A. Harding, K. Henrick, L. F. Lindoy, M. McPartlin and P. A. Tasker, *J. Chem. Soc., Chem. Commun.*, 1983, 1300.
101. K. R. Adam, L. G. Brigden, K. Henrick, L. F. Lindoy, M. McPartlin, B. Minnagh and P. A. Tasker, *J. Chem. Soc., Chem. Commun.*, 1985, 710.

Section A - Equilibrium Studies

2. Introduction

Analysis of equilibria in the solution chemistry of co-ordination compounds entails both an evaluation of the equilibrium constants for metal-ligand reactions and, where more than one metal complex is involved, determination of the species present in solution. [A description of the solution chemistry of a system which includes both these parameters is termed the chemical model]. The equilibrium constant of a metal complexation reaction (widely referred to as the stability or formation constant) provides a quantitative measure of the affinity of a ligand for particular metal ions. Comparisons between such parameters can therefore yield information about the metal ion selectivity displayed by ligands and may thereby demonstrate the success or failure of directed ligand design.

The need for accurate measurement of stability constants led to the development of a computer-controlled titration apparatus in these laboratories, capable of yielding potentiometric data under conditions of high thermal and electrochemical stability. The apparatus, described in Chapter 3, has been used in a number of speciation studies in a variety of solvent media (described in Chapters 4 and 5), and the following sections outline the conventions and principles applied to stability constant determinations in these studies.

2.1 Stepwise formation of complexes.^[1,2]

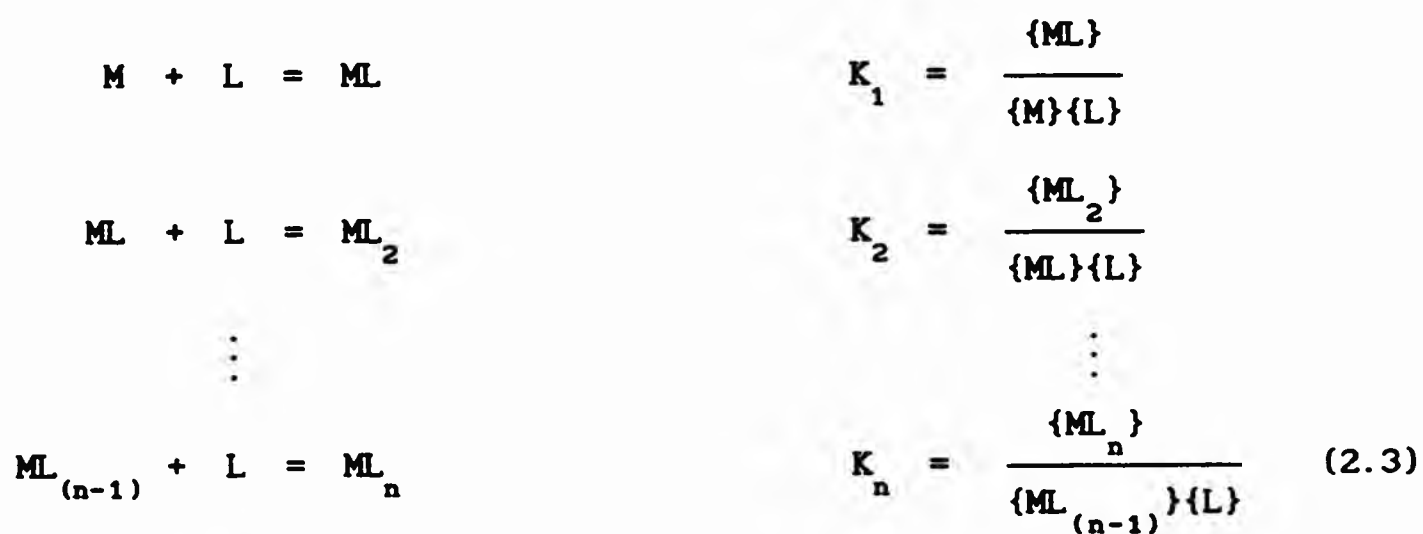
The formation of a complex ML can be expressed by the equilibrium,



The equilibrium constant, K , for this reaction is given by applying the law of mass action,

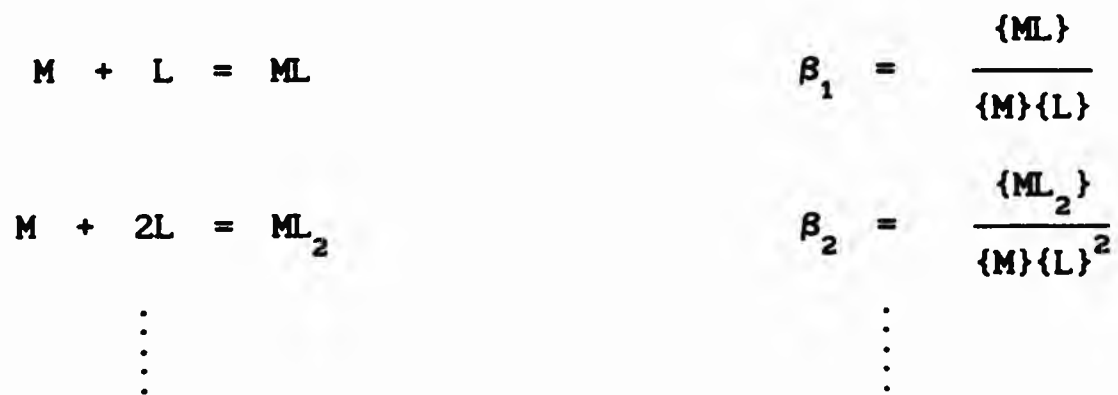
$$K = \frac{\{ML\}}{\{M\}\{L\}} \quad (2.2)$$

where $\{A\}$ is the activity of species A (the product of the concentration of A and its activity coefficient). The stepwise formation of complexes implies that the formation of the mononuclear complex ML_n is accompanied by the intermediate species $ML_{(n-1)}$, $ML_{(n-2)}$...etc. The system is described by the following equilibria and equilibrium constants.



The constants K_i are known as the stepwise stability constants for the i th species.

The system may also be described by considering the formation of the complexes by combination of metal and ligand units.





The constants β_i are known as the overall stability constants of the i th species. The overall and stepwise constants are related by Eqn. 2.5.

$$\beta_i = K_1 K_2 K_3 \dots K_i = \prod_{i=1}^i K_i \quad (2.5)$$

If the Lewis acid M is the hydrogen ion then the stability constants are known as the protonation constants for the ligand.

Protonated and hydrolysed complexes. ^[1,2]

The protonation of a multidentate ligand at one or more of its electron-donating groups can yield a protonated metal complex if the metal ion is able to bind simultaneously with other basic sites in the ligand. The general reaction,

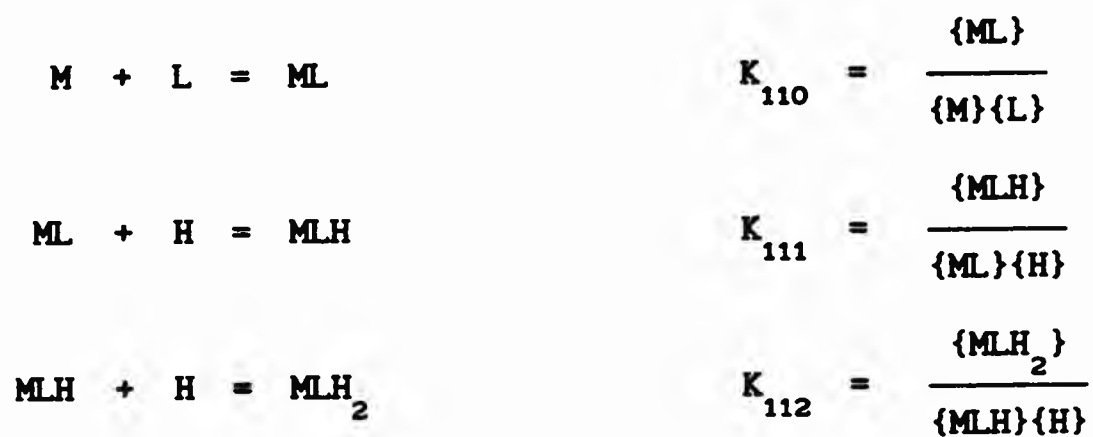


describes the formation of the protonated complex $M_l H_h$. The overall stability constant for the species $M_l H_h$ is therefore given by,

$$\beta_{mlh} = \frac{\{M_l H_h\}}{\{M\}^m \{L\}^l \{H\}^h} \quad (2.6)$$

This convention for describing the overall stability constant of the species, $M_l H_h$ will be employed throughout this work.

Formation of protonated complexes may also be regarded as a stepwise process. The formation of the complex MLH_2 may be described by the following equilibria,



and clearly,

$$\log \beta_{112} = \log K_{110} + \log K_{111} + \log K_{112} \quad (2.7)$$

Hydrolysis equilibria can also be conveniently expressed within this convention by considering deprotonation reactions. The proton contribution to the stoichiometry of the hydrolysed species is considered as 'negative', *e.g.* formation of $[\text{CuOH}]^+$ would correspond with $\log \beta_{10-1}$. In the case of metal complexes, such reactions may represent either the loss of a ligand-based proton or from deprotonation of water in the metal co-ordination sphere (*i.e.* hydrolysis). In order to overcome this ambiguity, it is usual to define the 'most hydrolysed' form of the ligand as the reactant (L);^[3] *e.g.* the glycinate anion ($\text{H}_2\text{NCH}_2\text{CO}_2^-$) is defined as L whereas glycine itself ($\text{H}_2\text{NCH}_2\text{CO}_2\text{H}$) is denoted by LH. Hydrolytic equilibria for metal complexes in this convention therefore arise from deprotonation of metal hydrates (Eqn. 2.8) and the formation constants for the deprotonation reaction may be directly related to the formation constant for the hydrolysed metal complex (Eqn. 2.9) via the dissociation constant for H_2O .

$$[\text{ML}(\text{H}_2\text{O})_n]^{z+} = [\text{ML}(\text{OH})_n]^{(z-n)+} + n\text{H}^+ \quad \beta_{\text{ml-h}} = \frac{\{\text{ML}(\text{OH})_n\} \{\text{H}\}^n}{\{\text{ML}(\text{H}_2\text{O})_n\}} \quad (2.8)$$

$$[\text{ML}]^{z+} + n\text{OH}^- = [\text{ML}(\text{OH})_n]^{(z-n)+} \quad \beta_{\text{ml(OH)}} = \frac{\{\text{ML}(\text{OH})_n\}}{\{\text{ML}\} \{\text{OH}\}^n} \quad (2.9)$$

$$\text{Since } K_w = \{\text{H}^+\} \{\text{OH}^-\}$$

$$\beta_{\text{ml(OH)}} = \frac{\{\text{ML}(\text{OH})_n\}}{\{\text{ML}\}} \frac{\{\text{H}\}^n}{K_w^n} = \frac{\beta_{\text{ml-h}}}{K_w^n}$$

Taking logs,

$$\log \beta_{\text{ml(OH)}} = \log \beta_{\text{ml-h}} + npK_w \quad (2.10)$$

2.2 Mass balance

Each reactant in a system at equilibrium will, in general, be present in a number of different species. The total activity of each reactant is the sum of the activities of the unco-ordinated reactant and its co-ordinated species.

In the general case, with $\text{M}_m\text{L}_l\text{H}_h$ as the highest species formed, total activities of M, L and H are given by, ^[1,2]

$$\{\text{M}\}_{\text{tot}} = \{\text{M}\} + \sum_{m=1}^{m=\text{M}} \sum_{l=1}^{l=\text{L}} \sum_{h=1}^{h=\text{H}} m \{\text{M}_m\text{L}_l\text{H}_h\} \quad (2.11)$$

$$\{\text{L}\}_{\text{tot}} = \{\text{L}\} + \sum_{m=1}^{m=\text{M}} \sum_{l=1}^{l=\text{L}} \sum_{h=1}^{h=\text{H}} l \{\text{M}_m\text{L}_l\text{H}_h\} \quad (2.12)$$

$$\{\text{H}\}_{\text{tot}} = \{\text{H}\} + \sum_{m=1}^{m=\text{M}} \sum_{l=1}^{l=\text{L}} \sum_{h=1}^{h=\text{H}} h \{\text{M}_m\text{L}_l\text{H}_h\} \quad (2.13)$$

Since $\{M L H\}_{m l h} = \beta_{m l h} \{M\}^m \{L\}^l \{H\}^h$ these expressions become,

$$\{M\}_{tot} = \{M\} + \sum_{m=1}^{m=M} \sum_{l=1}^{l=L} \sum_{h=1}^{h=H} m \beta_{m l h} \{M\}^m \{L\}^l \{H\}^h . \quad (2.14)$$

$$\{L\}_{tot} = \{L\} + \sum_{m=1}^{m=M} \sum_{l=1}^{l=L} \sum_{h=1}^{h=H} l \beta_{m l h} \{M\}^m \{L\}^l \{H\}^h . \quad (2.15)$$

$$\{H\}_{tot} = \{H\} + \sum_{m=1}^{m=M} \sum_{l=1}^{l=L} \sum_{h=1}^{h=H} h \beta_{m l h} \{M\}^m \{L\}^l \{H\}^h . \quad (2.16)$$

These equations may be employed for plots of species distribution as a function of pH, allowing direct evaluation of equilibrium solution composition. The concentrations of each species in the system are generally given as mole fractions of total metal or ligand concentrations and are usually deduced with computer algorithms.^[4] Species distribution plots for this study have been generated using Martell and Motekaitis's SPE program.^[5]

2.3 Thermodynamic and stoichiometric stability constants

The law of mass action is strictly valid only when species activities are used in Eqn. 2.2. The activity of a species is the product of its concentration and activity coefficient. Thermodynamic stability constants, also known as activity quotients, are calculated using species activities and are independent of the ionic medium.

Most detection methods employed for stability constant determination measure species concentrations instead of activities. Stoichiometric stability constants (concentration quotients) result from the use of species

concentrations in Equation 2.6 and are medium dependent. However, if concentration quotients are determined in the presence of a large excess of a suitable salt (the 'background electrolyte') it may be assumed^[1,2] that the activity coefficients of the species are independent of the concentrations of the reacting species and depend only on the nature and the concentration of the bulk electrolyte. The ionic strength (I) of the background electrolyte is given by the expression,

$$I = 0.5 \sum_i [i] z_i^2 \quad (2.17)$$

where [i] is the concentration of the ion i and z_i is its charge.

An effective background electrolyte has to meet the following criteria:^[2]

- (i) it must be a strong electrolyte;
- (ii) its cation or anion must not interact with the ligand or with complex species;
- (iii) redox reactions must not occur between the constituents of the electrolyte and the metal, ligand or complex species;
- (iv) its solubility must be large enough, and
- (v) its contribution to the measured physical or chemical property must be negligible.

In practice criterion (ii) may not be fulfilled; e.g. metal complexes of nitrate and perchlorate anions (widely employed as background ions due to their 'weak' affinity for metal ions) are well known.^[6] However, if the background electrolyte is present in sufficient excess, its equilibrium concentration may be regarded as constant and formally included in the equilibrium constant [solvent concentrations are treated similarly in solvent dissociation constants (e.g. K_w)].

Stoichiometric stability constants are exclusively reported in this study; species concentrations, denoted [A], therefore replace activities, {A}, in Eqns. 2.2-2.16.

2.4 Potentiometry in analysis of equilibria

In potentiometry, an electrode responding to one of the species (A) is used to measure its activity or concentration depending on the experimental conditions. The potential of the cell (E) is given by the Nernst equation,^[7]

$$E = E'_0 + (RT/nF)\ln\{A\} + E_j \quad (2.18)$$

where E'_0 is a constant for the cell, R is the gas constant, T is the temperature, F is the faraday, n is the number of electrons participating in the cell reaction and E_j is the term representing liquid-liquid junction potentials of any such junctions in the cell. In media containing an excess of background electrolyte, the activity coefficient term of Eqn. 2.18 is considered constant^[1,2] and may be included in the constant term E_0 yielding:

$$E = E_0 + (RT/nF)\ln[A] + E_j \quad (2.19)$$

The observed concentration of the electroactive ion is then used to evaluate the stability constants and compositions of the complex species using Eqns 2.14-16.

2.5 Computational methods for determining equilibrium constants

Pre-computer methods of data reduction are covered in a number of texts,^[1,2,8] of which that of Rossotti and Rossotti^[1] is regarded as

the definitive work. However, the complexity of equilibrium systems containing even relatively few species has been causal in the widespread adoption of computer methods for data treatment. The majority of general programs are based on the least-squares principle, calculating the 'best' values for the set of n desired parameters (e.g. β_{min} values) which minimise the residual squares sum (U) given by,

$$U = \sum_1^I w_1 (y_{\text{obs},1} - y_{\text{calc},1})^2 = \sum_1^I w_1 r_1^2 \quad (2.20)$$

where w_1 is the statistical weight, $y_{\text{obs},1}$ is the observed data at the i th data point, $y_{\text{calc},1}$ is the corresponding calculated value based on estimates of the n parameters and r_1 is the error residual for the i th data point. The principle relies on certain assumptions about the observed data;^[3] that it contains no systematic errors, that the random errors in the dependent variable have a normal (Gaussian) distribution, and that weights assigned are an exact measurement of the inherent accuracy of an observation. A number of programs based on this principle are currently available and the more widely used programs have been the subjects of a number of reviews.^[9,10,11,12,13,14] The minimum in the function of U with respect to the n desired parameters may be obtained from a number of established mathematical algorithms.^[15] Derivative methods (such as the Newton-Raphson and Newton-Gauss methods), based on the assumption that $\partial U / \partial n = 0$ at the minimum, have found wide application in this field. Small shifts are applied to input estimates of the n desired parameters and the minimum in the function of U corresponding to the 'best' set of the n parameters is found via an iterative procedure.

2.5.1 The programs MINIQAD and SUPERQUAD.

MINIQAD (mini quadrati)^[16] was developed by Gans, Sabatini and Vacca as a

general program for computation of stability constants from potentiometric titration data. It is based on least-squares algorithms for data reduction used in Sabatini and Vacca's program LEAST^[17] for refinement of stability constants and calculates the values of formation constants which minimise the residual squares sum of observed and calculated analytical reactant concentrations from an estimated chemical model. The titre volume is used as the independent variable during minimisation. Preliminary calculation of unknown 'free' reactant concentrations at each data point is achieved by non-linear regression (with the Newton-Raphson method) from the mass balance equations (Eqns. 2.14-16) using the potentiometrically-determined concentrations of the electroactive ion. These observed concentration values are then employed during the main minimisation (Newton-Gauss) in order to obtain the 'best' β_{mlh} values. Data points are not weighted during minimisation (in order to circumvent problems in accurately weighting data observed with the earlier program LEAST^[17]). After successful convergence, the calculated stability constants, along with parameters which characterise the quality of the 'fit' of the constants to the experimental data (the 'fit' parameters), and a graphical display of the residuals for each data point are produced as output. MINIQAD generates an R-factor to indicate the quality of fit for the calculated equilibrium model. The R-factor is defined by,

$$R = \left[\frac{\sum_1^1 w_1 (y_{obs,1} - y_{calc,1})^2}{\sum_1^1 w_1 (y_{obs,1})^2} \right]^{\frac{1}{2}} \quad (2.21)$$

and refinements for which $R/m < 0.002$ (m is the number of refined β values) are regarded as acceptable.^[18]

A second version of MINIQAD - MINIQAD-75^[19] - has been introduced giving faster and more reliable convergence and an automated model selection

procedure. In addition, a number of variants of MINQUAD have appeared in the literature; Meloun *et al.* have employed a version allowing refinement of E_0 in order to overcome inaccuracies in cell calibration procedures,^[14] Sylva and co-workers describe versions adapted to allow further refinement of β_{mlh} values that become negative (and therefore meaningless) during a refinement cycle and to refine the total proton concentration,^[20] and Arnold *et al.* have reported a microcomputer version.^[21] An unpublished MINQUAD version adapted to refine the total proton concentration, developed by Adam^[22] and widely applied by Lindoy *et al.* in a number of equilibrium studies, was used in the studies reported here.

Sabatini and Vacca described a subsequent program, MIQUV,^[23] which computes optimum values of β_{mlh} values from potentiometric data by minimising the residual squares sum of the observed and calculated cell emf values. Differing substantially from MINQUAD, the program assigns weighting factors to each data point (obtained from the reciprocal of estimated variances) for minimisation and allows refinement of certain group parameters (*i.e.* those that are unique to each titration; *e.g.* analytical concentrations, cell calibration parameters) as well as refining the common parameters (*i.e.* those that are identical in all titrations; *e.g.* β_{mlh} values). The authors noted that this facility proved to be useful in many systems and essential in some cases for successful refinement of data. Different fit parameters from those of MINQUAD are generated in MIQUV; the program uses Pearson's χ^2 statistic to evaluate the validity of the Gaussian assumptions about the titration data (*vide supra*) - a fit with an experimental $\chi^2 < 12.60$ implies that the model can be accepted at a confidence level of $> 95\%$ ^[24] - and a sample standard deviation (σ) defined as,

$$\sigma = \left(\frac{\sum w_i r_i^2}{m - n} \right)^{\frac{1}{2}} \quad (2.22)$$

where m is the number of data observations and n is the number of refined parameters. The σ statistic is of primary importance in model selection since the 'best' model is that which yields the lowest σ value.^[25]

These features of MIQUV are employed in SUPERQUAD^[25] (designed by Gans, Sabatini and Vacca to supercede MINIQVAD) which incorporates improvements in differential evaluation procedures, automated model selection facilities and revised data input and output formats. SUPERQUAD can treat data obtained for substances which cannot be obtained pure (by refining the appropriate group parameter) and can be used to account for non-Nernstian electrode response. Optional use of data weighting schemes allows less weight to be given to data near end points where larger errors in the measured potential are inevitable. In contrast to MINIQVAD and MIQUV, SUPERQUAD does not reject β values that become negative in an iteration cycle. An unmodified version of SUPERQUAD has been used in the majority of stability constant determinations in this study.

Both MINIQVAD and SUPERQUAD are widely used and their application to a variety of equilibrium systems is widely reported in the literature e.g. the Science Citation Index of 1989 lists over 50 references to such applications.

3. Experimental methods

3.1 Aminomethylenephosphonate syntheses.

3.1.1 Starting materials

Origins and purities of reagents used in syntheses of α -alkylaminomethylenephosphonic acids are summarised in Table 3.1.1.

Table 3.1.1 Origin and estimated purity of reagents used in synthesis of α -alkylaminomethylenephosphonic acids.

Compound	Source	Purity ^a
Diethylamine	BDH	GPR as 70 % aqueous solution
Ethylamine	BDH	GPR as 70 % aqueous solution
Hydrochloric acid	BDH	^b
Formaldehyde	BDH	AR as 40 % aqueous solution
Phosphorous acid	BDH	GPR
Propylene oxide	Aldrich	99 %

^a Manufacturer's estimate. ^b GPR concentrated HCl was diluted with an equivalent quantity of H₂O to give ca. 6 mol dm⁻³.

3.1.2 Physical measurements

Proton and carbon-13 nmr spectra were recorded for solutions of alkylaminomethylene phosphonic acids in D₂O with a Bruker AM250 spectrometer. General conditions for proton and carbon-13 spectra are given in Section 6.3.2 and 6.3.3 respectively. Chemical shifts were referenced to internal sodium

trimethylsilylpropionate [TSP- d_4 , sodium salt of 3-(trimethylsilyl)propionic-2,2,3,3- d_4 acid] in all cases. Phosphorus-31 nmr spectra were obtained in D_2O solution using a Bruker WP80; ^{31}P chemical shifts were referenced to external 85% *aqu.* phosphoric acid (H_3PO_4) contained in a coaxial tube. All nmr spectra were recorded at ambient probe temperature and, unless otherwise stated, at the natural pH of the ligand solution.

Analyses for carbon, hydrogen and nitrogen content of samples were obtained using a Carlo Erba 1106 Elemental Analyzer. All melting points are uncorrected.

3.1.3 Preparation of diethylaminomethylenephosphonic acid

Diethylaminomethylenephosphonic acid (DEAMPA) was prepared using a method developed from a general procedure described by Moedritzer *et al* for synthesis of α -aminomethylenephosphonic acids.^[26]

Aqueous diethylamine (70%, 23.3 g, 0.25 mol) was dissolved in iced water (250 cm^3) and treated with a stoichiometric quantity of hydrochloric acid (6 mol dm^{-3} , 40 cm^3) in portions with stirring and cooling. Phosphorous acid (16.4 g, 0.20 mol) was added and the mixture was brought to reflux. Aqueous formaldehyde (40%, 22 cm^3 , 0.30 mol) was added to the refluxing mixture over 60 min and refluxing was continued for a further 8 h. The reaction mixture was concentrated under reduced pressure, then treated with propylene oxide at 40 °C until gas evolution had ceased. The mixture was further concentrated under reduced pressure yielding a pale yellow oil. The oil was treated with an equal volume of mixed ethanol and acetone (ca. 3:1 v/v), the vessel stoppered and stored for 3 months. A white, hygroscopic, crystalline solid was isolated at the pump, washed with 2 portions of chilled ethanol and

desiccated *in vacuo* over phosphorus pentoxide for 24 h.

Yield = 13.20 g (40%). M.p. = 195–197 °C. Microanalysis: Found: C, 34.4;

H, 8.4; N: 8.4 %. Calculated for $C_5H_{14}NO_3P$: C, 35.9; H, 8.4; N, 8.4 %.

1H NMR (80.02 MHz, D_2O): δ /ppm 3.37 [q, $^3J_{HH} = 7.3$ Hz, $(CH_3CH_2)_2N-$]; 3.29 [d, $^2J_{HP} = 13.2$ Hz, $-NCH_2P-$]; 1.31 [t, $^3J_{HH} = 7.3$ Hz, $(CH_3CH_2)_2N-$].

^{13}C bb- $\{^1H\}$ NMR (D_2O , pH = 8.0): δ /ppm 53.46 [d, $^1J_{CP} = 126.7$ Hz, $-NCH_2P-$]; 51.90 [d, $^3J_{CP} = 3.8$ Hz] $(CH_3CH_2)_2N-$; 11.12 [s, $(CH_3CH_2)_2N-$].

^{31}P bb- $\{^1H\}$ NMR (D_2O): δ /ppm 7.91 ppm ($-CH_2PO_3H_2$). ^{31}P NMR (CD_3OD): δ /ppm 6.59 (t, $^2J_{PH} = 13.0$ Hz).

3.1.4 Preparation of Ethyliminodimethylenephosphonic Acid.

Ethyliminodimethylenephosphonic acid ($EIDMPH_4$) was prepared using the general procedure described by Moedritzer *et al* for synthesis of α -aminomethylenephosphonic acids.^[26]

Aqueous ethylamine (70%, 16.0 cm³, 0.10 mol) was diluted with water (200 cm³) and hydrochloric acid (6 mol dm⁻³, 40 cm³, 0.20 mol) was added over 30 minutes with stirring and cooling. Phosphorous acid (16.40 g, 0.20 mol) followed by hydrochloric acid (conc., 50 cm³) were added and the solution was brought to reflux. Formaldehyde solution (40% aq., 30 cm³ 0.40 mol) was added to the mixture over 90 min and reflux was continued for a further 2 h. The reaction mixture was concentrated under reduced pressure and then treated with an equal volume of ethanol. A white crystalline solid was isolated at the pump after 2 days, washed with ethanol, diethyl ether, and air dried.

Yield = 15.70 g (67%). M.p. = 205–207 °C (lit.,^[26] 205 °C).

Microanalysis: Found: C, 21.0; H, 5.7; N, 6.0 %. Calculated for $C_4H_{13}NP_2O_6$:

C, 20.6; H, 5.6; N, 6.0 %.

^1H Nmr (D_2O): δ/ppm 3.58 [q, $^3J_{\text{HH}} = 7.3$ Hz, $\text{CH}_3\text{CH}_2\text{N-}$]; 3.55 [d, $^2J_{\text{HP}} = 12.8$ Hz, $-\text{N}(\text{CH}_2\text{PO}_3\text{H}_2)_2$]; 1.36 [t, $^3J_{\text{HH}} = 7.3$ Hz $\text{CH}_3\text{CH}_2\text{N-}$].

^{13}C bb- $\{^1\text{H}\}$ Nmr (D_2O): δ/ppm 11.34 [s, $\text{CH}_3\text{CH}_2\text{N-}$]; 53.58 [dd, $^1J_{\text{CP}} = 137.1$ Hz, $^3J_{\text{CP}} = 4.4$ Hz, $-\text{N}(\text{CH}_2\text{PO}_3\text{H}_2)_2$]; 55.36 [t, $^3J_{\text{CP}} = 4.4$ Hz, $\text{CH}_3\text{CH}_2\text{N-}$].

^{31}P Nmr (D_2O): δ/ppm 7.78 (t, $^3J_{\text{PH}} = 12.9$ Hz).

3.2 Determination of protonation and metal complex stability constants by potentiometric titration.

3.2.1 Reagents used during potentiometric titrations.

Origins and purities of reagents routinely used for potentiometric titrations are summarised in Table 3.2.1. Samples of ligands used for titrations were of the highest quality available. The purity of ligands was confirmed using C, H, and N elemental analysis, ^1H , ^{13}C and, where appropriate, ^{31}P nmr.

3.2.2 Solvents

Water used for preparation of solutions was obtained in the following ways:

- (i) 'ANALSPEC' water ('electronic grade' water prepared by Micro-Image Technology Ltd.) was obtained from Interlox plc and used without further purification (except for preparation of base solutions).
- (ii) Deionised water, produced by ion exchange, was further purified by double distillation under nitrogen.
- (iii) Deionised water, produced by reverse osmosis, was used without further purification (except for preparation of base solutions).

Degassed water (for base solutions) was obtained after refluxing for at least 2 h followed by cooling the sample under a stream of nitrogen. Water prepared in this way was stored under nitrogen in sealed bottles for up to 2 weeks.

Table 3.2.1 Origin and estimated purity of compounds routinely used in potentiometric acid-base titrations.

Compound	Source	Purity
Hydrochloric acid	BDH	Concentrated solution ^a
Nitric acid	BDH	Concentrated solution ^a
Perchloric acid	Aldrich	69-72 % aqueous solution ^b
Potassium chloride	BDH	ARISTAR, > 99.5 % ^c
Potassium nitrate	BDH	ARISTAR, > 99.5 % ^c
Potassium hydroxide	BDH	Concentrated solution ^a
Tetraethylammonium perchlorate	d	
Tetraethylammonium hydroxide	e	
Tetraethylammonium chloride	Aldrich	Supplied as hydrate ^f
Mercury	Elgar	Doubly distilled
Mercurous chloride	Aldrich	> 95 % ^b
Ethylenediamine-tetraacetic acid, disodium salt	BDH	AnalaR, > 99.5 %
Disodium tetraborate decahydrate	BDH	AnalaR, > 99.5 % ^g
Nitrogen	BOC	'Oxygen-free', ^h
Soda lime ⁱ	BDH	-

^a 'CONVOL' solutions (prepared from AnalaR grade reagents). ^b Conforms to A.C.S. specification. ^c Dried at 120 °C for 24-48 h and stored over silica gel before use. ^d Prepared from tetraethylammonium bromide (Aldrich, 98 %); see Section 3.2.9. ^e Prepared from tetraethylammonium perchlorate; see Section 3.2.9. ^f Desiccated *in vacuo* over P₂O₅ for 24 h before use. ^g Recrystallised according to a standard procedure^[27a] before use. ^h Passed over soda lime and saturated with solvent before use. ⁱ Mesh size 3-9 or 10-16, self-indicating type used.

Methanol (Aldrich, > 99.9 %, HPLC grade) was pre-dried before use.

A portion of dry methanol (150 cm³, dried using the following method) was added to magnesium turnings (15.0 g) in a pre-dried distillation apparatus (dried at 120 °C for 2 h, and flamed out after assembly) incorporating a ca. 1 m vigreux column and fitted with silica gel guard tubes. Addition of iodine crystals (0.5 g) followed by gentle warming of the solution produced effervescence in the mixture and, once all solid had dissolved, HPLC grade methanol (2 dm³) was added. The solution was heated and refluxing was continued for 2-3 h. The solution was then distilled and the fraction boiling at 64.5-65.0 °C was collected in a dry flask. Solvent prepared in this way was stored under nitrogen in sealed bottles for up to 1 month. Where required solutions were degassed by sonication under suction. Dilution to give 95% (v:v) methanol/water solution was made with appropriate quantities of water purified as described above.

3.2.3 Preparation of acid solutions

Aqueous solutions

Stock solutions (ca. 0.1 mol dm⁻³) of hydrochloric acid and nitric acid were obtained by dilution of appropriate 'Convol' vials with water (500 cm³). Solutions were standardised against borax (disodium tetraborate decahydrate, Na₂B₄O₇·10H₂O) using methyl red indicator, according to a standard procedure. [27a]

Acid solutions for titrations were prepared from aliquots of stock solution diluted to give final acid concentrations of ca. 0.004 mol dm⁻³. Appropriate quantities of backing electrolyte (KCl for HCl solutions, and KNO₃ for HNO₃ solutions) were included to give KCl and KNO₃ concentrations of 0.096 mol dm⁻³ and hence total ionic strengths of 0.1 mol dm⁻³.

95 % Methanol-water solutions

Concentrated HClO_4 (ca. 70 %) was diluted with water to give a stock solution of ca. 1.0 mol dm^{-3} which was standardised against borax (disodium tetraborate decahydrate, $\text{Na}_2\text{B}_4\text{O}_7 \cdot 10\text{H}_2\text{O}$) using methyl red indicator, according to a standard procedure. [27a]

The acid solution for a titration was prepared by pipetting an aliquot of the acid stock solution, sufficient to give an acid concentration of $0.004 \text{ mol dm}^{-3}$, into a volumetric flask. A quantity of water, sufficient to make the final solution 5 % in water (v/v), was added. Tetraethylammonium perchlorate (sufficient to give a concentration of $0.096 \text{ mol dm}^{-3}$ in the final solution and $I = 0.1 \text{ mol dm}^{-3}$) and the majority of the required volume of methanol were added to the flask. The solution was then sonicated until the solid dissolved, cooled to room temperature and diluted to the final volume with methanol.

3.2.4 Preparation of base solutions

Base solutions were prepared with degassed solvents in all cases and manipulations were performed under nitrogen to minimise exposure to air (and hence to CO_2).

Aqueous solution

'Convol' vials containing concentrated KOH were diluted with water (500 cm^3) to give solutions of ca. 0.1 mol dm^{-3} . Solutions were then transferred to the motorised burette reservoir which had been pre-flushed with nitrogen and fitted with a soda lime guard tube.

95 % Methanol-water solutions

The hydroxide concentration of the concentrate derived from the preparation of $(C_2H_5)_4NOH$ (see Section 3.2.9) was estimated by titration against standard HCl solution (ca. 0.1 mol dm^{-3}) using methyl red as indicator. Aliquots of concentrate required to give a concentration of ca. 0.1 mol dm^{-3} of $(C_2H_5)_4NOH$, and of water required to give 5 % $H_2O/MeOH$ (v/v) in the final solution, were pipetted into a volumetric flask. Sufficient methanol was added to give the required volume of solution. The solution was then transferred to the motorised burette reservoir which had been pre-flushed with nitrogen and fitted with a soda lime guard tube.

In both of the above cases, the hydroxide concentration of the final solution was accurately determined by titration against aliquots of standard HCl solution (0.1 mol dm^{-3}) containing methyl red indicator.

3.2.5 Preparation of metal salt solutions

Solutions of metal ions (ca. $0.05\text{--}0.1 \text{ mol dm}^{-3}$) were prepared from hydrated metal salts containing chloride, nitrate, and perchlorate anions as appropriate. Concentrations of metal ion solutions were obtained from complexometric titrations with standard aqueous EDTA solution according to established procedures.^[27b] Solutions were prepared in the appropriate solvent and aliquots of stock solution ($< 1 \text{ cm}^3$) were introduced to the potentiometric titration cell with a micropipette.

3.2.6 Preparation of calomel reference electrodes

Calomel reference electrodes were prepared for each titration environment using methods adapted from that described by Vogel.^[27c] Electrodes were prepared using the solvent employed in each titration environment and their

compositions are summarised in Table 3.2.2. A schematic diagram of the calomel electrode is shown in Fig. 3.2.1.

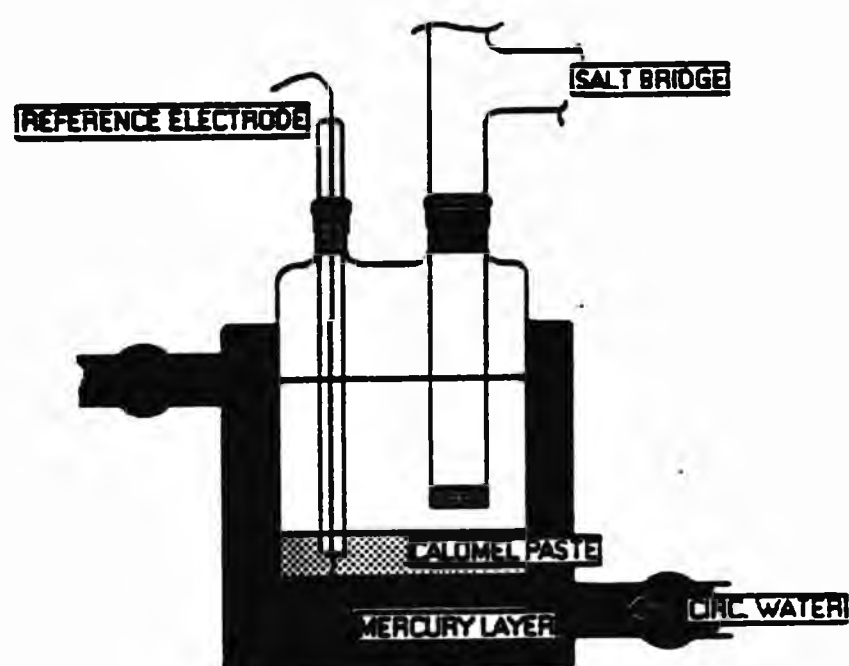


Figure 3.2.1 The calomel electrode.

Table 3.2.2 Composition of calomel reference electrodes prepared for titrations in aqueous and 95 % methanol-water media.

Solvent	Electrolyte ^a	Calomel half cell ^b
H ₂ O	KCl	KCl(0.10), Hg ₂ Cl _{2(s)} Hg _(s)
H ₂ O ^c	KNO ₃	KNO ₃ (0.095), KCl(0.005), Hg ₂ Cl _{2(s)} Hg _(s)
95 % MeOH ^d	Et ₄ NCIO ₄	Et ₄ NCIO ₄ (0.095), Et ₄ NCl(0.005), Hg ₂ Cl _{2(s)} Hg _(s)

^a Ionic strength = 0.1 mol dm⁻³. ^b Concentrations (mol dm⁻³) are given in parentheses. ^c Reference electrode also used for titrations in 3 % and 10 % H₂O₂/H₂O (v/v) solutions. ^d v/v aqueous solution.

3.2.7 Preparation of salt bridge solutions

Solutions for salt bridges were prepared using quantities of background electrolyte diluted with the appropriate volume of solvent to give solutions of ionic strength (0.10 mol dm^{-3}) equal to those of the titration solution.

3.2.8 Potentiometric titrations in dilute hydrogen peroxide solutions.

Titration were performed in both 3% and 10% (w/w) aqueous H_2O_2 solution using a similar cell composition to that employed for aqueous titrations using $\text{HNO}_3/\text{KNO}_3$. In these cases, however, acid solutions ($[\text{HNO}_3] = 0.004 \text{ mol dm}^{-3}$, $[\text{KNO}_3] = 0.096 \text{ mol dm}^{-3}$) were prepared using the appropriate aqueous H_2O_2 solution as solvent. Peroxide solutions were prepared by dilution of unstabilised, analytical grade aqueous H_2O_2 (35%, w/w obtained from Interlox plc) with 'ANALSPEC' water. All glassware (including the glass electrode) was treated with concentrated HNO_3 for 24 hours before use.

3.2.9 Preparation of tetraethylammonium salts for titrations in 95 % methanol-water medium.

Commercially available tetraethylammonium hydroxide and perchlorate were found to be unacceptably contaminated with halide ions (aqueous solutions of these compounds gave insoluble white precipitates when treated with AgNO_3 solution) and preparation of compounds with sufficient purity was therefore necessary.

Preparation of tetraethylammonium perchlorate.

Et_4NClO_4 was prepared by treating Et_4NBr (Aldrich, 98 %, 300g, 1.42 mol) in water (500 cm^3) with *aqu.* HClO_4 (1.0 mol dm^{-3}) until precipitation of white product was complete. The product was repeatedly recrystallised (typically 3 times) from hot *aqu.* HClO_4 (1.0 mol dm^{-3}) until free of bromide ion (AgNO_3 test), then from CH_3OH (typically 3 times) until free of acid (washings at pH 7). The resulting colourless crystals were dried over P_2O_5 under vacuum

for 24 hours before use.

CAUTION: Samples of Et_4NClO_4 prepared in this way detonated on contact with a hot spatula and therefore this compound should be handled as a potential explosive.

Yield = 120.6 g (37%). Microanalysis: Found: C, 41.9; H, 8.7; N, 6.2 %.

Calculated for $\text{C}_8\text{H}_{20}\text{NO}_4\text{Cl}$: C, 41.8; H, 8.8; N, 6.1 %.

Preparation of tetraethylammonium hydroxide.

Et_4NOH was prepared by warming (ca. 50 °C) and stirring Et_4NClO_4 (*vide supra*, 0.30 g, 0.13 mol) in dry methanol (250 cm³) with KOH pellets (7.3 g, 0.13 mol) under N_2 for 1.5 hours. The mixture, which contained suspended solids, was cooled, filtered under N_2 and the solid was washed with chilled, dry methanol. The filtrate was concentrated under reduced pressure and cooled in ice-water for ca. 45 min. Further solid precipitated, and this was filtered off (under N_2) and washed with chilled, dry methanol. The filtrate was again concentrated, and the cooling/filtering/washing/concentrating cycle was repeated until no further precipitation occurred. The concentrate was then dissolved in absolute ethanol and a further cooling/filtering/washing/concentrating cycle was repeated using ethanol as solvent, again until no precipitation of solid occurred on cooling. The resulting pale yellow oil was finally dissolved in degassed water and concentrated under reduced pressure. The hydroxide content of the solution was determined by titration against *aqu.* HCl (0.1 mol dm⁻³) using methyl red as indicator.

3.2.10 Data Acquisition.

Potentiometric, acid-base titrations were performed using an 'in-house' built automated titration apparatus based on a motorised piston burette (Metrohm Dosimat 655 fitted with an anti-diffusion tip) driven by a microcomputer (BBC Model B with 6502 second processor). All titrations were performed under an atmosphere of solvent-saturated, CO_2 -free nitrogen. Solution potential was measured using a glass electrode (Corning 003 11 101J) referenced to a thermostatted calomel electrode via a salt bridge composed of electrolyte solution (0.1 mol dm^{-3}). Liquid-liquid junctions between the salt bridge and the calomel and titration solutions were maintained by glass sinters (porosity 4). The titration environment was maintained at $25.0 \pm 0.1^\circ\text{C}$ by a circulating water system driven by a water bath (Grant SE15). Sample, circulating and ambient temperatures, obtained from platinum resistance thermometer probes (SDL Pt-100/3 glass encased, SDL Pt-100 steel encased and RS Pt-100 respectively), were calculated and displayed during execution of the titration program, S.SCMITR.⁷⁰ Titrations were suspended if the sample temperature exceeded a preset tolerance of $\pm 0.2^\circ\text{C}$. (In some cases, both water bath level and circulating water flow were monitored during titrations; failure of either resulted in titration suspension). Titration data (solution potential, volume of delivered base and sample temperature) were computer logged and saved to disc after every 5 titration points.

Solution potential measurements were calculated from the mean of a number (input variable; 30-99) of electrode readings separated by a time delay (input variable; typically 60-1500 s). Data points were recorded when successive potential measurements differed by less than 0.05 mV. If this criterion was not achieved before the read limit (input variable; 50-300) was exceeded, data points were recorded from the the final potential measurement and indicated as

such in the hard copy output.

3.2.11 Cell calibration.

Cell calibration was carried out according to a standardised procedure applicable to all solvent systems studied. The cell parameters (E_0 and pK_w) were obtained by titration of strong acid solution ($[H^+] = 0.004 \text{ mol dm}^{-3}$, in the presence of the appropriate electrolyte, $0.096 \text{ mol dm}^{-3}$) against standard base solution ($[OH^-] = 0.1 \text{ mol dm}^{-3}$) added in 0.025 cm^3 increments. Titrations were performed over same the potential range used for sample titrations. E_0 and pK_w were calculated from the computer-logged data by the program S.SCMCAL.⁸ Routine inspection of calibration titration curves revealed no evidence of carbonate contamination.

Standard calibration titration conditions:

Number of readings/point = 30, time delay = 30 s, read limit = 50 points, tolerance for recording data points = $\pm 0.05 \text{ mV}$, temperature tolerance = $\pm 0.2 \text{ }^\circ\text{C}$.

3.2.12 Conditions for ligand and metal-ligand titrations.

Preparation of solutions for sample titrations were generally carried out using a standardised procedure. A solid sample of ligand (weighed by difference using a 5-figure digital balance, Mettler AE163), sufficient to give the desired ratio of $H^+ : L$, was placed into the titration vessel and an aliquot (25 cm^3) of the appropriate acid solution ($[H^+] = 0.004 \text{ mol dm}^{-3}$; in the presence of the appropriate electrolyte, $0.096 \text{ mol dm}^{-3}$; $I = 0.1 \text{ mol dm}^{-3}$) added. For metal-ligand titrations, small aliquots of stock metal solution, sufficient to give the desired ratio of $M : L$, were delivered to the titration solution using a micropipette (Gilson Microman M250). The titration vessel

was then placed in position on the titration apparatus; nitrogen and base solution delivery tubes, a temperature probe and the salt bridge liquid-liquid junction were introduced into the solution (see Fig. 3.2.2) and the solution temperature was stabilised to within the preset tolerance of 25 °C. The potential of the solution was then recorded at 5 min intervals and the automated titration procedure was initiated once two successive measurements agreed to ± 0.2 mV (this latter stage was performed during execution of S.SCMITR⁷⁰).

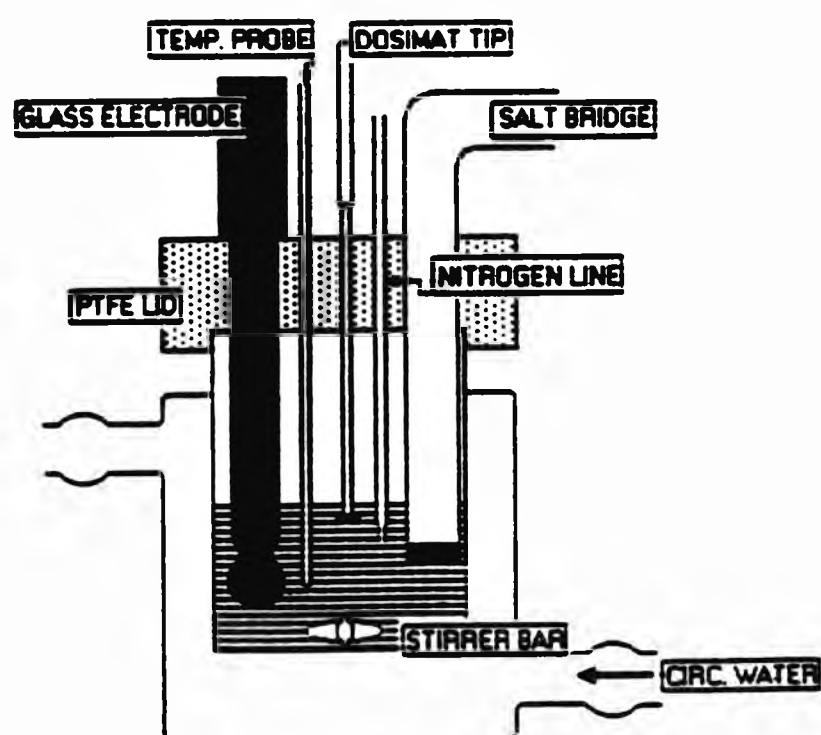


Figure 3.2.2 The sample titration vessel.

Glycine with Ni(II) in aqueous solution ($I = 0.1 \text{ mol dm}^{-3}$, KCl)

Typical conditions for titration of ligand

Number of readings/point = 30, time delay = 30 s, read limit = 50 points,
tolerance for recording data points = ± 0.05 mV, temperature
tolerance = ± 0.4 °C.

Typical conditions for titration of ligand with metal

Number of readings/point = 30, time delay = 90 s, read limit = 50 points,
tolerance for recording data points = ± 0.05 mV, temperature
tolerance = ± 0.2 °C.

Table 3.2.3 Experimental conditions for glycine titrations.

Data file	Ligand ^a			Metal salt		[M]:[L]
	/mg	/mmol	[L]/mol dm ⁻³	V ^b /cm ³	[M]/mol dm ⁻³	
GL31	c		0.003002			
GL32	c		0.003002			
GL33	3.9	0.05197	0.002078			
GL34	3.4	0.04530	0.001812			
				NiCl ₂ (aq) ^d		
NG30	3.4	0.04530	0.001727	1.230	0.001901	1:0.91
NG31	3.2	0.04264	0.001664	0.615	0.000973	1:1.71
NG32	3.8	0.05063	0.001976	0.615	0.000973	1:2.03
NG33	3.9	0.05197	0.002045	0.410	0.000654	1:3.12
NG34	3.8	0.05063	0.001992	0.410	0.000654	1:3.04

^a AnalAR glycine (BDH, >99.0 %) dried at 120 °C and stored over P₂O₅.

^b Volume of stock solution delivered from micropipette. ^c 25 cm³ aliquot of ligand solution [0.1127 g in 500 cm³ of 0.004 mol dm⁻³ aqu. HCl (including 0.096 mol dm⁻³ KCl)] titrated. ^d BDH AnalAR NiCl₂·6H₂O (>99 %); stock solution, [Ni²⁺] = 0.04056 mol dm⁻³.

1-aminopropylphosphonic acid with Cu(II) and Ni(II) in aqueous solution
(I = 0.1 mol dm⁻³, KNO₃)

Typical conditions for titration of ligand

Number of readings/point = 30, time delay = 30 s, read limit = 50 points,
tolerance for recording data points = ± 0.05 mV, temperature

tolerance = ± 0.2 °C.

Typical conditions for titration of ligand with metal

Number of readings/point = 30, time delay = 150 s, read limit = 50 points,

tolerance for recording data points = ± 0.05 mV, temperature

tolerance = ± 0.2 °C.

Table 3.2.4 Experimental conditions for 1-aminopropylphosphonic acid titrations.

Data file	Ligand ^a			Metal salt		[M]:[L]
	/mg	/mmol	[L]/mol dm ⁻³	V ^b /cm ³	[M]/mol dm ⁻³	
DG11	4.70	0.03379	0.001351			
DG12	4.62	0.03321	0.001328			
DG13	4.66	0.03350	0.001339			
				Cu(NO ₃) ₂ (aq) ^c		
DGC2	4.56	0.03278	0.001296	0.2778	0.000440	1:2.94
DGC3	4.32	0.03105	0.001228	0.2778	0.000440	1:2.79
DGC5	4.63	0.03328	0.001309	0.4167	0.000657	1:1.99
DGC6	4.56	0.03278	0.001268	0.8334	0.001294	1:0.98
				Ni(NO ₃) ₂ (aq) ^d		
DGN1	4.47	0.03213	0.001264	0.4124	0.000655	1:1.93
DGN2	4.42	0.03177	0.001250	0.4124	0.000655	1:1.91

^a Sample of 1-aminopropylphosphonic acid [CH₃CH₂CH(NH₂)PO₃H₂, M_R = 139.11] synthesized by D. St.C. Green at PNL. ^b Volume of stock solution delivered from micropipette. ^c BDH AnalaR Cu(NO₃)₂·6H₂O (>99 %); stock solution, [Cu²⁺] = 0.04012 mol dm⁻³. ^d BDH AnalaR Ni(NO₃)₂·6H₂O (>99 %); stock solution, [Ni²⁺] = 0.04040 mol dm⁻³.

Diethylaminomethylenephosphonic acid with Cu(II) and Ni(II) in aqueous solution ($I = 0.1 \text{ mol dm}^{-3}$, KNO_3)

Typical conditions for titration of ligand

Number of readings/point = 60, time delay = 45 s, read limit = 150 points,
tolerance for recording data points = $\pm 0.05 \text{ mV}$, temperature
tolerance = $\pm 0.2 \text{ }^\circ\text{C}$.

Typical conditions for titration of ligand with metal

Number of readings/point = 60, time delay = 150 s, read limit = 150 points,
tolerance for recording data points = $\pm 0.05 \text{ mV}$, temperature
tolerance = $\pm 0.2 \text{ }^\circ\text{C}$.

Table 3.2.5 Experimental conditions for diethylaminomethylenephosphonic acid titrations.

Data file	Ligand ^a			Metal salt		[M]:[L]
	/mg	/mmol	[L]/mol dm ⁻³	V ^b /cm ³	[M]/mol dm ⁻³	
IS14	8.47	0.05068	0.002027			
IS15	3.90	0.02333	0.000933			
IS16	4.10	0.02453	0.000981			
				Cu(NO ₃) ₂ (aq) ^c		
IS1CU1	4.17	0.02495	0.000973	0.6231	0.000975	1:1.00
IS1CU2	3.97	0.02375	0.000938	0.3116	0.000493	1:1.90
IS1CU3	4.41	0.02639	0.001046	0.2077	0.000330	1:3.17
				Ni(NO ₃) ₂ (aq) ^d		
IS1NI2	6.13	0.03668	0.001449	0.3094	0.000493	1:2.93
IS1NI3	4.08	0.02441	0.000970	0.1547	0.000248	1:3.91

^a Diethylaminomethylenephosphonic acid ($M_r = 167.14$); this work (see Section 3.1.3). ^b Volume of stock solution delivered from micropipette.

^c BDH AnalaR Cu(NO₃)₂·6H₂O (>99 %); stock solution, [Cu²⁺] = 0.04012 mol dm⁻³.

^d BDH AnalaR Ni(NO₃)₂·6H₂O (>99 %); stock solution, [Ni²⁺] = 0.04040 mol dm⁻³.

Ethyliminodimethylenephosphonic acid with Cu(II) and Ni(II) in aqueous solution ($I = 0.1 \text{ mol dm}^{-3}$, KNO_3)

Typical conditions for titration of ligand

Number of readings/point = 60, time delay = 45 s, read limit = 150 points,
tolerance for recording data points = $\pm 0.05 \text{ mV}$, temperature
tolerance = $\pm 0.2 \text{ }^\circ\text{C}$.

Typical conditions for titration of ligand with metal

Number of readings/point = 60, time delay = 150 s, read limit = 150 points,
tolerance for recording data points = $\pm 0.05 \text{ mV}$, temperature
tolerance = $\pm 0.2 \text{ }^\circ\text{C}$.

Table 3.2.6 Experimental conditions for ethyliminodimethylenephosphonic acid titrations.

Data file	Ligand ^a			Metal salt		[M]:[L]
	/mg	/mmol	[L]/mol dm ⁻³	V ^b /cm ³	[M]/mol dm ⁻³	
IS2B5	4.57	0.01961	0.000784			
IS2B6	4.71	0.02021	0.000808			
IS2B7	4.48	0.01922	0.000768			
				Cu(NO ₃) ₂ (aq) ^c		
M060	5.93	0.02544	0.000992	0.6231	0.000975	1:1.02
M061	6.17	0.02647	0.001045	0.3116	0.000493	1:2.12
M062	5.91	0.02535	0.001005	0.2077	0.000330	1:3.04
				Ni(NO ₃) ₂ (aq) ^d		
IS2N1	4.81	0.02063	0.000817	0.2475	0.000396	1:2.06
IS2N2	4.66	0.01999	0.000784	0.4950	0.000784	1:1.00

^a Ethyliminodimethylenephosphonic acid ($M_R = 233.10$); this work (see

Table 3.2.6 continued

Section 3.1.4). ^b Volume of stock solution delivered from micropipette.

^c BDH AnalaR $\text{Cu}(\text{NO}_3)_2 \cdot 6\text{H}_2\text{O}$ (>99 %); stock solution, $[\text{Cu}^{2+}] = 0.04012 \text{ mol dm}^{-3}$.

^d BDH AnalaR $\text{Ni}(\text{NO}_3)_2 \cdot 6\text{H}_2\text{O}$ (>99 %); stock solution, $[\text{Ni}^{2+}] = 0.04040 \text{ mol dm}^{-3}$.

A dibenzo-pyrido-pentaaza macrocycle with Cu(II) , Ni(II) , Zn(II) , and Cd(II) in 95 % methanol-water (v/v) ($I = 0.1 \text{ mol dm}^{-3}$, Et_4NClO_4)

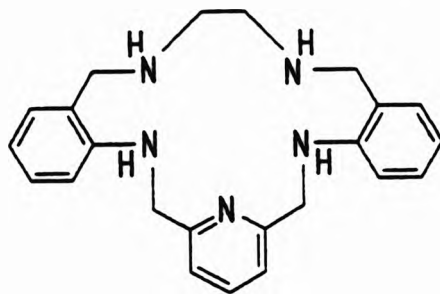


Figure 3.2.3 The dibenzo-pyrido-pentaaza macrocycle NpynNenH_4 .

Typical conditions for titration of ligand

Number of readings/point = 99, time delay = 150 s, read limit = 300 points,
tolerance for recording data points = $\pm 0.05 \text{ mV}$, temperature
tolerance = $\pm 0.2^\circ\text{C}$.

Typical conditions for titration of ligand with metal ($M = \text{Cu}^{2+}$, Zn^{2+} , Cd^{2+})

Number of readings/point = 99, time delay = 600 s, read limit = 300 points,
tolerance for recording data points = $\pm 0.05 \text{ mV}$, temperature
tolerance = $\pm 0.2^\circ\text{C}$.

Typical conditions for titration of ligand with metal ($M = \text{Ni}^{2+}$)

Number of readings/point = 99, time delay = 1500 s, read limit = 750 points,
tolerance for recording data points = $\pm 0.05 \text{ mV}$, temperature
tolerance = $\pm 0.2^\circ\text{C}$.

Table 3.2.7 Experimental conditions for NpynNenH₄ titrations.

Data file	Ligand ^a			Metal salt		[M]:[L]
	/mg	/mmol	[L]/mol dm ⁻³	V ^b /cm ³	[M]/mol dm ⁻³	
N5P1 ^d	6.30	0.01687	0.000670			
N5P3 ^d	5.67	0.01518	0.000600			
N5P4 ^d	7.34	0.01965	0.000786			
N5P5 ^d	7.39	0.01979	0.000783			
N5P6 ^d	7.26	0.01944	0.000769			
N5P9 ^d	7.53	0.02016	0.000802			
				Cu(ClO ₄) ₂ (s) ^e		
N5CA ^c	6.25	0.01673	0.000664	0.1728	0.000623	1:1.07
N5CB ^c	9.22	0.02469	0.000985	0.0460	0.000166	1:5.91
N5CC ^c	9.42	0.02522	0.000997	0.2766	0.000993	1:1.00
				Ni(ClO ₄) ₂ (s) ^f		
N5NA ^c	9.02	0.02415	0.000956	0.2600	0.000998	1:0.96
N5NB ^c	7.76	0.02078	0.000823	0.2230	0.000857	1:0.96
N5NC ^c	9.24	0.02474	0.000984	0.1198	0.000462	1:2.13
				Zn(ClO ₄) ₂ (s) ^g		
N5Z1 ^d	6.77	0.01813	0.000717	0.2600	0.001073	1:0.67
N5Z2 ^d	7.04	0.01885	0.000750	0.1000	0.000415	1:1.81
N5Z3 ^d	7.60	0.02035	0.000810	0.1000	0.000415	1:1.95
				Cd(ClO ₄) ₂ (s) ^h		
N1CD ^d	7.18	0.01922	0.000762	0.2000	0.000789	1:0.97
N2CD ^d	6.99	0.01872	0.000745	0.1000	0.000396	1:1.88
N8CD ^d	7.21	0.01930	0.000766	0.2000	0.000789	1:0.97

^a Two batches of NpynNenH₄ (Fig. 3.2.3, M_R = 373.49) were supplied by S. J. Kitchen of the University of Sheffield. ^b Volume of stock solution delivered from micropipette. ^c 1st ligand batch. ^d 2nd ligand batch. ^e BDH AnalaR Cu(ClO₄)₂·6H₂O (>99 %); stock solution, [Cu²⁺] = 0.09083 mol dm⁻³. ^f BDH AnalaR Ni(ClO₄)₂·6H₂O (>99 %); stock solution, [Ni²⁺] = 0.09700 mol dm⁻³. ^g BDH AnalaR Zn(ClO₄)₂·6H₂O (>99 %); stock solution, [Zn²⁺] = 0.1043 mol dm⁻³. ^h BDH AnalaR Cd(ClO₄)₂·6H₂O (>99 %); stock solution, [Cd²⁺] = 0.09948 mol dm⁻³.

A series of dibenzo-pyrido-triazadioxo macrocycles with Zn(II), and Cd(II) in 95 % methanol-water (v/v) ($I = 0.1 \text{ mol dm}^{-3}$, Et_4NClO_4)

Titration results were obtained using apparatus that has been described previously.^[23]

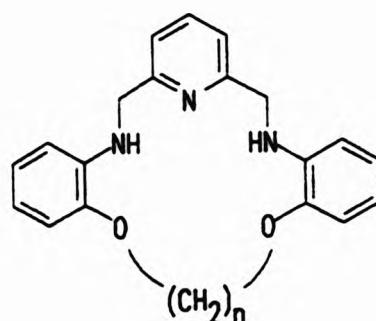
Typical conditions for titration of ligands

Number of readings/point = 100, time delay = 300 s, read limit = 150 points, tolerance for recording data points = $\pm 0.05 \text{ mV}$.

Typical conditions for titration of ligand with metal

Number of readings/point = 100, time delay = 900 s, read limit = 500 points, tolerance for recording data points = $\pm 0.05 \text{ mV}$.

Table 3.2.8 Experimental conditions for titrations of members of a series of dibenzo-pyrido-triazadioxo macrocycles.^a



Data file		Ligand		Metal salt		[M]:[L]
	/mg	/mmol	[L]/mol dm ⁻³	V ^b /cm ³	[M]/mol dm ⁻³	
n=2	BPM70 ^c					
B2P1	d		0.001355			
				Zn(ClO ₄) ₄ 2(s) ^e		
B2ZN1	d		0.001355	0.2000	0.001234	1:1.10
				Cd(ClO ₄) ₄ 2(s) ^f		
B2CD1	d		0.001355	0.2600	0.002035	1:0.67

Table 3.2.8 continued

n=3		BPM73 ^g					
B3P1	10.75	0.02974	0.001180				
				$\text{Zn}(\text{ClO}_4)_2(\text{s})^e$			
B3ZN1	12.37	0.03423	0.001358	0.2000	0.001234	1:0.96	
				$\text{Cd}(\text{ClO}_4)_2(\text{s})^f$			
B3CD1	12.62	0.03633	0.001442	0.1750	0.001374	1:1.05	
B3CD2	12.04	0.03466	0.001382	0.0750	0.000591	1:2.34	
B3CD3	11.87	0.03417	0.001360	0.1200	0.000944	1:1.44	
B3CD4	11.98	0.03448	0.001369	0.1750	0.001374	1:1.00	
n=4		BPM83 ^h					
B4P1	12.72	0.03382	0.001342				
B4P2	11.60	0.03085	0.001233				
				$\text{Zn}(\text{ClO}_4)_2(\text{s})^e$			
B4ZN1	11.67	0.03103	0.001231	0.2000	0.001234	1:1.09	
				$\text{Cd}(\text{ClO}_4)_2(\text{s})^f$			
B4CD1	12.82	0.03409	0.001354	0.1750	0.001374	1:0.98	

^a Ligands synthesized by B. P. Murphy at the University of Sheffield.

^b Volume of stock solution delivered from micropipette. ^c $\text{C}_{21}\text{H}_{21}\text{N}_3\text{O}_2$, $M_R = 347.41$. ^d 25 cm³ aliquot of ligand solution [0.4709 g in 100 cm³ of 0.004 mol dm⁻³ HClO₄ (in 95 % MeOH-H₂O (v/v) including 0.096 mol dm⁻³ Et₄NClO₄)] titrated. ^e Stock solution [Zn²⁺] = 0.1555 mol dm⁻³. ^f Stock solution [Cd²⁺] = 0.1978 mol dm⁻³. ^g $\text{C}_{22}\text{H}_{23}\text{N}_3\text{O}_2$, $M_R = 361.43$. ^h $\text{C}_{23}\text{H}_{25}\text{N}_3\text{O}_2$, $M_R = 376.07$.

3.2.13 Data Processing.

Sample titration data files (containing values for E_0 , pK_w , initial reactant concentrations, the mean sample temperature, and data for potential vs. volume of added base) were created on disc during execution of S.SCMTITR.^[29] These files were converted into ASCII format using the DECDATA^[30] program. Data was then transferred on to the mainframe computer (VAX 11/780) using the

TERMULATOR^[31] file transfer facility.

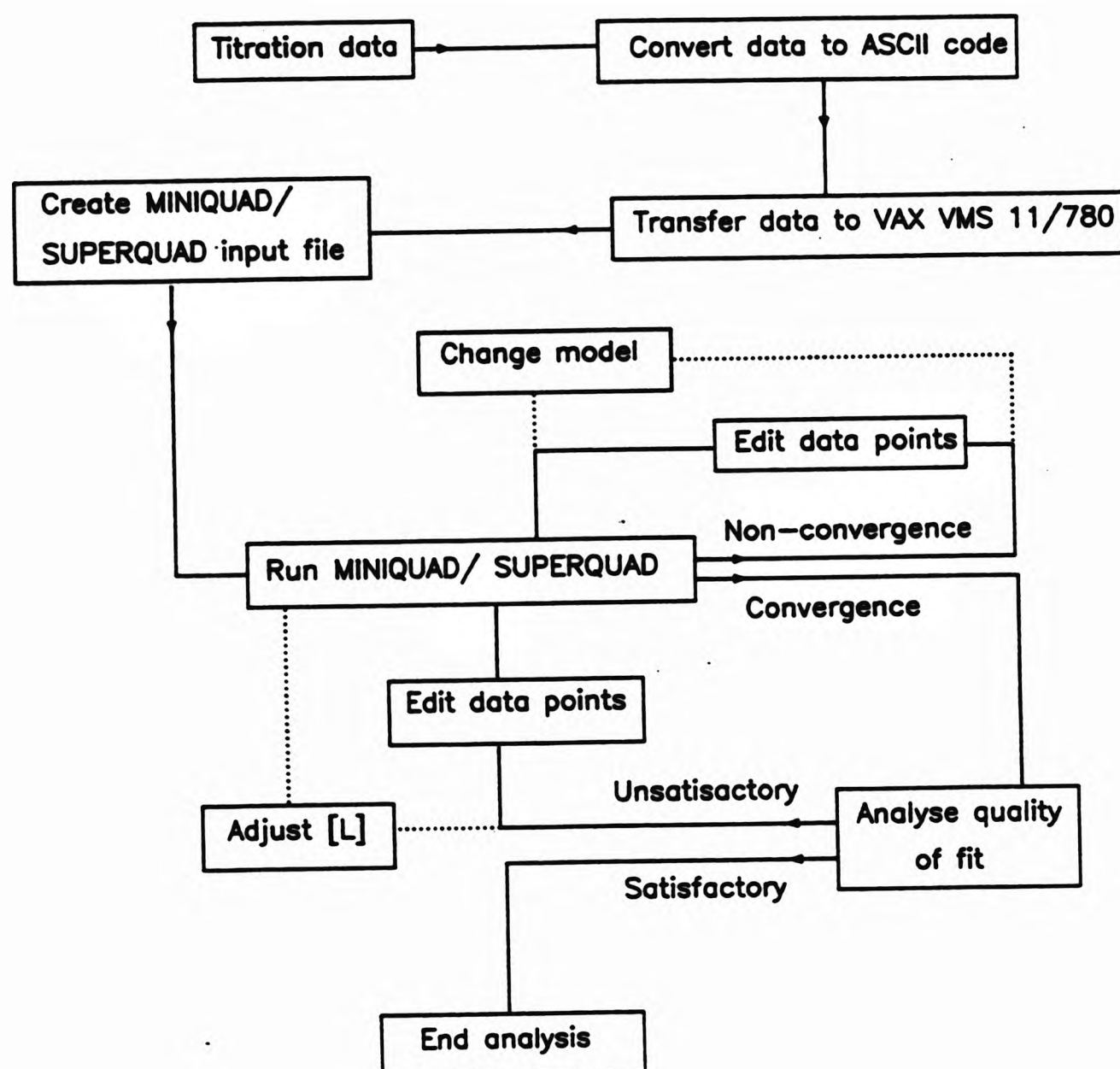


Figure 3.2.4 Flow diagram of the data refinement strategies employed with MINIQAD and SUPERQUAD.

Equilibrium constants were obtained from the data using MINIQAD^[16,22] and SUPERQUAD^[25] computer programs. Refinement of data for a particular equilibrium model was achieved by minimisation of the 'fit parameters' (R-factor for MINIQAD and chi-squared/sigma for SUPERQUAD) generated as part of each program's output. Variation of the pH range under study, by elimination of data points from the full data set, was generally required for

an acceptable fit. Metal, ligand and base concentrations were held constant during data analysis whilst acid concentration was not fixed and was recalculated during execution of the processing program.

Ligand protonation constants, obtained from analysis of titration data for the ligand only, were included as constants during analysis of data for ligand in the presence of metal ions. A flow diagram for the data processing strategy is given in Figure 3.2.4.

3.3 Nmr studies of phosphonic acids in aqu. hydrogen peroxide solutions

Reagents used were of the highest grade available and ligand purity was confirmed by phosphorus-31 nmr spectroscopy immediately prior to use. Glassware for hydrogen peroxide solutions was pre-treated by pickling in either concentrated nitric acid or concentrated hydrogen peroxide solution (70%). Solution pH was measured using a Data-Sci PTI-20 pH meter and a glass-calomel combination electrode (Russell CWL). The electrode was calibrated using pH 4.0 and 7.0 buffer solutions (prepared from BDH buffer tablets dissolved in deionised, boiled-out water). Phosphorus-31 broad band proton decoupled spectra were recorded on a Bruker WP80 nmr spectrometer, shifts being referenced to external 85% phosphoric acid (H_3PO_4) by sample substitution. Carbon-13 spectra were recorded on a Bruker WP80 and, where indicated, AM250 nmr spectrometers. Shifts were referenced to internal TSP- d_4 (sodium salt of 3-(trimethylsilyl)proprionic-2,2,3,3- d_4 acid) in both cases.

3.3.1 Interaction of disodium 1-hydroxyethyl-1,1-diphosphate with hydrogen peroxide.

A solution of disodium 1-hydroxyethyl-1,1-diphosphate [$\text{HEDPH}_2\text{Na}_2$, $\text{CH}_3\text{C}(\text{OH})(\text{PO}_3\text{H})_2\text{Na}_2$, 5000 ppm] in aqu. hydrogen peroxide solution (70% w:w, 50 cm^3) was divided into four portions (a-d) each of 10 cm^3 volume.

(a) The peroxide was destroyed immediately after dissolution of $\text{HEDPH}_2\text{Na}_2$ by adding a platinum wire catalyst and heating the solution at ca. 40 °C until bubble evolution had ceased (ca. 2 h). The solution was then diluted with an equal volume of water and a portion (2.5 g) was spiked with deuterium oxide (125 mg). The phosphorus-31 nmr spectrum was recorded; δ/ppm : 3.00, 19.20.

(b) The portion was diluted with an equal volume of water and refluxed for 24 hours. The peroxide was destroyed as above and a sample (2.5 g) of the solution was spiked with deuterium oxide (125 mg). The ^{31}P nmr spectrum was recorded; δ/ppm : 0.03.

(c) The portion was diluted with an equal volume of water and stored for 4 days at room temperature. Peroxide decomposition and nmr sample preparation were then carried out as above. δ/ppm : 0.60, 19.02.

(d) The portion was stored at room temperature for 4 days before dilution with an equal volume of water and preparation for nmr spectroscopy as above. δ/ppm : 0.60, 18.99.

3.3.2 Interaction of diethylaminomethylenephosphonic acid and hydrogen peroxide

(i) Diethylaminomethylenephosphonic acid (DEAMPH_2 Section 3.1.3, 0.40 g) was dissolved in aqu. hydrogen peroxide-deuterium oxide solution [20 cm^3 ; 19 cm^3

of aqu. H_2O_2 (10 % v/v) and 1 cm^3 of D_2O]. Carbon-13 spectra were recorded thereafter at 2 h intervals for 12 hours. A final ^{13}C spectrum was obtained after 48 h. The pH values of the solution on mixing and after completion of the study were recorded. The solution was then stored at room temperature for 3 months and, after this period, its ^{31}P spectrum was recorded.

(ii) DEAMPH_2 (0.0520 g) was dissolved in aqueous hydrogen peroxide (20.0 g, 35 % w/w) spiked with D_2O (1.00 g). Aliquots (2 cm^3) of this stock solution were taken and adjusted to pH 2, 4, 6, 8, 10 and 12 using, as appropriate, 0.880 ammonia or concentrated nitric acid. After storing the solutions at room temperature for 72 h, the hydrogen peroxide was decomposed on platinum wire as described above and the solution pH was measured. The ^{31}P nmr spectrum of each solution was recorded (Table 3.3.1) and the ^{13}C nmr spectrum of the solution at ca. pH 8 was recorded.

^{13}C bb- $\{^1\text{H}\}$: δ/ppm 65.96 [d, $^1J_{\text{CP}} = 117.4 \text{ Hz}$]; 63.65 (s); 10.48(s).

Table 3.3.1 Conditions for the determination of the pH dependence of the ^{31}P chemical shift of DEAMPH_2 after treatment with aqu. 35 % H_2O_2

Solution	pH Adjustment	Adjusted pH	pH after H_2O_2 decomposition	^{31}P Shift/ppm
a	HNO_3	1.92	2.20	8.40
b	n/a	4.00	4.65	7.88
c	NH_3	5.73	6.47	6.89
d	NH_3	7.70	8.26	5.25
e	NH_3	9.85	10.96	4.31
f	NH_3	10.44	10.56	4.21

(iii) A solution of DEAMPH₂ (0.520g, 2500 ppm) in H₂O/D₂O (95:5 v/v) was divided into aliquots (2 cm³) and treated with 0.880 ammonia solution or concentrated nitric acid to give a series of solutions covering the pH range ca. 2-12 (Table 3.3.2). $\delta(^{31}\text{P})$ for each solution, and the ¹³C spectrum of the solution at approximately pH 8 were recorded.

¹³C bb-{¹H}: δ/ppm 53.46 [d, $^1J_{\text{CP}} = 126.7 \text{ Hz}$]; 51.90 [d, $^3J_{\text{CP}} = 3.8 \text{ Hz}$]; 11.12 (s).

Table 3.3.2 Conditions for the determination of the pH dependence of the ³¹P shift of DEAMPH₂ in aqueous solution.

Solution	pH Adjustment	pH after Adjustment	³¹ P Shift/ppm
a'	HNO ₃	2.21	7.98
b'	n/a	3.80	7.83
c'	NH ₃	6.18	6.51
d'	NH ₃	8.32	6.38
e'	NH ₃	10.10	6.46
f'	NH ₃	11.75	8.28

3.4 Studies of the pH dependence of phosphorus-31 nmr chemical shifts for alkylaminomethylenephosphonic acids.

Small-volume acid-base potentiometric titrations were performed on aqueous solutions of the alkylaminomethylenephosphonic acids DEAMPH₂ (Section 3.1.3) and EIDMPH₄ (Section 3.1.4) contained in nmr tubes. The ³¹P nmr spectrum of the solution was recorded at each titration point in order to establish the pH dependence of $\delta(^{31}\text{P})$ for the phosphonate moiety in these compounds. Stock acid and base solutions were prepared using similar procedures to those

described in Section 3.2.3 and Section 3.2.4, respectively, using water deionised by reverse osmosis. Reagents employed were as described in Table 3.3.2; in addition, deuterium oxide (^2H , 99.9 %) was obtained from Goss Scientific Instruments Ltd. and KOH was obtained as a BDH 'CONVOL' vial giving a 1.0 mol dm^{-3} solution on dilution.

A solution of the alkylaminophosphonic acid (100 cm^3 , ca. 0.02 mol dm^{-3} in the phosphonic acid group, $-\text{PO}_3\text{H}_2$) was prepared in acidic $\text{H}_2\text{O}/\text{D}_2\text{O}$ medium ($[\text{HNO}_3] = 0.04 \text{ mol dm}^{-3}$, $[\text{KNO}_3] = 0.96 \text{ mol dm}^{-3}$, 5 % D_2O v/v) of ionic strength $I = 1.0 \text{ mol dm}^{-3}$. An aliquot (3 cm^3) of this solution was pipetted into an nmr tube (10 mm o.d.) and was titrated against aqu. KOH solution ($0.7840 \text{ mol dm}^{-3}$) delivered from a motorised piston burette (Metrohm Dosimat 655) fitted with an anti-diffusion tip. Aliquots of base were 0.012 cm^3 in buffer regions of the titration curve, but smaller aliquots (0.006 cm^3) were delivered over end point regions.

Solution pH was recorded in the nmr tube using a thin stem combination electrode (Russell CMAWL/3.7/200) linked to a Corning 150 pH/ion meter. The electrode was pre-calibrated using NBS standard 0.05 mol dm^{-3} -potassium hydrogenphthalate^[27d] (pH ca. 4.0) and $0.025 \text{ mol dm}^{-3}$ -phosphate^[27 d] (pH ca. 6.9) buffers, prepared according to standard procedures;^[27d] and corrected for temperature.^[27d] Solutions in nmr tubes were isolated from atmospheric CO_2 by flushing with nitrogen gas before adding the tube cap and, where possible, manipulations of solutions used in the titration were performed under a stream of nitrogen.

After each addition of base, proton-decoupled phosphorus-31 spectra were obtained at 32.392 MHz using a Bruker WP80 nmr spectrometer. Chemical shifts

were referenced to external 85% *aqu.* phosphoric acid (H_3PO_4) by sample substitution. This method was used in order to overcome the unfavourable dynamic ranges encountered when the reference solution was contained in a coaxial tube within the titration solution. The reference was contained in 5 mm (o.d.) coaxial tube within a second aliquot of the ligand-containing solution used at the start of the titration. Reference signals were recorded every 5 data points and showed variations of < 0.04 ppm. At the end of the titration, a volume of base solution, equal to the total delivered in the titration, was added to the solution surrounding the *aqu.* H_3PO_4 reference solution. In this way, the position of the H_3PO_4 reference signal was found to be independent of the pH of the phosphonate solution surrounding the coaxial tube. (Downfield shifts are denoted by positive signs for δ). Typically > 20 data points were recorded.

Typical spectrometer operating conditions: number of transients, 200; pulse length, $1.0 \mu\text{s}$; offset (f_1) 2500 Hz; delay 1.0 s; spectral width, 3012.0 Hz; acquisition time, 2.72 s; data points, 16 k; decoupling frequency 5800 Hz; line broadening, 3 Hz; temperature, 298 K.

4. A Potentiometric titration system

4.1 Introduction

Determination of stability constants of metal complexes is commonly achieved using potentiometric titration procedures and standard methods for such determinations have been described in detail.^[32] In cases where the organic substrate is a Brønsted base, metal complexation is sensitive to the hydrogen ion concentration of the solution and potentiometric titrations of acidified metal-ligand solutions against base are commonly used to generate data for determination of stability constants.^[1,2,3] The concentration of 'free' hydrogen ions in such solutions may be conveniently measured with a glass electrode and applications of the electrode to this field have been reviewed.^[33] However, manual acquisition of potentiometric titration data is time-consuming, tedious and prone to operational errors. The increase in availability of efficient and inexpensive microcomputers has enabled the titration procedures to be automated and several computer-controlled systems have been described.^[21,28,34,35]

Design, construction and development^[36] of an automated potentiometric titration system, based on the Acorn BBC B microcomputer, was commenced in the School of Chemistry at the Polytechnic of North London in 1985 as part of a collaborative project with the University of Sheffield, James Cook University of North Queensland, and ICI Colours and Fine Chemicals. The apparatus was designed to perform fully automated potentiometric titrations and used as its basis an earlier computer-controlled apparatus developed at James Cook University.^[28] System refinement and development of a menu-driven suite of dedicated programs was carried out over 1985 and 1987; this work enabled some preliminary stability constant measurements to be carried out. After a period

of inactivity during 1987, extensive recommissioning and refinement of the system hardware and software was required in order to achieve stability constant measurements comparable with those obtained in other laboratories working to widely accepted standards^[37,38] (see Section 4.7). The recommissioning and refinement formed a substantial part of the work presently described.

A second, identical system was built and commissioned over the period 1987-89.^[36] Both systems have provided potentiometric titration results for the several titration environments for this study. The hardware and software components of these systems are described the following sections.

4.2 Automated titration system

The microcomputer system provides for fully automated titrations by interacting with a number of external hardware devices via electronic interface circuitry (see Fig. 4.2.1). The hardware/software system enables both rapid sampling and self-compensatory control of the titration environment.

The BBC B microcomputer is expanded in the system by linking to a 6502 Second Processor using the Tube (an external connection providing selected address and data bus lines direct the internal bus). In this configuration the microcomputer acts as an I/O processor for the system, the controlling software being located in RAM of the second processor. The microcomputer is connected to output devices (VDU, lineprinter (Epson LX 800), plotter (Hewlett Packard ColorPro 7440A), and magnetic disk drives) and a Cambridge Microprocessor Systems (CMS) rack interface unit. A series of 'in-house' designed and built modules act as specialised interfaces between the various

sensors (e.g. electrodes) and controlled devices (e.g. the motorised burette) and the CMS interface unit.

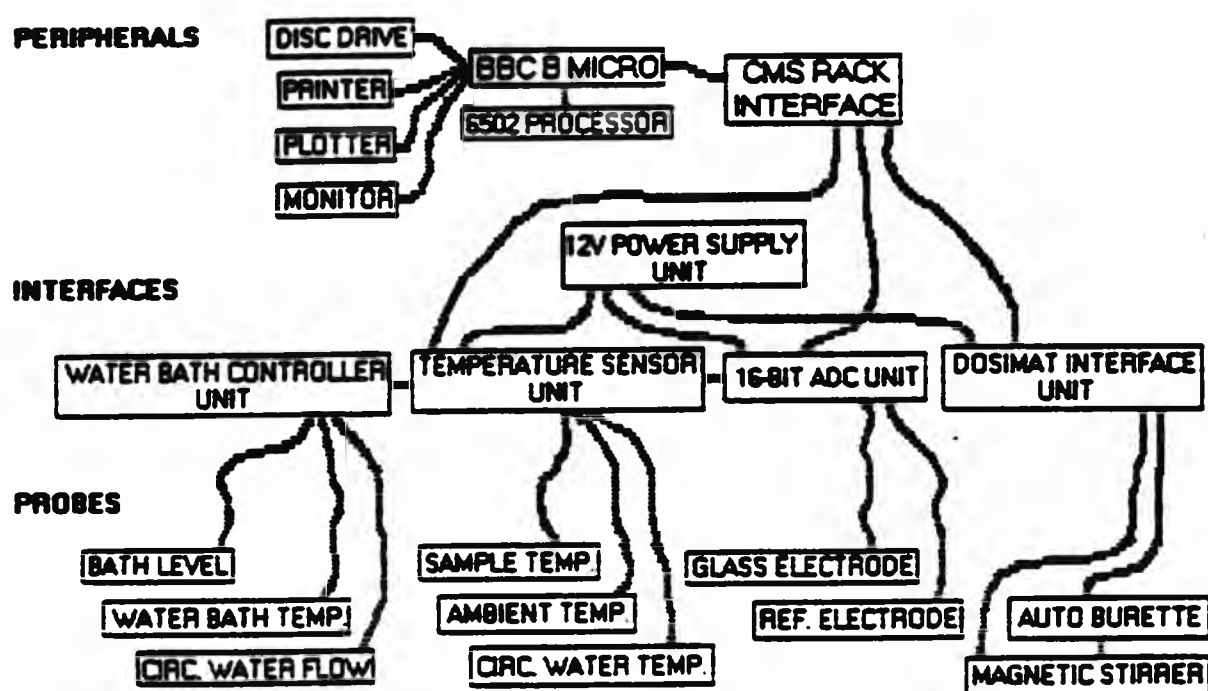


Figure 4.2.1 Interconnection of hardware devices in the automated titration system.

Cambridge Microprocessor Systems (CMS) rack interface unit.

The CMS unit interfaces hardware units through 6522 Variable Interface Adaptors (VIAs) located on cards in the rack, and is connected to the I/O processor (i.e. the BBC micro 6502 processor) via the 1 MHz Bus (an external connection giving direct access to 6502 address and data busses of the I/O processor). The Versatile Interface Card in the rack uses three 6522 VIAs to interface the 16-Bit ADC Unit, the automated burette and stirrer interface, and the water bath control unit. The temperature sensor unit is interfaced separately using the Analogue Interface Card which comprises 8 multiplexed ADC input channels giving rapid conversion to 12-bit accuracy. Signals from these cards pass through the BEEBEX Processor Card containing address decoding circuitry and timing circuitry matching the the 2 MHz 6502 processor to the

1 MHz Bus.

The power supply unit

Power supplies (+5 V and ± 15 V) for the temperature sensor and the water bath control units are obtained from purpose-built power supply unit (PSU).

The temperature sensor unit

The temperature sensor unit comprises Wheatstone bridge circuitry for four input channels. Resistance-temperature conversion uses a reduced form of the Callender-Van Dusen equation. During operation, the separate analogue channels are multiplexed into a single channel by digital circuitry controlled by the system software. Although up to three channels of the temperature sensor unit have been used for recording sample, circulating water, and ambient temperatures during experiments during development work, the sample temperature alone is required for data processing and therefore only one channel is employed during routine titrations. Each channel is regularly calibrated using a software-driven procedure (Section 4.3.3).

The water bath control unit

The water bath control unit monitors the temperature of water in the water bath, and the rate of flow of the circulating water. The analogue temperature reading, obtained from circuitry similar to that used in each channel of the temperature sensor unit, is multiplexed through the temperature sensor unit together with the other temperature channel readings. Pulses generated by the flow sensor are conditioned within the unit prior to counting by the VIA Variable Interface Card. The water bath control unit also contains relays for software control of the water bath heater in order to maintain constant water temperature, and, in addition, provides fail-safe features extra to those

standard for the water bath.

The 16-bit analogue-to-digital converter

The analogue-to-digital converter (ADC) is a purpose-built , high specification 16-bit ADC with internal power supply used to measure the potential of the titration solution using the potential of the calomel cell as a reference. Analogue signals from the glass electrode are digitised by a 16-bit converter pair of integrated circuits which constitute a dual slope integrating ADC. Output ADC readings are averages of two separate conversions, one of 0.64 s duration (incorporating a full auto-zero cycle), the second a short conversion of 0.48 s.

The Dosimat 655 interface unit

The unit enables full handshaking between the system and the Dosimat 655 automatic burette without the need for edge-sensitive input from the microcomputer. (The circuitry is applicable to other systems incorporating CMOS or TTL ports). The unit controls signals for burette fill and dispense operations and detects, and prevents issue of commands, when the burette is active.

The stirrer interface

This interface allows software control of the stirring rate of the Metrohm E649 magnetic stirrer positioned beneath the sample cell.

4.3 Titration software

The automated titration system includes a suite of dedicated programs written in BBC BASIC and Assembler languages. The programs control the operation of the titration apparatus and provide a number of hardware settings and data

processing options. Program selection is achieved via an autoboot procedure and interaction with a multi-screen menu program. The boot procedure issues various preliminary system settings, loads the HIBASIC version of BBC BASIC from ROM and chains in the menu program.

4.3.1 The menu program - S.SCMENU^[39a]

The menu program provides an interface between the user and the titration system. Its first function is to call the machine code module SCMMC (assembled by the BASIC program D.SCMSRC) which provides additional operating system commands to operate and interrogate the system hardware. The system hardware is then initialised by the menu program, placed into appropriate idle mode, and the main menu is displayed on the VDU. The menu and sub-menu options are shown in Fig. 4.3.1. Options from the menus, selected by return of the appropriate option number, are accessed by ON GOTO structures which call the appropriate procedures or run the relevant system programs.

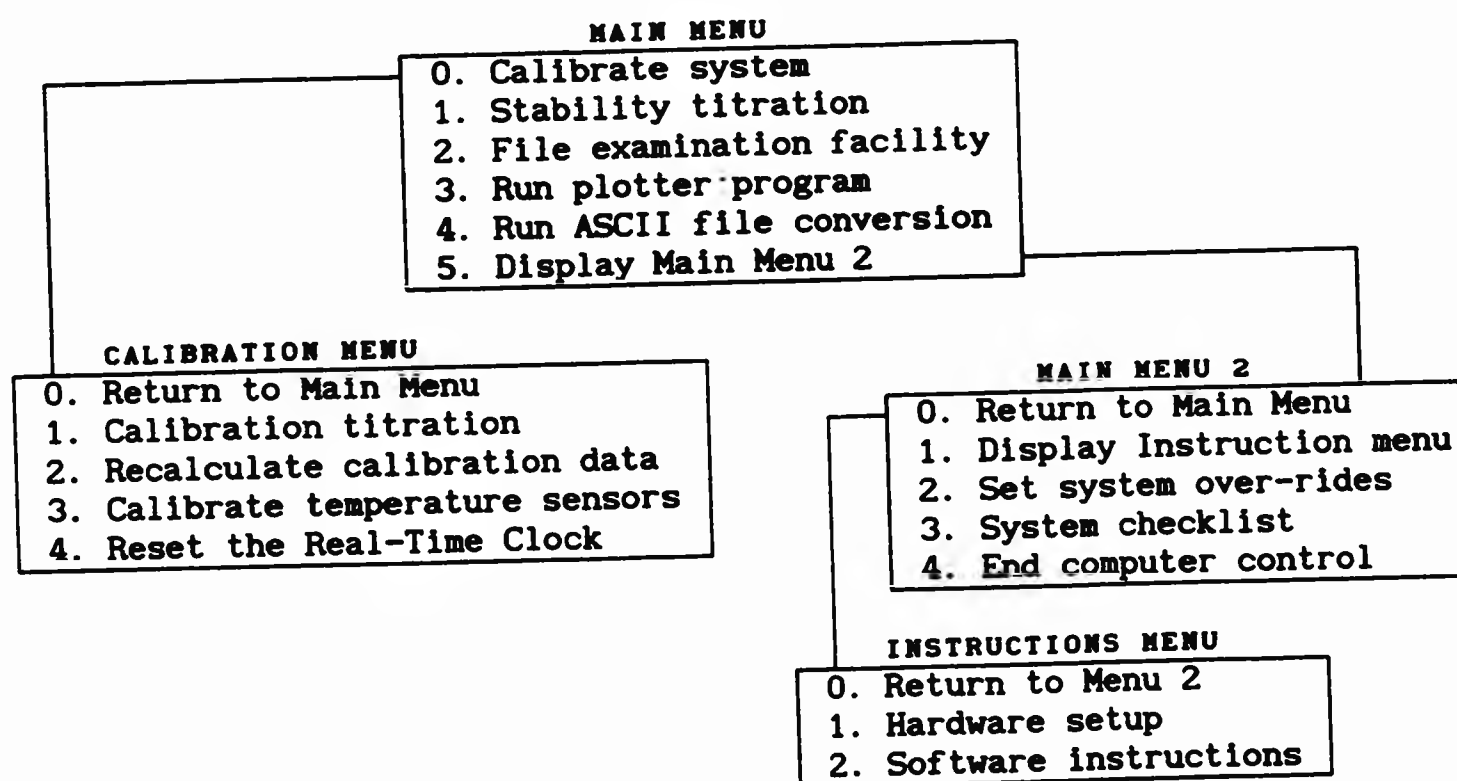


Figure 4.3.1 Schematic representation of menus in S.SCMENU

A second version of the menu program,^[39b] allowing selection of options via pull-down menus, has been introduced on one titration apparatus.

4.3.2 The titration program - S.SCMTITR^[29]

Selection of either titration option from the menu program calls the titration program S.SCMTITR. The program provides active computer control of the titration procedure through two separate modules controlling either calibration or sample titrations. The titration module is selected by the program using a variable setting issued on selection of the appropriate choice in the menu program. Many of the procedures called during execution of the respective titration options are common to both modules and the modular design of the program therefore allows efficient use of disc space and avoids repeated use of IF..THEN..ELSE structures. The structure of the titration program is shown schematically in Fig. 4.3.2.

Each module of S.SCMTITR executes an interactive session for input of pertinent titration parameters thereby offering significant flexibility in the conditions that may be employed in the respective titrations. Standard conditions are given during these sessions as default values for appropriate titration variables. Different formats for calibration and sample titration data files are required for subsequent data manipulations; calibration data files provide input for a program (S.SCMCAL^[40]) to calculate constants for the potentiometric cell, and sample data files are converted into ASCII format (DECDDATA^[30]) before transfer to mainframe computer. These files are created with the relevant titration parameters during execution of the appropriate module. Fully automated titrations are performed within each module by the TITRATE subroutine (*vide infra*) and the titration data is written to the appropriate disc file. For calibration data, a program to calculate E_0 and

pK_w for the titration cell is called from within the module before the system returns to the Main Menu. After data acquisition has been completed for sample titrations, a file compression procedure is performed to maximise available disc space on the data disc before the menu program is recalled.

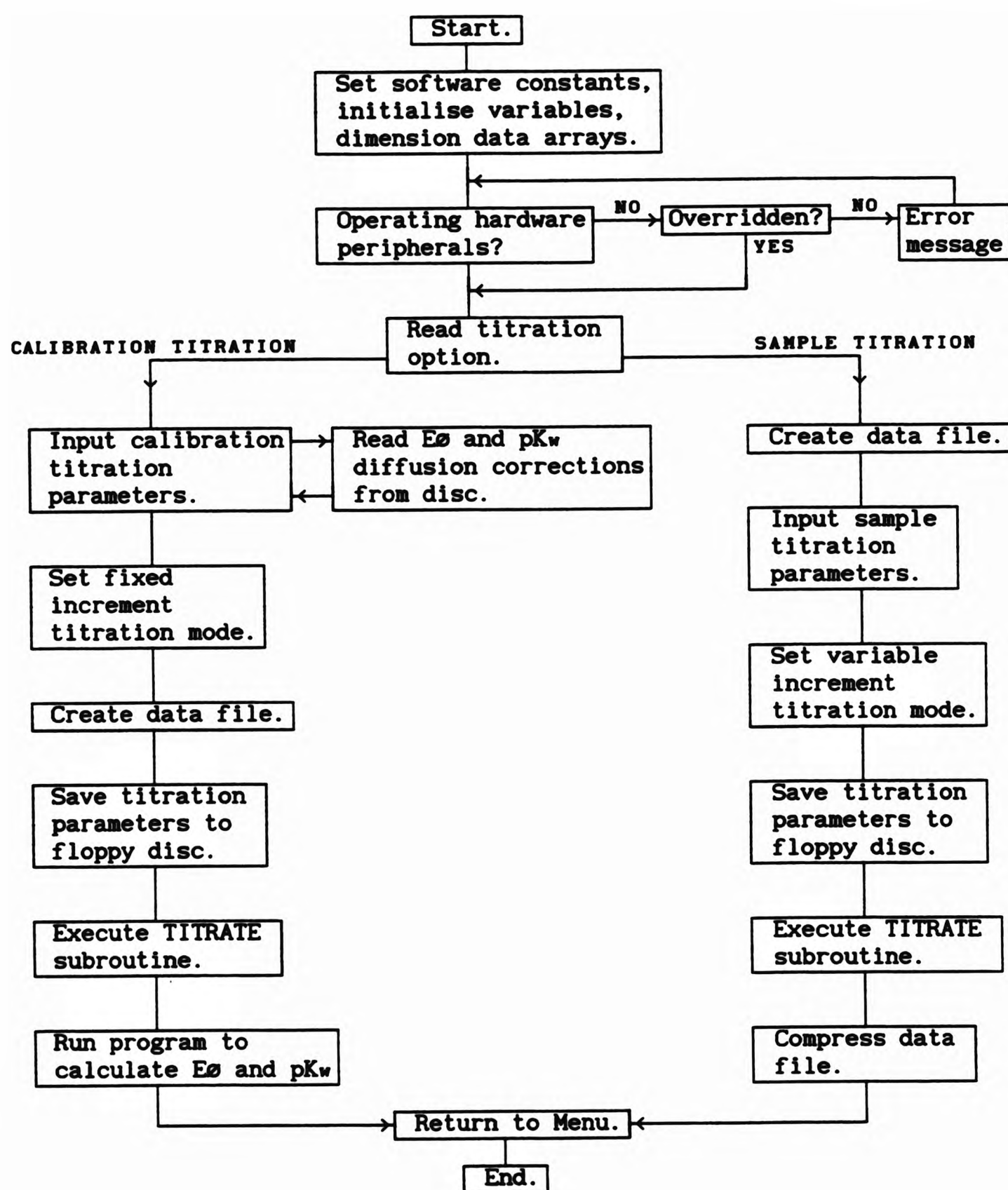


Figure 4.3.2 Schematic representation of the structure of S.SCMITR.

The TITRATE subroutine.

The TITRATE subroutine controls data acquisition during execution of both the calibration and sample titration modules. The routine employs a number of nested REPEAT..UNTIL loops to interact with system hardware, to execute criteria controlling data point measurements, to control delivery of base to the titration solution, and to write accepted data point measurements to appropriate disc files. The REPEAT..UNTIL structures engender flexibility in the titration procedure by using many of the titration parameters set during the preceding interactive set-up session as exit conditions for the appropriate loops. The logical sequence of instructions executed within the TITRATE subroutine is shown in Fig. 4.3.3.

The use of the REPEAT..UNTIL loops results in rapid update of measurements taken from hardware peripherals and displayed on the graphics screen; the innermost loop of the structure, and therefore most frequently executed code, returns measurements from each channel of the temperature sensor unit, the solution potential, the volume of base delivered to the titration solution, and the flow rate (measured on an arbitrary scale) of the circulating water system. These measurements are continuously available through Assembler routines which control and monitor the functions using the interrupt facilities of the computer. The temperature of the water bath is also controlled at this level; machine code is called to pulse the heater unit if the measured water bath temperature lies outside software-set tolerances.

Several safeguards to ensure that the titration solution is fully equilibrated before data is recorded are incorporated into the subroutine code. Storage of solution potential readings in computer RAM (for subsequent use in recording a data point) is initiated only when a user-specified time delay has elapsed

after the base aliquot from motorised burette has been delivered or, in the case of the first reading, after the titration was initiated. Furthermore, the potential reading is only stored if the solution temperature, recorded on the latest pass of the innermost REPEAT..UNTIL loop, lies within a user-specified tolerance of 25 °C. On the first pass of these criteria, i.e. before any base has been added to the solution, TITRATE invokes a procedure to ensure that the initial titration solution is fully stabilised. Using a similar REPEAT..UNTIL structure to that used in TITRATE, the procedure reads the potential of the solution at 5 min intervals and compares successive readings while maintaining and monitoring the titration environment. Program execution returns to TITRATE once successive readings coincide within a user-specified tolerance [a tolerance of 0.2 mV has generally proved satisfactory for this test; it should be noted that this is not the tolerance applied before recording data points (*vide infra*)].

Titration data points are recorded in the following way: A user-specified number of potential readings [the maximum number (99) is imposed by limitations on the dimensions of the array], satisfying time delay and sample temperature criteria, are averaged and the standard deviation of their mean (σ) is calculated. Readings outside a tolerance of 3σ are removed from the set and a second average of the accepted potential readings is calculated. The average of accepted readings is then compared with the average of accepted readings from the previous loop and recorded as a data point (with the volume of base delivered, temperatures from each channel of the TSU, and the elapsed time) if the two means coincide to within a user-specified tolerance (typically 0.05 mV). If the two means do not agree within the tolerance an extra test is used to prevent continuous looping for non-convergent data points. If a user-specified number of attempts to obtain convergent data is

exceeded, a data point is recorded using the mean of accepted readings from the most recent set.

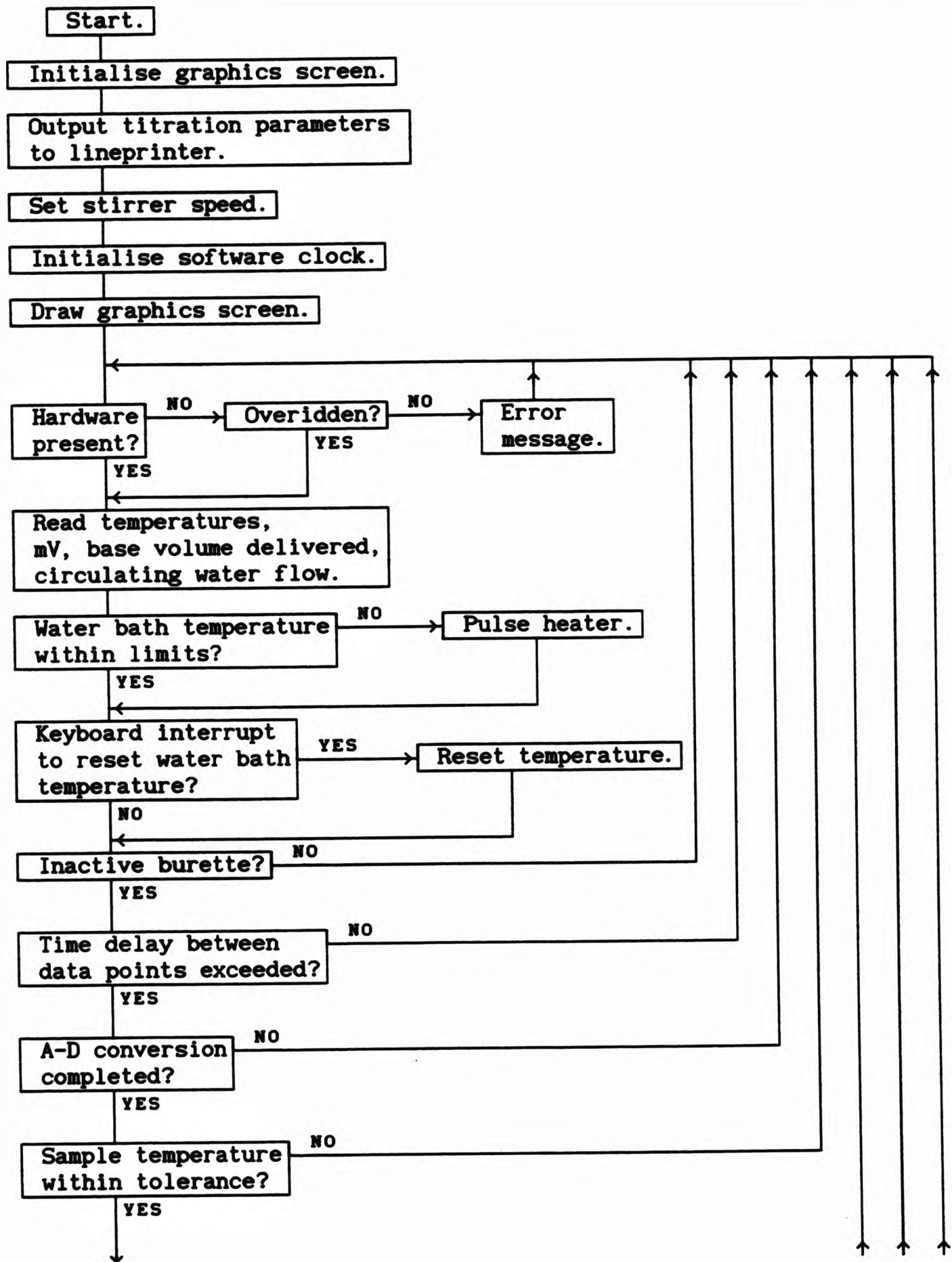


Figure 4.3.3 Logical sequence of the TITRATE subroutine. Continued overleaf.

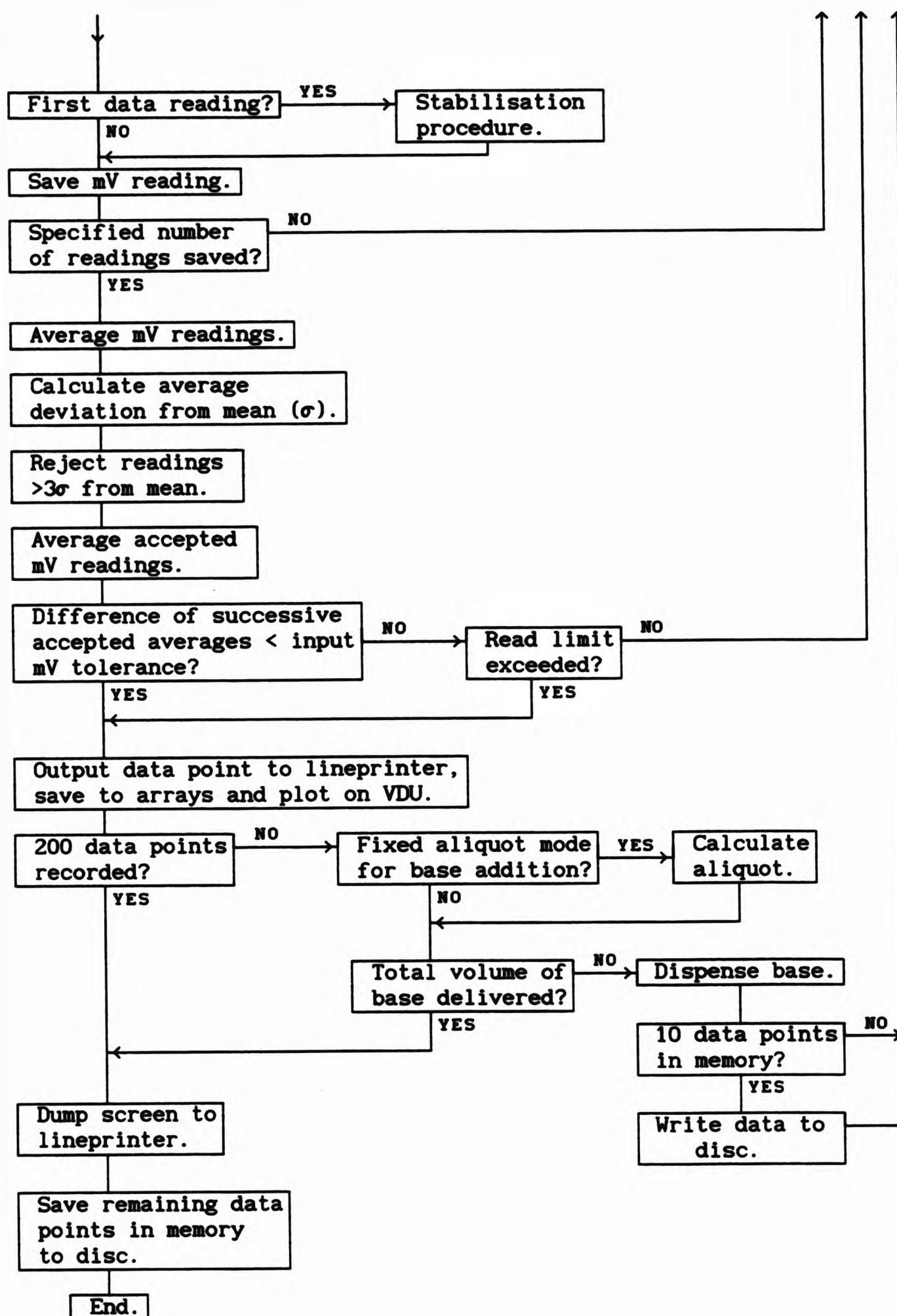


Figure 4.3.3 Logical sequence of the TITRATE subroutine.

Judicious choice of user-specified titration parameters, in conjunction with the safeguards imposed on data recording, allows accurate titration of potentially problematic systems, e.g. those for which equilibration times are long or those with unfavourably large heats of reaction, using this apparatus. It should be recognised however that unnecessary extension of titration times may result in increased measurement errors arising from evaporation, diffusion, and contamination effects.

Variable volumes for base additions, dependent on the change of solution potential with the previous addition, are calculated in TITRATE when the appropriate flag is detected. The flag is set during execution of the sample titration module (titrations executed by the calibration titration module used fixed increment additions) and variable increments within user-specified maximum and minimum aliquots are calculated from $\text{increment} = 2 \times \text{previous increment} / \Delta E$, where ΔE is the change in solution potential from delivery of the previous aliquot. (Clearly, fixed increment titrations within this mode are achieved by specifying equal maximum and minimum aliquots for the addition). Variation of the volume of base aliquot in this way has two main advantages; base additions become smaller approaching end point regions of the titration curve (where $\Delta E / \Delta V$ is large) yielding more data and, to some extent, anticipating the end point. Larger base aliquots are delivered over buffer regions in the curve resulting in reduced times for completion of a titration run and minimisation of errors arising from solvent evaporation, solution diffusion and contamination effects.

4.3.3 Auxiliary programs

Temperature Sensor Unit calibration facility - S.TEMPCAL^[41a]

S.TEMPCAL is an interactive BBC BASIC program used in conjunction with the calibration procedure for each channel of the Temperature Sensor Unit. The program gives a VDU display of current ADC readings from each temperature channel and values for calibration parameters contained in its associated data file D.TCOEFS. Each channel of the TSU is calibrated by introducing, in turn, two high accuracy resistors as the 'unknown' resistance in the Wheatstone Bridge circuit and adjusting zero and gain controls to give ADC values corresponding to the known resistance. Existing calibration parameters are replaced by the new ADC readings via interaction with the VDU display using cursor and return keys, and the new readings are saved to a data file (D.TCOEFS) on request. The calibration parameters are used to calculate temperatures during execution of the titration program S.SCMTITR.

Flat-bed data plotting facility - PLOTX^[41b]

PLOTX is a multi-option BBC BASIC plotting routine to drive a Hewlett Packard HP 7440A flat-bed plotter connected to a BBC B microcomputer via the RS432 serial port. The program accepts data from formatted sample and calibration data files (generated by S.SCMTITR) and plots pH or solution potential vs. volume of delivered base using user-selected display options (e.g. point plotting, line plotting, selected data ranges).

4.4 Cell calibration in aqueous solution

A potentiometric cell consisting of a glass electrode and a standard calomel electrode provides a convenient apparatus for measurement of the hydrogen ion concentration in a test solution and its use is recommended by IUPAC in 'Guidelines for the Determination of Stability Constants'.^[32] The electrochemical potential derived from these components is shown schematically in Fig. 4.4.1. In order that such cells give accurate measurements of proton concentrations in test solutions a number of different methods for cell calibration have been suggested.^[32, 33a, 42, 43, 44, 45, 46] These methods can be separated into two different approaches; calibration against buffer solutions of known pH, and calibration against solutions of known hydrogen ion concentration. Titrations of strong acid against strong alkali in the presence of high concentrations of a background electrolyte under similar conditions to those used for sample titrations are generally employed in the latter approach. Calibration methods employing buffer solutions are regarded as inappropriate for metal-ligand equilibrium studies, introducing uncertainties arising from the different ionic compositions of buffer and test solutions,^[33a] and cell calibration using titrations of strong acid against strong base are recommended,^[32] and widely used, for studies at constant ionic strength.

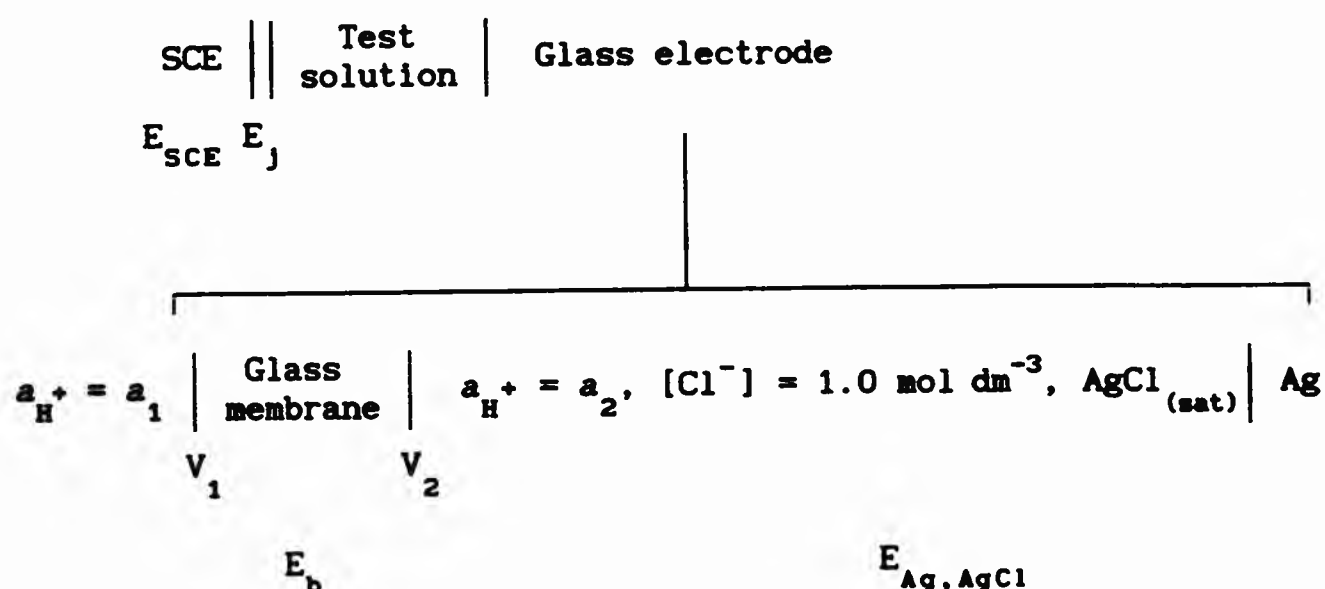


Figure 4.4.1 Schematic representation of the glass electrode-standard calomel electrode (SCE) cell.^[47] [V_1 and V_2 are the potentials generated at the respective membrane surfaces; a_i is the activity of the i th species].

4.4.1 Theory

The potential of glass electrode-calomel electrode cell (Fig 4.4.1) may be separated into a number of discrete contributions^[47]

$$E_{\text{cell}} = E_{\text{Ag, AgCl}} - E_{\text{SCE}} + E_{\text{asy}} + E_j + E_b \quad 4.4.1$$

where $E_{\text{Ag, AgCl}}$ is the potential of the internal Ag, AgCl reference in the glass electrode, E_{SCE} is the potential of the standard calomel electrode, E_{asy} is a potential deriving from asymmetry effects in the glass membrane, E_j is the junction potential at the salt bridge-test solution interface, and E_b is the boundary potential of the glass membrane. The first three terms of Eqn. 4.4.1 are independent of pH and may therefore be combined into a single constant, (E_0) giving

$$E_{\text{cell}} = E_0 + E_j + E_b \quad 4.4.2$$

The boundary potential of the glass membrane is related to the hydrogen ion activities of solutions in contact with each surface of the glass membrane and is made up from the potentials, V_1 and V_2 , generated at the respective membrane surface (see Fig. 4.4.1). The potentials at the membrane surfaces are given by^[47]

$$E_b = V_1 - V_2 = \left(j_1 + \frac{RT}{F} \ln (a_1/a'_1) \right) - \left(j_2 + \frac{RT}{F} \ln (a_2/a'_2) \right) \quad 4.4.3$$

where a_1 and a_2 are the hydrogen ion activities of the solutions in contact with the membrane surfaces and, a'_1 and a'_2 are the hydrogen ion activities in the gel layers of the electrode in contact with the solutions. The expression for E_b may be simplified if it is assumed that the gel surfaces of the membrane are identical; the constants j_1 and j_2 become identical when the gel surfaces of the membrane have equal numbers of sites from which protons can leave,^[47] and the hydrogen ion activities in the gel, a'_1 and a'_2 , become approximately equal when the equilibria at each membrane surface,

$H^+_{(soln)} + Na^+Gl^- = Na^+_{(soln)} + H^+Gl^-$ (where Gl^- represents a cation binding site of the membrane), lie far to the right hand side.^[47] These assumptions yield

$$E_b = \frac{RT}{F} \ln (a_1/a_2) \quad 4.4.4$$

and indicate that the boundary potential depends only on the activities of the hydrogen ion in the solutions in contact with the membrane surfaces. However, hydrogen ion activity solution of the internal HCl solution in the electrode is fixed in practice and therefore a factor of $-(RT/F)\ln a_2$ may be included in the constant term of Eqn. 4.4.2.

$$E_{cell} = E_0 + E_j + \frac{RT}{F} \ln a_1 \quad 4.4.5$$

Under conditions of constant ionic strength the activity of hydrogen ion in the test solution (a_1) may be expressed in terms of hydrogen ion concentration by including the activity coefficient in the constant term of the equation. [32,33a]

$$E_{\text{cell}} = E_0 + E_j + \frac{2.303 RT}{F} \log [H^+] \quad 4.4.6$$

4.4.2 Calibration of the computer-controlled apparatus

Automated strong acid-strong base titrations are employed to calibrate the BBC microcomputer-controlled potentiometric titration system. Titrations are controlled within software using a module of the S.SCMTITR^[29] program. The module controls fixed increment titrations and records the solution potential and volume of added base at each data point within the TITRATE procedure (see Section 4.3.2). On completion of the titration procedure the module calls the BBC BASIC program S.SCMCAL^[40] in order to calculate calibration parameters from the stored data. In order to minimise errors arising from differing ionic compositions of calibration and sample solutions, common stock acid and base solutions were used in both types of titration and data acquired over comparable ranges of $\log [H^+]$. (Experimental conditions employed for calibration titrations are described in Section 3.2.11).

4.4.4 A program to calculate cell parameters from strong acid-strong base titration data - S.SCMCAL^[40]

S.SCMCAL^[40] calculates the titration endpoint and the cell parameters E_0 (Eqn. 4.6.6) and pK_w (the apparent ionic product of the solvent) from strong acid-strong base titration data. These cell parameters are required for sample titration data processing using the MINIQAD^[16,22] and SUPERQUAD^[25] programs. A number of programs for calculating parameters pertinent to electrode calibration are described in the literature, including

some featuring least-squares refinement of one or more cell calibration parameter.^[33a,45,46] S.SCMCAL is based on a similar program written for the automated titration employed by Lindoy and co-workers^[28] and, as such, uses a similar approach for calculation of E_0 and pK_w . Calculations for E_0 and pK_w include considerations for liquid-liquid junction potential (E_j) derived from those described by Anderegg in EICHU.^[48]

The sequence of operations performed by S.SCMCAL is shown in Fig. 4.4.2. The program calculates the end point of the titration using the second derivative of the E vs. volume of delivered base (v) curve. The second derivative is obtained numerically at the i th titration point using Eqn. 4.4.7,^[49]

$$\frac{\partial^2 E}{\partial v^2} = A_0 E_1 + A_1 (E_{1+1} + E_{1-1}) + A_2 (E_{1+2} + E_{1-2}) \quad 4.4.7$$

where $A_0 = -0.2857$, $A_1 = -0.1429$, and $A_2 = 0.2857$. The end point for the acid-base titration is given at the point of inflexion of the sigmoid E vs. v curve; at this point the second derivative of the function is zero.^[1,27e,47]

S.SCMCAL interpolates between the data points describing the minimum value of the second derivative and the subsequent point where the second derivative becomes positive in order to estimate the volume where $\partial^2 E / \partial v^2 = 0$ (the volume of equivalence for the titration). From an accurate base concentration (input during the interactive setup session for calibration titration parameters in S.SCMTITR), the proton concentration at each data point is readily calculated.

E_0 , incorporating a correction for E_j , is calculated in S.SCMCAL^[40] as follows: an estimate of E_0 is calculated at the first (i.e. the most acidic) data point using Eqn. 4.4.6. A second estimate is obtained similarly at the second data point of the set. If this second estimate lies within a specified

tolerance (preset at ± 1.0 mV) of the first, the two estimates are averaged to give a 'running' mean for E_0 . This process is repeated for each datapoint in the data set - the estimate of E_0 at a particular data point is included in the running mean, which is then recalculated, if it lies within the specified tolerance. These conditions result in a final E_0 value derived entirely from measurements in acid environments. The final E_0 , its standard deviation and the number of datapoints contributing to the final average are output to a lineprinter.

The apparent ionic product for the solvent is calculated via E_{pKw} which is pK_w multiplied by the factor $2.303RT/F$. E_{pKw} is initially calculated using Eqn. 4.4.8 at the final (i.e. the most alkaline) data point of the titration. Subsequent estimations of E_{pKw} at each data point are included in a running average using similar conditions to those employed in E_0 calculations. The conditions in this case however, result in mean E_{pKw} , and hence pK_w values derived from data measured in alkaline solutions. The overall pK_w is calculated from the final average of E_{pKw} , and its value, standard deviation and the number of datapoints contributing to the final average of E_{pKw} are output to a lineprinter.

$$E_{pKw} = -E_{cell} + E_0 + E_j - \frac{2.303 RT}{F} \log [OH^-] \quad 4.4.8$$

4.4.5 Correction for liquid-liquid junction potentials

Calculations for both E_0 and E_{pKw} include corrections for the junction potential, E_j (Eqn. 4.2.6 and 4.2.8). Such potentials arise at the salt bridge-test solution interface from the differing diffusion rates of ionic species across the liquid-liquid junction. A similar junction potential at the salt bridge-calomel electrode interface is assumed to be independent of the composition of the test solution and is therefore included in E_0 for the

cell. Estimations of the magnitude of E_j may be made from long established theoretical bases,^[50,51] and relationships derived from the Henderson equation^[51] have been shown to successfully approximate measured junction potentials during potentiometric titrations in constant ionic media.^[52,53]

EICHU^[48] calculates junction potentials in acid and base solution using an adaptation of the Henderson equation based on the assumption that since ions of a common univalent background electrolyte are present in equal concentration on each side of the junction, the value of E_j is determined solely by the presence of H^+ or OH^- in the test solution. Estimates of the junction potentials in acid solution (E_j^a) and in base solution (E_j^b) used in S.SCMCAL are given by^[33b,53]

$$E_j^a = \frac{RT}{F} \ln \left(1 + \frac{(u_H - u_{cat}) [H^+]}{(u_{an} + u_{cat}) I} \right) \quad 4.4.9$$

$$E_j^b = \frac{RT}{F} \ln \left(1 + \frac{(u_{OH} - u_{cat}) [OH^-]}{(u_{an} + u_{cat}) I} \right) \quad 4.4.10$$

where u_x is the ionic mobility of the ion X at temperature T . ($X = an, cat$ imply respectively, the anion and cation of the background electrolyte). The constant terms of Eqns. 4.4.7 and 4.4.8 relating u_x are calculated within a separate program of the system software, DIFFCORR,^[54] containing a small data base of ionic mobilities taken from EICHU.^[48] These parameters are automatically input into S.SCMTITR during operation of the calibration titration module. Output from EICHU suggests, as might be expected, that the respective E_j corrections are most significant at the extremes of the $\log [H^+]$ range.^[48]

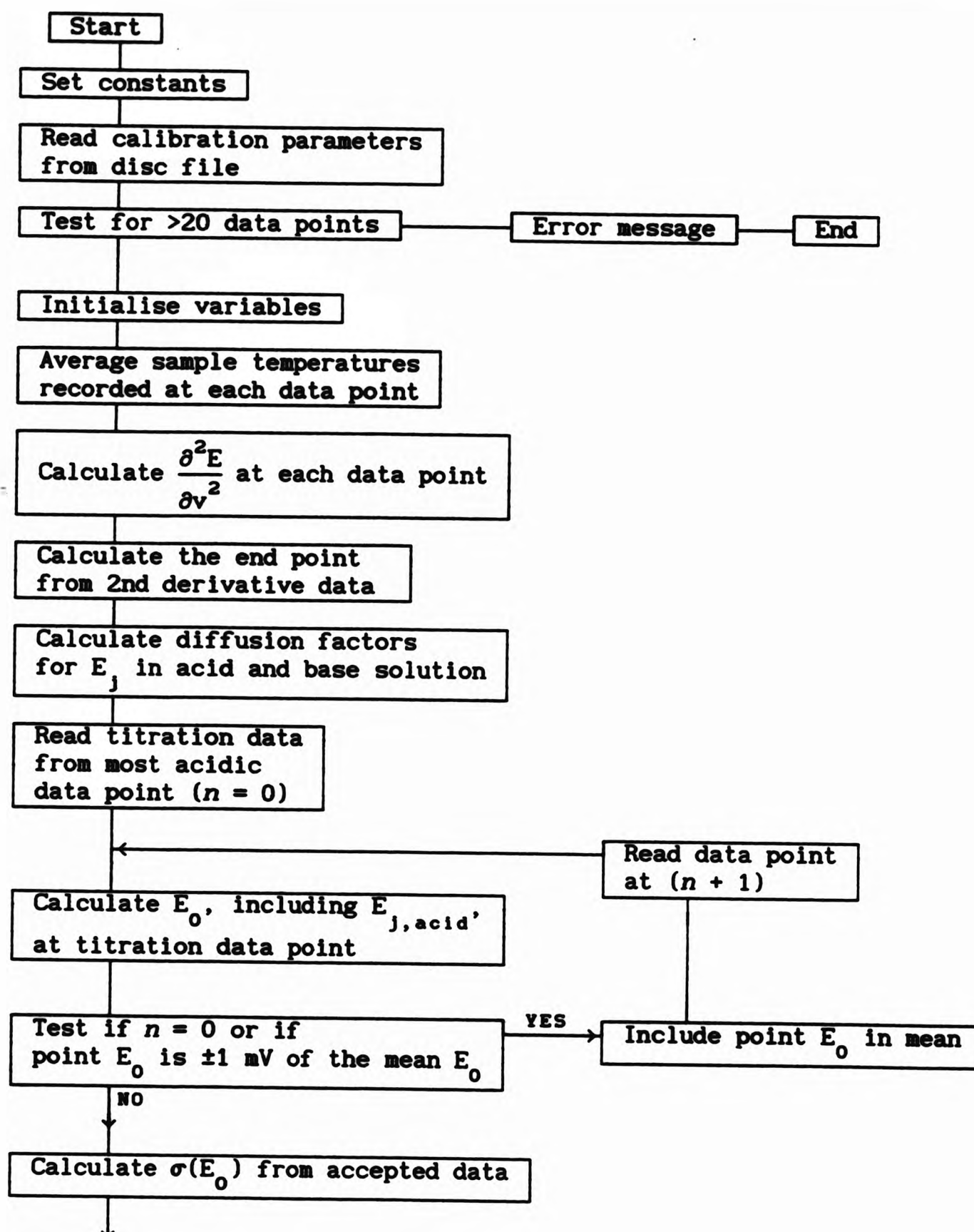


Figure 4.4.2 Logical sequence of operations in S.SCMCAL (continued overleaf)

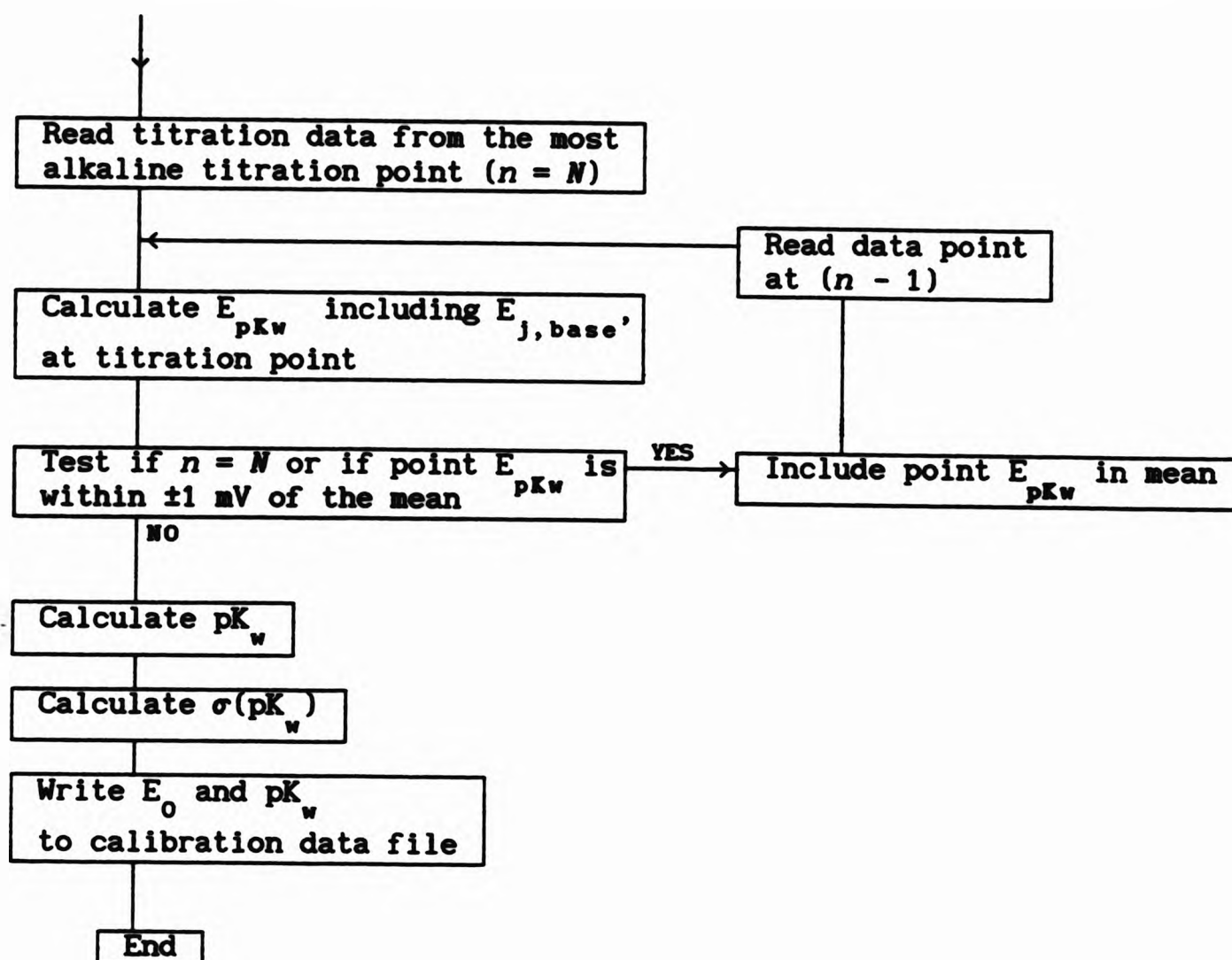


Figure 4.4.2 Logical sequence of operations in S.SCMCAL

4.4.6 Cell calibration for a potentiometric cell ($I = 0.1 \text{ mol dm}^{-3}$, KNO_3)

The potentiometric cell employed in the automated titration system was calibrated regularly; calibration titrations to obtain the cell constants E_0 and pK_w were generally performed at least once a day. The variation of E_0 and, less importantly, pK_w with time was used as a qualitative assessment of the stability of the potentiometric cell. Several origins for cell instability were identified (*vide infra*) and these were rectified by, as appropriate, reconditioning, replacement or redesign of components in the system.

The cell constants show the expected sensitivity to variations in the temperature of the titration solution and improvements to the stability of cell and room temperatures resulted in significantly smaller variation of the cell constants between titrations. The most significant improvements in cell thermostasis were achieved by; efficiently lagging the circulating water system, introducing cooling coils (carrying a steady flow of cold tap water) into the water bath of the system to reduce overshooting of the bath temperature following a heating cycle, and redesigning the titration vessel to incorporate a larger water jacket. Improvements to the stability of ambient temperature, including introduction of an air conditioning unit (which had the most dramatic effect), resulted in better cell temperature stability and enhanced reliability for the electronic hardware of the titration system.

Significant variation of the cell constants in temperature-stable solutions was commonly caused by clogging of the glass sinter at the sample/salt bridge liquid-liquid junction. Such blockages were often caused by precipitation from titration solutions and were particularly evident in solutions where insoluble metal hydroxide species were formed. In one exceptional example, severe drift of E_0 was traced to virtual disintegration of the glass frit induced by chemical attack on the glass. In cases where cleaning and replacement of the salt bridge were not effective, drift was often cured by reconditioning the glass electrode according to the manufacturer's recommended procedure - an overnight soak in *aqu.* HCl (0.1 mol dm^{-3}) was applied in these cases.

Cell parameters derived from a series of ten strong acid-strong base titrations acquired over a 15 day period are presented in Table 4.4.1. The series of titrations of HNO_3 ($0.004 \text{ mol dm}^{-3}$) against KOH (0.1 mol dm^{-3}) in

aqu. KNO_3 ($0.096 \text{ mol dm}^{-3}$) are representative of routine cell calibrations performed for the automated titration system. Cell parameters derived from consecutive calibration titrations frequently showed better agreements than those presented, but these data were chosen to fairly represent data available from the automated system throughout the period of study. The relative standard deviation of \bar{E}_0 for this data set ($\bar{E}_0 = 141.97$, $\sigma = 2.71 \text{ mV}$) is considerably larger than that of \bar{pK}_w ($\bar{pK}_w = 13.76$, $\sigma = 0.014$). Similarly, larger intertitration variations for E_0 than pK_w were routinely observed throughout the period of study. It is interesting to note that similar intertitration dependence of these parameters has been observed for data obtained with an automated potentiometric titration system and has been identified as the largest source of error for stability constant determinations. [55,56,57]

Braibanti and co-workers, during their studies of the contributions to errors in stability constant determinations, have considered the effect of variance of cell constant parameters within a calibration titration - the intratitration variability - and between calibration titrations - the intertitration variability. [55,56,57] These authors conclude that the parameters E_0 and pK_w show a distribution where the intertitration error is larger than the intratitration error. Consideration of the standard deviations for E_0 and pK_w values shown in Table 4.4.1 gives some indication of the intratitration variation of these parameters during calibration titrations. Although the standard deviations have not been derived with error propagation analysis, as used by Braibanti et al, [55,56,57,58] it is clear that the intratitration variation of E_0 and pK_w is considerably smaller than that between titrations. It is reasonable to assume that variations between calibration titrations show some time dependence and, since E_0 shows the

larger intertitration variation, changes in the asymmetry potential of the glass electrode are likely to have a significant, and unpredictable, influence. Frequent calibration of the apparatus is therefore required to limit errors induced by such uncertainty.

Table 4.4.1. Cell parameters calculated from a series of calibration titrations in aqueous solution.^a

File	End point/cm ³				E ₀ ^{b, c} /mV	pKw ^{b, c}	T ^d /°C
	2nd derivative method ^b	Gran function					
		acid	base	mean			
CALI300	0.950	0.961	0.952	0.957	141.27(0.27)	13.75(0.005)	24.96
CALI301	0.962	0.971	0.950	0.961	141.16(0.29)	13.74(0.004)	24.96
CALI302	0.961	0.967	0.951	0.959	140.83(0.31)	13.73(0.004)	25.00
CALI303	0.961	0.970	0.979	0.974	139.04(0.30)	13.74(0.008)	24.99
CALI304	0.963	0.979	0.966	0.972	139.24(0.18)	13.77(0.005)	24.99
CALI305	0.942	0.959	0.941	0.950	138.79(0.17)	13.76(0.005)	25.02
CALI306	0.963	0.977	0.989	0.983	142.95(0.24)	13.76(0.008)	25.00
CALI307	0.963	0.980	0.991	0.986	143.02(0.20)	13.77(0.007)	25.04
CALI308	0.987	1.012 ^e	0.991	1.002	144.45(0.31)	13.76(0.007)	25.01
CALI309	0.940	0.966 ^e	0.945	0.956	145.52(0.20)	13.76(0.005)	25.03
CALI310	0.962	0.988 ^e	0.958	0.973	145.41(0.31)	13.77(0.005)	24.99

^a Data obtained from titrations of HNO₃ (0.004 mol dm⁻³) against KOH (0.1 mol dm⁻³) in aqueous solution (25 cm³, I = 0.1 mol dm⁻³, KNO₃) over a 15 day period. ^b Calculated by S.SCMCAL.^[40] ^c Standard deviation in brackets.

^d Mean of sample temperatures at each data point. Data was collected with a preset temperature tolerance of ±0.1 °C. ^e Correlation coefficient < 0.999

The validity of cell constants calculated by S.SCMCAL (Section 4.4.4) are fundamentally dependent upon accurate determination of the end point from the

cell potential (E) vs. volume of added base (v) data [Fig. 4.4.3(i)]. The program employs a second derivative procedure to estimate the end point; a plot of $\Delta^2 E / \Delta v^2$ against v [Fig. 4.4.3.(ii)] yields the end point at $\Delta^2 E / \Delta v^2 = 0$.^[1,27e,47] The titration end point is also commonly estimated from plots of Gran functions^[59,60] against v. Such manipulations of potentiometric data yield functions with linear branches from data derived from acidic or basic solution which intersect the abscissa at the titration end point. The Gran functions described by Rossotti and Rossotti,^[42]

$$\psi = (V_0 + v)10^{-EF/2.303RT} \quad 4.4.9$$

$$\psi' = (V_0 + v)10^{EF/2.303RT} \quad 4.4.10$$

were plotted against v [Figs. 4.4.3(i) and (ii) respectively] for each data file of the set presented in Table 4.4.1. Titration end points were estimated the v-axis intercept of the least squares line for branches of $\psi(v)$ in acidic solution (i.e. where $v < v_e$) and $\psi'(v)$ in basic solution (where $v > v_e$). Gran plots can also provide useful diagnostic tests for the validity of the titration method, in particular non-linearity can arise from metal ion or carbonate contamination of solutions.^[42] However, least squares fits for titration data sets of Table 4.4.1 demonstrated good linearity; correlation coefficients for the respective branches of $\psi(v)$ and $\psi'(v)$ plots were greater than 0.995 in all cases, and better than 0.999 in the majority.

Comparison of titration end point estimates from second derivative and Gran functions (Table 4.4.1) show reasonable agreement between the grand mean for each set [\bar{v}_e (2nd deriv.) = 0.959, $\sigma = 0.013 \text{ cm}^3$; \bar{v}_e (Gran) = 0.970, $\sigma = 0.017 \text{ cm}^3$]. Agreements between end point estimations within the titrations (i.e. from comparison of end point estimations from different regions of the E vs. v curve) are somewhat poor in some cases although such

differences appear to be substantially smaller than those of the respective intertitration variations. These differences presumably arise from operational errors in solution preparation although there does not seem to be any obvious correlation with the intertitration variation of E_0 .

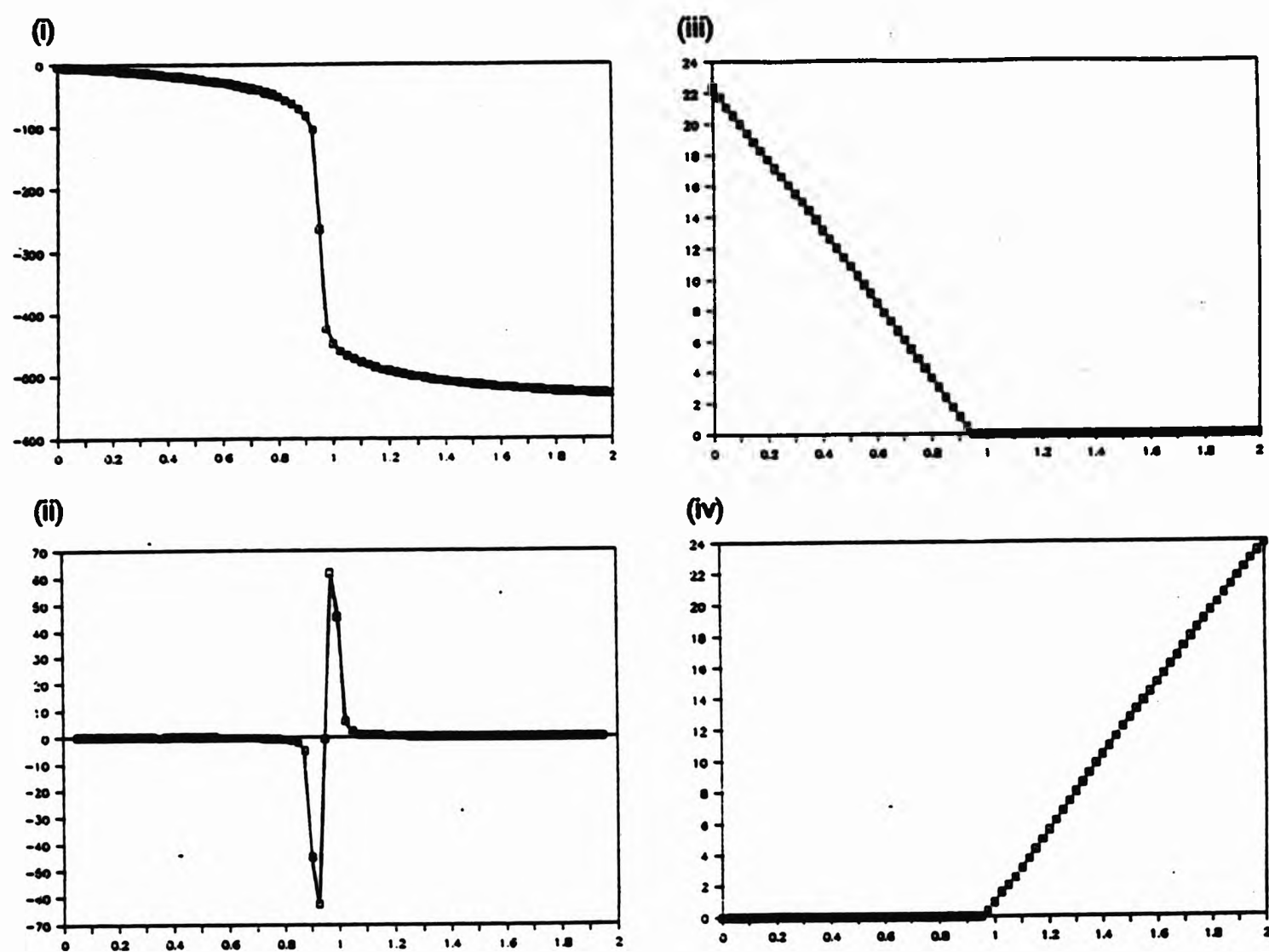


Figure 4.4.3 Plot of (i) cell potential (E) vs. volume of added base (v);
(ii) $\partial^2 E / \partial v^2$ vs. v ; (iii) $(V_0 + v)10^{-EF/2.303RT}$ vs. v ;
(iv) $(V_0 + v)10^{EF/2.303RT} \times 10^{-9}$ vs. v for titration of aqu. HNO_3 ($V_0 \text{ cm}^3$) against aqu. KOH at constant ionic strength (KNO_3 ; $I = 0.1 \text{ mol dm}^{-3}$).

4.5 The aqu. nickel-glycine system - a bench standard

The aqu. nickel-glycine system has been studied thoroughly by a number of laboratories,^[37,38,61,62] and comparison with these results is used as a measure of apparatus and technique accuracy.^[38] The protonation and complexation schemes are well established for this system. The glycinate anion ($L = \text{NH}_2\text{CH}_2\text{CO}_2^-$) forms two protonated species $[\text{H}_2\text{L}]^+$ and $[\text{HL}]$ and three nickel(II) complexes, $[\text{NiL}]^+$, $[\text{NiL}_2]$ and $[\text{NiL}_3]^-$. Although hydroxy species are almost certainly formed at higher pH, concentrations of these are regarded^[38] as being negligible at intermediate pH (2.5 - 9.0).

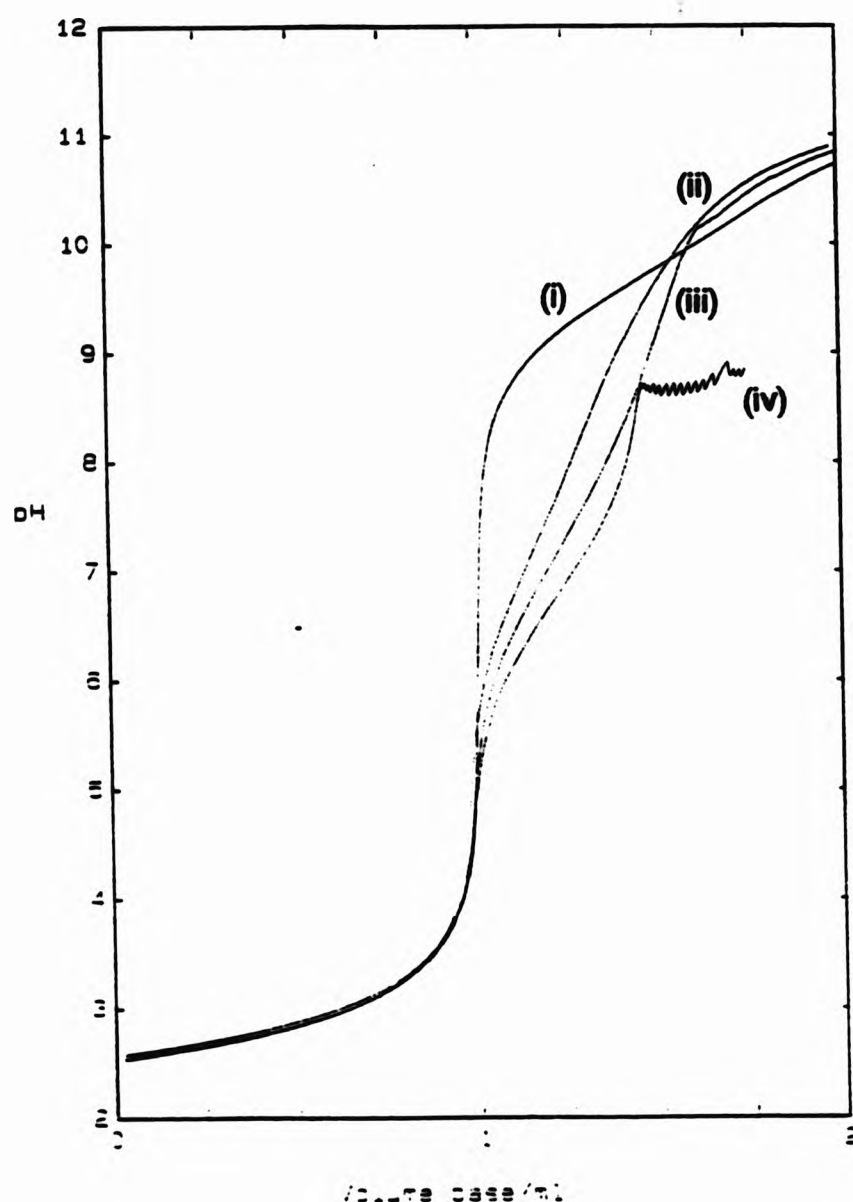


Figure 4.5.1 Titration curves (pH vs. volume of added base) for acidified aqu. solutions of (i) glycine ($[\text{L}] = 2 \text{ mmol dm}^{-3}$), and nickel(II) chloride with glycine; (ii) $[\text{M}]:[\text{L}] = 1:1$, (iii) $[\text{M}]:[\text{L}] = 1:2$, (iv) $[\text{M}]:[\text{L}] = 1:3$.

The potentiometric titration system developed for the present studies was tested against the nickel-glycine system. Plots of pH vs. volume of added base derived from ligand-only and metal-with-ligand titration data are shown in Fig. 4.5.1. Experimental data within the pH range ca. 2.5-9.0 were analysed using the FORTRAN program MINQUAD.^[16,22] Titration data for glycine in the presence of Ni²⁺ (M:L = 1:1, 1:2 and 1:3) was analysed with fixed ligand protonation constants.

Table 4.5.1 Protonation constants for glycine.^a

Datafile	$\log \beta_{011}$	$\log \beta_{012}$	$\log K_{012}$	R-factor ^b
GL31	9.53(0.003)	11.82(0.006)	2.29	0.002511
GL32	9.59(0.002)	11.94(0.006)	2.35	0.001876
GL33	9.57(0.003)	11.94(0.008)	2.37	0.002294
GL34	9.56(0.005)	11.97(0.012)	2.41	0.004549
Mean ^c	9.56 \pm 0.06	11.92 \pm 0.15	2.36 \pm 0.12	

^a Data obtained at constant ionic strength; I = 0.1 mol dm⁻³, KCl. Data analysed using the MINQUAD program. Figures in parentheses represent standard deviations calculated during execution of the program. Data files combined for refinement with SUPERQUAD: $\log \beta_{011} = 9.62$ (0.006), $\log \beta_{012} = 12.12$ (0.023) [$\chi^2 = 25.22$, $\sigma = 0.2182$]. ^b 'Crystallographic' R-factor; $R = \sqrt{[\sum(E_{\text{obs}} - E_{\text{calc}})^2 / \sum E_{\text{obs}}^2]}$. ^c Unweighted mean of values from each datafile; error limits are derived from the range for each value.

Formation constants for [NiL]⁺ and [NiL₂] were obtained at all the metal/ligand ratios investigated; the formation constant for [NiL₃]⁻ was obtained solely on refinement of data for titrations with M:L = 1:3. Titration data obtained at pH values above 9.0 was removed from each metal/ligand data set before

refinement. Irregularities in titration curves, presumably arising from precipitation of metal hydroxy species, were apparent for M:L = 1:1 and 1:2 at higher pH (ca. pH 8.6 and 10 respectively, see Fig. 4.5.1) and data points above ca. 8.5 were removed in the former case.

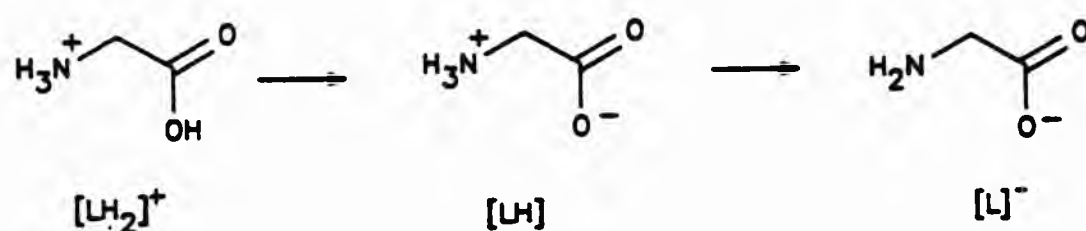


Figure 4.5.2 The protonation scheme of glycine.

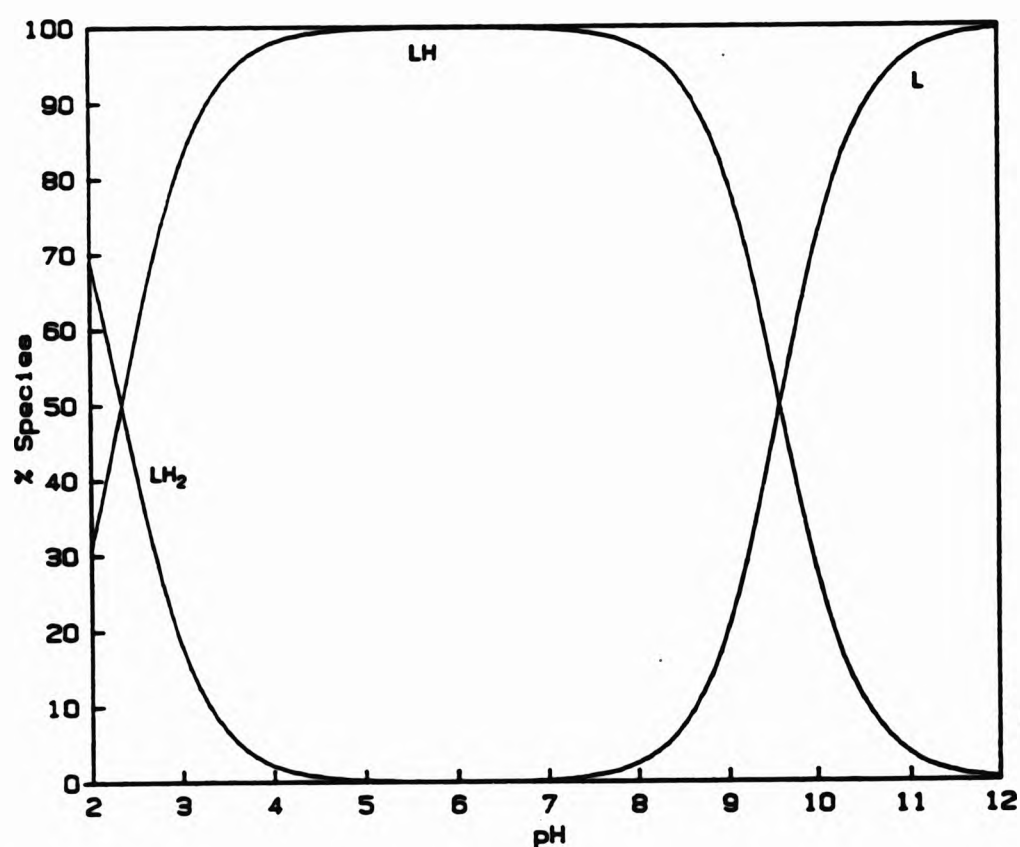


Figure 4.5.3 SPE^[5] computation of species distribution in the aqu. glycine-proton system ($[\text{H}^+] = 4 \text{ mmol dm}^{-3}$; $[\text{L}] = 2 \text{ mmol dm}^{-3}$).

The accepted protonation micro-equilibria for glycine^[63] (Fig. 4.5.2) are

consistent with the expected site basicities. The first deprotonation occurs at the carboxylic acid site giving the zwitterion structure, $\text{H}_3\text{N}^+-\text{CH}_2-\text{CO}_2^-$; X-ray^[64] and neutron diffraction studies^[65] indicate that this structure is stabilised in the solid state by intermolecular hydrogen bonding between the functional groups. Similar interactions are assumed to operate in solution, and a species distribution plot, generated using SPE^[5] (Fig. 4.5.3), shows [LH] as the dominant species over a wide pH range. Deprotonation of the quaternary cationic amine occurs only in more strongly basic solution and the titration curve shows a distinct inflexion at pH 9.6.

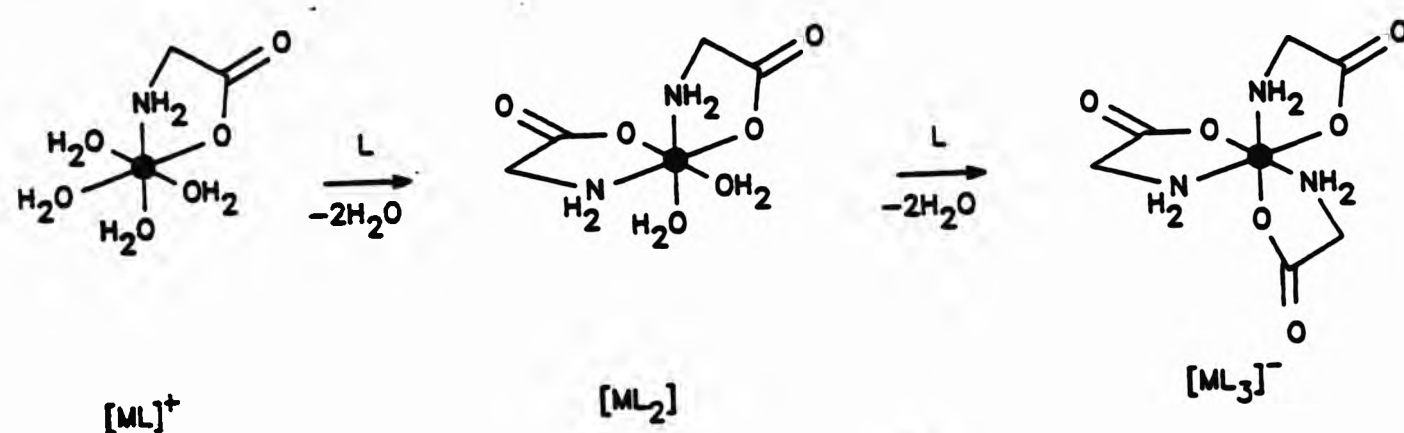


Figure 4.5.4 The stepwise formation of $[\text{NiL}_3]^-$.

The absence of equilibria involving protonated nickel-glycine complexes in the accepted^[37,38] complexation scheme suggests that the metal is co-ordinated to both the amine nitrogen and the carboxylate oxygen of the ligand in the complexes. The solid state structure of diaquabisglycinatonickel(II) $\{[\text{NiL}_2(\text{H}_2\text{O})_2]\}$ shows the metal chelated by the terminal N- and O-donors of the ligand and indicates that the structure is further stabilised by a network of intermolecular hydrogen bonds.^[66] Complex formation in solution occurs by a stepwise replacement of solvent on the metal by ligand leading to a mononuclear, tris-chelate species, $[\text{NiL}_3]^-$. Measurement of the thermodynamic functions, ΔG , ΔH , and ΔS for the stepwise equilibria [(i) and (ii) in Fig. 4.5.4]^[67] showed that complex formation is accompanied by favourable

entropy changes, consistent with bidentate structures for the complexes in solution.^[67] The observed fall in stepwise stability constant ($\log K_{110} > \log K_{120} > \log K_{130}$) on formation of the successive complexes is consistent with, among several factors, a reduction of available co-ordination sites on the metal after chelation of one or more ligands.

Table 4.5.2 Formation constants for nickel(II)-glycine complexes.^a

Datafile	$\log \beta_{110}$	$\log \beta_{120}$	$\log \beta_{130}$	R-factor ^b
NG30	5.57(0.008)	c	-	0.004219
NG32	5.56(0.015)	10.36(0.028)	-	0.003036
NG33	5.61(0.013)	10.34(0.010)	13.97(0.016)	0.003202
NG34	5.68(0.0003)	10.36(0.0002)	14.03(0.0003)	0.003058
Mean	5.60 \pm 0.12	10.35 \pm 0.02	14.00 \pm 0.06	

^a Data obtained at constant ionic strength; $I = 0.1 \text{ mol dm}^{-3}$, KCl. Data analysed using the MINIQAD program. Figures in parentheses represent standard deviations calculated during execution of the program.

^b 'Crystallographic' R-factor; $R = \sqrt{[\sum(E_{\text{obs}} - E_{\text{calc}})^2 / \sum E_{\text{obs}}^2]}$.

^c $\log \beta_{120} = 9.62(0.056)$ ($R = 0.003818$) obtained with value of $\log \beta_{110}$ input as a fixed constant. ^d Unweighted mean of values from each datafile; error limits are derived from the range of refined values.

Equilibrium constants for the nickel-glycinate system obtained in this study (Tables 4.5.1 and 4.5.2) compare favourably with those quoted in the literature (a selection of which are shown in Table 4.5.3). Minor variations in the values can be attributed to differences in types and concentrations of background electrolytes used; indeed, the constants reported here appear to be the first values for this system obtained in aqu. KCl at $I = 0.1 \text{ mol dm}^{-3}$.

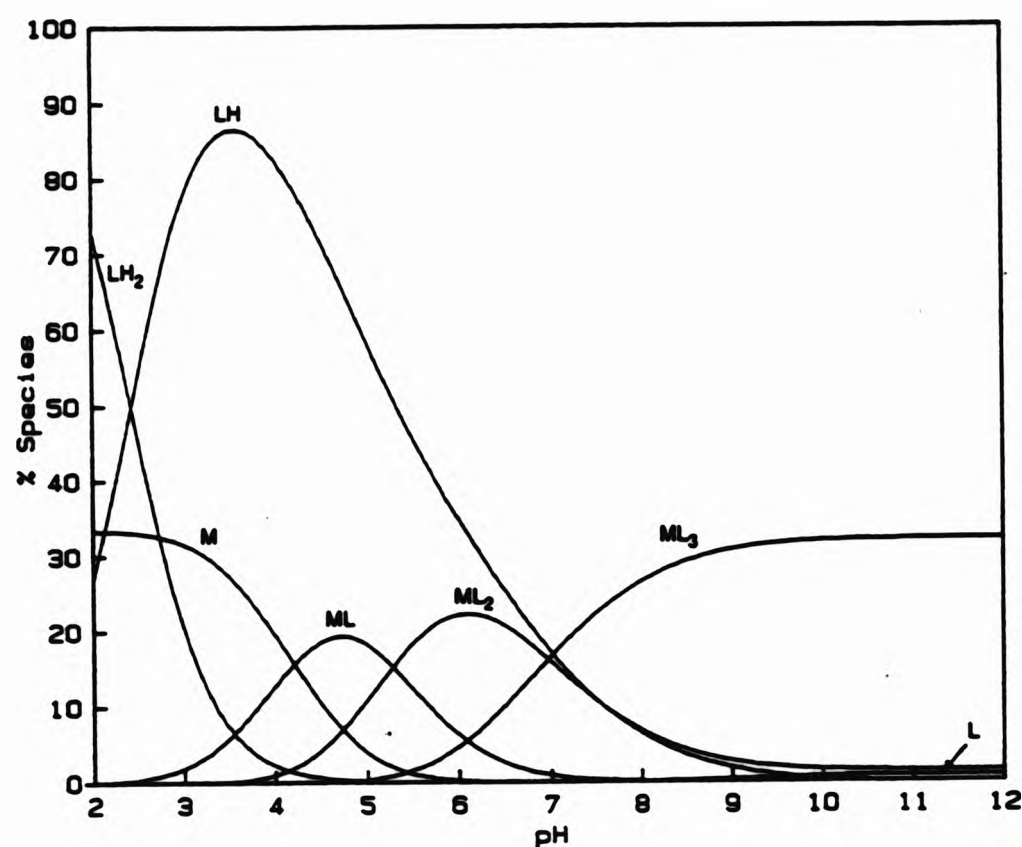


Figure 4.5.5 SPE^[5] computation of species distribution in the nickel(II)-glycine-proton system as percentages of total ligand concentration ($[H^+] = 4 \text{ mmol dm}^{-3}$; $[L] = 2 \text{ mmol dm}^{-3}$; $[M^{2+}] = 0.67 \text{ mmol dm}^{-3}$).

Table 4.5.3 Comparison of protonation and stability constants for the aqu. nickel-glycine system.

	^a	Ref. [37] ^b	Ref. [38] ^c	Ref. [76] ^d	Ref. [62] ^e
$\log \beta_{011}$	9.56 ± 0.06	9.65	9.65	9.61	9.57
$\log \beta_{012}$	11.92 ± 0.15	12.08	12.08	11.87	11.93
$\log \beta_{110}$	5.60 ± 0.12	5.64	5.64	5.73	5.78
$\log \beta_{120}$	10.35 ± 0.02	10.39	10.39	10.56	10.58
$\log \beta_{130}$	14.00 ± 0.06	13.92	13.92	14.00	14.00

^a This work; $I = 0.1 \text{ mol dm}^{-3}$ (KCl), 25°C . Error limits represent the range of values averaged for $\log \beta_{\text{mlh}}$. ^b $I = 1.0 \text{ mol dm}^{-3}$ (NaCl), 25°C .

^c $I = 1.0 \text{ mol dm}^{-3}$ (NaCl), 25°C . ^d $I = 0.1 \text{ mol dm}^{-3}$ (KNO₃), 25°C .

^e $I = 0.1 \text{ mol dm}^{-3}$ (electrolyte not quoted), 25°C .

The variation of $\log \beta_{\text{mlh}}$ between titrations observed during this study is less than 0.1 log units for $\log \beta_{011}$, $\log \beta_{120}$, and $\log \beta_{130}$. The wider range for values of $\log \beta_{012}$ is likely to result from the comparatively low α_{max} values (ca. 0.4) observed for the diprotonated ligand in the pH range of the studies, leading to larger calculated σ values for these constants. This uncertainty may also account for the larger range observed for the $\log \beta_{110}$ values obtained. The species distribution plot for nickel(II)-glycine-proton (Fig. 4.5.5) shows a narrow pH range (ca. 3.5-4.0) in which the species $[\text{H}_2\text{L}]^+$, $[\text{HL}]$ and $[\text{NiL}]^+$ have significant abundance. Uncertainty in the equilibrium concentration of $[\text{H}_2\text{L}]^+$ in this region (due to the relatively large error of $\log \beta_{012}$) is likely to correspond with some uncertainty in calculated concentrations of $[\text{NiL}]^+$ and may possibly account for the moderate inter-titration variation observed for $\log \beta_{110}$.

In conclusion, the comparability of constants obtained in this study with those available in the literature demonstrates the validity of the potentiometric titration system and titration techniques employed.

4.6 Potentiometric Titration in Dilute Hydrogen Peroxide Solution

4.6.1 Composition of the potentiometric cell

Hydrogen peroxide is a strong oxidising agent^[68] and readily decomposes in the presence of catalysts in aqueous solution.^[69] Therefore its inclusion in a potentiometric cell required careful consideration. In order to replicate standardized aqueous titration procedures, the titration solutions for these investigations were composed to yield titrations at constant ionic strength ($I = 0.1 \text{ mol dm}^{-3}$). Potassium nitrate was chosen as the backing electrolyte instead of KCl (Section 4.5) since chloride ion catalyses decomposition of *aq.* H_2O_2 solutions via a cyclical oxidation-reduction route.^[70] Isolation of the reference electrode solution from hydrogen peroxide was also considered to be desirable and therefore the salt bridge was composed of a solution of *aq.* KNO_3 (0.1 mol dm^{-3}) only. The resulting cell (Fig. 4.6.1) is similar to the glass electrode-Ag,AgCl combination described by Mitchell and Wynne-Jones.^[71]

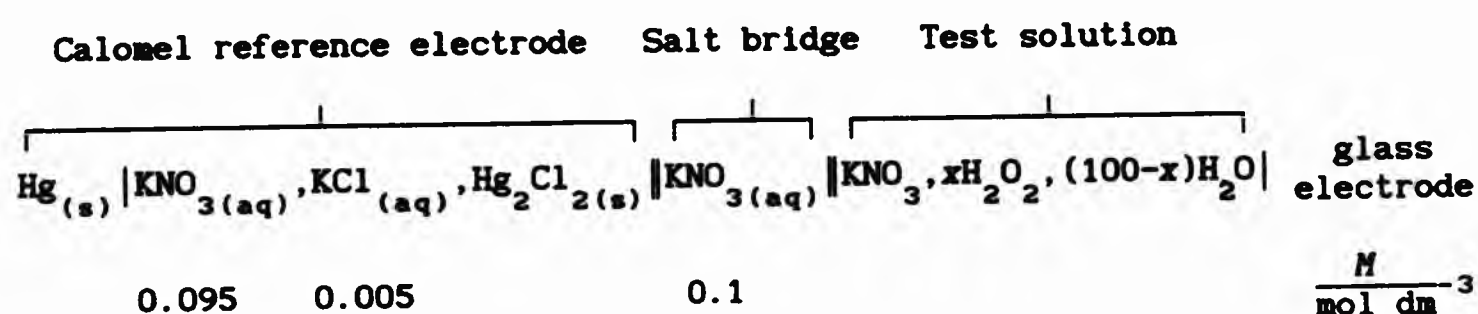


Figure 4.6.1 Schematic diagram of the potentiometric cell used for acid base titrations in dilute *aq.* hydrogen peroxide solutions.

In order to minimise H_2O_2 decomposition at glass surfaces, glassware in contact with the titration solution was pre-treated with concentrated nitric

acid. Glass electrodes used in the study were pre-soaked in acid stock solutions containing appropriate quantities of hydrogen peroxide (see Section 3.2.8).

4.6.2 Cell calibration

The glass electrode-calomel electrode cell in *aqu.* H_2O_2 solutions has been shown^[72] to yield stable and reproducible potentials which vary reproducibly with proton concentration. In a parallel study,^[71] erratic cell potentials were observed for a glass electrode-Ag,AgCl cell at higher H_2O_2 concentrations [$> 60\%$ (v/v)]. The instability was thought to arise from changes in the asymmetry potential of the glass electrode induced by dehydration of the glass membrane and was cured by pre-treatment of the electrode in 50% (v/v) H_2O_2 solution.^[71] Kolczynski *et al* noted that the emf of the glass electrode-calomel electrode couple shifts, E_0 becoming more negative with increasing peroxide concentration, resulting in lowered apparent pH readings on conventional pH meters.^[72] This effect was ascribed to differences in solvation energies of the proton in aqueous and *aqu.* hydrogen peroxide solutions.^[73] During the same study the effective ionic product (pK_w^*) of the respective solutions was calculated and these showed a depression of 3-5 log units from the pK_w for water at all concentrations, reaching a minimum ($\text{pK}_w^* = 8.7$) in approximately 50% peroxide-water mixtures.

As part of this study a series of calibration titrations were performed using acid solutions of differing H_2O_2 concentration. The results for the series of 5 titrations are shown in Table 4.6.1. While pK_w^* shows the expected depression at higher peroxide concentrations, E_0 becomes more positive. This is reflected in a positive translation on the y-axis for the respective E vs. v plots [Fig. 4.6.2(a)].

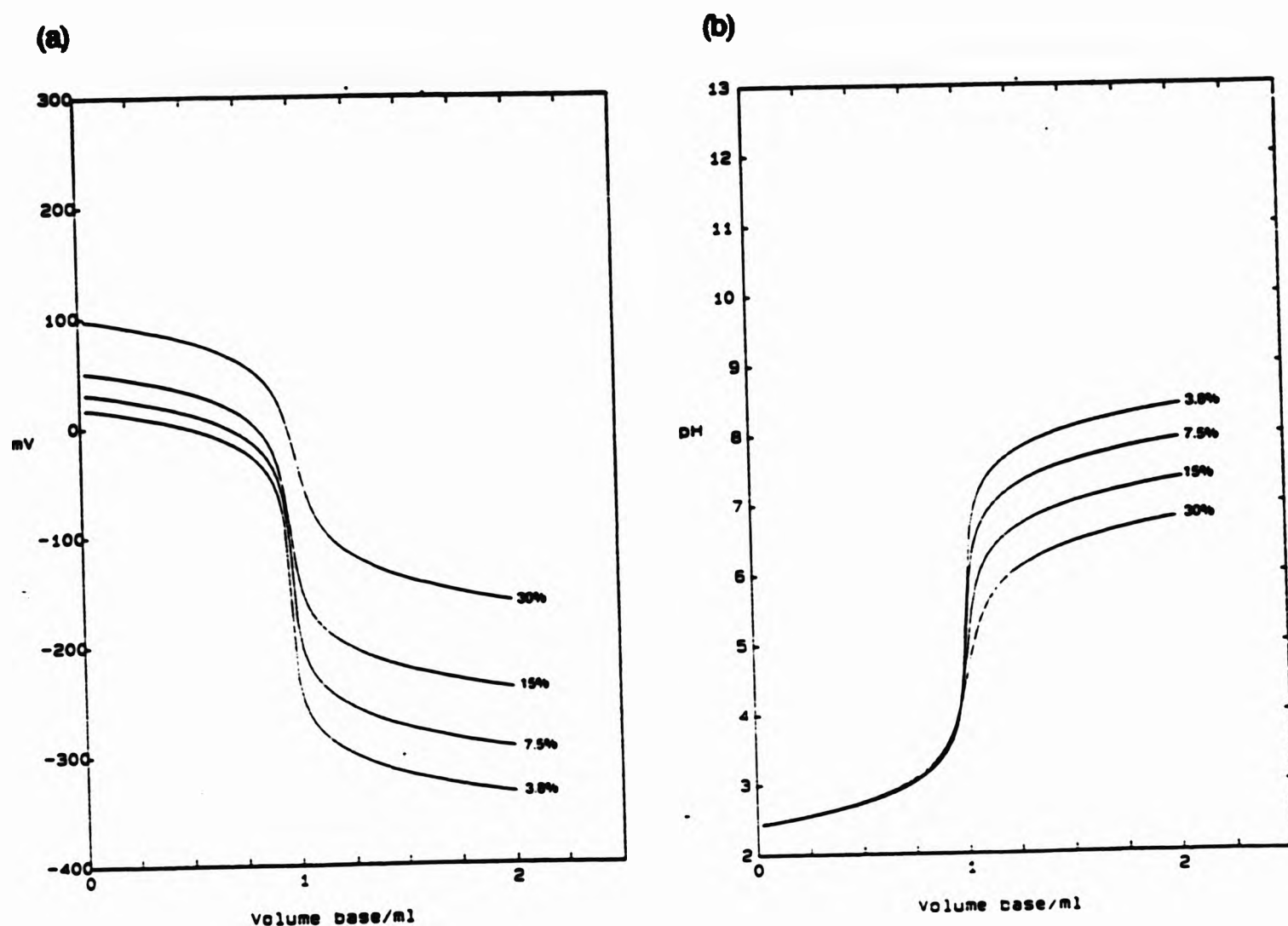


Figure 4.6.2 Plots of a) solution potential (E) vs. volume of added base (v) and b) pH vs. v for titration of HNO_3 (0.004 mol dm⁻³) in (i) 30 %, (ii) 15 %, (iii) 7.5 %, and (iv) 3.8 % (v/v) aqu. H_2O_2 ($I = 0.1$ mol dm⁻³, KNO_3) against aqu. KOH (0.1 mol dm⁻³)

However, plots of pH vs. v, derived using E_0 and pK_w^* values calculated from the titration data using S.SCMCAL,^[40] are virtually coincident in acid solution [Fig. 4.6.2(b)] (inter-titration errors for v_e presumably account for these minor deviations) suggesting that the system truly measures the proton concentration in these solutions. The decrease in pK_w^* with increasing peroxide concentration results in a progressive shortening of the equivalence region of the pH vs. v curve. In a discussion of the suitability of non-aqueous solvents for acid-base titrations, Budevsky points out that a

shortening of the equivalence region has a deleterious effect on the applicability of some solvents and solvent mixtures in acid-base titrimetry.^[74] The sigmoid curves of Fig. 4.6.2 indicate that conditions for acid-base titrimetry are therefore less favourable at the higher peroxide concentrations.

Table 4.6.1 Cell parameters calculated from acid-base titration data in *aqu.* hydrogen peroxide solutions.^a

H_2O_2 concentration ^b /%	E_0^c /mV	#readings averaged ^d	pK_w^* ^c	#readings averaged ^e
30.00	242.17(0.60)	19	9.239(0.010)	9
15.00	196.03(0.42)	25	9.797(0.009)	11
7.50	176.22(0.49)	26	10.371(0.008)	13
3.8	162.46(0.36)	32	10.847(0.009)	20
1.50	156.38(0.39)	30	11.262(0.009)	21
0 ^f	157.31(0.18)	38	13.766(0.004)	34

^a *Aqu.* H_2O_2 solutions of HNO_3 ($0.004 \text{ mol dm}^{-3}$; $I = 0.1 \text{ mol dm}^{-3}$, KNO_3) titrated against *aqu.* KOH (0.1 mol dm^{-3}). Cell parameters calculated using S.SCMCAL.^[40] ^b v/v. ^c Standard deviation in parentheses. ^d Number of point E_0 measurements averaged. ^e Number of point pK_w^* measurements averaged.

^f Cell parameters calculated from titration of *aqu.* HNO_3 ($0.004 \text{ mol dm}^{-3}$; $I = 0.1 \text{ mol dm}^{-3}$, KNO_3) against *aqu.* KOH (0.1 mol dm^{-3}) with identical cell equipment.

It is interesting to note that calculated standard deviations of E_0 and pK_w^* (Table 4.6.1) increase with peroxide concentration and that smaller numbers of data points are used in evaluation of both parameters at higher peroxide concentrations. These observations indicate that the intra-titration

variability of the cell constants in *aqu.* H_2O_2 mixtures is considerably larger than that in a purely aqueous system (Section 4.4.6) and increases with the peroxide concentration. It seems likely that the presence of H_2O_2 in the solvent will not only affect mobilities of ionic species (most importantly those of H^+ and OH^-) in the matrix but may also introduce additional ionic species. For example, H_2O_2 dissociates more readily than water [$\text{H}_2\text{O}_2 = \text{H}^+ + \text{O}_2\text{H}^-$, $\text{pK} = 11.65$ (25 °C)]^[69] and significant quantities of the hydroperoxide ion, which has a higher mobility than OH^- in *aqu.* H_2O_2 ,^[75] will interfere with E_j calculations in basic solution. Differing compositions of solutions each side of the sample-salt bridge liquid-liquid junction, as well as the factors outlined above, undermine the assumptions used in estimating the junction potential (E_j ; Section 4.4.5) and presumably underpin the larger errors of calculated E_0 and pK_w^* values.

Routine investigations in hydrogen peroxide solution were performed in 3 % and 10 % (w/w) *aqu.* H_2O_2 . Results from series of 5 calibration titrations obtained at both peroxide concentrations are presented in Table 4.6.2. Data was taken over a 5 day period in both cases. The data demonstrates that inter-titration variability of the cell calibration parameters in both peroxide solutions is significantly larger than that observed in the analogous aqueous system (Section 4.4.6). As observed in the aqueous system, the inter-titration variation of pK_w^* , although larger at the higher peroxide concentration, is substantially smaller than that for E_0 . In contrast to pK_w^* the variation of E_0 does not show an obvious dependence on the peroxide concentration. The E_0 data presented for the 3 % peroxide solution shows an overall drift. Such drifting of the standard cell potential was commonly observed at both peroxide concentrations but was generally cured by replacement of the salt bridge in the cell. This observation suggests that

diffusion of H_2O_2 across the liquid-liquid junction into the salt bridge solution during a titration may significant and that the drift in E_0 may originate from increasing amounts of H_2O_2 in the salt bridge solution. It is interesting to note that Wynne-Jones and co-workers used agar gel to support KCl as a salt bridge for measurements of pH in concentrated H_2O_2 solutions.^[71] This modification was used to reduce the uptake of water from conventional salt bridge solutions by the H_2O_2 solution.^[41]

Table 4.6.2 Cell constants obtained for aqueous hydrogen peroxide solutions.^a

	v_e^b/cm^3	E_0^c/mV	pK_w^{*d}
3% H_2O_2^e			
CALIB67	1.016	249.43(0.44)	11.296(0.011)
CALIB68	1.019	247.24(0.42)	11.297(0.009)
CALIB69	1.038	245.36(0.47)	11.317(0.011)
CALIB71	1.034	244.47(0.40)	11.286(0.009)
CALIB72	1.049	242.81(0.39)	11.282(0.009)
Mean ^f	1.031(0.012)	245.86(2.29)	11.296(0.012)
10% H_2O_2^e			
CALIB104	0.990	245.97(0.51)	10.433(0.010)
CALIB105	1.026	246.26(0.47)	10.432(0.010)
CALIB106	1.047	242.50(0.48)	10.389(0.009)
CALIB107	0.981	246.72(0.46)	10.504(0.008)
CALIB108	1.034	241.63(0.41)	10.399(0.010)
Mean ^f	1.015(0.030)	244.62(2.11)	10.431(0.040)

^a Aqu. H_2O_2 solutions of HNO_3 (0.004 mol dm⁻³; I = 0.1 mol dm⁻³, KNO_3) titrated against aqu. KOH (0.1 mol dm⁻³). Cell parameters calculated using S.SCMCAL.^[40] ^b Volume of equivalence estimated from second derivative

procedure with S.SCMCAL.^[40] ^c Standard deviation in parentheses.

^d Effective ionic product. Standard deviation in parentheses ^e w/w.

^f Grand mean for values presented. Standard deviations in parentheses.

The end point of the titrations also show larger variation at the higher peroxide concentration. This variation may possibly arise from errors in delivery of accurate volumes of titrand - solutions containing the higher concentration of peroxide were notably less viscous and pipetting accurate volumes of acid stock solution was more problematic with these solutions.

In order to account for the larger inter-titration variation of calibration parameters, calibration titrations were performed before and after each sample titration and the cell parameters obtained from these titrations were averaged before subsequent data processing.

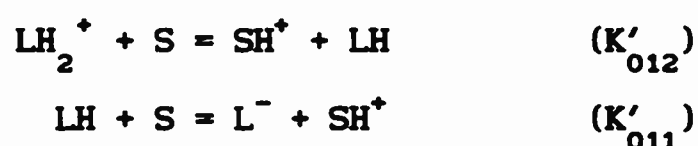
4.6.3 Nickel glycinate in 3% and 10% aqu. hydrogen peroxide solution

Potentiometric titrations were performed for glycine and nickel/glycine mixtures in both 3% and 10% (w/w) hydrogen peroxide solutions in order to determine the effect of H_2O_2 on the protonation and complexation equilibria of the systems. Although KCl was used as the electrolyte for titrations in aqu. media (see Section 4.5), KNO_3 was employed as the backing electrolyte for studies in peroxide solution in order to overcome the destabilising effect of the chloride ion on peroxide solutions. Reported values^[76] for glycine and nickel glycinate in aqueous KNO_3 (Table 4.5.3) show little difference to those obtained in chloride solution.

Ligand-only and ligand-with-metal titration data were refined using MINIQAD. The protonation and complexation models and $\log \beta$ values obtained for the aqueous system were used as initial estimates for the peroxide data analysis. In all cases, it was necessary to lower the ligand concentration was required to achieve acceptable convergence. In this way, 'best fit' parameters were obtained for ligand-only files at both peroxide concentrations and for

metal-with-ligand data obtained in the 3% solution. For nickel/glycine data in 10% H_2O_2 however, better fits were obtained on lowering the ligand concentration beyond that considered reasonable to account for modest sample impurity alone. Substantial gas evolution in the titration solution was also noted on termination of titrations at this concentration.

Values for the protonation constants in peroxide, given in Table 4.9.2, show significant depression from those for aqueous solution. Interestingly, $\log \beta_{011}$ decreases and $\log K_{012}$ increases at the higher H_2O_2 concentration. Considerable effort has applied in relating acid pK_a 's obtained in non-aqueous solvents and solvent mixtures^[77] and Budevsky describes four factors controlling the relative strength of an acid in a solvent (S);^[74] the intrinsic acidity of the acid, the intrinsic basicity of the solvent, the charge type of the acid, and the electric permittivity of the solvent. Equilibria for transfer of proton between glycine and the solvent (S),



demonstrate that the first deprotonation (K'_{012}) is isoelectric - the overall charge remains constant - while the second step (K'_{011}) is ionogenic. A relative increase in the electric permittivity of the solvent is expected to stabilise formation of charge, resulting in an increase in K_{011} but exerting no on the value of K_{012} . Clearly factors other than the electric effect of the medium assume significance for glycine protonation in the *aqu.* H_2O_2 mixtures considered. This is not entirely unexpected since *aqu.* H_2O_2 mixtures show little change of permittivity from that of water^[78] and have even been described as 'iso-dielectric'.^[79]

Nickel data yielded constants for $[ML]^+$ and $[ML_2]$ only, although titrations were performed with M:L = 1:3 in both peroxide media. Stepwise constants for the formation of $[ML]^+$ and $[ML_2]$ in 3 % peroxide show similar depression compared to values in aqueous solution. $[ML]^+$ showed a larger deviation in 10% solution, but the value for $[ML_2]$ was little different from that in aqueous solution.

Table 4.6.2 Protonation and stability constants for glycine and nickel/glycine in aqueous and dilute aqu. H_2O_2 solutions.

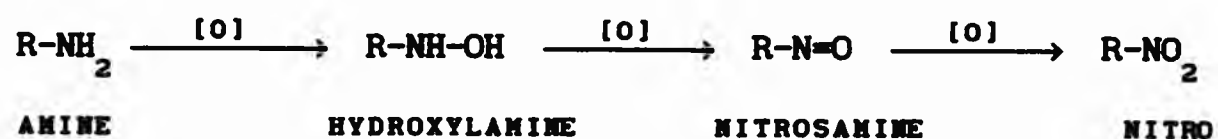
	Aqueous ^a	3% H_2O_2 ^b	10% H_2O_2 ^b	Methanol ^c	Dioxan ^d
$\log \beta_{011}$	9.56	8.93	8.73	9.29	9.58
$\log \beta_{012}$	11.92	11.33	11.57	e	e
$\log K_{012}$	2.36	2.40	2.84	2.97	3.25
$\log \beta_{110}$	5.60	5.06	4.68	6.16	6.51
$\log \beta_{120}$	10.35	9.27	9.33	e	e
$\log K_{120}$	4.75	4.21	4.65	5.27	5.62

^a This work (see Section 4.5); $I = 0.1 \text{ mol dm}^{-3}$ (KCl), 25 °C. ^b Aqueous solutions (w/w), $I = 0.1 \text{ mol dm}^{-3}$ (KNO_3), 25 °C. ^c From Ref. [80], 54.3 % (w/w) aqueous solution; $I = 0.5 \text{ mol dm}^{-3}$ ($NaClO_4$), 25 °C. ^d From Ref. [80], 48.1 % (w/w) aqueous solution; $I = 0.5 \text{ mol dm}^{-3}$ ($NaClO_4$), 25 °C. ^e Values not quoted.

Comparison of results in the three media reveals a general depression of formation constants with increasing peroxide concentration. Although the hydrogen peroxide solutions are relatively dilute, deviations of both proton and Ni(II) complex formation constants appear to be comparable in magnitude

with those induced by substantial quantities [ca. 50 % (w/w)] of methanol and dioxan (See Table 4.6.2).^[80] Clearly, the presence of hydrogen peroxide has a significant influence on the complexation behaviour of glycine.

Depression of log K values for $[ML]^+$ and $[ML_2]$ may result from increased stability of protonated ligand species in peroxide solutions, characterised by the increase of log K_{012} with increasing peroxide concentration. The anomalous deviation for ML_2 in 10% solution may be due to either ligand oxidations or medium breakdown. Rapid decomposition of peroxide, probably induced by both the added base and the presence of a redox-active metal ion, was apparent for titrations at the higher H_2O_2 concentration investigated. Oxidation of amines by hydrogen peroxide is well known; primary amines oxidise sequentially^[81] to a number of products in excess peroxide.



Ligand oxidation in acid solution is likely to be hampered by protonation of the amine nitrogen but the oxidation rate is likely to increase as the abundance of free amine becomes significant at higher pH.^[81] Variation in ligand concentration and uncertainty about the presence, quantity and identity of any decomposition products with co-ordinating ability, along with the inevitable uncertainty of the cell constants for a decomposing titration medium, probably account for the poor quality of fit for the data obtained at the higher H_2O_2 concentration.

These experiments demonstrate that reproducible values for proton and metal complex formation constants can be obtained in 3 % and 10 % *aqu.* H_2O_2

solutions and that the presence of hydrogen peroxide has a small but significant effect on the formation constants for glycine and nickel glycinate. Two roles for H_2O_2 in the cell can be envisaged. Firstly, inclusion of H_2O_2 will cause changes in the physical properties of the medium affecting solvation and electrostatic interactions in the solvent. Secondly, H_2O_2 may act as a reactive species in solution, possibly causing oxidation of ligand and undergoing decomposition induced by the presence of metal ions. This latter effect underpins the concerns that measurements may be subject to medium decomposition in 10 % *aqu.* H_2O_2 solution.

5. Stability and solution speciation of some aminomethylenephosphonic acids and their complexes with metal ions.

5.1 Introduction

The structures of polyaminophosphonic acids in solution have been the subject of a number of recent studies.^[82] Compounds of this class are of increasing importance as they replace the polyaminocarboxylic acids as metal sequestrants in a number of industrial processes;^[83] of particular interest is their remarkably effective stabilisation of hydrogen peroxide solutions.

Trace amounts of metal ions such as copper(II), nickel(II), and manganese(II) in hydrogen peroxide solutions cause catalytic decomposition to hydrogen and water.^[69] Such losses of peroxide, especially in paper bleaching and metal finishing processes, where consumption of H_2O_2 is a major cost, are minimised by the inclusion of stabilisers in the solution. Diethylenetriaminepenta-methylenephosphonic acid has been shown to be effective in the prevention of H_2O_2 decomposition in the presence of Fe(III) and Mn(II) ions,^[84] and several other tertiary aminomethylenephosphonic acids are in current use in this way as hydrogen peroxide stabilisers.^[85]

The mechanism by which aminomethylenephosphonic acids effect hydrogen peroxide stabilisation is still unknown although a number of possible contributory processes have been discussed.^[86] For example, the compounds may act primarily as metal-ion sequestrants or, as pure compounds or derivatives formed in hydrogen peroxide solution, as inhibitors of radical reactions. The metal sequestant rôle of these ligands in the stabilisation process is thought to be of some importance.^[86] Such co-ordination chemistry can be

investigated with a combination of potentiometric and nmr techniques, although the equilibria involved with multifunctional aminomethylenephosphonates of the types commonly used commercially are expected to be complex and difficult to elucidate.

In an effort to understand the stabilisation process, aqueous and *aqu.* H_2O_2 solution chemistries of some simpler aminomethylenephosphonic acids which could be regarded as model systems have been studied. To this end, two aminomethylenephosphonic acids (shown in Figure 5.1.1) have been synthesized and characterised. In addition, analogues of these model systems with different functionalities, *i.e.* a primary aminoalkylphosphonic acid (1-APP H_2 , Fig. 5.1.1) and a hydroxyalkyldiphosphonic acid (HEDPH $_4$, Fig. 5.1.1), have been investigated in order to establish the 'special' properties of the tertiary aminomethylene phosphonic acids.

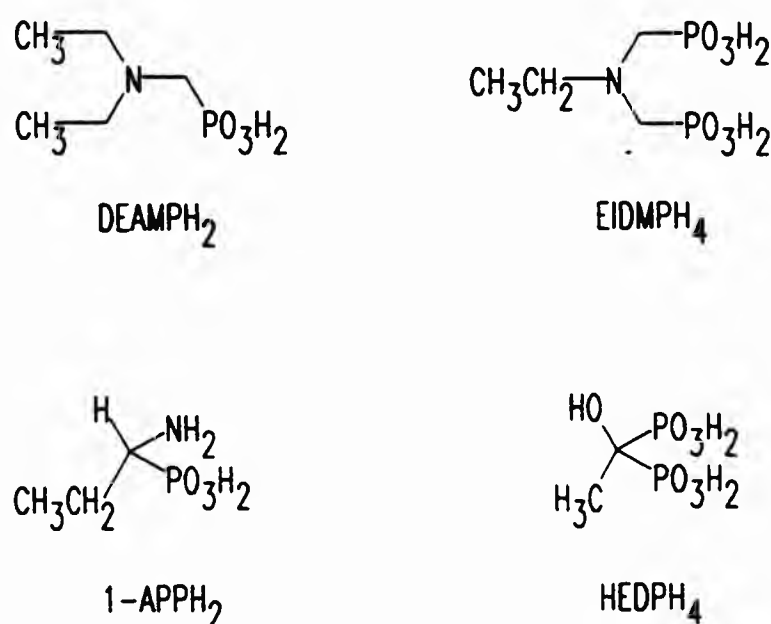


Figure 5.1.1 Diethylaminomethylenephosphonic acid (DEAMPH $_2$), ethyliminobis(methylenephosphonic acid) (EIDMPH $_4$), 1-aminopropylphosphonic acid (1-APPH $_2$) and 1-hydroxyethyl-1,1-diphosphonic acid (HEDPH $_4$).

5.2 Synthesis and characterization of diethylaminomethylene- phosphonic acid and ethyliminobis(methylenephosphonic acid)

The tertiary aminomethylenephosphonic acids, diethylaminodimethylene-
phosphonic acid (DEAMPH₂) and ethyliminobis(methylenephosphonic acid)
(EIDMPH₄), were prepared by direct reaction of the appropriate amine with
ortho-phosphorous acid and formaldehyde according to the general reaction
(R = Et, n = 1 for DEAMPH₂ and 2 for EIDMPH₄):^[26]



EIDMPH₄ precipitated in good yield from the reaction mixture as a white
microcrystalline solid. Recrystallisation from EtOH:H₂O (1:1 v/v) yielded a
white solid, the m.p., elemental analysis and ¹H, ¹³C and ³¹P nmr spectrum of
which confirmed formulation as EIDMPH₄.

Analyses of reaction products during initial attempts to prepare DEAMPH₂ were
carried out with ³¹P nmr spectroscopy (Fig. 5.2.1). Products prepared using
stoichiometric reactant ratios showed two persistent phosphorus-containing
contaminants. These were assigned on the basis of phosphorus-31 chemical
shift and ³¹P-¹H coupling information as unreacted *ortho*-phosphorous acid (at
δ = 4.71 ppm)^[87a] and hydroxymethylenephosphonic acid (at δ = 22.48
ppm).^[87b] Adjustment of the reactant ratios to 1.25 Et₂NH :

1.5 CH₂O : 1.0 H₃PO₃ and doubling the reflux time yielded a yellow oil with a
single signal in the ³¹P bb-¹H spectrum. After treating the oil with
EtOH/(CH₃)₂CO (3:1 v/v), the solution was stored for three months. Towards
the end of this period, DEAMPH₂ crystallised as a white solid.

Mono-methylenephosphonic acid derivatives of simple secondary alkylamines
reported previously^[26,88] have normally been obtained as syrupy liquids which
resisted crystallisation (see, for example, Refs. [26] and [88]). Analytical
results [elemental analysis and multinuclear nmr (¹H, ¹³C and ³¹P)] confirmed

the formulation as DEAMPH₂.

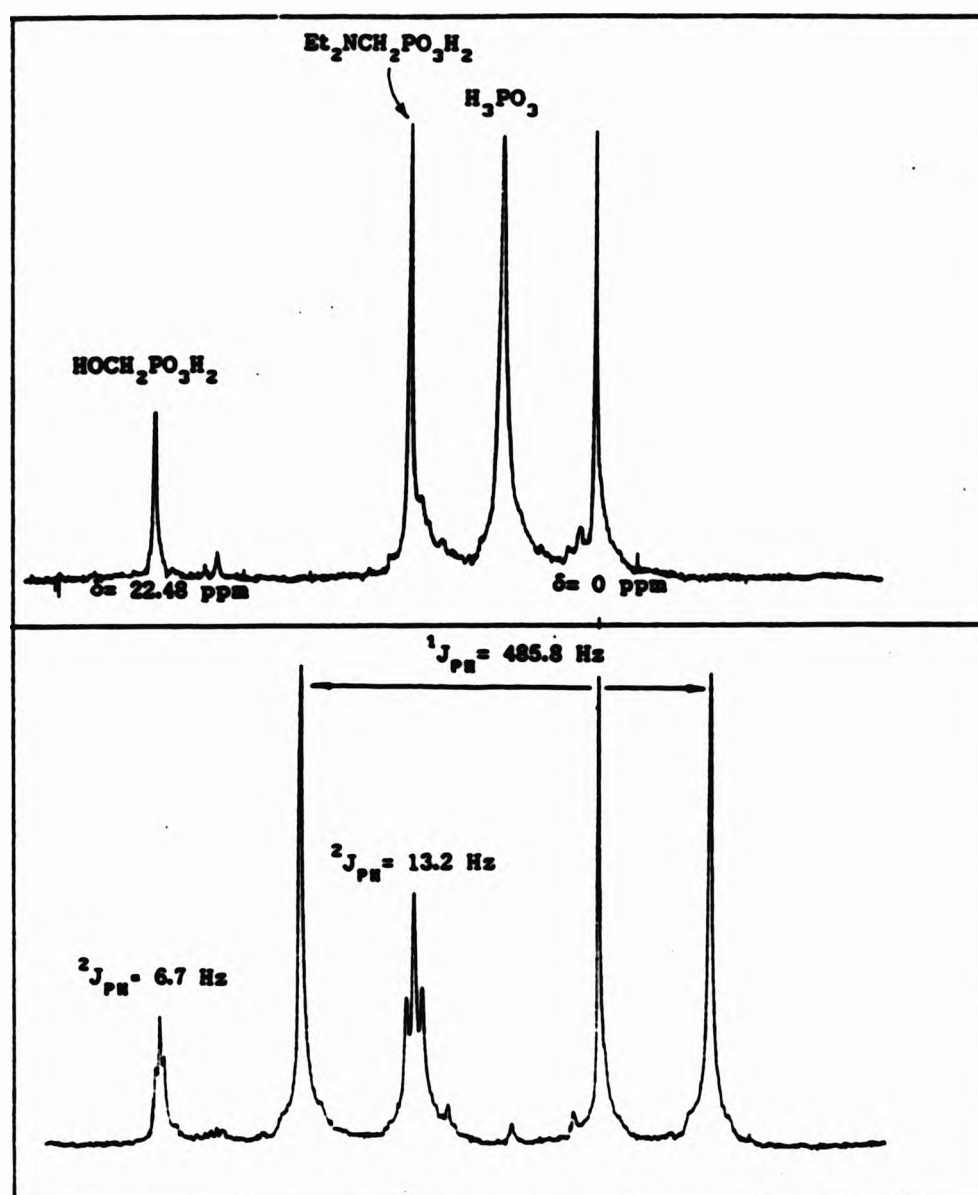


Figure 5.2.1 The ³¹P proton-coupled and broad-band proton-decoupled spectra of a reaction mixture obtained during synthesis of DEAMPH₂ using stoichiometric reactant ratios.

The ¹H nmr spectra for both DEAMPH₂ and EIDMPH₄ show a doublet in the region 3.3-3.6 ppm from coupling of the methylene protons to the phosphorus-31 nucleus. The respective coupling constants are repeated for the triplet in the ³¹P proton-coupled nmr spectra. Such signals are characteristic of α-aminomethylenephosphonic acids. [26,89] Whereas the ¹H spectrum of DEAMPH₂ shows discrete methylene multiplets, that of EIDMPH₄ is somewhat complicated by overlap of the ethyl quartet with the doublet from the bis-methylene

phosphonate hydrogens. In both cases signals were readily assigned using first-order splitting rules. The single peak of the ^{31}P spectrum of EIDMPH_4 implies equivalent environments for each phosphorus nucleus in the molecule.

5.3 Protonation equilibria for 1-aminopropylphosphonic acid

1-Aminopropylphosphonic acid (1-APPH_2) is of considerable interest as a fungicide^[90] and, as it contains a single α -aminomethylenephosphonic acid function, it provides a useful comparison with the tertiary aminomethylene-phosphonic acids employed as model compounds. As the ligand was readily available from other work in these laboratories and has been well characterised,^[91] it was employed in this study.

Although the mode of action of 1-APPH_2 as a fungicide is unknown, co-ordination of copper(II) has been implicated in the fungicidal action of the dithiocarbamates and 8-hydroxyquinoline.^[92] The metal complexing abilities of 1-APPH_2 are therefore of some interest. Furthermore, the metal complexation stability constants of 1-APPH_2 have not been reported and to this end a potentiometric investigation was undertaken. In addition, although protonation constants for 1-APPH_2 have been reported,^[93,94,95] a protonation scheme for the compound has not been firmly established. Phosphorus-31 nmr shift vs. pH data^[96] are reported herein to substantiate a proposed protonation scheme.

5.3.1 Protonation constants for 1-aminopropylphosphonic acid

The free base of 1-APPH_2 [$\text{L} = \text{EtCH}(\text{NH}_2)\text{PO}_3^{2-}$] contains three basic sites, the primary amino nitrogen and two oxygens of the phosphorus oxyanion, and each may potentially donate an electron pair on complexation with metal ions (H^+ can be considered as a unipositive metal ion in this context). Acid-base

titrations of ligand in the absence of metal ions (see Fig. 5.4.1) yielded three datafiles from which up to three protonation constants were obtained with the FORTRAN programs MINIQAD^[16,22] and SUPERQUAD^[25] (see Table 5.3.1). Data acquisition for one data set was terminated (by instrument failure) above pH ca. 8.0. In this case, refinement of two protonation constants was achieved by including one equivalent of labile proton from the ligand with the free acid concentration (instead of two equivalents). The constants obtained correspond with $\log K_{012}$ and (by subtraction) $\log K_{013}$ of the full model.

The relatively large inter- and intra-titration variation of $\log K_{013}$ presumably arises because the tri-protonated ligand is almost completely dissociated at the starting pH of the titration (an SPE^[5] generated speciation plot shows the abundance of $[LH_3]^+ < 20\%$ at pH 2.5). The values for $\log \beta_{011}$ and $\log \beta_{012}$ compare well with published values (see Table 5.4.1).

The value of $\log \beta_{011}$ is in the range expected for a primary amine.^[61,62] The second stepwise protonation constant, $\log K_{012}$, is of the same order as the first protonation constant for the anion of trimethylammoniummethylenephosphonic acid ($\log \beta_{011} = 5.10$).^[97] As the latter may only protonate on the phosphonate group, $\log K_{012}$ may be assigned, by analogy, to single protonation of the phosphonate group. The large difference between successive stepwise protonations of the phosphonate function, i.e. between $\log K_{012}$ and $\log K_{013}$, suggests stabilisation of the monoprotonated moiety. The ability of the phosphonate group to stabilise the single negative charge by delocalisation over the three P-O bonds of the group has been cited^[98] as the probable stabilising effect. The acidity of carboxylic acids has been explained in similar terms, the stability of the carboxylate anion deriving

from charge delocalisation over the C-O bonds. Furthermore, stabilisation of the phosphonate dianion by a similar mechanism is likely, suggesting that the proton of the $[\text{LH}]^-$ species resides predominantly at the amine site.

Table 5.3.1 Protonation constants for 1-aminopropylphosphonic acid
 $[\text{L} = \text{EtCH}(\text{NH}_2)\text{PO}_3^{2-}]$.^a

Datafile	$\log \beta_{011}$	$\log \beta_{012}$	$\log K_{012}$	$\log \beta_{013}$	$\log K_{013}$
DG11					
b	10.20(0.011)	15.95(0.023)	5.75	17.53(0.078)	1.58
b,c	10.16(0.009)	15.91(0.018)	5.75	17.55(0.055)	1.64
d	10.23(0.018)	15.99(0.030)	5.76	17.59(0.061)	1.60
e	10.13(0.011)	15.89(0.022)	5.76	-	-
DG12					
f	5.76(0.009) ^g	7.62(0.034)	1.86 ^h		
DG13					
i	10.16(0.007)	15.91(0.014)	5.75	17.08(0.014)	1.17
j	10.18(0.014)	15.93(0.022)	5.75	17.43(0.074)	1.50
k	10.13(0.013)	15.84(0.022)	5.71	-	-
MEAN ¹	10.17 ±0.06	15.92 ±0.08	5.75 ±0.04	17.44 ±0.36	1.56 ±0.39

^a Data obtained at constant ionic strength, $I = 0.1 \text{ mol dm}^{-3}$, KNO_3 ; 25 °C. Figures in parentheses are standard deviations obtained from data refinement programs. ^b Three species refined using MINIQAD.^[16,22] ^c Ligand concentration adjusted (within ±10 % w/w) to find 'best fit'. ^d Three species refined using SUPERQUAD;^[25] pH 2.42-10.88, 174 data points. ^e Two species refined using SUPERQUAD;^[25] pH 6.04-10.54, 75 data points. ^f Two species refined using SUPERQUAD.^[25] ^g Constant corresponds with stepwise formation of $[\text{LH}_2]$. ^h Constant corresponds with stepwise formation of $[\text{LH}_3]^+$. ⁱ Three species refined using MINIQAD;^[16,22] pH 2.47-10.53, 160 data points. ^j Three species refined using SUPERQUAD;^[25] pH 2.43-10.30, 154 data points. ^k Two species refined using SUPERQUAD;^[25] pH 3.92-10.30, 113 data points. ¹ Unweighted mean of values from each refinement; error limits are derived from the ranges obtained for each $\log \beta_{m1h}$ (and $\log K_{m1h}$).

These observations lead to a proposed stepwise protonation scheme (Fig. 5.3.1). The labile proton of the monoprotonated ligand is expected to bind at the amine nitrogen site, while the higher protonated species involve successive protonation at the phosphonate function. Some support for the zwitterion nature of $[LH_2]$ derives from the single crystal X-ray structure of 2-aminoethylphosphonic acid.^[99] The two protons conferring electroneutrality on the molecule were located and shown to be bound respectively to one phosphonate oxygen and the primary amine.

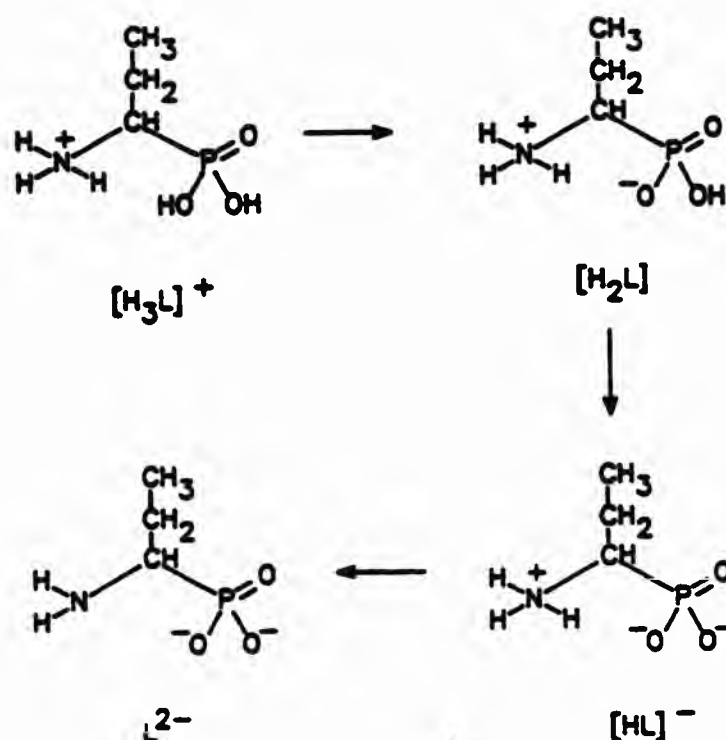


Figure 5.3.1 Protonation scheme of 1-aminopropylphosphonic acid.

5.3.2 Phosphorus-31 nmr studies

Aminomethylenephosphonic acids have pH-dependent nmr spectra. In particular, changes in phosphorus-31 nmr shifts of these compounds with pH can be related to neutralisation of specific labile protons of their acids. It has been established that deprotonation of the phosphonic acid function shields the ^{31}P nucleus^[26,100,101,102,103,104,105,106,107,108] whilst deprotonation of amine sites ($\text{R}_3\text{NH}^+ \longrightarrow \text{R}_3\text{N}$; $\text{R} = \text{alkyl, H}$) causes deshielding.^[26,100,101,104,105,106,107]

The pH dependence of the ^{31}P nmr shift of 1-APP H_2 was investigated^[96] using similar titration and spectral acquisition conditions to those described for EIDMP H_4 and DEAMP H_2 in this study (see Section 3.4). The broad band proton decoupled spectra, recorded for solutions in the pH range ca. 1.2-11.3, each showed a single signal corresponding to a single 'averaged' environment for the ^{31}P nucleus. Under such fast-exchange conditions, the observed shift is given by,^[109]

$$\delta_{\text{obs}} = \sum_i \chi_i \delta_i$$

where δ_i is the intrinsic shift of the i th species and χ_i is its mole fraction. As expected, the ^{31}P shift of 1-APP H_2 is sensitive to pH [Fig. 5.3.2(i)] and inflexions in this curve appear to correlate with a distribution plot of ligand species [calculated with pK_a 's from the preceding potentiometric study; Fig. 5.3.2(ii)] confirming the protonation model. Two inflexions are apparent in the $\delta(^{31}\text{P})$ vs. pH curve below pH 7 and both are in regions of the curve where the ^{31}P signal moves to higher field with increasing pH. This is consistent with stepwise deprotonation of the phosphonic acid function of 1-APP H_2 [Fig. 5.3.1; steps (i) and (ii)], in accord with the proposed protonation scheme. Larger changes in $\delta(^{31}\text{P})$ above pH 9, but this time to lower field with increasing pH, correlate with the increasing abundance of 'free' anion (*i.e.* the fully deprotonated form of 1-APP H_2 , L). Since such changes are indicative of amine deprotonation [Fig. 5.3.1; step (iii)], these observations are similarly consistent with the proposed protonation scheme.

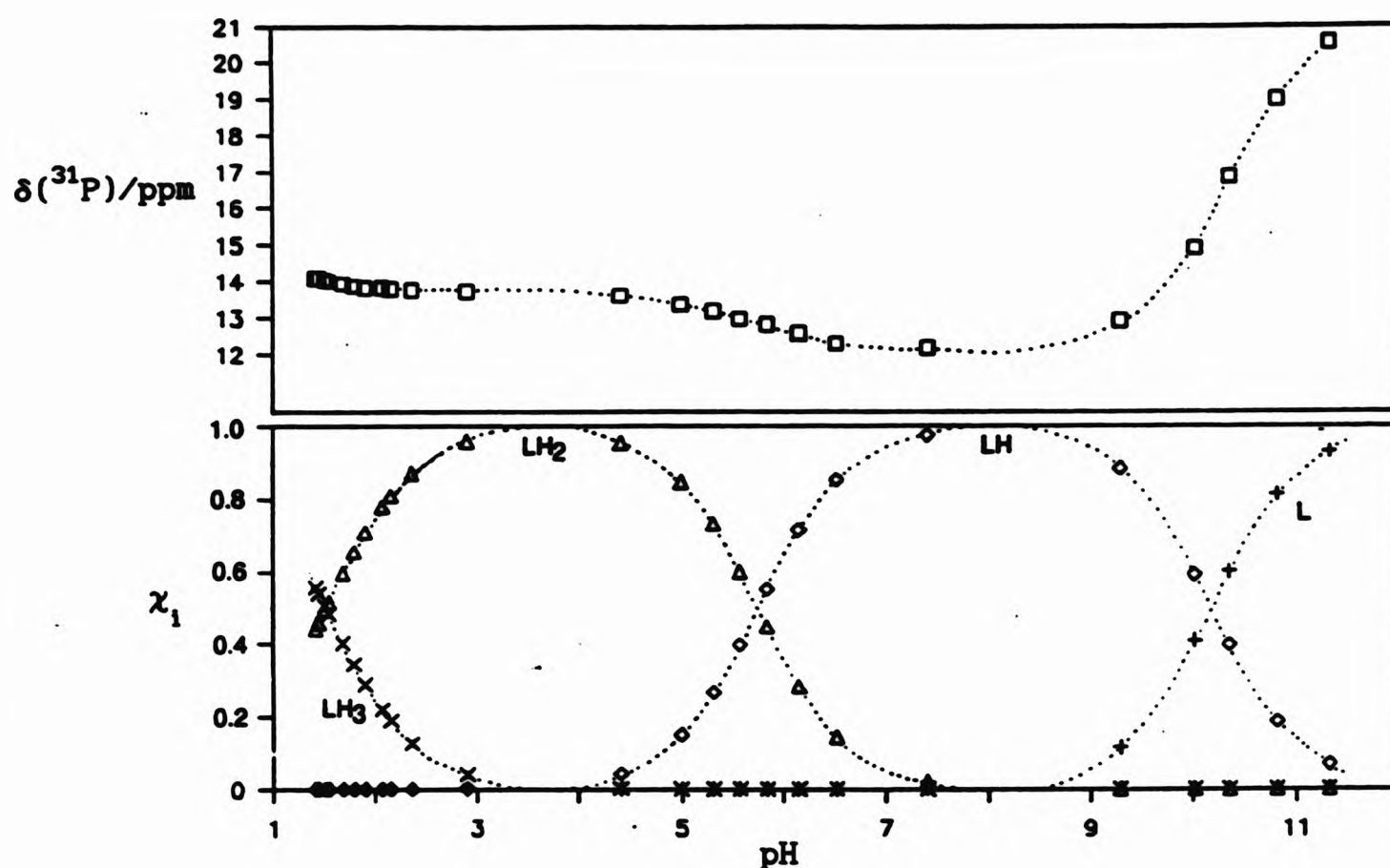


Figure 5.3.2 Correlation of (i) the variation of $\delta(^{31}\text{P})$ and (ii) the distribution of ligand species with pH for 1- APPH_2 . [The latter was calculated using free proton concentrations from the 'small volume' nmr titration in conjunction with formation constants from the preceding potentiometric study (Section 5.3.1)].

5.4 Stability of copper(II) and nickel(II) complexes of 1-aminopropylphosphonic acid

The complexation equilibria of 1- APPH_2 with both Cu(II) and Ni(II) in aqueous solution were investigated. A number of corresponding studies of structurally similar ligands with these metals have been reported (Table 5.4.1). A feature of the co-ordination chemistry of these ligands is their propensity for formation of protonated metal complexes. For Cu(II) a general equilibrium model seems to have been established.^[93,94,98] The metal ion forms *mono-* and *bis-* complexes ($[\text{MLH}]^+$ and $[\text{ML}_2\text{H}_2]$) with monoprotated ligand moieties

([LH]⁻). These undergo a series of deprotonation steps with increasing pH before yielding the species [ML] and [ML₂]²⁻. A general scheme describing this model is shown below:

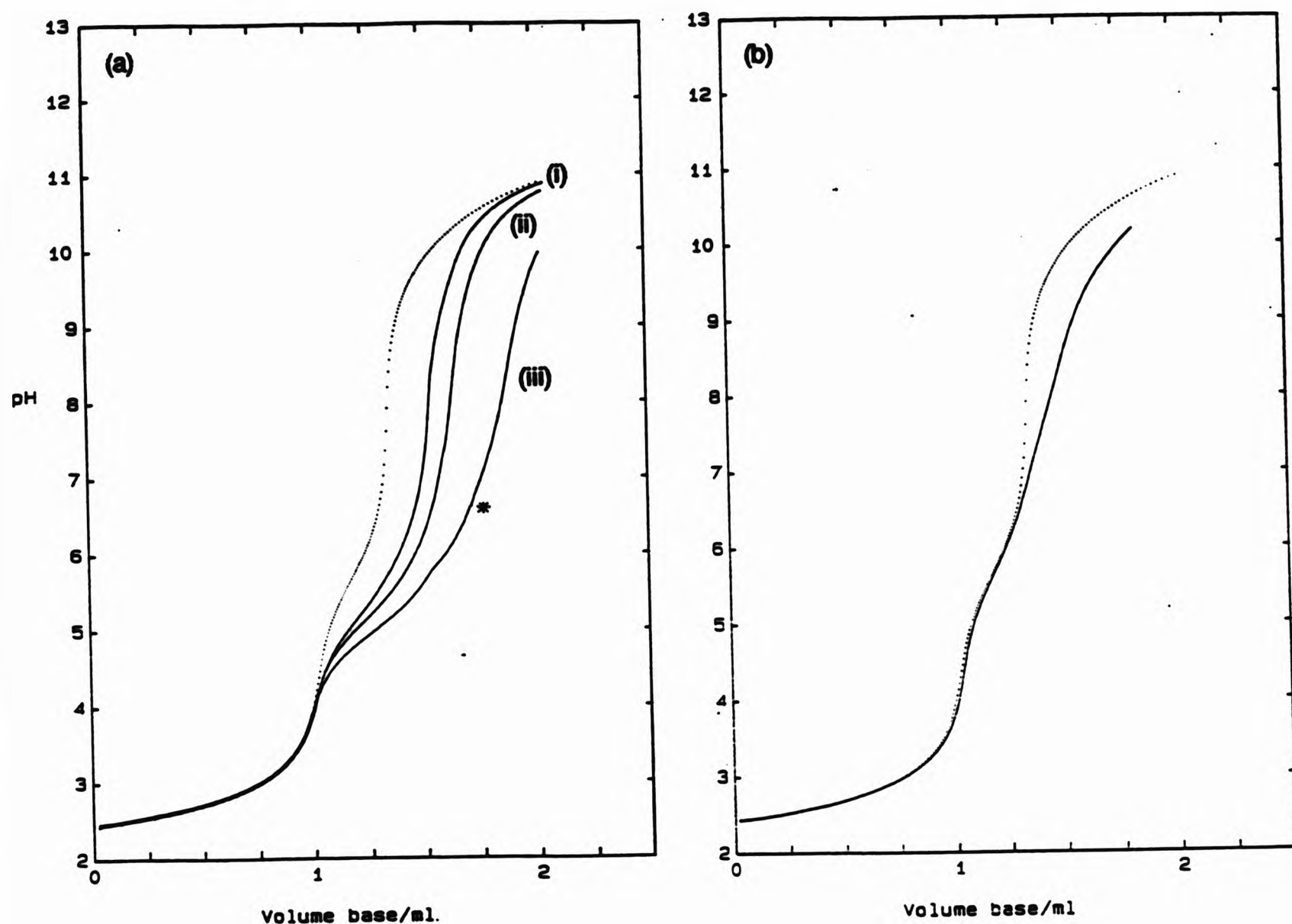
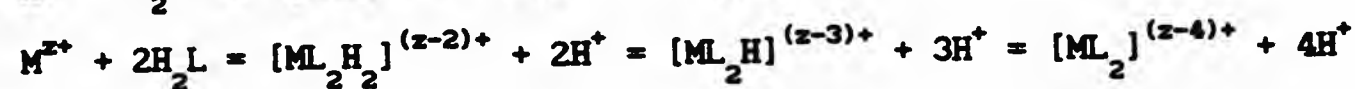
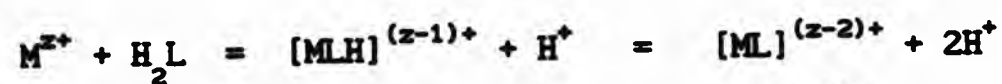


Figure 5.4.1. Titration curves (pH vs. volume of added base) for acidified aqu. solutions of: (a) 1-APPH₂ ([L] = 2 mmol dm⁻³, dotted line) and copper(II) nitrate with 1-APPH₂; (i) [M]:[L] = 1:3, (ii) [M]:[L] = 1:2, (iii) [M]:[L] = 1:1, curve discontinuity indicated with an asterisk; (b) 1-APPH₂ ([L] = 2 mmol dm⁻³, dotted line) and nickel(II) nitrate with 1-APPH₂; (i) [M]:[L] = 1:2.

Table 5.4.1 Formation constants for $[M L_1 H_n]$ complexes derived from primary aminoalkylphosphonic acids.

		<div> $\begin{array}{c} \text{NH}_3^+ \\ \\ ^-\text{HO}_3\text{P}-\text{CH}_2 \\ \text{AMPH}_2 \end{array}$ $\begin{array}{c} \text{NH}_3^+ \\ \\ ^-\text{HO}_3\text{P}-\text{CH}-\text{CH}_3 \\ \text{1-AEPH}_2 \end{array}$ $\begin{array}{c} \text{NH}_3^+ \\ \\ ^-\text{HO}_3\text{P}-\text{CH}-\text{CH}_2\text{CH}_3 \\ \text{1-APPH}_2 \end{array}$ $\begin{array}{c} \text{NH}_3^+ \\ \\ ^-\text{HO}_3\text{P}-\text{CH}-\text{CH}_2\text{CH}_2\text{CH}_3 \\ \text{1-ABPH}_2 \end{array}$ </div>							
		<div> $\begin{array}{c} \text{NH}_3^+ \\ \\ ^-\text{HO}_3\text{P}-\text{CH}-\text{CH}_2\text{CH}_2\text{CH}_2\text{CH}_3 \\ \text{1-APEPH}_2 \end{array}$ $\begin{array}{c} \text{NH}_3^+ \\ \\ ^-\text{HO}_3\text{P}-\text{CH}-\text{CH}-\text{CH}_3 \\ \\ \text{CH}_3 \\ \text{1-AMPrPH}_2 \end{array}$ $\begin{array}{c} \text{NH}_3^+ \\ \\ ^-\text{HO}_3\text{P}-\text{CH}_2\text{CH}_2-\text{NH}_3^+ \\ \text{2-AEPH}_2 \end{array}$ $\begin{array}{c} \text{NH}_3^+ \\ \\ ^-\text{HO}_3\text{P}-\text{CH}_2\text{CH}_2\text{CH}_2-\text{NH}_3^+ \\ \text{3-APPH}_2 \end{array}$ </div>							
M^{z+}	mlh	$\log \beta_{mlh}^a$							
		AMP	1-AEP	1-APP	1-ABP	1-APeP	1-AMPrP	2-AEP	3-APP
H^+ ^b	011	-	10.15	10.22	10.24	10.25	10.31	-	-
	012	-	15.72	15.85	15.90	15.93	16.08	-	-
	013	-	-	-	-	-	-	-	-
H^+ ^c	011	10.05	10.20	10.26	10.29	10.29	10.36	11.04	11.07
	012	15.44	15.78	15.91	15.96	15.99	16.15	17.29	17.95
	013	15.88	16.25	-	-	16.57	16.77	18.41	19.58
H^+ ^d	011	11.01	-	10.28	10.32	10.35	-	11.04	11.07
	012	17.98	-	16.03	16.15	16.17	-	17.29	17.95
	013	19.93	-	17.98	18.10	18.00	-	18.41	19.58
H^+ ^e	011	-	-	10.17	-	-	-	-	-
	012	-	-	15.92	-	-	-	-	-
	013	-	-	17.44	-	-	-	-	-
Cu^{2+} ^b	110	7.95	8.24	-	-	8.80	9.17	-	-
	111	12.58	13.11	-	-	13.34	13.70	-	-
	120	14.6	15.3	-	-	16.1	17.0	-	-
	121	20.4	21.1	-	-	21.8	22.4	-	-
	122	25.5	26.2	-	-	26.7	27.5	-	-
Cu^{2+} ^c	110	8.12	8.50	8.65 ^e	-	8.97	9.47	8.50	7.15
	111	12.56	12.82	12.88 ^e	-	13.25	13.71	13.75	13.97
	120	14.65	15.40	15.40 ^e	-	16.27	17.32	14.3	-
	121	20.20	21.0	21.62 ^e	-	21.60	22.53	21.4	-
	122	24.8	25.9	27.24 ^e	-	25.9	26.7	27.1	-
	11-1	(-0.4)	-0.1	(1.35) ^e	-	0.8	1.7	1.04	0.1
	21-2			(-1.41) ^e					

Table 5.4.1 continued

M ²⁺	mlh	log β _{mlh} ^a							
		AMP	1-AEP	1-APP	1-ABP	1-APeP	1-AMPrP	2-AEP	3-APP
Ni ²⁺	110	5.29 ^c	-	5.73 ^e	-	-	5.65 ^f	5.20 ^c	-
	111	11.69 ^c	-	13.04 ^e	-	-	13.33 ^f	12.80 ^c	-
	120	8.98 ^c	-	10.17 ^e	-	-	10.98 ^f	10.1 ^c	-
	121	16.4 ^c	-	18.72 ^e	-	-	-	18.8 ^c	-
	122	(22.6) ^c	-	-	-	-	-	25.6 ^c	-
	11-1	-	-	-	-	-	-	(-3.9) ^c	-
	12-1	-	-	0.34 ^e	-	-	-	-	-
	12-2	-	-	-10.63 ^e	-	-	-	-	-

^a Error limits generally $< \pm 0.5$ log units. Larger uncertainty is associated with values in parentheses. ^b From Ref. [93]; $I = 0.1 \text{ mol dm}^{-3}$, KNO_3 ; 25.0 °C. ^c From Ref. [94]; $I = 0.1 \text{ mol dm}^{-3}$, KNO_3 ; 25.0 °C. ^d From Ref. [95]; conditions not quoted. ^e This study; $I = 0.1 \text{ mol dm}^{-3}$, KNO_3 ; 25.0 °C. ^f Cited in Ref. [98]; $I = 0.1 \text{ mol dm}^{-3}$, KCl ; 25.0 °C.

5.4.1 Copper(II) studies

Potentiometric data from a number of titrations (see Fig. 5.4.1) with differing initial M:L ratios were refined using SUPERQUAD^[25] (Table 5.4.2). Preliminary investigations were performed for an equilibrium model including constants for the species $[ML]$ and $[MLH]^+$ as refinable variables with the protonation constants for the ligand (Table 5.3.1) as fixed variables. Successful convergence during these initial studies was achieved only after inclusion of the $[ML_2H_2]$ species in the model. Significantly better fits for the titration data (characterised by lower χ^2 and σ values) were found on inclusion of the species $[ML_2]^{2-}$ and $[ML_2H]^-$ in the model, confirming the general scheme shown above. Two separate final refinement strategies were adopted: the initial proton concentration (including two equivalents due to labile ligand protons) was treated as a refinable parameter and, to account for possible protic ligand impurities, the initial proton and ligand

concentrations were constrained (by setting the appropriate refinement keys within SUPERQUAD) to refine in similar directions.

For 1-APPH₂, precipitation of metal hydroxy species, characterised by irregularities in the titration curve, was apparent only at M:L = 1:1. In a parallel study of simple phosphonic acids, Wozniak and Nowogrocki isolated precipitates with the general formula $\text{RPO}_3\text{Cu} \cdot y\text{Cu}(\text{OH})_2$ ($y \approx 1$ at pH 7, $y \approx 4$ at pH 9) from basic solution,^[97] although the same authors, in a study of aminoalkylphosphonic acids, did not report^[94] any precipitation in the presence of an excess of ligand ($\text{M:L} \leq 0.5$). Formation constants were obtained^[94] for hydroxy complexes of aminophosphonic acids with the general formula $[\text{CuLOH}]^-$ (corresponding to species stoichiometry 11-1 shown in Table 5.4.1). Inclusion of the formation constants for copper hydroxy species $\text{Cu}(\text{OH})^+$ and $\text{Cu}_2(\text{OH})_2^{2+}$ ($\log \beta_{10-1} = -7.34$, $\log \beta_{20-2} = -10.60$; $I = 0.1 \text{ mol dm}^{-3}$, KNO_3)^[110] as fixed variables in the model, allowed separate refinement of values for $\log \beta_{11-1}$ and $\log \beta_{21-2}$. However, as these constants could not be obtained simultaneously in a single refinement, the existence of such species is open to some doubt. It is interesting to note that Wozniak and Nowogrocki considered only one copper hydroxide species, $\text{Cu}_2(\text{OH})_2^{2+}$, during their studies.^[94]

The results obtained (summarised in Table 5.4.2) show good inter- and intra-titration agreement. The final results for the system were derived by averaging values of $\log \beta_{\text{min}}$ from three data files (DGC2, DGC3 and DGC5); values from DGC6 were omitted as outliers and because a large error was associated with $\log \beta_{120}$ on refinement of the full model.

Table 5.4.2 Refinement summary for titrations of 1-APPH₂ with copper(II).^a

mlh	log β_{mlh}							
	DGC2		DGC3		DGC5		DGC6	
	b	c	b	c	b	c	b	
110	8.65	8.65	8.61	8.63	8.66	8.68	8.57	} ^e
111	13.03	13.02	12.73	12.79	12.83	12.89	13.26	
120	15.57	15.56	15.38	15.48	15.13	15.30	^d	
121	21.76	21.76	21.67	21.73	21.31	21.48	22.37	
122	27.21	27.21	27.37	27.37	27.14	27.14	27.07	
11-1	-	-	-	-	-	-	-	1.35 ^f
21-2	-	-	-	-	-	-	-	-1.41 ^g
χ^2	5.77	5.77	6.00	6.00	4.56	4.14	6.44	
σ	0.0164	0.0164	0.0141	0.0141	0.0206	0.0223	0.0169	
pH ^h	3.8-6.1		3.7-6.0		3.7-6.3		3.9-5.7	3.8-6.6
np ⁱ	64		63		76		53	83
DGC2/DGC3/DGC5				DGC2/DGC3/DGC5/DGC6				
	mean ^j		range		mean ^j		range	
110	8.65		0.07		8.64		0.11	
111	12.88		0.30		12.94		0.53	
120	15.40		0.44		15.40		0.44	
121	21.62		0.45		21.73		1.06	
122	27.24		0.23		27.22		0.30	

^a Data obtained at constant ionic strength; $I = 0.1 \text{ mol dm}^{-3}$, KNO_3 ; 25 °C.

^b Data refined with SUPERQUAD.^[25] Initial proton concentration treated as a refinable parameter. ^c Data refined with SUPERQUAD.^[25] Initial proton and ligand concentrations constrained to refine in the same direction. ^d Large error ($> 3\sigma$) obtained for $\log \beta_{120} = 15.79$. ^e $\log \beta_{mlh}$ ($h \geq 0$) fixed during refinement. ^f $\chi^2 = 10.20$, $\sigma = 1.2948$. ^g $\chi^2 = 12.20$, $\sigma = 1.2839$. ^h pH range of data points refined. ⁱ Number of data points used in refinement. ^j Unweighted mean of values.

Consideration of the available data has revealed an empirical linear relationship between $\log \beta_{110}$ and $\sum \log K_{01h}$ for Cu(II) and Ca(II) complexes with α -aminoalkylphosphonic acids.^[98] For the copper(II) chelates, this

relationship has the form,

$$\log \beta_{110} = 1.44 \sum_h pK_{01h} - 14.80$$

where the summation is across all the protonated ligand species. Putting the value of $\log \beta_{013}$ obtained for 1-APPH₂ (Table 5.3.1) into this equation yields an estimate of $\log \beta_{110} = 10.3$. Curiously, a much closer estimate to the experimentally determined value ($\log \beta_{110} = 8.65$) is obtained with $h = 2$. This latter case yields an estimate of $\log \beta_{110} = 8.3$.

5.4.2 Nickel(II) studies

Interaction of Ni(II) with this type of aminophosphonate ligand is less well characterised. Available data is summarised in Table 5.4.1 and previous studies employing KNO₃ (0.1 mol dm⁻³)^[94] as the background electrolyte yielded speciation analogous to the corresponding Cu(II) systems.

Interestingly, a study of the interaction of 1-amino-2-methylpropylphosphonic acid (AMPrP, Table 5.4.1) with Ni(II) in the presence of KCl

(I = 0.1 mol dm⁻³) yielded formation constants for [ML], [MLH]⁺ and [ML₂]²⁻ only.^[98]

Initial refinements of data for the 1-APPH₂/Ni(II) system [Fig. 5.4.1(b)] were attempted using similar regions of the titration curve to those used in the Cu(II) study. An acceptable 'fit' for the data could be obtained with a model describing the formation of [ML], [MLH]⁺ and [ML₂H₂] species. Inclusion of further bis-complexes, [ML₂]²⁻ and [ML₂H]⁻, in the model led to improved fits, although relatively large calculated standard deviations for $\log \beta_{122}$ were observed. Data refinements are summarised in Table 5.4.3.

The titration curve remained smooth throughout the pH range investigated,

indicating an absence of precipitation of hydroxy species at higher pH for the M:L ratios employed (ca. 1:2). In light of this, the formation constant of $[\text{Ni}(\text{OH})]^+$ ($\log \beta_{10-1} = -9.86$)^[110] was included as a constant in the equilibrium model and refinement of values for formation of metal complex hydroxy species was attempted. Although an acceptable fit for models including the $[\text{ML}(\text{OH})]^-$ species was not achieved (in contrast to the study of $\text{Ni}(\text{II})/2\text{-aminoethylphosphonic acid}$; see Table 5.4.1), consistent values for the formation of $[\text{ML}_2(\text{OH})]^{3-}$ and $[\text{ML}_2(\text{OH})_2]^{4-}$ were obtained in conjunction with equilibrium models including $[\text{ML}]$, $[\text{MLH}]^+$, $[\text{ML}_2]^{2-}$ and $[\text{ML}_2\text{H}]^-$. The results from these refinements are summarised in Table 5.4.3.

Table 5.4.3 Refinement summary for titrations of 1-APP₂ with nickel(II).^a

	log β_{mlh}						
mlh	DGN1			DGN2			Mean ^b
	c	c, d	c, d	c, d	c	c	
110	5.73	5.75	} ^f	5.70	5.88	5.48	5.73
111	13.05	13.11		12.97	13.49	-ve ^e	13.04
120	10.29	10.29		10.05	10.30	10.18	10.17
121	18.89	18.88		18.56	18.84	18.78	18.72
122	g	-	-	-	-ve ^e	26.07	
12-1	-	-	0.41	0.26	0.22	-	0.34
12-2	-	-	-10.39	-10.87	-9.69	-	-10.63
χ^2	0.61	2.80	9.90	12.43	4.50	7.93	
σ	0.0061	0.0062	0.0372	0.1386	0.0714	0.0196	
pH ^h	6.1-8.6		9.4-10.2	6.1-10.2	6.4-9.3	6.3-8.9	
np ⁱ	60		28	98	59	53	

^a Data obtained at constant ionic strength; $I = 0.1 \text{ mol dm}^{-3}$, KNO_3 ; 25 °C.

^b Unweighted mean of values. ^c Data refined with SUPERQUAD.^[25] Initial proton concentration treated as a refinable parameter. ^d Values contributing to mean. ^e Negative β obtained during refinement therefore model rejected.

^f $\log \beta_{\text{mlh}}$ ($h \geq 0$) fixed during refinement. ^g Large error ($> 3\sigma$) obtained for $\log \beta_{122} = 25.14$. ^h pH range of data points refined.

ⁱ Number of data points used in refinement.

Final values for $\log \beta$ were obtained by averaging results from the 'best fit' refinements for each data file. Values from refinements in which any β assumed a negative value or showed an excessive calculated standard deviation were excluded from this average.

5.4.3 Discussion

Species distribution plots (Fig. 5.4.2) for complexation of 1-APPH₂ with copper(II) and nickel(II) show the predominance of protonated metal complex species in acidic and neutral solutions. Although the potentiometric studies yielded macroscopic complexation models, the stoichiometries of the species described by each model are consistent with a number of different microscopic forms for each complex. This is illustrated for the deprotonation of an [MLH]⁺ species [Fig. 5.4.3(a)] but may equally be applied to each ligand moiety for the stepwise deprotonations of [ML₂H₂].

The pathway adopted for deprotonation of [MLH]⁺ depends on the relative stabilities of the two possible protonated complexes, and the deprotonated complexes (I), (II) and (III). Protonation studies of 1-APPH₂ indicate that phosphonate-bound protons are more acidic, and therefore more readily displaced by a metal ion, than those bound to the amine group. It seems reasonable to assume that for [MLH]⁺ the predominant form involves co-ordination of the metal via the phosphonate group and protonation at the amine site. Although direct structural evidence is not available for this compound, the single crystal X-ray structures of Co(II),^[111] Cu(II)^[112] and Zn(II)^[113] complexes of aminomethylenephosphonic acid (AMP, Table 5.4.1), the Zn(II) complex of ethylenediaminemethylenephosphonic acid^[114]

(⁺H₃NCH₂CH₂NH₂⁺CH₂PO₃²⁻) and the Mn(II) complex of aminomethylenephosphonic acid^[115] all show similar N-protonated ligand configurations. Spectral

evidence for metal-oxygen binding in protonated Co(II) complexes of 1-aminoethylphosphonic acid (1-AEP, Table 5.4.1) has also been presented.^[116] Furthermore, structures of protonated metal complexes of tertiary aminomethylenephosphonic acids also show a similar co-ordination mode.^[117]

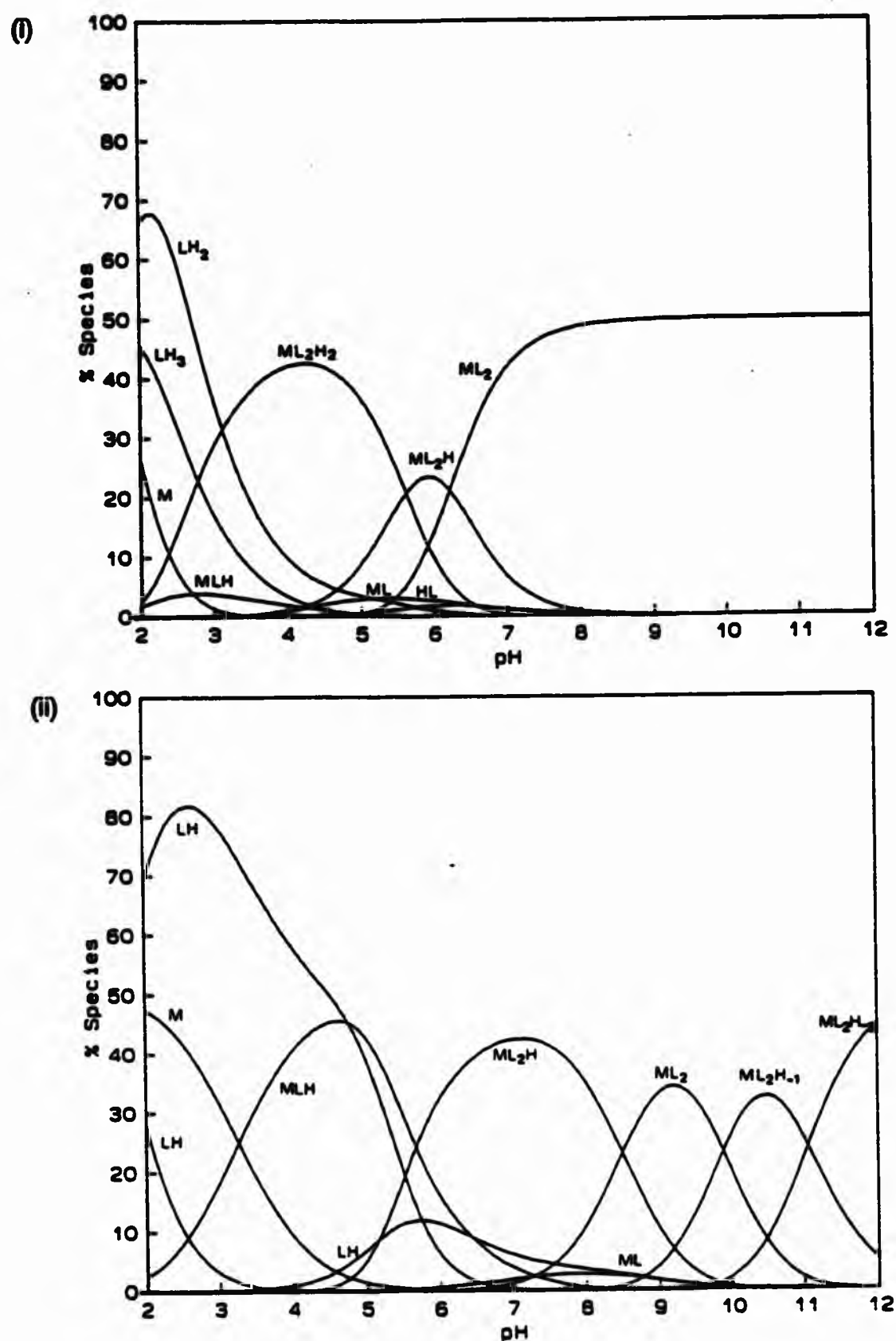


Figure 5.4.2 SPE^[5] computation of species distribution in the $M^{2+}/1-APPH_2$ /proton system ($[H^+] = 4 \text{ mmol}$; $[L] = 2 \text{ mmol}$; $[M^{2+}] = 1 \text{ mmol}$); (i) $M = Cu$, (ii) $M = Ni$.

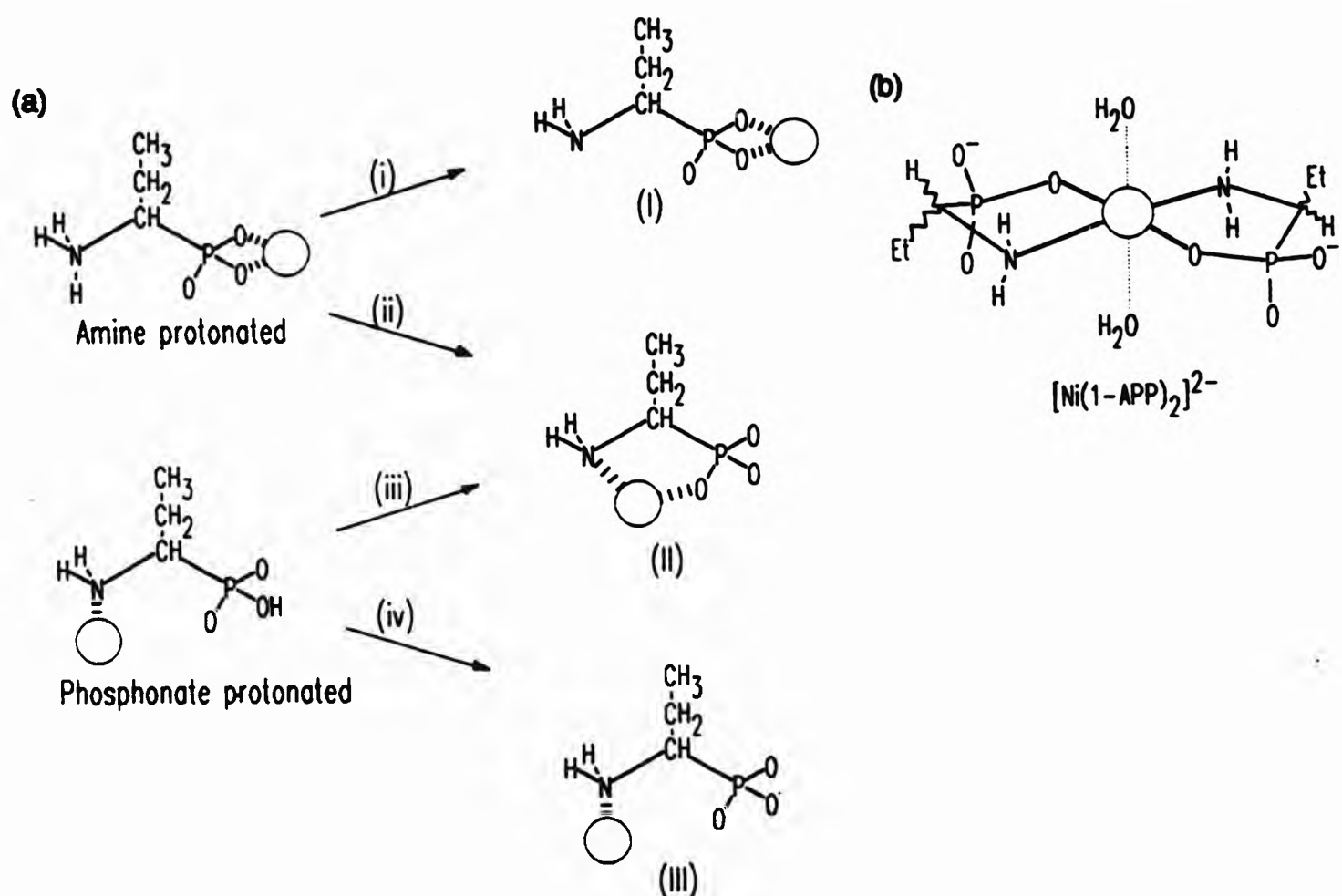


Figure 5.4.3 (a) Possible microscopic forms of species formed during deprotonation of $[MLH]^+$ ($L = CH_3CH_2CH(NH_2)PO_3^{2-}$).
 (b) A possible structure of $[NiL_2(H_2O)_2]^{2-}$.

X-ray crystallographic structural studies of metal complexes with a range of phosphonic acids have revealed several types of metal-phosphonate interactions in the solid including ion-pair interactions^[118,119] and co-ordination involving the phosphonate group in a variety of mono-, bi- and tri-dentate, and chelating modes.^[111,112,113,114,120] The latter modes feature in structures which may be best described as phosphonate-bridged metal polymers; the $\mu_2\eta^2$ bridging mode^[111,112,113,114] may be considered to describe co-ordination where the phosphonate is non-chelating and bidentate, the $\mu_2\eta^3$ mode^[120] where the phosphonate is tridentate with both chelating and

non-chelating interactions, while the less common $\mu_2\eta^1$ mode^[121] represents the interaction of two metals with a single phosphonate oxygen. Schematic representation of these metal-bridging modes is shown in Figure 5.4.4.

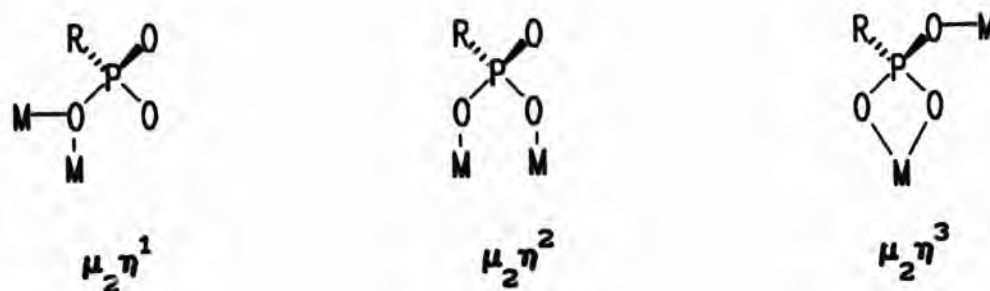


Figure 5.4.4 Schematic representation of metal bridging modes for phosphonate dianions.

Although polymeric alternatives may be discounted for this solution study (protonated polymetallic complexes do not feature in the final equilibrium model), it is impossible to distinguish between the chelate and non-chelate co-ordination modes on current evidence. However, the bite angle presented by the phosphonate group in forming a four-membered chelate ring is expected to impose severe distortion on the metal ion co-ordination sphere and this type of structure is probably destabilised with the d-block metal ions. As with complexes of amino acids (e.g. glycine, see Section 3.5), intermolecular hydrogen bonding almost certainly plays an important rôle in stabilising these metal complex structures (unidentate metal co-ordination of PO_3^{2-} leaves two phosphonate oxygens available for H-bonding as well as for metal bridging interactions) and complicated hydrogen bonded networks are widely observed in the solid state.^[111,112,113,114,120] The solid state structures show frequent involvement of H_2O in the metal co-ordination sphere^[115,118,120] and it is therefore expected that in aqueous solution solvent molecules will complete the metal co-ordination sphere. Furthermore, solvent molecules are likely to interact with the $-\text{NH}_3^+$ and PO_3^{2-} via hydrogen bonding in aqueous

solution.

Deprotonation of $[\text{MLH}]^+$ could, in principle, lead to any of structures (I), (II) or (III) [Fig. 5.4.3(a)]. There are reasons for postulating that $[\text{ML}]$ has the chelate structure (II), with the metal bonded in a 5-membered ring containing nitrogen, phosphorus and an oxygen donor of the phosphonate group. There appears to be an absence of crystal structure data for deprotonated complexes of aminophosphonic acids (available data is for protonated complexes only), although the structure of the copper(II) complex of hydroxymethylenephosphonic acid^[122] demonstrates that chelate formation with donor atoms in the alkyl side chains of phosphonic acids is feasible. Infrared spectroscopic evidence for complexes of the type $[\text{ML}]$ suggests that the metal is bound simultaneously to the phosphonate and amine groups.^[113] For $[\text{1-APP}]^{2-}$, ligand donor atoms in close proximity to the metal are unlikely to be sterically restrained from co-ordination and structure (II) [Fig. 5.4.3(a)], stabilised by chelate formation, is expected to be the dominant microscopic form for $[\text{ML}]$. The corresponding *bis*-complex, $[\text{ML}_2]^{2-}$, is expected to involve a similar type of ligand co-ordination, possibly adopting a structure similar to that shown for $[\text{NiL}_2(\text{H}_2\text{O})_2]^{2-}$ [Fig 5.4.3(b)]. Stepwise deprotonation of the water molecules of the latter is consistent with formation of the hydroxy species, $[\text{NiL}_2(\text{OH})]^{3-}$ and $[\text{NiL}_2(\text{OH})_2]^{4-}$, observed in the equilibrium model. Alternative (III) is unlikely to form because of charge separation (opposing charges would be expected to be localised on the metal ion and the phosphonate group), but a structure (I) in which the metal ion is co-ordinated to the phosphonate group is consistent with formation of both $[\text{ML}]$ and $[\text{ML}_2]^{2-}$. However in the light of the structural evidence for 'non-restriction' of the amine group from co-ordination, the chelate structure (II) is preferred.

5.5 Protonation equilibria of diethylaminomethylenephosphonic acid and ethyliminobis(methylenephosphonic acid)

A knowledge of the aqueous chemistry of the aminomethylenephosphonates is expected to underpin an understanding of their speciation in *aqu.* H_2O_2 solutions. Identification of plausible protonated forms of the ligands in aqueous solution may give some insight into the possibility that the ligands undergo a chemical transformation in *aqu.* H_2O_2 contributing to their ability to stabilise peroxide solutions. To this end, a study of the aqueous chemistries of the tertiary aminomethylenephosphonic acids, diethylaminomethylenephosphonic acid (DEAMPH_2 , Fig. 5.1.1) and ethyliminobis(methylenephosphonic acid) (EIDMPH_4 , Fig. 5.1.1), employed as model compounds, was undertaken in order to establish protonation schemes for each compound, including identification of the microscopic forms of the species in equilibrium.

Furthermore, as some equilibrium data was previously available,^[94,105] studies of these systems allowed further testing of the potentiometric titration system and experimentation with data refinement techniques. The need for structural information over the pH range used for potentiometric studies prompted development of a 'small-scale' titration system to record potentiometric and phosphorus-31 nmr data for solutions contained in an nmr tube.

5.5.1 Potentiometric studies

Titration of acidified aqueous solutions of DEAMPH_2 and EIDMPH_4 with *aqu.* KOH under conditions of constant ionic strength ($I = 0.1 \text{ mol dm}^{-3}$, KNO_3) yielded three datafiles for each compound. Titration curves (Fig. 5.5.1) were smooth in all cases and showed steps at around pH 6 corresponding to one equivalent

of base for DEAMPH_2 , and two equivalents for EIDMPH_4 . As these occurred after sufficient base had been added to neutralise acid added to the titrand as HNO_3 , the inflexions were assumed to arise from neutralisation of ligand-based protons in the sample. Discernable inflexions, however, were absent from both the acid and alkaline extremities of each curve. Titration data was refined in all cases using various modes of the FORTRAN program SUPERQUAD^[25] and the protonation constants obtained are summarised in Tables 5.5.1 (DEAMPH_2) and 5.5.2 (EIDMPH_4).

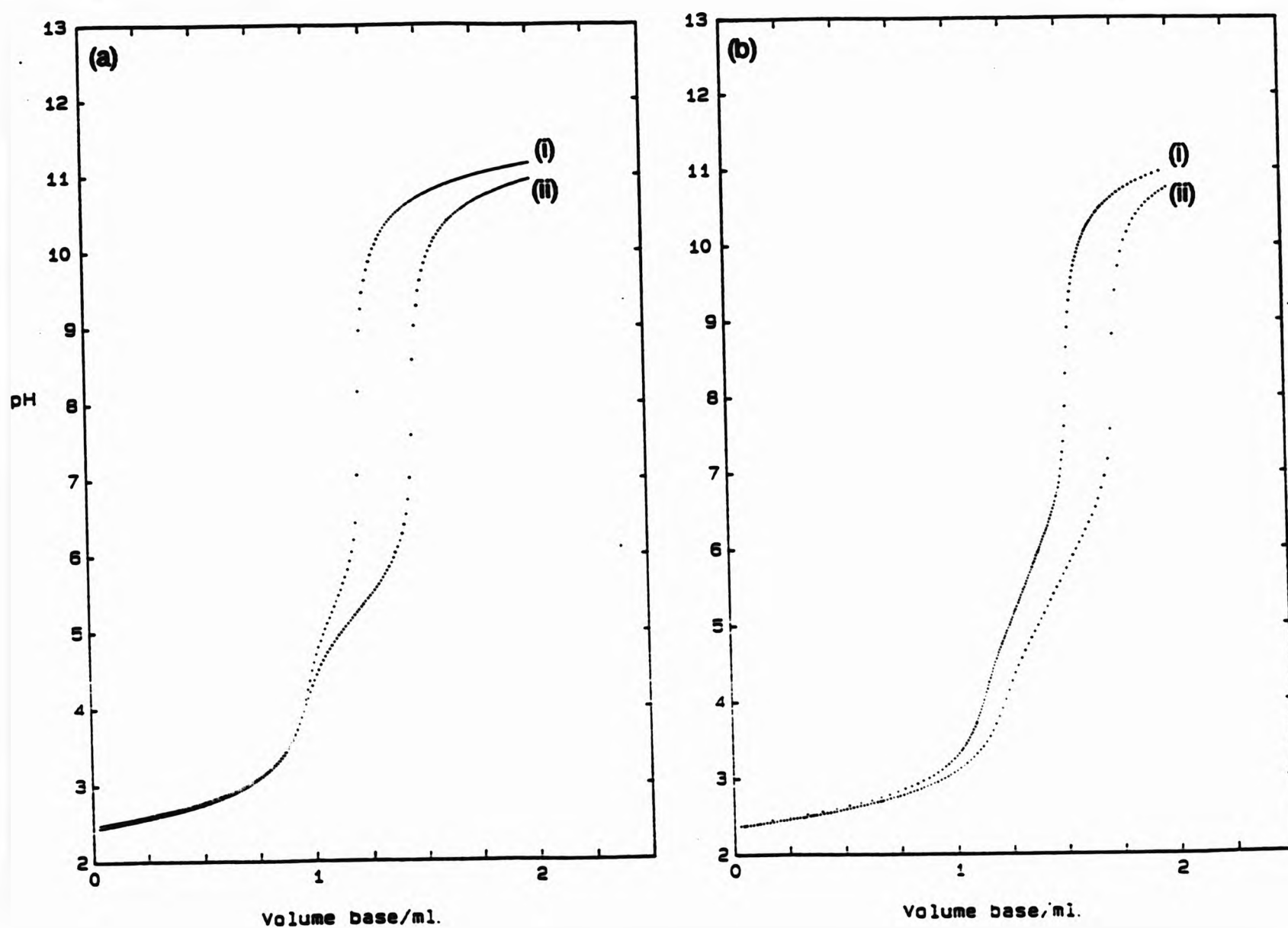


Figure 5.5.1. Titration curves (pH vs. volume of added base) for acidified *aqu.* solutions of (a) DEAMPH_2 ; (i) $[\text{L}] = 1 \text{ mmol dm}^{-3}$ (ii) $[\text{L}] = 2 \text{ mmol dm}^{-3}$, and (b) EIDMPH_4 ; (i) $[\text{L}] = 0.8 \text{ mmol dm}^{-3}$ and (ii) $[\text{L}] = 1 \text{ mmol dm}^{-3}$.

The dianion, DEAMP^{2-} , has similar functionality to 1-APP^{2-} and a similar equilibrium model, describing formation of the species $[\text{L}]^{2-}$, $[\text{LH}]^{-}$, $[\text{LH}_2]$, and $[\text{LH}_3]^{+}$, was used to describe protonation of its three basic sites. Initial refinements of data files for DEAMP_2 were executed with L defined as the free base, $[\text{Et}_2\text{NCH}_2\text{PO}_3]^{2-}$, and two moles of proton per mole of ligand were added to the initial proton concentrations required as input to SUPERQUAD.^[25] It was subsequently found that re-definition of L as the monoprotonated species $[\text{Et}_2\text{NHCH}_2\text{PO}_3]^{-}$, inclusion of only one mole of proton per mole of ligand in the initial acid concentration, and refinement of a protonation model described by $\log \beta_{01-1}$, $\log \beta_{011}$ and $\log \beta_{012}$, facilitated finding the 'best fit' data range for each file. In all cases investigated, both definitions of L yielded comparable stepwise protonation constants and identical 'fit' parameters from the 'best fit' data range. (One example, for datafile IS16, is given in Table 5.5.1.). In alternative refinement strategies, as well as refinement of initial proton concentrations ($[\text{H}]_1$), initial ligand concentrations ($[\text{L}]_1$) were also treated as refinable parameters. Two approaches were used; $[\text{L}]_1$ was either refined independently of $[\text{H}]_1$ or the relative shifts of $[\text{L}]_1$ and $[\text{H}]_1$ were constrained to be equal during refinement. The latter approach is expected to better reflect the true situation because changes in $[\text{L}]_1$ necessarily result in changes in $[\text{H}]_1$ as labile ligand-based protons are formally included in $[\text{H}]_1$ for data refinement. The results from each datafile (Table 5.5.1) show that formation constants obtained with each strategy are closely similar although it was noted that better fits were obtained on refinement of $[\text{L}]_1$, particularly when constraints were imposed on $[\text{L}]_1$ and $[\text{H}]_1$.

Previous potentiometric investigations of the protonation equilibria of DEAMP^{2-} ,^[94,105] yielded formation constants for $[\text{LH}]^{-}$ and $[\text{LH}_2]$ only. Not

surprisingly, the results of this study (Table 5.5.1) compare most favourably with the values obtained by Wozniak and Nowogrocki [$\log K_{011} = 11.81(\pm 0.03)$, $\log \beta_{012} = 17.09(\pm 0.03)$ ($\log K_{012} = 5.28$)]^[94] under corresponding conditions, i.e. $I = 0.1 \text{ mol dm}^{-3}$ (KNO_3), and less so with those reported by Carter *et al* [$\log K_{011} = 12.32(\pm 0.19)$, $\log K_{012} = 5.79(\pm 0.11)$]^[105] from solutions of higher ionic strength [$I = 1.0 \text{ mol dm}^{-3}$ (KNO_3)]. The latter authors point out that complexation of K^+ by the ligand may significantly affect the magnitude of $\log K_{011}$ in these experiments. It may therefore be the case that the observed differences in values obtained at different ionic strengths can be attributed to differences in the K^+ concentrations of the solutions. It is noted that the latter study was performed with the mono-potassium sesquihydrate salt of the ligand.

Although the free base of EIDMPH_4 nominally contains five potentially basic sites, refinement of titration data with SUPERQUAD^[25] using a model based on five protonation constants was unsuccessful; either $\log \beta_{014}$ and $\log \beta_{015}$ were associated with unacceptably large standard deviations or $\log \beta_{015}$ assumed a negative value on convergence. However, an equilibrium model describing the formation of four protonated species yielded successful refinements for each datafile (Table 5.5.2). These observations probably reflect the extreme acidity of an $[\text{LH}_5]^+$ species, which is presumably dissociated in even the most acidic solutions used in this study. Similarly, the intra- and inter-titration variations observed for $\log \beta_{014}$ reflect the ready deprotonation of $[\text{LH}_4]$; a species abundance plot [Fig. 5.5.4(ii)] shows this species to be less than 30 % abundant over the pH range of the study (pH 2.5-11).

As observed during refinement of DEAMPH_2 protonation data, values of the first

protonation constant $[-\log \beta_{01-1}$ for DEAMP²⁻ (Table 5.5.1); $\log \beta_{011}$ for EIDMP⁴⁻ (Table 5.5.2)] were especially sensitive to the data range chosen for

Table 5.5.1 Protonation constants for diethylaminomethylenephosphonic acid
(L = [Et₂NHCH₂PO₃]⁻).^a

File	$\log \beta_{01-1}$	$\log \beta_{011}$	$\log \beta_{012}$	$\log K_{012}$
IS14 ^b				
c	-11.59(0.013)	5.34(0.008)	6.81(0.029)	1.47
d	-11.48(0.009)	5.36(0.005)	7.09(0.017)	1.73
d,e	-11.49(0.008)	5.36(0.005)	7.10(0.011)	1.74
IS15 ^f				
c,g	-11.60(0.018)	5.36(0.020)	^h	
d	-11.51(0.017)	5.38(0.015)	6.67(0.089)	1.29
d,e	-11.51(0.013)	5.38(0.015)	6.65(0.059)	1.27
IS16 ^{i,j}				
c	-11.67(0.012)	5.38(0.012)	6.37(0.089)	0.99
d	-11.60(0.011)	5.38(0.011)	6.53(0.080)	1.15
d,e	-11.57(0.013)	5.40(0.013)	6.81(0.040)	1.41
IS16 ^{g,k}				
c		11.62(0.013)	16.97(0.022)	5.35
d		11.58(0.023)	17.00(0.027)	5.42
d,e		11.59(0.023)	16.99(0.027)	5.40
Mean ^l	-11.55±0.12	5.37±0.03	6.75±0.38	1.4±0.4

^a Data obtained at constant ionic strength; I = 0.1 mol dm⁻³, KNO₃. All $\log \beta$ values calculated with SUPERQUAD;^[25] figures in parentheses are standard deviations estimated during refinements. ^b Refinement for three species; pH 2.53-10.94, 189 data points. ^c Initial proton concentration treated as a refinable parameter. ^d Initial proton and ligand concentrations treated as refinable parameters. ^e Relative shifts of initial proton and ligand concentrations constrained during refinement. ^f Refinement for three species; pH 2.48-11.16, 128 data points. ^g Omitted from mean. ^h Large error (> 3 σ) obtained for $\log \beta_{012} = 6.00$. ⁱ Refinement for three species; pH 2.27-11.16, 195 data points. ^j Refinement for three species also carried out for L defined as [Et₂NCH₂PO₃]²⁻ yielding $\log \beta_{011} = 11.67(0.012)$, $\log \beta_{012} = 17.06(0.020)$, $\log \beta_{013} = 18.05(0.098)$. ^{c,g} ^k Refinement for two species with L defined as [Et₂NCH₂PO₃]²⁻; pH 4.88-11.16, 97 data points.

Table 5.5.1 continued

¹ Unweighted mean of values from each refinement; error limits are derived from the ranges obtained for each $\log \beta_{\text{min}}$ (and $\log K_{\text{min}}$). Stepwise equilibria are summarised in Table 5.5.3. For L defined as $[\text{Et}_2\text{NCH}_2\text{PO}_3]^{2-}$, $\log \beta_{011} = 11.55 \pm 0.12$, $\log \beta_{012} = 16.92 \pm 0.15$, $\log \beta_{013} = 18.3 \pm 0.5$.

refinement, and constants derived from 'best-fit' data ranges (i.e. those given in Tables 5.5.1 and 5.5.2) exhibit somewhat large inter- and intra-titration variations. A number of factors are expected to contribute to this behaviour including, relatively low abundances of the fully deprotonated ligand (< 30 %) in the pH range of the titration, interaction of the ligand with the background electrolyte (the large excess of KNO_3 in the solutions leads to the expectation that co-ordination of K^+ by the ligand will be significant), as well as the inherent unreliability of measurements with the glass electrode in strongly alkaline solutions. [33,47]

Protonation constants for EIDMP^{4-} reported previously ($\log K_{011} = 12.42$, $\log K_{012} = 5.92$, $\log K_{013} = 4.70$, $\log K_{014} < 2$) [105] were obtained in *aqu.* KNO_3 solution ($I = 1.0 \text{ mol dm}^{-3}$) and comparison with the results of this study show that stepwise protonation constants are slightly dependent on ionic strength. As well as effects due to differing concentrations of K^+ in the solutions (*vide supra*), it is worth noting that the constants reported by Carter *et al.* [105] were obtained from fewer data points than this study and their constants were calculated with a single estimate of pK_w . This latter assumption is expected to impinge on the reliability of the pH data in alkali solution (where dissociation of $[\text{LH}]^{3-}$ occurs) and therefore most affect values of $\log \beta_{011}$. Inconsistencies between reported values of $\log \beta_{011}$ in other aminomethylenephosphonic acid systems, particularly for the widely

studied ligands nitrilotris(methylenephosphonic acid) (NTMPH₆) and ethylenediaminetetrakis(methylenephosphonic acid) (EDTMPH₈), have been noted and attributed to differences in sample purity.^[104,123,124]

Table 5.5.2 Protonation constants for ethyliminobis(methylenephosphonic acid) (L = [EtN(CH₂PO₃)₂]⁴⁻).^a

File	log β ₀₁₁	log β ₀₁₂	log K ₀₁₂	log β ₀₁₃	log K ₀₁₃	log β ₀₁₄	log K ₀₁₄
IS2B5 ^b							
c	11.80(0.054)	18.14(0.060)	6.34	23.08(0.065)	4.94	24.86(0.098)	1.78
d,e	11.73(0.056)	18.00(0.063)	6.27	23.05(0.069)	5.05	24.99(0.093)	1.94
IS2B6 ^f							
c	11.79(0.049)	18.16(0.049)	6.37	23.04(0.060)	4.88	25.00(0.083)	1.96
d	11.70(0.043)	18.06(0.049)	6.36	23.01(0.052)	4.95	25.13(0.077)	2.12
d,e	11.65(0.040)	18.01(0.046)	6.36	22.98(0.051)	4.97	25.20(0.064)	2.22
IS2B7 ^g							
c	11.72(0.074)	18.06(0.087)	6.34	23.15(0.100)	5.09	25.54(0.129)	2.39
d,h	12.17(0.107)	18.56(0.113)	6.39	23.51(0.115)	4.95	25.52(0.135)	2.01
d,e	11.74(0.087)	18.08(0.103)	6.34	23.22(0.116)	5.14	25.70(0.140)	2.48
Mean ⁱ	11.73 ±0.08	18.07 ±0.09	6.34 ±0.07	23.08 ±0.14	5.00 ±0.14	25.2 ±0.5	2.1 ±0.4

^a Data obtained at constant ionic strength; I = 0.1 mol dm⁻³, KNO₃. All log β values calculated with SUPERQUAD;^[25] figures in parentheses are standard deviations obtained from the program. Values were obtained on refinement of equilibrium models describing the formation of four protonated species in all cases. ^b pH 2.57-10.96, 164 data points. ^c Initial proton concentration treated as a refinable parameter. ^d Initial proton and ligand concentrations treated as refinable parameters. ^e Relative shifts of initial proton and ligand concentrations constrained during refinement. ^f pH 2.64-10.97, 163 data points. ^g pH 2.55-10.97, 165 data points. ^h Omitted from mean. ⁱ Unweighted mean of values from each refinement; error limits are derived from the ranges obtained for each log β_{nlh} (and log K_{nlh}).

Using similar arguments to those applied to 1-APPH₂ (section 5.2), the

protonation scheme [Fig. 5.5.2(i)] based on potentiometric measurements of DEAMPH₂ is readily proposed. Of the microscopic forms possible for [LH]⁻, a species featuring localisation of the single proton at the amine site is expected to predominate. Subsequent protonations of this species at the phosphonate sites leads initially to formation of a zwitterion, stabilising [LH₂] to the extent that [LH₃]⁺ is only present in significant quantities in strongly acid solutions. Similar arguments can be extended to the protonation behaviour of EIDMPH₄, although its protonation behaviour may be complicated by the presence of an additional methylenephosphonate arm in the molecule [Fig. 5.5.2(ii)]. However, as log β₀₁₁ of EIDMP⁴⁻ is of a similar order to that of both 1-APP²⁻ and DEAMP²⁻, single protonation of the tetraanion may be assigned, by analogy, as protonation at the amine site of the molecule. Furthermore, the increase of log β₀₁₁ for EIDMP⁴⁻ over that of DEAMP²⁻ (and 1-APP²⁻) coincides with increasing phosphonate substitution at the nitrogen atom. The increase in basicity is consistent with an increase of electron density at the amine nitrogen due to the influence of an extra, 'electron-rich' PO₃²⁻ group in the molecule which appears to more than compensate for the loss of the inductive influence due to the ethyl group. Further substitution at the nitrogen with an additional methylenephosphonate group, exemplified by the ligand nitrilotris(methylenephosphonic acid) (NTMPH₆), also induces an increase in ligand basicity [log K₀₁₁ = 12.8, I = 0.1 mol dm⁻³ (KNO₃); ^[104] log K₀₁₁ = 12.34, I = 1.0 mol dm⁻³ (KNO₃) ^[105]]. Similar arguments have been applied to account for the observed increase in basicity of the polyaminophosphonates over their aminocarboxylate analogues. ^[101,125,126]

The values of log K₀₁₂ and log K₀₁₃ are indicative of single protonation of each PO₃²⁻ moiety in EIDMPH³⁻ and the comparability of the values suggests

there is little interaction between the groups, reflecting the flexibility of the phosphonate arms in the molecule and the likelihood that charge repulsions maximise their separation. Similarly, the three protonation constants in this range observed for NIMPH₆ are attributed to single protonation of its three $-\text{PO}_3^{2-}$ groups.^[104,105] The stepwise formation constant of $[\text{EIDMPH}_4]$ can only correspond to double protonation of one $-\text{PO}_3^{2-}$ group in the molecule, and further demonstrates the weak proton affinity of the $-\text{PO}_3\text{H}^-$ function.

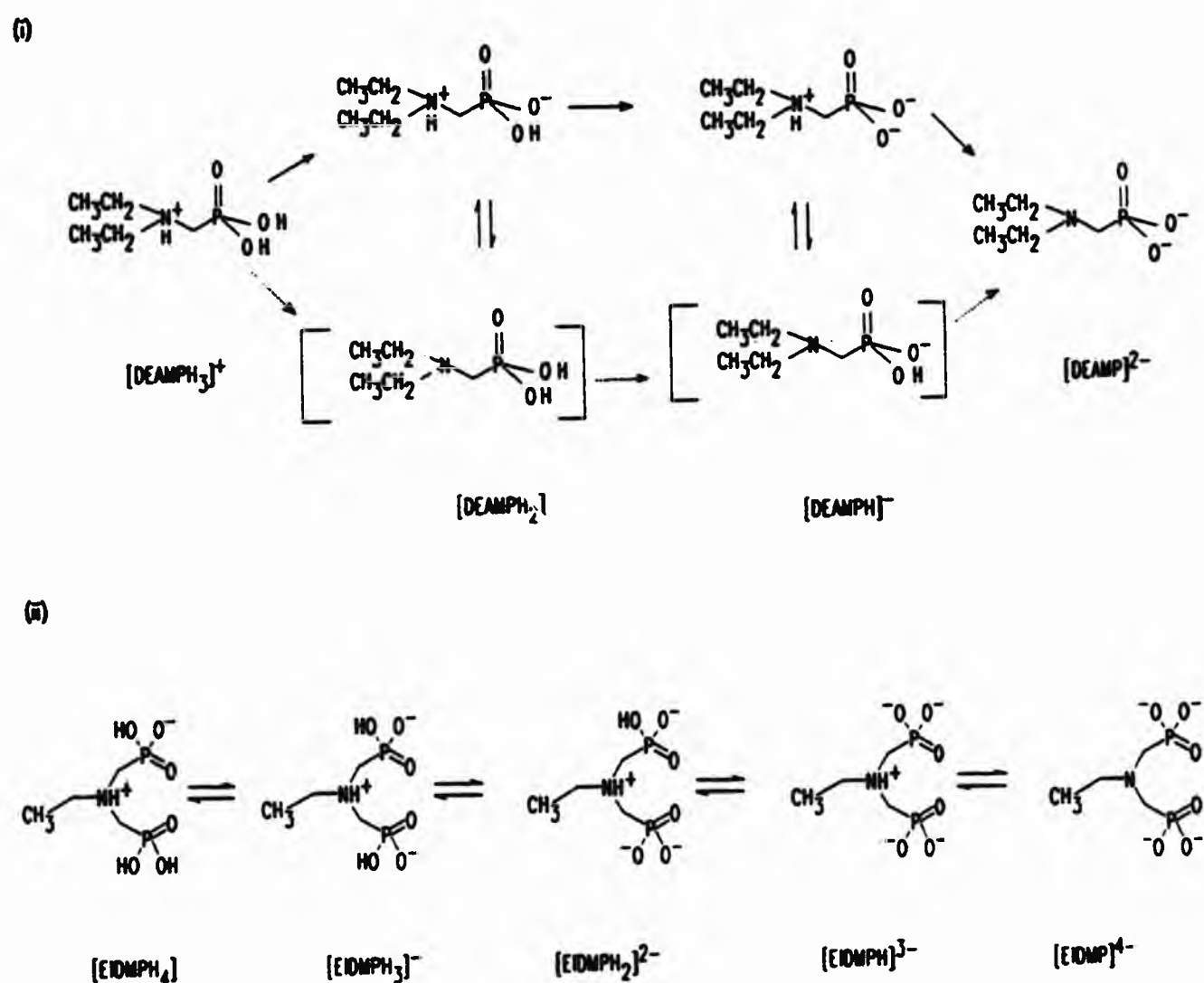


Figure 5.5.2 Protonation scheme of (i) diethylaminomethylenephosphonic acid (minor species featuring in micro-equilibria are shown in brackets) and (ii) ethyliminobis(methylenephosphonic acid).

5.5.2 Phosphorus-31 nmr studies

Positive confirmation of microscopic forms of protonated ligand species proposed on the basis of potentiometric data requires investigation of changes of molecular states instead of those of the bulk solution (as in potentiometric studies). Spectroscopic methods provide convenient detection of such changes in solution and, although uv-vis spectroscopy is widely applied in this field,^[3,34,128] the suitability of the ^{31}P nucleus for nmr study prompted an investigation of the pH dependence of $\delta(^{31}\text{P})$ for DEAMP_2 and EIDMP_4 in aqueous solution. The sensitivity of $\delta(^{31}\text{P})$ of phosphorus oxyanions to pH is well known and a number of comparable studies using aminophosphonic acids have been described.^[26,82,100,101,102,103,104,105,106,107,128]

Qualitative data for the pH dependence of $\delta(^{31}\text{P})$ for DEAMP^{2-} and EIDMP^{4-} has been reported^[105] and provided useful comparison data for the development of an experiment under conditions of constant ionic strength. Although employment of reagent concentrations comparable to the preceding potentiometric studies (Section 5.5.1) was desirable, preliminary ^{31}P nmr studies indicated that spectral acquisition using such solutions was unfeasably time-consuming. A 'ten-fold' scale-up of solution concentrations (i.e. $[\text{RPO}_3^{2-}]$ ca. 0.02 mol dm^{-3} ; $[\text{H}^+] = 0.04 \text{ mol dm}^{-3}$; $[\text{OH}^-] = 1.0 \text{ mol dm}^{-3}$; $I = 1.0 \text{ mol dm}^{-3}$; KNO_3) was therefore employed and proved to be more suitable for spectral acquisition while still retaining a measure of comparability with the potentiometric study. Solution pH was obtained *in situ* using a thin-stem glass electrode allowing the titration to be performed on a single solution in an nmr tube. Such an approach eliminates uncertainties associated with batch titrations.^[1,129] Shift referencing of $\delta(^{31}\text{P})$ to 85 % aq. H_3PO_4 using a coaxial tube, the standard method,^[130] resulted in unacceptably large

spectral dynamic ranges, and an alternative approach was required.

Referencing by sample substitution via a ^2D lock signal provided an effective solution and therefore titration solutions were prepared in 5 % (v/v) $\text{aq. D}_2\text{O}$. Although corrections for pH readings in D_2O solution have been described,^[131] the relatively low concentration of D_2O in these solutions was assumed to have a negligible influence on pH meter readings and these were used uncorrected.

In both cases, a single ^{31}P signal was observed throughout the pH ranges investigated. As noted for 1-APP H_2 (Section 5.3.2), the single signal is consistent with rapid exchange between species resulting in a single 'time-averaged' environment for the phosphorus-31 nuclei. Some broadening of the signal was noted over intermediate pH (ca. 4.5-10.5) for DEAMP H_2 while the signal for EIDMP H_4 broadened from pH 4.5 until the titration was completed. Broadening of the signal is attributed to slower exchange but whether the mechanism involves intramolecular or intermolecular proton scrambling between basic sites [see, for example, the micro-equilibria for DEAMP H_2 and [DEAMP H] $^-$ in Fig. 5.5.2(1)] remains unclear. Physical changes in the sample solution, such as changes in solution viscosity or homogeneity, that might induce signal broadening were not apparent.

Changes in $\delta(^{31}\text{P})$ for DEAMP H_2 and EIDMP H_4 with pH (Figs. 5.5.3 and 5.5.4) broadly correlate those previously reported;^[105] the curve for EIDMP H_4 also shows some similarity to those obtained for its close analogues, $\text{HN}(\text{CH}_2\text{PO}_3\text{H}_2)_2$ and $\text{CH}_3\text{N}(\text{CH}_2\text{PO}_3\text{H}_2)_2$.^[107] Curves for DEAMP H_2 and EIDMP H_4 are compared with species abundances calculated on the basis of potentiometrically derived pK_a values (Figs. 5.5.3 and 5.5.4). The pH values at which two predominant species are present in approximately equal amounts (the 'half-neutralisation' points) correspond approximately to inflexion points on the $\delta(^{31}\text{P})$ vs. pH

curves; naturally, these pH values also correspond approximately to pK_a values for the species involved. [Changes in $\delta(^{31}\text{P})$ corresponding to stepwise protonations of the ligands are summarised in Table 5.5.3.]. Shifts of $\delta(^{31}\text{P})$ to higher field are generally associated^[26,100,101,102,103,104,105,106,107,108] with stepwise deprotonation of the phosphonic acid function; for example, shielding of the ^{31}P nucleus is observed on deprotonation of $\text{CH}_3\text{PO}_3\text{H}_2$.^[103,106] The origins of this upfield shift have been investigated by *ab initio* methods.^[103] Quantum mechanical calculations^[132] have suggested that, for four co-ordinate phosphorus, ^{31}P shielding originates in two terms; a σ -bond contribution (δ_σ) determined solely by the p-orbital occupation of the phosphorus atom, and a π -bond contribution (δ_π) determined by occupation of the phosphorus d-orbitals. The δ_σ term depends on both the bond angles around the phosphorus atom and electronegativity differences between the phosphorus atom and its substituents. For polarities in the range of P-O interactions, the theory predicts^[103] that an increase in the electronegativity of the oxygen atom leads to shielding of the ^{31}P nucleus. The δ_π term is proportional to changes in the electron occupation of the phosphorus d-orbitals, although it is independent of the distribution of this total π -character among the various bonds to phosphorus. For $\text{CH}_3\text{PO}_3^{2-}$, Moedritzer deduced^[103] that, upon acidification, the σ and π contributions to the chemical shift are expected to act in opposing directions and that the upfield shift of $\delta(^{31}\text{P})$ on acidification is predominantly due to an increase in the electron occupancy of phosphorus d-orbitals; the increase in π -bonding is thought to outweigh effects due to changes in the σ -bond structure although significant contributions to changes of chemical shift are possible with relatively small changes in phosphorus bond angles.

Table 5.5.3 Changes in phosphorus-31 chemical shift ($\Delta\delta$) on stepwise protonations of DEAMP²⁻ and EIDMP⁴⁻.

Equilibrium	log K ^a	$\Delta\delta^b$ /ppm
[DEAMPH ₂] + H ⁺ = [DEAMPH ₃] ⁺	1.4	> 0.24
[DEAMPH] ⁻ + H ⁺ = [DEAMPH ₂]	5.37	1.53
[DEAMP] ²⁻ + H ⁺ = [DEAMPH] ⁻	11.55	> -5.51
[EIDMPH ₄] + H ⁺ = [EIDMPH ₅] ⁺	< 2	c
[EIDMPH ₃] ⁻ + H ⁺ = [EIDMPH ₄]	2.1	> 0.26
[EIDMPH ₂] ²⁻ + H ⁺ = [EIDMPH ₃] ⁻	5.00	} 0.94
[EIDMPH] ³⁻ + H ⁺ = [EIDMPH ₂] ²⁻	6.34	
[EIDMP] ⁴⁻ + H ⁺ = [EIDMPH] ³⁻	11.73	> -3.63

^a Titration data obtained at constant ionic strength, I = 0.1 mol dm⁻³, KNO₃.

^b Titration data obtained at constant ionic strength, I = 1.0 mol dm⁻³, KNO₃.

$\Delta\delta = \delta(\text{reactant}) - \delta(\text{product})$. ^c Potentiometric studies indicate that abundance of [LH₅]⁺ is negligible in the pH range of this study.

While deprotonations in acid solution cause $\delta(^{31}\text{P})$ to move to higher field, consistent with stepwise deprotonation of phosphonic acid functions, the deprotonation steps of both DEAMPH⁻ and EIDMPH³⁻ occur in basic solution and are accompanied by relatively large movements of the ³¹P signal to lower field. As noted previously (Section 5.3.1), such changes in $\delta(^{31}\text{P})$ have been widely observed and indicate deprotonation of amine functions in simple aminophosphonic acids. [26,100,101,104,105,106,107] Appleton *et al* [106] demonstrated that while curves of ³¹P chemical shift vs. pD for NH₂CH₂PO₃²⁻, NH₂(CH₂)₂PO₃²⁻ and NH₂(CH₂)₃PO₃²⁻ all show relatively large shifts of $\delta(^{31}\text{P})$ to low field above pD 7, the ³¹P shift of methylphosphonic acid is approximately constant in the same region. Furthermore, changes below pD 7 in the latter case are all to higher field. Although the association of amine

deprotonation with shifts of $\delta(^{31}\text{P})$ to lower field is widely made (*vide supra*), the origin of the deshielding of the phosphorus nucleus has been the subject of some debate.

Commonly, the downfield shift of $\delta(^{31}\text{P})$ on deprotonation of amine sites is associated with deshielding of the phosphorus nucleus due to a breakdown of intramolecular electrostatic and hydrogen bonding interactions between the positive ammonium centre and the negatively charged phosphonate group. [100,101,102,106] Considerable discussion has surrounded the effect of the alkyl chain length separating the amine and phosphonate groups on the magnitude of this downfield shift. Appleton *et al.* [106] observed that the difference between phosphorus-31 shifts of $\text{NH}_2(\text{CH}_2)_n\text{PO}_3^{2-}$ and $^+\text{NH}_3(\text{CH}_2)_n\text{PO}_3^{2-}$ sharply decreases as n changes from one to two, $\Delta\delta = 9.9$ for $n = 1$ and $\Delta\delta = \text{ca. } 2.8$ for $n = 2$. A further increase of the chain to $n = 3$ has a far less dramatic effect, in this case $\Delta\delta = 2.1$. The authors attribute these observations to the presence of cyclical configurations stabilised by hydrogen bonding and coulombic interactions in the monoprotonated species. Cacheris *et al.*, [101] in accounting for the changes in $\delta(^{31}\text{P})$ with pH for a series of N-substituted polyaza macrocyclic methylenephosphonic acids, reiterated Appleton's observations by highlighting the relative stabilities of hydrogen bonded, 5-, 6- and 7-membered rings. Martell and Sponganicz also explained shifts to lower field for $\delta(^{31}\text{P})$ on full deprotonation of some simple aminocarboxylic alkylphosphonates in terms of changes in hydrogen bonding. [100] However, on the basis that the paramagnetic contribution to nuclear shielding predominates for heavier atoms, Sawada *et al.* explained the shift changes during deprotonation of $[\text{H}_3\text{N}(\text{CH}_2)_n\text{PO}_3]^-$ in terms of changes in the electronic structure of the ^{31}P atom induced by changes at the nitrogen. [104] They contest that Appleton's results are consistent with a

through-bond interaction between the nitrogen and phosphorus atoms which diminishes as the carbon chain separating them increases.

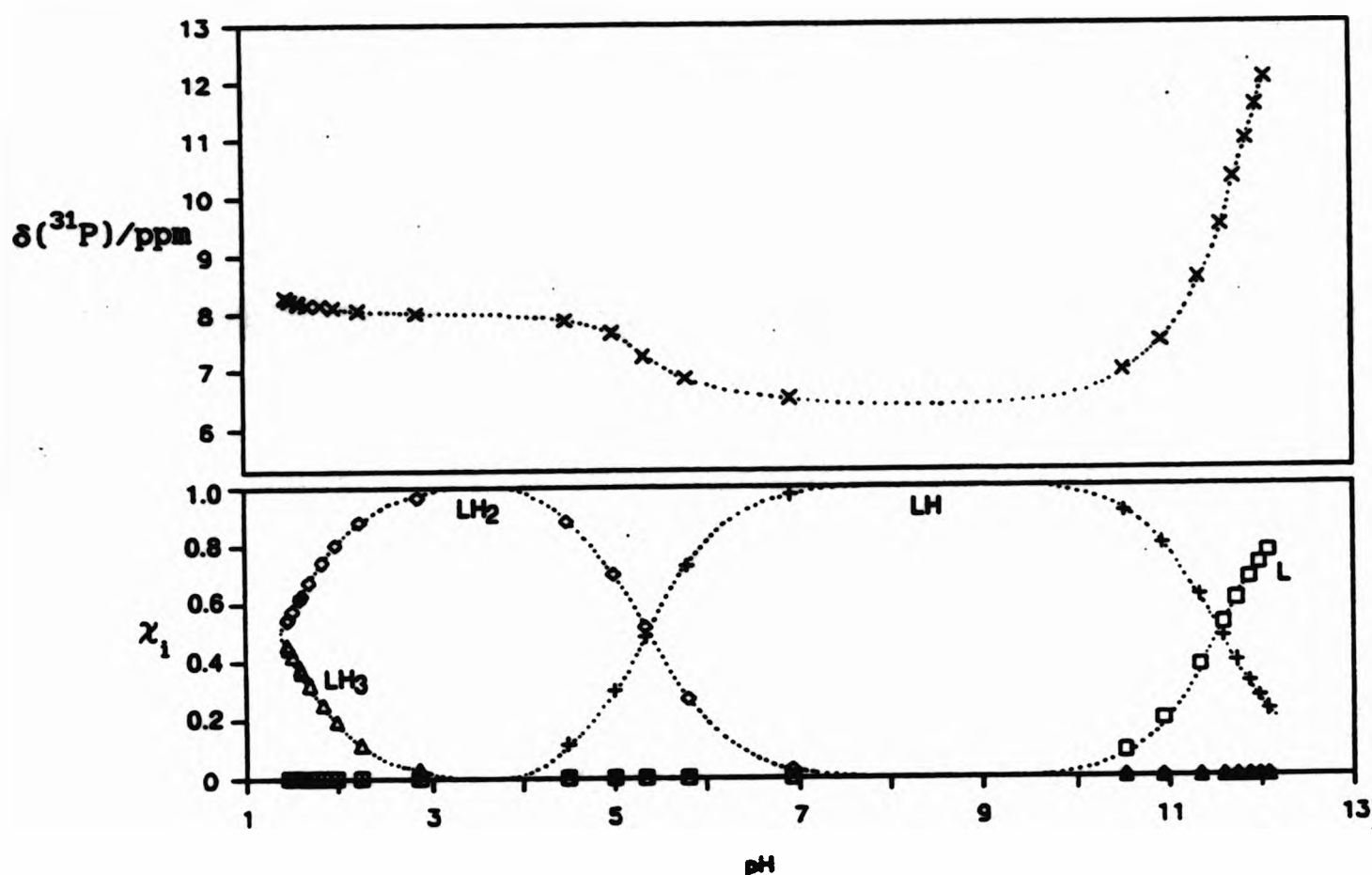


Figure 5.5.3 Correlation of (i) the variation of $\delta(^{31}\text{P})$ and (ii) the distribution of ligand species with pH for DEAMPH_2 . [The latter was calculated using free proton concentrations from the 'small volume' nmr titration in conjunction with formation constants from the preceding potentiometric study (Section 5.5.1)].

Moedritzer and Irani observe^[26] that the downfield shift of $\delta(^{31}\text{P})$ during the final deprotonation step of NTMPH_6 is comparable with those accompanying the corresponding deprotonations of the iminobis(methylenephosphonate) and nitrilotris(methylenephosphonate) ethoxy esters.^[133] They suggest that the shifts originate from changes in electronic structures.^[26] It might be expected that intramolecular hydrogen bonding and coulombic interactions between the phosphonic oxygen atoms and the ammonium nitrogen of monoprotonated species would be weakened after esterification of the PO_3^{2-}

groups and result in a substantial reduction in the magnitude of $\Delta\delta$ for these compounds. However, $\Delta\delta$ marginally increases over that of NTMPH^{5-} suggesting that through-bond interactions play an important rôle in these cases. Although ^{31}P shielding in the aminophosphonic acids is likely to depend on similar diamagnetic and paramagnetic terms to those of simple phosphonic acids (*vide supra*), the multiplicity of effects arising from both bonded and non-bonded interactions precludes a definitive conclusion.

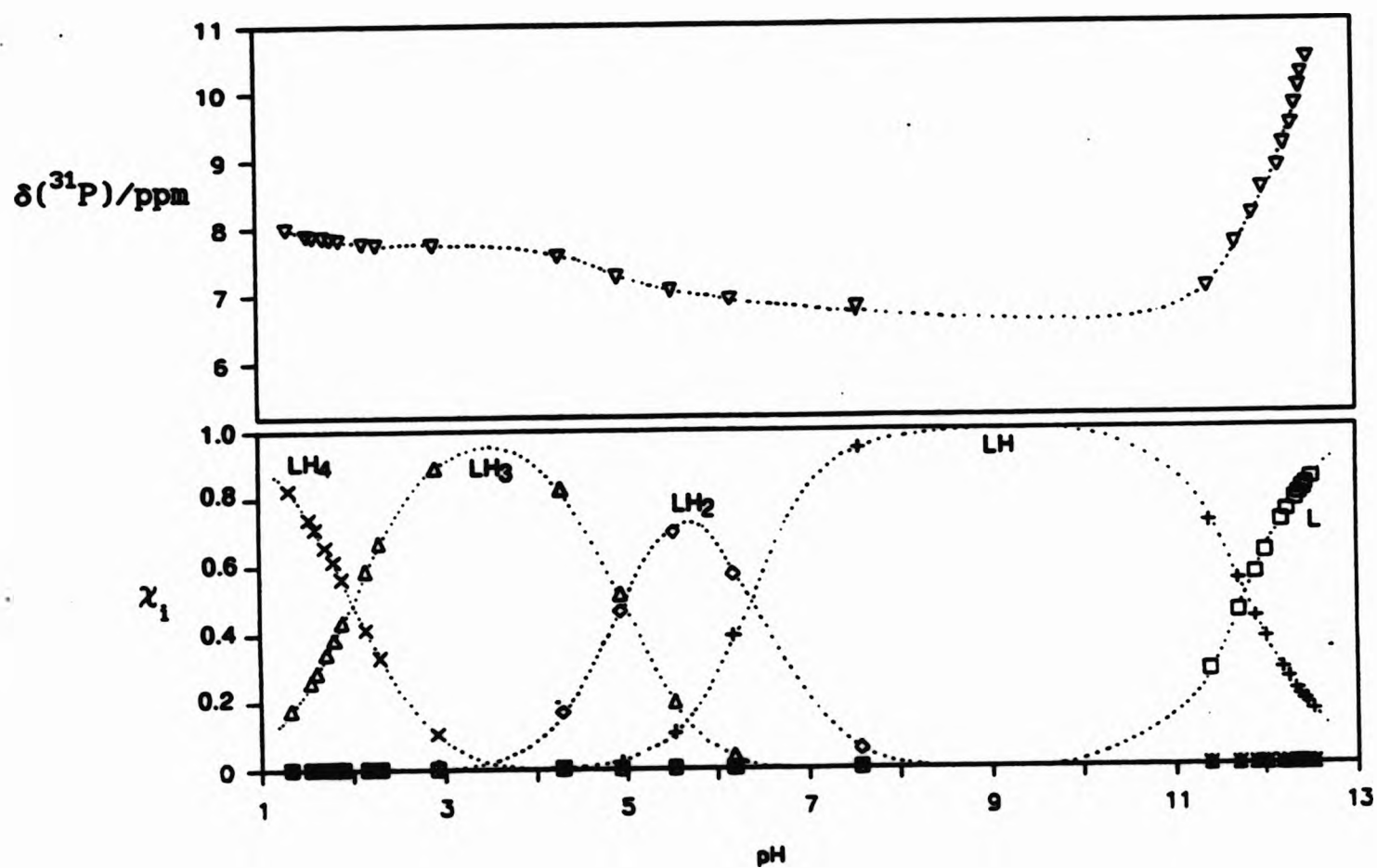


Figure 5.5.4 Correlation of (i) the variation of $\delta(^{31}\text{P})$ and (ii) the distribution of ligand species with pH for EIDMPH_4 . (The latter is calculated as for Fig. 5.5.3).

5.6 Stability of transition metal complexes of diethylaminomethylenephosphonic acid and ethyliminobis(methylenephosphonic acid)

Following the study of the acid-base behaviour of diethylaminomethylene-phosphonic acid (DEAMPH_2 , Fig. 5.5.1) and ethyliminobis(methylenephosphonic acid) (EIDMPH_4 , Fig. 5.5.1) in *aqu.* KNO_3 solutions (Section 5.5), a potentiometric investigation of the interaction of these ligands with copper(II) and nickel(II) under similar conditions ($I = 0.1 \text{ mol dm}^{-3}$) was undertaken. Such a study was expected to yield information about the relative stabilities of protonated metal complexes in these systems and identify the rôle of the potentially chelating second methylenephosphonate arm in complexes of EIDMP^{4-} .

The Cu(II) co-ordination chemistry of DEAMPH_2 and its close analogue N,N'-dimethylaminomethylenephosphonic acid (DMAMPH_2) have been established in *aqu.* KNO_3 media ($I = 0.1 \text{ mol dm}^{-3}$).^[94,134] The latter case yields analogous complex species to those of the 1- $\text{APPH}_2/\text{Cu(II)}$ system (see Section 5.4) in addition to a hydroxy complex, $[\text{MLOH}]^-$. The range of metal complexes reported for the interaction of DEAMPH_2 with Cu(II) is more limited; formation constants were obtained for $[\text{CuL}]$, $[\text{CuLH}]^+$, $[\text{CuL}_2\text{H}_2]$ and $[\text{CuLOH}]^-$ only.^[94] Deprotonation routes for $[\text{CuLH}]^+$ to give $[\text{CuL}]$ in these systems (and by analogy the stepwise deprotonation of each ligand moiety of $[\text{CuL}_2\text{H}_2]$ to give $[\text{CuL}]^{2-}$) are expected to feature similar species to those discussed for 1- $\text{APPH}_2/\text{Cu(II)}$ system (Section 5.4.3). In particular, lack of substantial steric restraint of the co-ordinating groups in these ligands is expected to allow formation of O,N-bonded metal chelates.

Unfortunately, at all concentrations investigated, acid-base titrations of DEAMPH_2 in the presence of $\text{Cu}(\text{NO}_3)_2$ and $\text{Ni}(\text{NO}_3)_2$ were beset by observable precipitation in basic solution. This phenomenon led to the occurrence of

discontinuities curves for pH vs. volume of added base; initial breaks in the titration curves are observed at ca. pH 6.5 for Cu(II) and ca. pH 8.5 for Ni(II). Although data refinement was precluded by the lack of suitable data points to model metal-ligand interactions (the discontinuities appear soon after the metal-ligand curves deviate from the ligand-only trace), comparison between curves obtained at each M:L ratio indicate that Cu(II) displaces ligand-bound protons more readily than Ni(II) and therefore, as might be expected, forms the more stable complexes. In the case of Cu(II), a granular grey-black solid giving an inconclusive elemental analysis was isolated from the titration at M:L = 1:1.

The metal ion co-ordination mode of the iminobis(methylenephosphonate) moiety is of interest as it features in a number of important polyaminomethylene-phosphonate sequestrants, notably EDTMPH₈, cyclohexane-1,2-diaminetetrakis-(methylenephosphonic acid) (CDTMPH₈) and diethylenetriaminepentakis-(methylenephosphonic acid) (DTPMPH₁₀). EIDMPH₄ provides an ideal system for such an investigation because its N-ethyl substituent is expected to resemble the C-C bridges of the more complicated sequestrants.

Interactions of iminobis(methylenephosphonate) ligands with several transition metal ions have been investigated,^[107,135] and potentiometric studies of EIDMPH₄ with several first row transition [Mn(II), Co(II), Cu(II), Ni(II)]^[136] and alkaline earth metals [Mg(II)]^[105] and Ca(II)^[105,136] have been reported. However, the majority of these studies have concentrated only on the formation of 1:1 metal/ligand complexes and the existence 1:2 complexes in systems employing excess quantities of EIDMPH₄ has not been established. Deployment of reactant ratios with [M]:[L] > 1:1 in order to establish the extent of formation of such species may shed light on likely species involved

in the sequestration of trace amounts of metal ions by the aminomethylene-phosphonic acids.

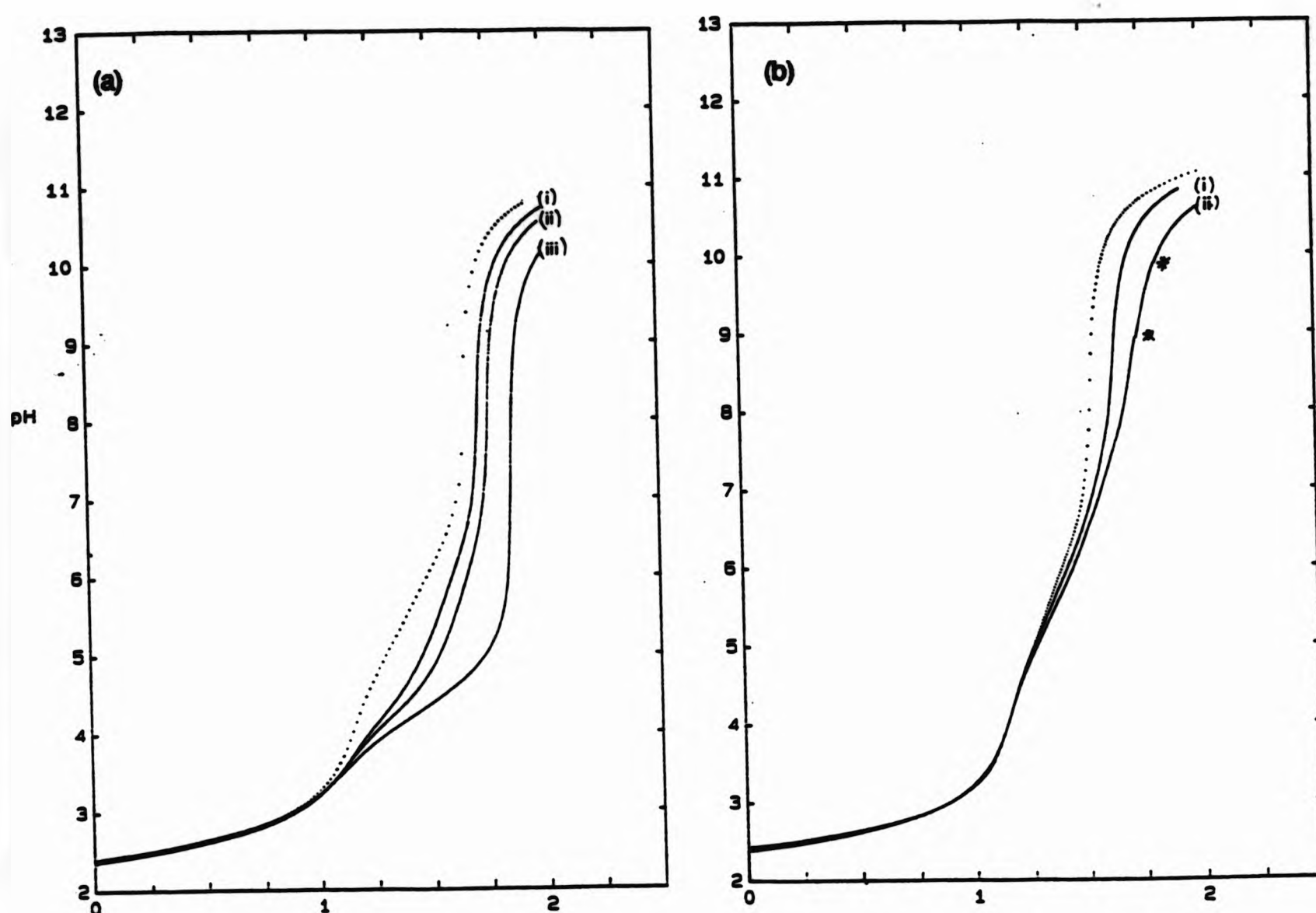


Figure 5.6.1. Titration curves (pH vs. volume of added base) for acidified aqu. solutions of: (a) EIDMPH_4 (dotted line, $[\text{L}] = 1 \text{ mmol dm}^{-3}$) and $\text{Cu}(\text{NO}_3)_2$; (i) $[\text{M}]:[\text{L}] = 1:3$, (ii) $[\text{M}]:[\text{L}] = 1:2$, (iii) $[\text{M}]:[\text{L}] = 1:1$ and (b) EIDMPH_4 (dotted line $[\text{L}] = 0.8 \text{ mmol dm}^{-3}$) and $\text{Ni}(\text{NO}_3)_2$; (i) $[\text{M}]:[\text{L}] = 1:2$, (ii) $[\text{M}]:[\text{L}] = 1:1$.

5.6.1 Copper(II)

Titration data sets for the $\text{EIDMPH}_4/\text{Cu}(\text{II})$ system were obtained at three different initial concentrations of metal ion corresponding with $[\text{M}]:[\text{L}] = 1:1$, $1:2$ and $1:3$. Smooth titration curves [Fig. 5.6.1(a)] were

recorded in each case and each data set was refined using SUPERQUAD.^[25] For refinement, the most hydrolysed form of the ligand (EIDMP^{4-}) was defined as L and initial proton concentrations were incremented by four moles of H^+ per mole of ligand to account for ligand-bound labile protons in the sample. Refinement of each data set was attempted using a number of different equilibrium models describing the formation of various combinations of both mono- and bis-metal complexes. Metal hydrolysis constants^[110] accounting for formation of $[\text{CuOH}]^+$ and $[\text{Cu}_2(\text{OH})_2]^{2+}$ were included as fixed values in all metal complexation models. The most successful refinements in each case are summarised in Table 5.6.1; successful models were selected by comparing the magnitudes of fit parameters (χ^2 and σ) and from a qualitative examination of the distribution of error residuals. In the latter case, equilibrium models giving a more random (Gaussian) distribution of residuals were preferred. For each data set, large error residuals were associated with data recorded over end point regions of the titration curves and elimination of such data for files M060 and M061 yielded excellent fits for models describing the formation of $[\text{ML}]^{2-}$, $[\text{MLH}]^-$ and $[\text{MLH}_2]$ in acidic solutions. However, once these $\log \beta$ values were established it was found that acceptable refinements were possible when data from more basic regions of each curve and describing the formation of $[\text{MLOH}]^{3-}$ for M:L = 1:1 (M060) and $[\text{ML}_2]^{6-}$ (and its protonated forms $[\text{ML}_2\text{H}]^{5-}$ and $[\text{ML}_2\text{H}_2]^{4-}$) for M:L = 1:2 (M061) was included. In these cases, selection of the weighted data points mode of SUPERQUAD^[25] (each data point is assigned a weight according to the ratio $\Delta E/\Delta v$ before refinement in order to account for larger uncertainty for data in end point regions) greatly aided the refinement process.

Table 5.6.1 Refinement summary for titrations of EIDMPH₄ with copper(II).^a

Datafile	log β_{mlh}^b log K_{mlh}^d						np ^c pH range	σ χ^2
	110	111	112	120	121	122	11-1	
M060 ^e	13.37	18.03	21.54				3.01	61
		4.66	3.51				16.80 ^f	3.90-10.13
								0.1771
								8.64
$\left\{ \begin{array}{l} 13.54 \\ 18.10 \\ 21.97 \end{array} \right.$							48	0.0433
		4.56	3.87				3.67-5.44	2.00
M061 ^h	13.63	18.08	22.01				42	0.0127
		4.45	3.93				3.88-5.59	5.24
	13.45	17.96		18.39			58	0.1232
		4.51		4.94			4.22-10.54	16.71
$\left\{ \begin{array}{l} 13.72 \\ 18.14 \\ 22.13 \end{array} \right.$				18.94	28.41	34.28 ⁱ	58	0.0444
		4.42	3.99	5.22	9.47	5.87	4.22-10.54	20.94
M062 ^j	13.64	17.99	22.03	18.45			80	0.1150
		4.35	4.04	4.81			3.74-10.59	15.40
$\left\{ \begin{array}{l} 13.74 \\ 18.05 \\ 22.14 \end{array} \right.$				18.91	28.51	34.19	80	0.0988
		4.31	4.09	5.17	9.60	5.68	3.74-10.59	35.60
	13.78	18.00	22.20	18.88	28.38		80	0.1006
		4.22	4.20	5.10	9.50		3.74-10.59	11.40
MEAN ^k								
log β	13.66	18.09	22.08	18.92	28.46	34.23 (3.01)		
	±0.13	±0.05	±0.11	±0.03	±0.07	±0.10		
log K		4.43	3.98	5.20	9.54	5.77		
		±0.13	±0.11	±0.03	±0.07	±0.10		

^a Data obtained at constant ionic strength; $I = 0.1 \text{ mol dm}^{-3}$, KNO_3 ; 25 °C. Log β values obtained with SUPERQUAD;^[25] initial proton concentrations treated as refinable parameters. ^b Overall formation constant for the species $[\text{M}_m\text{L}_l\text{H}_h]$. ^c Number of data points used in refinement. ^d Stepwise protonation constant ($K_{mlh} = [\text{M}_m\text{L}_l\text{H}_h]/[\text{M}_m\text{L}_l\text{H}_{h-1}][\text{H}]$ except for $K_{120} = [\text{ML}_2]/[\text{ML}][\text{L}]$).

Table 5.6.1 continued

^e Reactant ratio M:L = 1:1.02. ^f Overall formation constant for $[\text{MLOH}]^-$ ($\log \beta_{\text{ML(OH)}} = \log \beta_{11-1} + \text{pK}_w$). ^g 'Best fit' refinements; $\log \beta$ values included in mean. ^h Reactant ratio M:L = 1:2.12. ⁱ Large relative error associated with $\log \beta$ value. ^j Reactant ratio M:L = 1:3.04. ^k Unweighted mean of selected values. Error limits represent the maximum deviation from the mean value. Figures in parentheses represent values obtained from one data set refinement

Refinements of the data set recorded at M:L = 1:3 (M062) were attempted using similar equilibrium models to those successfully refined at M:L = 1:2. The model describing the formation of $[\text{ML}]^{2-}$, $[\text{MLH}]^-$, $[\text{MLH}_2]$ and $[\text{ML}_2]^{6-}$, $[\text{ML}_2\text{H}]^{5-}$, $[\text{ML}_2\text{H}_2]^{4-}$ in the latter case gives rise to a single ill-defined constant ($\log \beta_{122}$), normally grounds its rejection. However, its close agreement with the 'best fit' refinement for M061 and the more random distribution of its residuals allied to its lower σ value compared with the alternative model (i.e. that excluding $\log \beta_{122}$), warranted its inclusion as the 'best fit' refinement for this data set.

Average values of $\log \beta_{110}$, $\log \beta_{111}$ and $\log \beta_{112}$ from this study are comparable with those reported in a previous study of this system ($I = 1.0 \text{ mol dm}^{-3}$, KNO_3).^[136] However, the latter study addressed the formation of $[\text{ML}]^{2-}$, $[\text{MLH}]^-$ and $[\text{MLH}_2]$ ($\log \beta_{110} = 13.09$, $\log \beta_{111} = 18.49$ and $\log \beta_{112} = 22.09$)^[136] from initial concentrations of M:L = 1:1 only. Under similar initial metal-ligand ratios, Martell and co-workers describe the formation of $[\text{ML}]^{2-}$, $[\text{MLH}]^-$, $[\text{MLH}_2]$ and $[\text{MLH}_{-1}]^{3-}$ for iminobis(methylenephosphonic acid) $[\text{IDMPH}_4, \text{M} = \text{Cu(II)}]$, a close analogue of EIDMPH_4 .^[135] Significantly, a similar model best describes the $\text{EIDMPH}_4/\text{Cu(II)}$ system at M:L = 1:1 when points from basic solution are

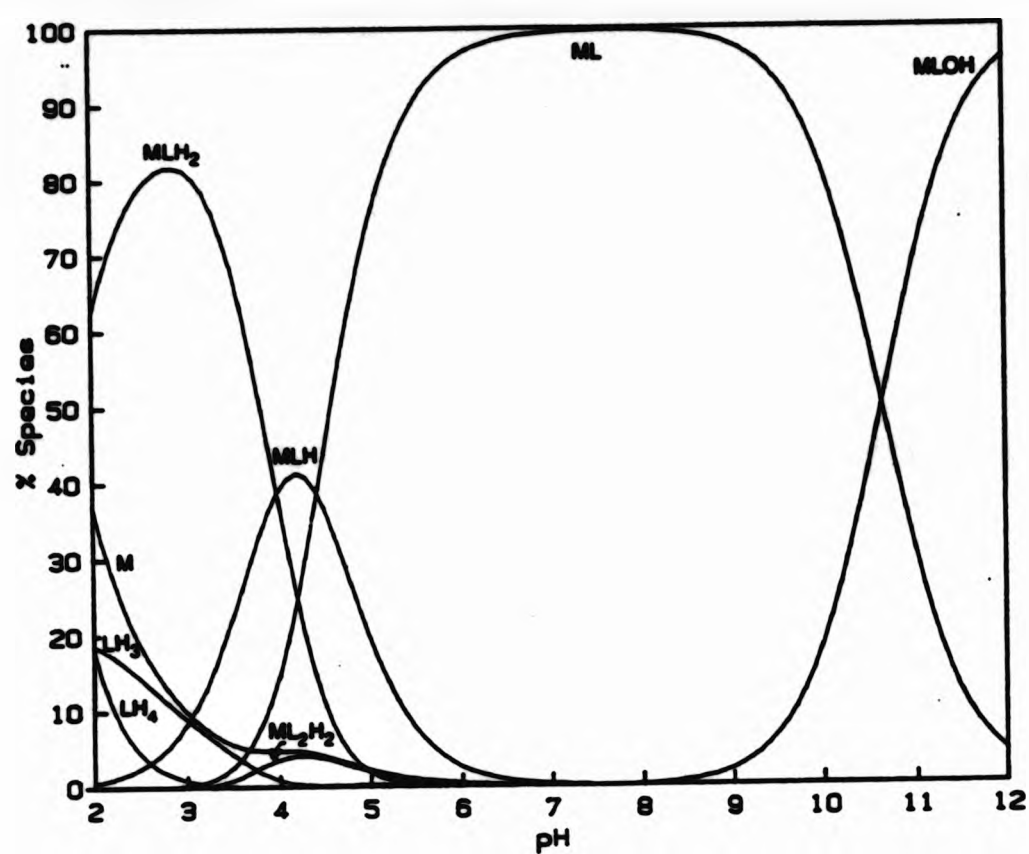
included in refinements. However, that bis-complexes are required for effective refinement of data obtained with initial concentrations of $\text{Cu:EIDMPH}_4 < 1:1$ (this study) and that such species dominate species distribution plots calculated with excess ligand concentrations [see, for example, Fig. 5.6.2(ii)], emphasizes their importance in fully describing the system.

5.6.2 Nickel(II)

Two datafiles were obtained for titration of EIDMPH_4 in the presence of Ni(II) , at initial concentrations corresponding to $\text{M:L} = 1:1$ and $1:2$ [Fig. 5.6.1(b)]. The curve obtained for $\text{M:L} = 1:1$ showed two discontinuities (indicated with asterisks in Fig. 5.6.1(b)(ii)) attributed to gas bubbles in the titrant delivery tube. Data at the point of the first discontinuity (increasing pH) and above were excluded before data refinement. Data was analysed with SUPERQUAD^[25] via a similar strategy to that employed for the Cu(II)-EIDMPH_4 system; a single metal hydrolysis constant $[\text{Ni}^{2+} + \text{H}_2\text{O} = \text{Ni(OH)}^+ + \text{H}^+; \log \beta_{10-1} = -9.86]^{[110]}$ was fixed during all data refinements. As observed in the corresponding Cu(II) systems, sharp end-points in the titration curves corresponded with large error residuals, reflecting greater uncertainty for data in these regions. Weighting data points before refinement again led to improved fits. Models yielding acceptable fits are summarised in Table 5.6.2.

Complexation models which refined successfully at both M:L ratios for the Ni(II)-EIDMPH_4 system broadly followed those refined in the Cu(II) system. For $\text{M:L} = 1:1$, formation constants for $[\text{ML}]^{2-}$, $[\text{MLH}]^-$ and $[\text{MLH}_2]$ were obtained in the absence and, over a wider pH data range, in the presence of $[\text{MLOH}]^{3-}$.

(i)



(ii)

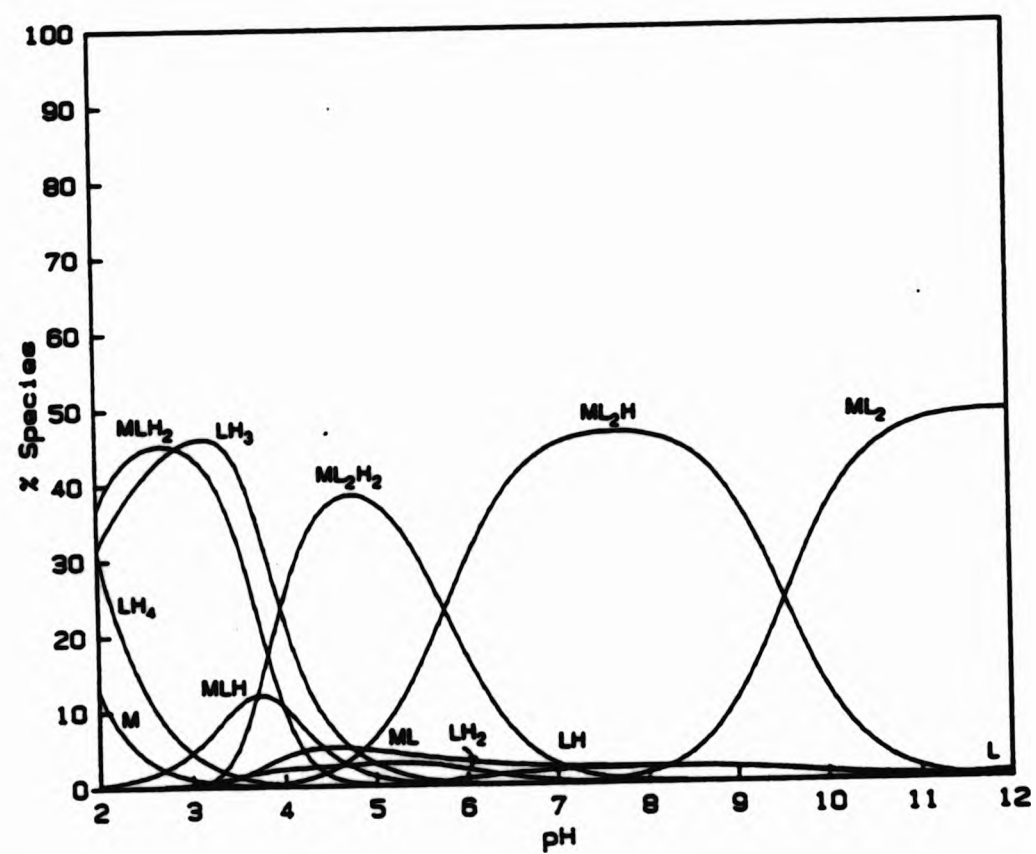


Figure 5.6.2 SPE^[5] computation of species distribution in the $M^{2+}/EIDMPH_4$ /proton system; (i) $M = Cu^{2+}$ ($[H^+] = 4 \text{ mmol}$; $[L] = 2 \text{ mmol}$; $[M^{2+}] = 2 \text{ mmol}$); (ii) $M = Cu^{2+}$ ($[H^+] = 4 \text{ mmol}$; $[L] = 2 \text{ mmol}$; $[M^{2+}] = 1 \text{ mmol}$).

(iii)

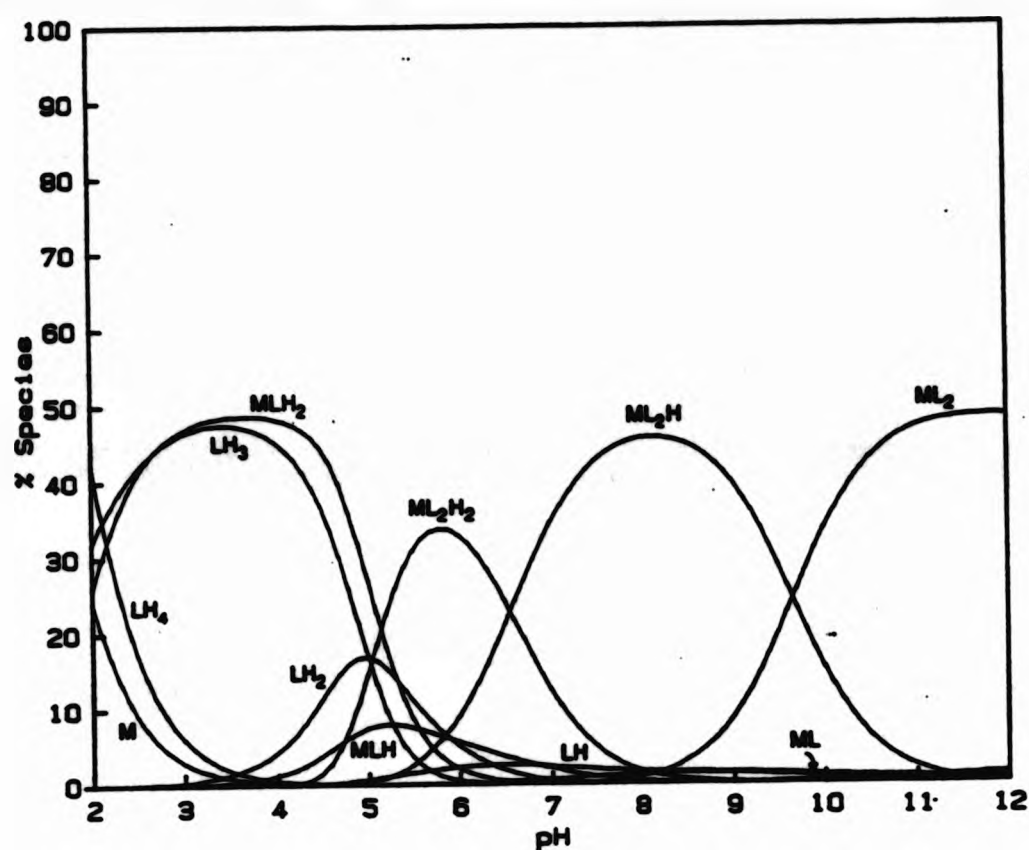


Figure 5.6.2 SPE^[5] computation of species distribution in the $M^{2+}/EIDMPH_4$ /proton system; (iii) $M = Ni^{2+}$ ($[H^+] = 4 \text{ mmol}$; $[L] = 2 \text{ mmol}$; $[M^{2+}] = 1 \text{ mmol}$).

However, better fits for the $M:L = 1:1$ data were obtained by including the formation of the *bis*-complex species $[ML_2H]^{5-}$ in the equilibrium model, indeed the 'best fit' model for this data includes $\log \beta_{121}$. (Including $\log \beta_{120}$ and $\log \beta_{122}$ in complexation models resulted in unacceptable data refinement). In an excess of ligand ($M:L = 1:2$), formation constants for the *bis*-complex species, $[ML_2]^{6-}$, $[ML_2H]^{5-}$ and $[ML_2H_2]^{4-}$ were modelled successfully in conjunction with $\log \beta_{110}$, $\log \beta_{111}$ and $\log \beta_{112}$. In this case, however, inclusion of metal complex hydrolysis equilibria in complexation models ($\log \beta_{11-1}$ was particularly investigated) led to ill-defined (or negative) constants on convergence.

Table 5.6.2 Refinement summary for titrations of EIDMPH₄ with nickel (II).^a

Datafile	log β_{mlh}^b log K_{mlh}^d						np ^c pH range	σ χ^2
	110	111	112	120	121	122	11-1	
IS2N1 ^e	8.63	16.29	21.85	14.01	23.83		90	0.3955
		7.66	5.56	5.38	9.82		4.60-9.37	13.11
f {	8.62	16.26	21.86	13.96	23.80	30.18	88	0.0864
		7.64	5.60	5.34	9.84	6.38	4.68-9.37	3.64
IS2N2 ^g	8.63	15.88	21.40				106	0.1278
		7.25	5.52				4.34-8.61	21.07
	8.54	15.69	21.25		23.16		106	0.0548
		7.15	5.56		-		4.34-8.61	4.18
	8.53	15.82	21.33				109	0.1339
		7.29	5.51				11.66 ^h	30.38
							4.42-8.93	
f {	8.54	15.84	21.35		23.44		99	0.0387
		7.30	5.51		-		12.19 ^h	4.03
							4.75-8.93	
MEAN ⁱ								
log β	8.58	16.05	21.61	(13.96)	23.62	(30.18)	(-1.62)	
	±0.04	±0.21	±0.25		±0.18			
log K		7.47	5.56	(5.38)	9.66	(6.56)		
		±0.21	±0.25		±0.18			

^a Data obtained at constant ionic strength; $I = 0.1 \text{ mol dm}^{-3}$, KNO_3 ; 25 °C.

Log β values obtained with SUPERQUAD; ^[25] initial proton concentrations

treated as refinable parameters. ^b Overall formation constant for the

species $[\text{ML}_i\text{H}_j]$. ^c Number of data points used in refinement. ^d Stepwise

protonation constant ($K_{mlh} = [\text{ML}_i\text{H}_j]/[\text{ML}_i\text{H}_{j-1}][\text{H}]$) except for

$K_{120} = [\text{ML}_2]/[\text{ML}][\text{L}]$. ^e Reactant ratio M:L = 1:2.06. ^f 'Best fit'

refinements; log β values included in mean. ^g Reactant ratio M:L = 1:1.00.

^h Overall formation constant for $[\text{MLOH}]^-$ ($\log \beta_{\text{ML(OH)}} = \log \beta_{11-1} + \text{p}K_w$).

ⁱ Unweighted mean of selected values. Error limits represent the maximum deviation from the mean value. Figures in parentheses represent values obtained from one data set refinement.

It is interesting to compare the inter-titration variability of each $\log \beta$ in this study and that of the preceding Cu(II) study. Data collection for the two systems was separated by some 2 years and the somewhat better reproducibility of the Cu(II) constants may be attributed to improvements to apparatus stability (following, for example, installation of an air conditioning unit and deployment of a redesigned titration vessel) achieved over this period.

The speciation deduced in this study bears little relation to that reported previously for acid-base titration of Ni(II)-EIDMPH₄ [$\log \beta_{110} = 7.97$ and $\log \beta_{111} = 10.69$; M:L = 1:1, I = 1.0 mol dm⁻³ (KNO₃)];^[136] remarkably, it agrees more closely, as do the $\log \beta$ values, with that of Ni(II)-IDMPH₄ [$\log \beta_{110} = 8.32$, $\log \beta_{111} = 14.23$, $\log \beta_{112} = 19.01$, $\log \beta_{120} = 9.84$, and $\log \beta_{11-1} = -2.48$; M:L = 1:1 and 1:2, I = 0.1 mol dm⁻³ (KNO₃)].^[135] It seems unlikely that changing the ionic strength of the solution could cause such a dramatic effect and therefore the differences can only be attributed to different data refinement techniques or sample purities. It is noteworthy that neither of these alternative models provide completely satisfactory fits for the titration data of this study.

5.6.3 Discussion

The influence of the second methylenephosphonic acid arm in EIDMPH₄ on Cu(II) co-ordination is revealed by comparing the magnitudes of $\log \beta$ from this study with those of Cu(II)-DEAMPH₂ and Cu(II)-MEAMPH₂; Wozniak and Nowogrocki report $\log \beta_{110}$ values of 7.46 and 7.99 for these systems respectively.^[94,134] A substantial increase in stability results in the iminobis(methylenephosphonic acid) system, for example $\log \beta_{110}$ is ca. 6 log units more stable, consistent with the presence of an extra donor group in the ligand, increased basicity of

ligand (see Section 5.5) due to methylenephosphonate substitution at the amine nitrogen, and the possibility that potentially terdentate ligands form metal complexes containing an extra 5-membered chelate ring. Possible metal co-ordination modes for EIDMP^{4-} (and its protonated forms) are shown in Figure 5.6.1(a).

Comparison of $\log \beta_{110}$ values in Cu(II)-EIDMPH_4 and Ni(II)-EIDMPH_4 systems shows that while Cu(II) forms the more stable $[\text{ML}]^{2-}$ complexes, as might be expected from the Irving-Williams series,^[137,138] the increase in stability over the Ni(II) system is substantial ($\Delta \log K_{110} = 5.08$). Addition of a second deprotonated ligand to $[\text{ML}]^{2-}$ giving $[\text{ML}_2]^{6-}$ is considerably less favourable. This observation is consistent with the Ni(II)-IDMPH_4 system, in which the destabilisation of $[\text{ML}_2]^{6-}$ was attributed to the influence of coulombic repulsion;^[135] charge interaction between L^{4-} and the anionic complex $[\text{ML}]^{2-}$ may be expected to restrict formation of $[\text{ML}_2]^{6-}$. Remarkably, $\log K_{120} ([\text{ML}]^{2-} + \text{L}^{4-} = [\text{ML}_2]^{6-})$ for Ni(II)-EIDMPH_4 is slightly larger than the corresponding stepwise constant in the Cu(II) system. Such effects may originate in the ability of Cu(II) to adopt a planar, 4-co-ordinate geometry [a structure for $[\text{ML}]^{2-}$ such as I (Fig. 5.6.3) can be envisaged with the fourth co-ordination site of the metal occupied by a water molecule] and thereby stabilise $[\text{ML}]^{2-}$ relative to $[\text{ML}_2]^{6-}$, in contrast to the propensity of 'high spin' Ni(II) to adopt 6-co-ordinate octahedral geometries, stabilising $[\text{ML}_2]^{6-}$ [which, in the absence of other influences could adopt a structure similar to Fig. 5.6.3(b)]. Deprotonation of the water molecule of the 4-co-ordinate complex described above ($[\text{ML}(\text{H}_2\text{O})]^{2-}$) giving the hydrolysed metal complex $[\text{ML}(\text{OH})]^{3-}$, is consistent with complexation models obtained for both systems. The alternative microscopic form for $[\text{ML}]^{2-}$ (structure II Fig. 5.3.1) involving non-co-ordination of one phosphonate group of the

ligand, may be of some importance, particularly if the terdentate (endo) form of the ligand (e.g. I, Fig. 5.3.1) is destabilised by intramolecular charge repulsion between the phosphonate groups or steric requirements of the external substituents of the O,N-chelate rings. Inspection of molecular models suggests that eclipsing of methylene hydrogens with both phosphorus and nitrogen substituents is significant in several conformations.

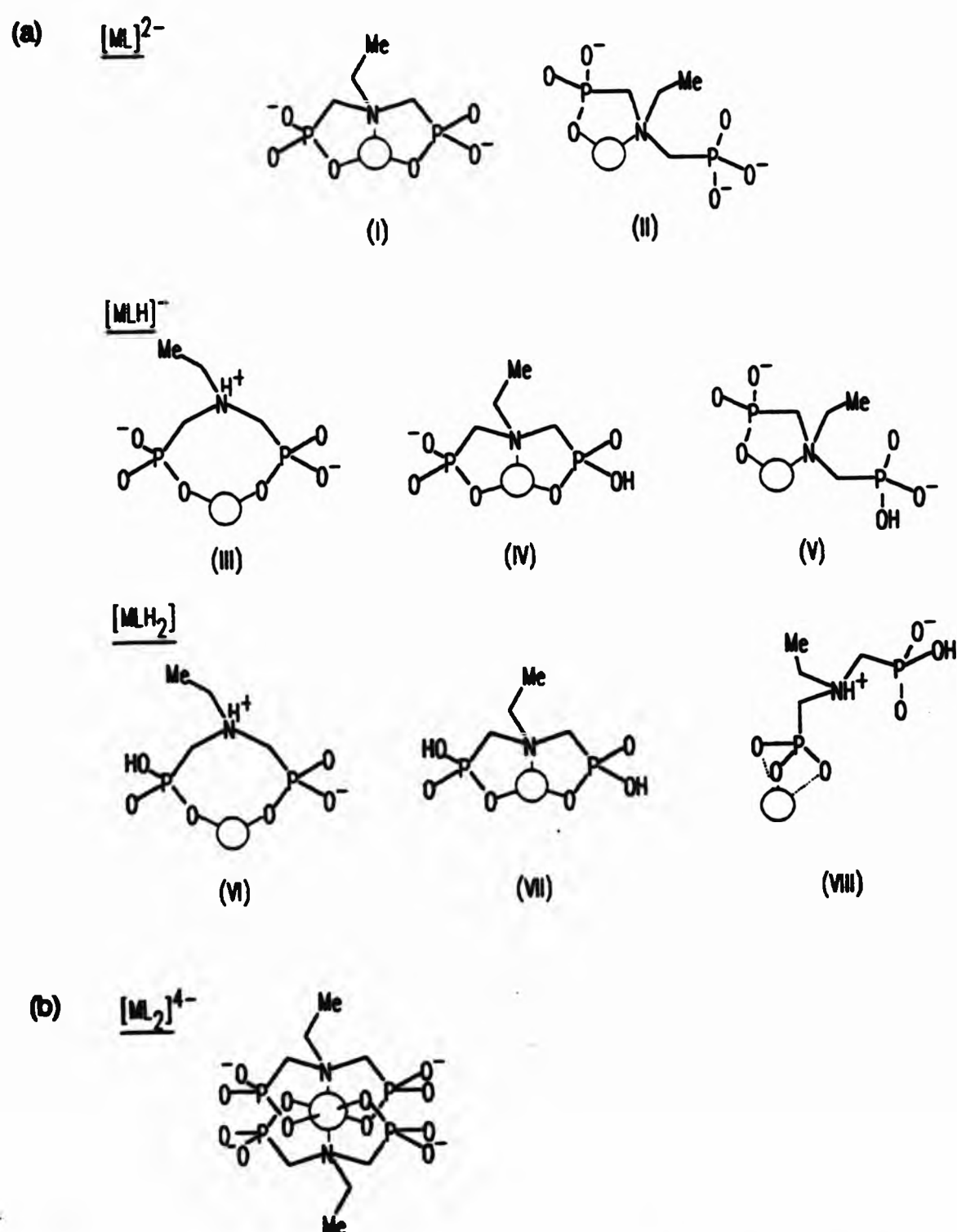


Figure 5.6.3 (a) Possible microscopic forms of species involved in deprotonation of $[MLH_2]$ [$L = CH_3CH_2N(CH_2PO_3)_2^{4-}$].
(b) A possible microscopic form for $[ML_2]^{6-}$.

Proton affinities

As might be expected, the inclusion of an extra methylenephosphonate group in EIDMPH₄ gives rise to a larger range of protonated metal complexes compared to DEAMPH₂. In this case complexes are formed with two different protonated forms of the ligand, giving rise to the species [MLH]⁻ and [MLH₂], for the Cu(II) and Ni(II) systems whereas both Cu(II)-DEAMPH₂ and Cu(II)-MEAMPH₂^[94,134] yield only one such complex, [MLH]⁺. These observations presumably result from the ability of the iminobis(methylenephosphonate) ligand to support larger positive charges than its amino-mono-methylenephosphonate analogues and, since substantial steric restriction of the ligand is not expected, maximise the charge separation between positive centres (e.g. VIII Fig. 5.6.3).

It is interesting to compare the stepwise protonation constants of EIDMPH₄ with those of [ML]²⁻; for the ligand, the second and third stepwise constants ($\log K_{011} = 6.34$, $\log K_{012} = 5.00$) correspond with single protonations of each phosphonate function (i.e. $-\text{PO}_3^{2-} + \text{H}^+ = -\text{PO}_3\text{H}^-$). The value of $\log K_{111}$ for Ni(II)-EIDMPH₄ (Table 5.6.2) is larger than either of these constants. If it is assumed that metal co-ordination does not increase the proton affinities of either phosphonate function in the molecule, this observation can only correspond with protonation at the nitrogen site in [MLH]⁻ eliminating structures IV and V (Fig. 5.6.2) from possible protonation schemes. Significantly, the preferred structure III corresponds with N-protonated structures proposed for alkaline earth metal complexes of NTMPH₆ from multinuclear nmr measurements.^[104] The value of $\log K_{112}$ in this system is comparable to those of the 'free' phosphonate groups in the ligand, suggesting a configuration such as VIII predominates for [MLH₂].

For Cu(II)-EIDMPH₄, both $\log K_{111}$ and $\log K_{112}$ are smaller than phosphonate protonations in the free ligand indicating that a deprotonation route from VII to IV to I may be feasible in addition to the routes outlined for the Ni(II) system. Interestingly, protonated O,N-chelating aminopropylphosphonate groups (essentially C-dimethyl substituted aminomethylenephosphonate arms) featuring protonation at the phosphonate function have been observed for Cu(II) in the solid state.^[139] Such co-ordination corresponds with structures VII and IV of Fig. 5.6.3.

For the bis-complexes modelled in both Cu(II)- and Ni(II)-EIDMPH₄, systems the vast number of co-ordination modes possible [each ligand may adopt any of the structures of Fig. 5.6.1(a) on co-ordination] precludes discussion of possible microspecies without further evidence. However, the high negative charge density in these complexes suggests that endo-, tridentate co-ordination of the each ligand, such as that shown for $[ML_2]^{6-}$ in Figure 5.6.1(b), is unlikely without some external charge stabilisation from interaction of $-PO_3^{2-}$ with either proton or other cationic species present in solution.

5.7 Studies of simple alkylphosphonic acids in dilute aqu. hydrogen peroxide solution

Having established the aqueous solution chemistry of some simple aminomethylenephosphonic acids, it was envisaged that similar techniques would allow their characterisation in aqu. H_2O_2 solution. Preliminary investigations into the possibility of obtaining potentiometric data from dilute aqu. H_2O_2 solutions (Section 4.6) were largely favourable, although it was observed that the reliability of the data diminished as concentrations of H_2O_2 in the solutions increased. Several factors, including ligand oxidation, were implicated in accounting for these observations. In order to establish whether similar problems affect titrations with aminomethylenephosphonic acids, a protonation study of 1-APP H_2 (Fig. 5.5.1) in 10 % aqu. H_2O_2 was undertaken.

5.7.1 A potentiometric study of 1-aminopropylphosphonic acid in 10% hydrogen peroxide solution

In contrast to protonation studies for 1-APP H_2 in aqueous solution, where three $\log \beta$ values were obtained (Section 5.3.1), those in aqu. hydrogen peroxide (10 % v/v; $I = 0.1 \text{ mol dm}^{-3}$, KNO_3) yielded only two constants, $\log \beta_{011} = 8.44 \pm 0.08$ and $\log K_{012} = 5.27 \pm 0.03$. Calibration and sample titrations were performed under analogous conditions to those employed during the study of glycine in 10% aqu. H_2O_2 (Section 4.6.3) and similar experimental effects were noted; e.g. stable and reproducible solution potential measurements were obtained from pre-treated glass electrodes yielding smooth titration curves although bubble evolution was observed in alkaline solution (above pH ca. 8.5-9.0). Similarly, apparent ionic products (pK_w^*) were depressed (to ca. 10.4) from those of aqu. solutions of KNO_3 .

The deviation of $\log \beta_{011}$ (-1.71 log units) from the value in aqueous solution

is somewhat larger than the analogous difference for glycine (-0.83). As observed for glycine, the depression of $\log \beta_{011}$ may indicate that a significant chemical change to the ligand occurs on contact with the peroxide medium. Although tertiary aminomethylenephosphonates are known to convert cleanly to their corresponding amine oxides in H_2O_2 ,^[140] oxidation of primary amines can lead to a number of products^[81] (Section 4.6.3); reaction of 1-APP H_2 with the titration solution is therefore possible. Indeed, substantial adjustment of ligand concentration [achieved by manual adjustment of (fixed) input ligand concentrations during SUPERQUAD^[25] refinement] was required for full refinement. A large standard deviation, calculated as part of SUPERQUAD^[25] output, was associated with $\log \beta_{011}$. The large difference between $\log \beta_{011}$ values in 10% aqu. H_2O_2 and in aqueous solution, compared to the smaller deviation for $\log \beta_{012}$ between the two solvent systems would be consistent with a chemical change on the ligand (e.g. oxidation by H_2O_2) occurring at the primary amine site, and may account for the difficulties encountered during data refinement.

Clearly the aqu. H_2O_2 chemistry of the aminomethylenephosphonic acids does not directly mirror their behaviour in aqueous solution. In particular, an understanding of interactions between the ligand and solvent is required before metal sequestering species in solution can be identified.

5.7.2 Chemical stability of 1-hydroxyethyl-1,1-phosphonic acid in aqu. hydrogen peroxide solution.

Potentiometric experiments in aqu. H_2O_2 have hinted that chemical changes may occur for organic substrates (see Sections 4.6.2, 4.6.3 and 5.7.1) on contact with solutions. In order to understand the modes of action by which the aminomethylenephosphonic acids stabilise aqu. H_2O_2 solutions, it is important to identify species present in solution and, in particular, investigate the

possibility that potential metal sequestrant ligands may be generated by chemical reaction with the solvent medium. A simple diphosphonic acid, 1-hydroxyethyl-1,1-diphosphonic acid (HEDPH_4 , Fig. 5.1.1), was chosen in order to directly probe the effects of H_2O_2 on the phosphonic acid function, in the absence of effects from potentially oxidisable amine groups. The compound was chosen as it has a widely studied chemistry^[141,142,143] and is commercially available in good purity [confirmed by preliminary ^{31}P nmr studies in $\text{H}_2\text{O}-\text{D}_2\text{O}$ (5 % D_2O v/v)] as its disodium salt (Warwick Chemicals MYKON P062, $\text{Na}_2\text{HEDPH}_2$). Furthermore, the compound has found commercial application as a stabiliser for *aqu.* H_2O_2 solutions although its long-term efficacy compares poorly with the aminomethylenephosphonic acids.^[144]

Phosphorus-31 nmr spectra were recorded for aqueous solutions derived from samples of $\text{Na}_2\text{HEDPH}_2$ which were subjected to different temperatures and concentrations of *aqu.* H_2O_2 (experimental conditions are summarised, and the resulting spectra are shown, in Figure 5.7.1). Phosphorus-31 chemical shifts were referenced to an external sample of *aqu.* H_3PO_4 (85 %) via sample substitution in this study. This 'non-standard' approach was used in this case so that signals due to reaction products would not be obscured by the reference signal.

Preliminary ^{31}P nmr spectra of $\text{Na}_2\text{HEDPH}_2$ were recorded as a function of concentration to establish the purity of the sample and deduce appropriate concentrations for subsequent study. Each showed a single resonance, consistent with a single 'time-averaged' environment for the phosphorus nuclei due to the anticipated 'fast exchange' conditions, and peaks attributable to phosphorus-containing sample impurities were absent. The ^{31}P chemical shift of HEDP^{4-} has been shown to be dependent on the degree of neutralisation of

the tetra-anion;^[108] measurements at 24.3 MHz on tetramethylammonium (Me_4N^+) salts of the acid give a range for $\delta(^{31}\text{P})$ between 19.8 ppm for the free acid and 18.6 ppm for the tetrakis-tetramethylammonium salt.^[108]

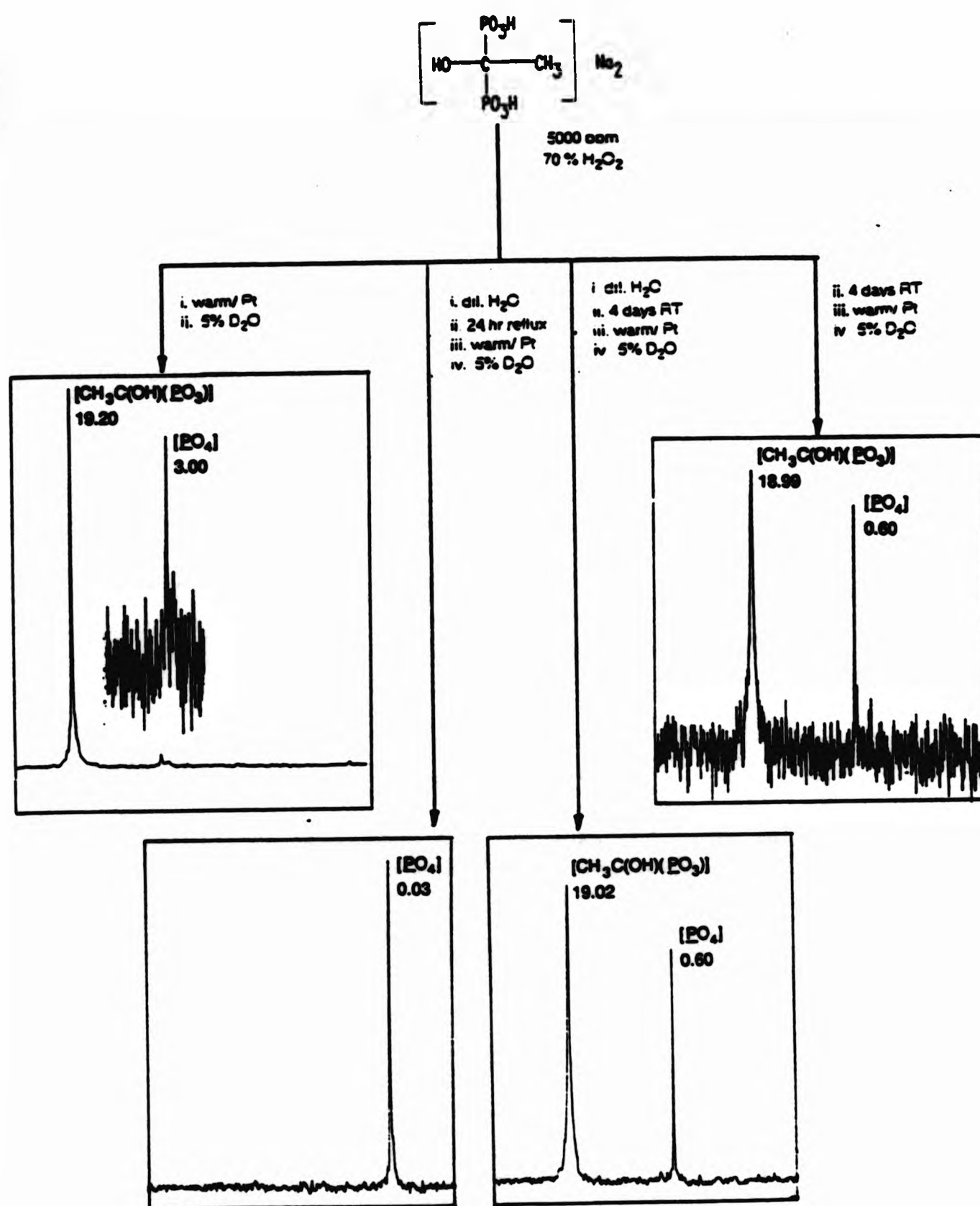


Figure 5.7.1 ^{31}P nmr spectra (showing chemical shifts in ppm) for samples of $\text{Na}_2\text{HEDPH}_2$ after treatment with hydrogen peroxide.

Phosphorus-31 nmr spectra of $\text{Na}_2\text{HEDPH}_2$ solutions prepared in 35 % and 70 % (v/v) *aqu.* H_2O_2 and stored at room temperature for ca. 96 hours [samples (3) and (4) respectively, Fig. 5.7.1], as well as the sample in which the peroxide was destroyed shortly after mixing [sample (1), Fig. 5.7.1], all showed two resonances. The major resonances in these spectra all lie within the chemical shift range for salts of HEDPH_4 ,^[108] and hence are assigned to HEDP^{4-} species. The minor peaks in these spectra indicate formation of a second phosphorus-containing species in the solutions. In contrast, the spectrum of the solution obtained after refluxing for 24 h [sample (2), Fig. 5.7.1] showed only one phosphorus-containing species; $\delta(^{31}\text{P})$ in this case corresponds with the minor signals observed in the other spectra. [Although intensities (heights) of these minor peaks apparently depend on the exposure time to peroxide, quantitative deduction of species' concentrations on this basis, or by peak integration, must be excluded because differences in longitudinal relaxation times (T_1) in the two ^{31}P environments^[145] may lead to attenuation of signals]. The upfield signals in the spectra appear around 0 ppm and hence are assigned to orthophosphate (PO_4^{3-}) species. Studies of the pH dependence of $\delta(^{31}\text{P})$ for orthophosphoric acid show signals moving to lower field, from 0 ppm to 6 ppm, as H_3PO_4 deprotonates.^[146,147] All shifts of the upfield resonances in this study lie within this range. Significantly, shifts of oligo- and polyphosphates lie upfield from this region; e.g. $\delta(^{31}\text{P})$ for $\text{P}_3\text{O}_{10}^{5-}$ varies between -11 ppm and -4 ppm between pH 2 and 13.^[147]

In a parallel study,^[148] each solution was analysed by ion chromatography. The results confirmed the presence of both phosphonate and orthophosphate anions in samples (1), (3) and (4), and negligible concentrations of phosphonate in comparison with orthophosphate for sample (2). Chromatograms recorded before and after H_2O_2 was decomposed with a platinum metal catalyst

indicated that phosphonate and phosphate concentrations in each solution remained essentially unchanged. Concentrations of species deduced in this latter study broadly correlate with qualitative assessments that can be derived from peak heights of ^{31}P signals. Both sets of results indicate that a chemical transformation involving cleavage (possibly by hydrolysis/peroxidolysis) of the phosphorus-carbon bonds of HEDP^{4-} occurs in $\text{aqu. H}_2\text{O}_2$ solutions and that more forcing conditions increase the amounts of phosphate formed. Clearly, more detailed experimentation is required before the mechanism of the reaction can be understood.

5.7.3 Multinuclear nmr studies of DEAMPH_2 in aqueous and $\text{aqu. H}_2\text{O}_2$ hydrogen peroxide.

Studies of the behaviour of diethylaminomethylenephosphonic acid (DEAMPH_2) as a function of pH and its interaction with hydrogen peroxide under similar conditions were performed using both carbon-13 and phosphorus-31 nmr spectroscopy. (Proton nmr studies were unfortunately precluded by the unavailability of deuterated H_2O_2). The model compound, DEAMPH_2 (Fig. 5.1.1) was chosen for these studies because its nmr spectra are uncomplicated; the ^{13}C nmr spectrum is simplified by equivalence of the ethyl carbons while the ^{31}P spectrum shows one peak and the pH dependence of $\delta(^{31}\text{P})$ in aqueous solution, and the speciation of DEAMPH_2 in aqueous solution, has been established (Section 5.5.2). Additionally, DEAMPH_2 contains a tertiary amine site and is therefore expected to give only one oxidation product, i.e. the amine oxide, ^[81,142] on reaction with H_2O_2 .

Broad band ^1H -decoupled carbon-13 spectra of DEAMPH_2 in 10 % $\text{aqu. H}_2\text{O}_2$ solution were recorded on mixing and thereafter at two-hourly intervals for 12 h, in the expectation that any reaction of the phosphonic acid with the solution would lead to the appearance of extra carbon-13 signals in the

spectrum. The ^{13}C spectrum of DEAMPH_2 obtained under these conditions (the apparent pH = 3.0 on dissolution and remained approximately constant throughout the study) was readily assigned; methylene carbon signals, split into doublets from coupling to the phosphorus atom, were separated by comparing the relative magnitudes of the observed ^{13}C - ^{31}P couplings ($^3J_{\text{CP}} = 4.3 \text{ Hz}$ and $^1J_{\text{CP}} = 137.9 \text{ Hz}$), while methyl resonances, unsplit by long range ^{13}C - ^{31}P coupling, appeared as singlets at higher field. Carbon-13 spectra of the solution did not change significantly throughout the investigation and, furthermore, its ^{31}P nmr spectrum remained unchanged after three months.

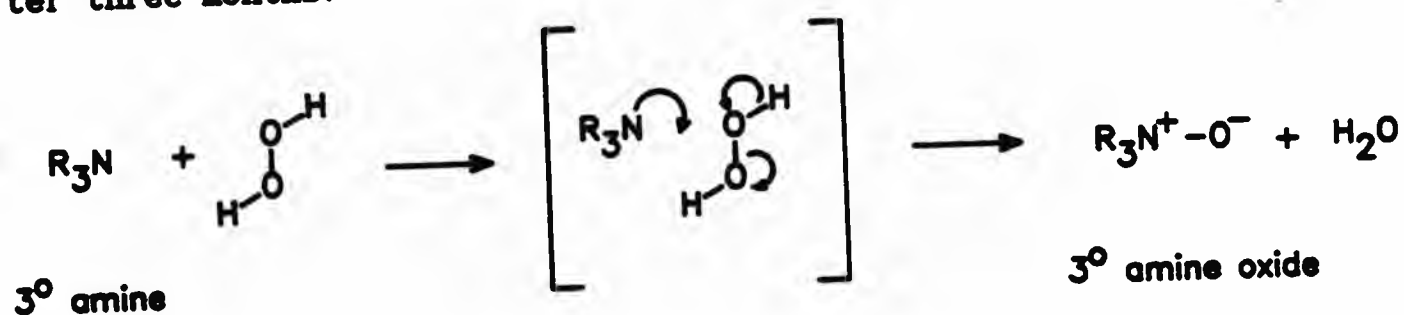


Figure 5.7.2 Mechanism for oxidation of a tertiary amine by hydrogen peroxide. [81]

The molecule clearly resists attack by H_2O_2 at this concentration and pH. Amine oxidation is slowed in acidic solution and is dependent on the availability of the nitrogen lone pair for attack on H_2O_2 . [81] A study of the kinetics of N-oxidation of EDTMPH_8 [and its carboxylic acid analogues, ethylenediaminetetrakis(acetic acid) EDTA and diethylenetriaminepentakis(acetic acid) DTPA] by substituted peroxybenzoic acids indicated a mechanism involving nucleophilic attack of the nitrogen of the substrate on the outer peroxidic oxygen of the perbenzoic acids. [149] For N-oxidation with H_2O_2 , a corresponding scheme (Fig. 5.7.2) [81] presumably applies. If the amine of DEAMP^{2-} is protonated, as is probable at this pH (see Section 5.5.2), its lone pair is no longer available for attack on H_2O_2 , implying that oxidation will only occur at higher pH than those employed here. These observations

naturally suggested that nmr techniques should be used to study possible aminomethylenephosphonic acid interactions as a function of pH.

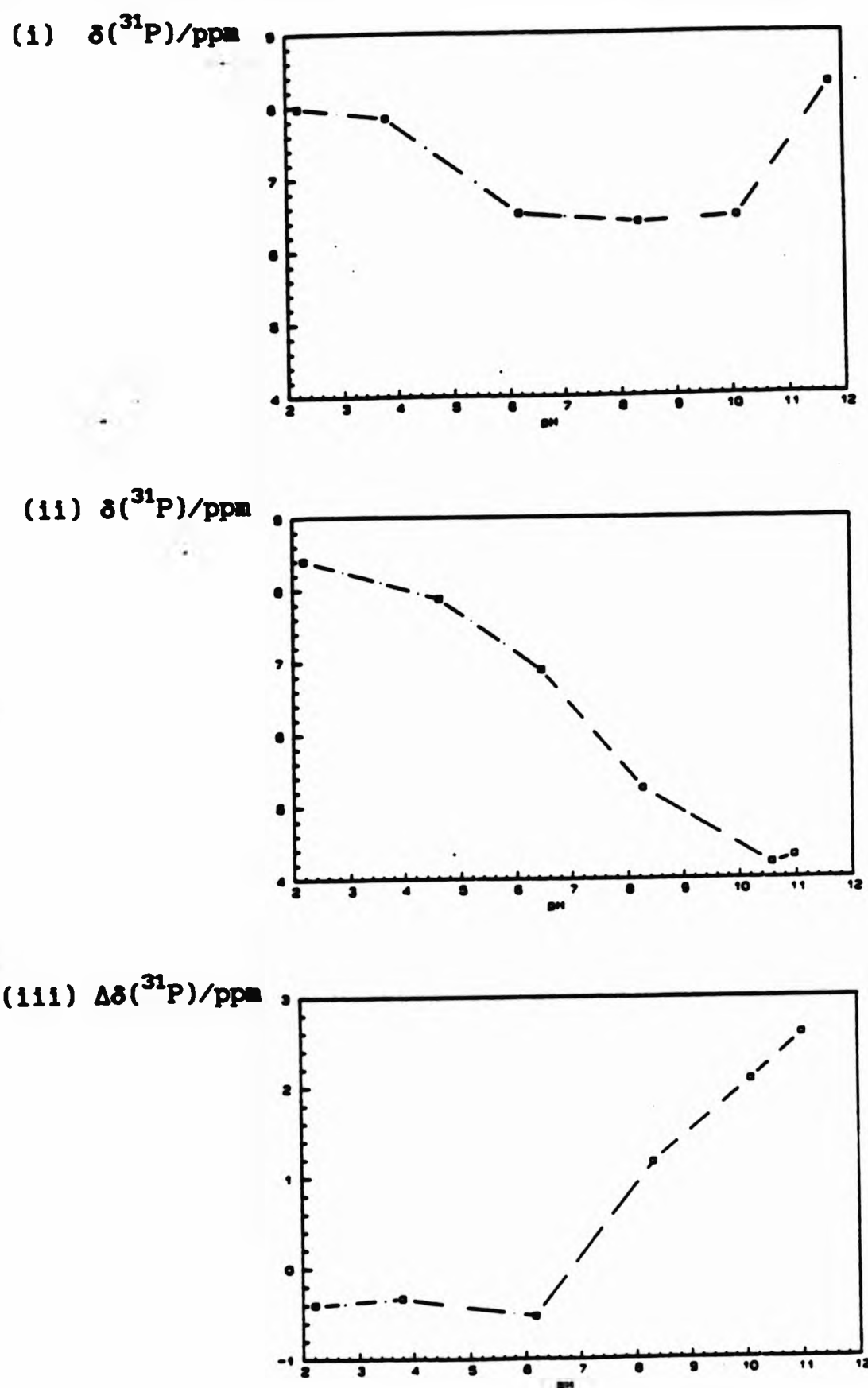


Figure 5.7.3 Plots of $\delta(^{31}\text{P})$ vs. pH for solutions of DEAMPH₂ in (i) aqu. D₂O (5 % v/v) and (ii) aqu. D₂O (5 % v/v) after treatment with H₂O₂. Induced changes in $\delta(^{31}\text{P})$ [$\Delta\delta = \delta_{\text{'aqueous'}}$ - $\delta_{\text{'peroxide'}}$] are plotted vs. pH in (iii).

Aminomethylenephosphonates have pH-dependent ^{31}P nmr shifts. As noted in Section 5.5.2, it has been widely observed that ^{31}P signals of these compounds shift downfield on protonation at the phosphonate site [26,82,100,101,102,103,104,105,106,107,108] whilst protonation at the amine induces larger upfield shifts for $\delta(^{31}\text{P})$. [26,100,101,104,105,106,107] Investigation of any pH dependence of the H_2O_2 interaction with DEAMPH_2 using ^{31}P nmr therefore required an investigation of the pH dependence of $\delta(^{31}\text{P})$ of DEAMPH_2 under analogous conditions in aqueous solution.

The investigation was carried out in water containing 5% deuterium oxide to give a ^2D lock signal and thereby enable ^{31}P shifts to be referenced to external 85 % aqu. H_3PO_4 via sample substitution. In this qualitative investigation, solution pH was adjusted with aqu. HNO_3 or aqu. NH_3 solutions. Although pH was not corrected for any effects of the ^2D isotope, [131] the low concentration of ^2D in the solution was assumed have a negligible effect on pH meter readings. In contrast to the preceding study (Section 5.5.2), these experiments were carried out without control of solution ionic strength and aqueous ammonia was employed as base in order to overcome possible metal complexation effects. Geraldès and co-workers have noted that the presence of alkali metal ions can affect magnitudes of $\Delta\delta$ in this type of experiment. [101] Broad-band ^1H -decoupled phosphorus-31 spectra were obtained for DEAMPH_2 under these conditions for 6 solutions between pH 2 and 12, and, as expected, all spectra showed a single peak; the variation of $\delta(^{31}\text{P})$ with pH is shown in Figure 5.7.3.(1).

The ^{31}P shift plotted against pH [Fig. 5.7.3(1)] shows a similar pH dependence to that observed for DEAMPH_2 under more controlled conditions [Fig. 5.5.3(1)], and resembles variations of $\delta(^{31}\text{P})$ observed in other simple

aminomethylenephosphonate systems.^[103,105,106] The ^{31}P signal shifts upfield as neutralisation of the acidic solution proceeds, consistent with deprotonation of the phosphonic acid group in the molecule, with the largest rate of change being seen at ca. pH 5.2. Little change in $\delta(^{31}\text{P})$ is observed over the region from pH 6 to 10, before a large downfield shift (ca. 2 ppm), indicative of deprotonation of the ammonium function of DEAMPH^+ , occurs between pH 10 and 12. The correlation between regions of the curve with the largest gradient ($\Delta\delta/\Delta\text{pH}$) and protonation constants for DEAMPH_2 ($\log \beta_{011} = 11.55$, $\log K_{012} = 5.28$; Section 5.5.1) further confirms the protonation sequence deduced for DEAMPH_2 (Fig. 5.5.2).

The ^{31}P shift for DEAMPH_2 after treatment with 35 % aqu. H_2O_2 over a similar range of pH is significantly different to the profile for the untreated ligand. As observed in the $\text{Na}_2\text{HEDPH}_2/\text{H}_2\text{O}_2$ study (Section 5.7.2), shift referencing by sample substitution is advantageous in this case as emergent peaks around 0 ppm, corresponding to formation of phosphate species, are not obscured by the reference signal. However, each spectrum showed only one signal, downfield from this region, and the dependence of $\delta(^{31}\text{P})$ on pH is shown in Figure 5.7.3.(ii). Increases in sample pH, up to 1.11 pH units, were observed after reaction periods and procedures to destroy H_2O_2 had been completed. These changes may arise from a number of effects including the depression of apparent pH readings in H_2O_2 solution.^[73] Observations during the preceding study of $\text{Na}_2\text{HEDPH}_2$ in H_2O_2 (Section 5.7.2) suggest that organic species in these solutions are unlikely to be affected by the peroxide decomposition procedures employed. Other workers have found organic substrates to be unaffected by decomposition of H_2O_2 with various heterogenous catalysts including platinum.^[150]

The ^{31}P shifts in solutions below pH 7 are closely similar to the corresponding shifts of DEAMPH_2 . The $\delta(^{31}\text{P})$ vs. pH plot [Fig. 5.7.3(i)] shows a smooth upfield change in $\delta(^{31}\text{P})$ with pH consistent with deprotonation of phosphonic acid sites. The comparability of $\delta(^{31}\text{P})$ for the aqueous and H_2O_2 -treated solutions below pH 7 supports the observation from the preceding ^{13}C nmr study that DEAMP^{2-} remains intact in acid solution. Changes in $\delta(^{31}\text{P})$, attributed to exposure of DEAMPH_2 to H_2O_2 , may be highlighted by plotting the difference between $\delta(^{31}\text{P})$ for the aqueous and peroxide systems at the same pH [i.e. $\Delta\delta$, Fig. 5.7.3(iii); $\delta(^{31}\text{P})$ for the aqueous system at a specified pH was obtained by interpolation from a smooth curve through the points of Fig. 5.7.3(i)].

Significant changes in ^{31}P shift after exposure to H_2O_2 are apparent above pH 8, and $\Delta\delta$ increases with pH in this region. The sharp downfield shift of $\delta(^{31}\text{P})$ expected on deprotonation of DEAMPH^- is not observed in peroxide-exposed solutions of DEAMPH_2 suggesting that either the amine proton has become substantially more basic or that the proton is absent altogether. The latter would be consistent with N-oxide formation. Although within experimental error, the small shift to higher frequency between pH 10 and 11 (ca. 0.1 ppm) is reminiscent of similar shift effects observed on removal of the final proton of nitrilotris-(methylenephosphonic acid)-N-oxide (assigned as the -NOH deprotonation of the amine oxide).^[102] Over the majority of the pH range 8-11, unreacted ligand species are expected to be singly protonated (i.e. DEAMPH^-). Studies in aqueous solution indicate that the zwitterion form of this species is predominant (Section 5.5). Protonation at the nitrogen site in this species presumably inhibits N-oxidation of the ligand, contrary to the observations above. However, broadening of ^{31}P signals in this pH region (Section 5.5.2) suggests slow exchange and hence that the nucleophilic

molecular form of DEAMPH⁻ [the minor species in the micro-equilibrium; Fig. 5.5.2(i)] may be present in sufficient abundance to drive the reaction. Davis and Jones account^[149] for the oxidation of EDTMPH₈ by substituted perbenzoic acids on this basis and observe that its oxidation rates are more rapid than those of its aminocarboxylic acid analogue, EDTA, despite the higher basicity of the aminomethylenephosphonate ligand.

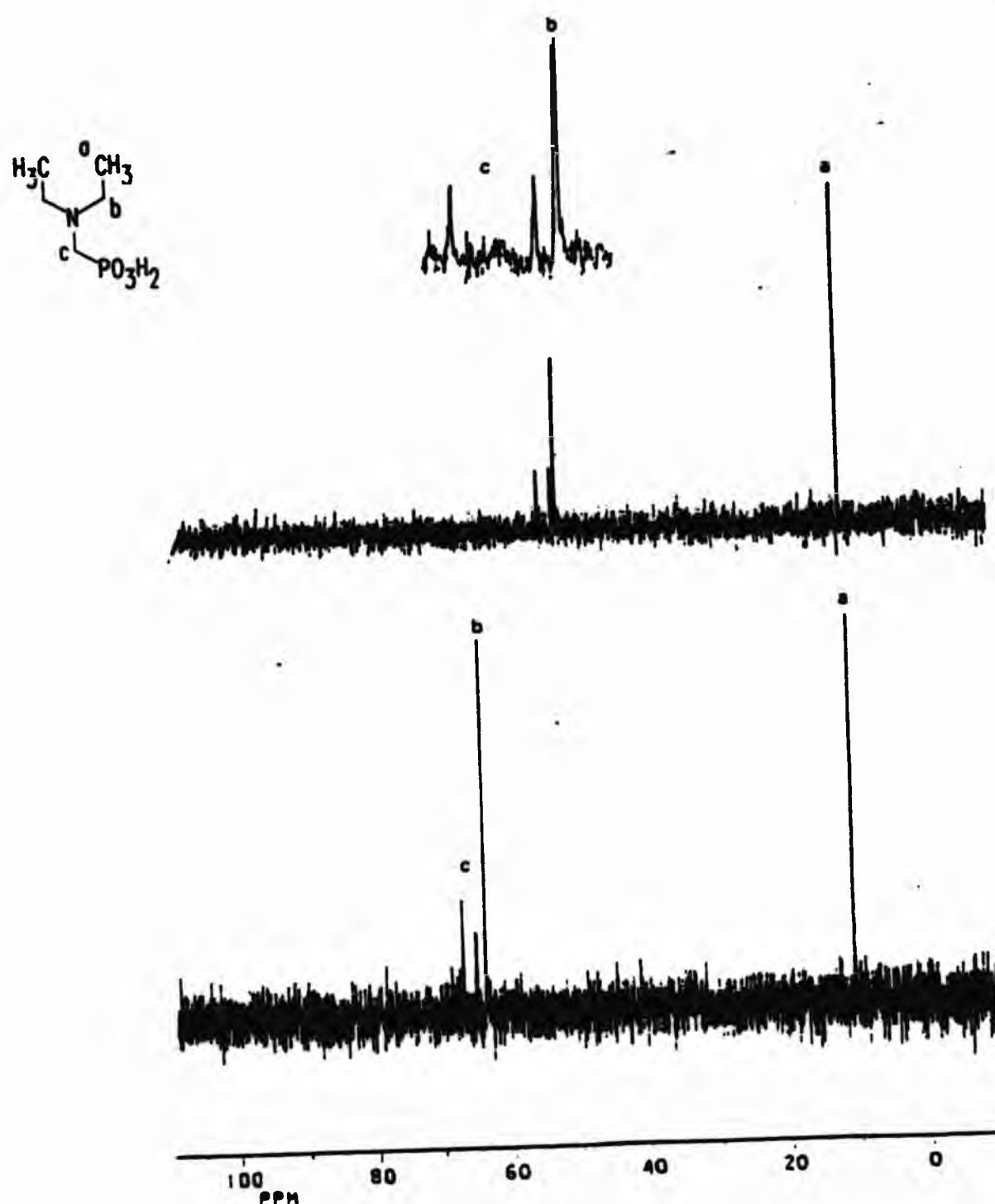


Figure 5.7.4 Carbon-13 spectra of solutions of DEAMPH₂ in (i) aqu. D₂O (5 % v/v) and (ii) aqu. D₂O (5 % v/v) after treatment with H₂O₂.

Comparison of carbon-13 spectra for aqueous and H_2O_2 -treated solutions at pH 8 [where $\Delta\delta(^{31}\text{P})$ becomes significant] provides further evidence for chemical reaction at the amine site of the ligand. The spectra (Fig. 5.7.4) show significant deshielding (ca. 12 ppm) for both methylene carbons connected to the amine nitrogen in the peroxide-treated solution. A much smaller shielding effect (0.67 ppm) is seen for the methyl carbons. Retention of the one bond phosphorus coupling to the adjacent methylene carbon in the H_2O_2 -treated solution confirms that the P-C bond in the molecule remains intact although, interestingly, the three bond ^{13}C - ^{31}P coupling observed for methylene carbons of ethyl groups in the unreacted ligand disappears after exposure to H_2O_2 .

The signs of $\Delta\delta(^{13}\text{C})$ [$= \delta(\text{H}_2\text{O}_2) - \delta(\text{H}_2\text{O})$] for are in agreement with those quoted^[151] for the α - and β -piperidine carbons on N-oxidation of a series of N-(4-substituted phenyl)piperidines. The magnitude of the 'oxidation effect', $\Delta\delta = +19$ ppm for the α carbons and -4 ppm for the β carbons, is somewhat larger than that observed for DEAMPH_2 . [Some pH dependence is expected for the ^{13}C spectrum of DEAMPH_2 , as is the case for its ^1H ^[105] and ^{31}P (Section 5.5.2) nmr spectra, which may affect comparisons of $\Delta\delta(^{13}\text{C})$ in this study.]

The results obtained from this study indicate that hydrogen peroxide interacts with DEAMPH_2 at the nitrogen site of the molecule, probably leading to the formation of the N-oxide. Oxidation of the ligand in this way seems to be significant only in basic solution (under the reaction conditions employed).

The metal ion catalysed decomposition of H_2O_2 is characterised by one electron steps involving formation of radical intermediates by alternate oxidation and reduction. The main features of decomposition catalysed by iron(III) have

been explained with an extended version ^[152] of the Haber-Weiss cycle [reactions (1), (2) and (3)]. ^[153] Reaction (2) of the cycle proceeds slowly, if at all, in the absence of metal ions, ^[154] but is catalysed by reaction (4) and reaction (5) (the so-called Fenton reaction) when metal ions are present.



In order to inhibit decomposition, one or more of these reactions must be retarded by the action of the stabiliser (or its derivatives in solution). Sequestration of the metal ion by the stabiliser may result in slowing reactions (1), (4) and (5) although simple co-ordination of the metal is not sufficient to achieve its deactivation; indeed Wang ^[155] demonstrated that the triethylaminetriamine complex of iron(III) is an efficient catalyst for H_2O_2 decomposition. Alternatively, the stabiliser (or its derivatives) may scavenge hydroxyl and hydroperoxide radical intermediates formed during decomposition, thereby interrupting the cycle.

Gilbert and co-workers ^[156] have suggested that in stabilising the higher (III) oxidation state of the metal, the aminomethylenephosphonic acids retard reactions (1) and (4). The high negative charges that can be supported by the aminomethylenephosphonate ligands presumably play some rôle in stabilising Fe^{III} . Interestingly, by stabilising the higher oxidation state, substantial increases in the rate of the Fenton reaction (5) over those of Fe^{II} in the

presence of EDTA, and even hydrated Fe^{II} , are observed in these phosphonate systems. [86]

While this mechanism applies when the aminomethylenephosphonic acids remain intact in solution, the observations recorded in this study suggest that the ligands form their corresponding N-oxides in basic solution. Significantly, the oxides of aminocarboxylic acids are known to stabilise $\text{aq. H}_2\text{O}_2$ solutions [156] and Gilbert and co-workers have investigated the potential of these compounds and the N-oxides of the aminomethylenephosphonic acids as radical scavengers. [86] They observe that while the N-oxides of EDTMPH_8 and diethylenetriaminepentakis(methylenephosphonic acid) scavenge hydroxyl radicals efficiently, forming stable nitroxide radicals such as $[\text{ON}(\text{CH}_2\text{PO}_3^{2-})_2]^\cdot$, in the process, the N-oxide of NTMPH_6 shows negligible reactivity towards $\cdot\text{OH}$. The authors conclude that radical scavenging, via transformation of the aminomethylene- phosphonic acid to the N-oxide in H_2O_2 solution, is unlikely to be the primary mode of action for these ligands given the dilute solutions that affect stabilisation [HO^\cdot is more likely to encounter H_2O_2 and perpetuate the chain via reaction (3)] and that NTMPH_6 is an efficient stabiliser for H_2O_2 solutions despite the unreactivity of its N-oxide towards $\cdot\text{OH}$.

The amine oxides retain the ability to co-ordinate metals. Indeed NTMP and NTMP-N-oxide have similar affinities for Mg^{2+} and Ca^{2+} , [102,105] and as the ligands retain the overall charge of the parent aminomethylenephosphonates, it is possible that they may stabilise higher oxidation states in complexation. This suggests that they may stabilise H_2O_2 via a similar mode to that of the unoxidised acids. Furthermore, their stabilising action in some cases may be enhanced by holding the radical generating centre (i.e. the metal ion) in

close proximity to a radical trap and thereby reduce initiation of chain reactions by limiting the diffusion of radicals into the bulk solvent.

6. Potentiometric investigations into functionalised pyridine macrocycles in 95 % methanol-water solution

6.1 Potentiometric titrations in methanol/water medium

As organic ligands become more complicated in design, their solubility in water often diminishes as a consequence. Traditional, aqueous-based potentiometric methods for determination of stability constants are inappropriate for equilibrium studies with such compounds. As a result, non-aqueous solvents and solvent mixtures are becoming more widely adopted to circumvent problems of this type.^[74,157] The similarity of the protolytic behaviour of water and the low molecular weight alcohols has led to the adoption of *aqu.* methanol and ethanol mixtures for a number of acid-base potentiometric studies.^[28,80,158]

The solution chemistry of some macrocyclic ligands and their metal complexes is described in the following sections. As a result of their insolubility in aqueous media, *aqu.* methanol media were used to establish protonation and metal-ion stability constants for these ligands by potentiometric acid-base titration. Definitive procedures for stability constant determinations by potentiometry in solvents other than water^[32] have yet to be established and therefore, a description of the composition of the potentiometric cell and results of cell calibrations is presented to establish the validity of the potentiometric method adopted herein.

6.1.1 Composition of the potentiometric cell

The potentiometric cell employed for these studies is derived from that developed by Anderegg and Lindoy in studies of dibenzomacrocycle-metal

systems in 95 % aqu. methanol solution.^[28] The cell comprises a glass electrode (pretreated by soaking in 95 % aqu. methanol) referenced to calomel electrode via a salt bridge containing a solution of a background electrolyte salt in aqu. methanol (95 %, v/v). Although Lindoy and co-workers have deployed a range of alkylammonium salts as background electrolytes in cells of this type, the majority of their recent studies^[159] use $(C_2H_5)_4NClO_4$. Similar conditions are adopted for these studies and the results reported herein are directly comparable with the growing body of data obtained for macrocyclic ligands under these conditions.

Liquid-liquid junctions at the salt bridge-test solution and salt bridge-calomel electrode interfaces are maintained with porous glass sinters. The calomel electrode employs a 'non standard' solution phase, $(C_2H_5)_4NClO_4$ (0.095 mol dm⁻³) and $(C_2H_5)_4NCl$ (0.05 mol dm⁻³) in 95 % methanol-water, which is expected to minimise diffusion effects at the salt bridge-calomel interface. Braibanti and Fisicaro have noted the importance of using compatible solvents at liquid-liquid junctions;^[57] in their studies of cell performance in 90 % aqu. MeOH, discontinuities in branches of Gran plots obtained for strong acid-strong base titrations were attributed to precipitation of KCl at the liquid junction of the mixed solvent and the aqueous KCl solution of a saturated KCl/calomel reference electrode.

The cell employed in this study yields stable and reproducible potential readings. A strong indication of the validity of the potentiometric method for these cells derives from the excellent linearity observed for Gran plots of strong acid-strong base titration data; for example, linear least squares analysis of each branch of the Gran plots derived from typical calibration data (CALIBII40, Fig. 6.1.1) yields correlation

coefficients in excess of 0.999.

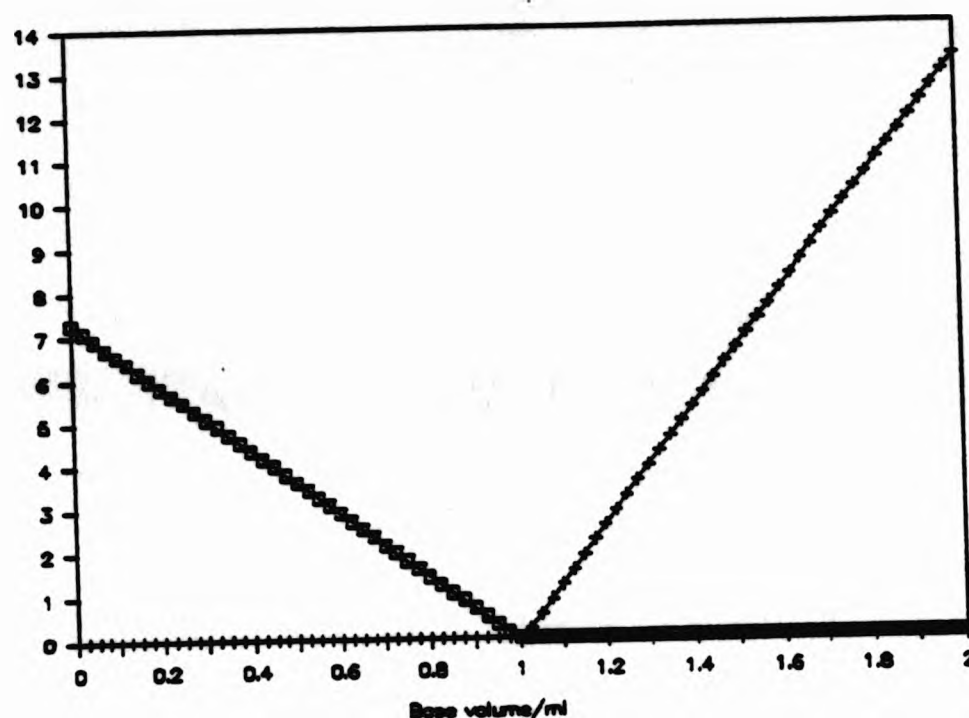


Figure 6.1.1 Plots of Gran functions vs. volume of added base for a strong acid-strong base titration (CALIBII40) in 95 % aqu. methanol solution [$I = 0.1$, $(\text{C}_2\text{H}_5)_4\text{NClO}_4$; 25°C]. [\square shows $(V_0 + v)10^{-EF/2.303RT} \times 10^{-3}$; $+$ shows $(V_0 + v)10^{EF/2.303RT} \times 10^{-8}$].

6.1.2 Cell calibration

Calibration of cells with 95 % methanol-water solution was achieved using strong acid-strong base titration procedures closely analogous to those deployed for aqueous and aqu. H_2O_2 solutions (see Sections 4.4 and 4.6.2 respectively). Cell parameters calculated from calibration titration data sets obtained in 95 % aqu. CH_3OH are shown in Table 6.1.1. These data sets were obtained during routine operation of the automated titration system over a 25 day period and show typical inter- and intra-titration variations of the cell parameters observed for the methanol-water medium deployed. Comparison of the cell constants with those obtained in aqueous and aqu. H_2O_2 systems (see Tables 4.4.1 and 4.6.2) reveals, as might be expected, a substantial

increase of the effective ionic product of the medium, pK_w^* consistent with the higher pK_a of pure methanol compared with those of H_2O and H_2O_2 .^[62,69] Comparisons of the magnitudes of E_0 between the titration media are inappropriate as the different sampling and reference electrodes involved in the respective studies lead to different contributions of E_{SCE} and E_{asy} to E_0 (see Eqns. 4.4.1 and 4.4.2).

Table 6.1.1 Cell constants obtained for *aqu.* methanol solutions.^a

	v_e^b/cm^3	E_0^c/mV	pK_w^{*d}
CALIBII37	0.9877	288.52(0.55)	15.038(0.007)
CALIBII38	0.9950	288.80(0.62)	15.007(0.010)
CALIBII40	0.9950	290.43(0.58)	15.051(0.007)
CALIBII41	1.0086	290.66(0.56)	15.052(0.011)
CALIBII42	0.9890	290.84(0.54)	15.064(0.008)
CALIBII43	1.0631	290.68(0.55)	14.974(0.008)
CALIBII45	1.0746	288.75(0.54)	15.021(0.009)
Mean ^e	1.0161(0.0403)	289.81(1.16)	15.030(0.034)

^a *Aqu.* CH_3OH solutions (95 %, v/v) of $HClO_4$ [0.004 mol dm^{-3} ; $I = 0.1$ mol dm^{-3} , $(C_2H_5)_4NClO_4$] titrated against $(C_2H_5)_4OH$ [0.1 mol dm^{-3} in *aqu.* CH_3OH (95 %, v/v)]. Cell parameters calculated using S.SCMCAL.^[40] ^b Volume of equivalence estimated from second derivative procedure with S.SCMCAL.^[40]

^c Standard deviation in parentheses. ^d Effective ionic product. Standard deviation in parentheses. ^e Grand mean for values presented. Standard deviations in parentheses.

The intra-titration variation of cell parameters is characterised by standard deviations for the cell constants calculated for each data set. Comparing these values for E_0 in 95 % *aqu.* methanol with those for aqueous media (see Table 4.4.1) reveals somewhat larger intra-titration variations. Similarly, larger intra-titration variations are obtained for pK_w^* in methanol-water. In

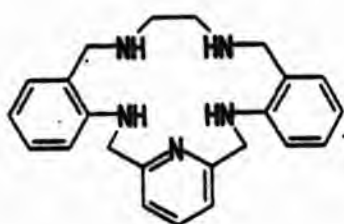
the absence of suitable ionic mobility data in methanol-water solution, junction potentials are calculated in S.SCMCAL^[40] (see Section 4.4.4) using ionic mobilities for the respective ions in aqueous solution. Thus, the larger intra-titration variations of E_0 and pK_w^* in methanol-water are attributed to poorer estimates of junction potentials generated at the sample-salt bridge interface in this medium.

In contrast, the differences in inter-titration variations, characterised by the standard deviations of averaged values of cell parameters, between the two media are less obvious (see Section 4.4.6). It was noticed, however that the long term stability of cells using methanol-water medium can be severely affected by deposition of the background electrolyte on salt bridge sinters. In such instances, serious drifts of E_0 values resulted which were rectified only by cleaning/replacement of the salt bridge. The moderate solubility of $(C_2H_5)_4NClO_4$ in methanol [samples were recrystallised from this solvent during preparation (see Section 3.2.9)] is presumably responsible for these effects.

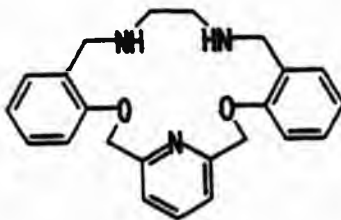
These results further demonstrate that, while the accuracy of calibration parameters obtained in methanol-water system is somewhat poorer than that of a purely aqueous system, cell constants obtained in this medium are reliable and reproducible to a good level of accuracy.

6.2 Complexes of a pentaaza macrocycle

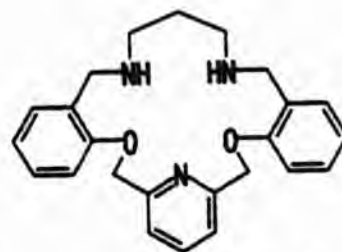
The dibenzo-pyrido penta-aza macrocycle (NpynNenH₄) was synthesised as part of a matrix of quinquedentate macrocycles developed by Fenton and co-workers.^[160,161] Copper, nickel, zinc, cadmium, mercury and silver complexes of the macrocycle have been isolated and characterised and X-ray structural studies indicate that the ligand imposes distorted co-ordination geometries in its complexes.^[162] Imposition of such distortions can form the basis for metal-ion selectivity by 'dislocation discrimination'.^[163] A potentiometric investigation into the stability of the Cu(II), Ni(II), Zn(II) and Cd(II) complexes in aqu. methanol (95 % v/v) solution was undertaken in order to establish metal-ion affinities for the ligand. The poor aqueous solubility of the ligand precludes its study in aqueous solution but the development of methanol-based titration environments (see above) allowed its solution chemistry to be investigated. The conditions used in this study mirror those deployed by Lindoy and co-workers^[28,164] and as such allow direct comparison with a substantial volume of data obtained for a 'matrix' of macrocyclic compounds.



NpynNenH₄



OpynNenH₄



OpynNtnH₄

6.2.1 The protonation constants for NpynNenH₄.

The protonation constants were determined for the ligand by titration of an acidified solution of the free base with Et₄NOH (experimental details are given in Section 3.2.12). The sample of ligand used was doubly recrystallised from ethanol and its purity, particularly the absence of any [2+2] product,

was established by ^1H and ^{13}C nmr, microanalysis and FAB mass spectrometry.^[162a] Titration curves were obtained for two different proton to ligand ratios (4:1 and 3:1) and each showed two inflections corresponding to the neutralisation of three protonated functions in the ligand. In both cases, the inflection around pH 9 corresponds to a single ligand equivalent of base, while the broader deviation at pH 3.5-5.6 includes two overlapping end points. Titrations with proton to ligand ratios of ca. 4:1 were performed during the development of the titration apparatus and as such were subject to larger thermal and electrochemical variability during data collection. Therefore detailed refinements, using both MINIQAD^[16,22] and SUPERQUAD^[25] were performed with data sets with H:L = 1:3 only and the results from these are summarised in Table 6.2.1. Small inter-titration variations are observed for $\log \beta_{011}$ and $\log \beta_{012}$, while the variation of $\log \beta_{013}$ is somewhat larger though still acceptable. Significantly, the formation constants obtained are independent of the refinement program employed. Although the titrations were performed with initial proton to ligand concentrations in ratios of ca. 3:1, a tetraprotonated species, $[\text{LH}_4]^{4+}$, was modelled successfully in two data files. In all other cases, however refinement of models including this species were unsuccessful; either $\log \beta_{014}$ assumed a negative value during a refinement iteration and was therefore rejected (MINIQAD) or was reported as negative on convergence (SUPERQUAD). Clearly, amounts of $[\text{LH}_4]^{4+}$ are negligible in the pH ranges investigated, (presumably due to destabilising charge repulsions within the constrained macrocyclic ring) and models corresponding to the formation of $[\text{LH}]^+$, $[\text{LH}]^{2+}$ and $[\text{LH}_3]^{3+}$ best describe the system at these concentrations. These observations were confirmed using data generated under similar conditions with an established titration system.^[26] In two data files (N5P3 and N5P4) SUPERQUAD refinements yielded χ^2 values greater than 12.6, the 95 % confidence level.^[24] However these were included in the final average

because alternative models yielded either a higher χ^2 value or returned negative (and therefore meaningless) $\log \beta$ values.

Table 6.2.1 Refinement summary for protonation of NpynNenH₄.^a

	log							pH range ^b	dp ^c	χ^2	σ
	β_{011}	β_{012}	K_{012}	β_{013}	K_{013}	β_{014}	K_{014}				
N5P1											
d, e	9.08	14.19	5.11	17.78	3.59			3.05-9.09	48	9.00	0.3650
f	9.11	14.26	5.15	17.82	3.56	19.73	1.91	3.05-9.09	48	12.67	0.3414
N5P3											
d, e	9.05	14.06	5.01	17.31	3.25			2.76-9.62	61	13.10	0.3905
f	9.05	14.08	5.03	17.29	3.21	18.74	1.45	2.76-9.62	61	15.72	0.3847
g	9.11	14.17	5.06	17.46	3.29	18.62	1.16	2.74-9.62	62	0.004845 ^h	
N5P4											
d, e	9.09	14.06	4.97	17.05	2.99			3.15-9.30	54	13.56	0.4835
f	9.17	14.17	5.00	17.47	3.30	i		3.15-9.30	54	6.74	0.2569
g	9.15	14.16	5.01	17.22	3.06	j		3.15-9.30	54	0.005537 ^h	
N5P5											
d, e	9.07	14.03	4.96	17.03	3.00			3.08-9.57	60	10.13	0.5817
f	9.15	14.16	5.01	17.50	3.34	i		3.08-9.57	60	8.00	0.3017
g	9.14	14.16	5.02	17.25	3.09	j		3.08-9.57	60	0.006591 ^h	
N5P6											
d, e	9.12	14.11	4.99	16.95	2.84			2.97-9.49	60	8.00	0.5352
f	9.20	14.23	5.03	17.38	3.15	i		2.97-9.49	60	27.73	0.3379
g	9.19	14.23	5.04	17.17	2.94	j				0.006627 ^h	
N5P9 ^k											
i	9.16	13.97	4.81	16.14	2.17			2.80-9.45	64	0.001272 ^h	
j	9.23	13.93	4.70	16.04	2.11	20.03	3.99	2.98-8.97	55	3.62	0.4983
Grand mean ⁿ											
	9.08	14.09	5.01	17.22	3.13	<19.22	<2				
	±0.04	±0.10	±0.10	±0.56	±0.46						

^a Titration data obtained in aqu. methanol (95 % v/v); I = 0.1 mol dm⁻³, Et₄NC10₄, 25 °C. ^b Range of data points used in final refinements.

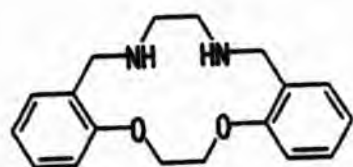
Table 6.2.1 continued.

^c Number of data points used in final refinements. ^d Three species refined with SUPERQUAD. ^[25] Initial proton concentration treated as a refinable parameter. ^e Values included in grand mean. ^f Four species refined with SUPERQUAD. ^[25] Initial proton concentration treated as a refinable parameter. ^g Four species refined with MINQUAD. ^[16,22] Initial proton concentration treated as a refinable parameter. ^h R-factor; $R = \sqrt{[\sum(E_{\text{obs}} - E_{\text{calc}})^2 / \sum E_{\text{obs}}^2]}$. ⁱ Value negative in final refinement cycle. ^j Species rejected - $\log \beta_{014}$ assumed a negative value during an iteration cycle. ^k Titration data obtained in aqu. methanol (95 % v/v); $I = 0.1 \text{ mol dm}^{-3}$, Et_4NClO_4 , 25 °C using a system described previously. ^[28] ^l Three species refined with MINQUAD. ^[16,22] Initial proton concentration treated as a refinable parameter. ^m Four species refined with SUPERQUAD. ^[25] Initial proton and ligand concentrations treated as refinable parameters. ⁿ Unweighted mean of selected values. Error limits represent the maximum deviation from the mean value.

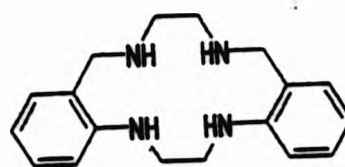
Proton binding constants have been reported for a number of penta-aza macrocyclic systems in aqueous solution ^[165] but, to date, no data exists for penta-aza systems in methanol solutions. The difference in the titration media somewhat limits comparisons between $\log \beta$ values of these systems and those reported herein for NpynNenH_4 .

However, the first and second protonation constants of NpynNenH_4 (Table 6.2.1) are comparable with those reported by Lindoy and co-workers in quadridentate and quinquedentate macrocyclic systems containing ethane-bridged benzylamine functions, e.g. dibenzo- N_2O_2 (OenNenH_4), ^[164] dibenzo- N_4 (NenNenH_4) ^[166] and dibenzopyrido- N_3O_2 (OpynNenH_4) ^[161] macrocycles. In these systems $\log \beta_{011}$ is in the range 9-9.5 and $\log K_{012}$ lie between 4 and 6. Interestingly, the first protonation constant obtained for NpynNenH_4 is identical to that reported for its dioxo analogue, suggesting that any intramolecular hydrogen bonding interactions, stabilising either the free or monoprotonated ligands,

are of a similar order. Indeed, weak intramolecular interactions between amine hydrogens and ether oxygens were observed in the solid state by X-ray analysis of the OpynNenH_4 ligand.^[161]



OenNenH_4



NenNenH_4

No values for $\log K_{013}$ are reported for either OpynNenH_4 or OpynNtnH_4 despite the presence of the pyridine donor atom in these ligands; in contrast, $\log K_{013}$ was obtained for NpynNenH_4 . The value of $\log K_{013}$ is significantly larger than the corresponding values for the series of anilino N-donor-containing dibenzo-tetraaza macrocycles (e.g. NenNenH_4).^[166] The difference in $\log K_{013}$ is attributed to the presence of the pyridyl- N_3 unit in the penta-aza ligand. Accordingly, the first protonation constants^[160] for the series of N_3O_2 macrocycles, which contain a similar 2,6-pyridinedimethylamine unit, lie in the range 3.0-3.5, which corresponds to $\log K_{013}$ for NpynNenH_4 . Furthermore, $\log K_{014}$ for NpynNenH_4 (where obtained) is of a similar magnitude as $\log K_{013}$ in the tetra-aza systems and $\log K_{012}$ in the N_3O_2 macrocycles and therefore appears to correspond with protonation of a weakly basic anilino nitrogen site. [A second factor, the increased ring size of NpynNenH_4 over the tetra-aza ligands, may also contribute the differences in $\log K_{013}$ between the tetra-aza and penta-aza systems. The increase in ring size in the latter ligand may partially offset the destabilising influence of charge repulsions between three protons constrained in the macrocycle.]

A microprotonation scheme for NpynNenH_4 may be proposed on the basis of the relative basicities of the different N-donor types in the macrocycle. In solution these are expected in the order, benzylamine > pyridine > aniline,^[62] and therefore the dominant mono-protonated and di-protonated species are therefore expected to feature protonation at the benzylamine sites [Fig. 6.2.1 (I)-(IV)]. Similarly, the dominant tri-protonated micro-species is expected to feature protonation at the pyridyl N-donor atom instead of at the anilino donor sites [Fig. 6.2.1 (V)-(VII)]. The proximity of non-co-ordinated N-donors to positive ammonium centres in such protonated species suggests that hydrogen bonding networks may influence the structure of such species.

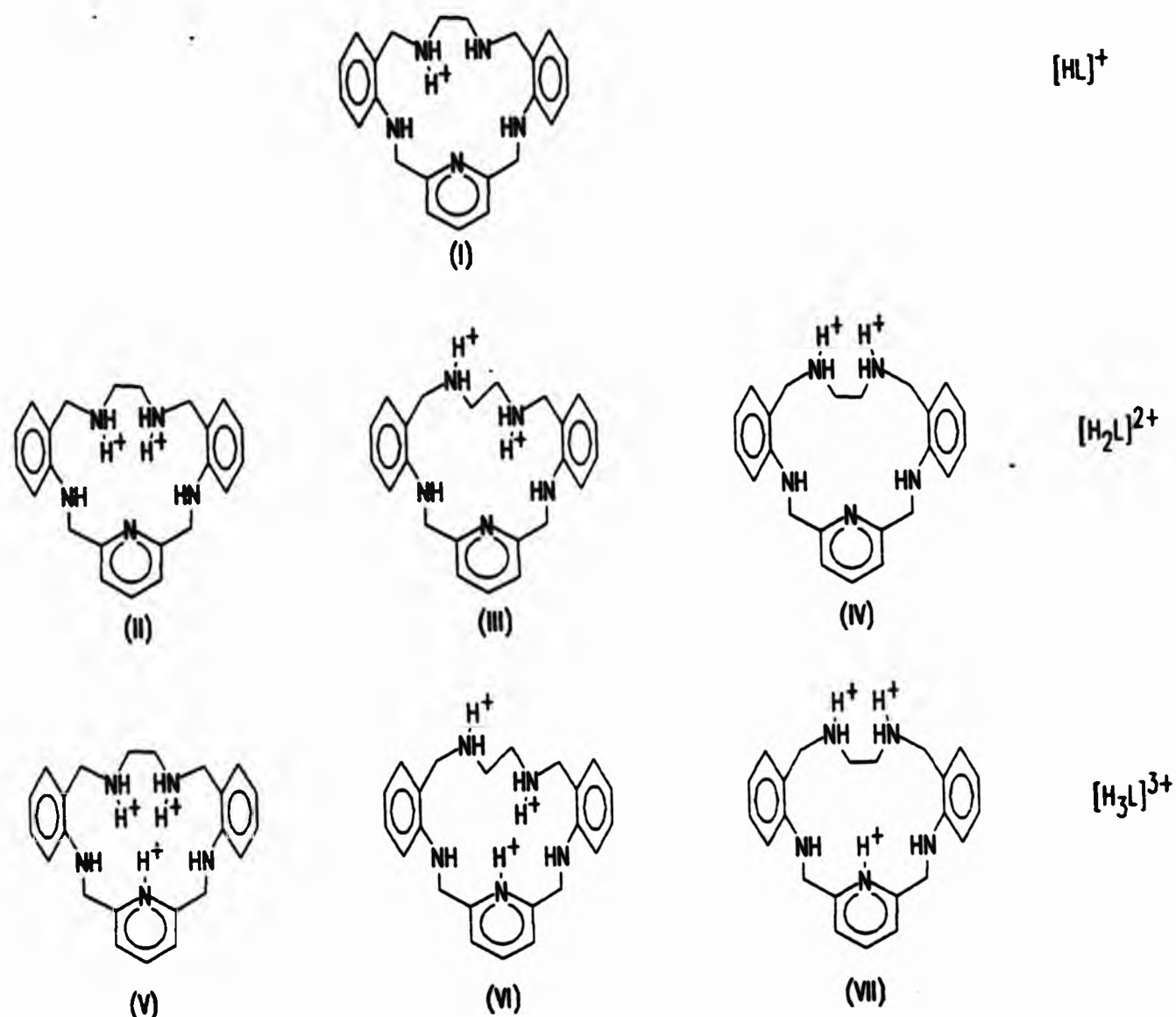


Figure 6.2.1 Possible configurations of dominant species featuring in the protonation microequilibria for NpynNenH_4 .

While some data exists for protonations of penta-aza macrocycles exists,^[165] the protonation behaviour of the related tetra-aza systems has received more detailed discussion. Kaden and co-workers have suggested that proton affinities of the series of tetra-aza macrocycles [12]aneN₄ to [16]aneN₄ are predominantly determined by the influence of electrostatic repulsions and that intramolecular H-bonds in the tetra-aza systems are weak or non-existent.^[167] Indeed, an X-ray crystallographic study of the dihydroperchlorate of cyclam ([14]aneN₄) indicated the existence of only weak intramolecular hydrogen bonds.^[168] In a detailed thermodynamic study of the protonations of [14]aneN₄, its tetra N-methyl analogue and [15]aneN₄,^[169] Paoletti and co-workers, while recognizing the possibility of hydrogen bond formation within the macrocyclic ring and with polar solvents, highlighted the rôle of nitrogen inversion as a mechanism for increasing the separation of ammonium sites and thereby reducing unfavourable electrostatic repulsions in di-, tri and tetra-protonated species.

Support for the scheme shown in Figure 6.2.1 derives from comparability of $\log K_{011}$ and $\log K_{012}$ of NpynNenH₄ with those of the dibenzo-N₂O₂ macrocycles (e.g. OenNenH₄).^[164] These ligands bear considerable structural similarity to the N₅ system but contain just two N-donor sites, the alkyl-bridged benzylamine atoms. Thus the two protonation constants of N₂O₂ macrocycles reveal the relative affinities of benzylamine sites in ligands of this type and their similarity with $\log K_{011}$ and $\log K_{012}$ of NpynNenH₄ support the microprotonation scheme proposed. Although NpynNenH₄ is rigidified by the presence of aromatic ring substituents some flexibility remains in the ligand which may allow an arrangement maximising the separation of the benzylamine donor atoms [such as that in Fig. 6.2.1 (III)], thereby offsetting the electrostatic repulsions between adjacent protonated functions in [LH₂]²⁺;

indeed orientations of the benzylamine lone pairs away from the macrocyclic cavity [similar to Fig. 6.2.1 (IV)] has been observed in the exomacrocyclic Ni(II), Zn(II) and Hg(II) complexes of its close analogue OpynNenH₄.^[170,171] The value of log K₀₁₃ obtained for NpynNenH₄ is comparable with log K₀₁₁ values of the N₃O₂ ligands^[160] but significantly larger than log K₀₁₃ values of the dibenzo-N₄ ligand series^[166] (e.g. NenNenH₄). Thus the dominant [LH₃]³⁺ species is expected to feature protonation at the pyridyl nitrogen rather than at either anilino site. The proximity of the latter N-donors, however, presumably plays some rôle in stabilising the tri-protonated species as a formation constant for such a species in the dioxo analogues of NpynNenH₄ was not reported. As inferred for [LH₂]²⁺, exomacrocyclic orientation of the protonated benzylamine functions [e.g. Fig. 6.2.1 (VI) and (VII)] may offset electrostatic repulsions in [LH₃]³⁺.

6.2.2 NpynNenH₄ - Copper(II) Titrations.

Titration of NpynNenH₄ in the presence of Cu(II) gave rise to a number of effects which suggest that the Cu(II)-NpynNenH₄ complex is too stable to be studied directly.

During preparation of the titration solution, addition of *aqu.* Cu(ClO₄)₂ solution to the acidified ligand solution was accompanied by a rapid colour change from pale blue (due to the [Cu(H₂O)₆]²⁺ ion) to deep green. This deep green colouration corresponds with solutions of [Cu(NpynNenH₄)]²⁺,^[162] indicating that the abundance of the Cu(II) complex is significant and possibly complete in even the most acidic solutions deployed with this technique (ca. pH 2.5). Furthermore, the acid-base titration curves obtained with this system replicate the strong acid-strong base curves obtained during cell calibration and the titration data defied analysis with any sensible

complexation model. The superimposibility of sample and calibration titration curves in this case suggests that all protons that would be associated with ligand binding sites in the absence of Cu(II) are displaced by formation of the metal complex. As the H^+ ions are effectively 'free' in solution at the start of the titration, a strong acid-strong base titration curve results for the system. In such cases, on the assumption that complexes of 1:1 metal-ligand stoichiometry are formed, β_{110} can be assigned as greater than 10^{14} .^[172] Comparable studies are not available for penta-aza systems in methanol titration media but binding constants of this order have been reported for comparable N_3O_2 macrocyclic ligands.^[161] In the light of the stability of the Zn(II) and Cd(II) complexes of this ligand (*vide infra*), the stability constant of the Cu(II) complex may be predicted to be well above 10^{14} , assuming a conventional Irving-Williams^[137,138] dependence for the $\log \beta$ values with this ligand.

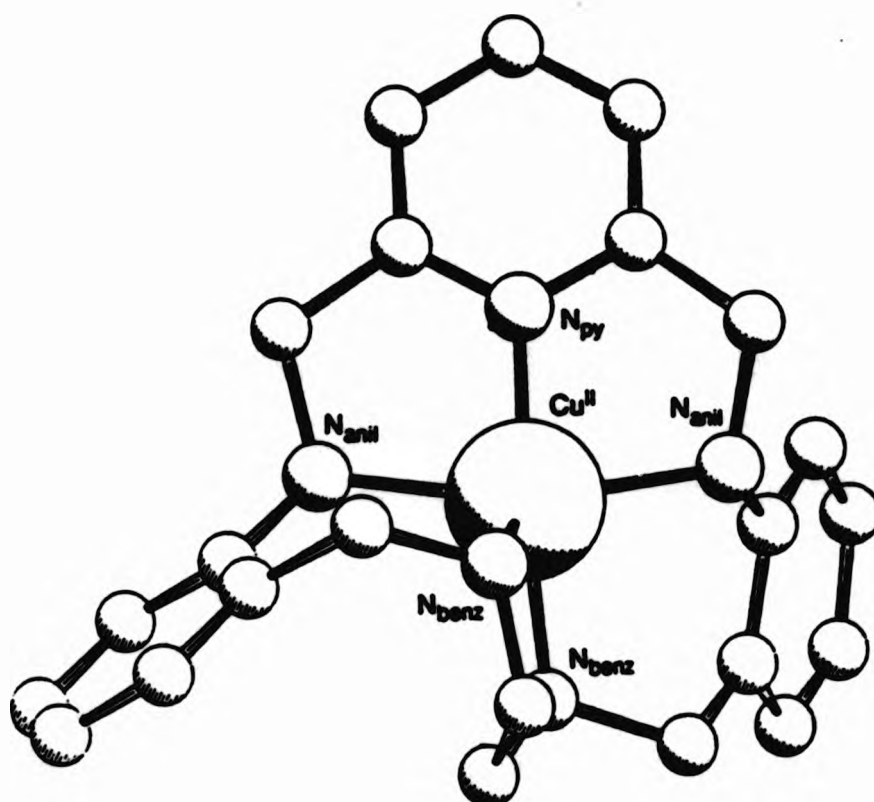


Figure 6.2.2 A view of the $[Cu(NpynNenH_4)]^{2+}$ cation.

Dark green crystals, isolated from an ethanolic solution of the ligand and

$\text{Cu}(\text{ClO}_4)_2$, have been characterised as the Cu(II) complex. Single crystal X-ray analysis of the complex showed the metal to be bound by all five donors of the macrocycle in a co-ordination geometry intermediate between square-based pyramidal and trigonal bipyramidal. A view of the complex is given in Figure 6.2.2. Conductometric and uv-vis spectrophotometric measurements suggest that a similar structure exists in solution^[162] and the relatively high stability constant for the complex presumably results from the involvement of all five donor atoms in co-ordinating the metal-ion.

6.2.3 Nickel(II)-NpynNenH₄ titrations

Acid-base titrations of solutions containing $\text{Ni}(\text{ClO}_4)_2$ and NpynNenH₄ yielded uneven curves throughout the pH range. Discontinuities above pH 7 are commonly observed during metal complexation studies in aqu. methanol solutions, often resulting from precipitation of metal hydroxide species, and do not preclude data analysis. However, discontinuities below pH 7, as observed with here, affect data in regions that correspond to complex formation and as such preclude data refinement. Conceivably, the discontinuities below pH 7 may arise from non-equilibration of titration solutions, indeed stability constant titrations involving Ni(II) commonly require longer delays between base additions to overcome the relatively inert nature of $[\text{Ni}(\text{H}_2\text{O})_6]^{2+}$.^[164] However, in this case, lengthening delays between base additions to as much as 25 minutes did not result in smoother titration curves but instead caused noticeable evaporation of the solvent from the titration vessel due to the very long times taken to complete titrations under these conditions.

In addition to these effects, a marked darkening of the titration solution was noted ca. pH 6. Similar effects were noted in titrations involving Ni(II) and

some other anilino N-donor macrocycles in identical titration environments (i.e. 95 % aqu. methanol with Et_4NClO_4 as the background electrolyte);^[173] these colour changes were attributed to metal-catalysed ligand decompositions, similar to metal-catalysed oxidations that have been identified in other anilino ligand systems.^[174]

In the light of these problems it was concluded that this system was unsuitable for study by potentiometric acid-base titration under these conditions and no further work was attempted.

6.2.4 Zinc(II)-NpynNenH₄ titrations.

Titration of acidified solutions of NpynNenH₄ in the presence of Zn(II) yielded three titration curves at two different metal to ligand ratios. Two datafiles were obtained with initial metal and ligand concentrations in the ratio ca. 1:2 (N5Z2 and N5Z3) and one at ca. 1:1 (N5Z1). Except for N5Z2, where data below pH 3.25 was affected by unacceptable sample temperature variation and excluded before refinement, curves obtained were smooth throughout the titration. In the absence of hydrolysis constants for metal-ions in this medium, data from basic solutions were excluded from refinement. Data was analysed using the SUPERQUAD program^[25] and a number of different equilibrium models for this system were investigated. Refinements from models giving the best fits for each data file are summarised in Table 6.2.2.

Table 6.2.2 Refinement summary for titrations of NpynNenH₄ with Zn(II).^a

Datafile	log β_{110}	log β_{111}	log K_{111}	pH range ^b	np ^c	χ^2	σ
N5Z1							
	11.89(8)			2.81-4.62	38	37.37	2.2815
^d	12.06(3)	15.71(2)	3.65	2.81-4.62	38	6.21	0.2051
N5Z2							
	11.66(6)			3.25-5.41	16	7.00	0.4525
	12.04(8)	15.21(13)	3.17	3.25-5.41	16	5.00	0.1595
N5Z3							
	12.21(8)			2.72-5.18	44	8.00	1.2729
^d	12.07(5)	15.52(3)	3.45	2.72-5.18	44	5.09	0.2792
Mean ^e	12.07±0.01	15.62±0.10	3.55±0.10				

^a Data obtained in *aqu.* methanol (95 % v/v); $I = 0.1 \text{ mol dm}^{-3}$, $(\text{C}_2\text{H}_5)_4\text{NClO}_4$; 25 °C. Log β values obtained with SUPERQUAD;^[25] initial proton concentrations treated as refinable parameters. Numbers in parentheses represent standard deviations calculated by the refinement program. ^b Range of data points used in final refinements. ^c Number of data points used in final refinements. ^d Values included in mean. ^e Unweighted mean of selected values. Error limits represent the maximum deviation from the mean value.

Synthetic and structural studies have revealed that NpynNenH₄ forms a 1:1 complex with Zn(II) where the metal-ion is encapsulated by the macrocycle (see Fig. 6.2.3).^[162] However, the titration data sets gave only moderate fits for an equilibrium model describing the formation of $[\text{Zn}(\text{NpynNenH}_4)]^{2+}$ alone and relatively large inter-titration variations result for log β_{110} values obtained with this model. In two cases (N5Z1 and N5Z3) the fit parameters generated on refining this model over the data range chosen were unacceptably

large and it was concluded that further species were required in the equilibrium model.

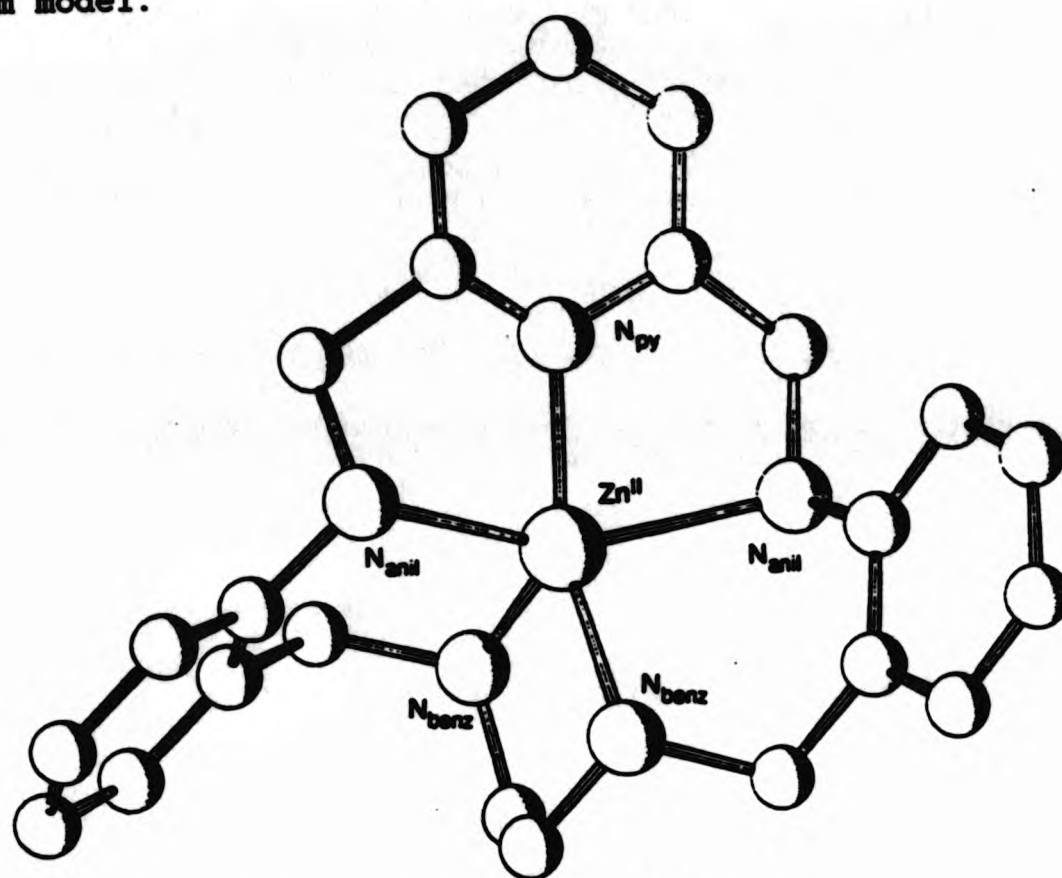


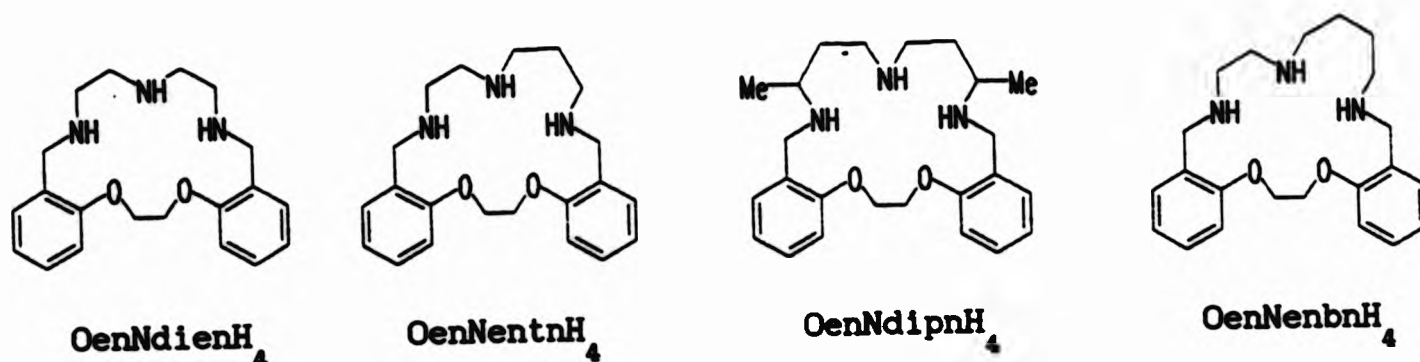
Figure 6.2.3 A view of the $[Zn(NpynNenH_4)]^{2+}$ cation.

In the light of the exomacrocyclic co-ordination of the metal-ion observed with the N_3O_2 analogue of NpynNenH₄ in its complex $[Zn(OpynNenH_4)I_2]$,^[171] and identification of complexes of formulation $[M(OpynNenH_4)_2]^{2+}$ ($M = Ni^{II}$, Cu^{II})^[170] with each ligand co-ordinated through the aliphatic nitrogen donors, similar *bis*-complexes with Zn(II) were envisaged. However inclusion of such $[ML_2]^{2+}$ species in equilibrium models were unsuccessful, even with files with initial metal and ligand concentrations in the ratio 1:2.

Inclusion of protonated metal complexes of formulation $[MLH]^{3+}$ in the equilibrium model led to substantially better fits than models with $[ML]^{2+}$ alone (see Table 6.2.2); indeed models describing the formation of these species gave the best fits in each data file. The formation constants obtained show excellent inter-titration reproducibility for $\log \beta_{110}$ and

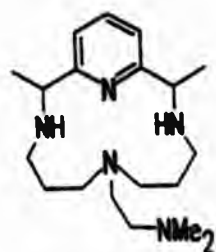
reasonable variations of $\log \beta_{111}$ between files. Exclusion of data from the acidic region for data file N522 (see above) results in a larger estimated standard deviation for $\log \beta_{111}$ as might be expected, and for this reason $\log \beta$ values from this data file were not included in the final averages (see Table 6.2.2).

Protonation of zinc complexes of penta-aza macrocycles in aqueous solution is well known,^[175,176] e.g. the protonation constants for Zn(II) complexes of [15]aneN₅, [16]aneN₅ and [17]aneN₅ lie in the range 3.1-4.3,^[176] but, as studies of penta-aza systems in *aqu.* methanol solutions have not been reported to date, comparisons for this study are limited to the quinquedentate N₃O₂ systems.^[171,177] While potentiometric studies of the closest analogues of NpynNenH₄, OpynNenH₄ and OpynNtnH₄, with Zn(II) in this medium yielded constants for formation of [ML]²⁺ only, protonation constants in the range 2.69-3.72 have been reported for the Zn(II) complexes of OenNdienH₄, OenNentnH₄, OenNdipnH₄ and OenNenbnH₄.^[177b] The value of $\log K_{111}$ for NpynNenH₄ lies within this range.

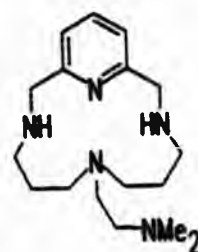


It is interesting to speculate on a possible structure for the protonated $[Zn(NpynNenH_5)]^{3+}$ cation. Significantly, the stepwise protonation constant ($\log K_{111}$) for the co-ordinated ligand is somewhat larger than $\log K_{013}$ for the 'free' ligand (Table 6.2.1) which is associated with protonation of the pyridyl donor of the macrocycle (see Fig. 6.2.1). Thus, unless metal complex

formation confers 'extra' basicity to this site, a dominant microscopic form for $[\text{MLH}]^{3+}$ featuring metal co-ordination by the aliphatic nitrogen donors and protonation at the pyridyl site [Fig. 6.2.4(I)] seems unlikely. Inspection of models suggests that an alternative configuration for $[\text{MLH}]^{3+}$ is possible. Exomacrocyclic orientation of one aliphatic nitrogen lone pair leaves the metal co-ordinated in the macrocyclic cavity in a four-co-ordinate geometry. Protonation of the exodentate aliphatic nitrogen effectively separates the metal-ion and the proton and such a configuration maybe the the dominant microscopic form for $[\text{MLH}]^{3+}$ [e.g. Fig. 6.2.4(II)]. This latter arrangement is reminiscent of the protonated Ni(II) and Cu(II) complexes of the quinquedentate pendant arm macrocycles (1) and (2).^[178,179] In these cases protonation results in decomplexation of the pendant arm and a change from a 5-co-ordinate metal-ion species to square planar $[\text{MLH}]^{3+}$ species.



(1)



(2)

Further support for protonated forms of $[\text{Zn}(\text{NpynNenH}_4)]^{2+}$ such as Fig. 6.2.3(II) derives from the comparability of $\log K_{111}$ for the penta-aza system with constants reported for zinc(II) complexes of OenNdienH_4 and its analogues.^[177b] Clearly these systems protonate at aliphatic nitrogen sites, as is the case for the dominant form predicted for $[\text{Zn}(\text{NpynNenH}_5)]^{3+}$.

The formation constant for $[\text{Zn}(\text{NpynNenH}_4)]^{2+}$ is some 6 orders of magnitude higher than the corresponding values for the Zn(II) complexes of its triaza-dioxa analogues,^[171] OpynNenH_4 ($\text{Alog } K_{110} = 6.18$) and OpynNtnH_4 .

($\Delta \log K_{110} = 6.32$). The penta-aza complex is also some 5 orders of magnitude more stable than the Zn(II) complex of the 17-membered macrocycle OenNdienH₄^[177] ($\Delta \log K_{110} = 4.59$). As the change in stability cannot be attributed to a change in the hole size of the macrocycles, it seems that a structural dislocation occurs on substituting the anilino donors of NpynNenH₄ for the phenoxyether oxygen donors of the N₃O₂ systems; in particular NpynNenH₄ and OpynNenH₄ are directly comparable in this context. While the relative co-ordinating ability of these different donor types is regarded as comparable in macrocycles of this type,^[166] it appears some co-operativity between the anilino and pyridyl donors on co-ordination, perhaps in moderating the steric demands of the 5-membered chelate rings, affords the N₃-donor unit of NpynNenH₄ a higher affinity for Zn(II) than the corresponding O₂N-donor unit of OpynNenH₄.

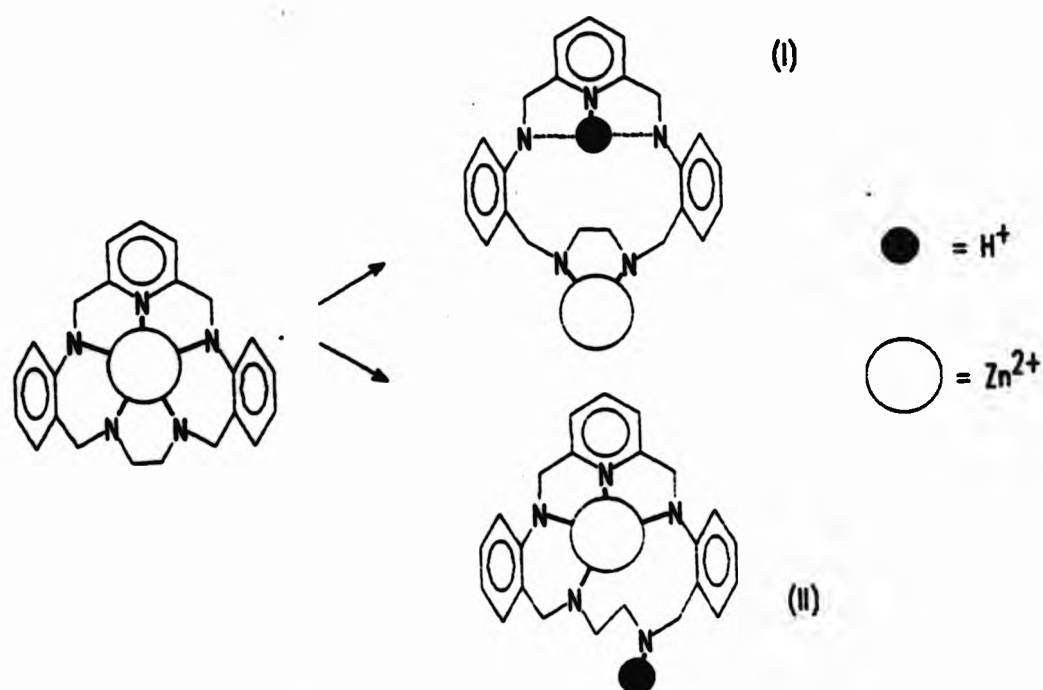


Figure 6.2.4 Alternatives for microscopic species formed on protonation of $[\text{Zn}(\text{NpynNenH}_4)]^{2+}$.

Some support for these observations may be gleaned from the solid state structures of the respective complexes. The X-ray crystal structure of

$[\text{Zn}(\text{NpynNenH}_4)]^{2+}$ (Fig. 6.2.3) shows the metal-ion co-ordinated to all five donors of the macrocycle in a geometry intermediate between square-based pyramidal and trigonal bipyramidal. No counterions or solvent molecules are involved in the metal co-ordination sphere indicating the metal is fully encapsulated by the ligand. Two distinct Zn(II) complexes of OpynNenH_4 have been observed in the solid state;^[171] an endomacrocyclic complex with the Zn(II) ion in an irregular 6-co-ordinate trigonal prismatic geometry involving the 5 donor atoms of the macrocycle and a unidentate nitrate ion and, an exomacrocyclic complex with the Zn(II) ion co-ordinated in a pseudo-tetrahedral geometry by the two aliphatic N-donors of the ligand and two iodide anions. While the latter of these structures shows a clear dislocation (the O_2N bridge is dissociated from the metal-ion) compared with the penta-aza system, it is noteworthy that the endomacrocyclic complex shows significantly longer metal-ligand bonds for the pyridyl-diphenoxy donor unit in comparison to the pyridyl-dianilino donor unit in $[\text{Zn}(\text{NpynNenH}_4)]^{2+}$. The shorter bonds in the latter suggest a stronger metal-ligand interaction which presumably translates into higher stability in solution.

6.2.5 Cadmium(II)- NpynNenH_4 titrations.

Titration of the acidified ligand in the presence of cadmium(II) perchlorate yielded three acceptable data sets; two data sets were obtained with initial metal and ligand concentrations in ratios ca. 1:1 and a single file was obtained at ca. 1:2. Further attempts at replicating these files were dogged by ambient temperature variation resulting in electrochemical instability although notably these experiments were executed before major improvements to the apparatus environment were completed.

Two Cd(II) complexes of NpynNenH_4 , $[\text{Cd}(\text{NpynNenH}_4)](\text{ClO}_4)_2$ and

$[\text{Cd}(\text{NpynNenH}_4)](\text{NO}_3)_2$, have been isolated from ethanolic solutions and characterised by microanalysis, infrared spectroscopy and fast atom bombardment mass spectrometry.^[162] Although suitable crystals could not be prepared for X-ray analysis, the diperchlorate complex was sufficiently soluble in acetonitrile- d_3 to enable multinuclear nmr experiments (^1H , ^{13}C , ^{15}N and ^{113}Cd) to be performed. The spectra have been assigned^[162] and while ^{13}C and ^{15}N spectra indicated the presence of a single, symmetrical complex, the more sensitive ^1H nmr probe indicated the presence of two complex species in solution [see Fig. 6.2.5(i)], consistent with the two signals observed in the ^{113}Cd spectrum [Fig. 6.2.5(ii)]. The major symmetrical species was assigned in the proton spectrum with the assistance of homonuclear COSY experiments; the relatively low intensity of the spectrum of the minor, non-symmetrical complex species and signal overlap precluded full analysis.

Significant deviations from strong acid-strong base (calibration) curves is apparent for only the most acidic regions of the titration curves obtained with this system indicating strong complexation between the metal-ion and the ligand. Accordingly, data in these regions were selected for refinement - data above pH 7 was excluded before refinement for the reasons outlined for the $\text{Zn(II)}-\text{NpynNenH}_4$ system (Section 6.2.4). Initial refinements of the data with SUPERQUAD^[25] were attempted with a complexation model describing the formation of $[\text{ML}]^{2+}$ only. Good fits were obtained with this model for each data file and the resulting $\log \beta$ values show acceptably small inter-titration variations (see Table 6.2.3).

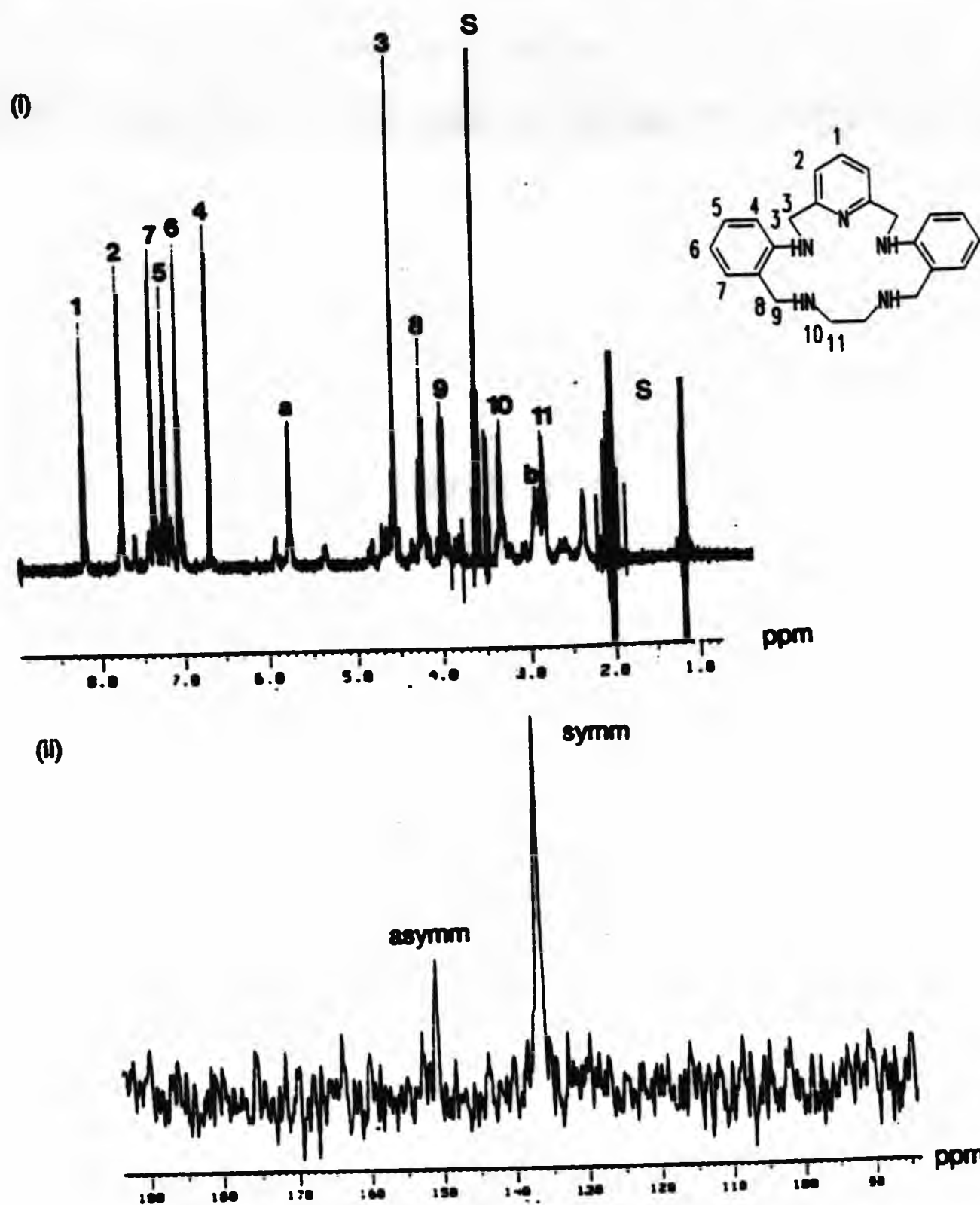


Figure 6.2.5 Nmr spectra of $[\text{Cd}(\text{NpynNenH}_4)](\text{ClO}_4)_2$ in acetonitrile- d_3 ;
 (i) ^1H nmr (signals due to residual solvent protons are denoted S) and (ii) ^{113}Cd nmr.

Refinement of the potentiometric data with SUPERQUAD¹⁴ for models containing two complex species of different stoichiometry was largely unsuccessful. Inclusion of either protonated complexes, $[\text{MLH}]^{3+}$, or bis-complexes, $[\text{ML}_2]^{2+}$, in schemes including $[\text{ML}]^{2+}$ caused refinement convergence with acceptable fits for each data set but poor inter-titration reproducibility of $\log \beta$ values

(see Table 6.2.3). Attempts at refining more elaborate equilibrium models led to non-convergence, negative $\log \beta$ values or $\log \beta$ values with excessively large estimated standard deviations. It was thus concluded that a model describing the formation of $[\text{Cd}(\text{NpynNenH}_4)]^{2+}$ only provides the best overall fit for data obtained under the conditions employed.

Table 6.2.3 Refinement summary for titrations of NpynNenH_4 with $\text{Cd}(\text{II})$.^a

Datafile	$\log \beta_{110}$	$\log \beta_{111}$	$\log \beta_{120}$	pH range ^b	np ^c	χ^2	σ
N1CD							
d	13.63(4)			2.83-3.52	21	11.38	0.2345
	12.34(8)	16.36(3)		2.53-3.30	23	3.78	0.0556
	13.89(5)		•	2.53-3.71	33	14.27	0.6924
N2CD							
d	13.59(16)			2.66-4.17	35	9.11	0.3511
	12.43(11)	20.19(15)		3.36-4.68	20	4.80	0.1062
	13.65(11)		21.23(17)	2.72-6.24	48	7.57	0.3448
N8CD							
d	13.74(1)			2.62-3.45	23	7.96	0.0845
	13.86(3)	16.02(8)		2.55-4.53	36	16.00	0.1989
	13.74(1)		23.35(10)	2.63-4.53	34	2.24	0.0912
Mean ^f							
	13.65±0.09						

^a Data obtained in *aqu.* methanol (95 % v/v); $I = 0.1 \text{ mol dm}^{-3}$, $(\text{C}_2\text{H}_5)_4\text{NClO}_4$; 25 °C. $\log \beta$ values obtained with SUPERQUAD; ^[25] initial proton concentrations treated as refinable parameters. Numbers in parentheses represent standard deviations calculated by the refinement program. ^b Range of data points used in final refinements. ^c Number of data points used in final refinements. ^d Values included in mean. ^e Value negative in final refinement cycle. ^f Unweighted mean of selected values. Error limits represent the maximum deviation from the mean value.

The presence of a second (asymmetric) complex indicated by ^1H and ^{113}Cd nmr experiments (Fig. 6.2.5) is consistent with the equilibrium model described. Although species with different stoichiometries were not predicted from potentiometric studies, the existence of a microequilibrium such as,



with a slow exchange rate on the nmr timescale is possible. As these two species have the identical macroscopic stoichiometries their separate identities will not be detectable using potentiometric methods. Integration of the ^1H nmr spectrum indicates the species are present in the ratio 3:1 (symmetrical:asymmetrical)^[162] and, given the presence of four chiral nitrogens in the macrocyclic complex, it seems likely that inversion of one or more nitrogen configurations may effect the conversion from symmetrical to asymmetrical species.

As noted for the $\text{Zn(II)}-\text{NpynNenH}_4$ system (Section 6.2.4), comparisons of complex stabilities of NpynNenH_4 are limited to analogous N_3O_2 systems. Similarly, the formation constant of $[\text{Cd}(\text{NpynNenH}_4)]^{2+}$ indicates the complex is substantially more stable than those of comparable N_3O_2 ligands; for example, $[\text{Cd}(\text{NpynNenH}_4)]^{2+}$ is 4.92 log units more stable than the directly comparable 17-membered macrocyclic complex $[\text{Cd}(\text{OpynNenH}_4)]^{2+}$ and 9.46 log units more stable than the 18-membered macrocyclic complex $[\text{Cd}(\text{OpynNtnH}_4)]^{2+}$. The drop in stability on increasing the ring size in the N_3O_2 complexes ($\Delta \log K_{110} = 4.54$) was associated with non-co-ordination of one or more donor atoms of the macrocycle, probably the less basic phenoxy or pyridyl donors.^[171] Accordingly, a stronger interaction of the metal-ion with all donors of the macrocycle is expected in the $\text{Cd(II)}-\text{N}_5$ system than in these $\text{Cd(II)}-\text{N}_3\text{O}_2$ systems; presumably substitution of the phenoxy donor atoms with

anilino donor atoms facilitates the interaction of the pyridyl-containing terdentate unit of the macrocycle with the metal-ion in the penta-aza system. Clearly more detailed structural study of this system is required before the origin of the stabilising factor in the penta-aza system can be identified.

6.2.6 Cadmium vs. zinc selectivity.

The increased affinity of NpynNenH_4 for cadmium over zinc is worthy of note. The 'natural' order of Zn(II) over Cd(II) selectivity shown in simple polyamine systems such as ethylenediamine and diethylenetriamine reflects the stronger electrostatic interaction expected on the basis of metal-ion radii of the d^{10} ions. An emerging feature of the larger (17- and 18-membered) dibenzo macrocycles is their ability to reverse this order showing, in common with NpynNenH_4 , higher affinities for Cd(II) over Zn(II) . For example, in a series of dibenzo tetra-aza macrocycles, the 15-membered macrocycle NenNtnH_4 favours Zn(II) over Cd(II) by ca. 3.2 log units but the 17-membered macrocycle, NenNpentnH_4 , shows a greater affinity for Cd(II) than Zn(II) by ca. 2.2 log units.^[166,180] Similarly, the 17- and 18-membered macrocycles of the series of N_3O_2 ligands including OenNdienH_4 and its analogues (changes in ring sizes and stereochemical degrees of freedom are achieved by systematic variation of alkyl chains spanning aliphatic nitrogen donors in these systems yielding e.g. OenNentnH_4 , OenNditnH_4 , OenNenbnH_4)^[177] show preferences for Cd(II) over Zn(II) . Selectivities in these systems are linked with full participation of all donor atoms in the Cd(II) complexes in contrast to non-coordination of one or more donors in the Zn(II) complexes (see Fig. 6.2.6).^[177] Reassertion of the 'normal' polyamine order of selectivity in the 19-membered ligands of this series is thought to coincide with the occurrence of amine-only modes of co-ordination with both metal-ions.

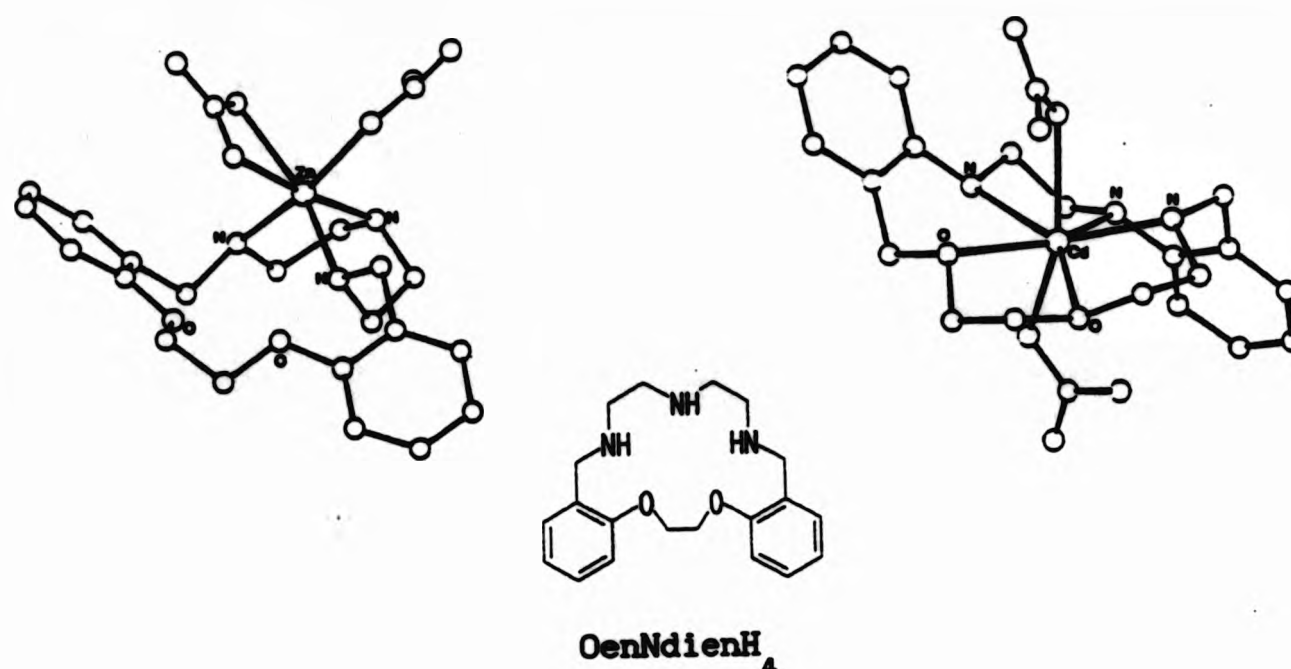


Figure 6.2.6 X-ray crystal structures of Zn(II) and Cd(II) complexes of OenNdienH₄, showing non-coordination of O-donor atoms in the Zn(II) complex; in solution the ligand shows selectivity for Cd(II) over Zn(II) ($\Delta \log K_{110} = 1.2$).^[177]

The origin of the Cd(II) over Zn(II) selectivity with NpynNenH₄ ($\Delta \log K_{110} = 2.58$) is less clear, although it is probable that the 17-membered macrocyclic ring of the ligand accommodates the larger Cd²⁺ ion with less strain than the smaller Zn²⁺ ion. Some twisting of the ligand is evident in the solid state structure of [Zn(NpynNenH₄)]²⁺ (Fig.6.2.3) and it might be expected that co-ordination to the larger Cd²⁺ ion would not cause such severe contortion. The incorporation of aromatic rings to the external structure of the macrocycle ring imposes limitations on the number of donor orientations available for the ligand. Thus the ligand may more readily adopt orientations of the donor set better suited to the size and preferred coordination geometry of Cd²⁺ ion. Such 'preorganisation' of the donor set has been cited^[181] as a basis for enhancing co-ordination selectivity.

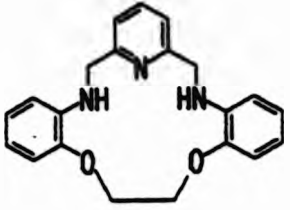
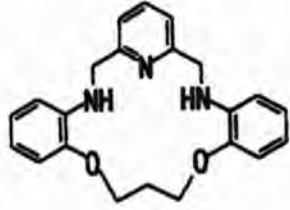
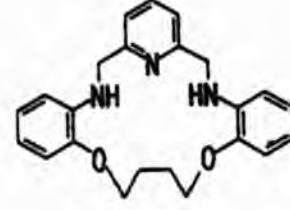
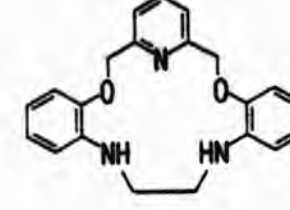
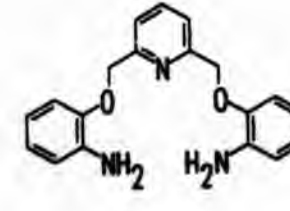
6.3 Protonation and metal complexation studies of a series of triaza-dioxo macrocycles

Proton, zinc(II) and cadmium(II) binding affinities of a series of dibenzo-pyrido triaza-dioxo [ligands (1)-(3), Table 6.3.1] were investigated in aqu. methanol (95 %, v/v). Acid-base titrations were performed using an established automated titration system at James Cook University of North Queensland. As this apparatus formed the basis for a similar system developed in these laboratories (see Chapter 4), this study provided an excellent opportunity to consolidate established sample preparation and data refinement procedures. The protonation constants of macrocycles (1)-(3) and their close analogues (4) and (5) have been reported along with their Co(II), Ni(II) and Cu(II) stability constants.^[160] In addition, the Zn(II) and Cd(II) complexes of (4) and (5) have been investigated by potentiometric methods.^[182] The results from these studies are summarised in Table 6.3.1; these ligands further extend the 'matrix' used by Lindoy and co-workers to probe metal-ion selectivity by dislocation discrimination.^[163]

Acid-base titrations of (1), (2) and (3) in the absence of metal-ions yielded smooth curves for which deviations from strong acid-strong base behaviour (revealed by the calibration curve for the system) were only apparent below pH 6. These differences appeared as broad deviations without easily discernible inflections. Titration data from each data file obtained was refined using a local version of MINIQAD^[16,22] using an estimated protonation model derived from published data.^[160] Data files for ligands (1) and (3) were also refined with SUPERQUAD^[25] using identical model estimates to those employed for MINIQAD refinements. Results from these refinements compare well with the published data (see Table 6.3.1) - the larger differences between $\log \beta_{012}$ values are consistent with larger errors associated with the published values,

notably values of $\log K_{012}$ in these systems are quoted only as estimates. [160]

Table 6.3.1 Protonation and metal complex stability constants for some macrocyclic and open chain triazadioxo macrocycles.^a

Ligand	$\log \beta_{011}$	$\log \beta_{012}$	$\log \beta_{110}$					Ref.
			Co ²⁺	Ni ²⁺	Cu ²⁺	Zn ²⁺	Cd ²⁺	
 (1)	2.98(1)	5.36(1)						b c d [160]
	2.97(1)	5.37(1)						
	3.00	5.15	<4	<4	8.83	<4	<4	
 (2)	3.43(1)	5.80(1)						e f d [160]
	3.44(1)	5.81(1)						
	3.50	5.90	<4	<4	9.48	<4	<4	
 (3)	3.75(1)	6.31(2)						g h d [160]
	3.69(1)	5.98(1)						
	3.73	5.53	<4	<4	7.36	<4	<4	
 (4)	4.41	6.59	<4	<4	6.84			[160] [182]
						3.90	i	
 (5)	4.80	8.74 ^j	<3	<3	3.60	<3	<3	[182]

^a Data obtained in aqu. methanol (95 %, v/v) at constant ionic strength.

Table 6.3.1 continued.

$I = 0.1 \text{ mol dm}^{-3}$, Et_4NClO_4 ; 25°C . Values in parentheses are standard deviations generated by refinement programs. ^b This work; MINIQAD^[16,22] refinement, $R = 0.000439$. ^c This work; SUPERQUAD^[25] refinement, $\chi^2 = 4.00$, $\sigma = 0.0962$. ^d This work; values estimated from titration curve. ^e This work; MINIQAD^[16,22] refinement, $R = 0.000778$. ^f This work; SUPERQUAD^[25] refinement, $\chi^2 = 4.67$, $\sigma = 0.1154$. ^g This work (data file 1); MINIQAD^[16,22] refinement, $R = 0.002184$. ^h This work (data file 2); MINIQAD^[16,22] refinement, $R = 0.000988$. ⁱ Insoluble complex formed. ^j $\log \beta_{013} = 10.82$.

As a reflection of the weak basicity of these ligands and their inability, partially due to the rigidity of the macrocyclic substituents, to adopt regular co-ordination geometries these ligands show little affinity for the divalent metal-ions investigated, with the exception of Cu^{II} . The relatively large stability constants for the copper(II) complexes were attributed in part^[160] to the ability of the $\text{Cu}(\text{II})$ to exhibit 'plasticity' in its stereochemical requirements.^[183]

Accordingly, the titration curves obtained in this study for (1), (2) and (3) in the presence of $\text{Zn}(\text{II})$ and $\text{Cd}(\text{II})$ diperchlorates superimpose the ligand-only curves below pH 7. In basic solution the curves become discontinuous, presumably reflecting the formation of insoluble hydroxides of 'free' metal ions. Such curves are indicative of negligible metal-ion complexation under the conditions employed and, if it is assumed that only an $[\text{ML}]^{2+}$ species will form in any case, a value of $\log \beta_{110} < 4$ can be ascribed to these complexes.^[172] Thus, in common with analogues (4) and (5), weak affinities are shown by ligands (1)-(3) for the $\text{Zn}(\text{II})$ and $\text{Cd}(\text{II})$ ions.

References

1. F. J. C. Rossotti and H. Rossotti, *The Determination of Stability Constants*, McGraw-Hill, New York, 1961.
2. M. T. Beck, *Chemistry of Complex Equilibria*, Van Nostrand Reinhold, New York, 1970.
3. M. Meloun, J. Havel and E. Högfeld, *Computation of Solution Equilibria: A Guide to Methods in Potentiometry, Extraction, and Spectrophotometry*, Ellis Horwood, Chichester, 1988.
4. D. D. Perrin and I. G. Sayce, *Talanta*, 1967, 14, 833.
5. A. E. Martell and R. J. Motekaitis, *Determination and Use of Stability Constants*, VCH, New York, 1988, Appendix III.
6. M. R. Rosenthal, *J. Chem. Ed.*, 1973, 50, 331.
7. P. W. Atkins, *Physical Chemistry*, Oxford University Press, Oxford, 2nd edn., 1982, p. 355.
8. F. P. Dwyer and D. P. Mellor (eds.), *Chelates and Chelating Agents*, Academic Press, New York, 1964.
9. M. A. Gristina, A. Sabatini and A. Vacca, *Coord. Chem. Rev.*, 1972, 8, 45.
10. D. J. Leggett, *Talanta*, 1977, 24, 535.
11. W. A. E. McBryde and T. B. Field, *Can. J. Chem.*, 1978, 56, 1202.
12. F. Gazier, *Coord. Chem. Rev.*, 1979, 27, 195.
13. D. J. Leggett (ed.), *Computational Methods for the Determination of Formation Constants*, Plenum Press, New York, 1985.
14. M. Bartos, E. Högfeld and M. Meloun, *Talanta*, 1988, 35, 981.
15. P. Gans, *Coord. Chem. Rev.*, 1976, 19, 99.
16. P. Gans, A. Sabatini and A. Vacca, *Talanta*, 1974, 21, 53.
17. A. Sabatini and A. Vacca, *J. Chem. Soc., Dalton Trans.*, 1972, 1693.
18. A. J. Leong and L. F. Lindoy, personal communication.
19. P. Gans, A. Sabatini and A. Vacca, *Inorg. Chim. Acta.*, 1976, 18, 237.
20. P. L. Brown, J. Ellis and R. N. Sylva, *J. Chem. Soc., Dalton Trans.*, 1983, 31; M. R. Davidson and R. N. Sylva, *J. Chem. Soc., Dalton Trans.*, 1979, 233.
21. A. P. Arnold, S. A. Daignault and D. L. Rubenstein, *Anal. Chem.*, 1985, 57, 1112.
22. K. Adam, unpublished modified version of MINQUAD.

23. A. Sabatini and A. Vacca, in *Computational Methods for the Determination of Formation Constants*, ed. D. J. Leggett, Plenum Press, New York, 1985.
24. J. C. Miller and J. N. Miller, *Statistics for Analytical Chemistry*, Ellis Horwood, Chichester, 2nd Edn., 1988.
25. P. Gans, A. Sabatini and A. Vacca, *J. Chem. Soc., Dalton Trans.*, 1985, 1197.
26. K. Moedritzer and R. R. Irani, *J. Org. Chem.*, 1966, 31, 1603.
27. (a) A. I. Vogel, *Vogel's Textbook of Quantitative Inorganic Analysis*, eds. J. Bassett, R. C. Denney, G. H. Jeffery and J. Mendham, Longman, Harlow, 5th edn., 1989, p. 288; (b) pp. 314-329; (c) p. 551; (d) p. 569; (e) p. 576.
28. G. Anderegg, A. Ekstrom, L. F. Lindoy and R. J. Smith, *J. Am. Chem. Soc.*, 1980, 102, 2670; K. R. Adam, A. J. Leong, L. F. Lindoy, H. C. Lip, B. W. Skelton and A. H. White, *J. Am. Chem. Soc.*, 1983, 105, 4645.
29. P. L. Biggins, S. E. Edwards, T. A. Lucas, R. W. Matthews, I. J. Scowen and C. J. L. Silwood, *S.SCHTITR*, unpublished BBC BASIC program.
30. P. L. Biggins, S. E. Edwards, R. W. Matthews, I. J. Scowen and C. J. L. Silwood, *DECDATA*, unpublished BBC BASIC program.
31. *TERMULATOR*, Terminal emulation for the BBC micro, University of Surrey, 1984.
32. G. H. Nancollas and M. B. Tomson, *Pure and Appl. Chem.*, 1982, 54, 2675.
33. (a) P. W. Linder, P. M. May, R. G. Torrington and D. R. Williams, *Talanta*, 1982, 29, 249; (b) P. M. May, K. Murray and D. R. Williams, *Talanta*, 1985, 32, 483.
34. G. Hänisch, T. A. Kaden and A. D. Zuberbühler, *Talanta*, 1979, 26, 563.
35. See for example, A. H. B. Wu and H. V. Malmstat, *Anal. Chem.*, 1978, 50, 2090; V. Cerda, J. M. Estela, J. Maimo, G. Ramis and A. Salva, *Talanta*, 1988, 35, 667.
36. P. L. Biggins, S. E. Edwards, T. A. Lucas, R. W. Matthews, I. J. Scowen and C. J. L. Silwood, unpublished results.
37. E. Bottari, A. Braibanti, L. Ciavatta, A. M. Corrie, P. G. Daniele, F. Dallavallee, M. Grimaldi, A. Mastroianni, G. Mori, G. Ostacoli, P. Paoletti, E. Rizzarelli, S. Sammartano, C. Severini, A. Vacca and D. R. Williams, *Annali di Chimica*, 1978, 68, 813.
38. A. Braibanti, G. Ostacoli, P. Paoletti, L. D. Pettit and S. Sammartano, *Pure Appl. Chem.*, 1987, 59, 1712.
40. S. E. Edwards, T. A. Lucas and R. W. Matthews, *S.SCHNCAL*, unpublished BBC BASIC program.

41. (a) S. Edwards, S. *TEMPCAL*, unpublished BBC BASIC program; (b) *PLOTX*, unpublished BBC BASIC program.
42. F. J. C. Rossotti and H. Rossotti, *J. Chem. Ed.*, 1965, 42, 375.
43. F. J. C. Rossotti and H. Rossotti, *J. Phys. Chem.*, 1964, 68, 3773.
44. G. F. C. Camoes, A. K. Covington and M. Filomena, *Anal. Chem.*, 1974, 46, 1547.
45. F. Gazier and A. Puskas, *Talanta*, 1981, 28, 565.
46. G. Arena, C. Rigano, E. Rizzarelli and S. Sammartano, *Talanta*, 1979, 26, 1.
47. D. A. Skoog and D. M. West, *Fundamentals of Analytical Chemistry*, CBS College Publishing, New York, 4th Edn., 1982.
48. G. Anderegg, *EICHU - Programm für die Berechnung von Eichtitration*, Program Library of the Laboratorium für Anorganische Chemie, 1978, ETHZ, Zurich.
49. M. J. E. Golay and A. Savitsky, *Anal. Chem.*, 1964, 36, 1627.
50. M. Planck, *Ann. Phys.*, 1890, 39, 161; 40, 561.
51. P. Henderson, *Z. Phys. Chem.*, 1907, 59, 118; 1908, 63, 325.
52. G. Beidermann and L. G. Sillen, *Arkiv. Khemi.*, 1953, 5, 425.
53. G. T. Hefter, *Anal. Chem.*, 1982, 54, 2518.
54. P. L. Biggins, *DIFFCOR*, unpublished BBC BASIC program.
55. A. Braibanti, F. Dallavalle, G. Mori and B. Veroni, *Talanta*, 1982, 29, 725.
56. A. Braibanti, F. Dallavalle, G. Mori and M. Pasquali, *Gazz. Chim. Ital.*, 1983, 113, 407.
57. A. Braibanti, C. Bruschi, E. Fisicaro and M. Pasquali, *Talanta*, 1986, 33, 471.
58. A. Braibanti and E. Fisicaro, *Talanta*, 1988, 35, 769.
59. G. Gran, *Acta Chem. Scand.*, 1950, 4, 559.
60. G. Gran, *Analyst*, 1952, 77, 661.
61. D. D. Perrin, *Stability of Metal-Ion Complexes. Part B: Organic Ligands*, Pergamon Press, Oxford, 1979.
62. (a) A. E. Martell and R. M. Smith, *Critical Stability Constants, Volume 1: Amino Acids*, Plenum Press, 1974; (b) *Volume 2: Amines*, 1975; (c) *Volume 3: Other Organic Ligands*, 1977; (d) *Volume 4: Inorganic Complexes*, 1976; (e) *Volume 5: First Supplement*, 1982; (f) *Volume 6: Second Supplement*, 1989.
63. B. Dempsey, D. D. Perrin and E. P. Serjeant, *pK_a Prediction for Organic Acids and Bases*, Chapman and Hall, London, 1981, p. 18.

64. Y. Iitaka, *Acta Crystallogr.*, 1960, 13, 35.
65. P. G. Jönsson and A. Kvik, *Acta Crystallogr., Sect. B*, 1972, B28, 1827; W. M. Canning, T. F. Koetzele, A. Kvik, and G. J. B. Williams, 1980, B36, 115.
66. A. J. Stosick, *J. Am. Chem. Soc.*, 1945, 67, 365; H. C. Freeman and J. M. Guss, *Acta Crystallogr., Sect. B*, 1968, B24, 1133; R. Calvo, E. E. Castellano, and O. R. Nascimento, 1982, B38, 1303.
67. H. C. Lim and G. H. Nancollas, *Inorg. Chem.*, 1971, 10, 1957.
68. F. A. Cotton and G. Wilkinson, *Advanced Inorganic Chemistry*, Wiley, London, 3rd Edn., 1972, pp. 414-416.
69. W. C. Schumb, C. N. Satterfield and R. L. Wentworth, *Hydrogen Peroxide*, A.C.S. Monograph No. 128, Rheinhold, New York, 1955.
70. J. O. Edwards, in *Peroxide Reaction Mechanisms*, ed. J. O. Edwards, Wiley, New York, 1962, ch. 5.
71. A. G. Mitchell and W. K. F. Wynne-Jones, *Faraday Discuss. Chem. Soc.*, 1955, 51, 1690.
72. J. R. Kolzynski, E. M. Roth and E. S. Shanley, *J. Am. Chem. Soc.*, 1957, 79, 531.
73. E. S. Shanley, in *Peroxide Reaction Mechanisms*, ed. J. O. Edwards, Wiley, New York, 1962, ch. 7.
74. O. Budevsky, *Talanta*, 1989, 36, 1209.
75. M. Kilpatrick and T. J. Lewis, *J. Am. Chem. Soc.*, 1956, 78, 5186.
76. A. Gergely, *Acta Chim. Acad. Sci. Hung.*, 1969, 59, 309.
77. E. J. King, *Acid-Base Equilibria; The International Encyclopedia of Physical Chemistry and Chemical Physics*, Topic 15, Volume 4, Pergamon, Oxford, 1965.
78. M. Kilpatrick, G. M. Nichols, E. M. Roth and E. S. Shanley, *J. Am. Chem. Soc.*, 1956, 78, 5190.
79. A. G. Mitchell and W. K. F. Wynne-Jones, *Faraday Discuss. Chem. Soc.*, 1953, 15, 161.
80. G. Faraglia, F. J. C. Rossotti and H. Rossotti, *Inorg. Chim. Acta*, 1970, 4, 488.
81. S. N. Lewis, in *Oxidation*, Volume 1, ed. R. L. Augustine, Marcel Dekker, New York, 1969.
82. E. N. Rizkalla and G. R. Choppin, *Inorg. Chem.*, 1983, 22, 1478; J. Oakes and E. G. Smith, *J. Chem. Soc., Dalton Trans.*, 1983, 601; R. D. Gillard and P. D. Newman, *Polyhedron*, 1989, 8, 2077.

83. I. A. Boenig, M. M. Crutchfield and C. W. Heitsch, in *Kirk-Othmer Encyclopedia of Chemical Technology*, eds. H. F. Mark, D. F. Othmer, C. G. Overberger and G. T. Seaborg, Wiley-Interscience, New York, 3rd edn., 1982, vol. 17, pp. 536-537.
84. D. F. Evans and M. W. Upton, *J. Chem. Soc., Dalton Trans.*, 1985, 2525.
85. See for example, W. K. Kibbel and E. T. O'Neill, *US.Pat.*, 3 681 022; *Chem. Abstr.*, 1972, 77, 106133a; D. Postlethwaite, *Eur.Pat.*, Appl. 37 146, 1980; *Chem. Abstr.*, 1982, 96, 8529g; C. Guth and A. Stehlin, *Eur.Pat.*, Appl. 210 952, 1987; *Chem. Abstr.*, 1987, 106, 178074x; N. Kimura, Y. Machida, M. Watanabe and T. Yoshida, *Jap.Pat.*, 62 185 797; *Chem. Abstr.*, 1988, 108, 39593u.
86. S. Croft, B. C. Gilbert, J. R. Lindsay Smith, J. K. Stell and W. R. Sanderson, *J. Chem. Soc., Perkin Trans. 2*, 1992, 153; J. K. Stell, Ph.D. Thesis, University of York, 1991.
87. (a) M. M. Crutchfield, C. H. Dungan, J. H. Letcher, V. Mark and J. Van Wezer, *Topics in Phosphorus Chemistry: P^{31} Nuclear Magnetic Resonance*, Wiley-Interscience, New York, 1967, p. 290; (b) p. 310.
88. E. K. Fields, *J. Am. Chem. Soc.*, 1952, 74, 1528.
89. K. Moedritzer and R. R. Irani, *Inorg. Chem.*, 1963, 31, 1603.
90. C. R. Worthing and R. J. Hance, *The Pesticide Manual - a World Compendium*, British Protection Council, Farnham, Surrey, 9th edn., 1991, p.33; *The Agrochemicals Handbook*, The Royal Society of Chemistry, Cambridge, 3rd edn. 1991, A1212/Aug 91; D. Cameron, H. R. Hudson, I. Lagerlund and M. Planka, *Eur.Pat.* 153 284; *Chem. Abstr.*, 1986, 104, 207445k.
91. D. St.C Green, Ph.D. Thesis, Polytechnic of North London, 1991.
92. R. Cremlyn, *Pesticides - Preparation and Mode of Action*, Wiley, Chichester, 1978.
93. J. Nicole, G. Tridot and M. Wozniak, *Bull. Soc. Chim. Fr.*, 1972, 11, 4445.
94. G. Nowogrocki and M. Wozniak, *Talanta*, 1979, 26, 1135.
95. J. P. Berry, A. F. Isbell and G. E. Hunt, *J. Org. Chem.*, 1972, 37, 4396.
96. T. Fyfe, B.Sc. Project, Polytechnic of North London, 1991.
97. G. Nowogrocki and M. Wozniak, *Talanta*, 1979, 26, 381.
98. E. N. Rizkalla, *Rev. Inorg. Chem.*, 1983, 5, 223 and refs. therein.
99. Y. Okaya, *Acta Crystallogr.*, 1966, 20, 712.
100. A. E. Martell and B. Szpoganicz, *Inorg. Chem.*, 1989, 28, 4199.

101. W. C. Cacheris, C. F. G. C. Geraldès and A. D. Sherry, *Inorg. Chem.*, 1989, 28, 3336.
102. R. P. Carter, M. M. Crutchfield and R. R. Irani, *Inorg. Chem.*, 1967, 6, 943.
103. K. Moedritzer, *Inorg. Chem.*, 1967, 6, 936
104. K. Sawada, T. Araki and T. Suzuki, 1987, *Inorg. Chem.*, 26, 1199.
105. R. P. Carter, M. M. Crutchfield and R. R. Irani, *Inorg. Chem.*, 1967, 6, 939.
106. T. G. Appleton, J. R. Hall, A. D. Harris, H. A. Kimlin and I. J. McMahon, *Aust. J. Chem.*, 1984, 37, 1833.
107. T. G. Appleton, J. R. Hall and I. J. McMahon, *Inorg. Chem.*, 1986, 25, 726.
108. R. J. Grabenstetter, O. T. Quimby and T. J. Flautt, *J. Phys. Chem.*, 1967, 71, 4194.
109. See for example, J. Hine, J. H. Jensen and F. A. Via, *J. Org. Chem.*, 1971, 36, 2926; L. R. Isbrandt and R. P. Oertel, *J. Am. Chem. Soc.*, 1980, 102, 3144.
110. C. F. Baes Jr. and R. E. Mesmer, *The Hydrolysis of Cations*, Wiley, New York, 1976.
111. T. Glowiak, B. Jezowska-Trzebiatowska and W. Sawka-Dobrowolska, *Inorg. Chim. Acta*, 1980, 45, L105.
112. T. Glowiak, B. Jezowska-Trzebiatowska and W. Sawka-Dobrowolska, *J. Cryst. Mol. Struct.*, 1980, 10, 1.
113. A. Cassaigne, J. Darriet, P. Fenot and C. Garrigou-Lagrange, *J. Mol. Struct.*, 1978, 43, 49.
114. A. Clearfield, Y. Ortiz-Avila and P. R. Rudolf, *J. Coord. Chem.*, 1989, 20, 109.
115. T. Glowiak and W. Sawka-Dobrowolska, *Acta Crystallogr., Sect. B*, 1977, B33, 2648.
116. M. A. Busch and D. E. Pennington, *Inorg. Chem.*, 1976, 15, 1940.
117. N. Choi, I. Khan, M. McPartlin and R. W. Matthews, unpublished results.
118. S. Gamper, G. Müller and A. Schier, *Inorg. Chim. Acta*, 1990, 177, 179.
119. C-Y. Guo, R. L. Kirchmeier, B. Scott, J. M. Shreeve and R. D. Willet, *J. Am. Chem. Soc.*, 1990, 112, 3152.
120. E. T. Clarke, A. Clearfield, A. E. Martell and P. R. Rudolf, *Acta Crystallogr., Sect. C*, 1988, C44, 796.
121. N. Q. Dao, M. R. Lee, N. El Messbahi, A. Neuman, R. Rochdaoui and J. P. Silvestre, *Acta Crystallogr., Sect. C*, 1990, C46, 986.

122. J. C. Boivin, C. Houttemane, G. Nowogrocki, D. Thomas and M. Wozniak, *Mater. Res. Bull.*, 1981, 16, 801.
123. A. E. Martell, R. J. Motekaitis and I. Murase, *Inorg. Nucl. Chem. Lett.*, 1971, 7, 1103.
124. A. E. Martell, R. J. Motekaitis and I. Murase, *Inorg. Chem.*, 1976, 15, 2303.
125. A. E. Martell, K. S. Rajan and S. Westerback, *J. Am. Chem. Soc.*, 1965, 87, 2567.
126. G. Duc, D. Giron and G. Thomas, *Compte Rend. Acad. Sc. Paris Ser. C*, 1971, 272, 1022.
127. V. L. Hughes and A. E. Martell, *J. Am. Chem. Soc.*, 1953, 57, 694; K-P Ang, *J. Am. Chem. Soc.*, 1958, 62, 1109; W. A. E. McBryde, *Talanta*, 1974, 21, 979.
128. T. G. Appleton, J. R. Hall and I. J. McMahon, *Inorg. Chem.*, 1986, 25, 720.
129. M. Meloun, J. Havel and E. Hogfeld, *Computation of Solution Equilibria: A Guide to Methods in Potentiometry, Extraction, and Spectrophotometry*, Ellis Horwood, Chichester, 1988, p. 13.
130. K. R. Dixon, in *Multinuclear NMR*, ed. J. Mason, Plenum Press, New York, 1987.
131. P. K. Glasoe and F. A. Long, *J. Phys. Chem.*, 1960, 64, 188; K. Mikkelsen and S. O. Nielsen, *J. Phys. Chem.*, 1960, 64, 632.
132. J. H. Letcher and J. R. Van Wazer, *J. Chem. Phys.*, 1966, 44, 815; 45, 2916.
133. L. C. D. Groenweghe, L. Maier and K. Moedritzer, *J. Chem. Eng. Data*, 1962, 7, 307.
134. G. Nowogrocki and M. Wozniak, *Talanta*, 1978, 25, 693.
135. A. E. Martell and R. J. Motekaitis, *J. Coord. Chem.*, 1985, 14, 139.
136. F. I. Bel'skii, I. B. Goryunova, M. I. Kabachnik, P. V. Petrovskii and T. Ya. Medved, *Bull. Acad. Sci. USSR*, 1982, 31, 93.
137. H. Irving and R. J. P. Williams, *Nature*, 1948, 162, 746.
138. H. Irving and R. J. P. Williams, *J. Chem. Soc.*, 1953, 3192.
139. V. K. Bel'skii, N. M. Dyatlova, A. L. Poznyak, M. V. Rudomino and L. M. Shkol'nikova, *Koord. Khim.*, 1986, 12, 565 (Engl. translation).
140. J. Meisenheimer and K. Brating, *Liebigs Ann. Chem.*, 1913, 397, 286; D. Jerchel and G. Jung, *Chem. Ber.*, 1952, 85, 1130;
141. R. R. Irani and K. Moedritzer, *J. Phys. Chem.*, 1962, 66, 1349; R. L. Carroll and R. R. Irani, *J. Inorg. Nucl. Chem.*, 1968, 30, 2971.

142. B. H. Wiers, *J. Phys. Chem.*, 1971, 75, 682; Q. Fernando and H. Wada, *Anal. Chem.*, 1971, 43, 751; T. Miodusky, *Talanta*, 1980, 27, 299; D. J. Burton, T. Fonong and D. J. Pietrzyk, *Anal. Chem.*, 1983, 55, 1089.
143. R. A. Gloss and V. A. Uchtman, *J. Phys. Chem.*, 1972, 76, 1298; V. A. Uchtman, *J. Phys. Chem.*, 1972, 76, 1304.
144. G. W. Morris, personal communication.
145. T. Glonek, P. J. Wang and J. R. Van Wazer, *J. Am. Chem. Soc.*, 1976, 98, 7968.
146. R. A. Y. Jones and A. R. Katritzky, *J. Inorg. Nucl. Chem.*, 1960, 15, 193.
147. C. F. Callis, M. M. Crutchfield, R. R. Irani and G. C. Roth, *Inorg. Chem.*, 1962, 4, 813.
148. G. W. Morris, personal communication.
149. D. M. Davies and R. M. Jones, *J. Chem. Soc., Perkin Trans. 2*, 1989, 1323.
150. D. F. Evans and M. W. Upton, *J. Chem. Soc., Dalton Trans.*, 1985, 2525.
151. K-H Kuthier, J. M. A. Al-Rawi and S. J. Hanna, *Spectrosc. Lett.*, 1989, 22, 549.
152. W. G. Barb, J. H. Baxendale, P. George and K. R. Hargrave, *Trans. Faraday Soc.*, 1951, 47, 591.
153. F. Haber and J. Weiss, *Proc. R. Soc. London, Ser. A*, 1935, 147, 332.
154. B. Halliwell, *FEBS Lett.*, 1976, 72, 8.
155. J. H. Wang, *J. Am. Chem. Soc.*, 1955, 77, 4715.
156. A. Couer and J. Alory, *Tenside*, 1967, 4, 65.
157. B. Kratochvil, *Anal. Chem.*, 1982, 54, 105R; J. F. Coetzee, B. K. Deshmukh and C-C. Liao, *Chem. Rev.*, 1990, 90, 827.
158. See for example, J-M. Lehn, E. Kauffmann and J-P. Sauvage, *Helv. Chim. Acta*, 1976, 59, 1099; F. Arnaud-Neu, J-M. Lehn, M. Sanchez, M-J. Schwing-Weill and R. Yahaya, *Helv. Chim. Acta*, 1985, 68, 456; M-C. Alamasio, F. Arnaud-Neu, J-M. Lehn, M-J. Schwing-Weill and S. A. Sullivan, *Helv. Chim. Acta*, 1985, 68, 831; L. L. Diaddario, T. E. Jones, L. A. Ochrymowycz, D. B. Rorabacher and L. L. Zimmer, *J. Am. Chem. Soc.*, 1975, 97, 7163; R. B. Cruz, L. L. Diaddario, T. E. Jones, L. A. Ochrymowycz, D. B. Rorabacher, L. S. W. L. Sokol, E. L. Yee and L. L. Zimmer, *J. Am. Chem. Soc.*, 1975, 97, 7163; L. A. Ochrymowycz, D. B. Rorabacher and L. S. W. L. Sokol, *Inorg. Chem.*, 1981, 20, 3189.

159. K. R. Adam, M. Antolovich, D. S. Baldwin, A. Bashall, L. G. Brigden, P. A. Duckworth, L. F. Lindoy, M. McPartlin and P. A. Tasker, *J. Chem. Soc., Dalton Trans.*, 1992, 1869 and refs. therein.
160. A. Bashall, D. E. Fenton, A. J. Leong, L. F. Lindoy, M. McPartlin and B. P. Murphy, *J. Chem. Soc., Dalton Trans.*, 1987, 2543.
161. N. A. Bailey, D. E. Fenton, S. J. Kitchen, A. J. Leong, T. H. Lilley, L. F. Lindoy, P. A. Tasker and M. G. Williams, *J. Chem. Soc., Dalton Trans.*, 1991, 627.
162. (a) S. J. Kitchen, Ph.D Thesis, 1989, University of Sheffield; (b) N. A. Bailey, D. E. Fenton, K. W. Grabham, S. J. Kitchen, R. W. Matthews, B. P. Murphy, I. J. Scowen, P. A. Tasker and M. G. Williams, *J. Chem. Soc., Dalton Trans.*, in preparation.
163. L. F. Lindoy, in *Current Topics in Macrocyclic Chemistry in Japan*, ed. E. Kimura, Hiroshima School of Medicine (Publ.), 1987.
164. K. R. Adam, G. Anderegg, A. J. Leong and L. F. Lindoy, *J. Chem. Soc., Dalton Trans.*, 1988, 1733.
165. See for example P. Schultz-Grunou, *Helv. Chim. Acta*, 1978, 61, 2291; M. Kodama and E. Kimura, *J. Chem. Soc., Dalton Trans.*, 1978, 104; M. Kodama, E. Kimura and T. Yatsunami, *J. Am. Chem. Soc.*, 1982, 104, 3182; K. Ishizu, M. Kodama, E. Kimura and R. Machida, *Inorg. Chem.*, 1982, 21, 595.
166. K. R. Adam, C. W. G. Ansell, P. J. Baillie, K. P. Dancey, L. A. Drummond, K. Henrick, A. J. Leong, L. F. Lindoy, B. J. McCool, M. McPartlin, P. A. Tasker, and D. K. Uppal, *J. Chem. Soc., Dalton Trans.*, 1990, 3435.
167. A. P. Leugger, L. Hartli and T. A. Kaden, *Helv. Chim. Acta*, 1978, 61, 2296.
168. C. Nave and M. R. Truter, *J. Chem. Soc., Dalton Trans.*, 1974, 2351.
169. M. Micheloni, P. Paoletti and A. Sabatini, *J. Chem. Soc., Perkin Trans. 2*, 1978, 828; M. Micheloni, P. Paoletti and A. Vacca, *J. Chem. Soc., Perkin Trans. 2*, 1978, 945; M. Bartolini, A. Bianchi, M. Micheloni and P. Paoletti, *J. Chem. Soc., Perkin Trans. 2*, 1982, 1345.
170. N. A. Bailey, D. E. Fenton, S. J. Kitchen, P. A. Tasker and M. G. Williams, *J. Chem. Soc. Chem. Commun.*, 1988, 1575.
171. H. Adams, N. A. Bailey, D. E. Fenton, I. G. Ford, S. J. Kitchen, A. J. Leong, T. H. Lilley, L. F. Lindoy, P. A. Tasker and M. G. Williams, *J. Chem. Soc., Dalton Trans.*, 1991, 1665.
172. L. F. Lindoy, personal communication.

173. K. R. Adam, M. Antolovich, P. J. Baillie, L. G. Brigden, L. Fabrizzi, A. J. Leong, L. F. Lindoy, M. McPartlin, D. Proserpio, B. Shah, P. A. Tasker, and D. K. Uppal, *J. Chem. Soc., Dalton Trans.*, 1991, 2493.
174. E. B. Fleischer, A. E. Gebala and P. A. Tasker, *Inorg. Chim. Acta*, 1972, 6, 72.
175. R. Bhula, P. Osvath and D. C. Weatherburn, *Coord. Chem. Rev.*, 1988, 91, 82.
176. M. Kodama and E. Kimura, *J. Chem. Soc., Dalton Trans.*, 1978, 1081.
177. (a) K. R. Adam, K. P. Dancey, B. A. Harrison, A. J. Leong, L. F. Lindoy, M. McPartlin and P. A. Tasker, *J. Chem. Soc., Chem. Commun.*, 1983, 1351; (b) K. R. Adam, K. P. Dancey, A. J. Leong, L. F. Lindoy, B. J. McCool, M. McPartlin and P. A. Tasker, *J. Am. Chem. Soc.*, 1988, 110, 8471.
178. N. W. Allcock, R. G. Kingston, P. Moore and C. Pierpoint, *J. Chem. Soc., Dalton Trans.*, 1984, 1937.
179. T. J. Lotz and T. A. Kaden, *Helv. Chim. Acta*, 1978, 61, 1376.
180. P. J. Baillie, A. J. Leong and L. F. Lindoy, unpublished results.
181. S. B. Brown, D. J. Cram, R. C. Helgeson, T. Kaneda, E. Maverick and K. N. Trueblood, *J. Am. Chem. Soc.*, 1985, 107, 3645; D. J. Cram, *Angew. Chem. Int. Ed. Engl.*, 1986, 25, 1039.
182. K. R. Adam, A. Bashall, M. R. Dent, S. Donnelly, D. E. Fenton, A. J. Leong, L. F. Lindoy, B. J. McCool, M. McPartlin, B. P. Murphy and P. A. Tasker, *J. Chem. Soc., Dalton Trans.*, 1990, 1635.
183. I. B. Bersuker, J. Garaj, J. Gazo, M. Kabesova, J. Kohout, H. Langelderova, M. Melnik, M. Serator and F. Valach, *Coord. Chem. Rev.*, 1976, 19, 253.

**Section B - Synthetic and Structural Studies of Semi-rigid Mixed-donor
Schiff-base Macrocyclic Complexes**

7. Introduction

Condensation reactions between carbonyl compounds and primary amines have played a central role in the preparation of co-ordination compounds containing unsaturated nitrogen donor atoms. The use of such condensation reactions between dicarbonyl and α,ω -diamines in providing routes to synthetic macrocyclic ligands is well established.^[1] Indeed Schiff-base condensations figured in some of the earliest serendipitous^[2] and deliberate^[3] macrocyclic syntheses. Incorporation of a suitable metal ion in the reaction mixture provides an *in situ* approach to the synthesis of macrocyclic complexes and generally leads to markedly increased yields of cyclic product. The action of the metal ion in promoting cyclisation rather than polymerisation and oligomerisation, generally termed the metal-ion template effect,^[4] has been the subject of some debate.^[5] Influences due to the metal ion, such as co-ordinating and orientating reactants into suitable configurations and conformations for cyclisation (the kinetic template effect^[6]) and stabilisation of preformed cyclic structures (the thermodynamic template effect^[5]) have however been established.

The pyridine-based dicarbonyls, 2,6-diacetylpyridine (DAP) and pyridine-2,6-dicarbaldehyde (DFP), have been widely employed^[7] in reactions of this type, yielding an important class of imine macrocyclic complexes. The suitability of these dicarbonyls for participation in template reactions probably derives from their ability to co-ordinate to, and possibly be

activated by, the metal ion.^[7]

An interesting feature of these pyridine-based dicarbonyl compounds (in common with their furan, pyrrole and thiophen analogues) is their ability to participate in higher order condensations with α,ω -diamines yielding [2+2]^[8] (diamine + dicarbonyl) and, in some cases larger cyclars,^[9,10] depending on the metal employed. The [2+2] macrocycles are generally obtained using the larger metal ions as templates, e.g. Ag(I),^[11,12] Pb(II),^[13,14] Ba(II)^[15,16] and the actinide and lanthanide ions.^[17] Interestingly, higher order condensations (e.g. [4+4]) have been obtained in cases where polynuclear, small-ion 'cores', whose formation is facilitated by the structure of a reaction precursor, act as the templating device.^[18] The orders of condensation in reactions of this type are generally rationalised^[7,8] in terms of a match between the ionic radius of the templating ion and the cavity size of the resulting macrocycle.

Another interesting aspect of the influence of different metals on the chemistry of these systems is the occurrence of metal-induced contractions of the macrocyclic ring. Ring contractions of ligands containing =NH^[19] and -OH^[20] groups available for addition to imine double bonds of the ring are thought to be related to the size of the co-ordinated ion. Should a metal ion be too small to be effectively accommodated by these ligands, the macrocyclic ring may contract via intramolecular addition of the nucleophilic functions to one or more imine bonds producing smaller, more suitable cavities.

Schiff-base condensations of DFP and, more commonly, DAP with α,ω -diamines containing ether and thioether functions have yielded mixed-donor macrocyclic ligands in a large number of cases.^[5,7,8,21] Such ligands, in containing

rigid arrays of donors of differing character, have the potential for metal-ion recognition.^[22]

As part of a wider study into the metal ion discrimination of these rigid, mixed-donor systems, the aromatic diamines *bis*-(2-aminophenoxy)- and *bis*-(2-aminothiophenoxy)-*o*-xylene have been synthesised in order to produce novel macrocyclic ligands via condensation reactions employing DFP. Semi-rigid macrocyclic ligands with significantly different properties than their more flexible alkyl analogues^[23] were expected to result from these condensations. The condensation of α, α' -*bis*-(2-aminophenoxy)-*o*-xylene with DFP in the presence of s- and d-block metal perchlorates has yielded complexes of the same 34-membered [2+2] ligand (L^1 , Fig. 8.1.1).^[24] The apparent insensitivity of the condensation to the size of the templating ion is of significant interest. Complexes of L^1 with d- and p-block metals have been prepared in the course of the study reported here by both template and metal exchange (transmetallation) reactions. Structural investigations of the resulting complexes in the solid state and in solution have been undertaken in order to probe the co-ordination behaviour of L^1 with metal ions of different size and character. The results have implications for the design of selective complexing agents and highlight possible origins of the unusual template reactions.

Reductive demetallation of related [1+1] diimine complexes with sodium tetrahydridoborate has successfully yielded mixed-donor macrocycles suitable for investigation by potentiometric titration in 95 % methanol-water solution.^[23] To date, similar reductions with complexes of L^1 have not produced samples of the corresponding tetraamine with sufficient purity and solubility for such investigations.

Schematic representation of macrocyclic ligands derived from heterocyclic dicarbonyls

Conventional naming systems for organic ligands become increasingly more cumbersome with ligand complexity and even Melson's abbreviations for macrocyclic ligands^[1] become inappropriate for the larger cyclic structures. For this work, a simplified, schematic approach, especially suited to di- and tetra-imine ligands derived from heterocyclic dicarbonyls, will be adopted (see Fig. 7.1.1). Once the order of condensation for formation of the ligand is established (i.e. [1+1] for condensation of one molecule of dicarbonyl and one molecule of diamine, [2+2] for condensation of two molecules of dicarbonyl and two molecules of diamine), specification of the ring constituent chains (R^2), the imine carbon substituents (R^1) and the heterocyclic ring ($D = \text{py}$, fur, and th for 2,6-pyridine, 2,5-furan and 2,5-thiophen respectively) allows ready abbreviation for the majority of symmetrical structures. Open chain ligands may also be specified within this framework (e.g. [1+2] = diamine-diimine; [2+1] = dicarbonyl-diimine). Thus the 'N₆O₄', [2+2] ligand L^1 may be abbreviated as $D = \text{py}$, $R^1 = \text{H}$, $R^2 = o\text{-C}_6\text{H}_4\text{OCH}_2o\text{-C}_6\text{H}_4\text{CH}_2\text{Oo-C}_6\text{H}_4$.

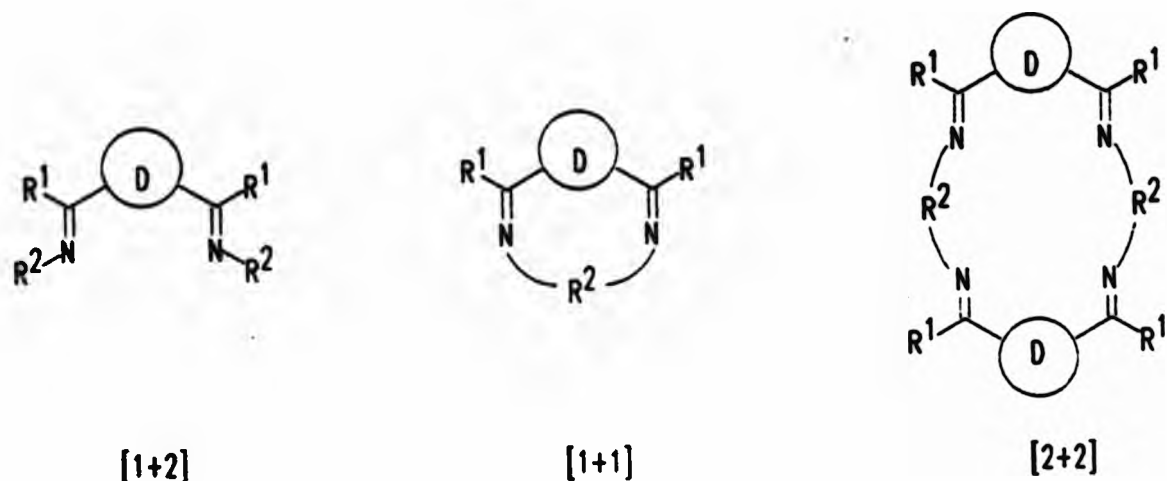


Figure 7.1 Schematic representations for Schiff-base ligands derived from heterocyclic dicarbonyls.

8. Experimental methods

8.1 List of compounds synthesised^a

^a (n) = compound label

8.1.1 Starting materials

Origins and purities of reagents used in syntheses of organic precursor compounds are summarised in Table 8.1.1.

Table 8.1.1. Origin and estimated purity of reagents used in synthesis of organic precursor compounds.

Compound	Source	Purity ^a
2-Nitrophenol	Aldrich	Moist solid containing 15 % H ₂ O
α,α' -Dibromo- <i>o</i> -xylene	Aldrich	96 %
2-Aminothiophenol	Aldrich	99 %
2,6-Pyridinedimethanol	Aldrich	98 %
Selenium dioxide	BDH	99 %
Hydrazine hydrate	Aldrich	Hydrazine content 55 %
Pd catalyst	Aldrich	10 % on carbon

^a Manufacturer's estimate.

8.1.2 Organic precursor compounds

α, α' -Bis(2-nitrophenoxy)-o-xylene	(1)
α, α' -Bis(2-aminophenoxy)-o-xylene	(M ³)
α, α' -Bis(2-aminothiophenoxy)-o-xylene	(2)
Pyridine-2,6-dicarbaldehyde	(3)

8.1.3 Template reaction products

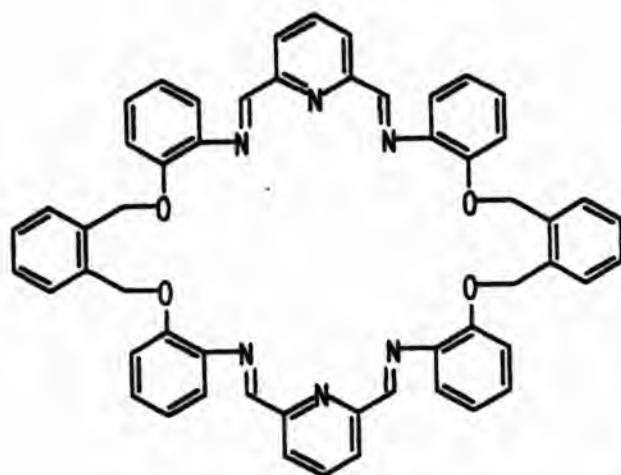


Figure 8.1.1 The hexaazatetraoxa macrocycle, L¹.

{(4,5:8,9:12,13:23,24:27,28:31,32,-hexabenz-3,14,22,33,39,40,-hexaaza-6,11,25,30-tetraoxatricyclo[34.3.1.1^[25]]tetraconta-1(39),4,8,12,16(40),17,19,23,27,31-decaene)manganese(II)}chlorate(VII)
([MnL¹][ClO₄]₂)

{(4,5:8,9:12,13:23,24:27,28:31,32,-hexabenz-3,14,22,33,39,40,-hexaaza-6,11,25,30-tetraoxatricyclo[34.3.1.1^[25]]tetraconta-1(39),4,8,12,16(40),17,19,23,27,31-decaene)disilver(I)}chlorate(VII)
([Ag₂L¹][ClO₄]₂)

{(4,5:8,9:12,13:23,24:27,28:31,32,-hexabenz-3,14,22,33,39,40,-hexaaza-6,11,25,30-tetraoxatricyclo[34.3.1.1^[25]]tetraconta-1(39),4,8,12,16(40),17,19,23,27,31-decaene)lead(II)}chlorate(VII)
([PbL¹][ClO₄]₂)

{(4,5:8,9:12,13:23,24:27,28:31,32,-hexabenz-3,14,22,33,39,40,-hexaaza-6,11,25,30-tetraoxatricyclo[34.3.1.1^[25]]tetraconta-1(39),4,8,12,16(40),17,19,23,27,31-decaene)lead(II)}thiocyanate
 $([\text{PbL}^1][\text{SCN}]_2)$

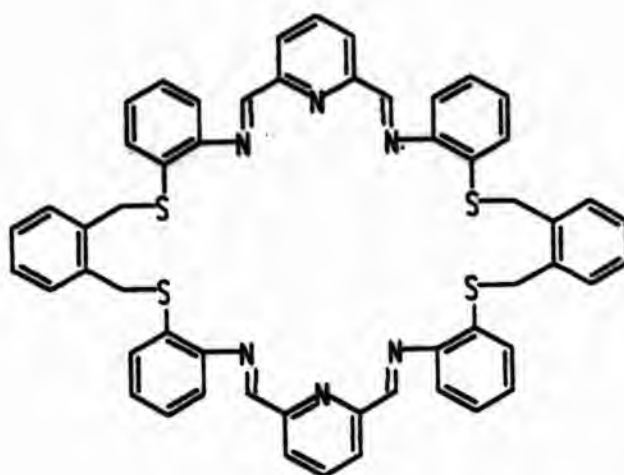


Figure 8.1.2 The hexaazatetrathia macrocycle, L^2 .

{(4,5:8,9:12,13:23,24:27,28:31,32,-hexabenz-3,14,22,33,39,40,-hexaaza-6,11,25,30-tetrathiatricyclo[34.3.1.1^[25]]tetraconta-1(39),4,8,12,16(40),17,19,23,27,31-decaene)lead(II)}chlorate(VII)
 $([\text{PbL}^2][\text{ClO}_4]_2)$

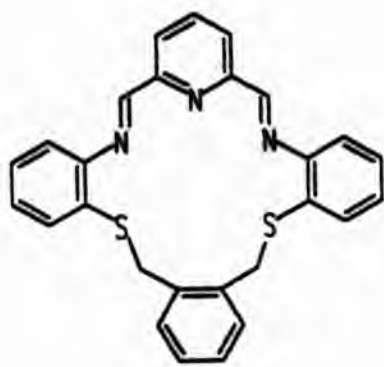


Figure 8.1.3 The triazadithia macrocycle, L^3 .

{(4,5:8,9:12,13-tribenz-13,14,20-triaza-6,11-dithiabicyclo[15.3.1]pentadeca-1(20),4,8,12-tetraene)silver(I)}chlorate(VII)
 $([\text{AgL}^3][\text{ClO}_4])$

8.1.4 Transmetalation reaction products

{(4,5:8,9:12,13:23,24:27,28:31,32,-hexabenz-3,14,22,33,39,40,-hexaaza-6,11,25,30-tetraoxatricyclo[34.3.1.1^[25]]tetraconta-1(39),4,8,12,16(40),17,19,23,27,31-decaene)cobalt(II)}chlorate(VII)

$$([CoL^1][ClO_4]_2)$$

{(4,5:8,9:12,13:23,24:27,28:31,32,-hexabenz-3,14,22,33,39,40,-hexaaza-6,11,25,30-tetraoxatricyclo[34.3.1.1^[25]]tetraconta-1(39),4,8,12,16(40),17,19,23,27,31-decaene)nickel(II)}chlorate(VII)

$$([NiL^1][ClO_4]_2)$$

{(4,5:8,9:12,13:23,24:27,28:31,32,-hexabenz-3,14,22,33,39,40,-hexaaza-6,11,25,30-tetraoxatricyclo[34.3.1.1^[25]]tetraconta-1(39),4,8,12,16(40),17,19,23,27,31-decaene)zinc(II)}chlorate(VII)

$$([ZnL^1][ClO_4]_2)$$

{(4,5:8,9:12,13:23,24:27,28:31,32,-hexabenz-3,14,22,33,39,40,-hexaaza-6,11,25,30-tetraoxatricyclo[34.3.1.1^[25]]tetraconta-1(39),4,8,12,16(40),17,19,23,27,31-decaene)cadmium(II)}chlorate(VII)

$$([CdL^1][ClO_4]_2)$$

8.1.5 Other materials used

α,α' -Bis-hydroxy-*o*-xylene (97 %, Aldrich) (M^4)

2,6-[1-(phenylimino)ethyl]pyridine [supplied by Prof. D. A. Edwards (University of Bath)] (see Fig. 11.1.1 for nmr numbering scheme) (M^1)

¹H Nmr (CDCl₃): δ /ppm 8.34 [A₂B multiplet, H11, ³J(H11-H12)], 7.87 [A₂B multiplet, H12) = 7.8 Hz]; ca. 7.38 [H32, second order multiplet approximating to triplet]; 7.12 [H33, second order multiplet approximating to triplet of triplets, ³J(H33-H32) = 7.4 Hz, ⁴J(H33-H31) = 1.2 Hz]; ca. 6.85 [H31, second order multiplet approximating to doublet of doublets]; 2.40 [s, H21].

¹³C Nmr (bb-{¹H}, CDCl₃): δ /ppm 167.32 (C2), 155.48 (C1), 151.31 (C3), 136.83 (C12), 129.01 (C32), 123.61 (C33), 122.32 (C11), 119.25 (C31), 16.19 (C21).

8.2 Solvents

General purpose grade solvents were used as supplied in most cases.

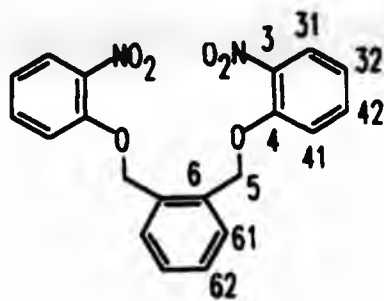
Chloroform was dried over activated 4 Å molecular sieves. Anhydrous dioxan was obtained by warming the GPR-grade reagent over potassium hydroxide pellets (3 molar equivalent) followed by filtration. The filtrate was subsequently heated at reflux under nitrogen with finely divided sodium metal and, in the preparation of 3, distilled at 103 °C directly into a pre-dried, 'flamed-out', reaction flask.

8.3 Synthesis of organic precursor compounds

8.3.1 Preparation of α,α' -Bis(2-nitrophenoxy)-o-xylene (1).

The preparative method employed was adapted from that described by Cannon et al for synthesis of 1,2-di-(o-nitrophenoxy)ethane.^[26]

Potassium carbonate (27.6 g, 0.20 mol) was added portionwise to o-nitrophenol (31.9 g, 0.195 mol, assuming 15 % H₂O impurity) in hot dimethylformamide (250 cm³). α,α' -Dibromo-o-xylene (26.4 g, 0.10 mol) was added to the refluxing mixture over 40 minutes. Refluxing was continued thereafter for 2 hours. The reaction mixture was cooled, concentrated under reduced pressure and poured into cold water (600 cm³). After cooling at 4°C for 24 hrs, a white precipitate was isolated at the pump. Concentration of the filtrate under reduced pressure yielded more white solid on cooling. Both crops were combined, washed with portions of methanol (3 × 50 cm³) and recrystallised from hot acetone. The resulting white flocculant solid was isolated at the pump, washed with chilled acetone (4 × 5 cm³) and desiccated in vacuo over phosphorus pentoxide for 24 h.



1

Yield 23.7 g (62%). M.p. = 135.7–136.4 °C. Microanalysis: Found: C, 63.3; H, 4.2; N, 7.4 %. Calculated for $C_{20}H_{16}N_2O_6$: C, 63.2; H, 4.2; N, 7.4 %.
 I.r. (FTIR, KBr 3 mm disc): $\bar{\nu}_{max}/cm^{-1}$ 3117w (Ar-H), 3070w (Ar-H); 1616s (Ar), 1581m (Ar), 1521s (NO_2), 1454m, 1345s (NO_2), 1316m, 1274s, 1250m, 1168m, 1019m, 985m, 865m, 858m, 752m, 738s (Ar-H).
 M.s. (e.i., positive ion): m/z 242 (11 %, $[M-C_6H_4NO_3]^+$), 196 (100, $[M-\{C_6H_4NO_3 + NO_2\}]^+$), 104 (29, $[M-2\{C_6H_4NO_3\}]^+$).
 1H Nmr ($CDCl_3$): δ/ppm 7.81 [H31, dd, $^3J(H31-H32) = 8.2$ Hz, $^4J(H31-H42) = 1.7$ Hz]; ca. 7.6–7.45 (H42 and H62, m); ca. 7.4 (H61, m); 7.23 [H41, dd, $^3J(H41-H42) = 8.3$ Hz, $^4J(H41-H32) = 0.9$ Hz]; 7.01 [H32, ddd, $^3J(H32-H42) \approx 8$ Hz]; 5.39 (H5, s).
 ^{13}C Nmr (bb- $\{^1H\}$, $CDCl_3$): δ/ppm 151.72 (C4), 139.85 and 133.83 (C3 and C6), 134.37 (C42), 129.10 and 128.88 (C61 and C62), 125.65 (C31), 120.61 (C32), 114.74 (C41), 69.61 (C5).

8.3.2 Attempted synthesis of α,α' -Bis(2-aminophenoxy)-o-xylene (M^3).

The reduction of 1 using hydrazine hydrate with catalytic palladium on activated charcoal as catalyst according to a procedure adapted from that described by Fleischer et al.^[27] yielded o-aminophenol instead of M^3 .

A slurry of 1 (9.5 g, 0.025 mol) in degassed ethanol and water (1.5:1 v/v, 250 cm^3) containing palladium on carbon as catalyst (2.5 g, Pd:C 10 % w/w) was

prepared. The mixture was brought to reflux under nitrogen and hydrazine hydrate (25 g, 0.43 mol, assuming 45 % H₂O) was added in portions over 3 h. Refluxing was continued thereafter for 14 h, whereupon the mixture was filtered, cooled and concentrated to ca. 150 cm³ under reduced pressure. After storage overnight, a white precipitate was isolated at the pump and washed with water (2 × 5 cm³) and chilled methanol (1 × ca. 1 cm³). Recrystallisation from ethanol and water (1.5:1 v/v) yielded colourless crystals which were collected at the pump, washed with water (2 × 5 cm³) and chilled methanol (1 × ca. 1 cm³), and dried in vacuo over P₂O₅ for 12 h.

Yield = 2.2 g (40 %). M.p. = 173.7–175.0 °C (lit.,^[28] 174 °C).

Microanalysis: Found: C, 66.0; H, 6.5; N, 12.9 %. Calculated for C₆H₇NO: C, 66.0; H, 6.5; N, 12.8 %.

I.r. (KBr 12 mm disc): $\bar{\nu}_{\text{max}}$ /cm⁻¹ 3380s (NH₂), 3320s (NH₂), 3060–2600s, br (OH), 1600s (Ar), 1510s (Ar), 1470s, 1400s, 1280s, 1270s, 1230m, 1220m, 930m, 900s, 850m, 800m, 770m, 750s.

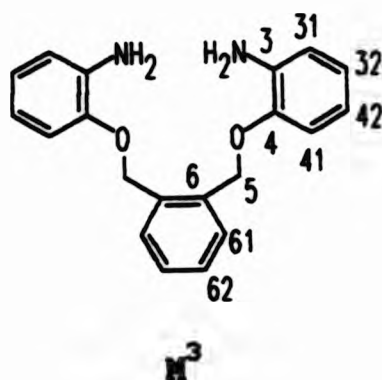
M.s. (e.i., positive ion): *m/z* 109 (100%, M⁺).

¹H Nmr [(CD₃)₂SO]: δ/ppm ca. 8.8 (OH, br); 6.65 [H31, dd, ³J(H31-H32) = 7.7 Hz, ⁴J(H31-H42) = 1.4 Hz]; 6.59 [H41, dd, ³J(H41-H42) = 7.7 Hz, ⁴J(H41-H32) = 2.0 Hz]; 6.54 [H42, td, ³J(H42-H41) ≈ ³J(H42-H32) ≈ 7.8 Hz, ⁴J(H42-H31) = 1.4 Hz]; 6.40 [H32, td, ³J(H32-H31) ≈ ³J(H32-H42) ≈ 7.4 Hz, ⁴J(H32-H41) = 2.0 Hz]; ca. 4.4 (NH₂, br).
¹³C Nmr [bb-{¹H}, (CD₃)₂SO]: δ/ppm 143.91 (C4) 136.39 (C3), 119.44 (C32), 116.42 (C42), 114.42 and 114.35 (C31 and C41).

8.3.3 Preparation of α,α'-Bis(2-aminophenoxy)-o-xylene (M³).

Reduction of 1 was achieved using a method adapted from that described by Bashall et al for reduction of 2,6-bis(2-nitrophenoxyethyl)pyridine.^[23]

α,α' -Bis(2-nitrophenoxy)-o-xylene (9.5 g, 0.025 mol) was slurried in ethanol-water (1.5:1 v/v, 500 cm³) containing iron filings (14.0 g, 0.25 mol) and brought to reflux. Glacial acetic acid (15 cm³) was added over 30 min and refluxing was continued for 18 h. The reaction mixture was filtered hot through cellulose floc (Whatman Ashless Floc) at the pump and refrigerated at 4 °C for 12 h. Beige crystals separated from the filtrate during storage and were collected at the pump. Concentration of the filtrate under reduced pressure yielded more product. The crops of crystals were combined and recrystallised twice from 2-propanol containing decolourising charcoal. Soft, beige, plate-like crystals were isolated at the pump after several days and washed with portions of chilled methanol (2 x 5 cm³) before desiccation in vacuo over phosphorus pentoxide for 24 h.



Yield = 3.60 g (45 %). M.p. = 98.0–98.7 °C. Microanalysis: Found: C, 75.6; H, 6.4; N, 8.8 %. Calculated for C₂₀H₂₀N₂O₂: C, 75.0; H, 6.3; N, 8.7 %.

I.r. (FTIR, KBr 3 mm disc): $\bar{\nu}_{\text{max}}$ /cm⁻¹ 3480s (NH₂), 3380s (NH₂), 2940w, 2880w, 1620s (Ar), 1590m (Ar), 1510s (Ar), 1460m, 1380m, 1300s, 1230s, 1215s, 1140m, 1050m, 1020m, 760s (Ar-H).

M.s. (e.i., positive ion): m/z 320 (15 %, [M]⁺), 212 (83, [M-C₆H₄NH₂O]⁺), 108 (51, [C₆H₄NH₂O]⁺), 104 (36, [M-2{C₆H₄NH₂O}]⁺), 70 (100).

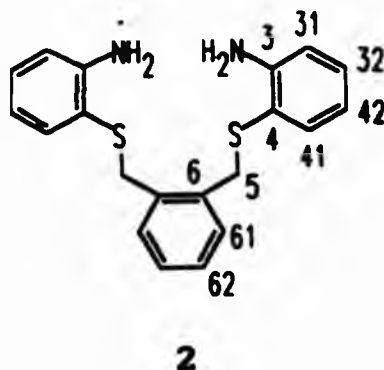
¹H Nmr (CDCl₃): δ /ppm ca. 7.52 and ca. 7.38 (H61 and H62, m); 6.88–6.65 (H31, H32, H41, H42, m); 5.19 (H5, s); 3.79 (NH₂, br).

¹³C Nmr (bb-{¹H}, CDCl₃): See Table 11.2.2.

8.3.4 Preparation of α,α' -Bis(2-aminothiophenoxy)-*o*-xylene (2).

The preparative method employed was adapted from that described by Cannon et al for synthesis of 1,2-di-(2-aminothiophenoxy)ethane. [26]

Degassed absolute ethanol (125 cm³) was treated with portionwise sodium (2.3 g, 0.1 mol) under a positive pressure of nitrogen. The solution was brought to reflux and, on dissolution of the sodium, 2-aminothiophenol (6.6 g, 0.053 mol) was added dropwise to the mixture via a pressure equalising funnel. α,α' -Dibromo-*o*-xylene (6.6 g, 0.025 mol) was added over 40 min to the mixture and refluxing was continued for a further 60 minutes. The reaction mixture was then filtered into cold water (250 cm³) and refrigerated at 4 °C for 12 h. The white solid precipitate was collected at the pump and recrystallised from hot ethanol. Pale purple crystals were isolated by suction filtration, washed with portions of ethanol (2 x 25 cm³) and diethyl ether (1 x 30 cm³) and dried in vacuo over P₂O₅ for 12 h.



Yield = 5.64 g (64 %). M.p. = 99.4-100.0 °C. Microanalysis: Found: C, 68.1; H, 5.8; N, 8.0 %. Calculated for C₂₀H₂₀N₂S₂: C, 68.1; H, 5.7; N, 8.0 %.
I.r. (FTIR, KBr 3 mm disc): $\bar{\nu}_{\text{max}}$ /cm⁻¹ 3446m (NH₂), 3352m (NH₂), 3065w (Ar-H), 3011w (Ar-H), 1606s (Ar), 1563sh (Ar), 1477s, 1447m, 1307m, 1254m, 1160m, 770m, 750s, 728m (Ar-H).

M.s. (e.i. positive ion): m/z 352 (68 %, $[M]^{+\cdot}$), 228 (93, $[M-C_6H_6NS]^{+\cdot}$), 194 (100, $[M-(C_6H_6NS + H_2S)]^{+\cdot}$), 124 (97, $[C_6H_6NS]^{+\cdot}$), 104 (75, $[C_6H_6]^{+\cdot}$).
 1H Nmr ($CDCl_3$): δ/ppm 7.17 [H41, ddd, $^3J(H41-H42) = 7.7$ Hz, $^4J(H41-H32) = 1.6$ Hz, $^5J(H41-H31) = 0.4$ Hz]; 7.09 [H32, ddd, $^3J(H32-H42) = 7.4$ Hz, $^3J(H32-H31) = 8.0$ Hz, $^4J(H32-H41) = 1.6$ Hz]; 7.03 (centre of AA'BB' multiplet, H61 and H62); 6.66 [H31, ddd, $^3J(H31-H32) = 8.0$ Hz, $^4J(H31-H42) = 1.4$ Hz, $^5J(H31-H41) = 0.4$ Hz]; 6.59 [H42, ddd, $^3J(H42-H41) = 7.7$ Hz, $^3J(H42-H32) = 7.4$ Hz, $^4J(H42-H31) = 1.4$ Hz]; 4.26 (NH_2 , s, br); 3.96 (H5, s).
 ^{13}C Nmr (bb- $\{^1H\}$, $CDCl_3$): δ/ppm 148.65 (C3), 136.55 (C41), 136.17 (C6), 130.49 (C62 or C61), 130.11 (C32), 127.28 (C61 or C62), 118.41 (C42), 117.25 (C4), 114.81 (C31), 36.59 (C5).

8.3.5 Preparation of pyridine-2,6-dicarbaldehyde (3).

Pyridine-2,6-dicarbaldehyde was obtained by oxidation of 2,6-pyridinedimethanol, based on the method of Jerchel *et al.* [29]

2,6-Pyridinedimethanol (12.5 g, 0.09 mol) was dissolved in anhydrous dioxan (250 cm^3) in a pre-dried apparatus fitted with silica gel guard tubes. Selenium dioxide (10.2 g, 0.09 mol) was added in portions and the mixture was heated at reflux for 2.75 h. The solution was filtered under nitrogen (pre-dried by passing over anhydrous $CaCl_2$) and concentrated under reduced pressure. A pale yellow solid precipitated from the solution overnight and was collected at the pump. Further reduction of the solution yielded more product and the two crops of solid were combined. The solid was dissolved in a minimum volume of dried chloroform, filtered and treated dropwise with petroleum ether (40-60 °C fraction) until precipitation was apparently complete. The cream coloured powder was collected at the pump and dried in

vacuo over P_2O_5 overnight.

On prolonged exposure to air, the surface of the powder developed a red colouration. Re-purification using the procedure described above afforded samples of dialdehyde with sufficient purity for subsequent use.

Yield: 10.1 g (75 %). Microanalysis: Found: C, 62.2; H, 3.8; N, 10.5 %. Calculated for $C_7H_5NO_2$: C, 62.2; H, 3.7; N, 10.4 %. M.s. (e.i., positive ion): m/z 135 (81 %, $[M]^{+\cdot}$), 107 (81, $[M-CO]^{+\cdot}$), 85 (100), 78 (94, $[M-2CO]^{+\cdot}$).

8.4 Metal template syntheses

The macrocyclic ligands L^1 , L^2 , and L^3 were obtained as metal complexes using *in situ* metal template syntheses adapted from the method described by Bashall et al.^[23] In general, a stoichiometric quantity of the appropriate diamine (M^3 or 2) in methanol was added over ca. 30-45 min to a refluxing solution of 3 and the appropriate metal salt in methanol. Refluxing was continued for 1-12 h whereupon the product was isolated and purified.

8.4.1 Preparation of $[MnL^1][ClO_4]_2 \cdot 2H_2O$

Manganese perchlorate hexahydrate (5.4 g, 0.015 mol) and 3 (2.0 g, 0.015 mol) were dissolved in methanol (200 cm^3) and the solution was brought to reflux. M^3 (4.8 g, 0.015 mol; in ca. 50 cm^3 methanol) was added over 45 min. and refluxing was continued thereafter for 2 h. The mixture was then cooled, concentrated under reduced pressure and treated with diethyl ether (ca. 5 cm^3). A yellow, microcrystalline precipitate was isolated at the pump after 48 h, washed with diethyl ether (2 \times 10 cm^3) and dried under suction.

Yield = 5.40 g (32 %). Microanalysis: Found: C, 57.1; H, 3.9; N, 7.2 %.

Calculated for $C_{54}H_{46}N_6O_{14}Cl_2Mn$: C, 57.4; H, 4.1; N, 7.4 %.

I.r. (FTIR, KBr 3 mm disc): $\bar{\nu}_{max}/cm^{-1}$ 3467br,s (H_2O), 3067w (Ar-H), 3030w (Ar-H), 2952w, 1640m (C=N), 1589s (Ar, py), 1486s (Ar), 1463m, 1451m, 1283m, 1242s, 1211m, 1145s, 1119vs and 1088vs ($\nu_3 ClO_4^-$), 1050m, 1009m, 950m, 804m, 787m, 755s (Ar-H) and 627s ($\nu_4 ClO_4^-$).

M.s. (fab, positive ion): m/z 993 (100 %, $[MnL^1][ClO_4]^+$), 894 (58, $[MnL^1]^+$).

8.4.2 Preparation of $[Ag_2L^1][ClO_4]_2 \cdot 0.5CH_3CN$

Silver perchlorate monohydrate (4.1 g, 0.02 mol) and 3 (2.0 g, 0.015 mol) were dissolved in methanol (200 cm³) and heated to reflux. M^3 (4.8 g, 0.015 mol; in 70 cm³ methanol) was added over 40 minutes (accompanied by development of an intense yellow colouration of the solution) and refluxing was continued for 12 h. A yellow-green precipitate was isolated at the pump which, after twice recrystallising from acetonitrile-diethyl ether (approximately 10:1 v/v), yielded yellow, efflorescent needles. On exposure to air, the crystals disintegrated into yellow microcrystals. These were washed with diethyl ether (2 × 5 cm³) and dried under suction.

Yield = 4.12 g (35 %). Microanalysis: Found: C, 51.6; H, 3.5; N, 7.3 %.

Calculated for $C_{55}H_{43.5}N_{6.5}O_{12}Cl_2Ag_2$: C, 51.8; H, 3.4; N, 7.2 %.

I.r. (FTIR, KBr 3 mm disc): $\bar{\nu}_{max}/cm^{-1}$ 3064m (Ar-H), 2883w, ca. 2000vw (C=N), 1628m (C=N), 1585s (Ar, py), 1486s, 1455s, 1373w, 1366w, 1290m, 1267m, 1241s, 1205m, 1162m, 1091vs,br ($\nu_3 ClO_4^-$), 1032m, 999s, 956m, 947m, 802m, 778m, 750s (Ar-H), 623s ($\nu_4 ClO_4^-$).

M.s. (fab, positive ion): m/z 1154 (29 %, $[Ag_2L^1][ClO_4]^+$), 1055 (7, $[Ag_2L^1]^+$), 948 (100, $[AgL^1]^+$), 842 (6, $[AgL^1-C_8H_8]^+$), 527 (20, $[Ag_2L^1]^{2+}$).

1H Nmr (CD_3CN): See Table 11.1.9. ^{13}C Nmr (bb- $\{^1H\}$, CD_3CN): See Table 11.2.3

8.4.3 Preparation of $[\text{PbL}^1][\text{ClO}_4]_2 \cdot \text{H}_2\text{O}$

Diamine M^3 (3.2 g, 0.01 mol; in ca. 50 cm^3 methanol) was added over ca. 40 minutes to a refluxing solution of lead(II) perchlorate trihydrate (4.6 g, 0.01 mol) and 3 (1.3 g, 0.01 mol) in methanol (200 cm^3). A microcrystalline yellow solid precipitated from the reaction solution on addition of the diamine. Refluxing was terminated after the dropwise addition of the diamine had been completed. After cooling, the solid was isolated at the pump and then dissolved in hot acetonitrile (25 cm^3). The solution was allowed to cool and diethyl ether (ca. 3 cm^3) was added. Yellow, efflorescent plates were isolated after 48 h. The crystals were washed with chilled methanol (2 \times 5 cm^3) and diethyl ether (1 \times ca. 2 cm^3), and dried *in vacuo* over P_2O_5 for 24 h.

Yield = 8.40 g (67 %). Microanalysis: Found C, 51.7; H, 3.3; N, 6.7 %.

Calculated for $\text{C}_{54}\text{H}_{44}\text{N}_6\text{O}_{13}\text{Cl}_2\text{Pb}$: C, 51.4; H, 3.5; N, 6.7 %.

I.r. (FTIR, KBr 3 mm disc): $\bar{\nu}_{\text{max}}/\text{cm}^{-1}$ ca. 3500m,br (H_2O), 3067w (Ar-H), 1632m (C=N), 1586s (Ar, py), 1492s, 1457m, 1269m, 1234s, 1205m, 1164m, ca. 1095vs,br ($\nu_3 \text{ClO}_4^-$), 1037s, 1013s, 1003s, 777m, 753s (Ar-H), 624s ($\nu_4 \text{ClO}_4^-$).

M.s. (fab, positive ion): m/z 1145 (29 %, $[\text{PbL}^1(\text{ClO}_4)]^+$), 1046 (11, $[\text{PbL}^1]^+$), 818 (65), 718 (47), 523 (33), 507 (100).

^1H Nmr (CD_3CN): See Table 11.1.6. ^{13}C Nmr (bb- $\{^1\text{H}\}$, CD_3CN): See Table 11.2.3.

8.4.4 Preparation of $[\text{PbL}^1][\text{NCS}]_2$

Diamine M^3 (1.6 g, 0.005 mol; in 50 cm^3 MeOH) was added over 45 minutes to a suspension of $\text{Pb}(\text{NCS})_2$ (2.6 g, 0.01 mol) in a methanol solution (125 cm^3) of 3 (0.68 g, 0.005 mol). The solution was heated at reflux for 1 h and filtered while hot through glass fibre. The filtrate was concentrated at reduced pressure to ca. 70 cm^3 and, after storage for 72 h at 4 $^\circ\text{C}$, an orange

precipitate was collected at the pump. A portion of the solid was dissolved in hot methanol (ca. 25 cm³) containing activated charcoal and filtered. Reduction of the volume of solution to ca. 20 cm³ by slow evaporation of the filtrate at 4 °C yielded orange efflorescent plates. These crystals were collected by gravity filtration and dried *in vacuo* over P₂O₅ for 24 h.

Microanalysis: Found C, 57.9; H, 3.5; N, 9.5 %. Calculated for

C₅₆H₄₂N₈O₈S₄Pb: C, 59.9; H, 3.5; N, 9.5 %.

I.r. (FTIR, KBr 3 mm disc): $\bar{\nu}_{\text{max}}$ /cm⁻¹ 3060w (Ar-H), 3020w (Ar-H), 2943w, 2879w, 2054vs (ν_1 NCS⁻), 1630m (C=N), 1584s (Ar, py), 1490s, 1456m, 1270m, 1232s, 1204m, 1163m, 1114m, 1039m, 1012m, 1005sh, 932m, 806m (ν_2 NCS⁻), 777m, 753s (Ar-H).

¹H NMR (CD₃CN): See Table 11.1.6. ¹³C NMR (bb-{¹H}, CD₃CN): See Table 11.2.3.

8.4.5 Preparation of [PbL²][ClO₄]₂

Lead perchlorate trihydrate (2.3 g, 0.005 mol) and 3 (0.68 g, 0.005 mol) in refluxing methanol (200 cm³) were treated dropwise with 2 (1.8 g, 0.005 mol; in ca. 50 cm³ methanol) over 40 minutes. Refluxing was continued thereafter for 20 minutes and a yellow, microcrystalline precipitate was isolated at the pump. Dissolution of the solid in N,N'-dimethylformamide (ca. 50 cm³) followed by portionwise addition of water to the mixture (ca. 2 cm³; sufficient volume to induce transient turbidity in the solution on mixing) yielded, after several weeks, small yellow needles which were collected at the pump, washed with acetone (3 × 5 cm³) and dried *in vacuo* for 4 h. Slow evaporation of filtrate from the reaction mixture over several weeks yielded small octahedral crystals of the same product.

Microanalysis: Found C, 49.7; H, 3.3; N, 6.4 %. Calculated for

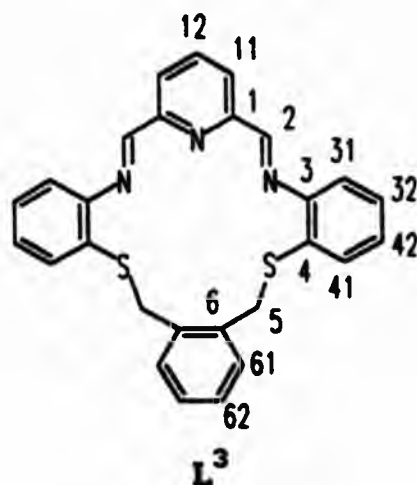
$C_{54}H_{42}N_6O_4S_4Cl_2Pb$: C, 49.5; H, 3.2; N, 6.4 %.

I.r. (FTIR, KBr 3 mm disc): $\bar{\nu}_{max}/cm^{-1}$ 3056m (Ar-H), 3002w (Ar-H), 2822w, 1629m (C=N), 1583s (Ar, py), 1568sh, 1470s, 1451m, 1274m, 1163s, ca. 1095vs,br (ν_3 ClO_4^-), 1039s, 1002m, 771m, 737s (Ar-H), 622s (ν_4 ClO_4^-).

M.s. (fab, positive ion): m/z 1209 (17 %, $\{[PbL^2][ClO_4]\}^{+}$), 1110 (10, $[PbL^2]^{+}$), 758 (100, $\{[PbL^2-C_{27}H_{21}N_3S_2][ClO_4]\}^{+}$), 659 (36, $[PbL^2-C_{27}H_{21}N_3S_2]^{+}$), 554 (37, $[PbL^2-C_{35}H_{29}N_3S_2]^{+}$), 420 (37), 346 (46, $[C_{19}H_{13}N_3S_2]^{+}$).

8.4.6 Preparation of $[AgL^3][ClO_4]$

Dropwise addition of 2 (0.67 g, 0.005; mol in 50 cm^3 methanol) to a refluxing solution of silver perchlorate monohydrate (2.3 g, 0.01 mol) and 3 (0.68 g, 0.005 mol) in methanol (125 cm^3) yielded a yellow precipitate after refluxing for 1 h. Dissolution of the solid in N,N'-dimethylformamide (ca. 50 cm^3) followed by dropwise addition of water (ca. 5 cm^3) to the mixture yielded, after storage for 48 h, a yellow, microcrystalline precipitate. The solid was isolated at the pump, washed with methanol (3×5 cm^3) and diethyl ether ($1 \times$ ca. 1 cm^3), and dried in vacuo over P_2O_5 for 24 h.



Microanalysis: Found: C, 49.5; H, 3.3; N, 6.5 %. Calculated for

$C_{27}H_{21}N_3O_5S_2ClAg$: C, 49.2; H, 3.2; N, 6.4 %.

I.r. (FTIR, KBr 3 mm disc): $\bar{\nu}_{max}/cm^{-1}$ 3054w (Ar-H), 3001w, 1621m (C=N), 1587s (Ar, py), 1472s, 1428m, 1277m, 1161m, 1098vs,br ($\nu_3 ClO_4^-$), 1034m, 949m, 799m, 761s (Ar-H), 736s, 623s ($\nu_4 ClO_4^-$).

M.s. (fab positive ion): m/z 560 (100 %, $[AgL^3]^+$), 399 (17).

1H Nmr (CD_3CN): δ /ppm 8.91 [H2, s]; 8.30 [H12, AB_2 multiplet,

$^3J(H11-H12) = 7.6$ Hz]; 8.05 [H11, AB_2 multiplet]; ca. 8.11 [H41, m]; 7.63-7.54 [H31, H32, H42, m]; ca. 7.41 and ca. 7.18 [H61 and H62, m]; 4.68 [H5, s].

The sample was insufficiently soluble for determination of its ^{13}C nmr spectrum.

A second batch of $[AgL^3][ClO_4]_2$ in CD_3CN gave an essentially identical spectrum except that the signal at 8.91 ppm appeared as a doublet ascribed to silver-proton spin-spin coupling [$^3J(^{107,109}Ag-H2) = 4.0$ Hz].

8.5 Transmetalation syntheses

Exchange of the two Ag(I) ions of $[Ag_2L^1][ClO_4]_2$ with Co(II), Ni(II), Zn(II) and Cd(II) was achieved using a procedure adapted from that described by Nelson *et al.*^[30] The appropriate hydrated metal perchlorate (ca. 0.5 mmol) was added in portions (over ca. 15 min) to a solution of $[Ag_2L^1][ClO_4]_2$ (ca. 0.1 mmol) in acetonitrile (25 cm³) at room temperature. Solutions were stored at room temperature for ca. 18 h, heated on a steam bath, filtered hot and concentrated to ca. 15 cm³ under reduced pressure. Slow evaporation of the solvent over several weeks yielded crystals of the appropriate metal complex of L^1 which were collected by gravity filtration, washed with methanol (3 x 1 cm³) and dried in vacuo for 24 h.

8.5.1 $[\text{CoL}^1][\text{ClO}_4]_2$

Treatment of $[\text{Ag}_2\text{L}^1][\text{ClO}_4]_2$ (0.1331 g, 0.11 mmol) with $\text{Co}(\text{ClO}_4)_2 \cdot 6\text{H}_2\text{O}$ (0.1831 g, 0.50 mmol) yielded orange-yellow needles.

Microanalysis: Found: C, 58.9; H, 3.5; N, 7.7 %. Calculated for

$\text{C}_{54}\text{H}_{42}\text{N}_6\text{O}_{12}\text{Cl}_2\text{Co}$: C, 59.1; H, 3.9; N, 7.7 %.

I.r. (FTIR, KBr 3 mm disc): $\bar{\nu}_{\text{max}}/\text{cm}^{-1}$ 3074w (Ar-H), 3026w (Ar-H), 2878w, 1630w (C=N), 1589s (Ar, py), 1495s, 1488s, 1448m, 1289m, 1250s, 1214m, 1164m, 1120sh, 1094vs,br ($\nu_3 \text{ClO}_4^-$), 1054s, 1007m, 969m, 952m, 784m, 756s (Ar-H), 624s ($\nu_4 \text{ClO}_4^-$).

M.s. (fab, positive ion): m/z 997 (100 %, $[\text{CoL}^1][\text{ClO}_4]^+$), 898 (77, $[\text{CoL}^1]^{+\cdot}$).

8.5.2 $[\text{NiL}^1][\text{ClO}_4]_2 \cdot \text{CH}_3\text{CN}$

Treatment of $[\text{Ag}_2\text{L}^1][\text{ClO}_4]_2$ (0.1141 g, 0.091 mmol) with $\text{Ni}(\text{ClO}_4)_2 \cdot 6\text{H}_2\text{O}$ (0.1866 g, 0.51 mmol) yielded red, octahedral crystals.

Microanalysis: Found: C, 58.1; H, 4.0; N, 8.8 %. Calculated for

$\text{C}_{56}\text{H}_{45}\text{N}_7\text{O}_{12}\text{Cl}_2\text{Ni}$: C, 59.1; H, 4.0; N, 8.6 %.

I.r. (FTIR, KBr 3 mm disc): $\bar{\nu}_{\text{max}}/\text{cm}^{-1}$ 3070w (Ar-H), 3025w (Ar-H), 2878w, ca. 2240w (C=N), 1631w (C=N), 1589s (Ar, py), 1489s, 1469m, 1447m, 1288m, 1251s, 1215m, 1163m, 1120sh, 1095vs,br ($\nu_3 \text{ClO}_4^-$), 1054s, 1008m, 974m, 954m, 809m, 755s (Ar-H), 624s ($\nu_4 \text{ClO}_4^-$).

M.s. (fab positive ion): m/z 1013 (23 %), 995 (100, $[\text{NiL}^1][\text{ClO}_4]^+$), 914 (30), 896 (90, $[\text{NiL}^1]^{+\cdot}$).

8.5.3 $[\text{ZnL}^1][\text{ClO}_4]_2 \cdot 2\text{CH}_3\text{CN}$

Treatment of $[\text{Ag}_2\text{L}^1][\text{ClO}_4]_2$ (0.1304 g, 0.10 mmol) with $\text{Zn}(\text{ClO}_4)_2 \cdot 6\text{H}_2\text{O}$ (0.1848 g, 0.50 mmol) yielded yellow octahedral crystals.

Microanalysis: Found: C, 58.9; H, 4.0; N, 9.4 %. Calculated for

$\text{C}_{58}\text{H}_{48}\text{N}_8\text{O}_{12}\text{Cl}_2\text{Zn}$: C, 58.8; H 4.1; N, 9.4 %.

I.r. (FTIR, KBr 3 mm disc): $\bar{\nu}_{\text{max}}/\text{cm}^{-1}$ 3074w (Ar-H), 3066w (Ar-H), 2878w, 2240w (C≡N), 1636w (C=N), 1628w (C=N), 1590s (Ar,py), 1496s, 1487s, 1453m, 1447m, 1287m, 1249s, 1214m, 1163m, 1144m, 1120sh, 1093vs,br ($\nu_3 \text{ClO}_4^-$), 1051m, 1008m, 971m, 952m, 825m, 812m, 783m, 756s (Ar-H), 624 ($\nu_4 \text{ClO}_4^-$).

M.s (f.a.b. positive ion): m/z 1002 (100 %, $[\text{ZnL}^1][\text{ClO}_4]^+$), 920 (20), 903 (52, $[\text{ZnL}^1]^+$).

$^1\text{H Nmr}$ (CD_3CN): See Table 11.1.3. $^{13}\text{C Nmr}$ (bb- $\{^1\text{H}\}$, CD_3CN): See Table 11.2.3.

8.5.4 $[\text{CdL}^1][\text{ClO}_4]_2 \cdot \text{CH}_3\text{CN} \cdot \text{H}_2\text{O}$

Treatment of $[\text{Ag}_2\text{L}^1][\text{ClO}_4]_2$ (0.1257 g, 0.10 mmol) with $\text{Cd}(\text{ClO}_4)_2 \cdot 6\text{H}_2\text{O}$ (0.2058 g, 0.49 mmol) yielded pale yellow crystalline plates.

Microanalysis: Found: C, 56.6; H, 3.7; N, 8.0 %. Calculated for

$\text{C}_{56}\text{H}_{47}\text{N}_7\text{O}_{13}\text{Cl}_2\text{Cd}$: C, 55.6; H 3.9; N, 8.1 %.

I.r. (FTIR, KBr 3 mm disc): $\bar{\nu}_{\text{max}}/\text{cm}^{-1}$ 3598-3419m,br (H_2O), 3068m (Ar-H), 3025m (Ar-H), 2876m, 2011w (C≡N), 1633m (C=N), 1589s (Ar, py), 1486s, 1457m, 1284m, 1240s, 1211m, 1163m, ca. 1095vs,br ($\nu_3 \text{ClO}_4^-$), 1045s, 1016s, 948m, 803m, 786s (Ar-H), 754s, 624s ($\nu_4 \text{ClO}_4^-$).

M.s (fab, positive ion): m/z 1051 (81 %, $[\text{CdL}^1][\text{ClO}_4]^+$), 952 (34, $[\text{CdL}^1]^+$), 848 (5, $[\text{CdL}^1-\text{C}_8\text{H}_8]^+$), 530 (18, $[\text{CdL}^1-\text{C}_{27}\text{H}_{21}\text{N}_3\text{O}_2]^+$), 476 (29, $[\text{CdL}^1]^{2+}$), 428 (100, $[\text{CdL}^1-\text{C}_{35}\text{H}_{29}\text{N}_3\text{O}_2]^+$).

$^1\text{H Nmr}$ (CD_3CN): See Table 11.1.4. $^{13}\text{C Nmr}$ (bb- $\{^1\text{H}\}$, CD_3CN): See Table 11.2.3.

8.6 Instrumental methods

8.6.1 ^1H nmr spectra

Proton nmr spectra were obtained using a Bruker AM250 operating at 250.134 MHz in Pulse Fourier Transform (PFT) mode. A ^2D solvent field-frequency lock was used in all cases. Routinely, spectra were run at ambient probe temperature (300 K) and sample temperatures (estimated error ± 1.0 K) for these and variable temperature spectra were estimated using an on-line Bruker Temperature Controller.

Samples for nmr analysis were dissolved in deuteriated solvents containing tetramethylsilane (SiMe_4) as the internal standard. Typical operating conditions, using $[\text{ZnL}^1][\text{ClO}_4]_2$ (saturated solution in CD_3CN) as an example, were:

number of transients, 364; pulse length, 2.0 μs ; delay 2.0 s; spectral width, 3546.099 Hz; acquisition time, 2.31 s; points, 16 k.

8.6.2 ^{13}C nmr spectra

Broad band proton decoupled (bb- $\{^1\text{H}\}$) carbon-13 nmr spectra were obtained using a Bruker AM250 operating at 62.896 MHz at ambient probe temperature (300 K). Samples were prepared in deuteriated solvents, containing internal SiMe_4 as the reference standard, and a solvent field-frequency lock was used in all cases. Typical operating conditions for a ^{13}C bb- $\{^1\text{H}\}$ spectrum, using $[\text{ZnL}^1][\text{ClO}_4]_2$ (saturated in CD_3CN) as an example, were: number of transients, 14886; pulse length, 2.5 μs ; offset f_1 2000.00 Hz; delay 2.0 s; spectral width, 15625.0 Hz; acquisition time, 1.049 s; data points, 32 k; decoupling frequency 5700.00 Hz;

8.6.3 2-D nmr spectra

Routine local procedures were employed using the following conditions:

COSY spectra

^1H - ^1H COSY spectra were collected with 256 t_1 FIDs of 16 scans each and a relaxation delay of 5 s per scan. The initial t_1 delay of 3 μs was incremented by 490 μs per experiment. Analogous parameters used for ^1H - ^{13}C COSY spectra were: 256 t_1 FIDs of 64 scans with 3 s relaxation delay per scan; initial t_1 delay of 3 μs , incremented by 245 μs per experiment. Delays D_1 and D_2 of 3.57 and 1.78 ms, respectively, assumed $^1J(\text{CH}) = 140$ Hz.

^1H - ^1H J-Resolved

Parameters used to determine ^1H - ^1H J-resolved spectra were: 128 t_1 FIDs of 32 scans with a 5 s relaxation delay; initial t_1 delay of 3 μs , incremented by 16.0 ms per experiment.

Quadrature detection in t_2 was used for all 2D experiments.

8.6.4 Infrared spectra

Infrared spectra were obtained variously using either of two instruments:

a) A Perkin-Elmer 781 spectrophotometer operating in transmission mode.

Samples were supported in pressed KBr discs (12 mm diameter) prepared by grinding pre-dried KBr with ca. 10 % (v/v) sample. Spectra were calibrated using the absorption at 1602 cm^{-1} of standard polystyrene film.

b) Fourier transform infrared (FTIR) spectra were recorded using a BIO-RAD FTS40 spectrometer linked to a 3240-SPC data station. Samples were supported in pressed microdiscs (3 mm diameter) prepared by grinding pre-dried KBr with ca. 1 % (w/w) of sample. Background spectra were obtained from KBr

of the same batch as that used in preparation of samples and re-run at bihourly intervals. Spectra were obtained in transmission mode and the corresponding absorbance spectrum was computed to allow estimation of peak positions (estimated error $\pm 5 \text{ cm}^{-1}$) by computer analysis. Spectra were calibrated using internal He-Ne laser calibration. Typical conditions employed for FTIR spectra were: range, $4500\text{--}500 \text{ cm}^{-1}$; number of scans, 64; resolution, 4 cm^{-1} .

All discs were prepared immediately prior to spectral determination.

8.6.5 C, H, and N analysis

Analyses for carbon, hydrogen and nitrogen content of samples were obtained using a Carlo Erba 1106 Elemental Analyzer.

8.6.6 Mass spectra

Electron impact (e.i.) spectra were obtained for the organic compounds using an AEI MS-9 or a Kratos Profile spectrometer operating in positive ion mode. Positive ion, fast atom bombardment (FAB) spectra were obtained for metal complexes in 2-nitrobenzyl alcohol matrices via the SERC service at the University of Swansea.

9. Synthesis and characterisation of mixed donor macrocyclic imine complexes

Complexes of the macrocyclic ligands L^1 , L^2 and L^3 have been prepared using *in situ* metal template condensations of pyridine-2,6-dicarbaldehyde and the diamines, M^3 and 2. The general synthetic routes for the oxa and thia systems are summarised in Figure 9.1(i) and 9.1(ii) respectively. Interestingly, during early studies of metal-templated macrocyclisations, Busch and co-workers reported Zn(II) and Cd(II) complexes of an ' N_3S_2 ' macrocycle [D = py, R^1 = Me, R^2 = $oC_6H_4SCH_2oC_6H_4CH_2SoC_6H_4$] similar to L^3 .^[31] The only difference between the macrocycles lies in the azomethine carbon substituent (L^3 has H in this position while Busch's macrocycle has methyl substituents). In contrast to the synthetic routes employed in this study, Busch prepared these complexes via neutral, open chain Schiff-base complexes [D = py, R^1 = Me, R^2 = $oC_6H_4S^-$], formed on condensation of 2,6-diacetylpyridine with *o*-aminothiophenol in the presence of the appropriate metal ion. Formation of the macrocyclic ring was then achieved on reaction with α,α' -dibromo-*o*-xylene.

9.1 Synthesis of diamine precursors M^3 and 2

Adaptions of the synthetic routes described by Cannon *et al*^[26] for synthesis of 1,2-bis(2-aminophenoxy)ethane and 1,2-bis(2-aminothiophenoxy)ethane provided successful routes to the xylenyl-based diamines, M^3 and 2 respectively. The properties of these compounds, as well as those of the dinitro precursor of M^3 , are reported for the first time.

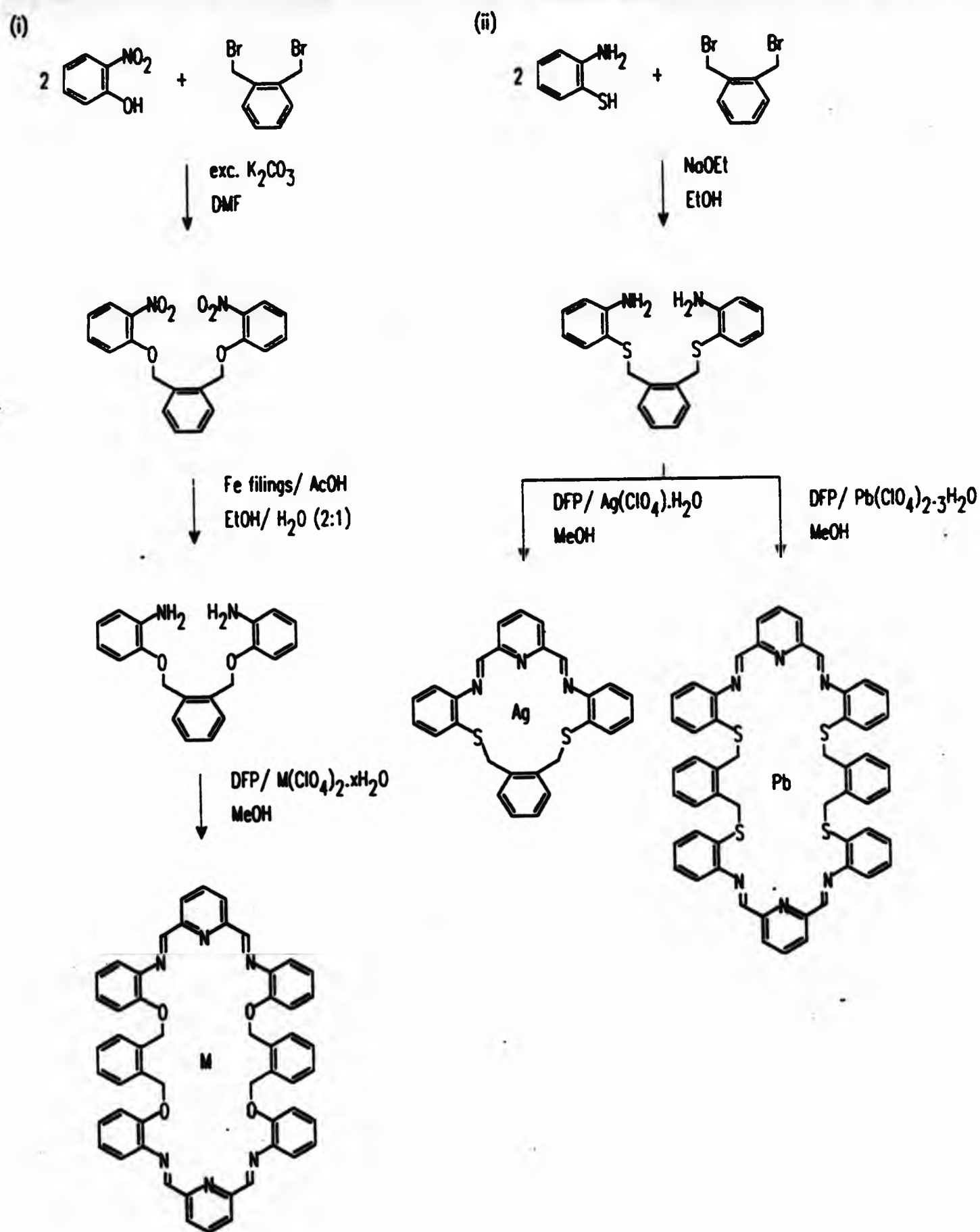


Figure 9.1 Synthetic routes for complexes of; (i) the hexaazatetraoxa macrocycle L^1 ; (ii) the hexaazatetrathia and triazadithia macrocycles L^2 and L^3 . [DFP is pyridine-2,6-dicarbaldehyde]

Synthesis of M^3 required preparation of its dinitro analogue, α,α' -bis(2-nitrophenoxy)-*o*-xylene (1). This was achieved by reaction of α,α' -dibromo-*o*-xylene with *o*-nitrophenol in *N,N'*-dimethylformamide. Treatment of a hot solution of *o*-nitrophenol with a slight excess of potassium carbonate (accompanied by a colour change from yellow to red which presumably reflects the formation of a nitrophenolate species), followed by addition of the dibromide and a short period of refluxing produced, after work-up and recrystallisation, pure samples of the required dinitro compound in good yield.

α,α' -Bis(2-aminophenoxy)-*o*-xylene, M^3 , was synthesised by reduction of the dinitro compound, 1, with metallic iron. Prolonged refluxing (> 12 h) was required to effect reduction of the nitro functions, and the separability of M^3 from the reaction mixture was poor, leading to low yields of product. Preparation of pure samples of M^3 required at least two recrystallisations from 2-propanol containing charcoal. In view of these difficulties, the reduction was attempted using hydrazine hydrate with catalytic palladium. Analytical and spectroscopic data for the colourless crystals obtained from this experiment are, however, consistent with isolation of 2-aminophenol from the reaction. It seems likely that the carbon-oxygen bonds of 1 are reduced along with its nitro functions. Notably, reduction of the related bis-nitrophenoxy compound, 2,6-bis(2-nitrophenoxy)methylpyridine using similar reaction conditions does not give the desired diamine.^[32]

The reactivity of the C-O bonds in 1 is reflected to some extent in the electron impact mass spectrum of the compound. The parent ion of the molecule ($m/z = 380$) is not observed in the spectrum, while peaks observed at $m/z = 242$ (the highest mass peak) and 104 correspond to the successive loss of

nitrophenoxyl radicals ($[\text{C}_6\text{H}_4\text{NO}_3]^\cdot$, $m/z = 138$) from 1. The base peak of the spectrum, at $m/z = 196$, corresponds to loss of neutral NO_2 from the highest mass fragment ($m/z = 242$). Primary fragmentation of 1 probably involves homolytic cleavage of the C-O bond yielding $[\text{C}_{14}\text{H}_{12}\text{NO}_3]^\cdot$ ($m/z = 242$) and the nitrophenoxyl radical $[\text{C}_6\text{H}_4\text{NO}_3]^\cdot$.

In contrast, the e.i. mass spectrum of M^3 shows a peak due the molecular ion ($m/z = 320$) although intense peaks at $m/z = 212$ and 104 correspond to the successive loss of aminophenoxyl radicals ($[\text{C}_6\text{H}_5\text{NO}]^\cdot$, $m/z = 108$) from $[\text{M}]^{+\cdot}$, again indicating that cleavage of the C-O bond is a likely fragmentation pathway. The observation of such fragmentations is of use in assigning the mass spectra of the metal complexes of L^1 .

The sulphur analogue of M^3 , α, α' -bis(2-aminothiophenoxy)-*o*-xylene (2), was prepared in one step, by reaction of 2-aminothiophenol with α, α' -dibromo-*o*-xylene in the presence of sodium ethoxide (prepared *in situ* using metallic sodium dissolved in absolute ethanol). Mild reaction conditions produced pure samples of the required diamine in good yields.

The e.i. mass spectrum of 2 shows a peak at $m/z = 352$ due to the molecular ion of the diamine. Intense peaks observed at $m/z = 228$ and 104 are consistent with, respectively, loss of one and two aminothiophenoxyl moieties (which, on turn, correspond with peaks at $m/z = 124$) from the molecular ion. These fragmentations presumably arise from cleavage of the C-S bond. The spectrum of 2 is more complicated than that of the oxygen analogue, M^3 , in the higher mass regions and it appears that more than one major fragmentation pathway may be operative.

9.2 Metal template reactions

9.2.1 Synthesis of $[\text{MnL}^1][\text{ClO}_4]_2$

Previous investigations into the condensation of M^3 with 3 in the presence of manganese(II) perchlorate have indicated the formation of a mononuclear complex of the [2+2] Schiff-base product L^1 .^[24] Using similar reaction conditions, 3 and $\text{Mn}[\text{ClO}_4]_2 \cdot 6\text{H}_2\text{O}$ in refluxing methanol were treated with M^3 in a 1:1:1 ratio. An intense yellow colour developed in the solution during addition of the diamine, presumably due to formation of a Schiff-base product. Addition of a small volume of diethyl ether to the concentrated reaction mixture yielded, after storage, a yellow, microcrystalline precipitate of pure product.

The infrared spectrum of the microcrystals contained a medium intensity band at 1640 cm^{-1} assigned to the imine ($\text{C}=\text{N}$) stretching mode. The imine stretching mode generally gives rise to diagnostic, medium intensity bands in metal complexes of related di- and tetra-imino ligands in the range ca. $1660\text{--}1600\text{ cm}^{-1}$.^[16,33] Low intensities for these bands have, however, been noted in several first row transition metal complexes.^[30,34] The presence of the band at 1640 cm^{-1} and absence of peaks attributable to carbonyl (at ca. 1720 cm^{-1}) and amine (ca. 3400 cm^{-1}) for this sample points to formation of a cyclised, Schiff-base product. Amine stretching modes could be obscured by the broad absorbance at ca. 3500 cm^{-1} (attributed to O-H stretching of lattice water) but, as N-H stretches generally give rise to strong bands (for example, the strong bands at 3480 and 3380 cm^{-1} of M^3), contamination of the product with amine impurities is not indicated.

The region between $1600\text{--}1400\text{ cm}^{-1}$ in the infrared spectrum is dominated by

strong absorbances at 1589 and 1487 cm^{-1} , and medium intensity bands at 1463 and 1451 cm^{-1} . These are attributed to carbon-carbon (and in the case of the pyridine ring, carbon-nitrogen) stretches of the aromatic pyridyl, iminophenoxy and xylenyl rings. Macrocyclic complexes containing 2,6-pyridinediimine head units as the sole aromatic component of the ligand also show strong absorbances at ca. 1590 cm^{-1} .^[30] The band at 1589 cm^{-1} in the spectrum is therefore tentatively assigned as a stretching mode associated with the 2,6-pyridyl ring.

Very strong and strong absorptions observed at ca. 1100 and 627 cm^{-1} respectively are within ranges associated with the asymmetric stretching mode [$\nu_3(\text{ClO}_4)$, see Fig. 9.2.1] and the asymmetric bending mode [$\nu_4(\text{ClO}_4)$, Fig. 9.2.1] of perchlorate.^[35,36] Evidence for metal complex formation may be inferred from the presence of these characteristic, strong absorptions.

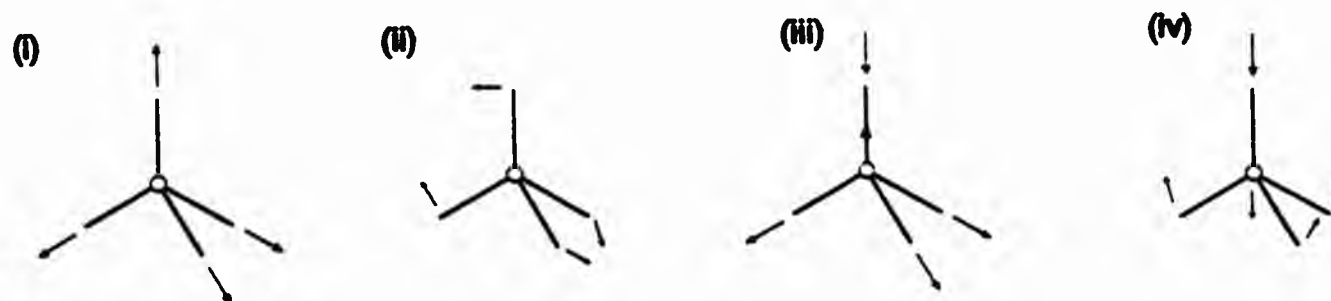


Figure 9.2.1 The four normal modes of vibration for tetrahedral $[\text{ClO}_4]^-$; ^[35] (i) $\nu_1(\text{ClO}_4)$, symmetric stretch; (ii) $\nu_2(\text{ClO}_4)$, symmetric bend; (iii) $\nu_3(\text{ClO}_4)$, asymmetric stretch; (iv) $\nu_4(\text{ClO}_4)$, asymmetric bend.

Splitting of the $\nu_3(\text{ClO}_4)$ band into two components, at 1119 and 1088 cm^{-1} , and the fine structure apparent in the $\nu_4(\text{ClO}_4)$ band, indicate^[36] lowering of the tetrahedral symmetry of the $[\text{ClO}_4]^-$ ion. In cases where perchlorate symmetry is lowered by association (either by co-ordination to a metal ion or through

hydrogen bonding), the $\nu_1(\text{ClO}_4)$ and $\nu_2(\text{ClO}_4)$ modes (Raman-only active in the free ion) become ir active, showing bands at ca. 930 and ca. 460 cm^{-1} respectively. [35,36] Absorbances due to these modes are not apparent in the spectrum although a weak band due to $\nu_1(\text{ClO}_4)$ might plausibly be obscured by ligand bands in the 950-900 cm^{-1} region. The observed reduction of perchlorate symmetry from that of the free ion may be due to association with either the metal ion or with the lattice water via hydrogen bonding. The two distinct bands in the region corresponding to $\nu_3(\text{ClO}_4)$ of the free ion, are assigned as ν_1 (at 1088 cm^{-1}) and ν_4 (1119 cm^{-1}) of unidentate perchlorate. [36] Co-ordination in this fashion lowers the symmetry of the group from T_d to C_{3v} . Bidentate co-ordination confers C_{2v} symmetry on the species and is accompanied by the appearance of three bands in this region. [36]

Splitting of the $\nu_3(\text{ClO}_4)$ band by ca. 70 cm^{-1} in the infrared spectrum of a Mn(II) complex of a related [1+1] 'N₅' macrocycle [D = py, R¹ = H, R² = $\text{oC}_6\text{H}_4\text{-N}(\text{CH}_2)_2\text{N-oC}_6\text{H}_4$] has been shown, by the determination of the crystal structure, to arise from monodentate perchlorate to metal co-ordination. [37] Hydrogen bonding of perchlorate, albeit to a secondary alcohol function, has also been observed for imine macrocyclic complexes in the solid state. [38] In the latter example $\nu_3(\text{ClO}_4)$ was split by 67 cm^{-1} . Such splittings are considerably larger than that observed for $[\text{MnL}^1][\text{ClO}_4]_2$ (31 cm^{-1}) and these observations, allied to the expectation that folding of the ligand around the metal will prevent approach of the anion towards the metal centre, lead to the conclusion that the perchlorate is unlikely to be co-ordinated to the metal. The C_{3v} symmetry of the ion therefore probably results from hydrogen bonding to the water molecules in the lattice.

Analyses for the carbon, hydrogen and nitrogen content of the yellow

microcrystals are consistent with the condensation of two molecules of diamine with two molecules of dicarbonyl per manganese(II) ion, presumably in a [2+2] cyclisation. The best fit for the data is given by inclusion of two moles of water per mole of $[\text{MnL}^1][\text{ClO}_4]_2$, consistent with the observation of $\nu(\text{H}_2\text{O})$ in the infrared spectrum.

The fab mass spectrum provides key evidence for the [2+2] nature of the Schiff-base condensation. The highest mass peak in the spectrum (at $m/z = 993$) corresponds to the species $[\text{MnL}^1][\text{ClO}_4]^+$, arising from loss of a perchlorate anion from the neutral parent molecule. This peak is also the base peak of the spectrum. The loss of the second perchlorate anion generates the species $[\text{MnL}^1]^+$ at $m/z = 894$. The remaining peaks of the spectrum are of insignificant intensity (<5 % in all cases) although the weak peak at $m/z = 790$ corresponds to the loss of $[\text{C}_8\text{H}_8]^+$ from $[\text{MnL}^1]^+$. This mirrors the cleavage of the $\text{PhO}-\text{CH}_2$ bond noted as a principal site for fragmentation in the electron impact mass spectra of the organic precursors of L^1 .

9.2.2 Synthesis of $[\text{Ag}_2\text{L}^1][\text{ClO}_4]_2$

The disilver(I) complex of L^1 was isolated during preliminary investigations^[24] into the condensation of M^3 with 3. A similar product has been isolated as part of this study, the reaction of M^3 and 3 in methanol yielding $[\text{Ag}_2\text{L}^1][\text{ClO}_4]_2$. As in the preparation of $[\text{MnL}^1][\text{ClO}_4]_2$, the reaction mixture developed an intense yellow colour on addition of the diamine to a solution containing 3 and the hydrated metal perchlorate ($\text{Ag}[\text{ClO}_4]\cdot\text{H}_2\text{O}$ in this case). A yellow-green precipitate was isolated after 12 h refluxing: evidence of precipitated metallic silver was noted on the sides of the reaction flask. Addition of diethyl ether to a near-saturated acetonitrile solution of the yellow-green material gave yellow crystals; a second 'recrystallisation' using

this method yielded yellow needles of pure product. On exposure to air the surfaces of these crystals dulled rapidly; indeed larger crystals disintegrated into a powder and were therefore unsuitable for single crystal X-ray studies. Attempts to prepare crystals suitable for such studies by using a range of solvent systems proved fruitless (see Chapter 10).

The infrared spectrum of $[\text{Ag}_2\text{L}^1][\text{ClO}_4]_2$ is broadly similar to that of $[\text{MnL}^1][\text{ClO}_4]_2$. The medium intensity band at 1628 cm^{-1} , attributed to the imine stretching mode, and the absence of strong absorbances at ca. 1720 and 3300 cm^{-1} , confirm the integrity of the Schiff-base product. (A broad weak band at ca. 3530 cm^{-1} is ascribed to water contamination, either of the KBr disc or, less likely, of the sample chamber of the spectrometer). The weak band at ca. 2000 cm^{-1} is attributed to the cyanide stretch of lattice acetonitrile. The weak nature of the band may arise from loss of solvent from the crystals during sample preparation and is consistent with the efflorescent nature of the crystals described above.

Absorbances due to perchlorate $\nu_3(\text{ClO}_4)$ and $\nu_4(\text{ClO}_4)$ modes appear as featureless, very strong and strong bands at 1091 and 623 cm^{-1} respectively. The presence of such absorbances and the absence of bands attributable to the $\nu_1(\text{ClO}_4)$ and $\nu_2(\text{ClO}_4)$ modes, are consistent with tetrahedral ClO_4^- in the complex, ^[35,36] presumably deployed in a counterionic rôle.

The spectrum shows ligand bands in similar positions to those observed for $[\text{MnL}^1][\text{ClO}_4]_2$. The spectrum contains bands which can be ascribed to the aromatic functions of the ligand; C-H stretching vibrations are assigned to weak bands at ca. 3000 cm^{-1} ; pyridine, iminophenoxy, and xylenyl ring stretching vibrations, to strong-medium bands at 1585 , 1486 and 1455 cm^{-1} ; and

aromatic C-H deformations to the medium-strong bands at 802, 778 and 750 cm^{-1} .

Analysis of the carbon, hydrogen and nitrogen content of the sample is consistent with the condensation of one mole of diamine with one mole of dicarbonyl per mole of Ag^+ . On the assumption that $[\text{Ag}_2\text{L}^1][\text{ClO}_4]_2$ is the reaction product, the closest fit to the analytical data is given by including one molecule of acetonitrile solvent per 2 molecules of complex. The presence of CH_3CN in the product was also inferred from its infrared spectrum.

Clearly, the infrared spectrum and the elemental analysis do not allow discrimination between a mononuclear $\text{Ag}(\text{I})$ complex of an N_3O_2 [1+1] cyclo-condensation product and a dinuclear [2+2] complex. Fab mass spectrometry, again, provides key evidence for formation of the [2+2] macrocycle L^1 . The highest mass peak in the spectrum ($m/z = 1154$) corresponds to loss of one perchlorate ion from the neutral parent complex, $[\text{Ag}_2\text{L}^1][\text{ClO}_4]_2$. Loss of a second perchlorate results in a weak peak at $m/z = 1055$, due to $[\text{Ag}_2\text{L}^1]^+$, and a rather more intense peak at $m/z = 527$, due to $[\text{Ag}_2\text{L}^1]^{2+}$. Loss of one silver ion from the dicationic complex generates the species $[\text{AgL}^1]^+$ giving the base peak of the spectrum at $m/z = 948$. This fragmentation pattern is closely similar to those of the analogous disilver complexes of the bibracchial tetraimine macrocycles derived from pyridine-2,6-dicarbaldehyde.^[12] In these cases, formation of [2+2] rings was confirmed by X-ray crystallography. Crystallographic evidence for the formation of the [2+2] ring in $[\text{Ag}_2\text{L}^1][\text{ClO}_4]_2$ may be inferred from crystal structures of $[\text{ZnL}^1][\text{ClO}_4]_2$ and $[\text{NiL}^1][\text{ClO}_4]_2$ (see Section 10.2). These compounds were obtained by transmetalation of the $\text{Ag}(\text{I})$ complex and, although an unusual ligand expansion has been observed during transmetalation of a [2+2] barium complex [$\text{D} = \text{py}$, $\text{R}^1 = \text{Me}$, $\text{R}^2 = \text{CH}_2\text{CH}(\text{OH})\text{CH}_2$] (yielding the corresponding [4+4]

tetramanganese(II) complex),^[18] it is expected that the [2+2] ring of $[\text{ZnL}^1]^{2+}$ and $[\text{NiL}^1]^{2+}$ is unchanged from that of the disilver derivative.

9.2.3 Syntheses of $[\text{PbL}^1][\text{ClO}_4]_2$ and $[\text{PbL}^1][\text{SCN}]_2$

The condensation of M^3 with 3 was attempted with Pb(II) present as both the perchlorate and thiocyanate salts.

Addition of M^3 to a solution of 3 and $\text{Pb}[\text{ClO}_4]_2 \cdot 3\text{H}_2\text{O}$ in refluxing methanol resulted in almost immediate precipitation of yellow, microcrystalline product. Recrystallisation of the yellow solid from acetonitrile-diethyl ether solution yielded yellow, efflorescent plate-like crystals.

The infrared spectrum of this product shows a medium intensity band at 1632 cm^{-1} , the presence of which, together with the absence of bands attributable to carbonyl and amine functions, indicated isolation of a cyclic Schiff-base product. A broad, featureless band at $\text{ca. } 3500\text{ cm}^{-1}$ is attributed to lattice water in the crystals, in agreement with the composition of the sample deduced from carbon, hydrogen and nitrogen microanalysis. The ir spectrum features a number of bands attributable to the aromatic ring systems of the molecule: weak absorbances at $\text{ca. } 3000\text{ cm}^{-1}$ are assigned as the aromatic C-H stretching modes; strong bands in the range $1600\text{--}1400\text{ cm}^{-1}$ as the aromatic C-C bond stretches; and medium to strong bands between $\text{ca. } 800\text{--}750\text{ cm}^{-1}$ to the aromatic C-H deformation modes.

The spectrum shows an intense band at 1095 cm^{-1} and strong band at 624 cm^{-1} , each devoid of fine structure. Again, these are readily assigned as the $\nu_3(\text{ClO}_4)$ and $\nu_4(\text{ClO}_4)$ modes of a tetrahedral perchlorate anion; the unsplit nature of both bands indicating a non-co-ordinating rôle for ClO_4^- in the

complex. [35,36]

The template synthesis of L^1 was also attempted in the presence of $Pb[SCN]_2$. It was hoped that the stronger co-ordinating ability of the thiocyanate ion compared with that of the perchlorate ion [36] would facilitate inclusion of two $Pb(II)$ ions in the 34-membered ring. A number of dilead(II) complexes of [2+2] tetraimine systems employing thiocyanate either as a co-ordinating ligand [14] or as a bridging ligand [13] have been reported. The thiocyanate anions, in co-ordinating the metal ions, presumably help to overcome charge repulsions between the two dipositive ions, allowing their proximity within these constrained systems. Significantly, the dilead(II) complex of a closely related N_6O_4 [2+2] macrocycle has been isolated as the tetra-thiocyanato complex using template procedures involving $Pb[NCS]_2$. [14]

Diamine M^3 was reacted with 3 and a suspension of $Pb[NCS]_2$ in methanol. The reactants were combined in the ratio 1:1:2 respectively. After a short period of refluxing, unreacted $Pb[NCS]_2$ was filtered from the solution and an orange-yellow precipitate of crude product developed in the filtrate after several hours. Pure samples of $[PbL^1][NCS]_2$ were obtained as orange-yellow plate-like crystals after recrystallisation of crude product from methanol.

The presence of a band at 1630 cm^{-1} (due to the C=N stretching mode) in the infrared spectrum and absence of absorbances due to amine or carbonyl functions again confirm the integrity of the Schiff-base product. Excepting regions corresponding to anion absorbances, the infrared spectrum of the thiocyanate derivative is essentially the same as that of the perchlorate. Microanalysis of the sample is consistent with the formation of a mononuclear

Pb(II) complex $[\text{PbL}^1][\text{NCS}]_2$.

The strong absorbance at 2054 cm^{-1} in the infrared spectrum of $[\text{PbL}^1][\text{NCS}]_2$ is assigned to the C-N stretching mode $[\nu_1(\text{SCN})]$ of the thiocyanate moiety. The C-S stretching mode of thiocyanate $[\nu_3(\text{SCN})]$ generally gives rise to a medium intensity band within the range $860\text{--}690\text{ cm}^{-1}$.^[39] In this case however, unambiguous assignment of the $\nu_3(\text{SCN})$ band is precluded by a profusion of bands due to aromatic C-H deformations of the ligand in the region $850\text{--}750\text{ cm}^{-1}$. The N-C-S bending frequency $[\nu_2(\text{SCN})]$, generally observed at ca. 450 cm^{-1} ,^[35,39] presumably lies beyond the spectral range investigated in this case ($4000\text{--}500\text{ cm}^{-1}$).

Ranges for $\nu_1(\text{SCN})$, $\nu_2(\text{SCN})$, and $\nu_3(\text{SCN})$ related to the anion-metal bonding mode of thiocyanate (*i.e.* monodentate co-ordination via either the nitrogen or sulphur donor atoms and bidentate bridging co-ordination via N-C-S or N-only bridges) have been proposed,^[35,39] although the unreliability of this approach has recently been highlighted.^[40] Although there is some danger in assigning a specific thiocyanate bonding mode based on the single ν_1 frequency observed for $[\text{PbL}^1][\text{NCS}]_2$, $\nu_1(\text{SCN})$ does lie within the range ($2060\text{--}2040\text{ cm}^{-1}$) quoted for the 'ionic' SCN^- counterions of Pb(II) thiocyanate complexes of the closely analogous triaza-dioxa and hexaaza-tetraoxa macrocycles.^[33] Additionally, the ν_1 band of $\text{K}[\text{NCS}]$ appears at 2053 cm^{-1} ,^[35] and these observations provide the basis for assigning the thiocyanate in $[\text{PbL}^1][\text{NCS}]_2$ as non-co-ordinating.

The fab mass spectrum of $[\text{PbL}^1][\text{ClO}_4]_2$ shows a highest mass peak at $m/z = 1145$, corresponding to loss of a perchlorate ion from the neutral parent complex. Loss of a second anion generates the peak at $m/z = 1046$, consistent

with the formulation $[\text{PbL}^1]^+$; the corresponding dicationic species ($[\text{PbL}^1]^{2+}$) is also present in the spectrum at $m/z = 523$. The remaining peaks of the spectrum apparently arise from a complicated breakdown pattern involving ligand fragmentation. Observed fragmentation products do not appear to correspond to α -cleavage of the phenyl ether bonds of the ligand, in marked contrast to the fragmentations observed for the dinitro- and diamino- organic precursor compounds (1 and M^3 respectively) and the sulphur analogue of $[\text{PbL}^1][\text{ClO}_4]_2$ (see Section 9.2.4).

Evidence for the formation of the [2+2] N_6O_4 ligand, L^1 , upon the template reaction of M^3 with 3 and $\text{Pb}[\text{NCS}]_2$ derives from the close similarity of its ^1H and ^{13}C nmr spectra with those of $[\text{PbL}^1][\text{ClO}_4]_2$ (see Section 11.1.4). Observation of essentially identical infrared spectra for the thiocyanate and perchlorate complexes supports this conclusion. From this evidence it appears that L^1 provides a specific one-ion binding site for $\text{Pb}(\text{II})$, in contrast to the dilead complexes isolated for significantly smaller [2+2] tetraimine macrocyclic rings,^[13,14] indicating a highly twisted conformation for the ligand. Further insight into the structures of the respective $[\text{PbL}^1]^{2+}$ complexes was obtained from ^1H and ^{13}C nmr (see Section 11.1.4).

9.2.4 Synthesis of $[\text{PbL}^2][\text{ClO}_4]_2$

The reaction of pyridine-2,6-dicarbaldehyde and the dithia-diamine 2 in methanol yielded a yellow solid after a short period of refluxing. Pure sample of $[\text{PbL}^2][\text{ClO}_4]_2$ was obtained on recrystallisation of the crude product from $\text{N,N}'$ -dimethylformamide and water. Crystalline samples of product giving essentially the same analyses were also obtained from slow evaporation of the reaction filtrate.

The infrared spectrum of the compound, in showing a medium intensity band at 1629 cm^{-1} (assigned to the C=N stretch) and absences of bands corresponding to carbonyl and amine functions, is consistent with the proposed formulation. Intense bands at 1095 and 622 cm^{-1} due to the $\nu_3(\text{ClO}_4)$ and $\nu_4(\text{ClO}_4)$ modes respectively, are unsplit, indicative of the perchlorate ion in T_d symmetry.^[36] Therefore, the perchlorate appears to be non-co-ordinating. The remainder of the spectrum is broadly similar with that of the analogous $[\text{PbL}^1][\text{ClO}_4]_2$ complex. Comparison of the spectra of these complexes provides useful insight into the origin of the separate bands ascribed to skeletal aromatic stretching modes in the respective complexes. The band at 1586 cm^{-1} in the spectrum of $[\text{PbL}^1][\text{ClO}_4]_2$, tentatively assigned as $\nu(\text{py})$ by comparison with spectra of Pb(II) complexes of non-benzenoid Schiff-base ligands,^[33] corresponds to the strong band at 1583 cm^{-1} in the spectrum of $[\text{PbL}^2][\text{ClO}_4]_2$. Positions of the two other principal bands in this region ($1600\text{--}1400\text{ cm}^{-1}$), however, appear to depend on the identity of the hetero-atom in the ligand, thereby supporting assignments of the $\nu(\text{py})$ stretch in the spectra of $[\text{PbL}^1][\text{ClO}_4]_2$ and $[\text{PbL}^2][\text{ClO}_4]_2$.

Elemental analysis and fab mass spectral data indicate formation of a mononuclear Pb(II) complex of the [2+2] cyclocondensation product L^2 . The mass spectrum shows a highest mass peak at $m/z = 1209$, corresponding to the loss of a perchlorate ion from the neutral parent complex, $[\text{PbL}^2][\text{ClO}_4]_2$. Loss of a second perchlorate generates the species $[\text{PbL}^2]^+$ at $m/z = 1110$. The remainder of the spectrum may be interpreted by assuming homolytic cleavage of the PhS-CH_2 bond as the principal fragmentation pathway (see Fig. 9.2.2). The complex apparently cleaves symmetrically at opposing S-CH_2 bonds yielding a fragment, $\{[\text{PbL}^2 - \text{C}_{27}\text{H}_{21}\text{N}_3\text{S}_2][\text{ClO}_4]\}^+$ at $m/z = 758$, the base peak of the spectrum. Loss of perchlorate from the fragment generates

the species $[\text{PbL}^2 - \text{C}_{27}\text{H}_{21}\text{N}_3\text{S}_2]^+$ at $m/z = 659$.

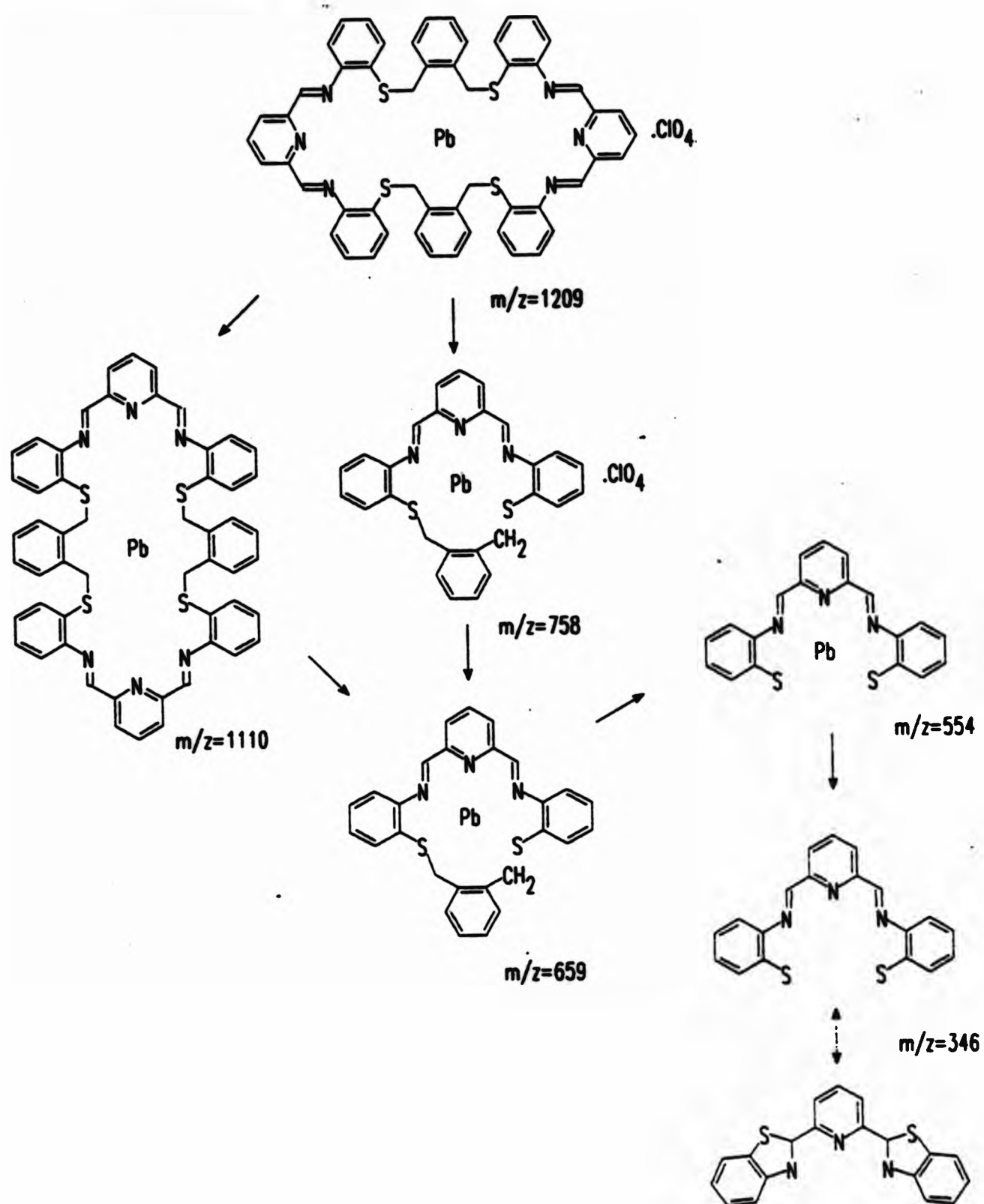


Figure 9.2.2 Proposed formulations for major fragments observed in the fab mass spectrum of $[\text{PbL}^2][\text{ClO}_4]_2$.

Organic fragments of these species are possibly stabilised by formation of a 17-membered macrocyclic ring (similar to L^3). Subsequent fragmentation apparently involves the loss of the xylenyl moiety from the ring-contracted

complex, presumably again involving cleavage of S-CH_2 , and ultimately loss of the Pb(II) ion. The resulting organic fragment may be stabilised by intramolecular rearrangement, possibly involving formation of a bis-thiazoline structure.

9.2.5 Synthesis of $[\text{AgL}^3][\text{ClO}_4]$

Condensation of 3 with the dithia-diamine 2 in methanol yielded a yellow powder after a short period of refluxing. Recrystallisation of the solid using N,N' -dimethylformamide and water yielded yellow microcrystals.

The infrared spectrum of the compound shows a medium intensity band at 1621 cm^{-1} assigned to the C=N stretch of the Schiff-base ligand. The absence of bands attributable to amine and carbonyl functions again confirms the integrity of the imine bonds in the product. Unsplit, intense bands at 1098 and 623 cm^{-1} are assigned to the $\nu_3(\text{ClO}_4)$ and $\nu_4(\text{ClO}_4)$ modes of perchlorate with T_d symmetry. Non-co-ordination of anion in the complex is deduced on this basis. The predominant features of the remainder of the spectrum are again attributable to aromatic functions. Weak bands at ca. 3000 cm^{-1} are assigned to C-H stretches of the respective aromatic rings; strong to medium bands at 1587 , 1472 , and 1428 cm^{-1} are assigned to skeletal stretches of the rings. The highest wavenumber peak of the latter group may be assigned to $\nu(\text{py})$ by comparison with the spectrum of $[\text{Ag}_2\text{L}^1][\text{ClO}_4]_2$, and those reported for analogous complexes derived from alkyl-bridged α,ω -diamines.^[41] Medium to strong bands in the region $800\text{--}730\text{ cm}^{-1}$ are assigned to C-H deformations of the same aromatic functions.

Microanalysis of the product is consistent with the condensation of one mole of diamine with one mole of dicarbonyl per mole of $\text{Ag}[\text{ClO}_4]$. As noted for $[\text{Ag}_2\text{L}^1][\text{ClO}_4]_2$, these observations are equally consistent with the formation

of a mononuclear complex of a [1+1] macrocycle ($[\text{AgL}^3][\text{ClO}_4]$) and of a binuclear complex of a [2+2] ligand (i.e. $[\text{Ag}_2\text{L}^2][\text{ClO}_4]_2$).

The fab mass spectrum of the sample is remarkably simple in comparison with those of $[\text{Ag}_2\text{L}^1][\text{ClO}_4]_2$ and $[\text{PbL}^2][\text{ClO}_4]_2$ and shows that Ag(I) directs the condensation specifically towards the [1+1] product, L^3 . The highest mass peak ($m/z = 560$) is the only significant feature in the spectrum and corresponds to loss of perchlorate from the neutral parent complex of the [1+1] macrocycle, $[\text{AgL}^3][\text{ClO}_4]$. Absences of peaks at higher mass numbers confirms identification of the [1+1] product.

The complex was sufficiently soluble in CD_3CN to enable its proton nmr spectrum to be obtained. Solubility was insufficient, however, for determination of useful ^{13}C nmr spectra. The proton spectrum shows groups of signals consistent with equivalence for sites comprising each half of the [1+1] product. (The numbering scheme for the asymmetric unit of $[\text{AgL}^3]^+$ is given in the experimental section). Absences of signals attributable to aldehydic and amine protons in the spectrum, indicate the integrity of the ligand in this solvent. Full assignment of the spectrum was precluded by overlap of signals due to a complicated second order subspectrum arising from the iminophenoxy ring protons. Discrete multiplets centred at ca. 7.41 and 7.18 ppm are distinguishable and approximate the separate components of an $\text{AA}'\text{XX}'$ subspectrum. Such spin systems are widely known for symmetrically 1,2-disubstituted benzenes;^[42] these signals are thus assigned to the xylenyl ring protons (H61 and H62). Assignment of separate multiplets in the $\text{AA}'\text{XX}'$ subspectrum are inappropriate without further comparative data for this macrocycle. The β - and γ -pyridyl protons give rise to an AB_2 subspectrum at low field. Analysis of the subspectrum using standard procedures^[42] yielded the parameters; $\delta(\text{H12}) = 8.30$ ppm, $\delta(\text{H11}) = 8.05$ ppm and $^3\text{J}(\text{H12-H11}) = 7.6$ Hz.

9.3 Transmetalation Syntheses

Metal exchange reactions have been widely employed^[8,21,43] to obtain transition metal complexes of imine macrocyclic ligands inaccessible via more traditional routes; direct reaction of ligands with metal salt solutions is often precluded by instability or unavailability of the 'free' imine ligand and template procedures often give differing products depending on the metal ion employed. In addition, first row transition metal ions are commonly ineffective as templating devices in preparations of [2+2] 2,6-pyridinediimine macrocycles^[8] in contrast to other macrocyclic and cryptate systems, e.g. the Co(II) template syntheses of sepulchrates and sarcophagines cages,^[44] and the Ni(II) template syntheses of salicylaldehyde derivatives.^[45]

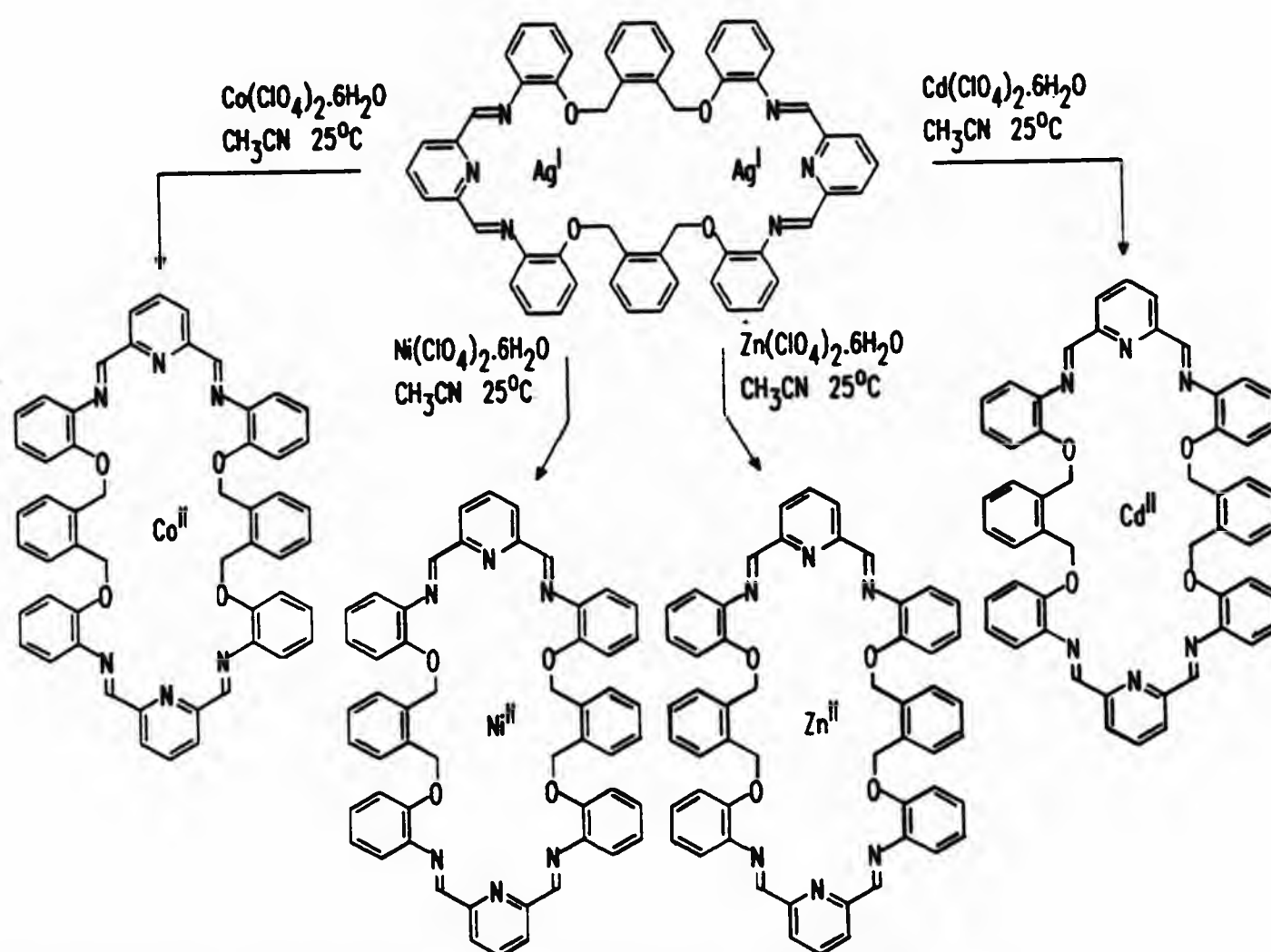


Figure 9.3.1 Transmetalation reactions of $[\text{Ag}_2\text{L}^1][\text{ClO}_4]_2$.

In this study, the lability of the disilver(I) complex of L^1 has been exploited to prepare cobalt(II) and nickel(II) complexes via facile, room temperature syntheses (See Fig. 9.3.1). The efficacy of $[Ag_2L^1][ClO_4]_2$ as a precursor for these syntheses obviated the need to resort to potentially problematic template procedures and also provided the basis for preparation of zinc(II) and cadmium(II) derivatives.

9.3.1 Preparation of $[CoL^1][ClO_4]_2$

Treatment of the disilver complex of L^1 with a 5 mole excess of hydrated cobalt(II) perchlorate in CH_3CN , yielded a mononuclear cobalt(II) complex. The metal exchange apparently proceeds rapidly at room temperature, the yellow solution of $[Ag_2L^1][ClO_4]_2$ turning to an orange colouration, presumably due to $[CoL^1][ClO_4]_2$, after a few minutes. The orange-yellow crystalline product was isolated after concentrating the solution by slow evaporation of solvent at room temperature.

The infrared spectrum of the solid is broadly similar to that of $[Ag_2L^1][ClO_4]_2$. Strong, sharp absorbances at 1094 and 624 cm^{-1} , assigned to $\nu_3(ClO_4)$ and $\nu_4(ClO_4)$ respectively, are unsplit and indicate non-association of perchlorate ions with the metal-ions. Bands in the range $1600\text{--}1400\text{ cm}^{-1}$ (associated with skeletal aromatic stretching modes) correspond to absorbances observed for the precursor disilver(I) complex and these were assigned accordingly. However, the strong band at 1486 cm^{-1} for $[Ag_2L^1][ClO_4]_2$ is replaced by two closely spaced bands at 1495 and 1488 cm^{-1} in the cobalt(II) derivative. The band due to the $C=N$ stretching mode of the cobalt(II) derivative (1630 cm^{-1}) is of significantly lower intensity is in comparison with those of the d^{10} metal complexes of L^1 . Infrared spectra of mononuclear Co(II) complexes of the related $[2+2]$ 'N₆O₄' [D = py, R¹ = Me,

$R^2 = (\text{CH}_2)_2\text{O}(\text{CH}_2)_2\text{O}(\text{CH}_2)_2$]^[30] and [2+2] 'N₆' [D = py, R¹ = Me,

$R^2 = (\text{CH}_2)_3\text{N}(\text{Me})(\text{CH}_2)_3$]^[46] macrocycles also show reduced intensities for these bands. In the latter case, the observation was associated with a low spin configuration (confirmed by magnetic moment measurements) for the Co(II) ion. Meridional co-ordination of the convergent terdentate 'head units' of the ligand is expected to give a sufficiently strong octahedral ligand field to overcome spin pairing repulsions for electrons in the metal d-orbitals. Unfortunately, determination of the magnetic moment of the complex was precluded by the relatively large amounts of sample required by the apparatus available. [Similar considerations also prohibited such measurements for the Mn(II) and Ni(II) complexes].

Reduced intensity imine bands have also been observed for a Co(II) transmetallated product of the barium complex of the [2+2] 'N₆' macrocycle [D = py, R¹ = H, R² = o-C₆H₄].^[47] In this case, however, X-ray crystallographic studies of the product revealed that the 18-membered ring had contracted to give a quinquedentate 15-membered macrocycle with an exo-macrocylic imidazoline ring, effectively halving the number of imine bonds in the ligand and thereby causing the reduction in imine absorbance.^[47] The driving force for the ring contraction is thought to derive from the improved fit of Co(II) in the smaller ring.

The absence of bands attributable to amine absorbances in the ir spectrum of [CoL¹][ClO₄]₂ is inconsistent with such rearrangements, further supporting the assumption that the L¹ backbone remains intact during the metal ion exchange.

Elemental analysis and fab mass spectral data confirm that the integrity of the ligand is retained during the transmetallation. The analyses for C, H,

and N content of the sample are consistent with the proposed formulation of a mononuclear cobalt(II) diperchlorate structure. The simplicity of the fab mass spectrum of $[\text{CoL}^1][\text{ClO}_4]_2$ contrasts with the complexity of that for $[\text{AgL}^1][\text{ClO}_4]_2$. The spectrum consists of peaks at $m/z = 997$ (the base peak of the spectrum) and $m/z = 898$, corresponding to loss of one and two perchlorates from the neutral complex respectively. It is noteworthy that these fragmentations mirror those observed of $[\text{MnL}^1][\text{ClO}_4]_2$.

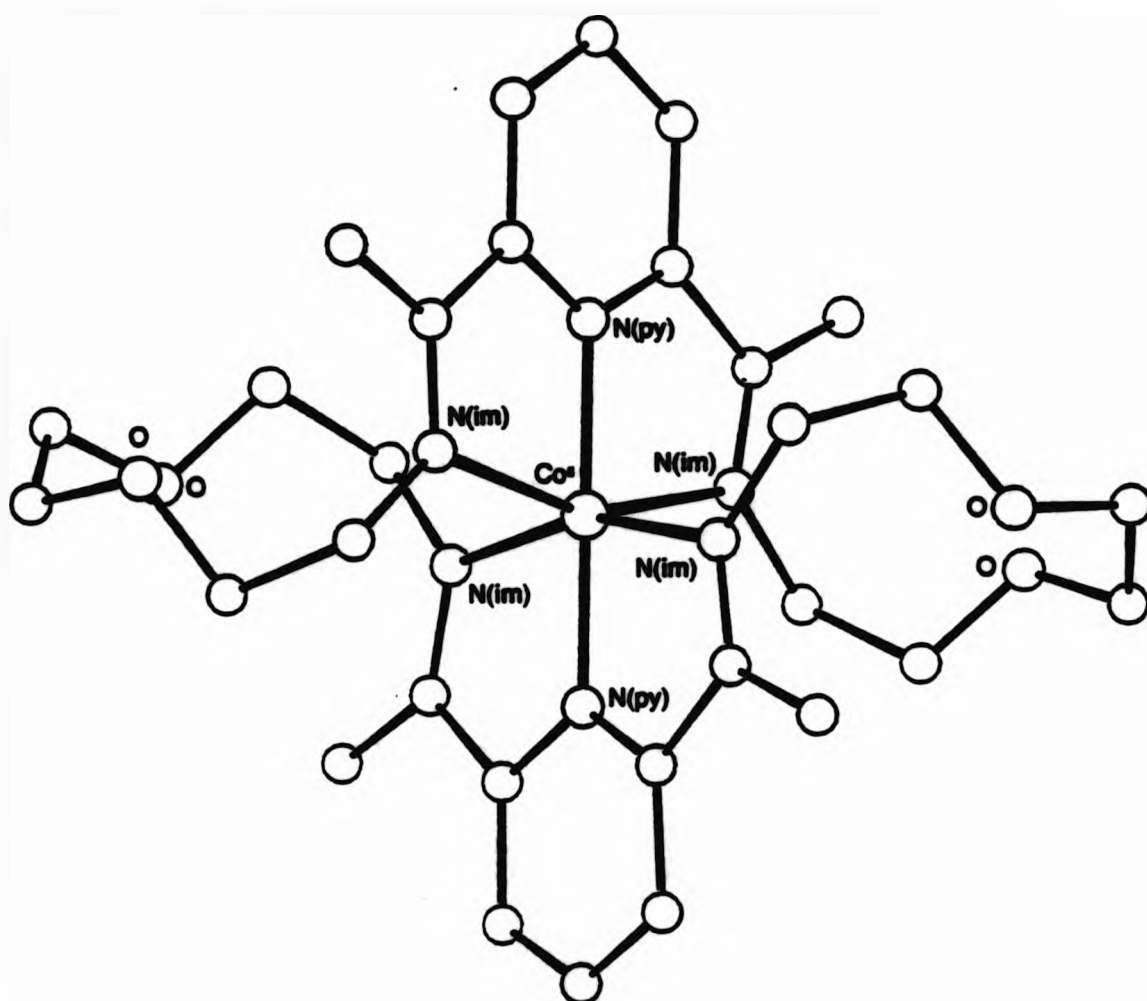


Figure 9.3.2 The solid state structure of a Co(II) complex of a 30-membered N_6O_4 macrocyclic analogue of L^1 . [48]

It is expected that L^1 accommodates the single cobalt(II) ion in a similar way to its 30-membered [2+2] ' N_6O_4 ' [$\text{D} = \text{py}$, $\text{R}^1 = \text{Me}$, $\text{R}^2 = (\text{CH}_2)_2\text{O}(\text{CH}_2)_2\text{O}(\text{CH}_2)_2$] analogue; the mononuclear cobalt(II) complex of which has been structurally characterised. [48] X-ray crystallography for this compound (see Fig. 9.3.2) showed the 30-membered ring to be arranged with the potentially dentitic ether

oxygen atoms displaced well away from the metal co-ordination sphere, the ligand employing all six nitrogen donors to bind to the metal. The two pyridine nitrogens are exactly trans co-ordinated in the complex although the two 2,6-pyridinediimine moieties (themselves planar) intersect at an angle of 80.0°. Deviation from idealised octahedral co-ordination was attributed to the steric demands of the ligand.^[48] In comparison, L^1 has a larger inner-great ring and, due to incorporation of aromatic rings in its superstructure, fewer degrees of freedom for spatial orientation of its rigid tridentate head units. It is therefore likely that the ligand will adopt a similar conformation to that observed in the solid state structures of $[NiL^1][ClO_4]_2$ and $[ZnL^1][ClO_4]_2$ (see Section 10.2), and co-ordinate Co(II) in a distorted 'N₆' octahedron.

9.3.2 Synthesis of $[NiL^1][ClO_4]_2$, $[ZnL^1][ClO_4]_2$, and $[CdL^1][ClO_4]_2$

Mononuclear Ni(II), Zn(II) and Cd(II) complexes of L^1 were prepared via metal exchange between $[Ag_2L^1][ClO_4]_2$ and the appropriate hydrated metal perchlorate in acetonitrile solution. These compounds have proved amenable to detailed structural analysis in the solid state [Ni(II) and Zn(II); Chapter 10] and in solution [Zn(II) and Cd(II); Chapter 11] and therefore only brief characterisation details are presented here. Transmetalation reaction conditions in each case were closely similar to the mild conditions used during preparation of $[CoL^1][ClO_4]_2$ described previously. Metal exchange appears to occur relatively rapidly in each case; yellow solutions of $[Ag_2L^1][ClO_4]_2$ changed to the colour of the transmetalation products [red for Ni(II) and pale yellow for Zn(II) and Cd(II)] within a few minutes at room temperature. Concentration of the solutions followed by slow evaporation over a period of several weeks yielded crystalline samples of product in each case. The Ni(II) and Zn(II) compounds were isolated as stable, octahedron-shaped

crystals and selected crystals from each sample proved to be suitable for X-ray analysis. The Cd(II) complex was isolated as pale yellow plate-like crystals, similar in appearance to those of $[\text{PbL}^1][\text{ClO}_4]_2 \cdot \text{H}_2\text{O}$. The crystals dull on exposure to air.

Microanalyses were consistent with formation of mononuclear complexes in each case; closest fits with analytical data are given with the formulations $[\text{NiL}^1][\text{ClO}_4]_2 \cdot \text{CH}_3\text{CN}$, $[\text{ZnL}^1][\text{ClO}_4]_2 \cdot 2\text{CH}_3\text{CN}$, and $[\text{CdL}^1][\text{ClO}_4]_2 \cdot \text{CH}_3\text{CN} \cdot \text{H}_2\text{O}$. (A second sample of the Cd(II) compound was produced using a similar procedure which, after vacuum desiccation, analysed as $[\text{CdL}^1][\text{ClO}_4]_2$). The presence of solvent in each sample was confirmed by the presence of appropriate bands in the respective infrared spectra. The infrared spectra are unremarkable and show close similarity with those of other complexes of L^1 described previously. The presence of imine stretching bands in each spectrum, observed at ca. 1630 cm^{-1} are consistent with the presence of the tetraimine macrocycle. Bands ascribed to the asymmetric stretching and bending modes of perchlorate [$\nu_3(\text{ClO}_4)$ and $\nu_4(\text{ClO}_4)$ respectively] are unsplit indicating non-coordination of the anion to the metal-ion.

Fab mass spectra of the Ni(II) and Zn(II) derivatives confirm the the proposed formulation of the complexes and show the simple fragmentation pattern observed for other first row transition metal complexes of L^1 . The spectra show two significant peaks corresponding to loss of one (yielding the base peak in both spectra) and two perchlorate ions, respectively, from the neutral parent complexes.

The spectrum of the Cd(II) complex is somewhat more complicated in comparison and shows species apparently resulting from ligand fragmentation. Highest

mass species in the spectrum correspond to the successive loss of perchlorate ions from the neutral parent complex and confirm the formulation of the complex. A peak at $m/z = 476$ corresponds to the $[\text{CdL}^1]^{2+}$ dication. Peaks at $m/z = 848$, 530, and 428 (the base peak of the spectrum) may be tentatively assigned to metal co-ordinated ligand fragments, apparently generated via α -cleavage of the phenoxy ether linkages of the macrocycle (See Fig. 9.3.3).

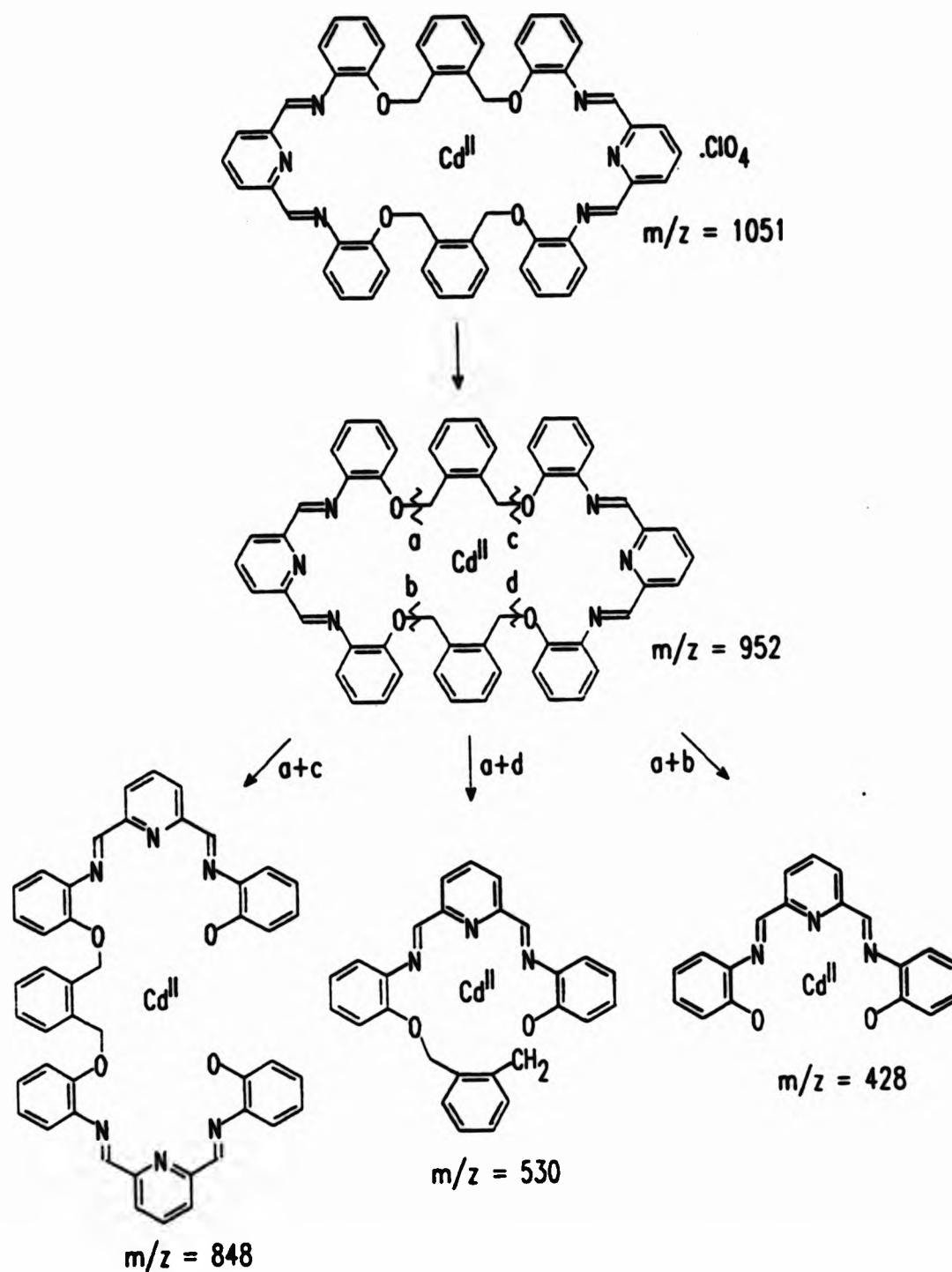


Figure 9.3.3 Fragmentation products identified in the fab mass spectrum of $[\text{CdL}^1][\text{ClO}_4]_2$. Generation of the products corresponds with α -cleavage of any two phenoxy ether bonds (a, b, c, d) of the parent macrocycle.

10. X-ray diffraction studies

Crystals of the zinc(II) and nickel(II) complexes of L^1 were successfully subjected to single crystal X-ray diffraction analysis. Suitable crystals of $[ZnL^1][ClO_4]_2 \cdot 2CH_3CN$ and $[NiL^1][ClO_4]_2 \cdot 2CH_3CN$ were prepared by slow evaporation of acetonitrile solutions of the complexes over several weeks. A similar procedure yielded a single plate of $[PbL^1][ClO_4]_2$ which, although strongly diffracting the X-ray beam during initial stages of data collection, appeared to decompose after several hours. Attempts at preparing suitable crystals of $[Ag_2L^1][ClO_4]_2$ from a variety of solvent systems yielded either unsuitable fine needle crystals (from slow evaporation of saturated solutions of the complex in acetone, methanol and methanol/dichloromethane) or efflorescent plates (from acetonitrile, acetonitrile/diethyl ether and nitromethane solutions). In the latter cases, attempts at mounting crystals over their respective mother liquors using Lindemann tubes were unsuccessful.

10.1 Structure solution and refinement

Collection and refinement of diffraction data was performed using a standardised local procedure. Intensity data were recorded by a Philips PW1100 four-circle diffractometer using graphite-monochromatised molybdenum-K α radiation ($\lambda = 0.7107 \text{ \AA}$). Data was refined using the SHELX-76 suite of programs^[49] running on a VAX 11/780 cluster with VMS 4.7.

10.1.1 Determination of crystal system and unit cell dimensions

A crystal of suitable dimensions (less than ca. $0.5 \times 0.5 \times 0.5 \text{ mm}$) was selected under a microscope and attached to a quartz fibre using epoxy resin. The crystal was then mounted in the goniometer head and, after centring in the

X-ray beam, the four circles were driven incrementally over the ranges $\omega = 4 - 15^\circ$, $\chi = -80 - +80^\circ$, and $\phi = 0 - 360^\circ$, to obtain 25 strong reflections. Optimum values of ω , χ , ϕ , and 2θ were recorded for each of these reflections and a primitive unit cell and an orientation matrix (the UB matrix) relating the geometry of the crystal to that of the goniometer were computed.^[50]

Preliminary inspection of these data allowed tentative identification of the crystal system for the crystals of $[\text{ZnL}^1][\text{ClO}_4]_2$ and $[\text{NiL}^1][\text{ClO}_4]_2$. Unit cell dimensions of $a = 14.894(3)$, $b = 18.800(4)$, $c = 19.753(4)$ Å; $\alpha = 90^\circ$, $\beta = 104.82(2)$, $\gamma = 90^\circ$ obtained for the crystal of $[\text{ZnL}^1][\text{ClO}_4]_2$ are closely similar to those for that of $[\text{NiL}^1][\text{ClO}_4]_2$; $a = 14.680(3)$, $b = 18.609(4)$, $c = 20.085(4)$ Å; $\alpha = 90^\circ$, $\beta = 104.08(2)$, $\gamma = 90^\circ$. The intensity relationships $I_{hkl} = I_{\bar{h}\bar{k}\bar{l}} = I_{h\bar{k}l} = I_{hkl}$ were observed in each case and these, together with the unit cell constraints $a \neq b \neq c$; $\alpha = \gamma = 90^\circ \neq \beta$, indicated monoclinic crystal systems (set with the b-axis as unique).

Reflections collected for the crystal of $[\text{PbL}^1][\text{ClO}_4]_2$ yielded the unit cell dimensions; $a = 20.465(4)$, $b = 20.461(4)$, $c = 23.667(4)$ Å; $\alpha = 90^\circ$, $\beta = 90^\circ$, $\gamma = 120^\circ$. Confirmation of the tentative assignment of the crystal system as trigonal or hexagonal was unfortunately precluded by crystal decomposition during data collection. Further studies of this system were not undertaken.

10.1.2 Data collection and reduction

Intensity data was collected for crystals of $[\text{ZnL}^1][\text{ClO}_4]_2$ and $[\text{NiL}^1][\text{ClO}_4]_2$ using a θ - 2θ scan technique at a constant scan speed of 0.05 s^{-1} . Scan widths of respectively, 0.7° and 0.9° were employed. The four circles of the diffractometer were computer-driven to angles corresponding to all possible

unique reflections in the θ range 3 - 15 °. Reflections deemed to be insignificant were skipped during collection. The criterion used to distinguish insignificant reflections was; $I_t - 2\sqrt{I_t} < I_b$, where I_t = count rate at the top of the reflection peak and I_b = the mean count of two preliminary 5 s background measurements at the extremities of the scan. Reflections were recorded as follows; the diffracted X-ray beam was scanned over the preset scan width by synchronous variation of ω and 2θ , and the total counts (I_t) were recorded. Background counts, made at the beginning and end of each scan, were recorded over times proportional to the ratio I_b/I_t (I_t is the initial count at the peak).

Three reference reflections were recorded at 5 h intervals during data collections. The measured intensities of these reflections for $[\text{ZnL}^1][\text{ClO}_4]_2$ did not vary significantly over the period of data collection. For $[\text{NiL}^1][\text{ClO}_4]_2$ however, one reference reflection was noted to drop by ca. 40 % in intensity during the latter stages of data collection. Loss of the crystal prevented recollection of the data but a reasonable refinement was achieved and the gross features of this novel structure were established.

Data reduction

I_{hkl} and $\sigma_c(I_{hkl})$ (the variance of I_{hkl} due to counting statistics) were corrected for Lorentz and polarisation factors using a local PW1100-dedicated program. Equivalent reflections collected were averaged^[49] giving a total of n data with $I_{hkl}/I_b > 3.0$.

10.1.3 Identification of space group

Inspection of the diffraction data (I_{hkl}) for systematic absences allowed the respective crystal systems (each previously assigned as monoclinic) and

lattice types to be unambiguously established for the crystals of $[\text{ZnL}^1][\text{ClO}_4]_2$ and $[\text{NiL}^1][\text{ClO}_4]_2$ investigated.

In each case, general absences were noted for reflections (I_{hkl}) with $h+k = 2n+1$ (i.e. odd) indicating C-face centred monoclinic lattice types. Special systematic absences of the types; $0\ k\ 0$ with $k = 2n+1$ and $h\ 0\ l$ with $l = 2n+1$, were also noted in each case. The former special systematic absences are a subset of the general absences caused by the C-face centred monoclinic lattice.

Observed absences of $h\ 0\ l$ data in the respective data sets, implying the presence of c-glide planes perpendicular to the respective b-axes, provides key evidence for identification of the space group for each of the crystals. C-Face centred monoclinic space groups including c-glide planes are restricted to two possible alternatives; $^{[51]}Cc$ (no. $9^{[51]}$), requiring equivalence of 4 asymmetric entities per unit cell, and $C2/c$ (no. $15^{[51]}$), for which 8 such entities are equivalent.

Determination of density

The density of each of the crystals was calculated from unit cell dimensions, in order to estimate the number of molecules in the respective unit cells. The volumes of the monoclinic unit cells were obtained from

$$V = abc \sin\beta$$

The calculated density was obtained thereafter using

$$D_c = \frac{M_r Z}{LV}$$

where M_r = relative molecular mass of the complex; Z the number of molecules in the unit cell; L = Avogadro's constant; and V = the volume of the unit

cell. Calculations were performed assuming either $Z_M = 4$ or 8 giving respectively, $D_c = 1.37$ and 2.74 g cm^{-3} for $[\text{ZnL}^1][\text{ClO}_4]_2$, and, $D_c = 1.37$ and 2.75 g cm^{-3} for $[\text{NiL}^1][\text{ClO}_4]_2$. Measured densities of ca. 1.5 g cm^{-3} are commonly associated with co-ordination compounds of first-row transition metals and therefore solutions for D_c based on 4 molecules per unit cell are most likely in both crystals.

The inference of the presence of 4 molecules of complex in the respective unit cells does not, however, provide a basis for the unambiguous assignment of the space groups of either crystal. In the case of Cc, the complex may occupy 4 general positions in the unit cell. For C2/c, four molecules of complex may give equivalent positions for 8 asymmetric portions in the unit cell if 2-fold point group symmetry is present. In view of the high symmetry of $[\text{ZnL}^1][\text{ClO}_4]_2$ in solution (inferred from ^1H and ^{13}C nmr), the centrosymmetric space group C2/c was assumed for, and confirmed by (*vide infra*), subsequent refinement of both crystal data sets. Assignment of the centrosymmetric space group (*i.e.* C2/c) implies that the metal atoms occupy a 'special' position in the unit cell coincident with the 2-fold rotation axis.

10.1.4 Structure solution and refinement for $[\text{ZnL}^1][\text{ClO}_4]_2 \cdot 2\text{CH}_3\text{CN}$

The position of the metal atom was located using a Patterson synthesis of the data. Partial assignment of the Patterson map calculated from the crystal data, in showing vector peaks between two atoms proportional in height to the product of their respective atomic numbers, yielded the position of the zinc atom of the complex. Equivalent positions for the $C_{2/c}$ space group are given as^[51]

$$\text{a) } x, y, z; \text{ b) } \bar{x}, \bar{y}, \bar{z}; \text{ c) } \bar{x}, y, \frac{1}{2} - z; \text{ d) } x, \bar{y}, \frac{1}{2} + z.$$

The unique Patterson vectors between atoms in equivalent positions are readily

calculated by subtraction,

$$a) - b) 2x, 2y, 2z; \quad a) - c) 2x, 0, \frac{1}{2} + z; \quad a) - d) 0, 2y, \frac{1}{2}.$$

The highest peak in the map (ignoring the origin), situated at $u = 0.000$, $v = 0.464$, $w = 0.500$, was assigned to the metal-metal vector due to a Zn atom on the 2-axis at $x_M = 0$, $y_M = 0.232$, $z_M = 0.25$. Clearly this peak in the map is equally attributable to the $a) - b)$, and the $a) - d)$ vectors, yielding identical estimates for y_M . The x - and z - co-ordinates define the special position of the metal atom and were therefore fixed in subsequent refinement; its position refining along the y -axis only.

An observed-Fourier map, calculated from the data using the position of the zinc atom, revealed the position of the chlorine atom of the perchlorate anion.

Difference-Fourier maps, calculated after two cycles of least-squares refinement for the scale factor and one cycle for atomic positions revealed, initially, two benzene rings and the remainder of the perchlorate anion and, subsequently, the remainder of the asymmetric unit of the complex. Further difference-Fourier syntheses revealed one molecule of CH_3CN in the asymmetric unit of the cell. Two further cycles of least-squares refinement were performed with the iminophenoxy ring atoms constrained to refine with idealised geometry ($\text{C}-\text{C} = 1.395 \text{ \AA}$, $\text{C}-\text{C}-\text{C} = 120^\circ$). Introduction of these constraints was necessary in order to overcome an unfavourable n/n_p ratio (n_p is the number of parameters refined) arising from the relatively low number of collected reflections. A difference-Fourier synthesis, calculated using structure factors of reflections for which $\sin\theta/\lambda < 0.35$, revealed peaks allowing estimation of hydrogen atom positions. Rejection of estimates giving unlikely local geometries allowed identification of the imine hydrogens (H2a

and H2b), one of the methylene hydrogens (H5a1), and one methyl proton of the acetonitrile solvate. The remaining hydrogen atoms were assigned to calculated positions constrained to 'ride' in idealised geometries at 1.08 Å from the corresponding carbon atoms. All hydrogen atoms were assigned a fixed isotropic thermal parameter (0.08 Å^2).

After refinement of all atoms with isotropic thermal parameters ($R = 0.0980$, $R_w = 0.0954$), an empirical absorption correction was made to the data using DIFABS.^[52] After three further cycles of refinement with all atoms assigned isotropic thermal parameters the R-factor dropped to $R = 0.0932$ ($R_w = 0.0874$). In the final cycles of full-matrix least-squares refinement, anisotropic thermal parameters were assigned to the 'heavy' atoms of the complex (Zn and Cl). The final refinement converged at $R = 0.0759$ and $R_w = 0.0696$. [It should be noted that the large drop in R-factor in the latter stage of refinement was due in part to correction of the structure factors attributed to C11a.]

10.1.5 Structure solution and refinement for $[\text{NiL}^1][\text{ClO}_4]_2 \cdot 2\text{CH}_3\text{CN}$

Location of the nickel atom was achieved using a similar procedure to that employed for $[\text{ZnL}^1][\text{ClO}_4]_2 \cdot 2\text{CH}_3\text{CN}$. A Patterson synthesis of the crystal data yielded a vector map with the highest peak (excluding the origin) at $u = 0.000$, $v = 0.452$, $w = 0.500$. Assignment of this peak as the $0, 2y_{\text{H}}, \frac{1}{2}$ vector, yielded the nickel co-ordinates; $x_{\text{H}} = 0.0$, $y_{\text{H}} = 0.227$, $z_{\text{H}} = 0.25$. Again, the x- and z-co-ordinates, in defining the 'special' position of the metal atom in the cell, were fixed during subsequent refinements.

The close similarity observed between the crystal parameters for derived for

$[\text{NiL}^1][\text{ClO}_4]_2$ at this stage of refinement and those obtained for $[\text{ZnL}^1][\text{ClO}_4]_2$ at the corresponding stage prompted estimation of positions of non-metal atoms (excluding hydrogen) in the former case using refined co-ordinates from the solution of the latter structure. A difference-Fourier map was calculated from the $[\text{NiL}^1][\text{ClO}_4]_2$ data with three cycles of least-squares refinement, blocked to refine the scale factor alone on the first cycle. The map revealed the carbon, nitrogen and oxygen atoms of the ligand, chlorine and oxygen atoms of the perchlorate anion, and one molecule of acetonitrile solvate. A subsequent difference-Fourier map calculated from reflections for which $\sin\theta/\lambda < 0.35$, did not reveal the appropriate positions for any hydrogen atoms and these were therefore assigned to geometrically idealised positions at 1.08 Å from the appropriate carbon atoms. A fixed isotropic thermal parameter (0.08 Å^2) was assigned to hydrogen atoms in each case.

Anisotropic thermal parameters were refined for the metal, perchlorate and acetonitrile atoms of the complex. Refinement of such parameters for ligand atoms was precluded by the size of the data set. Four cycles of least-squares refinement yielded a final structure solution with $R = 0.0684$ and $R_w = 0.0670$.

Table 10.1.1 Crystal data for $[\text{ZnL}^1][\text{ClO}_4]_2 \cdot 2\text{CH}_3\text{CN}$ and $[\text{NiL}^1][\text{ClO}_4]_2 \cdot 2\text{CH}_3\text{CN}$.

	$[\text{ZnL}^1][\text{ClO}_4]_2$	$[\text{NiL}^1][\text{ClO}_4]_2$
Molecular formula	$\text{C}_{58}\text{H}_{48}\text{N}_8\text{O}_{12}\text{Cl}_2\text{Zn}$	$\text{C}_{58}\text{H}_{48}\text{N}_8\text{O}_{12}\text{Cl}_2\text{Ni}$
Relative molecular mass ($M_r/\text{g mol}^{-1}$)	1185.34	1178.68
Crystal system	Monoclinic	Monoclinic
Lattice type	C-face centred	C-face centred
Space group	$C2/c$	$C2/c$
Unit cell dimensions		
a, b, c (\AA)	14.894, 18.800, 19.793	14.680, 18.609, 20.085
α, β, γ ($^\circ$)	90.0, 104.82, 90.0	90.0, 104.08, 90.0
Z	4	4
F(000)	2448	2440
Unit Cell Volume (\AA^3)	5346.99	5321.98
Density ($D_c/\text{g cm}^{-3}$)	1.472	1.471
Crystal dimensions (mm^3)	$0.30 \times 0.11 \times 0.13$	ca. $0.3 \times 0.1 \times 0.1$
μ (cm^{-1})	5.79	4.86
Unique data refined	1033	1829
No. of parameters refined	149	208
R	0.0759	0.0684
R_w	0.0696	0.0670

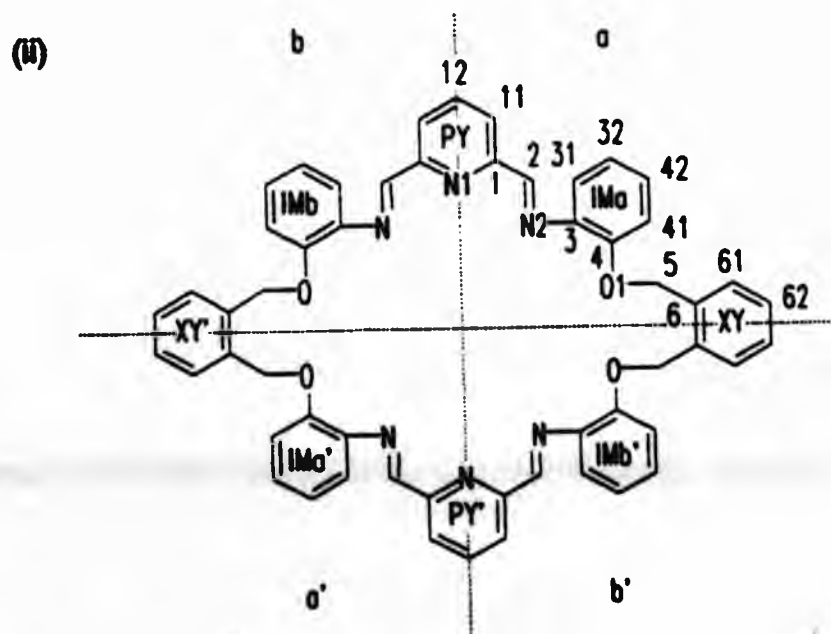
10.1.6 Mean plane calculations

Mean atomic planes and angles between normals to planes were calculated using XANADU. [49]

10.2 The solid state structures of metal complexes of L^1

10.2.1 Description of the structure of $[ZnL^1][ClO_4]_2$

Single crystal X-ray analysis of $[ZnL^1][ClO_4]_2 \cdot 2CH_3CN$ confirmed the formulation of the transmetalated product proposed from analytical data. In particular, the presence of a 34-membered macrocyclic ring (L^1) is unambiguously demonstrated by this technique. Fractional atomic co-ordinates, bond lengths, bond angles, inter- and intra-molecular distances for the structure are given in Tables 1-7 in Appendix 1. A general view of the complex with the numbering scheme employed for the ligand is shown in Figure 10.2.1. The asymmetric unit of the unit cell comprises one half of the complex, one perchlorate anion and one molecule of CH_3CN . The complex contains a crystallographically imposed 2-fold axis passing through the metal atom. Atoms of the ligand in the asymmetric unit are related by the 2-fold axis to their symmetry equivalents which describe the rest of the macrocycle - fractional co-ordinates for the equivalent atoms are generated by applying the symmetry transformation $-x, y, \frac{1}{2} - z$ to the co-ordinates of atoms in the asymmetric unit (i.e. at x, y, z). This operation also relates the perchlorate ion and acetonitrile molecule of the asymmetric unit to a second perchlorate ion and a second acetonitrile molecule respectively, giving the appropriate formulation of the crystal.



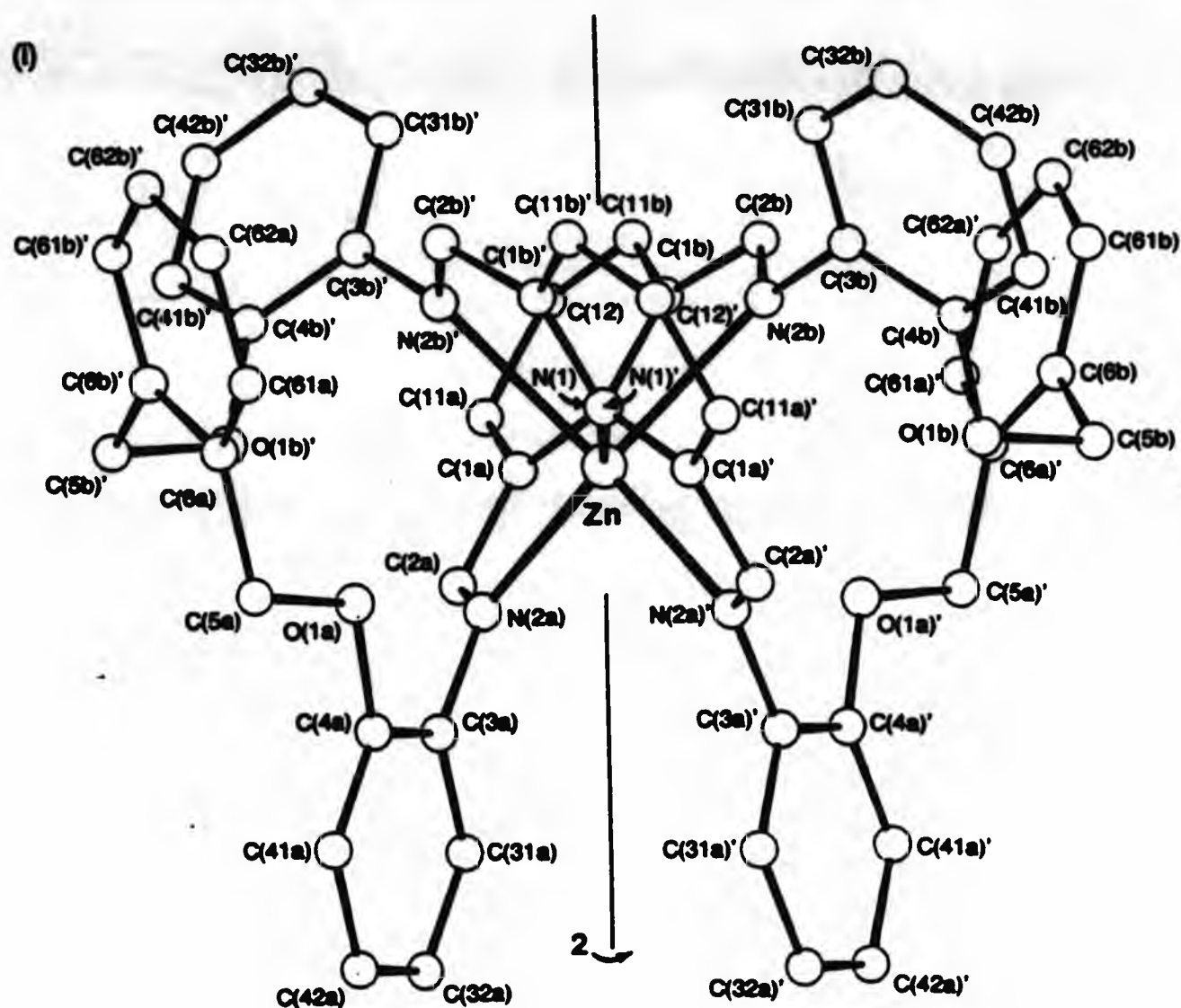


Figure 10.2.1. (i) ORTEP^[53] plot of the complex cation $[\text{ZnL}^1]^{2+}$ viewed perpendicular to the 2-fold axis;
(ii) ligand atom and aromatic ring labelling scheme used for structures of $[\text{ZnL}^1][\text{ClO}_4]_2 \cdot 2\text{CH}_3\text{CN}$ and $[\text{NiL}^1][\text{ClO}_4]_2 \cdot 2\text{CH}_3\text{CN}$.

The perchlorate ion is not associated with the metal atom and possesses essentially tetrahedral symmetry predicted from infrared data. The closest contact between the perchlorate and the complex is 3.02 Å from O2 to C11a. Intermolecular distances between other perchlorate oxygens and the complex are in the range 3.03–3.42 Å. The closest contact between the complex and lattice CH_3CN is 3.57 Å, between C12 and the cyanide nitrogen [Ns(1)] of the molecule at $1 - x, y, \frac{1}{2} - z$. While the distance between this nitrogen [Ns(1)] and the hydrogen atom (H12) associated with C12 is greater than the sum of their van der Waals radii, and therefore does not fulfil the basic condition for

hydrogen bonding,^[54] some contact distances between carbon-bound hydrogen atoms and oxygens of the perchlorate anions indicate potential C-H...O hydrogen bonds. However, using Taylor and Kennard's definition of significant 'nearest neighbour contact',^[55] only two of these C-H...O contacts can be considered close enough for hydrogen bonding - O(2) to H(11a) (2.28 Å) and O(3) to H(31b) of the asymmetric unit at $x + \frac{1}{2}$, $y + \frac{1}{2}$, z (2.36 Å). In the light of the non-distorted geometry of the perchlorate ion (hydrogen bonding might be expected to lower its symmetry from tetrahedral^[36]) and the relatively few close contacts it makes with hydrogen atoms of the complex, in association with relatively large complex to solvate distances, it is not expected that either counterions or solvate molecules play a significant rôle in determining the gross structure of the complex through hydrogen bonding interactions. The relative dispositions of anions and solvate molecules are shown in Figure 10.2.2.

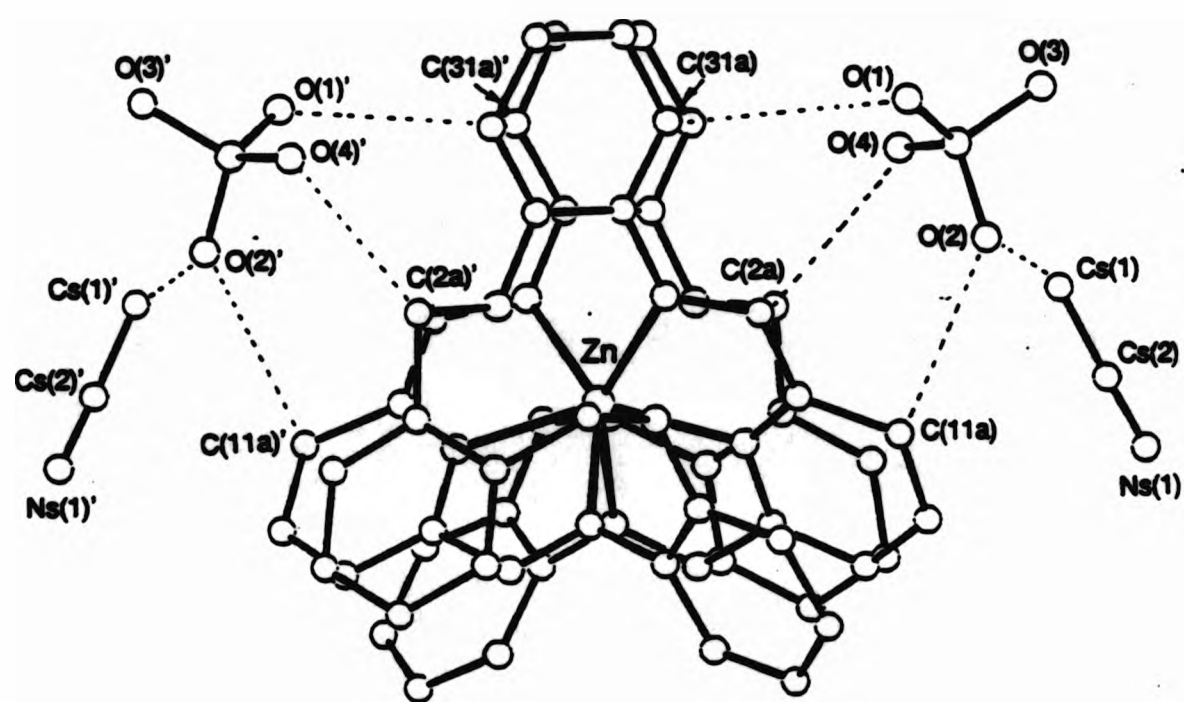


Figure 10.2.2. ORTEP^[53] plot of the relationship of perchlorate counterions and acetonitrile solvate molecules to the complex cation $[ZnL^1]^{2+}$ in the crystal lattice. [The view shown is perpendicular to the 2-fold axis and corresponds to a 90° rotation of Fig. 10.2.1(i) about this axis.]

The structure of $[\text{ZnL}^1][\text{ClO}_4]_2$ (Fig. 10.2.1) shows that the Zn(II) ion is co-ordinated to all six nitrogen donors of the ligand; the ether oxygen donor atoms of the asymmetric unit are, in each case, over 3 Å from the metal atom [(Zn..O1a = 3.240, Zn..O1b = 3.903 Å) and are therefore not included in the first co-ordination sphere of Zn(II) .

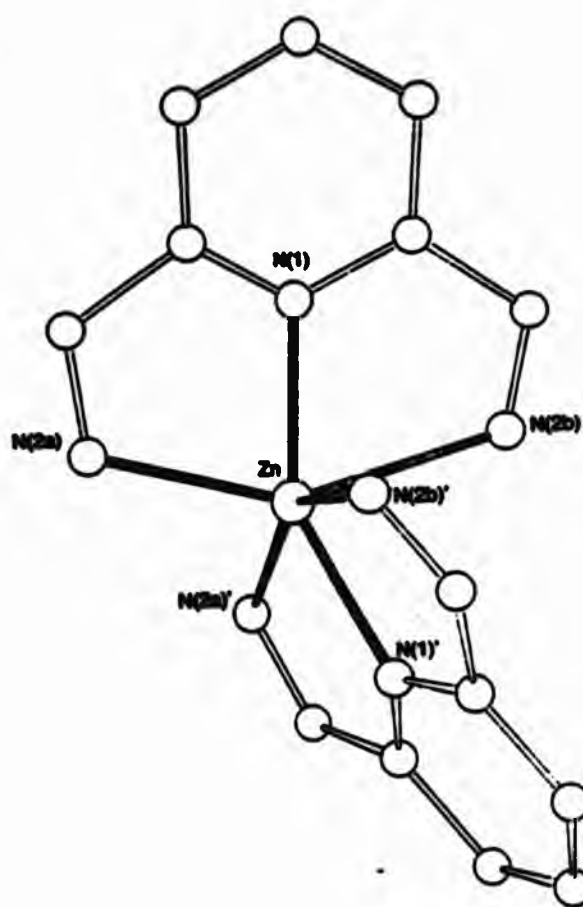
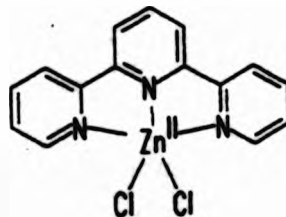


Figure 10.2.3. ORTEP^[53] plot of the metal co-ordination sphere in $[\text{ZnL}^1]^{2+}$.

The nitrogen donor atoms of L^1 may be considered to describe the vertices of a highly distorted octahedron (see Fig. 10.2.3) with the pyridine donors occupying axial positions [$\text{Zn-N1} = \text{Zn-N1}' = 2.023(12)$ Å] and the four imine nitrogens describing a 'ruffled' equatorial plane [$\text{Zn-N2a} = \text{Zn-N2a}' = 2.139(12)$; $\text{Zn-N2b} = \text{Zn-N2b}' = 2.373(13)$ Å] in the complex. Each 2,6-pyridinediimine head unit co-ordinates to the metal in an approximately meridional fashion. The two distal nitrogens of each head unit (N2a, N2b and N2a', N2b') lie to the same side of the equatorial plane of the octahedron.

The deviations of these imino nitrogens from their mean plane [N2a, +0.6221; N2a', -0.6221; N2b, +0.5793; N2b', -0.5793 Å] are substantial and constitute the considerable 'ruffling' of the equatorial plane. .

The foreshortening of the pyridyl nitrogen to metal bond in comparison to the metal to imine nitrogen bonds is a well established phenomenon in complexes containing 2,6-pyridinediimine donor units^[56] and originates in the demands imposed on spacial orientation of the 'N₃' donors by unsaturation. The crystal structure of [Zn(terpy)Cl₂]^[57] (where terpy is 2,2':6',2''-terpyridine) is worthy of consideration here. The rigid 'N₃' donor set of terpy is clearly comparable to those of the 2,6-pyridinediimine moieties in L¹, although significantly the three sp² nitrogen donors of terpy are of identical type and are therefore expected to have closely similar donor strengths. Thus, in the absence of ligand structural demands, Zn-N bond lengths in [Zn(terpy)Cl₂] might be expected to be equal. The terpy ligand co-ordinates Zn(II) via a planar array of three sp² nitrogens; the remainder of a pseudo-trigonal bipyramidal co-ordination sphere for the metal is completed by two co-ordinated chlorides. The Zn-N bond to the central pyridine ring in [Zn(terpy)Cl₂] is significantly shorter than those to the distal pyridine nitrogen donors (2.09 vs. 2.24 and 2.18 Å) which mirrors the situation observed in [ZnL¹]²⁺ and substantiates the view that shortening of the Zn-N1 bond in [ZnL¹]²⁺ derives from structural demands in the planar N₃ array.



[Zn(terpy)Cl₂]

The two pyridyl nitrogens (N1 and N1') in $[\text{ZnL}^1]^{2+}$ are significantly distorted from a mutually trans orientation ($\text{N1-Zn-N1}' = 146.34^\circ$). In the absence of other influences, repulsions within the metal co-ordination sphere are expected to maximise separation of the donor atoms and, in cases where 6-coordinate metal spheres are generated from two convergent 2,6-pyridinediimine 'head units', lead to maximum separation (i.e. $\text{N}_{\text{py}}-\text{M}-\text{N}_{\text{py}} = 180^\circ$) of the central pyridine donor atoms of each unit. The deviation from 180° for $\text{N1-Zn-N1}'$ in $[\text{ZnL}^1]^{2+}$ contrasts with the Co(II) and Fe(II) co-ordination spheres in mononuclear complexes of the 30-membered [2+2] 'N₆O₄' analogue of L¹ [D = py, R¹ = Me, R² = (CH₂)₂O(CH₂)₂O(CH₂)₂]^[48] where the corresponding N-M-N' angles are 179.2 and 179.6° respectively [a view of the Co(II) complex of this ligand is shown in Fig. 9.3.2]. A Ni(II) complex derived from two [1+2] open chain ligands [D = py, R¹ = Me, R² = (CH₂)₃Ph], containing an identical 'N₆' donor set to that of L¹, also demonstrates an essentially trans orientation for the pyridyl donors, in this case $\text{N-M-N}' = 178.7^\circ$.^[58] The deviation of the 2,6-py head units from a mutually trans orientation in $[\text{ZnL}^1]^{2+}$ presumably results from a combination of ligand-based influences as it folds to present the N₆-donor set. The geometry of the co-ordination sphere indicates a predominance of donors atoms on one side of the metal-ion and thus the metal co-ordination site may be viewed as a shallow cleft in the ligand. However the cleft does not approach that of the mononuclear Ba(II) complex of the bibracchial [2+2] Schiff base ligand [D = py, R¹ = Me, R² = (CH₂)₂N(2-py)(CH₂)₂]. In this case, the ligand is folded back upon itself to co-ordinate the metal-ion in a cleft formed by an offset face-to-face orientation of the 2,6-pyridinediimine units. The pyridine fragments which describe the cleft in this Ba(II) complex lie at an angle of 4.8°, whereas in $[\text{ZnL}^1]^{2+}$, the normals to the mean planes of the respective 2,6-pyridinediimine head units (themselves essentially planar, see

Fig. 10.2.6) which yield a comparable angle, intersect at 70.2° .

The co-ordination of Zn(II) by the 'N₆' donor array may alternatively be described as trigonal prismatic with N1, N2a, N2a' and N1', N2b, N2b' respectively describing the two triangles of a distorted prism. Distortions from regular trigonal prismatic geometry are substantial; normals to the respective mean planes of the trigonal faces intersect at an angle of 35.19° , the Zn(II) ion lies significantly closer to the N1, N2a, N2a' face of the 'prism' [reflected in shorter Zn-N2a (= Zn-N2a') bonds in comparison to Zn-N2b (= Zn-N2b')], and each of the trigonal faces deviates from a regular triangle. It is therefore difficult to obtain a single angle to describe the relative twist of the triangular faces of the prism and, hence, estimate the degree of distortion from the trigonal prism to the octahedron using criteria described by Fleischer et al. [59] [The twist angle between opposite triangular faces (ϕ , see Fig. 10.2.4) in geometrical solids thus described is 0° for regular trigonal prismatic geometry, 60° for regular octahedral geometry.] For [ZnL¹]²⁺, the angle between lines joining a vertex of each triangle (N1, N2a, N2a' and N1', N2b, N2b') to the midpoint of its respective base may be used as crude substitute for ϕ . With this approximation, ϕ is ca. 40° in [ZnL¹]²⁺, indicating a co-ordination geometry for the zinc atom intermediate between the trigonal prismatic and octahedral, albeit slightly closer to the latter.

Bite angles of the 5-membered nitrogen chelate rings in [ZnL¹]²⁺ deviate from the 90° expected for idealised octahedral geometry [N1-Zn-N2a = $77.4(5)^\circ$, N1-Zn-N2b = $72.7(4)^\circ$] as a result of the structural constraints of 2,6-pyridinediimine head unit mentioned above. The ligand atoms in each chelate ring are essentially planar, the atoms of each mean plane deviating by

less than 0.03 Å from the plane. The Zn(II) atom lies significantly above these planes (0.2074 Å above N1-C1a-C2a-N2a; 0.3798 Å above N1-C1b-C2b-N2b), which confers pseudo-envelope conformations^[60] on the respective 5-membered chelate rings.

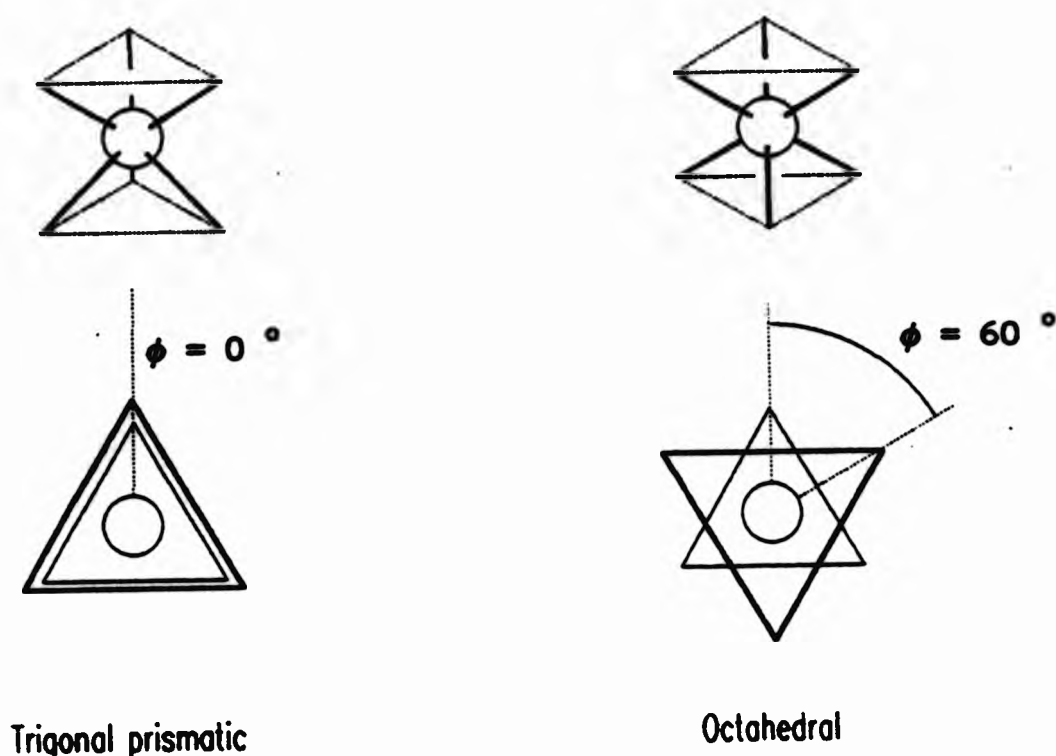


Figure 10.2.4 Characterisation of the twist angle between opposite triangular faces for regular trigonal prismatic and regular octahedral co-ordination geometries.

Relatively few Zn(II) complexes of ligands containing 2,6-pyridinediimine donor units have been structurally characterised; in particular, Zn(II)-nitrogen bond length data for complexes with an N_6 donor set derived from two 2,6-pyridinediimine residues is not available. However, the metal-pyridine nitrogen (N_{py}) bond lengths of $[ZnL^1]^{2+}$ are comparable with those reported for Zn(II) complexes of ' N_3 ',^[61] ' N_5 ',^[62,63,64] and ' N_3S_2 ',^[65] open chain [1+2] ligands that contain a 2,6-pyridinediimine donor unit. Bond lengths in the range 1.990(9)-2.117(6) Å are reported in these systems. In contrast, the two different metal-imine nitrogen bond lengths in $[ZnL^1]^{2+}$ lie beyond of the range of Zn- N_{imine} distances [2.170(7)-2.282(7) Å] observed in

these open chain systems^[61,62,63,64,65] although it is noteworthy that each of these ligands feature methyl substituents on their imine carbon atoms. Zinc(II) complexes of the [1+1] macrocyclic 'N₃S₂' ligands [D = py, R¹ = H, R² = oC₆H₄S-(CH₂)₂-oC₆H₄S] and [D = py, R¹ = H, R² = oC₆H₄S-(CH₂)₃-oC₆H₄S] give mean metal-imine bond lengths (M-N_{im}) of 2.211 and 2.338 Å respectively^[66] and, as they are derived from pyridine-2,6-dicarbaldehyde and thus do not feature imine carbon substituent functional groups, provide a closer comparison for L¹. Accordingly, the Zn-N_{imine} bond lengths in these N₃S₂ systems correlate more closely to those of [ZnL¹]²⁺.

To a good approximation, the open chain and macrocyclic Zn(II) complexes used for comparison above, show the metal atom co-ordinated symmetrically (i.e. with closely similar Zn-imino nitrogen bond lengths) within the 2,6-pyridinediimine unit. In contrast, the co-ordination of Zn(II) within the two 2,6-pyridinediimine residues in [ZnL¹]²⁺ is distinctly unsymmetrical [Zn-N1 = 2.023(12), Zn-N2a = 2.139(12), Zn-N2b = 2.373(13) Å] and, as all the nitrogen donor atoms are involved, is termed asymmetric endodentate. Asymmetric metal-ion co-ordination by 2,6-pyridinediimine units in other systems has been documented in relatively few cases, most remarkably in examples where 2,6-pyridinediimine shows bidentate co-ordination. The Mo(CO)₄ complex of an open chain 'N₃' ligand^[67] [D = py, R¹ = Me, R² = CH₂C(CH₃)₃] and the disilver(I) complex of a [2+2] tetraimine ligand bearing pendant pyridyl functions [D = py, R¹ = H, R² = (CH₂)₃N(2-py)(CH₂)₃].^[12] In an example of asymmetric endodentate 'N₃' co-ordination involving Cu(II), the asymmetry was attributed to the influence of strain induced by accommodating the 7-co-ordinate [1+2] open chain ligand [D = py, R¹ = Me, R² = (CH₂)₂NH(CH₂)₂NH₂] to a pentagonal bipyramidal geometry.^[68] It seems likely that the asymmetric co-ordination of Zn(II) has a similar origin;

considerable strain is anticipated if L^1 is orientated to give a more regular octahedral N_6 donor set and therefore it appears that the ligand imposes the metal co-ordination rather than *vice versa*. This theme will be more fully considered in Section 10.2.7.

Molecular helicity

The configuration adopted by the ligand in order to present the N_6 donor set to the metal atom imposes chirality on the complex. The two enantiomers present in the crystal are represented in diagrammatic form in Figure 10.2.5 where the co-ordination geometry of zinc has been idealised to approximate octahedral. It is assumed in this representation that the zinc atom and the three nitrogen atoms of the 2,6-pyridinediimine head unit are coplanar, and that these planes are orthogonal.

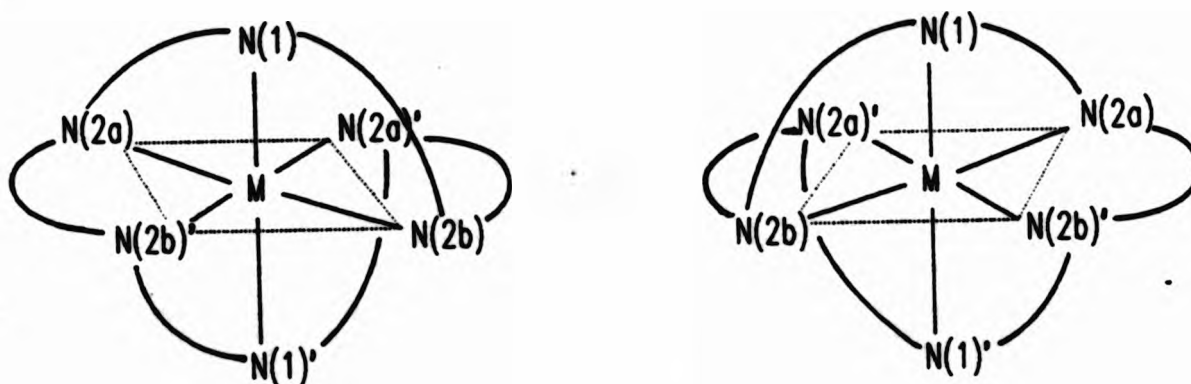


Figure 10.2.5. Schematic representation of the two enantiomers of $[ZnL^1]^{2+}$ present in the crystal. Geometries of the metal ion are idealised to approximate octahedral.

Identification of a centrosymmetric space group for the crystal implies that the two enantiomers of the complex are present in racemic proportions. The particular enantiomer studied (and shown in all ORTEP^[53] plots in this Section) corresponds to that shown in Fig. 10.2.5(a). Displacement of atoms in the asymmetric unit of the complex from the mean plane of the

2,6-pyridinediimine moiety (itself essentially planar) are shown in Fig. 10.2.6. The positions of C4a and C4b, respectively above and below the plane indicate a helical conformation for the ligand atoms of the asymmetric unit, similar to that observed for the Zn(II) complex of an open chain [1+2] 'N₃S₂' [D = py, R¹ = Me, R² = C₆H₄S⁻] analogue of L¹. [65]

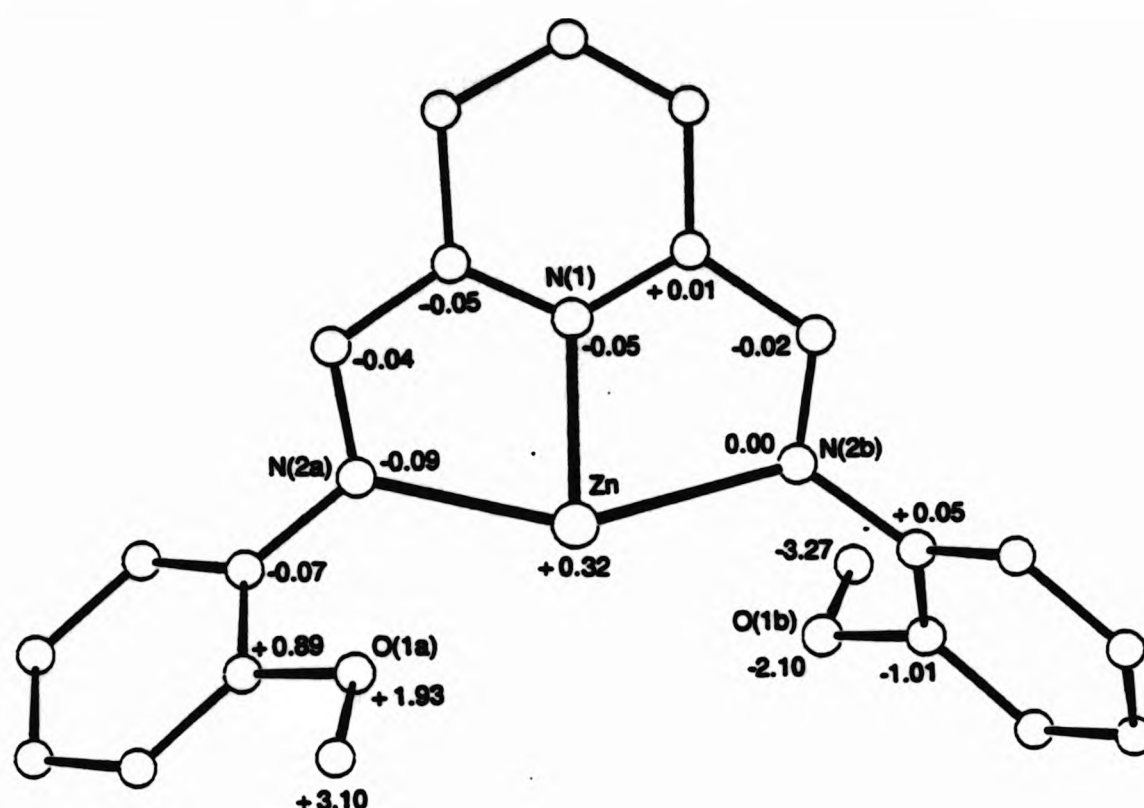


Figure 10.2.6. View of the asymmetric unit of [ZnL¹]²⁺ showing displacements (in Å) of ligand atoms from the 2,6-pyridinediimine mean plane.

The 2-fold symmetry relation between two halves of the ligand in the complex confers a similar helicity to the 'other half' of the ligand. Viewed parallel to the 2-fold axis, the inner great ring of the macrocycle describes a fragment of a double helix with each helical strand nominally joined at C5b and C5b' (see Fig. 10.2.7). In the enantiomer studied, each of these helical strands possesses right-handed helicity and, as they combine to generate double helix with the same screw sense, the gross configuration for this enantiomer is therefore assigned as right-handed or plus (P) (see Fig. 10.2.8). [69] As mentioned earlier, the centrosymmetric space group of

the crystal implies that it is a racemate and thus the opposite minus (M) enantiomorph is also present.

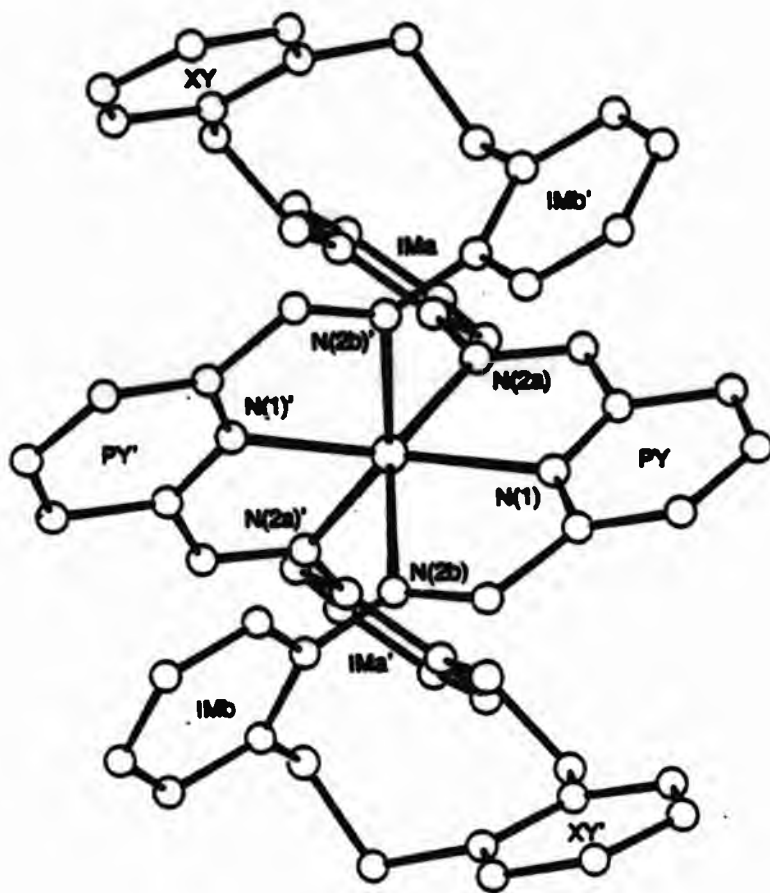


Figure 10.2.7. ORTEP^[53] plot of the $[\text{ZnL}^1]^{2+}$ cation viewed parallel to the two-fold axis.

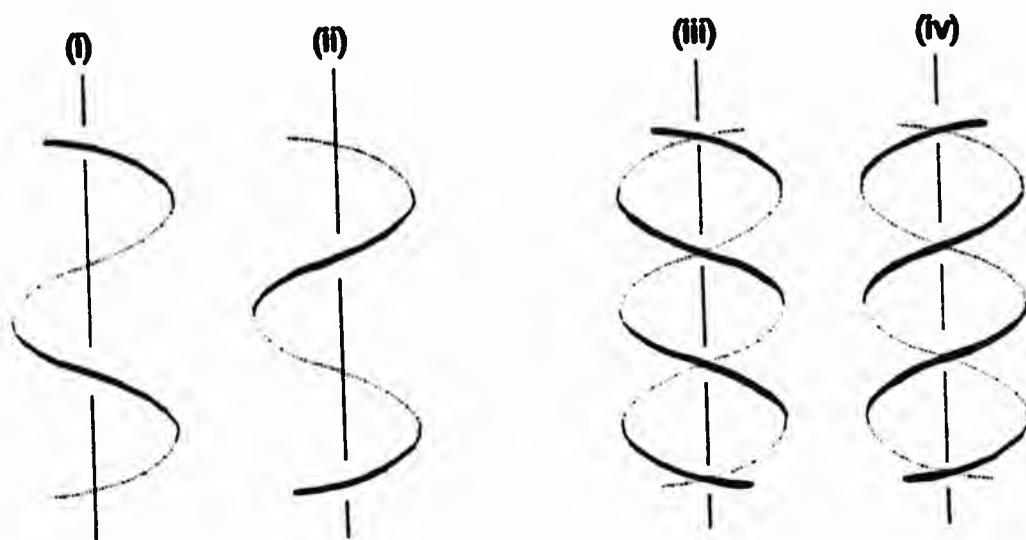


Figure 10.2.8. Handedness of single and double helices. The screw sense of (i) and (iii) is *dextroverse* [right-handed, denoted plus or (P)], that of (ii) and (iv) is *sinistroverse* [left-handed, denoted minus or (M)].^[69]

Arene stacking interactions

The conformation adopted by $[\text{ZnL}^1]^{2+}$ involves orientations for the aromatic rings of the ligand which suggest stabilising interactions between their π -systems. Attractive forces between non-bonded π -systems can play an important rôle in determining structures of large molecules, e.g. the tertiary structures of some proteins involve energetically favourable non-bonded interactions between phenyl rings,^[70] and a number of host-guest complexes involve π - π interactions for substrate binding.^[71] Interacting arene pairs are defined as those in which the distance between their ring centroids is less than 7 Å.^[70] The iminophenoxy rings (C3a-C4a and C3a'-C4a', IMa and IMa') are orientated to the same side of the metal co-ordination sphere such that their interplanar angle is 8.7° and the centroid-centroid distance is 4.35 Å indicating an interaction between them. Close contacts are observed between carbon atoms of these rings [i.e. C3a..C3a' = 3.56, C31a..C31a' = 3.61, C32a..C31a' = 3.90, C32a..C32a' = 3.95 Å]. The ring centroids (obtained from an average of the carbon atom co-ordinates of each ring) are horizontally displaced by ca. 2.5 Å, just under the ring diameter of benzene (2.80 Å for a regular hexagon with C-C = 1.40 Å), indicating that these rings do not lie directly over one another. Schematic representation of the parameters used to describe aromatic ring dispositions are shown in Fig. 10.2.9.

The 'b-side' iminophenoxy ring (IMb) occupies a position below the pyridine ring at $-x, y, \frac{1}{2} - z$ (PY') which is in the 'opposite' head unit of the ligand, i.e. the 2,6-pyridinediimine unit to which it is not attached. These two aromatic rings are displaced from a parallel orientation by an interplanar angle of 17.6° , although their disposition is approximately columnal with a horizontal displacement of their respective centroids of ca. 0.5 Å. The

closest contacts between the rings ($C3b..N1' = 3.207 \text{ \AA}$, $C4b..C1a' = 3.455 \text{ \AA}$, $C31b..C1b' = 3.430 \text{ \AA}$) are somewhat shorter than the mean deviation of the IMb ring carbons from the pyridyl (PY') plane (3.619 \AA). The stacking of the two planes is therefore compressed (resulting in the non-parallel interplanar angle) at the atoms closest to the metal centre. The 2-fold axis generates an identical disposition for the IMb' iminophenoxy ring over the pyridyl ring (PY) of the asymmetric unit at x, y, z .

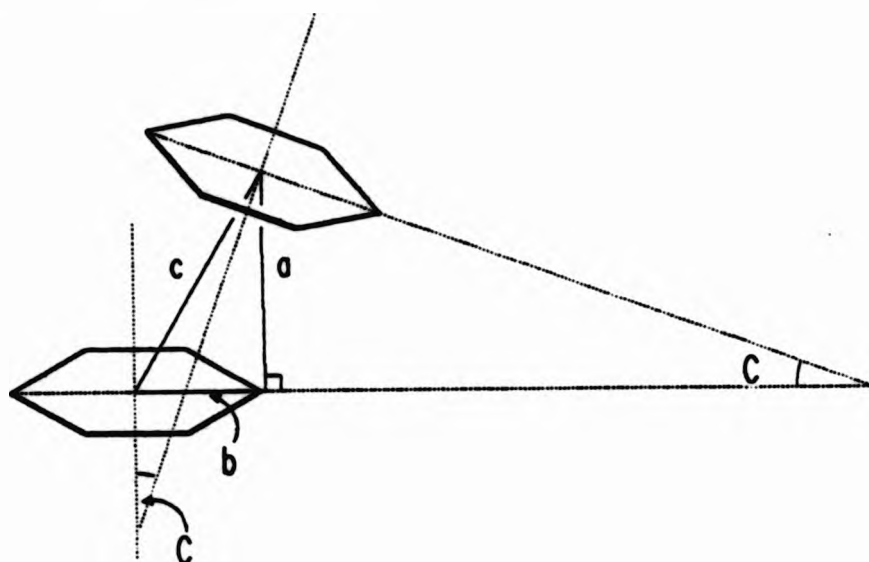


Figure 10.2.9. Schematic representation of parameters used to describe aromatic ring dispositions; a = mean atom displacement above the plane, b = horizontal displacement of centroids, c = centroid-centroid distance, C = interplanar angle (angle between normals to planes).

The xylenyl ring $C6a-C6b'$ (XY) of the macrocycle lies above the same pyridyl (PY') ring. The interplanar angle between these two π -systems is 17.1° , and their ring centroids are displaced from a columnar orientation by ca. 3.1 \AA . The centroid-centroid distance between these rings is 4.307 \AA , and the xylenyl ring carbon atoms are at a mean distance of 2.989 \AA above the pyridyl plane. The shortest contact distances between the rings are $C6a..C1b' = 3.661$, $C61a..C1b' = 3.442$, $C61a..C11b' = 3.530$, $C62a..C11b' = 3.622 \text{ \AA}$. There are, however, generally shorter contact distances between the imine atoms ($C2b'$ and $N2b'$) attached to this pyridine (PY') ring and other carbon atoms of the

xylene ring (e.g. $C2b' \dots C6b' = 3.334$, $C2b' \dots C61b' = 3.372$, $N2b' \dots C6b' = 3.344$, $N2b' \dots C61b' = 3.666$ Å). These shorter distances show the xylene aromatic ring (XY) is orientated above one side of the 2,6-pyridinediimine head unit (containing PY'). As for the IMb ring, the presence of the 2-fold axis in the complex implies equivalent orientations for the xylene (XY') ring over the other pyridyl (PY) ring.

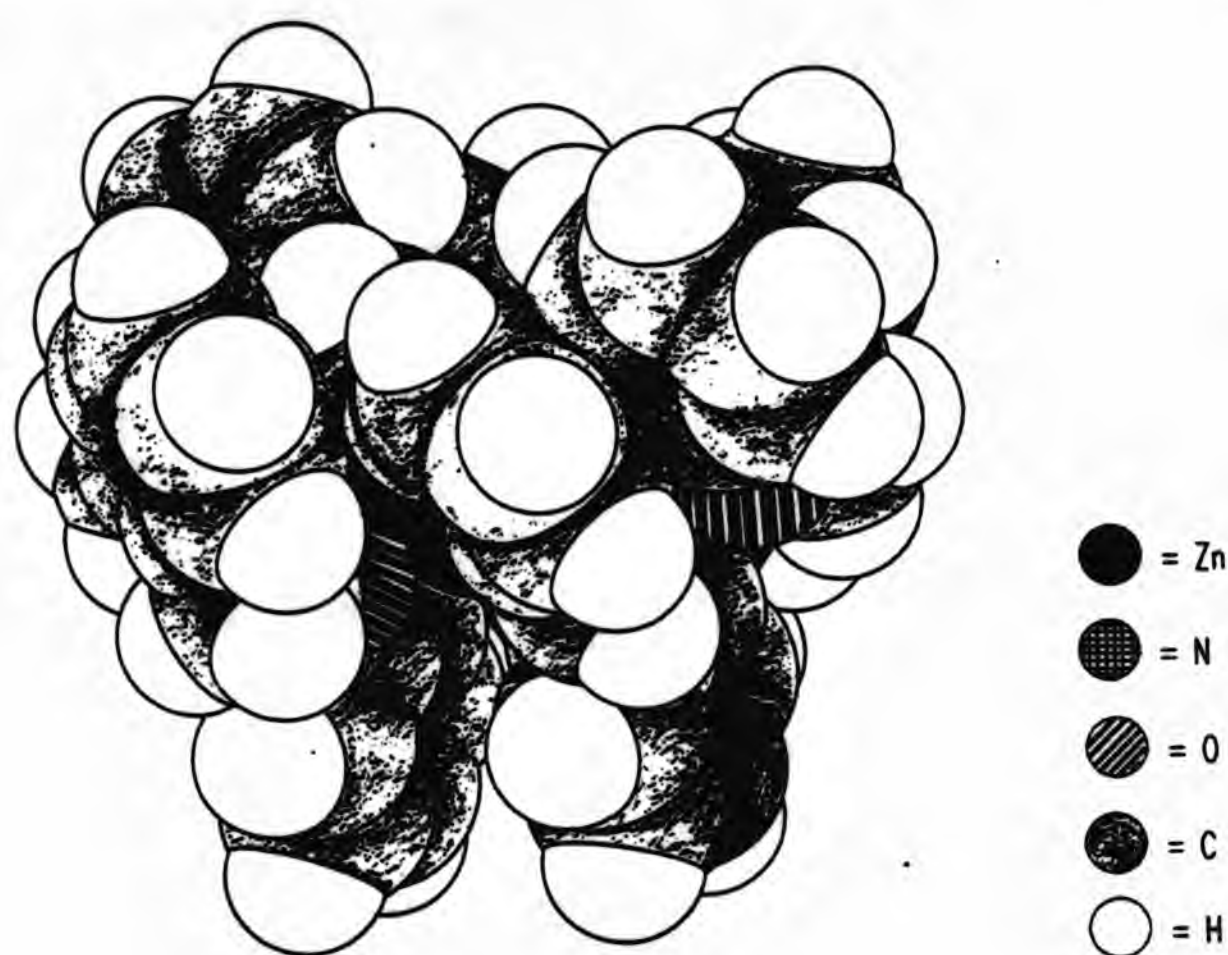


Figure 10.2.10. JACKAL^[72] space-filling view of $[ZnL^1]^{2+}$ cation showing orientations of interacting aromatic rings in a three tier stack (XY', PY, and IMb') and an arene pair (IMa and IMa'). [Atom spheres are van der Waals surfaces].

There are, therefore, five instances where pairs of aromatic rings lie within distances associated^[70] with arene-arene interactions. An offset face-to-face aromatic pair is formed by (symmetry related) iminophenoxy rings

(IMa and IMa') and two three-tier stacks (comprising the IMb, PY' and XY rings in one case and their symmetry equivalents in the other) are apparent. A space-filling representation of the complex (Fig. 10.2.10) highlights the juxtaposition of these aromatic systems and shows that the metal-ion is effectively embedded by the twisted ligand conformation adopted on co-ordination.

The shortest contact distances between the stacked aromatic systems of $[\text{ZnL}^1]^{2+}$ are similar to the interlayer distance in graphite (3.35 Å), where the lamellar structure is stabilised by van der Waals interactions between the layers.^[73] Interactions between face-to-face orientated benzene derivatives have been identified for some time; in 1961, Wallwork^[74] introduced the term 'polarisation bonding' for such interactions to include both the charge transfer bonding between polarised aromatic systems described earlier by Mulliken^[75] and the weaker van der Waals interactions between aromatic systems arising from the juxtaposition of polar groups of one nucleus with polarisable regions of the other.^[74] In principle, Mulliken's charge transfer complexes are stabilised by overlap between the highest energy occupied molecular orbital (HOMO) of the π -donating aromatic system with the lowest unoccupied molecular orbital (LUMO) of the π -accepting system.^[75] As these interactions and the van der Waals forces rely on overlap of the π -systems of the arene pairs, face-to-face columnar orientations of benzene derivatives maximise their contributions.

More recently, quantum mechanical studies^[76,77] of dibenzene have revealed the importance of electrostatic repulsion between the respective π -systems and have indicated that global minima in energies occur with 'T-stacked' arrangements of the arene pairs. The T-stacked arrangement involves the rings

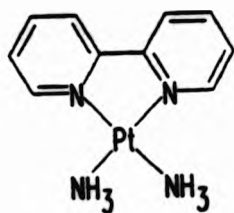
orientated orthogonally without any horizontal displacement of their centroids and allows the maximum interaction of positively-polarised (δ^+) ring hydrogens with the negatively-polarised (δ^-) π cloud of the partner molecule. In addition, local minima in the energetics of dibenzene were predicted for offset, face-to-face orientations of the interacting ring pairs. Statistical studies of the distribution of geometries of interacting arene pairs in proteins and amino acids are largely in accord with these predictions. [70,78]

Hunter and Sanders have reported^[79] an extensive study of π - π interactions including annulenes, kekulenes and porphyrins, based on a theoretical model where the (positive) σ -framework of the aromatic system is considered separately from the (negative) π -electrons. With this model,^[79] the charge distribution in the aromatic molecule is described by a set of point charges and the overall energy of interaction between species is estimated by combining terms due to electrostatic and van der Waals interactions. Geometries predicted with this model for non-polarised aromatic systems are broadly in accord with those obtained for dibenzene (see above); π - σ attractions are the resultant forces for T-stacked and offset face-to-face orientations, whereas π - π repulsions dominate in columnar, face-to-face orientations. Extending the studies to polarised π -systems, the authors observed that the presence of strongly-polarising atoms can exert a major influence on the electrostatic interactions between π -systems by offsetting the repulsions which disfavour face-to-face orientations. In this context, a set of rules was established within which strong geometrical requirements for face-to-face stacking were implied. In addition, the model implies that interactions between two π -deficient systems can be more favourable than between π -rich and a π -deficient systems, and charge transfer between the

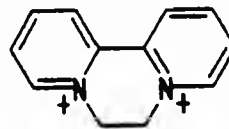
systems may exert relatively little to the overall energetic stability of juxtaposed π -systems.

Stacking interactions can play an important role in orientating organic substrates in co-ordination compounds^[80,81] and have been widely exploited in host-guest chemistry.^[71] The following examples, taken from the latter field, demonstrate complexation of pyridyl guest molecules within macrocyclic hosts via π -stacking interactions and provide interesting comparison with the conformation adopted by L¹.

The complex of the $[\text{Pt}(\text{bipy})(\text{NH}_3)_2]^{2+}$ dication (where bipy = 2,2'-bipyridyl) and dibenzo[30]crown-10 is stabilised by charge transfer interactions between the benzene rings of the crown ether (π -donors) with the comparatively electron-deficient pyridyl rings of bipy (π -acceptor).^[82] The host folds to form a U-shaped cavity such that the aromatic systems of host and guest adopt face to face orientations. Average separations of interacting aromatic systems in the complex are ca. 3.5 Å. Interplanar angles in the region 0.9 - 2.2 ° testify to the coplanarity of the respective aromatic nuclei.



$[\text{Pt}(\text{bipy})(\text{NH}_3)_2]^{2+}$



diquat

Orientations of interacting aromatic systems in complexes of the diquat di-cation with the members of the series of dibenzo[3n]crown-n ($n = 6 - 12$) (DB3nCn)polyether macrocycles are controlled by the structural demands of the

crown ligands.^[83] The larger crowns in the series are able to fold and form a U-shaped cavity on complexation with the diquat cation, similar to that of the $[\text{Pt}(\text{bipy})(\text{NH}_3)]^{2+}$ -DB30C10 complex described above. Such configurations for the larger macrocycles yield essentially parallel orientations for the aromatic systems of the host and guest. The average distances between the mean planes of a benzo-ring and the bipyridinium ring of the diquat-DB30C10 complex in the solid is 3.4 Å. The juxtaposition of the aromatic nuclei is believed to maximise charge transfer between the benzene (π -donor) substituents of the host and the bipyridine ring (π -acceptor) of the guest. Reduction of the macrocyclic ring size of the host leads to reduced charge transfer between the host and guest in the DB27C9-diquat complex. This arises from the inability of the smaller ligand to adopt a U-shaped cavity on complexation. The resulting V-shaped cavity reduces the overlap between the π -systems of the host and guest compared to the complexes of the larger macrocycles and results in less effective charge transfer. Smaller members of the dibenzocrown series (e.g. DB24C8) form termolecular complexes with diquat. The two molecules of diquat bind to different benzene rings of the host. The authors^[83] conclude that the abrupt change in co-ordination behaviour arises because the smaller rings are too small to form even a V-shaped cavity to bind a single diquat cation. This series, particularly the DB27C9-diquat complex, demonstrates that while structural demands of a ligand can take a predominant rôle in displacing aromatic systems from idealised charge transfer orientations, interactions between aromatic nuclei in non-ideal juxtaposition can still stabilise specific ligand conformations.

Thus the presence of aromatic substituents in the macrocyclic ring of L^1 plays a crucial rôle in determining the structure of its $\text{Zn}(\text{II})$ complex both through limiting the number of conformations that may be adopted by the ligand due to

rigidity and steric factors and by forming intramolecular arene stacking interactions. The following section describes the structure of the Ni(II) complex of L^1 . As the d^8 Ni(II) ion exerts stronger stereochemical preferences for its co-ordination sphere than d^{10} ions such as Zn(II), comparisons between the structures may provide further insight into the rôle of ligand-based influences in controlling complex structures.

10.2.2 The structure of $[NiL^1][ClO_4]_2 \cdot 2CH_3CN$ in the solid state

$[NiL^1][ClO_4]_2 \cdot 2CH_3CN$ crystallises in the $C2/c$ space group and is essentially isomorphous with $[ZnL^1][ClO_4]_2 \cdot 2CH_3CN$. As for the zinc complex, the asymmetric motif in the unit cell contains one perchlorate anion, one molecule of acetonitrile, and one half of the complex; similarly, the stoichiometry of the crystal is satisfied by 2-fold rotation axis passing through the metal atom. The single Ni(II) ion is co-ordinated solely to the six nitrogen donor atoms of the ligand and the gross conformation of the complex is closely similar the Zn(II) derivative. The atomic numbering scheme deployed for the ligand is shown in Figure 10.2.1(ii) and fractional atomic co-ordinates, bond lengths, bond angles, inter- and intra-molecular distances for the structure are given in Tables 1-7 of Appendix 2. A general view of the complex [corresponding to the view of $[ZnL^1]^{2+}$ shown in Figure 10.2.1(i)] is shown in Figure 10.2.11.

The most notable differences between the two structures lie in the dimensions of the respective metal co-ordination spheres and these are compared in Table 10.2.1. Meridional co-ordination of each 2,6-pyridinediimine head unit of L^1 confers a distorted, octahedral co-ordination sphere on Ni(II) in the complex. The four imine nitrogens again describe a 'ruffled' equatorial plane for the octahedron albeit with rather

smaller deviations for contributing imine atoms from their mean plane [N2a, +0.5034; N2a', -0.5034; N2b, +0.4802; N2b', -0.4802 Å] than in $[\text{ZnL}^1]^{2+}$.

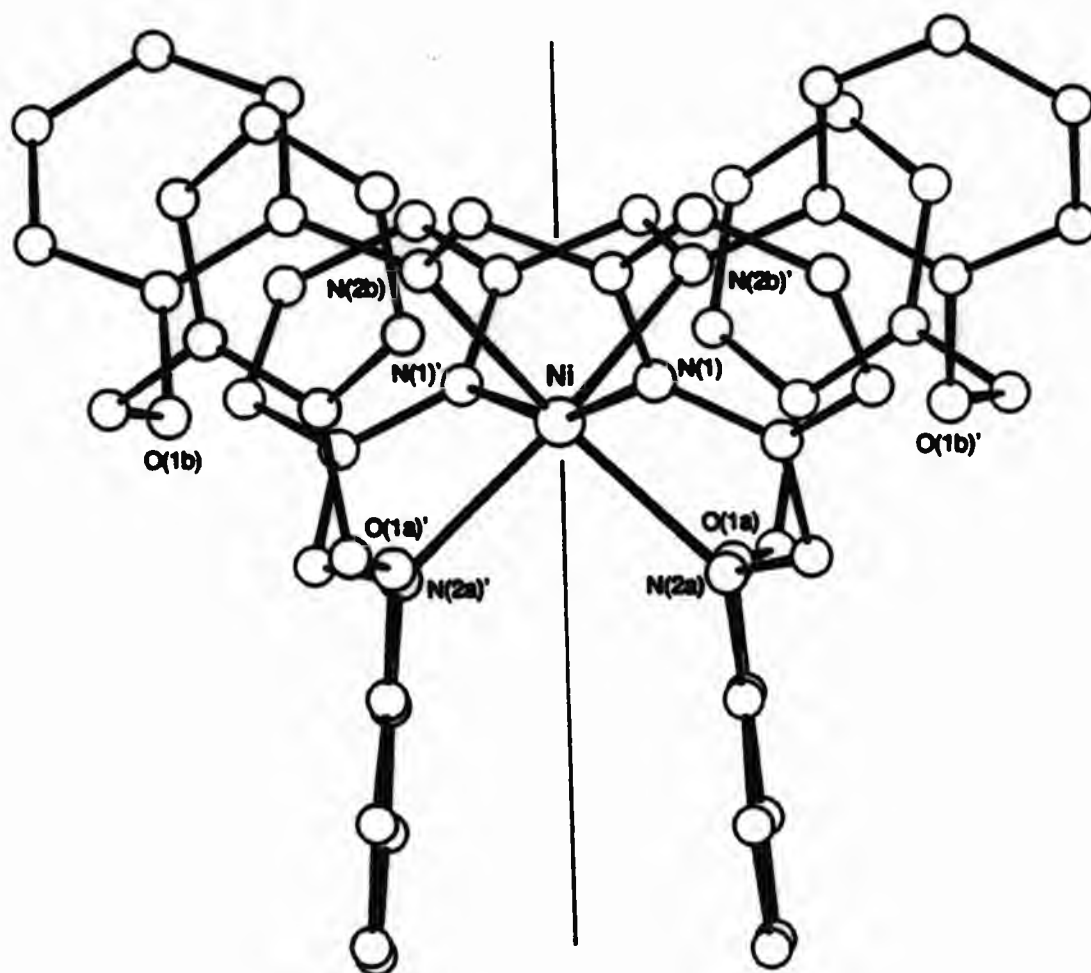


Figure 10.2.11. ORTEP^[53] plot of the complex cation $[\text{NiL}^1]^{2+}$ viewed perpendicular to the 2-fold axis.

In contrast to the clearly asymmetric co-ordination of the metal ion within the 2,6-pyridinediimine moiety of $[\text{ZnL}^1]^{2+}$, differences between the Ni(II)-imine bond lengths [Ni-N2a = 2.138(7), Ni-N2b = 2.168(7) Å] of $[\text{NiL}^1]^{2+}$ are barely significant and reflect the more common 'symmetrical' co-ordination behaviour of the 'N₃' residue (see above). The metal-pyridyl nitrogen bond [Ni-N1 = 1.996(7)] is significantly shorter than the metal-imine bonds and the bite angles of the 5-membered chelates (Ni-N1-N2a = 78.6(3), Ni-N1-N2b = 76.2(3) °) in each terdentate 'head unit' are significantly distorted from idealised octahedral geometry, again as is the case for the zinc complex.

Table 10.2.1 Comparison of metal ion co-ordination sphere dimensions for $[ML^1]^{2+}$.^a

	M = Zn(II)	M = Ni(II)
Bond lengths (Å) ^b		
N1 - M	2.023(12)	1.996(7)
N2a - M	2.139(12)	2.138(7)
N2b - M	2.373(13)	2.168(7)
Interbond angles (°)		
N1-M-N2a	77.4(5)	78.6(3)
N1-M-N2b	72.7(4)	76.2(3)
N2a-M-N2b	148.9(5)	153.5(3)
N1-M-N1'	146.34	158.50
N1-M-N2a'	127.51	117.20
N1-M-N2b'	83.34	89.26
N2a-M-N2a'	95.12	92.05
N2b-M-N2b'	88.97	95.00
Interplane angle (°)		
N1N2aN2b-N1'N2a'N2b'	75.52	84.18

^a See Fig. 10.2.1 for atom numbering scheme. Estimated standard deviations are given in parentheses. ^b Remainder of co-ordination sphere comprises atoms (N1', N2a', N2b') related to the asymmetric unit by the 2-fold rotation axis.

Nickel-nitrogen bond lengths in the complex are comparable with those for observed for a nickel(II) complex derived from two [1+2] 'N₃' open-chain ligands [D = py, R¹ = Me, R² = (CH₂)₂Ph] (mean Ni(II)-N_{py} = 1.99 Å, mean Ni(II)-N_{im} = 2.12 Å).^[58] Deviations from idealised octahedral co-ordination to Ni(II) in the latter bis-2,6-pyridinediimine complex are characterised by reduced bite angles of the 5-membered chelate rings and shortened Ni-pyridyl nitrogen bonds. The two pyridyl nitrogens of each ligand adopting an essentially *trans*-oid orientation across the metal. In contrast, the

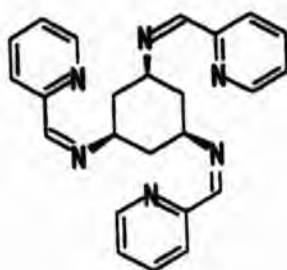
N1-N1-N1' angle (158.5°) in $[\text{NiL}^1]^{2+}$ reveals an extra deviation from octahedral symmetry in the complex similar, although slightly smaller, to that noted for $[\text{ZnL}^1]^{2+}$.

Somewhat shorter Ni(II) to nitrogen distances ($\text{Ni(II)}-\text{N}_{\text{py}} = 1.958$, mean $\text{Ni(II)}-\text{N}_{\text{im}} = 2.09 \text{ \AA}$) are observed in $[\text{Ni}(\text{NO}_3)_2 \text{M}^1] [\text{M}^1; [1+2], \text{D} = \text{py}, \text{R}^1 = \text{Me}, \text{R}^2 = \text{Ph}]$.^[84] Although incorporating a Ni(II)-bound 2,6-pyridinediimine residue, the 6 co-ordinate pseudo-octahedral complex also includes monodentate and bidentate co-ordinated nitrate, and does not therefore provide an ideal comparison for $[\text{NiL}^1]^{2+}$.

Bond angles within the co-ordination sphere of Ni(II) in $[\text{NiL}^1]^{2+}$ are somewhat closer to octahedral than for $[\text{ZnL}^1]^{2+}$. This is as expected since the crystal field stabilisation energy^[85] provides an 'extra' driving force towards octahedral co-ordination for the d^8 Ni(II) ion. However, the nickel atom of $[\text{NiL}^1]^{2+}$ does show significant deviation from octahedral geometry, most notably in the angle formed at the metal atom between the pyridyl nitrogen donor atoms ($\text{N1-Ni-N1}' = 158.50^\circ$). Thus, despite the CFSE for Ni(II) in a regular octahedral co-ordination sphere, it appears that the ligand 'forces' the metal into its apparently unfavourable geometry.

Distorted co-ordination geometries for Ni(II), intermediate between trigonal prismatic and octahedral have been observed in complexes derived from tris-pyridine-2-carboxaldimino ligands.^[59] Distortions from a regular co-ordination geometry in these complexes were rationalised on the basis of competing demands of ligand rigidity (promoting trigonal prismatic co-ordination for the metal) and the influence of crystal field stabilisation energy as a driving force towards octahedral metal geometries. As is the case

in complexes of L^1 , the Ni(II) geometry adopted on co-ordination of the semi-rigid ligand *cis,cis*-1,3,5-tris(pyridine-2-aldimino)cyclohexane^[59] is closer to octahedral ($\phi = 28^\circ$, see Fig. 10.2.4) than the geometry adopted by Zn(II) in the corresponding complex.^[86] In the latter complex, the co-ordination geometry of the metal approximates trigonal prismatic ($\phi = 4.6^\circ$).^[86] Distortions in the Ni(II) co-ordination sphere from this (ligand imposed) geometry towards octahedral was attributed to the influence of the CFSE.^[59]



cis,cis-1,3,5-tris(pyridine-2-aldimino)cyclohexane

The drive towards regular octahedral geometry for Ni(II) in $[NiL^1]^{2+}$ does have a small effect on the spacial arrangement of L^1 around the single metal ion but the gross features of the complexed ligand remain closely similar to those of $[ZnL^1]^{2+}$. In particular, $[NiL^1]^{2+}$ adopts a similar twisted structure with 'double helical' configuration for the ligand. The twisting of the ligand is emphasized in Fig. 10.2.7. As noted for $[ZnL^1]^{2+}$, identification of a centrosymmetric space group indicates that the crystal contains both enantiomers of the complex in racemic proportions; similarly the plus (P)^[69] enantiomer was studied during structure solution.

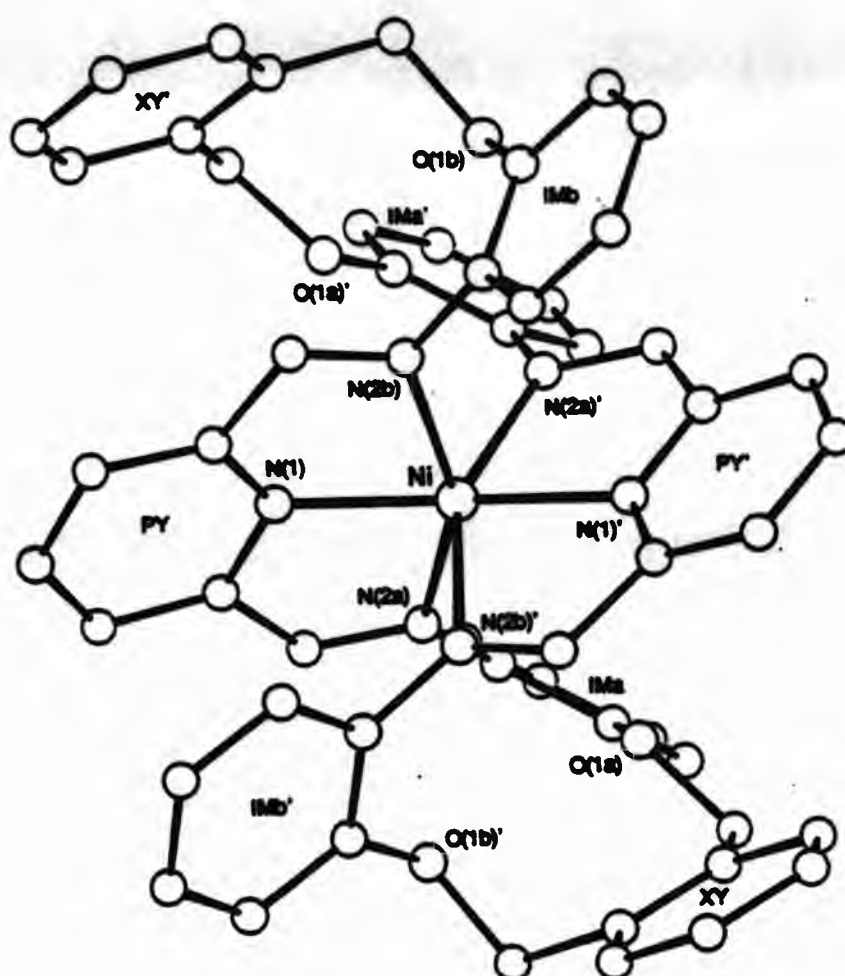


Figure 10.2.12. ORTEP^[53] plot of the $[\text{NiL}^1]^{2+}$ cation viewed parallel to the two-fold axis.

Arene stacking interactions

Offset face-to-face orientations for pairs of aromatic rings are again a noteworthy feature of the conformation adopted by L^1 in $[\text{NiL}^1]^{2+}$. Comparison of orientation parameters with those for rings in $[\text{ZnL}^1]^{2+}$ (Table 10.2.2), shows that the rings in $[\text{NiL}^1]^{2+}$ are slightly further displaced from parallel, columnar orientations, although the centroids of the pairs lie well within the maximum distance associated with interacting arene rings (7 Å).^[70] The orientation parameters leave little doubt that interaction between the rings, including possible charge transfer interactions in some cases, stabilises the juxtaposition of pairs of rings and therefore, presumably, the overall structure of the complex.

Table 10.2.2. Comparison of aromatic ring dispositions in $[ML^1]^{2+}$.^a

	M = Zn(II) ^b	M = Ni(II)
<u>IMa to IMa'</u>		
Interplanar angle ($^\circ$)	8.68	9.66
Shortest contact (\AA)	3.559 ^c	3.347 ^d
Centroid-centroid (\AA)	4.35	4.64
Mean displacement (\AA)	3.584	3.453
Horizontal displacement of centroids (\AA)	ca. 2.5	ca. 3.1
<u>IMb to PY'</u>		
Interplanar angle ($^\circ$)	17.6	17.7
Shortest contact (\AA)	3.207 ^e	3.215 ^e
Centroid-centroid (\AA)	3.65	3.70
Mean displacement (\AA)	3.619	3.599
Horizontal displacement of centroids (\AA)	ca. 0.51	ca. 0.84
<u>XY to PY'</u>		
Interplanar angle ($^\circ$)	17.1	23.1
Shortest contact (\AA)	3.442 ^f	3.501 ^f
Centroid-centroid (\AA)	4.30	4.27
Mean displacement (\AA)	2.989	2.655
Horizontal displacement of centroids (\AA)	ca. 3.1	ca. 3.3

^a See Fig. 10.2.1 for ligand numbering scheme; Fig. 10.2.9 for definition of orientation parameters. ^b Iminophenoxy rings were constrained to refine with idealised geometries (C-C = 1.395 \AA , C-C-C = 120 $^\circ$). ^c C3a..C3a'.

^d C31a..C31a'. ^e C3b..N1'. ^f C61a..C1b'.

The poorest overlap in both complexes, between the xylenyl C6a-C6b' ring and the pyridine PY' ring (and their symmetry equivalents), is characterized by the large horizontal displacement of the ring centroids. In addition, this

ring pair in the Ni(II) complex shows a large deviation from coplanarity. In both complexes, the xylenyl rings lie to one side of the 2,6-pyridinediimine head units and, in this position, interaction with the π -system of the imine double bonds is possible.

Interaction between the C3a-C4a (IMa) and C3a'-C4a' (IMa') iminophenoxy rings in both complexes is likely due to their approximately co-planar, face-to-face disposition. Their orientation is distinctly offset in both complexes with horizontal displacements of the ring centroids similar to the diameter of a benzene ring (see above); slightly larger in $[\text{NiL}^1]^{2+}$, somewhat less in $[\text{ZnL}^1]^{2+}$. The more pronounced offsetting of these rings in $[\text{NiL}^1]^{2+}$, in conjunction with the smaller deviation of the N2a-M-N2a' angle from 90° (i.e. idealised octahedral geometry), presumably are a manifestation of the rôle CFSE due to the metal-ion plays in determining the gross geometry of the complex.

The most significant overlap between aromatic systems in both complexes appears to involve the IMb and IMb' iminophenoxy rings with pyridine rings of the 'opposite' asymmetric unit, PY' and PY respectively. Small horizontal displacement of the rings as well as short inter-nuclear contacts indicate a significant interaction between these systems that is probably charge transfer in origin: the 'electron-rich' iminophenoxy rings (π -donor) donating to the 'electron-deficient', co-ordinated pyridine nuclei (π -acceptor). The noticeable deviation from parallel juxtaposition of these systems (giving non-ideal overlap between their respective π -orbitals) in both complexes probably results from a combination of the structural demands imposed by the ligand and inter-donor repulsions in the metal co-ordination sphere. (Metals with filled d-orbitals gravitate towards octahedral co-ordination in order to

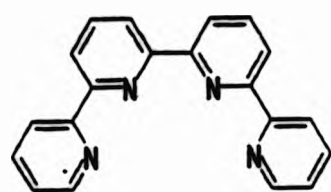
maximise charge separation around the metal sphere.^[87]) Interestingly, comparison between the relative positions of face-to-face aromatic systems between the two complexes shows that the pyridine-iminophenoxy stacks are the least affected by the co-ordination of Ni(II), suggesting a relatively strong interaction.

Molecular helicity

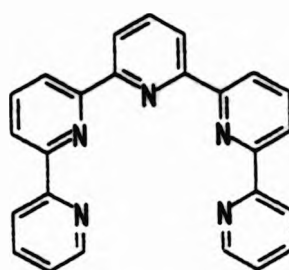
Molecular helicity in inorganic complexes is a topic of significant current interest and true double helical structures have been observed for a number of inorganic complexes.^[88] Particular interest has surrounded the double helical structures formed on co-ordination of two oligopyridine ligand chains,^[89] where the two ligand strands intertwine into a double helix stabilised by co-ordination to two or more metal ions. Lehn and co-workers have obtained double helical bi- to pentanuclear Cu(I) complexes (the so-called helicates) using ligands comprising two to five 2,2'-bipyridine units separated by ether 'spacer' groups.^[90,91] These complexes 'self-organize' to provide approximately tetrahedral co-ordination sites for each metal ion. Stacking interactions between bipy units of these complexes have been identified as significant factors in stabilising the double helical structures and in promoting the spontaneous assembly of the complexes in conjunction with the driving force provided by co-ordination of Cu(I) ions in approximately tetrahedral environments.^[90,91]

Double helical arrays of unbridged polypyridine chains have been observed in a number of binuclear metal complexes: quarterpyridine [M = Cu(I)^[92]], quinquepyridine [M = Cu(II)^[93], Ni(II)^[94], Pd(II)^[95]] and sexipyridine [M = Cd(II)^[96,97]]. Each ligand in the series adopts a helical configuration in order to co-ordinate to both metal centres in the complex,

the overall combination of two helical ligands arrays in the complexes yields a double helical configuration. In all cases, the ligands displayed only one major interannular twist resulting in co-ordination of essentially planar bipy, terpy and bipy, and terpy units respectively to metal ions of the complexes. Interestingly, one Ni(II) ion of $[\text{Ni}_2\text{quinquepy}_2(\text{OAc})]^{3+}$, is co-ordinated to two planar terpy units (thus describing an sp^2 nitrogen donor set analogous to that of L^1) of the double helical ligand array, resulting in a distorted Ni(II) co-ordination sphere of similar dimensions to that of $[\text{NiL}^1]^{2+}$.^[94] Constable has postulated that helical co-ordination of these oligopyridine chains arises when the conjugated polydentate systems 'compress' to accommodate metal ions that are smaller than the bonding cavity described by a planar ligand configuration.^[98]



quarterpy



quinquepy



sexipy

Double helical structures of these 'helicates' provide therefore interesting comparison with the twisted structures of $[\text{ZnL}^1]^{2+}$ and $[\text{NiL}^1]^{2+}$ where possible conjugation of the 2,6-pyridinediimine unit with the iminophenoxy rings is interrupted by significant twisting of the latter from the ' N_3 ' plane. As noted previously, these twists confer a helical configuration for each asymmetric unit of L^1 and, through the two-fold symmetry present in the each complex, result in the presentation of an apparently double helical ligand array at the metal centre.

The importance of interligand π -stacking interactions in stabilising helical polypyridine structures has been emphasized.^[92,93,94,95,96,97] In an example,^[94] similar solid state structures were observed for $[\text{Cu}_2\text{quinguepy}_2(\text{OAc})]^{3+}$ and $[\text{Ni}_2\text{quinguepy}_2(\text{OAc})]^{3+}$ despite different co-ordination spheres for corresponding metal centres in the complexes. [The metals occupy a four co-ordinate cavity described by bipy moieties of each ligand and complete their respective co-ordination spheres with a co-ordinated acetate ligand; monodentate for Cu(II) (5 co-ordinate) and bidentate for Ni(II) (6 co-ordinate).] The authors conclude that the gross geometries of the complexes result from a predominance of stacking interactions within the double helical bis-quinguepy array of the complexes over the electronic preferences of the metal ions.^[94]

In conclusion, the solid state structures show that the co-ordination of L^1 to Zn(II) and Ni(II) arises from preferential binding of the 2,6-pyridinediimine nitrogen donor sites in the ligand. The compression of the macrocycle required to produce a donor cavity of suitable size for these relatively small metal ions results in a twisted, double helical configuration stabilised by transannular π -stacking interactions between the aromatic rings of the ligand. These observations give invaluable insight into the co-ordination chemistry of L^1 and are extended to consideration of the solution phase structures of, in the first instance, $[\text{ZnL}^1]^{2+}$ and, by comparison of nmr data, other diamagnetic metal complexes of L^1 .

11. Nuclear magnetic resonance studies of the diamagnetic complexes of L^1

The diamagnetic complexes of the ligand L^1 (Fig. 11.1.1) were investigated using both proton and carbon-13 nmr spectroscopy in an attempt to characterise their solution structures. Applications of nmr spectroscopy in co-ordination chemistry are well known^[99] and have been widely applied to the conformational analysis of metal chelate compounds.^[64,100] Nmr studies of macrocyclic complexes are becoming increasingly widespread,^[101] although studies of tetraamine, [2+2] macrocyclic complexes remain limited to a few examples.^[10,102] A number of complexes of L^1 proved to be suitable for study by nmr spectroscopy and full assignment of their proton and carbon-13 was attempted in order to probe possible conformational and co-ordination changes in the ligand induced by the nature of the co-ordinated metal ion.

In the absence of nmr data for the un-complexed form of L^1 , assignment of the spectra, particularly the complicated aromatic regions, was aided by consideration of data for compounds containing similar functional groups to those in ligand, L^1 . These model compounds, M^1 , M^2 , M^3 , M^4 , are shown in Figure 11.1.1; nmr parameters for M^1 , M^3 and M^4 were determined during the course of this work.

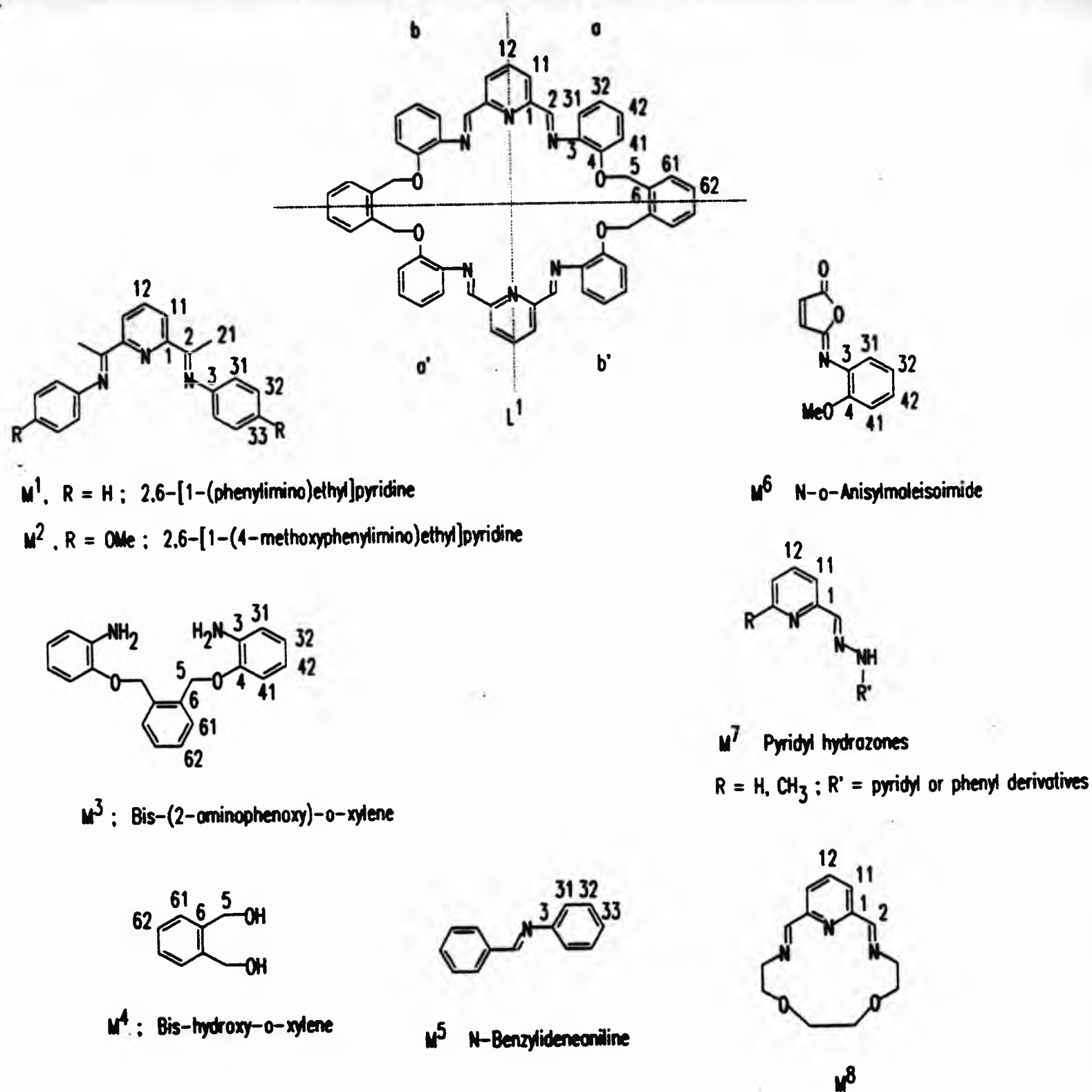


Figure 11.1.1. Ligand L¹ and model systems used in assignment of ¹H and ¹³C nmr spectra of complexes, [ML¹]²⁺. The numbering scheme for the asymmetric unit of each compound is consistent with that of L¹.

Assignments were further aided by calculation of predicted shifts for ¹H and ¹³C in aromatic environments from empirical parameters for substituent-induced

shifts (z_R^i relative to benzene, where i = *ortho*, *meta* or *para*) for mono-substituted benzene environments.^[103,104] This data allowed estimation of relative orders of shielding for the respective aromatic environments and provided a basis for assignment of the proton and carbon-13 spectra of $[ML^1]^{2+}$. Predicted 1H and ^{13}C shifts were obtained by summation of the appropriate substituent-induced shift (z_R^{ipso} (for ^{13}C only), z_R^{ortho} , z_R^{meta} , or z_R^{para}) for each functional group according to Equation 11.1.1. Proton and carbon-13 shifts of 7.27 ppm^[103] and 128.5 ppm^[104] respectively were used for $\delta(C_6H_6)$ throughout this work.

$$\delta = \delta(C_6H_6) + \sum_i z_R^i \quad (11.1.1)$$

11.1. Assignment of proton nmr spectra

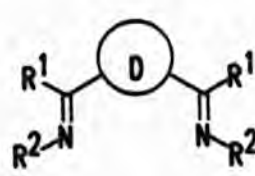
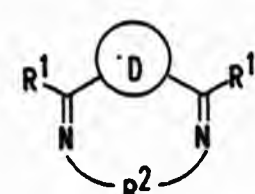
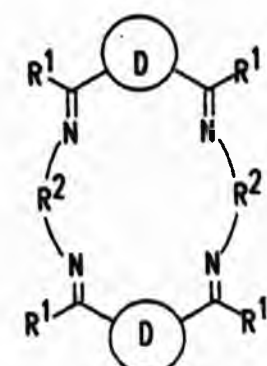
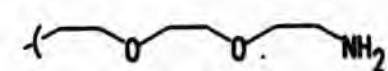
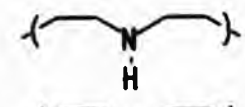


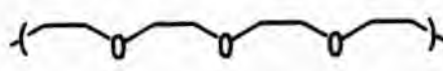
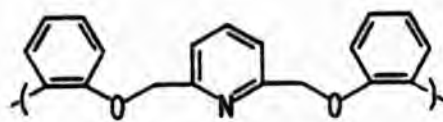
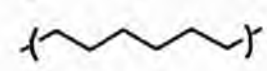
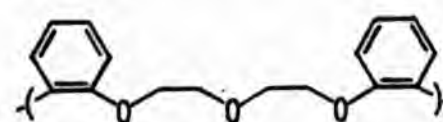
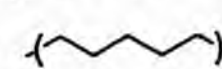
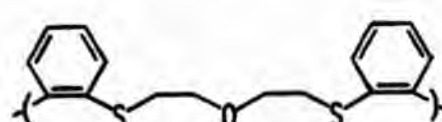
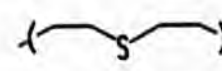
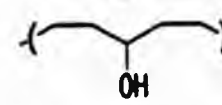
11.1.1 General features

Reports of metal complexes of Schiff-base ligands derived from either 2,6-pyridine-, 2,5-furan- or 2,5-thiophendicarbonyl compounds are widespread in the literature (*vide supra*) and a selection of reported proton nmr parameters are shown in Table 6.6.1. Identification of the pyridyl and imine proton resonances of $[ML^1]^{2+}$ was particularly aided by consideration of the coupling multiplicities given in the table. Imine resonances (corresponding to H2) appear as characteristic lowfield singlets whilst the γ - (H12) and β - (H11) protons of symmetrically 2,6-disubstituted pyridine rings frequently show triplet and doublet splittings respectively. Schematic representations of ligand structures are included in the table.

Differentiation of the aromatic signals arising, respectively, from the iminophenoxy and xylenyl rings of $[ML^1]^{2+}$ was generally achieved with 1H - 1H

correlation spectroscopy (^1H - ^1H COSY). Thereafter, comparison of nmr data with that of model compounds containing either xylenyl or iminophenoxy rings was helpful in assigning individual multiplets.

Table 11.1.1. Proton nmr parameters of some metal complexes of Schiff-base ligands derived from 2,5-furan-, 2,5-thiophen- and 2,6-pyridine-dicarbonyls.

					
open		1+1		2+2	
	R^2		R^2		R^2
	1		8		
	2		9		
	3		10		
	4		11		
	5		12		
	6				
	7				

M ^a	D ^b	R ¹	R ² Ring	Solvent	Chemical shift ^c			Reference
					$\delta(\beta\text{-py})$	$\delta(\gamma\text{-py})$	$\delta(\text{CH=N})$	
Ba	py	H	1 open	CD ₃ CN	7.85(m)		8.54(s)	[105]
Ba	fur	H	1 open	CD ₃ CN	-		8.20(s)	[105]
Ba	py	H	2 2+2	CD ₃ CN	7.88(m)		8.50(s)	[105]
Ba	fur	H	2 2+2	CD ₃ CN	-		8.45(s)	[105]
Ca	py	H	3 1+1	(CD ₃) ₂ SO	8.00-8.53(m)		8.80(s)	[106]
Sr	py	H	3 1+1	(CD ₃) ₂ SO	8.06-8.54(m)		8.85(s)	[106]
Ba	py	H	3 1+1	(CD ₃) ₂ SO	8.00-8.50(m)		8.75(s)	[106]
Pb ₂	py	Me	4 2+2	CD ₃ CN	8.55(m)		-	[13]
Pb ₂	py	Me	5 2+2	CD ₃ CN	8.35(m)		-	[13]
Ag ^I	th	H	6 2+2	CD ₃ CN	-		9.34(s)	[107]
Cu ^I	th	H	6 2+2	CD ₃ CN	-		8.65(s)	[107]
Ba	py	Me	7 2+2	CD ₃ OD	7.69(d)	7.87(t)	-	[15]
Ag ^I	py	Me	8 2+2	CD ₃ CN	8.26(m)		-	[46]
Ag ^I	py	Me	9 2+2	CD ₃ CN	8.30-8.54(m)		-	[46]
Pb	py	H	10 1+1	CD ₃ CN	8.27(d)	8.54(t)	9.66(s)	[23]
Pb	fur	H	10 1+1	CD ₃ CN	-		9.00(s)	[23]
Pb	py	H	11 1+1	(CD ₃) ₂ SO	8.44(d)	8.72(t)	9.87(s)	[108]
Pb	py	H	12 1+1	CD ₃ CN	8.87(d)	8.63(t)	9.63(s)	[109]

^a Metal ions are bivalent unless otherwise stated. ^b D = hetero-ring; py = pyridine, fur = furan, th = thiophen. ^c In ppm relative to SiMe₄; reported multiplicities are given in parentheses.

For the unsymmetrically 1,2-disubstituted rings of L¹, discrimination of the resonances due to aromatic protons *ortho* to the ring substituents (H31 and H41) and those *meta* to the substituents (H32 and H42) was achieved on the basis of differing first-order spin-spin coupling multiplicities arising from their respective environments. Multiplets due to protons *ortho* to the ring substituents are expected to give rise to a doublet of doublets, while those *meta* to the substituents are likely to approximate a triplet of doublets. If

the respective three-bond couplings (3J and $^3J'$) are resolved for the latter case, the multiplet will appear as a doublet of doublet of doublets. Perturbation of relative peak intensities and multiplicities by second order effects in such aromatic environments are widely known.^[110]

Application of Eqn. 11.1.1 to estimate the proton shifts for a series of *o*-substituted methoxybenzenes provided data to assist assignment of the iminophenoxy protons. In the absence of data for imino-substituted benzene rings, the proton parameters $z_{\text{H=C}}^{\text{ortho}}$, $z_{\text{H=C}}^{\text{meta}}$, and $z_{\text{H=C}}^{\text{para}}$ were deduced from the spectrum of M^1 (Ref. [61] and this work) and applied as above.

Proton nmr parameters were determined for M^1 in CDCl_3 . Insolubility of the compound in CD_3CN unfortunately precluded an nmr study in this solvent. Integration of the spectrum indicates six unique proton environments corresponding to the six environments of an asymmetric unit comprising one half of the molecule. The methyl protons (H21, see Fig. 11.1.1 for numbering scheme) give rise to a singlet at 2.40 ppm. Signals assigned to the γ - and β -pyridyl protons (H12 and H11 respectively) form an A_2B subspectrum at low field. Analysis using standard equations^[42] yields $\delta(\text{H11}) = 8.34$ ppm, $\delta(\text{H12}) = 7.87$ ppm, and $^3J(\text{H11-H12}) = 7.8$ Hz.

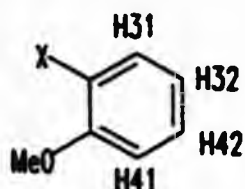
The phenylimino ring protons give rise to three complicated multiplets centred at ca. 7.38, 7.12, and ca. 6.85 ppm. The multiplet at 7.12 ppm may be unambiguously assigned to H33 on the basis of peak integration. The multiplet resembles a triplet of triplets although extra lines in the central component of the multiplet indicate some second order behaviour. The three- and four-bond coupling constants, $^3J(\text{H33-H32}) \approx 7.4$ Hz and $^4J(\text{H33-H31}) \approx 1.2$ Hz, were estimated from this multiplet. The multiplets at ca. 7.38 and ca.

6.85 ppm, in showing predominantly triplet and doublet of doublet splittings, are assigned to H32 and H31 respectively. Both multiplets show extra splittings and asymmetry consistent with second order character in the spectrum and the phenylimino protons should therefore be regarded strictly as an ABB'CC' spin system. Confirmation of this assignment and calculation of the coupling constants in the subspectrum requires computer simulation and further work was not undertaken.

Substituent-induced shifts due to imino ring substituents may be estimated from this data, giving $z_{\text{N=C}}^{\text{ortho}} = -0.42$, $z_{\text{N=C}}^{\text{meta}} = +0.11$ and $z_{\text{N=C}}^{\text{para}} = -0.15$ ppm. The shielding of the ortho and para protons induced by imino substitution contrasts with the predicted deshielding influence of -CHO ($z_{\text{N=C}}^{\text{ortho}} = +0.56$, $z_{\text{N=C}}^{\text{para}} = +0.29$)^[103a] and, less clearly, the influence of -CH=CH₂ ($z_{\text{N=C}}^{\text{ortho}} = +0.06$, $z_{\text{N=C}}^{\text{para}} = -0.10$)^[103a] at these sites. These latter substituent-induced shifts might have been used as estimates in the absence of data for imino-substitution. Estimates of the phenyl proton shifts for 2,6-bis[1-(4-methoxyphenylimino)ethyl]pyridine, M², using the parameters derived above and the reported^[103a] values for -OMe gives $\delta(\text{H31}) = 6.76$ and $\delta(\text{H32}) = 6.90$, in good agreement with the reported multiplet at 6.83-6.92 ppm in CDCl₃.^[61]

Assignment of the aromatic protons of L¹ was aided by estimating shifts for a series of o-substituted methoxybenzenes. Methoxy substitution of benzene is predicted to cause a general shielding of the phenyl protons with $z_{\text{OMe}}^{\text{ortho}} = -0.48$, $z_{\text{OMe}}^{\text{meta}} = -0.09$ and $z_{\text{OMe}}^{\text{para}} = -0.44$.^[103a] The predicted shifts for aromatic protons of the various o-substituted methoxybenzenes, calculated using Eqn. 11.1.1, are given in Table 11.1.2.

Table 11.1.2. Predicted influence of functional groups, X, on the chemical shifts of protons for *o*-substituted methoxybenzenes.^a



Group	Chemical shift			
X	$\delta(\text{H31})$	$\delta(\text{H32})$	$\delta(\text{H42})$	$\delta(\text{H41})$
$-\text{NH}_2$	6.43	6.58	6.53	6.54
$-\text{NH}_3^+$ ^b	7.58	7.03	7.38	6.99
$-\text{CHO}$	7.74	7.05	7.47	7.01
$-\text{CH}=\text{CH}_2$	7.24	7.80	7.08	6.76
$-\text{N}=\text{C}(\text{Me})\text{py}^c$	6.76	6.94	7.03	6.90

^a Shifts in ppm. Substituent shifts, relative to benzene ($\delta = 7.27$ ppm), from Ref. [103a] unless otherwise stated. ^b Substituent shifts from Ref. [103b].

^c Calculated from spectrum of 2,6-bis[1-(phenylimino)ethyl]pyridine (Ref. [61] and this work).

Amine substitution of methoxybenzene, e.g. $-\text{NH}_2$, is predicted to shift all resonances upfield relative to that of benzene. The upfield shift is largest for H31, *ortho* to the $-\text{NH}_2$ substituent. Protonation of the resulting aromatic amine, approximating the effect of metal coordination, causes a deshielding of H31 and H42 and shielding of H32 and H41 relative to the benzene resonance. Ring substitution with the α,β -unsaturated group $-\text{CHO}$, shifts the protons *ortho* and *para* to the substituent (H31 and H42 respectively) downfield and the *meta* protons (H32 and H41 respectively) upfield from benzene. For $o\text{-CH}_2=\text{CH}-\text{C}_6\text{H}_4\text{OMe}$, $\delta(\text{H31})$, $\delta(\text{H41})$ and $\delta(\text{H42})$, are predicted to be upfield from $\delta(\text{C}_6\text{H}_6)$ while $\delta(\text{H32})$ is expected at lower field. The small shielding due to $-\text{CH}=\text{CH}_2$ ($\delta_{\text{meta}}^{\text{CH}=\text{CH}_2} = -0.03$ ppm^[103a]) is presumably swamped by the *para*

deshielding effect of the methoxy substituent in the latter case. In contrast, substitution with $-N=C(Me)py$ causes a general shielding of the protons with the *ortho* proton (H31) shifted furthest upfield. If it is assumed that the substituent effects of the coordinated imine are best approximated by the $-N=C(Me)py$ parameters, the aromatic resonances of $[ML^1]^{2+}$ are predicted to separate with H31 upfield from H41 and H42 downfield from H32. More accurate prediction of the signal positions is clearly not warranted.

The *ortho*-xylenyl proton assignments for the macrocycle were aided by comparison with spectra for benzenedimethanol (M^4 ; α,α' -bis-hydroxy-*o*-xylene, in CD_3CN) and the diamine precursor of L^1 , α,α' -bis(2-aminophenoxy)-*o*-xylene (M^3 , in $CDCl_3$). The proton spectrum of M^3 (see Section 8.3.3 for a list of parameters) shows a broadened peak at ca. 3.8 ppm which disappears on exchange with D_2O and is assigned to the anilino protons. The signal at ca. 3.6 ppm in the spectrum of M^4 is assigned to the hydroxyl proton. The methylene protons, H5, give sharp singlets, at 5.19 ppm for M^3 and 4.62 ppm for M^4 .

The aromatic region of the spectrum of M^4 consists of two complex multiplets, at ca. 7.27 ppm and ca. 7.35 ppm, due to H61 and H62. The multiplets show line splittings, intensities and symmetries reminiscent of the AA'BB' spectra for other 1,2-symmetrically disubstituted benzenes^[42]. Application of Eqn. 11.1.1, in an attempt to estimate $\delta(H61)$ and $\delta(H62)$ using substituent-induced shifts for $-CH_2OH$ ($z_{ortho}^{N=C}$, $z_{meta}^{N=C}$, $z_{para}^{N=C} = 0.07^{[103a]}$), does not distinguish between the sites and further assignment was not attempted.

The aromatic region of the M^3 spectrum consists of overlapping multiplets from

eight protons at 6.65–6.88 ppm and two complex multiplets centred at ca. 7.38 and ca. 7.52 ppm respectively, due to two protons each. The upfield multiplet can be assigned to overlapping resonances from the aminophenoxy protons, H31, H32, H41 and H42; the range is in reasonable agreement with the estimated shifts for rings of this type (Table 11.1.2). The downfield multiplets approximate the AA'BB' pattern of the M⁴ o-xylenyl protons, H61 and H62 (*vide supra*). Though closely similar, the two multiplets are not identical, suggesting an ABCD spin system. The non-equivalence could be caused by intramolecular hydrogen bonding. These resonances are more widely separated and are shifted to lower field than the corresponding aromatic absorbances for M⁴. The ¹H-¹³C COSY spectrum of M³ indicated that this proton assignment is consistent with a carbon-13 assignment based on substituent-induced shift parameters for aromatic carbon environments (*vide infra*).

11.1.2 The ¹H nmr spectrum of [ZnL¹][ClO₄]₂.

The proton nmr spectrum of [ZnL¹][ClO₄]₂ in CD₃CN [Fig. 11.1.2(i)] shows sharp, well-separated peaks, and the ten discrete multiplets observed in the spectrum correspond to ten proton environments for the complex. The spectrum indicates equivalent protons such that, in solution, the asymmetric unit comprises one quarter of the molecule as shown in Fig. 11.1.1. Spectral assignments, using the numbering scheme of Fig. 11.1.1, are summarised in Table 11.1.3. Non-co-ordinating molecules of acetonitrile present in the crystal lattice are expected to exchange with the bulk solvent and their signal is therefore obscured by that at ca. 1.9 ppm due to residual proton impurities in the deuteriated solvent.

The triplet at 8.10 ppm is assigned to the proton (H12) in the γ-pyridyl position on the basis of shift (by comparison with data of Table 11.1.1),

spin-spin coupling to the equivalent protons H11a and H11b ($^3J(\text{H12-H11}) = 7.7$ Hz), and integration (all other peaks integrate for 4 or more protons compared to 2 for this triplet). The doublet at 7.66 ppm integrates for four protons and correlates to the H12 triplet in the ^1H - ^1H COSY spectrum of the complex [Fig. 11.1.2(ii)], and is hence assigned to H11. The ^1H - ^1H COSY spectrum also shows the doublet to be correlated to the singlet at 7.80 ppm. This latter signal can be unambiguously assigned to the imino proton, H2 although it is slightly upfield of resonances observed for related metal complexes (see Section 11.1.1). The correlation with H11, noted above and indicating a four bond coupling, is not reflected in observable splitting of the peak, presumably because $^4J(\text{H11-H2})$ is very small. Correlations between H12, H11, H2 and other aromatic resonances are notably absent from the ^1H - ^1H COSY spectrum.

Signals centered at ca. 4.65 ppm, and corresponding to 4 protons, are assigned to the methylene protons H5 by analogy with the methylene shifts of the precursor diamine (M^3) and benzene dimethanol (M^4). The ^1H - ^1H COSY spectrum shows an absence of correlation between these and other signals in the spectrum and the splitting therefore arises from geminal coupling between the two non-equivalent protons of the methylene group. The signals can be assigned as an AB spin system with $^2J = 11.4$ Hz. The chemical shift separation ($\nu_0 \Delta\delta$ where ν_0 is the operating frequency of the spectrometer and $\Delta\delta$ is the separation of the signals in ppm) for an AB system is calculated as^[110]

$$\nu_0 \Delta\delta = \sqrt{(a - d)(b - c)} \quad (11.1.2)$$

where $(a - d)$ and $(b - c)$ are the separations between the outermost and innermost pairs of lines of the spectrum. This yields chemical shifts for H5(1) and H5(2) of 4.65 and 4.63 ppm respectively. The intensity ratio of the

lines (stronger:weaker), I_s/I_w , may be calculated using^[110]

$$(I_s/I_w)_{\text{calc}} = (1 + J/\sqrt{(\nu_0\Delta\delta)^2 + J^2}) / (1 - J/\sqrt{(\nu_0\Delta\delta)^2 + J^2}) \quad (11.1.3)$$

giving $(I_s/I_w)_{\text{calc}} = 15.4$ [$(I_s/I_w)_{\text{obs}} = 10.3$].

Six discrete multiplets in the region 6.26–7.30 ppm, each corresponding to four protons, are assigned to phenyl protons. The ^1H – ^1H COSY, in showing correlations between the coupled signals of each ring, is particularly useful in determining the origin of each of the multiplets. The multiplets at $\delta = 7.27, 6.97, 6.86$ and 6.28 correlate to one another, and are therefore expected to originate from the four protons of the iminophenoxy ring. The iminophenoxy resonances are sufficiently separated ($\nu_0\Delta\delta/J \geq 3.1$) to approximate an AMPX spin system. Such first-order spin-spin coupling between these nuclei is expected to generate characteristic multiplets (Section 11.1.1). The ‘triplet of doublets’ pattern, expected for H42 and H32, is approximated by the signals centred at 7.27 and 6.86 ppm. Mean three-bond coupling constants of 8.0 and 7.6 Hz respectively may be deduced from these multiplets although asymmetry of the central peaks of each multiplet, particularly for the signals at ca. 7.27 ppm, suggests that the individual coupling constants are not equal. The signals at 6.97 and 6.29 ppm are split into the ‘doublet of doublets’ pattern and, significantly, do not generate a cross peak in the ^1H – ^1H COSY. The peaks are therefore assigned to the *ortho* protons H31 and H41 and the absence of correlation between the peaks suggests that coupling between them (5J) is not observed.

Consideration of the model systems, Section 11.1.1, indicates H41 and H42 to be the more deshielded proton of each pair and provides the basis of the assignment given in Table 11.1.3.

Table 11.1.3. ^1H nmr parameters for $[\text{ZnL}^1][\text{ClO}_4]$.^a

Assignment	δ^b /ppm	Multiplicity ^c	Integration	^1H - ^1H Coupling ^d		
				2J	3J	4J
H12	8.10	t	2H		7.7	
H2	7.80	s	4H			
H11	7.66	d	4H		7.7	
H42	7.27	ddd	4H		ca. 8.0 ^e	1.5
H61 (H62 ^f)	7.10	g	4H			
H41	6.97	dd	4H		8.2	1.2
H32	6.86	ddd	4H		ca. 7.6 ^e	1.2
H62 (H61 ^f)	6.36	g	4H			
H31	6.29	dd	4H		7.8	1.6
H5(1)	4.63	h	} 8H	11.4		
H5(2)	4.65	h		11.4		

- ^a Saturated solution of complex in CD_3CN at ambient temperature. See Fig. 11.1.1 for numbering scheme. ^b Chemical shift in ppm relative to internal SiMe_4 . Estimated error ± 0.002 ppm. Shifts are given as the mean position of the multiplet unless otherwise stated. ^c s = singlet, d = doublet, dd = doublet of doublets, ddd = doublet of doublets of doublets, t = triplet. ^d Coupling constants in Hz; estimated error ± 0.44 Hz. ^e Separate couplings not resolved. ^f Possible alternative assignment. ^g Symmetrical multiplet approximating to $\text{AA}'\text{XX}'$. ^h AB multiplet.

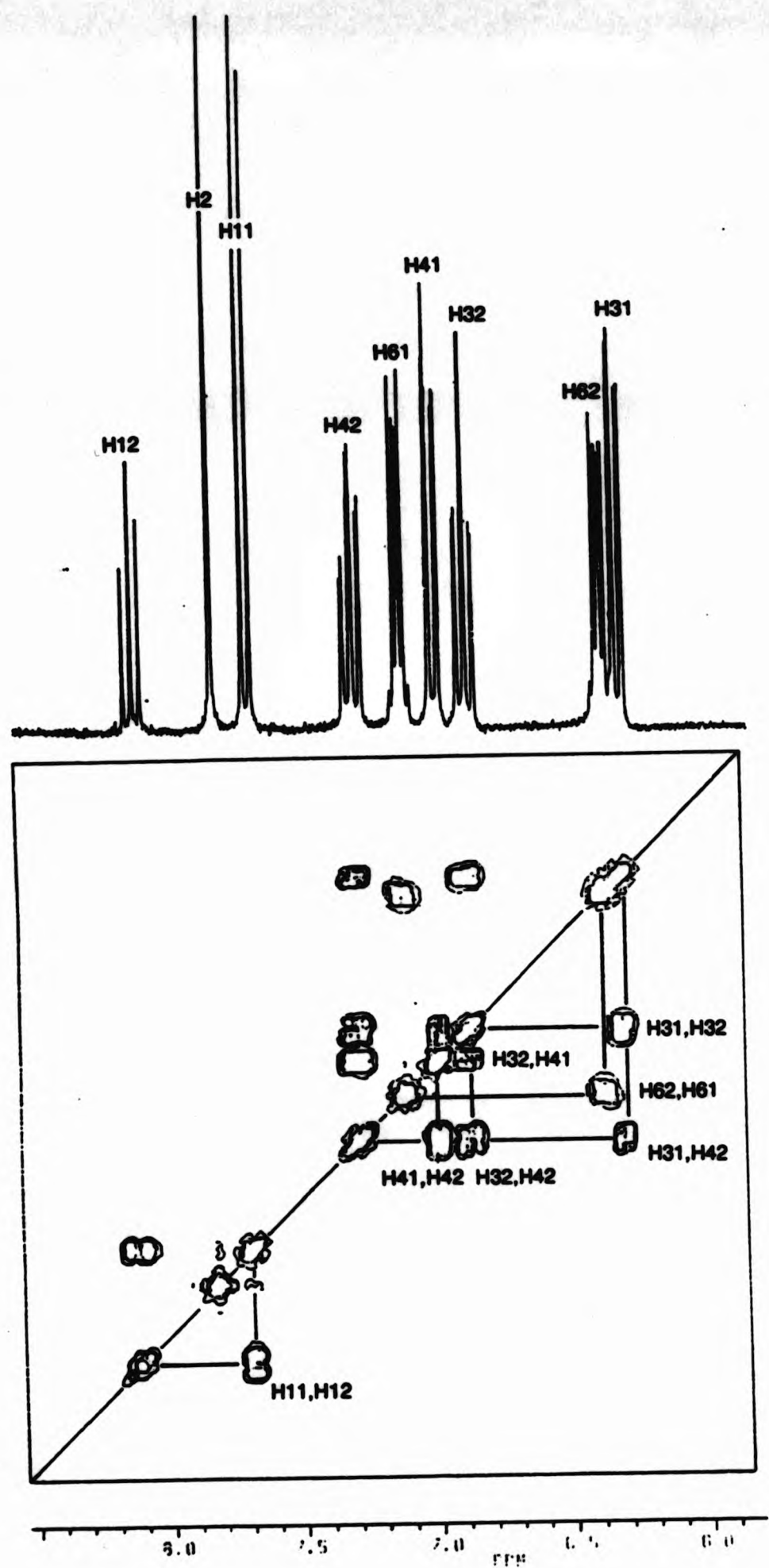


Figure 11.1.2 Proton nmr spectra of $[\text{ZnL}^1][\text{ClO}_4]_2$. (i) Range: 8.2–6.0 ppm;
(ii) ^1H - ^1H COSY contour plot

The ^1H - ^1H COSY spectrum of $[\text{ZnL}^1][\text{ClO}_4]_2$ [Fig. 11.1.2(ii)] shows the multiplets centred at 7.10 and 6.36 ppm to be correlated solely to one another. This is consistent with their assignment to protons H61 and H62 of the xylenyl ring. Unexpectedly, the multiplets are well separated ($\nu_0\Delta\delta = 185.5$ Hz) compared with the model xylenyl systems ($\nu_0\Delta\delta$ (M^3) = 35.0 Hz; $\nu_0\Delta\delta$ (M^4) = 20.0 Hz) and approximate the two parts of an AA'XX' spectrum. Despite the wide separation between ν_A ($=\nu_{A'}$) and ν_X ($=\nu_{X'}$), the multiplets appear to be complicated by second order character. The nearly identical multiplets of the spectrum (centred at ν_A and ν_X) are symmetric about their 'centre of gravity' $(\nu_A + \nu_X)/2$ and each is symmetric about ν_A and ν_X respectively, consistent with AA'XX' spectra of symmetrical 1,2-disubstituted benzene four spin systems.^[42] Ten lines are expected for each multiplet of this spin system but only 6 are discernable in the spectrum of $[\text{ZnL}^1][\text{ClO}_4]_2$. For this reason it was not possible to deduce the separate coupling constants, $^3J(\text{H61-H62})$, $^3J(\text{H62-H62}')$, $^4J(\text{H61-H62}')$ and $^5J(\text{H61-H61}')$. As noted for the proton spectra of M^3 and M^4 , while there is no basis for assigning H61 and H62 to particular multiplets, H61 is nominally assigned to lower field.

11.1.3 The ^1H nmr spectrum of $[\text{CdL}^1][\text{ClO}_4]_2$.

Proton nmr spectra of $[\text{CdL}^1][\text{ClO}_4]_2$ [Fig. 11.1.3(i)-(iv)] were obtained from saturated solutions of the complex in CD_3CN . Essentially identical spectra were obtained for two independent batches of the complex. Signals arising from non-co-ordinating acetonitrile and water molecules, inferred from microanalytical and infrared data for one batch of sample, are expected to be obscured by those arising from the solvent residual and aqueous impurities at ca. 1.9 ppm and ca. 2.2 ppm respectively. Integration of the spectra indicated ten unique proton environments for $[\text{CdL}^1]^{2+}$, in common with $[\text{ZnL}^1]^{2+}$, and hence the asymmetric unit of the complex in solution essentially

comprises one quarter of the molecule (shown in Fig. 11.1.1). Assignments are summarised in Table 11.1.4.

Table 11.1.4. ^1H nmr parameters for $[\text{CdL}^1][\text{ClO}_4]_2$.^a

Assignment	δ^b /ppm	Multiplicity ^c	Integration	^1H - ^1H Coupling ^d		
				2J	3J	4J
H12	8.10	s	2H		7.7	
H2	7.99	f	4H			
H11	7.63	g	4H		7.7	
H42	7.23	td	4H		ca. 7.9 ^h	1.5
H32	6.93 ⁱ	td	12H		ca. 7.8 ^j	1.1
H61 (H62 ^k)	6.90 ⁱ	s				
H41	6.85 ⁱ	dd			8.2	1.1
H31	6.65	dd	4H		7.8	1.5
H62 (H61 ^k)	6.08	s	4H			
H5(1)	4.79	m	4H	11.3		
H5(2)	4.57	m	4H	11.3		

- ^a Saturated solution of complex in CD_3CN at ambient temperature. See Fig. 11.1.1 for numbering scheme. ^b Chemical shifts in ppm relative to internal SiMe_4 . Estimated error ± 0.002 ppm. Shifts are given as the mean position of the multiplet unless otherwise stated. ^c s = singlet, d = doublet, dd = doublet of doublets, t = triplet, td = triplet of doublets. ^d Coupling constants in Hz. Estimated error ± 0.5 Hz. ^e t with overlapped td satellite spectrum; $^5J(^{111,113}\text{Cd-H12}) = 2.5$ Hz. ^f s overlapped with d satellite spectrum; $^3J(^{111}\text{Cd-H2}) = 34.4$ Hz, $^3J(^{113}\text{Cd-H2}) = 35.6$ Hz. ^g d with overlapped dd satellite spectrum; $^4J(^{111,113}\text{Cd-H12}) = 4.5$ Hz. ^h $^3J(\text{H42-H32}) \approx ^3J(\text{H42-H41})$. ⁱ Determined from J-resolved spectrum. ^j $^3J(\text{H32-H42}) \approx ^3J(\text{H32-H31})$. ^k Possible alternative assignment. ^l Symmetrical multiplet approximating to $\text{AA}'\text{XX}'$ subspectrum. ^m AB multiplet.

The methylene protons [H5(1) and H5(2)] give rise to an AB multiplet centred at 4.68 ppm with $^2J = 11.3$ Hz. The H5 resonances are separated by 51.9 Hz (0.21 ppm) (Eqn. 11.1.2) and the intensity ratio for the lines of the 'roofed' doublets of the multiplet ($(I_s/I_w)_{\text{obs}} = 1.46$) compares favourably with the calculated value, $(I_s/I_w)_{\text{calc}} = 1.54$ (Eqn. 11.1.3).

Assignment of the iminophenoxy and xylenyl proton resonances was aided by homonuclear J-resolved [Fig. 11.1.3(ii) and (iii)] and ^1H - ^1H -COSY spectra. The six signals appear as four multiplets with relative areas of 1:3:1:1 centred at $\delta = 7.23$, ca. 6.9, 6.65 and 6.08 ppm respectively. The triplet of doublets pattern, expected for both H32 and H42, is approximated by the most downfield of these signals. This multiplet is assigned to H42 on the basis of the shift arguments discussed in section 11.1.1. The doublet of doublets at 6.65 ppm is likewise assigned to H31.

The three overlapping signals forming the complex multiplet at 6.83-6.96 ppm were separated by a homonuclear J-resolved experiment [Fig. 11.1.3(ii)]. The central multiplet ($\delta = 6.90$ ppm) has a pattern identical to that of the multiplet at 6.08 ppm. Furthermore, the ^1H - ^1H -COSY spectrum shows that the latter multiplet correlates solely to the centre of the three proton multiplet at ca. 6.9 ppm. These signals are therefore ascribed to an AA'XX' spectrum arising from the xylenyl ring protons. As with the Zn(II) complex, detailed analysis and certain assignment of the signals to H61 and H62 was not possible.

The other components of the multiplet at ca. 6.9 ppm, a triplet of doublets at 6.93 ppm (due to H32) and a doublet of doublets at 6.85 ppm (H41) were assigned in accordance with the coupling patterns and the shift arguments of

Section 11.1.1, and, for H41, the lack of correlation in the ^1H - ^1H COSY between the multiplets at 6.85 ppm (H41) and 6.65 ppm (H31). Extra peaks, symmetrical about $f_1 = 0$, are observed in the J-resolved spectrum between the iminophenoxy resonances of the multiplet at ca. 6.9 ppm. Such peaks, indicative of second order coupling, are observed in J-resolved spectra when $\nu_0 \Delta\delta/J < 3$, although cross-sections near the true chemical shift remain accurate representations of the multiplets until $\nu_0 \Delta\delta/J$ becomes less than two. [111] The above assignment gives $\nu_0 \Delta\delta/J \approx 2.5$.

Table 11.1.5. Magnetic properties of selected nuclides.^a

Isotope	Spin	Magnetogyric ratio ^b	Natural abundance	Relative receptivity (D^c) ^c
^1H	1/2	26.7510	99.98	5.58×10^3
^{13}C	1/2	6.7283	1.108	1.00
^{107}Ag	1/2	-1.0828	51.82	0.195
^{109}Ag	1/2	-1.2448	48.18	0.276
^{111}Cd	1/2	-5.6714	12.75	6.93
^{113}Cd	1/2	-5.9328	12.26	7.6
^{207}Pb	1/2	5.5797	22.60	1.18×10^1

^a Taken from Ref. [113]. ^b $/10^7 \text{ rad T}^{-1} \text{ s}^{-1}$. ^c Relative to ^{13}C ; $D^c(^{13}\text{C}) = 1.00$.

The downfield triplet (8.10 ppm, $^3J = 7.7 \text{ Hz}$), singlet (7.99 ppm) and doublet (7.64 ppm, $^3J = 7.7 \text{ Hz}$), [Fig. 11.1.3(iv)] are assigned to the pyridyl and imine protons, H12, H2 and H11 respectively. Each of these lines shows

symmetrical satellites each with intensity approximately one-fifth that of the central peak. These satellites remain on the f_2 axis of the J-resolved spectrum [Fig. 11.1.3(ii)] and the diagonal of the ^1H - ^1H COSY spectrum, and arise from spin-spin coupling between protons and the nmr-active ($I = 1/2$) isotopes of cadmium, Table 11.1.5. Attempted selective decoupling experiments, in which the low frequency satellite of H2 was irradiated, were adversely affected by 'non-selectivity' of the decoupler frequency, and hence saturation transfer effects^[112] could not be determined.

The H2 satellites are sufficiently resolved to show both proton-cadmium-111 [$^3J(^{111}\text{Cd-H2}) = 34.4 \text{ Hz}$] and proton-cadmium-113 [$^3J(^{113}\text{Cd-H2}) = 35.5 \text{ Hz}$] couplings [Fig. 11.1.3(iv)]. The ratio, $^3J(^{111}\text{Cd-H2}):^3J(^{113}\text{Cd-H2}) = 0.969$ is in close agreement with the ratio of the magnetogyric ratios^[113] for the cadmium isotopes, i.e. $\gamma(^{111}\text{Cd}):\gamma(^{113}\text{Cd}) = 0.956$. The higher intensity of the innermost satellites reflects the higher natural abundance of the ^{111}Cd isotope. Couplings of $^4J(^{111,113}\text{Cd-H11}) = 4.5 \text{ Hz}$ and $^5J(^{111,113}\text{Cd-H12}) = 2.5 \text{ Hz}$ are apparent from the satellites of the signals assigned to H11 and H12. The small values of these coupling constants precluded resolution of the separate coupling to ^{111}Cd and ^{113}Cd and the quoted values therefore represent 'mean' proton-cadmium coupling constants.

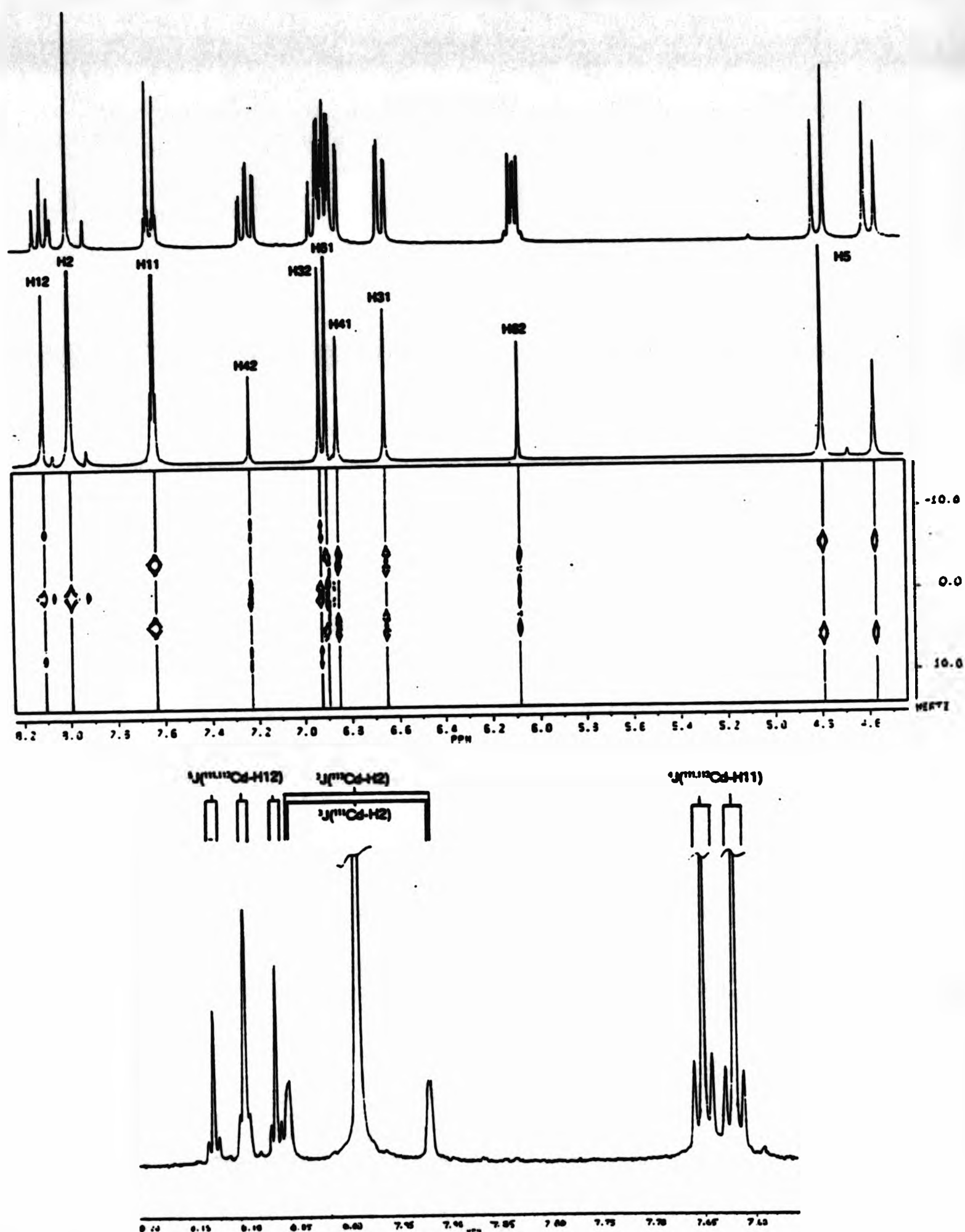


Figure 11.1.3 Proton nmr spectra of $[\text{CdL}^1][\text{ClO}_4]_2$. (i) Range: 8.2-4.5 ppm; (ii) ^1H - ^1H J-resolved f_2 projection; (iii) ^1H - ^1H J-resolved contour plot; (iv) Range: 8.2-7.55 ppm.

11.1.4. The ^1H nmr spectra of $[\text{PbL}^1][\text{ClO}_4]_2$ and $[\text{PbL}^1][\text{NCS}]_2$.

The lead thiocyanate and perchlorate complexes of L^1 were sufficiently soluble in CD_3CN to give well resolved proton nmr spectra. A variable temperature study of the perchlorate salt in this solvent was undertaken. The latter complex was also sufficiently soluble in $(\text{CD}_3)_2\text{CO}$ to yield a good quality spectrum. Assignments were aided by comparison with a ^1H - ^1H COSY spectrum of $[\text{PbL}^1][\text{ClO}_4]_2$ in CD_3CN and are summarised in Table 11.1.6. The aromatic region of the spectrum of $[\text{PbL}^1][\text{NCS}]_2$ is, within experimental error, identical to that of the perchlorate in CD_3CN and assignment of the latter (given below) may also be applied to the thiocyanate complex.

Integration of each spectrum indicates that the asymmetric unit of $[\text{PbL}^1]^{2+}$ in both CD_3CN and $(\text{CD}_3)_2\text{CO}$ essentially comprises one-quarter of the molecule (shown in Fig. 11.1.1), as observed for $[\text{ZnL}^1]^{2+}$ and $[\text{CdL}^1]^{2+}$. The methylene protons (H5(1) and H5(2)) of $[\text{PbL}^1][\text{ClO}_4]_2$ give rise to an AB subspectrum in both CD_3CN and $(\text{CD}_3)_2\text{CO}$. Results of the analysis of the AB spin systems are summarised in Table 11.1.6. In contrast, the spectrum of $[\text{PbL}^1][\text{NCS}]_2$ shows the methylene resonances as a broadened doublet centred at 4.84 ppm. Broadening of the expected AB pattern prevents observation of the geminal coupling.

The proton resonances of the 2,6-pyridinediimine 'head unit' are well separated in both solvents and were assigned from shift considerations and both 2D- and 1D-coupling correlations. Broadening of the central line of the γ -pyridyl 'triplet' and the β -pyridyl 'doublet', and 'roofing' of line intensities between these multiplets, observed in each spectrum of $[\text{PbL}^1]^{2+}$, suggests a slight deviation from first order behaviour, (i.e. AX_2) to give an AB_2 subspectrum, for H12 and H11. However, the second order perturbations

observed are slight; $\nu_0 \Delta\delta/J > 10$ in each case, and, in the absence of the extra (up to 9 in total) lines expected for AB_2 subspectra,^[42] signals due to H12 and H12 were analysed as AX_2 subspectra.

The imine singlets in both solvents, and for the thiocyanate derivative, are flanked by low intensity satellites (relative intensities 1:10:1) which are independent of the sample spinning rate. These signals are therefore assigned to doublets arising from ^{207}Pb -H2 spin-spin coupling. The spectrum of $[\text{PbL}^1][\text{ClO}_4]_2$ was also determined at higher field (500 MHz). The satellites were discernable as broad shoulders, the broadening presumably being due to T_1 -spin decoupling^[114] caused by the increased influence of chemical shift anisotropy on the relaxation rate of the ^{207}Pb nucleus at higher field.^[115]

Resonances due to the xylenyl ring protons were identified using the ^1H - ^1H COSY spectrum of the perchlorate complex in CD_3CN . The multiplet centred at 6.47 ppm is correlated solely to the peak at 6.66 ppm. Furthermore, these two multiplets have identical patterns and are therefore assigned to an $AA'XX'$ spectrum arising from the xylenyl ring protons ($\delta(\text{H61}) = 6.47$, $\delta(\text{H62}) = 6.66$ ppm). Interchange of assignments for H61 and H62 is possible, and indeed would be consistent with the Zn(II) and Cd(II) complexes, i.e. H61 nominally assigned to be the more deshielded of the two sites. However, arbitrary assignment of H61 and H62 in the zinc and cadmium complexes led, via ^1H - ^{13}C COSY experiments, to assignment of the signal for C62 downfield of that for C61. The pair of signals in the ^{13}C spectrum of the Pb(II) complex which can be assigned to C62 and C61 retain these shifts. This leads, through the ^1H - ^{13}C COSY experiment, to assignment of H62 downfield of H61 for $[\text{PbL}^1][\text{ClO}_4]_2$.

The remaining three multiplets arise from the four aromatic iminophenoxy protons. At 250 MHz, the multiplets are complicated and the homonuclear J-resolved spectrum of $[\text{PbL}^1][\text{ClO}_4]_2$ in CD_3CN shows extra peaks symmetrical about $f_1 = 0$, indicative of second order coupling.^[111] Assignment is provided from the ^1H - ^{13}C COSY spectrum of $[\text{PbL}^1][\text{ClO}_4]_2$ (*vide infra*). The ^{13}C shifts for C32 (125.06-123.83 ppm) and C42 (131.00-130.61 ppm) of the zinc, cadmium and disilver complexes of L^1 are well separated. Signals at 125.37 ppm and 131.40 ppm, assigned to C32 and C42 respectively, in the ^{13}C spectrum of $[\text{PbL}^1][\text{ClO}_4]_2$, correlate to closely-spaced proton multiplets at 7.18 and 7.15 ppm. These are therefore assigned to H32 and H42 respectively. The shift difference between these two multiplets is not easily deduced from the 1D-proton spectrum at 250 MHz, so $\delta(\text{H32})$ and $\delta(\text{H42})$ were estimated from the ^1H - ^{13}C COSY spectrum. The spectrum was subsequently obtained at 500 MHz and showed signals for H32 and H42 as overlapping triplets of doublets, allowing the chemical shift values for H32 and H42 to be confirmed. The signals centred at ca. 6.60 and ca. 7.30 ppm are therefore due to the *ortho* protons (H31 and H41) of the iminophenoxy ring and are assigned using the shift arguments outlined in Section 11.1.1, *i.e.* H41 downfield from H31. The patterns of these two multiplets are virtually mirror images of each other and exhibit second order character. At 500 MHz, signals for H31 and H41 appear as distinct doublets of doublets.

The spectrum of $[\text{PbL}^1][\text{ClO}_4]_2$ in $(\text{CD}_3)_2\text{CO}$ at 250 MHz is complicated by second order effects similar to those noted in CD_3CN at the same field. Shieldings of the iminophenoxy protons are apparently in the same order as in the spectrum in CD_3CN and the spectrum has been assigned accordingly. Interestingly, the H32 and H42 signals are precisely overlapped to give a symmetrical 6-line pattern.

Table 11.1.6. ^1H nmr parameters for $[\text{PbL}^1][\text{ClO}_4]_2$ and $[\text{PbL}^1][\text{NCS}]_2$.

Assignment	Chemical shift ^a		
	$[\text{PbL}^1][\text{ClO}_4]_2^b$	$[\text{PbL}^1][\text{ClO}_4]_2^c$	$[\text{PbL}^1][\text{NCS}]_2^c$
H2	9.20(s) ^d	8.86(s) ^e	8.88(s) ^f
H12	8.25(t) ^g	8.05(t) ^g	8.05(t) ^h
H11	7.92(d) ^g	7.64(d) ^g	7.66(d) ^h
H41	7.55(m) ⁱ	7.30(m) ^j	7.32(m) ⁱ
H32	} 7.22(m) ^{i k}	7.18(m) ^k	} 7.16(m) ^{i k}
H42		7.15(m) ^k	
H62(H61 ^l)	6.84(m)	6.66(m)	6.68(m)
H31	6.77(m) ^l	6.60(m) ^{l m}	6.62(m) ^l
H61(H62 ^l)	6.57(m)	6.47(m)	6.49(m)
H5(1)	5.12 ⁿ	4.93 ⁿ	4.92(br)
H5(2)	4.90 ⁿ	4.73 ⁿ	4.77(br)

^a In ppm relative to internal SiMe_4 . Estimated error ± 0.002 ppm. See Fig. 11.1.1 for numbering scheme. At 250 MHz unless otherwise noted. Multiplicities are given in parentheses: s = singlet, d = doublet, t = triplet, m = multiplet, br = broad. ^b Saturated solution in $(\text{CD}_3)_2\text{CO}$ at ambient temperature. ^c Saturated solution in CD_3CN at ambient temperature. ^d Lead-207 satellites present, $^3J(^{207}\text{Pb-H2}) = 3.4$ Hz. ^e Lead-207 satellites present, $^3J(^{207}\text{Pb-H2}) = 4.3$ Hz. ^f Lead-207 satellites present, $^3J(^{207}\text{Pb-H2}) = 4.0$ Hz. ^g $^3J(\text{H12-H11}) \approx 7.7$ Hz. ^h $^3J(\text{H12-H11}) \approx 7.8$ Hz. ⁱ Estimated centre of multiplet. ^j dd at 500 MHz; $^3J(\text{H41-H42}) = 7.4$ Hz, $^4J(\text{H41-H32}) = 2.0$ Hz. ^k Overlapping signals. ^l Possible alternative assignment. ^m dd at 500 MHz; $^3J(\text{H31-H32}) = 7.7$ Hz, $^4J(\text{H31-H42}) = 1.6$ Hz. ⁿ AB multiplet, $^2J = 11.4$ Hz.

Variable temperature ^1H spectra of $[\text{PbL}^1][\text{ClO}_4]_2$

In order to probe the origins of the broadening observed for the methylene AB subspectrum in the ^1H spectrum of $[\text{PbL}^1][\text{SCN}]_2$ at ambient temperature, the spectrum of the diperchlorate salt was recorded at elevated temperatures in an attempt to reproduce this effect. Four spectra were recorded in the temperature range 300–343 K for saturated solutions of $[\text{PbL}^1][\text{ClO}_4]_2$ in CD_3CN . Each of the spectra indicated that the complex retains the essentially four-fold symmetry observed at ambient temperature (Fig. 11.1.1). A ^1H spectrum of the sample (at 290 K) recorded on completion of the study confirmed that the ligand remained intact at the highest temperature employed.

Table 11.1.7. Temperature dependence of ^1H spectral parameters for $[\text{PbL}^1][\text{ClO}_4]_2$.^a

T^b	Chemical Shift ^c									
	H2	H12	H11	H41 ^d	H32, H42 ^{e, d}	H62 ^f	H31 ^d	H61 ^f	H5(1)	H5(2)
300	8.86 ^g	8.05	7.64	7.30	7.16	6.66	6.60	6.47	4.93 ^h	4.73 ^h
320	8.86 ⁱ	8.05	7.64	7.28	7.16	6.66	6.62	6.50	4.85 ^j	
330	8.86 ^k	8.05	7.65	7.28	7.17	6.66	6.63	6.51	4.85 ^j	
343	8.86 ^l	8.05	7.65	7.27	7.17	6.65 ^{e, d}		6.51	4.8 ^m	

- ^a Recorded for a saturated solution in CD_3CN . ^b Temperature /K. ^c In ppm relative to internal SiMe_4 ; estimated error ± 0.01 ppm. ^d Shifts given as estimated centres of multiplets. ^e Individual multiplets indistinguishable. ^f Possible alternative assignment; H61 and H62 may be reversed. ^g $^2J(^{207}\text{Pb}-\text{H2}) = 4.3$ Hz. ^h AB multiplet, $^2J = 11.4$ Hz. ⁱ $^2J(^{207}\text{Pb}-\text{H2}) = 3.7$ Hz. ^j Estimated centre of broadened doublet. ^k $^2J(^{207}\text{Pb}-\text{H2}) = 3.5$ Hz. ^l $^2J(^{207}\text{Pb}-\text{H2}) = 3.4$ Hz. ^m Broadened doublet close to coalescence.

The low field regions of the spectra, containing the pyridine, imine and aromatic resonances of the complex, are virtually identical to the corresponding regions in the ambient temperature spectra of $[\text{PbL}^1][\text{ClO}_4]_2$ and, significantly, $[\text{PbL}^1][\text{SCN}]_2$ described above. The individual multiplets in the variable temperature spectra were therefore assigned by direct comparison with the former spectrum although, as ^1H - ^{13}C data were not available, the shifts of H32 and H42 could not be differentiated. The spectral assignments are summarised in Table 11.1.7. A small downfield shift ($\Delta\delta \approx 0.04$ ppm) of the H31 multiplet (ca. 6.60 ppm at 300 K) was observed with increasing temperature. At 343 K this effect resulted in overlap of H31 signals with the multiplet due to H62 (ca. 6.66 ppm) and, in this case, the centres of the respective multiplets could not be estimated. In contrast, the H41 resonance was observed to undergo a small upfield shift of similar proportions.

Spin-spin coupling between the pyridyl protons does not appear to depend on the solution temperature; $^3\text{J}(\text{H12-H11}) \approx 7.7$ Hz in all the spectra obtained for $[\text{PbL}^1][\text{ClO}_4]_2$. The H2 singlets are overlapped with doublet satellite spectra from ^{207}Pb - ^1H coupling at all the temperatures. The small variations of $^2\text{J}(^{207}\text{Pb-H2})$ however, do not seem to be related to sample temperature and are ascribed to uncertainties in measuring the small value of $^2\text{J}(^{207}\text{Pb-H2})$ for doublets overlapped by the intense H2 signal.

The methylene AB subspectrum of $[\text{PbL}^1][\text{ClO}_4]_2$ (Table 11.1.7) shows considerable temperature dependence, broadening to approximate a doublet with increasing temperature before reaching near-coalescence at 343 K [Fig. 11.1.4(vi)]. Shifts for H5(1) and H5(2) at 300 K were obtained using AB analysis (Eqn. 11.1.2). The centre of the H5 resonances in each spectrum does not appear to shift significantly from ca. 4.83 ppm throughout the temperature range investigated.

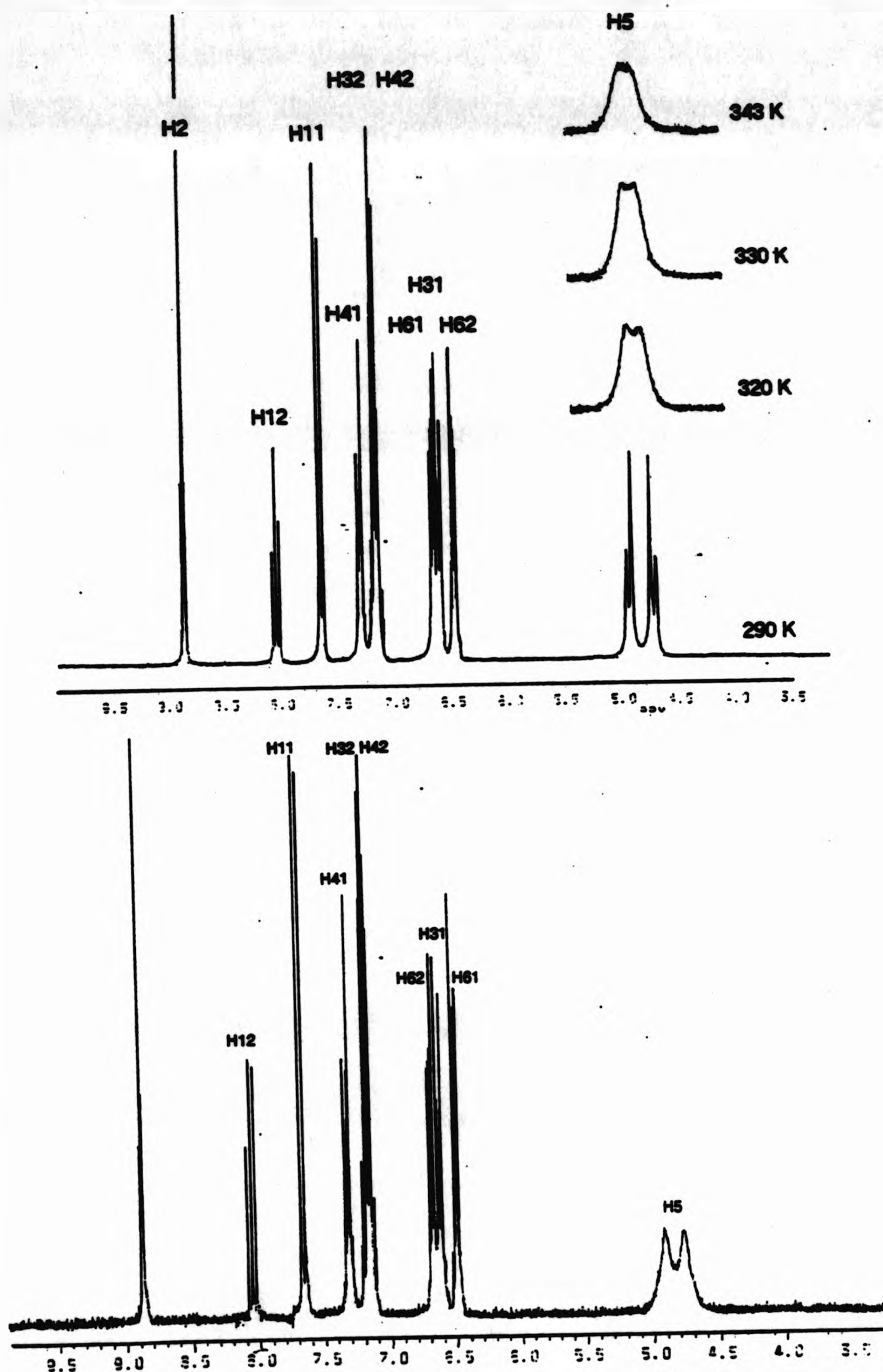


Figure 11.1.4 Proton nmr spectra of $[PbL^1]^{2+}$. Diperchlorate salt: (i) range 9.5-3.5 ppm at 300 K; range 5.0-4.5 ppm at (ii) 293 K; (iii) 300 K; (iv) 320 K; (v) 330 K; (vi) 343 K. Dithiocyanate salt (vii) range 9.5-3.5 ppm at 300K.

11.1.5. The ^1H nmr spectra of Group II metal complexes of L^1 .

High field (250 MHz) proton nmr spectra for the group II metal diperchlorate complexes $[\text{ML}^1][\text{ClO}_4]_2$, where $\text{M} = \text{Ca(II)}$, Sr(II) and Ba(II) were available.^[24] The spectra, determined on saturated solutions in CD_3CN , were assigned (Table 11.1.8) by comparison with the spectra of $[\text{ZnL}^1]^{2+}$, $[\text{CdL}^1]^{2+}$ and $[\text{PbL}^1]^{2+}$.

In common with the ^1H nmr spectra for other non-transition complexes of L^1 , the spectra of the Ca(II) , Sr(II) and Ba(II) complexes indicate ten unique proton environments, consistent with the asymmetric unit shown in Fig. 11.1.1. The spectra of $[\text{SrL}^1]^{2+}$ and $[\text{BaL}^1]^{2+}$ have many features in common, and are generally similar to the spectrum of $[\text{PbL}^1]^{2+}$ in terms of signal groupings and patterns.

Signals due to imino and pyridyl environments of L^1 were readily identified from their respective spin-spin coupling multiplicities. The intensity of the central component of the γ -pyridyl signal was substantially reduced from that expected for a first order (AX_2) spectrum and the multiplet was analysed as AB_2 . The imine signal is downfield of the β - and γ -pyridyl resonances in the spectra of $[\text{SrL}^1]^{2+}$ and $[\text{BaL}^1]^{2+}$ but overlaps the H12 triplet in the $[\text{CaL}^1]^{2+}$ spectrum.

The spectra show four-line multiplets, similar to those observed for $[\text{CdL}^1]^{2+}$ and $[\text{PbL}^1]^{2+}$, centred at ca. 4.8 ppm. These signals are assigned to H5 and analysed as AB multiplets (Table 11.1.8).

Resonances due to the xylenyl protons H61 and H62 were identified in the $[\text{CaL}^1]^{2+}$ and $[\text{BaL}^1]^{2+}$ spectra by their characteristic multiplet pattern; the multiplets centred at 6.77 and 6.26 ppm in the $[\text{CaL}^1]^{2+}$ spectrum and at 6.82

and 6.56 ppm in the $[\text{BaL}^1]^{2+}$ show, respectively, identical patterns and are therefore assigned as AA'XX' spectra arising from the protons of the 1,2-disubstituted rings. The downfield multiplet for $[\text{CaL}^1]^{2+}$ is arbitrarily assigned to H61 for consistency with ^1H nmr spectra of Zn(II) and Cd(II) complexes of L^1 . The opposite assignment, however, is preferred for the Ba(II) complex in view of the similarity between its proton spectrum and that of $[\text{PbL}^1]^{2+}$. In both spectra the separation between signals ascribed to H61 and H62 is small (ca. 0.2 ppm) and in the Pb(II) case, H62 is assigned to the lower field multiplet via the ^1H - ^{13}C COSY spectrum. For $[\text{CaL}^1]^{2+}$, the H61 multiplet at 6.77 ppm is partially overlapped by a doublet of doublets at 6.74 ppm. On the basis of shift (and again for consistency) this multiplet is assigned to H31.

The spectrum of $[\text{SrL}^1]^{2+}$ shows a complex multiplet at ca. 6.6 ppm due to three protons in aromatic environments. Other multiplets in the spectrum may be assigned to iminophenoxy protons (*vide infra*) and it is possible to distinguish signals arising from H31 in this multiplet. The remaining signals are therefore due H61 and H62 and the closely-spaced resonances are expected to give an AA'BB' spectrum. Signal overlap, with H31 and within the multiplet, and the complicated nature of AA'BB' spectra, precluded further assignment of these resonances.

Two multiplets in the spectrum of $[\text{CaL}^1]^{2+}$, centred at 7.15 and ca. 7.0, of relative intensity 1:2, are assigned to the remaining iminophenoxy protons. Severe deviations from first order intensity relationships are noted for these multiplets but they remain sufficiently recognisable to allow first-order analysis to aid their assignment. The two-proton multiplet at ca. 7.0 ppm approximates to a triplet of doublets somewhat overlapped by a doublet of

doublets. The doublet of doublets is assigned to H41. The four-bond coupling constants, $^4J(\text{H31-H42}) = 1.3 \text{ Hz}$ and $^4J(\text{H32-H41}) \approx 2.4 \text{ Hz}$ provide a basis for distinguishing between signals for H32 and H42. The triplet of doublets at 7.02 ppm shows a coupling constant of 1.3 Hz and is consequently assigned to H42. The low field multiplet of the aromatic region approximates to a doublet of doublets of doublets at 7.15 ppm with $^4J(\text{H32-H41}) \approx 2.4 \text{ Hz}$ and is therefore assigned to H32. This assignment contradicts the shift arguments of Section 11.1.1 but as $\delta(\text{H32})$ and $\delta(\text{H42})$ are not widely differentiated by the model systems (Table 11.1.2) and have been observed to 'cross over' in the $[\text{PbL}^1]^{2+}$ spectrum, the present assignment is preferred.

Multiplets due to iminophenoxy resonances of $[\text{SrL}^1]^{2+}$ and $[\text{BaL}^1]^{2+}$, centred at 7.28, ca. 7.1 and 6.56 (relative intensity, 1:2:1) and at ca. 7.38, ca. 7.2 and ca. 6.65 ppm (1:2:1) respectively, resemble those found in the spectrum of $[\text{PbL}^1]^{2+}$. The multiplets centred at 7.38 and 6.65 ppm in the spectrum of $[\text{BaL}^1]^{2+}$ are symmetric with respect to their centre of gravity at 7.02 ppm and are assigned to H41 and H31 respectively by analogy with the spectrum of $[\text{PbL}^1]^{2+}$. Similarly, signals in the $[\text{SrL}^1]^{2+}$ spectrum centred at ca. 6.56 ppm are the mirror image of those in the multiplet at ca. 7.28 ppm and these may also be assigned to H31 and H41 respectively by analogy with $[\text{PbL}^1]^{2+}$.

The two-proton multiplets at ca. 7.1 and ca. 7.2 ppm in the spectra of $[\text{SrL}^1]^{2+}$ and $[\text{BaL}^1]^{2+}$ respectively, arise from overlapping triplets of doublets. Again by analogy with the similar spectra of the two Pb(II) complexes, these two multiplets are assigned to H32 and H42 with H32 downfield. Eleven of the twelve expected lines are observed in each case and the line intensities of each triplet of doublets show the considerable 'roofing' effect expected for such closely-spaced coupled resonances.

Table 11.1.8. ^1H nmr parameters for $[\text{CaL}^1][\text{ClO}_4]_2$, $[\text{SrL}^1][\text{ClO}_4]_2$ and $[\text{BaL}^1][\text{ClO}_4]_2$.^a

Assignment ^b	Chemical Shift ^c		
	$[\text{CaL}^1][\text{ClO}_4]_2$	$[\text{SrL}^1][\text{ClO}_4]_2$	$[\text{BaL}^1][\text{ClO}_4]_2$
H2	8.04(s)	8.23(s)	8.34(s)
H12	8.06(m) ^d	7.96(m) ^e	7.96(m) ^e
H11	7.60(m) ^d	7.54(m) ^e	7.56(m) ^e
H41	6.97(dd) ^f	7.28(m)	7.38(m)
H32	7.15(ddd) ^g	7.15(td) ^h	7.22(td) ⁱ
H42	7.02(td) ^j	7.10(td) ^h	7.17(td) ⁱ
H31	6.74(dd) ^k	6.56(m)	6.65(m)
H61 (H62)	6.77(m) ^l	} 6.58(m) ^m	6.56(m) ^l
H62 (H61)	6.26(m) ^l		6.82(m) ^l
H5(1)	4.95 ⁿ	4.99 ^p	5.03 ^q
H5(2)	4.67 ⁿ	4.68 ^p	4.73 ^q

^a Obtained for saturated solutions in CD_3CN at ambient temperature. ^b See Fig. 11.1.1 for numbering scheme; possible alternative assignments are given in parentheses. ^c In ppm relative to internal SiMe_4 ; estimated error ± 0.02 ppm. Shifts are given as the mean position of the multiplet unless otherwise stated. Multiplicities are given in parentheses; s = singlet, d = doublet, dd = doublet of doublets, ddd = doublet of doublets of doublets, t = triplet, td = triplet of doublets, m = multiplet. ^d AB_2 multiplet, $^3\text{J}(\text{H12-H11}) = 7.9$ Hz for $\text{Ca}(\text{II})$, = 7.8 Hz for $\text{Sr}(\text{II})$. ^e AB_2 multiplet, $^3\text{J}(\text{H12-H11}) = 7.8$ Hz. ^f AB_2 multiplet, $^3\text{J}(\text{H41-H42}) = 7.8$ Hz, $^4\text{J}(\text{H41-H32}) = 2.4$ Hz. ^g $^3\text{J}(\text{H32-H42}) = 7.0$ Hz, $^3\text{J}(\text{H32-H31}) = 8.0$ Hz; $^4\text{J}(\text{H32-H41}) = 2.4$ Hz. ^h Overlapping multiplets; $^3\text{J}(\text{H32-H31}) \approx ^3\text{J}(\text{H32-H42}) \approx 7.1$ Hz, $^3\text{J}(\text{H42-H41}) \approx ^3\text{J}(\text{H42-H32}) \approx 7.5$ Hz, $^4\text{J}(\text{H32-H41}) \approx ^4\text{J}(\text{H42-H31}) \approx 2.0$ Hz. ⁱ Overlapping multiplets; $^3\text{J}(\text{H32-H31}) \approx ^3\text{J}(\text{H32-H42}) \approx 7.2$ Hz, $^3\text{J}(\text{H42-H41}) \approx ^3\text{J}(\text{H42-H32}) \approx 8.0$ Hz, $^4\text{J}(\text{H32-H41}) \approx ^4\text{J}(\text{H42-H31}) \approx 2.0$ Hz. ^j $^3\text{J}(\text{H42-H41}) \approx ^3\text{J}(\text{H42-H32}) \approx 7.2$ Hz, $^4\text{J}(\text{H42-H31}) = 1.3$ Hz. ^k $^3\text{J}(\text{H31-H32}) = 8.0$ Hz, $^4\text{J}(\text{H31-H42}) = 1.3$ Hz. ^l Symmetrical multiplets approximating to $\text{AA}'\text{XX}'$. ^m Overlapped multiplets. ⁿ AB multiplet, $^2\text{J} = 11.8$ Hz. ^p AB multiplet, $^2\text{J} = 11.5$ Hz. ^q AB multiplet, $^2\text{J} = 11.3$ Hz.

11.1.6 ^1H nmr spectra of $[\text{Ag}_2\text{L}^1][\text{ClO}_4]_2$.

The disilver complex of L^1 was sufficiently soluble in CD_3CN and $(\text{CD}_3)_2\text{CO}$ to allow proton nmr spectra to be obtained in both solvents. Assignments of both spectra are summarised in Table 11.1.9. The spectrum obtained in acetone shows signals, due to the sample, which are considerably broader than those in CD_3CN . Assignment of the spectrum of the complex in CD_3CN was assisted by consideration of the ^1H - ^{13}C COSY spectrum, obtained in the same solvent. The spectra indicate ten unique proton environments for the ligand and therefore the asymmetric unit of the complex essentially comprises one-quarter of the molecule, in common with the mononuclear complexes of L^1 (see Figure 11.1.1).

Signals from the methylene protons (H5) give a singlet at 5.12 ppm in CD_3CN . In contrast, these signals are split into a broad AB multiplet in $(\text{CD}_3)_2\text{CO}$, centred at 5.20 ppm. The imine resonances (H2) appear at lowest field in both solvents. Interestingly, a pair of broad signals at 8.71 and 8.69 ppm are observed for $[\text{Ag}_2\text{L}^1]^{2+}$ in $(\text{CD}_3)_2\text{CO}$.

The pyridyl resonances are readily assigned from shift and coupling considerations in both solvents. Signals due to H12 in CD_3CN might be expected to resemble the corresponding triplets observed for the AX_2 spin systems in $[\text{ZnL}^1]^{2+}$ and $[\text{CdL}^1]^{2+}$ but appear as a four-line multiplet significantly 'roofed' to the doublet at ca. 7.58 ppm (H11). This doublet, especially the upfield resonance, appears to be slightly broadened in comparison to the corresponding signals in ^1H spectra of $[\text{ZnL}^1]^{2+}$ and $[\text{CdL}^1]^{2+}$ and is strongly 'roofed' to the H12 multiplet. These spectral features are reminiscent of the AB_2 spectrum of 2,6-lutidine.^[116] Although only 6 of the 9 lines predicted^[42] for such AB_2 systems are resolved in the spectrum of $[\text{Ag}_2\text{L}^1]^{2+}$, analysis of the H12/H11 multiplet as AB_2 ^[42] yields $\delta(\text{H12}) = 7.81$,

$\delta(\text{H11}) \approx 7.58$ ppm and $^3J(\text{H12-H11}) \approx 7.7$ Hz. More accurate estimation of $\delta(\text{H11})$ and $^3J(\text{H12-H11})$ is precluded by signal overlap in the 'H11 doublet'.

The aromatic region of the spectrum obtained from acetonitrile solution shows a doublet of doublets of doublets at 7.30 ppm, a doublet of doublets at 7.15 ppm and a complex multiplet, originating from four protons of the asymmetric unit, at 6.98–6.81 ppm. Unusually, in the case of the multiplet (ddd) at 7.30 ppm, resolution was sufficient to allow determination of all coupling constants. This multiplet is assigned to H42 on the basis of the shift arguments of Section 11.1.1, and is 'roofed' to the doublet of doublets at 7.17 ppm. Assignment of the latter to H41 is consistent with the different four-bond coupling constants observed in these two multiplets, the 'roofing' between them, the shift arguments of Section 11.1.1, and the ^1H - ^{13}C COSY spectrum (see Section 11.1.7). The complex multiplet at 6.98–6.81 ppm includes a doublet of doublets at 6.83 ppm. Assignment of this multiplet to H31 is consistent with observed three- and, particularly, four-bond coupling constants. Significantly, the assignment is also in agreement with the shielding orders expected for iminophenoxy ring protons (Section 11.1.1). The remainder of the multiplet is assigned to overlapping multiplets for H32 and the AA'BB' spin system of the xylenyl ring protons (H61 and H62). Estimates of the shifts for these protons was obtained from the ^1H - ^{13}C COSY spectrum of $[\text{Ag}_2\text{L}^1][\text{ClO}_4]_2$ in CD_3CN .

The aromatic region of the acetone spectrum, 6.85–7.38 ppm, is broad and poorly resolved, but integration confirms that both the iminophenoxy and xylenyl ring resonances are contained in this region. A doublet at 7.22 ppm ($^3J = 7.4$ Hz) and a triplet at 7.38 ppm ($^3J = 7.5$ Hz) are discernible, but they are not sufficiently resolved to show the expected four-bond

proton-proton splittings. These signals are tentatively assigned to H41 and H42 respectively using the shift arguments outlined in Section 11.1.1. Further assignment in this region was not attempted.

Variable temperature study

In contrast to the methylene (H5) AB subspectra of the mononuclear complexes of L^1 , the ambient temperature spectrum of $[Ag_2L^1][ClO_4]_2$ in CD_3CN shows a singlet at 5.12 ppm. 1H nmr spectra of $[PbL^1][ClO_4]_2$ in CD_3CN show considerable temperature dependence in this region, the methylene AB multiplet collapsing to a broad singlet at ca. 343 K. In the light of these observations, spectra were obtained at 500 MHz for $[Ag_2L^1][ClO_4]_2$ in CD_3CN at 298, 253, and 233 K (See Fig. 11.1.6). Spectral assignments are summarised in Table 11.1.10.

The 500 MHz spectrum obtained at 298 K is closely similar to that obtained at 250 MHz and 300 K, and assignments for the latter spectrum (summarised in Table 11.1.9) are applied here. The spectrum of $[Ag_2L^1][ClO_4]_2$ obtained at higher field yields little more information than that obtained from the 250 MHz spectra. In particular the severe overlap observed for signals ascribed to H32, H61, and H62 at 250 MHz is not resolved at the higher field. At 500 MHz, these signals form a 15 line multiplet in the range 6.96–6.88 ppm and therefore assignments obtained from 1H - ^{13}C COSY correlations at 250 MHz remain the best estimates of $\delta(H32)$, $\delta(H61)$ and $\delta(H62)$. The β - and γ -pyridyl protons do however, give rise to an AX_2 subspectrum at the higher field, in contrast to the AB_2 pattern observed at 250 MHz, allowing accurate estimation of $^3J(H11-H12)$.

Table 11.1.9. ^1H nmr parameters for $[\text{Ag}_2\text{L}^1][\text{ClO}_4]_2$.

Assignment	Chemical shift ^a	
	CD_3CN^b	$(\text{CD}_3)_2\text{CO}^b$
H2	8.46(s)	$\left\{ \begin{array}{l} 8.71(\text{s}) \\ 8.69(\text{s}) \end{array} \right.$
H12	7.81 ^c	7.99(t)
H11	ca. 7.58 ^c	7.83(d)
H42	7.30(ddd) ^d	7.38(t)
H41	7.17(dd) ^e	7.22(d)
H62(H61 ^f)	ca. 6.94 ^g	$\left\{ \begin{array}{l} 7.08-6.85(\text{m})^h \end{array} \right.$
H32	ca. 6.92 ^g	
H61(H62 ^f)	ca. 6.89 ^g	
H31	6.84(dd) ⁱ	
H5(1)	$\left\{ \begin{array}{l} 5.12(\text{s}) \end{array} \right.$	5.32 ^j
H5(2)		5.09 ^j

^a Relative to internal SiMe_4 . Estimated error: in CD_3CN ± 0.002 ppm; in $(\text{CD}_3)_2\text{CO}$ ± 0.004 ppm. See Fig. 11.1.1 for numbering scheme. Multiplicities given in parentheses; s = singlet, d = doublet, dd = doublet of doublets, ddd = doublet of doublets of doublets, t = triplet, td = triplet of doublets, m = multiplet. ^b Saturated solution at ambient temperature. All signals substantially broad compared to SiMe_4 signal. AB_2 multiplet, $^3\text{J}(\text{H12-H11}) \approx 7.7$ Hz. ^d $^3\text{J}(\text{H42-H41}) = 8.3$ Hz, $^3\text{J}(\text{H42-H32}) = 7.2$ Hz, $^4\text{J}(\text{H42-H31}) = 1.7$ Hz. ^e $^3\text{J}(\text{H41-H42}) = 8.3$ Hz, $^4\text{J}(\text{H41-H32}) = 1.3$ Hz. ^f Possible alternative assignment. ^g Shifts estimated from ^1H - ^{13}C COSY spectrum. ^h Separate signals not resolved. ⁱ $^3\text{J}(\text{H31-H32}) = 7.9$ Hz, $^4\text{J}(\text{H31-H42}) = 1.7$ Hz. ^j AB multiplet, $^2\text{J} = 10.9$ Hz.

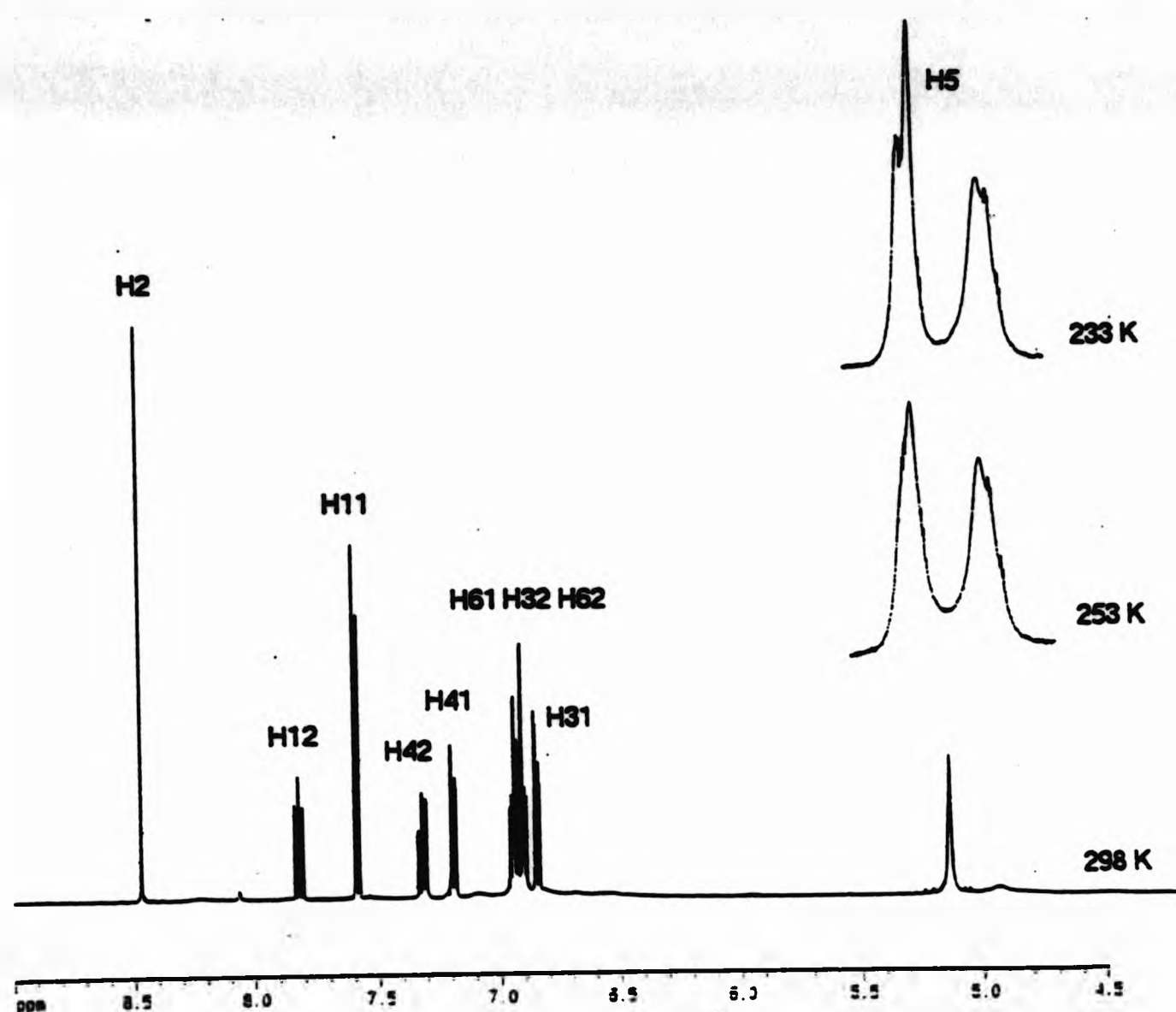


Figure 11.1 Proton nmr spectra of $[\text{Ag}_2\text{L}^1][\text{ClO}_4]_2$. Range 8.1–5.5 ppm; at (i) 298 K; range 5.3–4.7 ppm at (ii) 253 K and (iii) 233 K.

Signals due to the methylene protons (H5) in $[\text{Ag}_2\text{L}^1][\text{ClO}_4]_2$ do indeed show significant temperature dependence; the singlet at 5.13 ppm for a sample at ambient temperature becomes a broad doublet at 253 K which sharpens slightly to resemble a broadened AB multiplet at 233 K. The centres of these multiplets are shifted slightly downfield (0.04 ppm) from $\delta(\text{H5})$ at 298 K. Insignificant shifts with decreasing temperature (<0.02 ppm) are noted for the majority of the remaining signals in the spectra. However, signals assigned to H41 show a relatively large downfield shift of 0.06 over the temperature range investigated. Some movement of signals is also apparent in the H32/H61/H62 multiplet. The 15 discrete signals, evenly distributed in the region 6.96–6.88 ppm at 298 K, apparently broaden into two distinct groups of

signals, centred at ca. 6.96 and ca 6.89 ppm, in the sub-ambient spectra. All signals in the spectra become increasingly broadened with depression of temperature, eventually leading to loss of four-bond couplings for signals due to H31, H41 and H42.

Table 11.1.10. Temperature dependence of ^1H spectral parameters for $[\text{Ag}_2\text{L}^1][\text{ClO}_4]_2$.^a

Assignment ^b	Chemical Shift ^c		
	298 K	253 K ^d	233 K ^e
H2	8.47 (s)	8.51 (s)	8.51 (s)
H12	7.82 (t) ^f	7.80 (t)	7.80 (t)
H11	7.58 (d) ^f	7.58 (d)	7.59 (d)
H42	7.31 (ddd)	7.33 (td)	7.33 (t)
H41	7.18 (dd)	7.23 (d)	7.24 (d)
H61 } H32 } H62 }	6.96-6.88 (m) ^g	6.97-6.88 (m) ^g	6.97-6.88 (m) ^g
H31	6.84 (dd)	6.83 (dd)	6.83 (d)
H5(1)	} 5.13 (s)	5.23 (s)	5.25 (d)
H5(2)		5.10 (s)	5.09 (d)

^a Recorded for a near-saturated solution in CD_3CN at 500 MHz. ^b See Fig. 11.1.1 for numbering scheme. ^c In ppm relative to internal SiMe_4 ; estimated error ± 0.01 ppm. Shifts are given as estimated centres of multiplets. Multiplicities are given in parentheses; s = singlet, d = doublet, dd = doublet of doublets, ddd = doublet of doublets of doublets, t = triplet, td = triplet of doublets, m = multiplet, br = broad. ^d All signals substantially broader than those at 298 K. ^e All signals substantially broader than those at 253 K. ^f $^3\text{J}(\text{H11-H12}) = 7.7$ Hz. ^g Separate signals not resolved

11.2 Carbon-13 *nmr* spectra of diamagnetic complexes of L^1 .

The carbon-13 spectra of the zinc(II), cadmium(II), lead(II) and disilver(I) diperchlorate complexes of L^1 were recorded for saturated solutions of the complexes in acetonitrile at ambient temperature. The spectrum of the calcium(II) diperchlorate complex, obtained under analogous conditions, was also available.^[24] The broad-band proton-decoupled spectra of these complexes (see, for example the spectra of $[CdL^1][ClO_4]_2$ and $[PbL^1][ClO_4]_2$, Fig. 11.2.1) each consists of fourteen signals corresponding to the fourteen unique carbon environments of the asymmetric unit of the ligand (Fig. 11.1.1) and full assignments of the spectra are given in Table 11.2.3.

11.2.1 Spectral assignment

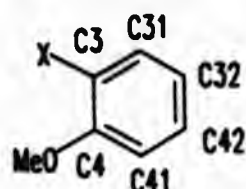
Signals due to non-protonated carbons (C1, C3, C4 and C6) were identified by elimination from DEPT-45 (Zn(II), Cd(II), Pb(II), and Ag(I) complexes), DEPT-90 (Ag(I)), DEPT-135 (Cd(II) and Ag(I)). Non-protonated carbons of $[CaL^1][ClO_4]_2$ were identified from a J-modulated spin-echo (APT) spectrum. Assignment of the protonated carbon environments of the Zn(II), Cd(II), Ag(I) and Pb(II) complexes was aided by 1H - ^{13}C correlation spectroscopy (1H - ^{13}C COSY). 1H - ^{13}C COSY data was not available for $[CaL^1][ClO_4]_2$ but, due to the very close similarity of its ^{13}C spectrum to that of $[PbL^1][ClO_4]_2$ assignment of the ^{13}C spectrum was achieved by applying the orders of shielding observed for carbon sites of the Pb(II) complex.

1H - ^{13}C COSY spectra were hence used to unambiguously assign (via unambiguous proton assignments) the methine carbon (C2) and the β - and γ -pyridyl carbons (C11 and C12 respectively). Assignment of the γ -pyridyl carbon in this way was consistent with the observation that this signal had the lowest intensity

in each spectrum, presumably because there are half the number of carbon atoms in C12 environments compared to other sites. The proton-carbon correlations also allowed assignment of the iminophenoxyl and xylenyl carbons to pairs signals without resort to proton chemical shift arguments; i.e. C31 and C41, C32 and C42, C61 and C62. Assignments within these pairs was considered using the chemical shift arguments detailed below.

Estimates of ^{13}C shifts for a number of *o*-substituted methoxybenzene compounds, obtained from combination of the substituent-induced shifts for carbon environments of monosubstituted benzenes according to Eqn. 11.1.1, are shown in Table 11.2.1. Parameters for imino substitution of benzene do not appear to have been reported but estimates of $z_{\text{N=CHPh}}^{\text{ipso}} = +23.5$, $z_{\text{N=CHPh}}^{\text{ortho}} = -7.7$, $z_{\text{N=CHPh}}^{\text{meta}} = +0.5$ and $z_{\text{N=CHPh}}^{\text{para}} = -2.7$ were deduced from ^{13}C data for N-benzylidene aniline^[117] (M^5 , Fig. 11.1.1) in CDCl_3 . It is not clear from this work (Ref. [117] and refs therein) that assignment of the signals for *ortho* and *meta* carbon is unambiguous; hence a measure of uncertainty attaches to these particular substituent shifts. However, these substituent-induced shifts broadly mirror the direction and magnitude of those reported^[104] for the N-phenylhydrazone substituent ($-\text{N=NPh}$), although the *para*-shielding influence of $-\text{N=CHPh}$ contrasts with the deshielding influence of $-\text{N=NPh}$ ($z_{\text{N=NPh}}^{\text{para}} = +2.2$). (The hydrazone function is expected to closely resemble the effect of an imino substituent on the electronic distribution of a derivatised benzene ring). Interestingly, the substituent-induced shifts for imine do not compare with with other α,β -unsaturated groups, eg. $-\text{CH=CH}_2$ and $-\text{CHO}$, but are similar to those of $-\text{NH}_2$, $-\text{NR}_2$, OH and $-\text{OMe}$ ^[104] in direction but somewhat smaller in magnitude.

Table 11.2.1. Predicted influence of functional groups, X, on the carbon-13 shifts of *o*-substituted methoxybenzenes.^a



Group	Chemical shift ^b					
	$\delta(\text{C3})$	$\delta(\text{C31})$	$\delta(\text{C32})$	$\delta(\text{C42})$	$\delta(\text{C41})$	$\delta(\text{C4})$
X						
-NH ₂	132.3	116.1	121.6	119.5	114.9	146.5
-CHO	122.5	130.7	121.3	135.2	114.6	161.1
-CH=CH ₂	123.0	127.2	120.7	128.7	114.0	157.6
-N=NPh	138.1	123.7	121.1	131.7	114.4	154.1
-N=CHPh ^c	137.6	121.8	121.3	126.8	114.6	152.2
-N=C(Me)py ^d	136.9	120.3	121.3	124.6	114.6	150.7

^a Shifts in ppm. Estimated by combining substituent shifts^[104] relative to benzene ($\delta = 128.5$ ppm) according to Eqn. 6.6.1. ^b See Fig. 11.1.1 for numbering scheme. ^c Substituent shifts estimated from spectrum of *N*-benzylidene aniline (M⁵, Fig. 11.1.1).^[117] ^d Substituent shifts estimated from the spectrum of M¹ in CDCl₃.

Equally appropriate estimates for substituent-induced shifts due to imino-substitution of benzene can be deduced from ¹³C data for M¹ in CDCl₃ (M¹ is insufficiently soluble in CD₃CN for determination of the ¹³C spectrum in this solvent). While suffering from the disadvantage, compared to the above estimate, that the imine is methyl substituted, the ambiguity of *ortho*- and *meta*-carbon signal is resolved. Determination of ¹H, ¹³C and ¹H-¹³C COSY nmr spectra for M¹ led, through unambiguous assignments for the aromatic proton signals, to unambiguous assignment of signals for the *ortho*- and

meta-carbons. The parameters for imine substitution so deduced are

$$Z_{\text{ipso}}^{\text{H=C(Me)py}} = +22.8, Z_{\text{ortho}}^{\text{H=C(Me)py}} = -9.3, Z_{\text{meta}}^{\text{H=C(Me)py}} = +0.5 \text{ and}$$

$Z_{\text{para}}^{\text{H=C(Me)py}} = -4.9$. These parameters are in good agreement with those derived from N-benzylidene aniline and confirm the *ortho*- and *meta*- carbon assignments for the latter compound.

Estimated shifts for iminophenoxy carbons using the parameters for imino-substitution derived above (see bottom row of Table 11.2.1), are in good agreement with assignments^[118] for the *anti*-isomer of N-*o*-anisylmaleisoimide [(M⁶, Fig. 11.1.1) δ /ppm in (CD₃)₂SO; C3, 130.3; C31, 122.6; C32, 120.3; C42, 127.0; C41, 112.1, and C4, 151.2 ppm].^[118]

Using the predicted shifts for *o*-phenyliminomethoxy benzene (Table 11.2.1) signals, the pairs C31 and C41, and C32 and C42 could, in principle, be differentiated. Support for these assignments derives from their consistency with detailed proton assignments for [ZnL¹]²⁺, [CdL¹]²⁺, and [Ag₂L¹]²⁺ (derived from proton chemical shift arguments, Section 11.1.1) via the ¹H-¹³C COSY spectra. Assignments of the C31 and C41 signals for [PbL¹][ClO₄]₂ (and, by analogy, [CaL¹][ClO₄]₂) using predicted ¹³C shifts for *o*-phenyliminomethoxy benzene are, however, inconsistent with assignments for H31 and H41 based on proton shift arguments. In this case, the separation of the H31 and H41 signals in the proton spectrum of [PbL¹]²⁺ is particularly large, while the corresponding ¹³C signals are separated by <1 ppm. Assignment of C31 and C41 was therefore based on the proton assignments correlated through the ¹H-¹³C COSY spectrum, yielding C41 *less shielded* than C31. The Pb(II) complex also provided an anomaly in the assignment of the 32 and 42 sites. The widely separated C32 and C42 carbon resonances were assigned according to the predicted shifts for *o*-phenyliminomethoxybenzene (Table 11.1.1) and the ¹H-¹³C

COSY was used to assign the closely-spaced H32 and H42 signals, yielding H32 less shielded than H42, contrary to proton shift predictions (Section 11.1.1).

Consideration of the reported spectra^[119,120] for substituted hydrazones of 2-acylpyridines (M^7 , Fig. 11.1.1) allowed estimation of the position of the quaternary pyridyl carbon (C1). These authors report shifts in the range 156.9–152.9 ppm for carbon environments corresponding to C1. Carbon-13 data has been reported^[121] for the Mg(II) complexes of M^8 in D_2O . Comparison with the unambiguous assignments of the imine and the β - and γ -pyridyl carbons in the present work shows the reported^[121] assignments to be incorrect and reassignment yields, by elimination, a chemical shift of 149.9 ppm for the α -pyridyl carbon, i.e. slightly upfield of the range observed for the hydrazone ligands. Three signals in the ^{13}C spectrum of M^1 could be attributed to non-protonated carbons. Assignment of the signal at 167.32 ppm to C2 by analogy with the complexes of L^1 and the signal at 151.31 ppm to C3 by analogy with M^5 , left a signal at 155.48 ppm to be assigned to C1, within the range noted above.

Assignment of the xylenyl resonances (especially C6) was obtained by comparison with the ^{13}C spectra of M^3 and M^4 (Figure 11.1.1). Assignment of the carbon-13 spectra of these model compounds was based on shifts calculated for *o*-aminomethoxybenzene and α,α' -bis-hydroxy-*o*-xylene (M^4) using Eqn. 11.1.1 (Table 11.2.2). Observed and estimated shifts are generally in good agreement.

Table 11.1.2. Observed carbon-13 chemical shifts for α,α' -bis(2-aminophenoxy)-*o*-xylene (M^3) and α,α' -bis-hydroxy-*o*-xylene (M^4) and comparison with calculated values.

Atom	M^3 ^a	M^4 ^b	M^4 ^c	<i>o</i> -aminomethoxybenzene ^d
C3	135.42			132.3
C31	115.26			116.1
C32	121.72			121.6
C42	118.39			119.5
C41	112.28			114.9
C4	146.27			146.5
C5	68.32	63.23		
C6	136.62	140.77	140.1	
C61 (C62) ^e	129.22	129.37	127.1	
C62 (C61) ^e	128.50	128.66	127.3	

^a Spectrum obtained in CDCl₃; chemical shifts (/ppm) referenced to internal SiMe₄. ^b Spectrum obtained in CD₃CN; chemical shifts (/ppm) referenced to internal SiMe₄. ^c Estimated using substituent-induced shifts (/ppm) from Ref. [103a]. ^d Substituent-induced shifts (/ppm) from Ref. [104]. ^e Possible alternative assignment.

Calculated shifts for C61 and C62 are almost identical, as are the observed shifts in M^3 and M^4 . There are therefore no grounds for matching C61 and C62 with either of the observed signals. In complexes of L^1 however, C62 is assigned to the downfield signal of the pair, reflecting the arbitrary attribution used for H61 and H62 of $[ZnL^1]^{2+}$ and correlated through its ¹H-¹³C COSY spectrum. The ¹³C signals for C61 and C62 show far less variation over the range of complexes than their corresponding proton signals and therefore provide the basis for assignment of H61 and H62 in the ¹H spectra,

again via correlations in the respective ^1H - ^{13}C COSY spectra, for the Cd(II), Pb(II) and Ag(I) complexes.

Noting shifts for C3 (137.6 ppm) and C6 (136.62 ppm) in o-phenyliminomethoxybenzene (Table 11.2.1) and M^3 respectively, it is not possible to assign signals due to quaternary carbons of the complexes of L^1 in the appropriate region (140-135 ppm) on the basis of shift arguments. Similarly, ambiguity remains in assignment of C1 and C4 to the two remaining signals in the region 145-155 ppm. $\delta(\text{C4})$ is predicted (Table 11.2.1, $\text{X} = -\text{N}=\text{CHPh}$) at 150.9 ppm, close to the range (157-149 ppm) expected for C1 as noted previously.

The assignment questions left unresolved by chemical shift considerations for the pairs C3, C6 and C1, C4 were resolved by observation of metal-carbon spin-spin coupling for the Cd(II) and Pb(II) complexes. Assignments of C3, C6 and C1, C4 for $[\text{ZnL}^1]^{2+}$ and $[\text{Ag}_2\text{L}^1]^{2+}$ were then made using the orders of shielding observed for the respective sites in $[\text{CdL}^1]^{2+}$, and for $[\text{CaL}^1]^{2+}$ by analogy with shieldings observed for $[\text{PbL}^1]^{2+}$.

Table 11.2.3. Carbon-13 parameters^a for the zinc(II), cadmium(II), calcium(II), lead(II) and disilver(I) diperchlorate complexes of L¹.

Atom ^b	Chemical shift ^c				
	[ZnL ¹] ²⁺	[CdL ¹] ²⁺	[CaL ¹] ²⁺	[PbL ¹] ²⁺ ^d	[Ag ₂ L ¹] ²⁺
C2	158.08	155.46 ^o	159.02	160.34 ^f	160.28
C4	151.90	152.14	152.50 ^g	153.34	152.09 ^g
C1	146.50	146.94 ^h	152.24 ^g	153.49 ⁱ	150.47 ^g
C12	144.33	143.49	142.42	142.10	140.87
C3	139.69	139.48 ^j	139.76	139.92 ^k	139.98
C6	136.74	136.28	135.34	135.59	136.60
C62 ^l	132.10	131.51	131.45	132.60	132.12
C11	131.15	} 131.00 ^m	130.11	130.36 ⁿ	131.45
C42	130.93		131.23	131.40	130.61
C61 ^l	130.19	130.23	129.73	129.70	129.87
C32	124.46	125.06	125.42	125.37	123.83
C31	121.72	120.35	119.05	119.10	121.41
C41	119.63	119.28	119.75	119.92	117.86
C5	73.97	74.37	75.29	75.10	71.95

^a Spectra obtained from saturated CD₃CN solutions at ambient temperature.

^b See Fig. 11.1.1. for numbering scheme. ^c In ppm relative to internal SiMe₄.

Estimated error ± 0.02 ppm. ^d Dithiocyanate complex: 160.47 (C2), 153.49 (C1,

²J(²⁰⁷Pb-C1) = 6.5 Hz], 153.43 (C4), 142.11 (C12), 140.01 (C3), 135.68 (C6),

132.62 (C62), 131.40 (C42), 130.44 (C11), 129.76 (C61), 125.35 (C32),

120.05 (C41), 119.10 (C31), 75.07 (C5). ^e ²J(^{111,113}Cd-C2) = 17.6 Hz.

^f ²J(²⁰⁷Pb-C2) = 10.1 Hz. ^g Possible alternative assignment, C4 and C1 may be

reversed. ^h ²J(^{111,113}Cd-C1) = 26.6 Hz. ⁱ ²J(²⁰⁷Pb-C1) = 5.7 Hz.

^j ²J(^{111,113}Cd-C3) = 4.3 Hz. ^k ²J(²⁰⁷Pb-C3) = 5.0 Hz. ^l Possible alternative

assignment, C62 and C61 may be reversed. ^m Overlapped signals,

³J(^{111,113}Cd-C11) = 10.3 Hz. ⁿ ³J(²⁰⁷Pb-C11) = 2.6 Hz

11.1.2 Metal-carbon-13 coupling.

Satellites, due to coupling between ^{13}C and the nuclei ^{111}Cd , ^{113}Cd and ^{207}Pb (see Table 11.2.3), were observed for certain sites in $[\text{CdL}^1]^{2+}$ and $[\text{PbL}^1]^{2+}$, and provided vital information for assignment of the quaternary carbon signals in these complexes.

The proton spectrum of $[\text{CdL}^1][\text{ClO}_4]$ showed cadmium coupling to the pyridine (H11 and H12) and imine (H2) environments and it is therefore reasonable to assume that the carbon signals showing satellites due to ^{111}Cd and ^{113}Cd coupling should be likewise assigned to pyridyl and imino environments. Satellites, ca. 15% of the central peak height, were observed flanking signals at 155.46 ppm (assigned to C2, $^2J(^{111,113}\text{Cd}-\text{C2}) = 17.6 \text{ Hz}$), 146.94 ppm, 139.48 and 131.01 ppm. Satellites were not resolved into the separate signals due ^{111}Cd and ^{113}Cd coupling, and the signs of the couplings were not determined. The quoted values therefore represent the magnitude of an 'average' coupling constant. The signal at 131.01 is unambiguously assigned to overlapping resonances from C42 and C11 (although in a separately prepared sample, these resonances were resolved, $\Delta\delta\text{C} = 0.07 \text{ ppm}$). Noting the observed cadmium coupling to H11, the satellites must be ascribed to $^3J(^{111,113}\text{Cd}-\text{C11}) = 10.3 \text{ Hz}$. The remaining two carbon signals showing satellites in the spectrum arise from non-protonated carbons and must therefore be assigned to carbons within, or close to, the pyridyl and imino environments, i.e. C1 at 146.94 ppm [$^2J(^{111,113}\text{Cd}-\text{C1}) = 26.6 \text{ Hz}$] and C3 at 139.48 ppm [$^2J(^{111,113}\text{Cd}-\text{C3}) = 4.3 \text{ Hz}$].

In contrast to the proton spectrum of $[\text{PbL}^1]^{2+}$, where $^{207}\text{Pb}-^1\text{H}$ coupling was resolved only for the imino proton signal, the ^{13}C spectrum showed satellites flanking the signals at 160.42 ppm (assigned to C2, $^2J(^{207}\text{Pb}-\text{C2}) = 10.1 \text{ Hz}$),

153.49 ppm (C1, $^2J(^{207}\text{Pb}-\text{C1}) = 5.7$ Hz), 139.92 ppm (C3, $^2J(^{207}\text{Pb}-\text{C3}) = 5.0$ Hz) and 130.36 ppm (C11, $^3J(^{207}\text{Pb}-\text{C11}) = 2.6$ Hz). Again, coupling to the metal provided an essential basis for assignment, particularly in the case of C1 which is less shielded than C4, in contrast to the Zn(II) and Cd(II) complexes.

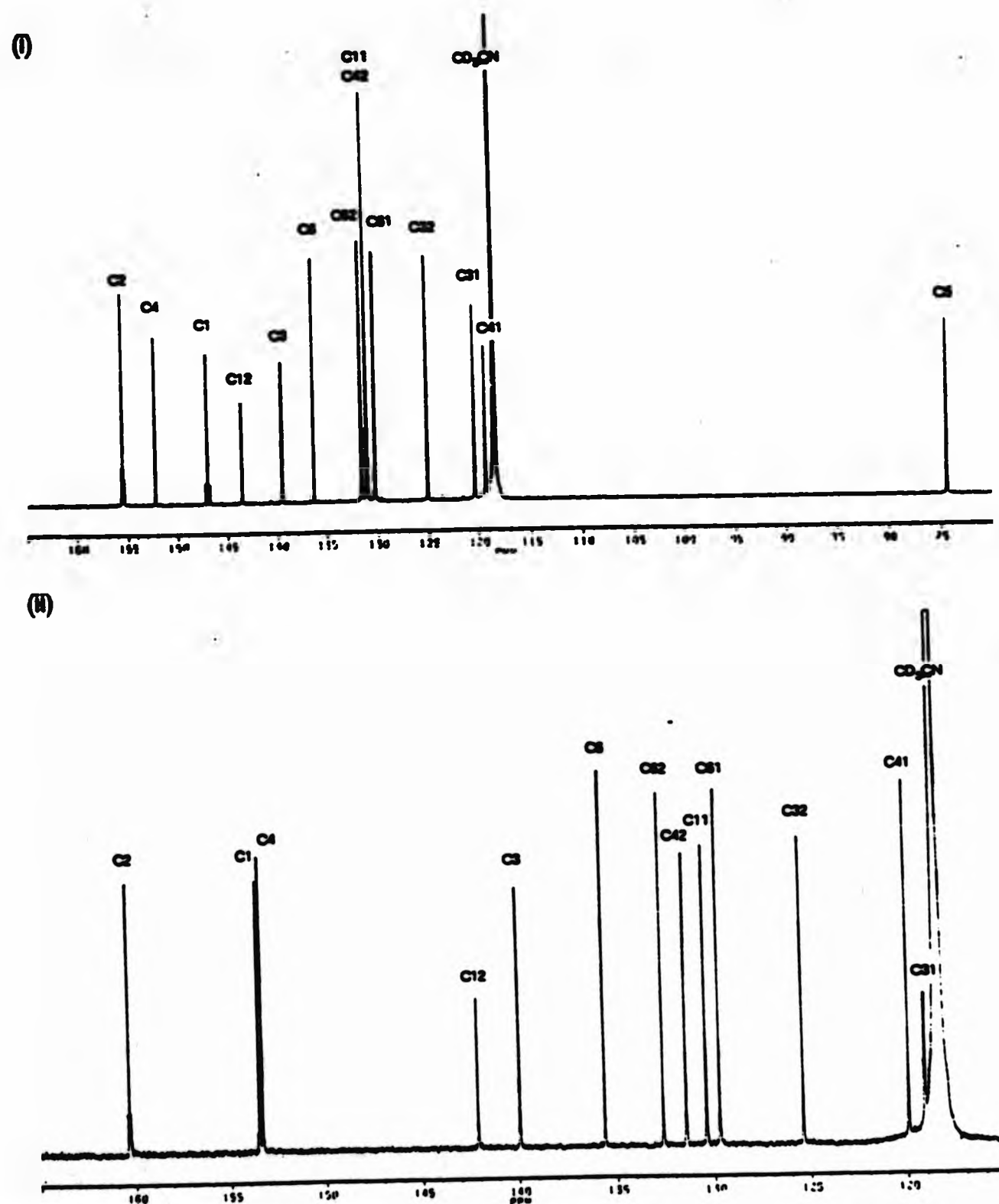


Figure 11.2.1 Carbon-13 spectra of (i) $[\text{CdL}^1][\text{ClO}_4]_2$ (range 170-70 ppm); and (ii) $[\text{PbL}^1][\text{ClO}_4]_2$ (range 165-115 ppm).

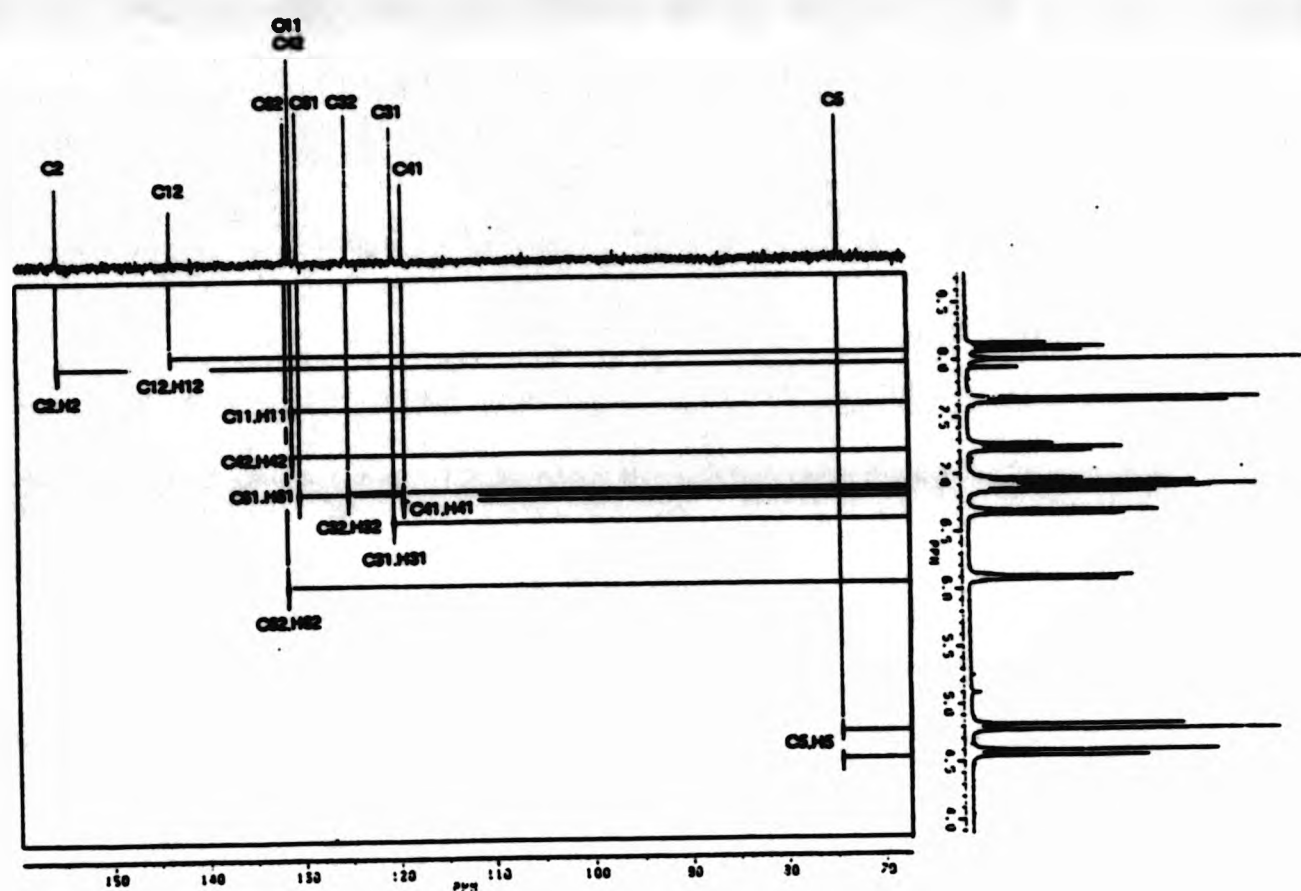


Figure 11.2.1 ^1H - ^{13}C COSY contour plot for $[\text{CdL}^1][\text{ClO}_4]_2$ (range: ^1H , 8.5-4.0 ppm; ^{13}C , 160-70 ppm).

11.3 Discussion

The carbon-13 and proton spectra of the diamagnetic complexes of L^1 further confirm the purity of the samples and, by the absence resonances attributable to aldehydic and/or amino functions, the structural integrity of the ligand in acetonitrile solution. Similarly, the proton spectra of $[PbL^1][ClO_4]_2$ and $[Ag_2L^1][ClO_4]_2$ in acetone- d_6 are consistent with formulations proposed for the complexes.

Spectral assignments, based on observed proton multiplicities and 1H - ^{13}C correlations, are unambiguous in the majority of cases. However, recourse to empirical substituent-induced shifts for benzene was required to distinguish between nuclei within each pair of *ortho*- and *meta*-positions in the iminophenoxy rings. Individual assignments of these sites are therefore somewhat less reliable particularly as they are based on data derived from non-complexed ring substituents and are also subject to uncertainties associated with predicting shifts of *ortho*-disubstituted aromatic nuclei using such parameters. [103,104]

11.3.1 Symmetry considerations.

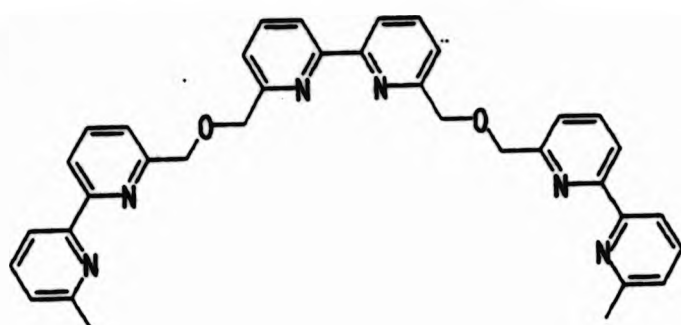
Solid state structural analysis of the $Zn(II)$ complex of L^1 reveals the presence of two enantiomers of the complex, each containing a crystallographically-imposed 2-fold axis. Except in the cases where the nmr solvent is chiral, corresponding nuclei of enantiomorphous complexes are in equivalent magnetic environments and are therefore indistinguishable in the spectrum. [99] These considerations alone imply that spectra will involve signals corresponding to each half of the ligand (giving 22 unique proton and 28 unique carbon environments).

However, only fourteen unique carbon environments were observed for complexes investigated $\{[ZnL^1][ClO_4]_2, [CaL^1][ClO_4]_2, [CdL^1][ClO_4]_2, [Ag_2L^1][ClO_4]_2, [PbL^1][ClO_4]_2 \text{ and } [PbL^1][SCN]_2\}$ and these complexes as well as the Sr(II) and Ba(II) complexes show signals corresponding to 11 unique proton environments. These observations apparently indicate the presence of four-fold symmetry for the complexes in solution. The asymmetric unit of the complexes comprises one quarter of the ligand, as shown in Fig. 11.1.1.

For such spectra to be consistent with the solid state configuration of L^1 observed in $[ZnL^1]^{2+}$ requires fluxional motion (approximating to a symmetry element) on a rate faster than the nmr timescale. Inspection of molecular models derived from the solid state structure of $[ZnL^1]^{2+}$ indicates that a motion corresponding to an exchange of iminophenoxy ring positions in the complex (i.e. $IMa \leftrightarrow IMb$ and $IMa' \leftrightarrow IMb'$ or $IMa \leftrightarrow IMb'$ and $IMa' \leftrightarrow IMb$) provides the apparent equivalence between each quadrant required by the nmr spectrum (see Fig. 11.1.1). As this interchange apparently requires only the non-bonded interactions (i.e. the intramolecular π -stacking interactions) to be disrupted and does not involve rupture of metal-ligand bonds, it is expected to be a relatively low energy process. Importantly, an interchange of this type results in retention of the helical configuration of the complex [Fig. 11.3.1(1)]. A similar dynamic 'helix bending-twisting' process, which interchanges the bipyridine units of the double-helicate $[Cu_3(1)_2]^{3+}$ in CD_2Cl_2 solution, has been assigned to account for higher symmetry apparently adopted by the complex in solution than was observed in the solid state.^[90]

Similarly, nmr studies of the helical dicadmium complex of the oligobipyridine ligand, sexipyridine, show 10 magnetically distinct proton resonances, i.e. equivalence for one half of each helical strand, indicating that the

double-helical geometry of the complex is retained in solution.^[96,97]



(1)



sexipy

Studies in the solid state indicated that the structure of the mononuclear complexes of L^1 is largely determined by ligand-based influences. In the absence of evidence to the contrary, it is expected that all the $[ML^1]^{2+}$ complexes will adopt a double-helical configuration in the solid state similar to that observed for $[ZnL^1]^{2+}$ and $[NiL^1]^{2+}$ and some support for this assumption derives from the similarities of the infrared spectra of the complexes. In solution, similar configurations for the ligand in all the mononuclear complexes are implied by the identical numbers of unique environments implied by 1H and ^{13}C nmr spectra of the complexes. Strong evidence for adoption of double-helical configurations in the complexes will be implied if it can be established that the complexes are chiral in solution.

Crucial evidence indicating that the mononuclear complexes of L^1 are indeed chiral in solution derives from the 1H subspectra due to the methylene protons (H5). The methylene sites of the ligand are prochiral assemblies and therefore provide probes for chirality in the complexes since paired ligands [in this case the protons H5] attached to a prochiral centre in a chiral compound are always diastereotopic.^[122] Thus, if complexes of L^1 are chiral in solution, the methylene protons would be diastereotopic, exhibit chemical shift non-equivalence^[123] (i.e. they would be anisochronous), and give rise

to AB subspectra. Such AB patterns were observed at ca. 4.8 ppm in ambient temperature ^1H spectra of each mononuclear complex studied. Some differences in the magnitude of the AB splitting ($\Delta\delta$) in the complexes are evident but it is well known that the factors controlling magnitudes of geminal non-equivalence are complex.^[122] That chemical shift non-equivalence is observed for the methylene protons in $[\text{ZnL}^1]^{2+}$ strongly indicates that it retains a chiral, double-helical configuration in solution. By analogy, the AB methylene subspectra observed in the other mononuclear complexes of L^1 suggests that similar double-helical configurations for the ligand are also adopted in these complexes and that these structures are retained in solution.

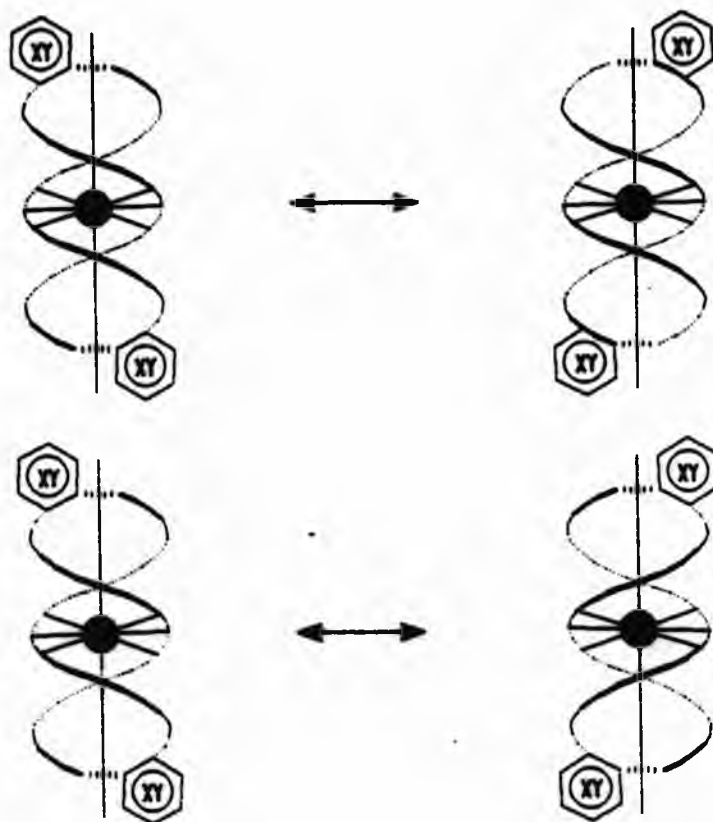
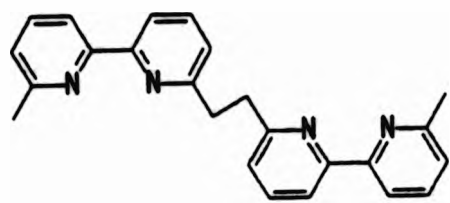


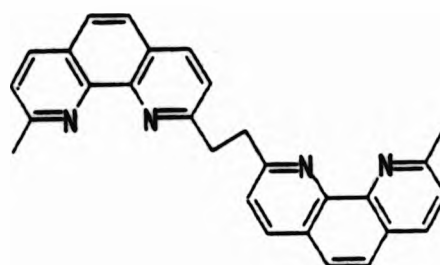
Figure 11.3.1 Schematic representation of exchange processes for mononuclear complexes of L^1 ; (i) helix bending-twisting involving retention of helical configuration and (ii) interchange of helical configuration.

Geminal non-equivalence in methylene groups is an emerging feature of kinetically-inert helicate complexes. Lehn and co-workers, in discussing

helicate formation from alkyl-bridged oligobipyridine^[90,91,124] [e.g. (1) and (2)] and oligophenanthroline^[125] [e.g. (3)] ligands, note that the aliphatic ¹H nmr resonances of helicate complexes are markedly different from the corresponding signals in ¹H spectra of the free ligands. Whereas the geminal protons are equivalent and give rise to singlets in the free ligands, second order spectra, arising from chemical shift non-equivalence of geminal protons, appear in the helicates; e.g. the -CH₂OCH₂- bridges of [Cu₃(1)₂]³⁺ give rise to overlapping AB patterns^[90] and the -CH₂CH₂- bridges of [Cu₂(2)₂]²⁺ and [Cu₂(3)₂]²⁺ yield ABCD subspectra.^[125] Observations of non-equivalence for the geminal protons led to assignment of chiral, helical structures for the complexes which were confirmed by single crystal X-ray analysis of [Cu₃(1)₂]³⁺ and [Cu₂(2)₂]²⁺.^[90,125]



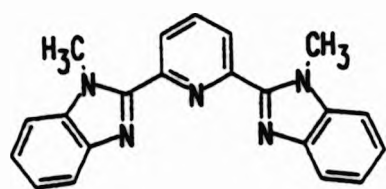
(2)



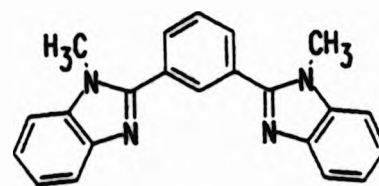
(3)

Observations of geminal non-equivalence in ¹H nmr can therefore be used as a test for retention of solid state helical configurations of suitable co-ordination compounds in solution. Although the chirality of some helical complexes has been demonstrated with the use of chiral shift reagents,^[90,126] the separation of nmr spectra that these compounds produce are often small due to the low association constants between the substrates. It is sometimes preferable to design ligands that incorporate prochiral centres that are covalently bonded to the ligand backbone and directly observe chemical shift non-equivalence to establish chirality in solution. To establish whether the

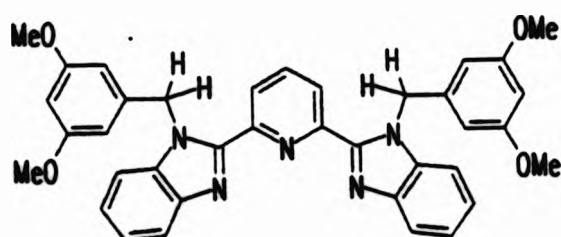
helical structure^[127] of $[\text{Cu}_2(\underline{4})_2]^{2+}$ and non-helical structure^[128] of $[\text{Cu}_2(\underline{5})_2]^{2+}$ in the solid state are retained in solution, Williams and co-workers designed the ligands (6) and (7) and investigated whether intramolecular diastereotopic effects^[122,123] were present for the prochiral benzyl protons.^[128] Proton nmr studies at sub-ambient temperatures revealed an AB pattern for the benzyl protons of $[\text{Cu}_2(\underline{6})_2]^{2+}$ indicating that this complex is chiral, and an A_2 pattern for the corresponding protons of $[\text{Cu}_2(\underline{7})_2]^{2+}$, indicating that it is non-chiral. The authors concluded by analogy that helical and non-helical configurations exist in solution for $[\text{Cu}_2(\underline{4})_2]^{2+}$ and $[\text{Cu}_2(\underline{5})_2]^{2+}$ respectively.



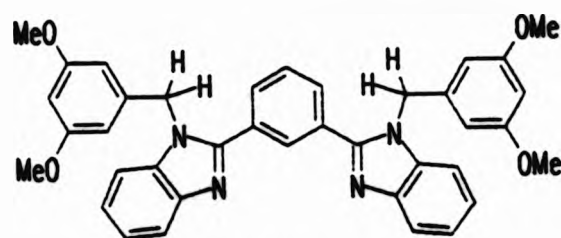
(4)



(5)



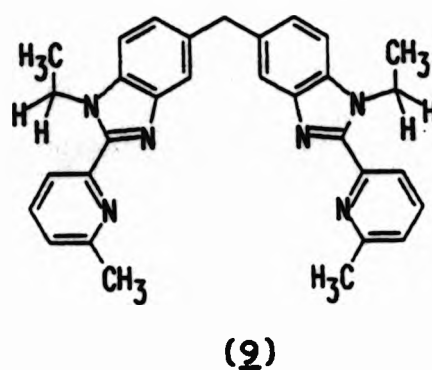
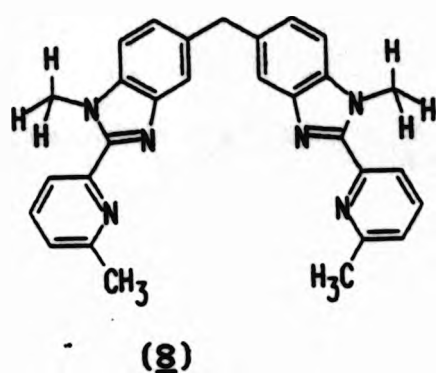
(6)



(7)

Similarly, Williams and co-workers established the helical nature of $[\text{Cu}_2(\underline{8})_2]^{2+}$ in solution by analogy with $[\text{Cu}_2(\underline{9})_2]^{2+}$ which contains CH_3CH_2 - groups bonded to the ligand backbone.^[129] Although the prochiral CH_2 probe of $[\text{Cu}_2(\underline{9})_2]^{2+}$ gives rise to the A_2 portion of an A_2X_3 subspectrum due to the ethyl substituent at ambient temperature, below 0 °C the multiplet becomes an ABX_3 spectrum. Thus the methylene protons become diastereotopic at low temperature, demonstrating that $[\text{Cu}_2(\underline{9})_2]^{2+}$ is chiral and, by analogy,

indicates that $[\text{Cu}_2(\underline{8})_2]^{2+}$ retains its helical structure in solution. The observation that the prochiral protons of $[\text{Cu}_2(\underline{9})_2]^{2+}$ become enantiotopic above 0°C was attributed to rapid interconversion between enantiomers on the nmr timescale. [129]

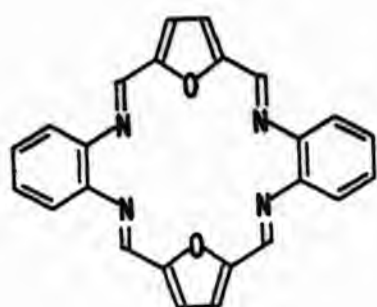


Other studies have revealed temperature-dependent exchange processes in helical complexes. [64,130] As part of this study, temperature dependence was observed for ^1H spectra of the disilver(I) complex and, as a representative of the mononuclear complexes, the lead(II) complex of L^1 (see Section 11.3.3).

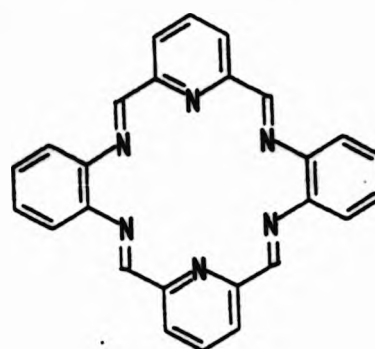
11.3.2 Metal-ligand spin-spin coupling and dynamic stability of complexes

The exchange rate of the metal-ion between the mononuclear complexes $[\text{ML}^1]^{2+}$ and $[\text{M}(\text{CD}_3\text{CN})_n]^{2+}$ is believed to be slow on the nmr timescale. In each case, $[\text{ML}^1]^{2+}$ complexes gave sharp, well resolved spectral signals and, in cases where the nmr-active metal nuclei ($I = \frac{1}{2}$) ^{111}Cd , ^{113}Cd and ^{207}Pb are present, coupling between these metal nuclei and both proton and carbon-13 nuclei was observed. Indeed, satellites from $^{207}\text{Pb}-^1\text{H}$ coupling remained evident around the azomethine resonance of $[\text{PbL}^1][\text{ClO}_4]_2$ even at the highest temperature (343 K) of a variable-temperature study. These observations are consistent with relatively long residence times for metal-ions in the complexed state and suggest that the spectra obtained represent the metal complexes and not an

average of complex and 'free' ligand spectra. Evidence for slow exchange in other mononuclear, tetraimine macrocycles is sparse but slow exchange of the normally labile Na^+ ion between the furan-based complex, $[\text{Na}(\text{10})][\text{ClO}_4]$ and $[\text{Na}((\text{CD}_3)_2\text{SO})_n]$ has been demonstrated^[102c] by ^{23}Na nmr.



(10)

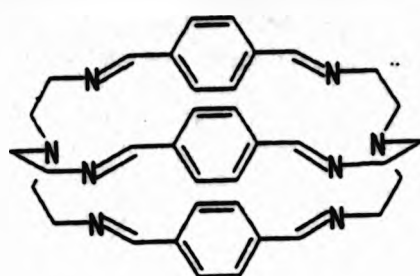


(11)

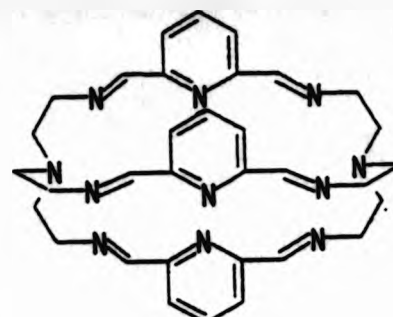
The observations of metal-proton and metal-carbon coupling in the $\text{Cd}(\text{II})$ and $\text{Pb}(\text{II})$ systems provides useful structural information about the complexation behaviour of L^1 . In both cases satellites due to metal coupling were associated with pyridyl and azomethine signals indicating that the metal-ions interact most strongly with an N_6 donor set of the ligand resulting from convergence of the 2,6-pyridinediimine head units. These observations, coupled with the symmetry implications of the spectra discussed above, suggest solution structures of these compounds that are similar to the double-helical structures of $[\text{ZnL}^1]^{2+}$ and $[\text{NiL}^1]^{2+}$ in the solid state. It should be noted that the absence of coupling satellites for signals attributable to proton or carbon sites proximal to the phenoxyether O-donors does not discount interaction between these donors and the metal-ion. However it seems likely that any metal-oxygen interaction in these complexes will be predominantly electrostatic in nature (similar to interactions described in alkali metal complexes of the crown ethers)^[131] and, as such, will be significantly weaker than the metal-nitrogen interactions. This theme is considered in more detail in Section 11.3.4.

The observations of metal-coupling satellites in the ^{13}C spectra of $[\text{CdL}^1]^{2+}$ and $[\text{PbL}^1]^{2+}$ proved particularly useful for identifying the pyridine α -carbon resonance. Except for one instance [coupling to the N-aryl carbon (C3)], J-values for Cd-X coupling were larger than the corresponding Pb-X splitting in these complexes despite the similarities of the gyromagnetic ratios of respective nuclei (see Table 11.1.5). Although these the differences in corresponding coupling constants can be attributed to differences in the metal-ligand bonding in the respective complexes, further analysis is beyond the scope of this study.

In contrast to the spectra obtained for divalent Cd(II) and Pb(II) complexes of L^1 , ^1H and ^{13}C spectra of the binuclear silver(I) complex in d_3 -acetonitrile show no evidence of metal-proton or metal-carbon-13 coupling. Silver possess two nmr-active ($I = \frac{1}{2}$) nuclei (see Table 11.1.5); ^{107}Ag and ^{109}Ag . Thus >99 % of the silver(I) complex molecules will contain nmr-active metal nuclei and, if resolved, superimposed doublet spectra due to resulting from coupling to both ^{107}Ag and ^{109}Ag will be observed for coupled proton and carbon-13 nuclei. Clearly, if the couplings to each $I = \frac{1}{2}$ nucleus are not resolved the coupled signals appear as doublets. Recently, Nelson and co-workers have identified silver- ^1H couplings in low temperature spectra (233 K) of the disilver complexes of the Schiff-base cryptands (12) and (13).^[132] Splittings of ca. 8 Hz for the azomethine proton signals were confirmed as $^3J(^{107,109}\text{Ag}-^1\text{H})$ in the case of $[\text{Ag}_2(13)]^{2+}$ by the observation of corresponding splitting for the ^{109}Ag signal in a ^{109}Ag INEPT spectrum of the complex.^[132b]



(12)



(13)

The absence of observable $^{107,109}\text{Ag}$ -proton coupling for $[\text{Ag}_2\text{L}^1]^{2+}$ in CD_3CN is attributed to a rapid exchange of the metal-ions between $[\text{Ag}_2\text{L}^1]^{2+}$ and $[\text{Ag}(\text{CD}_3\text{CN})]^+$ on the nmr timescale. However, the ^1H spectrum of the complex in $(\text{CD}_3)_2\text{CO}$ shows two signals due to the imine proton (H2) separated by 6.4 Hz which, in the light of the observations above, may be tentatively attributed to $^3J(^{107,109}\text{Ag-H2})$ coupling. Other features of the spectrum of $[\text{Ag}_2\text{L}^1]^{2+}$ in $(\text{CD}_3)_2\text{CO}$ are consistent with slowed exchange processes compared with the complex in CD_3CN (see Section 11.3.3) lending further support for this assignment. The structural implications of these observations are clear; although weak interaction of with O-donors cannot be discounted it appears that each Ag^+ ion in the complex is co-ordinated by an N_3 donor set from the 2,6-pyridinediimine head units of the ligand.

11.3.3 The effects of temperature and enantiomeric interchange

Having established that the presence of methylene AB subspectra in ^1H nmr spectra of the mononuclear complexes of L^1 is consistent with retention of complex chirality and strongly indicative of kinetically stable double-helical complex structures in solution, the observations of methylene signal broadening in ^1H spectra of $[\text{PbL}^1]^{2+}$ are worthy of note. The methylene AB 'doublet of doublets' pattern transforms into a broadened singlet (approaching A_2) on raising the temperature of CD_3CN solutions of $[\text{PbL}^1][\text{ClO}_4]_2$ and reaches

near-coalescence at ca. 343 K. As the temperature is increased, the methylene protons become enantiotopic (and are therefore equivalent in the achiral medium). Presumably, this could arise through fluxionality in the molecule corresponds to a symmetry plane bisecting the prochiral methylene assembly. Thus the collapse of the AB subspectrum corresponds to rapid interconversion between enantiomeric complexes on the nmr timescale. Inspection of models suggests that a number of processes that effect an interchange between the double-helical enantiomers are possible, *e.g.* decomplexation of one 2,6-pyridinediimine head unit followed by its re-attachment in the opposite configuration; untwisting of the co-ordinated ligand and retwisting in the opposite screw sense via a pseudo-planar transition state; exchange of the metal-ion between the ligand and the solvent. The latter possibility can be discounted as the metal-proton coupling satellites remain evident at all the temperatures studied, indicating the metal-ion remains bound to the ligand during the exchange process. Interestingly, the ^1H spectrum of $[\text{PbL}^1](\text{SCN})_2$ at ambient temperature also shows broadening for the methylene AB pattern suggesting that the enantiomeric exchange is dependent on the nature of the complex counterion. The spectrochemical series^[133] indicates that SCN^- has a higher metal-ion affinity than ClO_4^- , suggesting that the SCN^- may be involved in stabilising transition states in the exchange process perhaps through interaction with the metal-ion of the complex. Clearly more detailed experimentation is required before any mechanism can be elucidated.

In contrast to the mononuclear complexes of L^1 , the ambient temperature ^1H nmr spectrum of the disilver(I) complex in CD_3CN shows an A_2 (singlet) subspectrum due to the methylene protons. These enantiotopic environments for the methylene protons presumably arise from rapid dynamic exchange processes for the complex in this solvent. Greater flexibility is anticipated in this

bimetallic complex as the two 2,6-pyridinediimine head units are not 'anchored' to the same metal-ion, as is the case for the mononuclear complexes; indeed charge repulsions might be expected to maximise the separation between the metal-ions of the bimetallic complex leading to a more flexible arrangement for the ligand in the complex. Lowering the temperature of the solution led to resolution of the A_2 spectrum into a broadened doublet and, at 233 K, an AB spectrum indicating diastereotopic environments for the methylene protons. Thus, once the exchange processes are slowed to allow observation of separate species on the nmr timescale, it appears that $[Ag_2L^1]^{2+}$ is chiral, possibly adopting a double-helical structure resulting from similar orientational influences of the ligand (e.g. steric demands of the ligand backbone, arene π - π interactions) that were identified in the solid state structures of $[ZnL^1]^{2+}$ and $[NiL^1]^{2+}$ (see Chapter 10).

The 1H spectrum of $[Ag_2L^1][ClO_4]_2$ in $(CD_3)_2CO$ at ambient temperature provides an interesting comparison with the low temperature spectrum of the complex in CD_3CN . The spectrum in acetone- d_6 shows an AB subspectrum for the methylene protons (H5) indicating that they occupy diastereotopic environments which, as has been discussed previously, indicates chirality for the complex in the solution. Contrasting the rapid interconversion between enantiomers evidenced by the A_2 methylene spectrum at ambient temperature in CD_3CN , the complex therefore shows a substantially slower rate of exchange in acetone. In addition, the tentative assignment of ^{107}Ag - and ^{109}Ag - 1H coupling to the imine proton of the ligand in this solvent, indicating that metal exchange is slow on the nmr timescale, in contrast to the absence of similar coupling in CD_3CN , suggests that metal exchange between the complex and the solvent may play an important rôle in the exchange processes in solution. The rôle of acetonitrile in exchange processes in Cu(I) complexes has been

demonstrated^[127,134] and the compatibility of the 'soft' cyanide N-donor atom with the 'soft' Ag(I) ion may be of importance in this instance.

11.3.4 Analysis of chemical shifts.

The significant differences in chemical shifts of both proton and carbon-13 nuclei between complexes of L^1 are largely attributed to the influence of the co-ordinated metal-ions in the complexes. Spectra were obtained from saturated solutions in every case and some difference in the concentrations of samples is therefore inevitable. However, it seems likely that substrate-substrate interactions will be minimal in solutions at these relatively low concentrations and, on this basis, it is assumed that the observed shifts are predominantly due to intramolecular effects in the complexes. The symmetry and metal-coupling information discussed previously (see Sections 11.3.1 and 11.3.2) suggest that similar, double-helical structures are adopted by all the mononuclear complexes in solution. The fast-exchange 'helical twisting-bending' mechanism that confers equivalent environments on atoms in each quarter of the ligand in the $[ML^1]^{2+}$ complexes [see Fig. 11.3.1(1)], implies that the shifts observed at ambient temperature are a 'time-averaged' representation of the intrinsic 1H and ^{13}C shifts for the discrete a/a' and b/b' environments predicted in the solid state (see Fig. 11.1.1). However, the use of appropriate chemical shift values as probes of electronic structure in the complexes may reveal some differences in the gross structures and/or the co-ordination modes adopted in the complexes.

Convergence of the two 2,6-pyridinediimine 'head units' in the mononuclear complexes in order to co-ordinate single metal-ions is expected to involve severe twisting of the ligand [similar to the 'sweet wrapper' encapsulation of Zn(II) and Ni(II) observed in the solid state]. The incorporation of aromatic

rings in the superstructure of L^1 thus creates the possibility of substantial intramolecular interaction of ligand nuclei with anisotropic magnetic fields generated by the ring currents of unsaturated systems. These interactions are expected to play a significant rôle in determining chemical shift values.

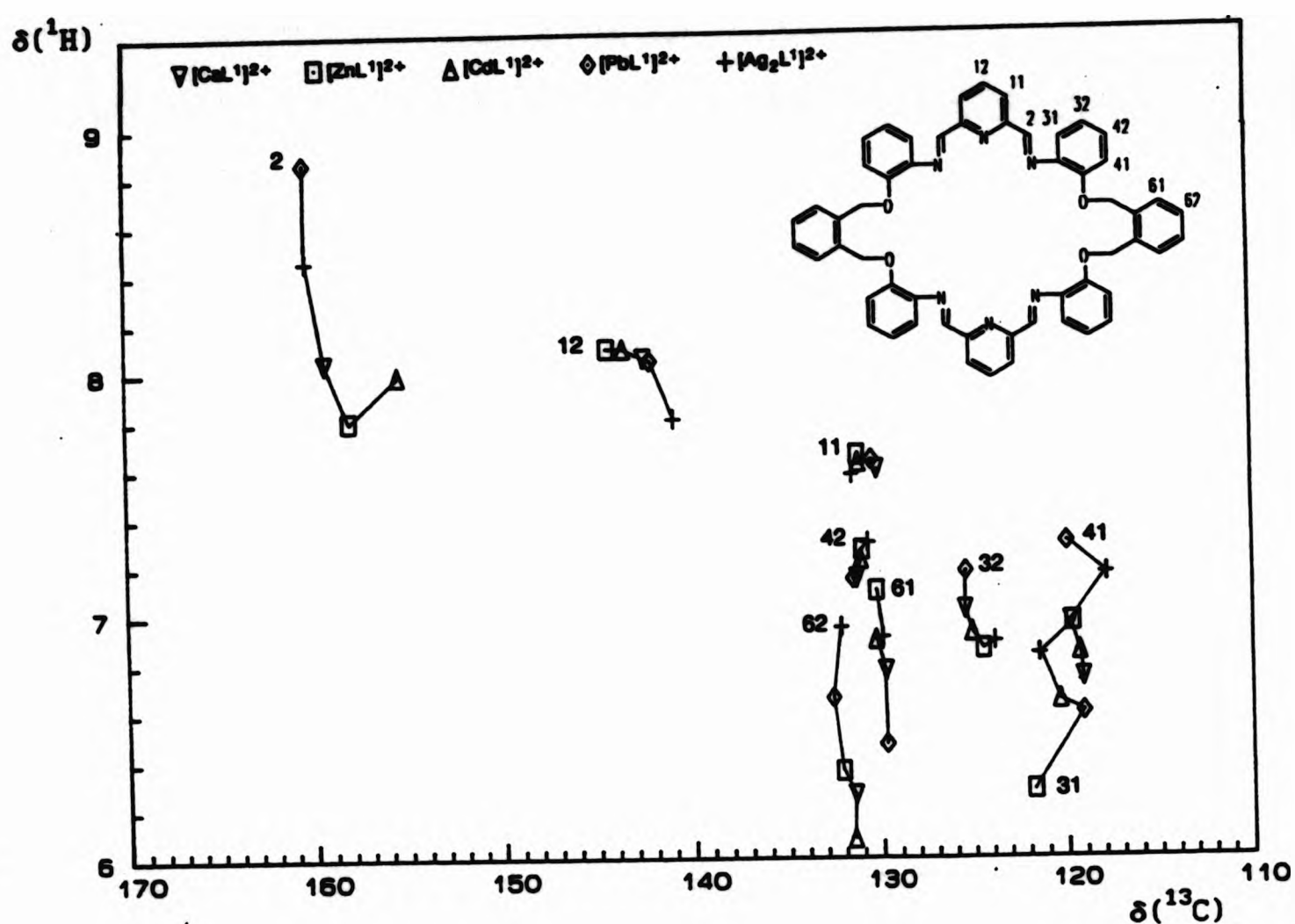


Figure 11.3.2 Correlation of ^1H and ^{13}C chemical shifts for diperchlorate complexes of $[\text{CaL}^1]^{2+}$, $[\text{ZnL}^1]^{2+}$, $[\text{CdL}^1]^{2+}$, $[\text{PbL}^1]^{2+}$ and $[\text{Ag}_2\text{L}^1]^{2+}$.

Possibly as a result of these influences, proton chemical shifts appear to be more sensitive to the different metal-ions in the complexes than the corresponding carbon signals (see Fig. 11.3.2). Since hydrogen atoms occupy positions on the peripheries of the macrocyclic structure, they are therefore more likely to be 'feel' the effects of these local fields. Pople has shown

that shielding due to aromatic ring currents is strongly dependent on the position of the nucleus relative to the aromatic ring; as well as a strong (\cos^2) dependence on the angle to the plane of the aromatic ring, the induced shift is also inversely proportional to the cube of the distance between the probe nucleus and the centroid of the aromatic ring.^[135] Thus small changes in the positions of protons with respect to aromatic ring currents are likely to lead to relatively large changes in ^1H chemical shifts in the L^1 complexes.

Any indication of differences in co-ordination modes of the complexes is expected to show in signal positions of the constituent nuclei of the 2,6-pyridinediimine 'head units'. In metal complexes of pyridine and its substituted analogues, Lavallo and co-workers have established that the γ -pyridine ^1H and ^{13}C chemical shifts provide reliable indications of the changes of electron density in the aromatic ring resulting from co-ordination of metal-ions.^[136] In these studies,^[136] deshielding of γ -sites [relative to $\delta(\text{pyridine})$] on complexation was associated with electron-withdrawal from the ring, and upfield shifts for the γ -signals with electron-donation, i.e. π back-bonding from N-coordinated metal-ions. In contrast, the reliability of chemical shift comparisons for α - and β -pyridine sites in this context is limited by local field and neighbour group anisotropy effects (due to their proximity to the co-ordination centre).^[136]

Orders of shielding of proton and carbon-13 γ -pyridyl sites in complexes of L^1 are similar; shieldings of γ -pyridyl protons (H12) are in the order $\text{Ag(I)} > \text{Ba(II)} = \text{Sr(II)} > \text{Pb(II)} \approx \text{Ca(II)} > \text{Cd(II)} = \text{Zn(II)}$ whereas shieldings of the corresponding ^{13}C nuclei (C12) are in the order $\text{Ag(I)} > \text{Pb(II)} > \text{Ca(II)} > \text{Cd(II)} > \text{Zn(II)}$. In comparison to the mononuclear divalent complexes, both ^1H and ^{13}C γ -pyridyl sites experience greater shielding in the disilver(I)

complex (see Fig. 11.3.2). The shielding at these sites is consistent both with a smaller inductive effect expected from the singly charged ion and the effects of the rapid complex-solvent metal exchange process in CD_3CN (see Section 11.3.2). This latter process results in 'time-averaged' signals with shifts intermediate between the intrinsic shifts of the complexed (downfield γ -pyridine signals) and uncomplexed (upfield γ -pyridine signals) ligand. Unfortunately, chemical shifts for the free ligand (L^1) were not available but, in common with other pyridine-containing ligands,^[25,128,136] metal co-ordination is expected to induce downfield shifts for γ -pyridyl signals.

Table 11.3.1 The ionic and Pauling radii of selected cations.

Metal	Ionic radius ^a		Pauling radius ^b
	CN = 6	CN = 8	
Zn(II)	72	84	-
Cd(II)	95	110	97
Ca(II)	100	112	99
Sr(II)	118	126	113
Ba(II)	135	142	-
Pb(II) ^c	119	129	-

^a In pm, from Ref. [137]. CN is the co-ordination number. ^b In pm, from Ref. [138]. ^c Stereochemically inactive electron lone-pair. Radius of Pb(II) with a stereochemically active electron lone-pair is ca. 74 pm.^[139]

Within the series of divalent mononuclear complexes, the orders of shielding appear to relate to the relative radii of the metal-ions (see Table 11.3.1). Co-ordination of smaller ions produces larger downfield shifts, suggesting that greater polarisation of the pyridyl π -cloud, and thus deshielding of γ -pyridyl sites, results from higher positive charge densities of co-ordinated metal-ions. These observations thus indicate that the strongest interactions

with the 2,6-pyridinediimine nitrogen donors of the ligand occur for the smaller metal-ions. Accordingly, the solid state structure of $[\text{ZnL}^1]^{2+}$ shows the metal bound solely by the N-donors of the ligand.

Bell and co-workers, in their studies of Group I and Group II metal-ion complexes of the [2+2] N_6 -tetraimine macrocyle $[\text{D} = \text{py}, \text{R}^1 = \text{H}, \text{R}^2 = \sigma\text{-C}_6\text{H}_4, (11)]^{[25,102d]}$ also noted that the smaller, more highly charged metal-ions shift the γ -pyridyl ^1H signals to lower field and similarly attributed these observations to the effects of electrostatic polarisation. In the same studies, these authors concluded that similar metal-ion based influences also underlie the shielding of imine proton sites in the complexes. Support for this view was derived from the observations of Nelson and co-workers regarding the order of shielding $[\text{K(I)} > \text{Na(I)} > \text{Sr(II)} > \text{Pb(II)}]$ of imine protons in mononuclear complexes of the [2+2] N_4O_2 macrocycle $[\text{D} = \text{fur}, \text{R}^1 = \text{H}, \text{R}^2 = \sigma\text{-C}_6\text{H}_4, (10)]^{[102c]}$.

Inspection of the values given in Table 11.1.1 for ^1H shifts of imine resonances suggests that while charge densities of the co-ordinated metal-ions undoubtedly play a rôle in determining shieldings of imine proton sites in the complexes, the predictive power of such a concept is limited. Notably, shifts of imine proton resonances in complexes with Pb(II) co-ordinated in trimethine 'head units' appear at significantly lower field than might be expected on the basis of an ionic radius of 1.19 Å [closely comparable with the Sr^{2+} radius of 1.18 Å].^[137] However, it is noteworthy that lead has a higher electronegativity than other comparable metals,^[138] and, in certain circumstances, is able to extrude a stereochemically-active lone pair of electrons from its 'inner core' electrons and behave as an ion with a radius of ca. 0.75 Å.^[139] Both these factors are likely to enhance polarisation of the co-ordinated $\text{C}=\text{N}$ bond and may therefore account for the comparatively

large deshielding noted in the Pb(II) complexes. Interestingly, in two instances X-ray studies have indicated the presence of stereochemically active lone pairs in Pb(II) complexes of 2,6-pyridinediimine-containing macrocycles^[108,140] and, in both cases, reported imine ¹H chemical shifts are greater than 9.5 ppm, and therefore at the lower end of the range indicated in Table 11.1.1.

The imine (H2) resonances in the mononuclear complexes of L¹ are somewhat upfield from comparable values in Table 11.1.1. The order of shielding in these complexes [Zn(II) > Cd(II) > Ca(II) > Sr(II) > Ba(II) > Pb(II)] appears to be reversed from that which might have been expected on the basis of metal-ion charge densities discussed above. While the order of shielding of azomethine carbon sites (C2) in the complexes [Cd(II) > Zn(II) > Ca(II) > Pb(II)] differs slightly from the proton data - the order of shieldings of [CdL¹]²⁺ and [ZnL¹]²⁺ are reversed - it is clear that shielding patterns rationalised on the basis of metal-induced polarisation of co-ordinated C=N bonds do not reflect the chemical shift data obtained in these complexes.

In the light of the arene stacking interactions observed in the Zn(II) complex in the solid state, it is highly likely that the positions of the imine resonances arise because intramolecular π - π interactions confer shielded environments on the nuclei. It is unclear from this evidence which benzene rings are involved in shielding the imine sites although in the solid state two xylenyl rings occupy sites directly over the imine bonds in [ZnL¹]²⁺. However these shieldings suggest that π -stacking interactions may persist in solution, further indicating that the complexes adopt double helical structures in which arene-stacking interactions play a significant stabilising rôle.

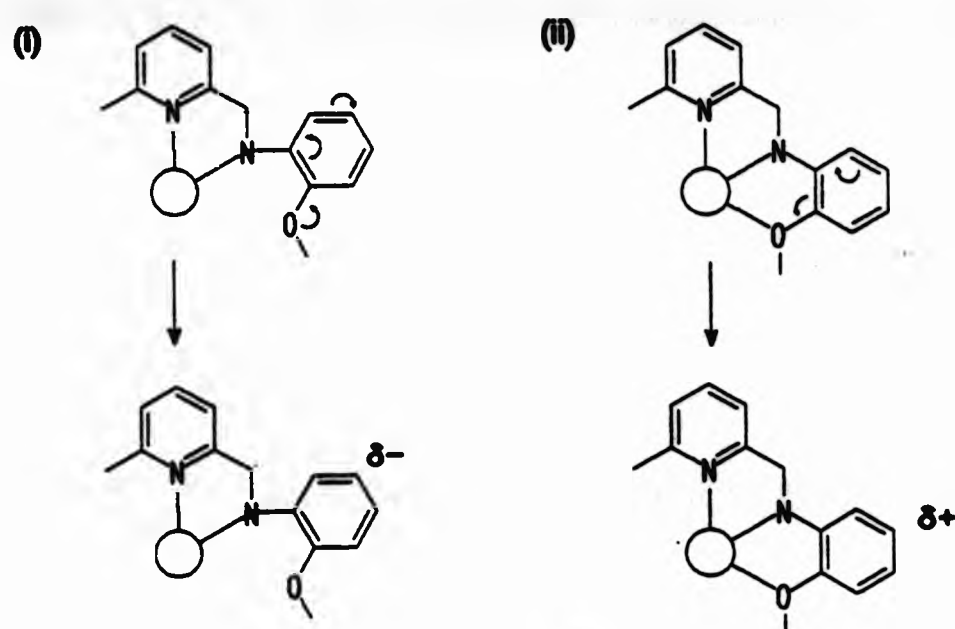


Figure 11.3.3 Transmission of the electronic effects of metal-oxygen co-ordination in iminophenoxy aromatic rings; (i) shielding of para sites due to np- π delocalisation of non-coordinated oxygen lone pairs and, (ii) withdrawal of electron density from para sites due to metal-oxygen co-ordination.

Of particular interest to this study is the possibility of interaction between the metal-ion and the ether donors of the macrocyclic ring. Co-ordination of one or more of the oxygen donors by the metal may enhance the thermodynamic stability of such a complex over metal-ions interacting solely with the N_6 donor set. Such 'structural dislocations' have been shown to provide a basis for metal-ion discrimination in mixed donor macrocyclic ligands.^[22] In the same way that electronic effects of different aromatic substituents influence the relative chemical shifts of ortho and para nuclei in substituted benzenes, it was envisaged that a comparison of the chemical shifts of the sites para to the ether oxygen substituents of the the iminophenoxy rings of L^1 (H32 and C32) might provide a probe for the extent of metal-oxygen interaction in the complexes. Unco-ordinated phenoxy ether aromatic substituents shield ortho and para sites through np- π delocalisation [Fig. 11.3.3(i)] and this effect is

characterised by negative values of the substituent effect parameters (as applied in Eqn. 11.1.1).^[103,104] Any interaction between the O-donors of the ligand with the d^{10} metal-ions under consideration here might be expected to increase the electron affinity of the oxygen atoms relative to the non-coordinated case and thus deshield the *ortho* and *para* sites [Fig. 11.3.3(ii)].

The order of shielding of H32 sites in the mononuclear complexes is $Zn(II) > Cd(II) > Ca(II) = Sr(II) > Ba(II) > Pb(II)$, shieldings of the corresponding C32 sites show a similar order; $Zn(II) > Cd(II) > Pb(II) > Ca(II)$. While these orders seem to indicate that stronger metal-oxygen interactions are present in complexes derived from the harder metal-ions (as might be expected from HSAB), the ranges encompassing shifts for all the complexes are rather small, ca. 0.4 ppm for H32 and ca. 1 ppm for C32. Therefore it can be concluded that if any metal-oxygen interactions are present in the complexes, they are relatively weak and probably electrostatic in nature.

Thus, it is clear from the nmr evidence presented that the structures of the complexes in solution are largely determined by (i) the convergence of the trimethine head units to co-ordinate to the single metal-ions and (ii) the resultant twisting of the ligand in order to adopt conformations that minimise steric repulsions of the macrocyclic superstructure. It is likely that the structures of the mononuclear complexes of L^1 involve double helical ligand arrays which are stabilised by intramolecular π -stacking interactions between the aromatic nuclei.

References

1. G. A. Melson, in *Coordination Chemistry of Macrocyclic Compounds*, ed. G. A. Melson, Plenum, New York, 1979.
2. D. A. House and N. F. Curtis, *Chem. Ind.*, 1961, 1708.
3. M. C. Thompson and D. H. Busch, *J. Am. Chem. Soc.*, 1964, **86**, 3651.
4. L. F. Lindoy and D. H. Busch, in *Preparative Inorganic Reactions*, ed. W. L. Jolly, Wiley-Interscience, New York, Vol. 6, 1971.
5. D. St.C Black, in *Comprehensive Coordination Chemistry*, ed. G. Wilkinson, Pergamon, 1987, vol. 6, pp.155-227 and refs. therein.
6. E. L. Blinn and D. H. Busch, *Inorg. Chem.*, 1968, **7**, 820.
7. S. M. Nelson, *Pure and Appl. Chem.*, 1980, **52**, 2461 and refs. therein.
8. D. E. Fenton, *Pure and Appl. Chem.*, 1986, **58**, 1437 and refs. therein.
9. D. E. Fenton, S. J. Kitchen, C. M. Spencer, S. Tamburini and P. A. Vigato, *J. Chem. Soc., Dalton Trans.*, 1988, 685.
10. V. McKee and W. B. Shephard, *J. Chem. Soc., Chem. Commun.*, 1985, 158.
11. M. G. B. Drew, S. G. McFall, S. M. Nelson and C. P. Waters, *J. Chem. Res. (S)*, 1979, 16.
12. H. Adams, N. A. Bailey, W. D. Carlise, D. E. Fenton and G. Rossi, *J. Chem. Soc., Dalton Trans.*, 1990, 1271.
13. M. G. B. Drew, B. P. Murphy, J. Nelson, S. M. Nelson and P. C. Yates, *J. Chem. Soc., Dalton Trans.*, 1987, 123.
14. M. G. B. Drew, M. McCann, S. M. Nelson and A. Rodgers, *J. Chem. Soc., Chem. Commun.*, 1978, 415.
15. N. A. Bailey, D. E. Fenton, I. T. Jackson, R. Moody and C. O. de Barbarin, *J. Chem. Soc., Chem. Commun.*, 1983, 1463.
16. M. G. B. Drew, F. S. Esho and S. M. Nelson, *J. Chem. Soc., Dalton Trans.*, 1983, 1857.
17. D. E. Fenton and P. A. Vigato, *Chem. Soc. Rev.*, 1988, **17**, 69.
18. S. Brooker, V. McKee, W. B. Shepherd and I. K. Pannell, *J. Chem. Soc., Dalton Trans.*, 1987, 2555.
19. M. G. B. Drew, J. Nelson and S. M. Nelson, *J. Chem. Soc., Dalton Trans.*, 1981, 1678.
20. N. A. Bailey, D. E. Fenton, R. J. Good, R. Moody and C. O. Rodriguez de Barbarin, *J. Chem. Soc., Dalton Trans.*, 1987, 207.
21. M. G. B. Drew, S. G. McFall, S. M. Nelson and A. H. bin Othman, *Proc. Royal Irish Acad.*, 1977, **77B**, 523.

22. L. F. Lindoy, in *Current Topics in Macrocyclic Chemistry in Japan*, ed. E. Kimura, Hiroshima School of Medicine (Publ.), 1987.
23. A. Bashall, D. E. Fenton, A. J. Leong, L. F. Lindoy, M. McPartlin and B. P. Murphy, *J. Chem. Soc., Dalton Trans.*, 1987, 2543
24. D. E. Fenton and B. P. Murphy, unpublished observations.
25. T. W. Bell, M. G. B. Drew and F. Guzzo, *J. Am. Chem. Soc.*, 1991, 113, 3115 and refs. therein.
26. R. D. Cannon, B. Chiswell and L. M. Venanzi, *J. Chem. Soc. A*, 1967, 1277.
27. E. B. Fleischer and P. A. Tasker, *J. Am. Chem. Soc.*, 1970, 92, 7072.
28. J. R. A. Pollock and R. Stevens (eds.), *Dictionary of Organic Compounds*, Eyre and Spottiswood, London, 4th edn., 1965, vol. 1, p. 193.
29. D. Jerchel, J. Heider and H. Wagner, *Liebigs Ann. Chem.*, 1958, 613, 153.
30. S. M. Nelson, *J. Chem. Soc., Dalton Trans.*, 1979, 1477.
31. D. H. Busch and L. F. Lindoy, *Inorg. Chem.*, 1974, 13, 2494.
32. B. P. Murphy and D. E. Fenton, unpublished observations.
33. D. H. Cook, M. G. B. Drew, D. E. Fenton, M. McCann, S. M. Nelson and A. Rodgers, *J. Chem. Soc., Dalton Trans.*, 1979, 414.
34. M. F. Cabral, B. P. Murphy and J. Nelson, *Inorg. Chim. Acta*, 1984, 90, 169.
35. K. Nakamoto, *Infrared Spectra of Inorganic and Coordination Compounds*, Wiley, New York, 2nd Edn., 1970.
36. M. R. Rosenthal, *J. Chem. Ed.*, 1973, 50, 331.
37. N. W. Alcock, D. C. Liles, M. McPartlin and P. A. Tasker, *J. Chem. Soc., Chem. Commun.*, 1974, 727.
38. S. S. Tandon and V. McKee, *J. Chem. Soc., Dalton Trans.*, 1989, 19.
39. A. H. Norbury and A. I. P. Sinha, *Quart. Rev.*, 1970, 24, 69.
40. J. L. Burmeister, *Coord. Chem. Rev.*, 1990, 105, 77.
41. C. Cairns, M. G. B. Drew, S. G. McFall and S. M. Nelson, *J. Chem. Soc., Dalton Trans.*, 2020.
42. F. A. Bovey, *Nuclear Magnetic Resonance Spectroscopy*, Academic Press, New York, 1969.
43. M. G. B. Drew, M. McCann and S. M. Nelson, *J. Chem. Soc., Dalton Trans.*, 1981, 1868.
44. A. M. Sargeson, *Pure and Appl. Chem.*, 1986, 58, 1511 and refs therein.
45. L. G. Armstrong and L. F. Lindoy, *Inorg. Chem.*, 1975, 14, 1322;
L. G. Armstrong and L. F. Lindoy, *Inorg. Nucl. Chem. Lett.*, 1970, 6, 675.
46. M. F. Cabral, B. P. Murphy and J. Nelson, *Inorg. Chim. Acta*, 1984, 90, 169.

47. P. Bird, M. G. B. Drew, F. S. Esho and S. M. Nelson, *J. Chem. Soc., Chem. Commun.*, 1979, 1035.
48. M. G. B. Drew, M. McCann and S. M. Nelson, *Inorg. Chim. Acta*, 1980, 41, 213.
49. G. M. Sheldrick, *SHELX Program for Crystal Structure Solution*, University of Cambridge, 1976.
50. J. Hornstra and B. Stubbs, *PW1100 Data Processing Program*, Philips Research Laboratories, Eindhoven, Holland, 1972.
51. N. F. M. Henry and K. Lonsdale (eds.), *International Tables for X-Ray Crystallography*, Kynoch Press, Birmingham, 2nd edn., 1965, vol. 1.
52. D. Stuart and N. Walker, *Acta Crystallogr., Sect. A*, 1983, A39, 158.
53. C. K. Johnson, *ORTEP II*, Report ORNL-5138, Oak Ridge National Laboratory, Oak Ridge, Tennessee, 1976.
54. J. A. Ibers and W. C. Hamilton, *Hydrogen Bonding in Solids*, W. A. Benjamin, New York, 1968.
55. O. Kennard and R. Taylor, *J. Am. Chem. Soc.*, 1982, 104, 5063.
56. C. Cairns, M. G. B. Drew, J. Nelson and S. M. Nelson, *J. Chem. Soc., Dalton Trans.*, 1981, 942.
57. F. W. B. Einstein and B. R. Penfold, *Acta Crystallogr.*, 1966, 20, 924.
58. A. J. Blake, A. J. Lavery, T. I. Hyde and M. Schröder, *J. Chem. Soc., Dalton Trans.*, 1989, 965.
59. E. B. Fleischer, A. E. Gebala, D. R. Swift and P. A. Tasker, *Inorg. Chem.*, 1972, 11, 2775.
60. N. L. Allinger, S. J. Angyal, E. Eliel, and G. A. Morrison, *Conformational Analysis*, Wiley Interscience, New York, 1967; W. L. Daux, D. C. Rohrer and C. M. Weeks, *Top. Stereochem.*, 1976, 9, 282.
61. D. A. Edwards, M. F. Mahon, W. R. Martin, K. C. Malloy, P. E. Fanwick and R. A. Walton, *J. Chem. Soc., Dalton Trans.*, 1990, 3161.
62. L. Casella, M. E. Silver and J. A. Ibers, *Inorg. Chem.*, 1984, 23, 1409.
63. I. Bernal, J. D. Korp, C. L. Merrill and L. J. Wilson, *J. Chem. Soc., Dalton Trans.*, 1981, 1951.
64. D. K. Coggin, J. A. Gonzalez, A. M. Kook, D. M. Stanbury and L. J. Wilson, *Inorg. Chem.*, 1991, 30, 1115.
65. V. L. Goedken and C. G. Christoph, *Inorg. Chem.*, 1973, 12, 2316.
66. D. C. Liles, M. McPartlin and P. A. Tasker, *J. Chem. Soc., Dalton Trans.*, 1987, 1631.
67. S. Lu and J. Selbin, *Inorg. Chim. Acta*, 1987, 134, 229.

68. M. G. B. Drew, J. Nelson and S. M. Nelson, *J. Chem. Soc., Dalton Trans.*, 1981, 1685.
69. R. S. Cahn, C. K. Ingold and V. Prelog, *Angew. Chem. Int. Ed. Engl.*, 1966, 5, 385.
70. S. K. Burley and G. A. Petsko, *Science*, 1985, 229, 23.
71. See for example, A. D. Hamilton, A. V. Muehldorf, D. Van Engen and J. C. Warner, *J. Am. Chem. Soc.*, 1988, 110, 6561; F. Diederich and D. Smithrud, *J. Am. Chem. Soc.*, 1990, 112, 339; C. A. Hunter, *J. Chem. Soc., Chem Commun.*, 1991, 749.
72. E. Keller, *SCHAKAL*, University of Freiberg, 1982.
73. A. G. Sharpe, *Inorganic Chemistry*, Longman, London, 1981, p. 292.
74. S. C. Wallwork, *J. Chem. Soc.*, 1961, 494.
75. R. S. Mulliken, *J. Am. Chem. Soc.*, 1950, 72, 600; 1952, 74, 811.
76. B. Jönsson, G. Karlström, P. Linse and A. Wallqvist, *J. Am. Chem. Soc.*, 1983, 105, 3777.
77. S. K. Burley and G. A. Petsko, *J. Am. Chem. Soc.*, 1986, 108, 7995.
78. R. O. Gould, A. M. Gray, P. Taylor and M. D. Walkinshaw, *J. Am. Chem. Soc.*, 1985, 107, 5921.
79. C. A. Hunter and J. K. M. Sanders, *J. Am. Chem. Soc.*, 1990, 112, 5525.
80. H. Sigel, *Angew. Chem., Int. Ed. Engl.*, 1975, 14, 394.
81. P. R. Mitchell, B. Prijs and H. Sigel, *Helv. Chim. Acta*, 1979, 62, 1723.
82. H. M. Colquhoun, J. F. Stoddart, D. J. Williams, J. B. Wolstenholme and R. Zarzycki, *Angew. Chem., Int. Ed. Engl.*, 1981, 20, 1051.
83. H. M. Colquhoun, E. P. Goodings, J. M. Maud, J. F. Stoddart, D. J. Williams and J. B. Wolstenholme, *J. Chem. Soc., Perkin Trans. 2*, 1985, 607.
84. E. C. Alyea, G. Ferguson, P. H. Merrel and R. J. Restivo, *J. Chem. Soc., Chem. Commun.*, 1975, 269; E. C. Alyea, G. Ferguson and R. J. Restivo, *Inorg. Chem.*, 1975, 14, 2491.
85. See for example, A. G. Sharpe, *Inorganic Chemistry*, Longman, London, 1981, pp. 465-472; D. S. Urch, *Orbitals and Symmetry*, Macmillan, London, 1979, pp. 165-176.
86. W. O. Gillum, J. C. Hoffmann, W. E. Streib and R. A. D. Wentworth, *J. Chem. Soc., Chem. Commun.*, 1969, 843; R. F. Childers, W. O. Gillum, and R. A. D. Wentworth, *Inorg. Chem.*, 1970, 9, 1825.
87. R. J. Gillespie, *Can. J. Chem.*, 1960, 38, 818; *Angew. Chem., Int. Ed. Engl.*, 1967, 6, 819.

88. J. F. Madder, G. von Koten, K. Vrieze and A. L. Speck, *Angew. Chem., Int. Ed. Engl.*, 1989, 28, 1698; G. Stackmeier, U. Thewalt and J-H. Furhop, *J. Am. Chem. Soc.*, 1976, 98, 278.; E. C. Constable and J. M. Holmes, *Inorg. Chim. Acta*, 1987, 126, 187; E. C. Constable, J. M. Holmes and P. R. Raithby, *Polyhedron*, 1991, 10, 127.
89. U. Koert, M. M. Harding and J-M. Lehn, *Nature*, 1990, 376, 339; E. C. Constable, *Nature*, 1990, 376, 314.
90. B. Chevrier, J. Harrowfield, J-M. Lehn, D. Moras, A. Rigault and J. Sigel, *Proc. Natl. Acad. Sci. USA*, 1987, 84, 2565.
91. J-M. Lehn and A. Rigault, *Angew. Chem., Int. Ed. Engl.*, 1988, 27, 1095.
92. J-P. Declercq, G. Germain, J-M. Lehn, M. Van Meersche, C. Piccinni-Leopardi, J-P. Sauvage, J. Simon and R. Zeissel, *Nouveau J. Chem.*, 1983, 7, 413.
93. E. C. Constable, M. G. B. Drew and M. D. Ward, *J. Chem. Soc., Chem. Commun.*, 1987, 1601; M. Barley, E. C. Constable, S. A. Corr, R. C. S. McQueen, J. C. Nutkins and M. D. Ward, *J. Chem. Soc., Dalton Trans.*, 1988, 2655.
94. E. C. Constable, M. G. B. Drew, G. A. Forsyth and M. D. Ward, *Polyhedron*, 1989, 8, 2551.
95. E. C. Constable, S. M. Elder, J. Healy and M. D. Ward, *J. Am. Chem. Soc.*, 1990, 112, 4590.
96. E. C. Constable, D. A. Tocher and M. D. Ward, *J. Am. Chem. Soc.*, 1990, 112, 1256.
97. E. C. Constable, D. A. Tocher and M. D. Ward, *J. Chem. Soc., Dalton Trans.*, 1991, 1675.
98. E. C. Constable, M. G. B. Drew, G. Forsyth and M. D. Ward, *J. Chem. Soc., Chem. Commun.*, 1988, 1451.
99. E. A. Abbot and R. H. Holm, in *Coordination Chemistry*, ed. A. E. Martell, ACS Monograph No. 168, Van Nostrand Reinhold, New York, 1971 vol. 1, ch. 5.
100. C. J. Hawkins and J. A. Palmer, *Coord. Chem. Rev.*, 1982, 44, 1115.
101. N. W. Alcock, P. Moore, H. A. A. Omar and C. J. Reader, *J. Chem. Soc., Dalton Trans.*, 1987, 2643; D. Baldwin, L. F. Lindoy and D. P. Graddon, *Aust. J. Chem.*, 1988, 41, 1347; C. W. G. Ansell, K. P. Dancey, L. F. Lindoy, M. McPartlin and P. A. Tasker, *J. Chem. Soc., Dalton Trans.*, 1983, 1789; L. Fielding and P. Moore, *J. Chem. Soc., Dalton Trans.*, 1989, 873.

102. (a) C. J. Gray and F. A. Hart, *J. Chem. Soc., Dalton Trans.*, 1987, 2289;
 (b) F. Benetollo, G. Bombieri, K. K. Fonda, A. Polo, J. R. Quagliano and
 L. M. Vallarino, *Inorg. Chem.*, 1991, 30, 1345; (c) M. G. B. Drew,
 F. S. Esho and S. M. Nelson, *J. Chem. Soc., Dalton Trans.*, 1983, 1857;
 (d) T. W. Bell and F. Guzzo, *J. Am. Chem. Soc.*, 1984, 106, 6111.
103. a) I. Fleming and D. H. Williams, *Spectroscopic Methods in Organic
 Chemistry*, 4th edn., McGraw-Hill, London, 1988; b) 3rd edn.,
 McGraw-Hill, London, 1980.
104. H-O Kalinowski, S. Berger and S. Braun, *Carbon-13 NMR Spectroscopy*, John
 Wiley, New York, 1988, pp. 311-336.
105. M. G. B. Drew, C. V. Knox, M. McCann and S. M. Nelson, *J. Chem. Soc.,
 Dalton Trans.*, 1981, 1669.
106. D. H. Cook and D. E. Fenton, *J. Chem. Soc., Dalton Trans.*, 1979, 266.
107. M. G. B. Drew, A. Lavery and S. M. Nelson, *J. Chem. Soc., Dalton Trans.*,
 1987, 2975.
108. A. Bashall, M. McPartlin, B. P. Murphy, D. E. Fenton, S. J. Kitchen and
 P. A. Tasker, *J. Chem. Soc., Dalton Trans.*, 1990, 505.
109. S. J. Kitchen, Ph.D. Thesis, University of Sheffield, 1989.
110. J. W. Akitt, *NMR and Chemistry - An Introduction to the Fourier
 Transform-Multinuclear Era*, Chapman and Hall, London, 2nd edn., 1983.
111. B. K. Hunter and J. K. M. Sanders, *Modern NMR Spectroscopy*, Oxford
 University Press, Oxford, 1987.
112. F. A. L. Anet, *Tetrahedron Lett.*, 1964, 46, 339.
113. J. B. Lambert and F. G. Riddell (eds.), *The Multinuclear Approach to NMR
 Spectroscopy*, Reidel, Dordrecht, 1982.
114. F. Brady, M. J. Forster, D. G. Gillies and R. W. Matthews, *J. Chem. Soc.,
 Chem. Commun.*, 1981, 911.
115. K. Horchler and B. Wrackmeyer, *Ann. Rep. N.M.R. Spectrosc.*, 1990, 22,
 249.
116. H. J. Bernstein, J. A. Pople and W. G. Schneider, *Can. J. Chem.*, 1957,
 35, 65.
117. R. Akaba, H. Sakuragi and K. Tokumaru, *Bull. Chem. Soc. Jpn.*, 1985, 58,
 301.
118. C. K. Sauers and H. M. Relles, *J. Am. Chem. Soc.*, 1973, 95, 7731.
119. R. H. Butler and S. M. Johnston, *J. Chem. Soc., Perkin Trans. 1*, 1984,
 2109.
120. A. T. Casey and I. P. Traverso, *Magn. Reson. Chem.*, 1990, 28, 660.

121. D. H. Cook, M. G. B. Drew, D. E. Fenton, S. G. McFall and S. M. Nelson, *J. Chem. Soc., Dalton Trans.*, 1977, 446.
122. W. B. Jennings, *Chem. Rev.*, 1975, 75, 307.
123. K. Mislow and M. Raban, *Top. Stereochem.*, 1967, 1, 1.
124. J. Fischer, T. M. Garrett, U. Koert, J-M. Lehn, D. Meyer and A. Rigault, *J. Chem. Soc., Chem. Commun.*, 1990, 557.
125. J-M. Lehn, M-T. Youinou and R. Zeissel, *Inorg. Chem.*, 1991, 30, 2144.
126. D. K. Mitchell and J-P. Sauvage, *Angew. Chem., Int. Ed. Engl.*, 1988, 7, 930.
127. G. Bernardinelli, C. Piguet and A. F. Williams, *Inorg. Chem.*, 1989, 28, 2920.
128. G. Bernardinelli, B. Bocquet, C. Piguet, S. Rüttimann and A. F. Williams, *J. Am. Chem. Soc.*, 1992, 114, 4230.
129. G. Bernardinelli, B. Bocquet, C. Piguet, A. Quattropiani and A. F. Williams, *J. Am. Chem. Soc.*, 1992, 114, 7440.
130. P. D. Beer, C. P. Moore and J. W. Wheeler, *J. Chem. Soc., Dalton Trans.*, 1992, 2667.
131. J-M. Lehn and A. I. Popov, in *Coordination Chemistry of Macrocyclic Compounds*, ed. G. A. Melson, Plenum, New York, 1979, ch. 9.
132. (a) M. G. B. Drew, D. McDowell and J. Nelson, *Polyhedron*, 1988, 7, 2229;
(b) ; M. G. B. Drew, D. Marrs, V. McKee and J. Nelson, Poster 113, 16th International Symposium on Macrocyclic Chemistry, Sheffield, 1991;
(c) M. G. B. Drew, J. Hunter, D. Marrs and J. Nelson, *J. Chem. Soc., Dalton Trans.*, 1992, 11.
133. J. E. Huheey, *Inorganic Chemistry*, Harper and Row, New York, 3rd edn., 1983, pp. 382-386
134. A. L. Crumbliss and A. T. Poulos, *Inorg. Chem.*, 1975, 14, 1529.
135. J. A. Pople, *J. Chem. Phys.*, 1956, 24, 1111.
136. M. D. Baughman, D. K. Lavalley and M. P. Phillips, *J. Am. Chem. Soc.*, 1977, 99, 718.
137. R. D. Shannon, *Acta Crystallogr., Sect. A*, 1976, A32, 751.
138. L. Pauling, *The Nature of the Chemical Bond*, Cornell University Press, New York, 3rd edn., 1960.
139. R. D. Hancock and A. E. Martell, *Chem. Rev.*, 1989, 89, 1857.
140. S. Waikar, Ph.D Thesis, University of North London, 1992.

Appendix I

TABLE 1 Fractional atomic coordinates and thermal parameters (\AA^2) for $[\text{ZnL}^1][\text{ClO}_4]_2 \cdot 2\text{CH}_3\text{CN}$

Atom	x	y	z	U_{iso} or U_{eq}
Zn	0.00000	0.23236(17)	0.25000	0.0348(21)
Cl(1)	0.3525(4)	0.4183(3)	0.3039(3)	0.054(4)
N(1)	0.1291(8)	0.2012(6)	0.2474(6)	0.019(3)
C(12)	0.3032(13)	0.1446(10)	0.2702(10)	0.047(6)
C(11a)	0.2901(12)	0.2053(9)	0.3049(9)	0.039(5)
C(1a)	0.2002(10)	0.2319(9)	0.2907(8)	0.029(4)
C(2a)	0.1740(12)	0.2952(9)	0.3262(9)	0.035(5)
N(2a)	0.0865(9)	0.3092(7)	0.3158(7)	0.032(4)
C(3a)	0.0592(8)	0.3734(5)	0.3405(6)	0.029(5)
C(31a)	0.0963(8)	0.4385(5)	0.3273(6)	0.043(5)
C(32a)	0.0648(8)	0.5015(5)	0.3506(6)	0.055(6)
C(42a)	-0.0038(8)	0.4994(5)	0.3872(6)	0.059(6)
C(41a)	-0.0409(8)	0.4343(5)	0.4004(6)	0.073(7)
C(4a)	-0.0094(8)	0.3713(5)	0.3771(6)	0.036(5)
O(1a)	-0.0438(8)	0.3052(6)	0.3867(6)	0.046(4)
C(5a)	-0.0966(13)	0.2989(10)	0.4390(10)	0.053(6)
C(6a)	-0.0947(12)	0.2220(10)	0.4595(9)	0.041(5)
C(61a)	-0.1795(13)	0.1847(10)	0.4454(10)	0.051(6)
C(62a)	-0.1845(13)	0.1150(10)	0.4642(10)	0.054(6)
C(11b)	0.2299(12)	0.1119(10)	0.2249(9)	0.040(6)
C(1b)	0.1427(11)	0.1402(8)	0.2143(8)	0.027(5)
C(2b)	0.0569(11)	0.1111(8)	0.1651(8)	0.029(5)
N(2b)	-0.0171(8)	0.1423(6)	0.1635(6)	0.025(4)
C(3b)	-0.1015(6)	0.1136(6)	0.1200(6)	0.029(5)
C(31b)	-0.1368(6)	0.0490(6)	0.1365(6)	0.038(5)
C(32b)	-0.2228(6)	0.0248(6)	0.0969(6)	0.045(6)
C(42b)	-0.2735(6)	0.0653(6)	0.0409(6)	0.050(6)
C(41b)	-0.2382(6)	0.1299(6)	0.0244(6)	0.048(6)
C(4b)	-0.1522(6)	0.1540(6)	0.0640(6)	0.038(5)
O(1b)	-0.1210(7)	0.2195(6)	0.0503(6)	0.047(4)
C(5b)	-0.0768(12)	0.2209(10)	-0.0078(9)	0.054(6)
C(6b)	0.0140(12)	0.1853(9)	0.0068(9)	0.034(5)
C(61b)	0.0227(14)	0.1151(11)	-0.0103(10)	0.059(6)
C(62b)	0.1046(14)	0.0810(11)	0.0041(10)	0.061(6)

TABLE 1 Fractional atomic coordinates and thermal parameters (\AA^2) for
 $[\text{ZnL}^1][\text{ClO}_4]_2 \cdot 2\text{CH}_3\text{CN}$ continued.

Atom	x	y	z	U_{iso} or U_{eq}
O(1)	0.3248(8)	0.4528(7)	0.3593(7)	0.064(4)
O(2)	0.3857(9)	0.3484(8)	0.3260(7)	0.080(5)
O(3)	0.4260(9)	0.4570(7)	0.2878(7)	0.080(5)
O(4)	0.2767(10)	0.4149(8)	0.2450(8)	0.083(5)
Cs(1)	0.3982(13)	0.3061(11)	0.1581(11)	0.071(7)
Cs(2)	0.4350(16)	0.2388(13)	0.1449(12)	0.078(7)
Ns(1)	0.4638(13)	0.1892(10)	0.1312(10)	0.089(7)
H(2a)	0.21940	0.34070	0.34480	0.0800
H(5a1)	-0.07200	0.33010	0.48560	0.0800
H(2b)	0.07800	0.06740	0.13440	0.0800
H(1sx)	0.34340	0.33290	0.11860	0.0800

TABLE 2 Fractional atomic coordinates for the hydrogen atoms for
 $[\text{ZnL}^1][\text{ClO}_4]_2 \cdot 2\text{CH}_3\text{CN}$

Atom	x	y	z
H(12)	0.3718	0.1216	0.2803
H(11a)	0.3489	0.2321	0.3386
H(31a)	0.1494	0.4402	0.2989
H(32a)	0.0935	0.5519	0.3403
H(42a)	-0.0282	0.5482	0.4053
H(41a)	-0.0940	0.4326	0.4288
H(5a2)	-0.1639	0.3219	0.4160
H(61a)	-0.2420	0.2111	0.4164
H(11b)	0.2386	0.0626	0.1993
H(31b)	-0.0975	0.0177	0.1799
H(32b)	-0.2501	-0.0252	0.1097
H(42b)	-0.3401	0.0465	0.0103
H(41b)	-0.2774	0.1612	-0.0189
H(5b1)	-0.1226	0.1952	-0.0523
H(5b2)	-0.0672	0.2758	-0.0204
H(61b)	-0.0389	0.0868	-0.0380
Hs(1y)	0.4554	0.3432	0.1711
Hs(1z)	0.3694	0.2996	0.2026
H(62a)	-0.2514	0.0898	0.4541
H(62b)	0.1048	0.0255	-0.0080

TABLE 3 Anisotropic thermal parameters (\AA^2) for $[\text{ZnL}^1][\text{ClO}_4]_2 \cdot 2\text{CH}_3\text{CN}$

Atom	U_{11}	U_{22}	U_{33}	U_{23}	U_{13}	U_{12}
Zn	0.032(2)	0.035(2)	0.038(2)	0.000	0.008(2)	0.000
Cl(1)	0.048(4)	0.053(4)	0.061(4)	0.004(4)	0.020(3)	-0.005(3)

TABLE 4 Bond lengths (Å) for $[\text{ZnL}^1][\text{ClO}_4]_2 \cdot 2\text{CH}_3\text{CN}$

Zn	-N(1)	2.023(12)	Zn	-N(2a)	2.139(12)
Zn	-N(2b)	2.373(13)	N(1)	-C(1a)	1.313(18)
N(1)	-C(1b)	1.361(20)	C(12)	-C(11a)	1.37(3)
C(12)	-C(11b)	1.367(23)	C(11a)-C(1a)		1.389(23)
C(1a)	-C(2a)	1.484(25)	C(2a)	-N(2a)	1.293(22)
C(2a)	-H(2a)	1.093(16)	N(2a)	-C(3a)	1.402(17)
C(3a)	-C(31a)	1.395(15)	C(3a)	-C(4a)	1.395(19)
C(31a)-C(32a)		1.395(15)	C(32a)-C(42a)		1.395(19)
C(42a)-C(41a)		1.395(15)	C(41a)-C(4a)		1.395(15)
C(4a)	-O(1a)	1.376(15)	O(1a)	-C(5a)	1.454(25)
C(5a)	-C(6a)	1.50(3)	C(5a)	-H(5a1)	1.074(18)
C(6a)	-C(61a)	1.41(3)	C(61a)-C(62a)		1.37(3)
C(11b)-C(1b)		1.369(24)	C(1b)	-C(2b)	1.496(21)
C(2b)	-N(2b)	1.242(21)	C(2b)	-H(2b)	1.113(17)
N(2b)	-C(3b)	1.434(14)	C(3b)	-C(31b)	1.395(16)
C(3b)	-C(4b)	1.395(14)	C(31b)-C(32b)		1.395(12)
C(32b)-C(42b)		1.395(14)	C(42b)-C(41b)		1.395(16)
C(41b)-C(4b)		1.395(12)	C(4b)	-O(1b)	1.366(16)
O(1b)	-C(5b)	1.461(24)	C(5b)	-C(6b)	1.471(24)
C(6b)	-C(61b)	1.38(3)	C(61b)-C(62b)		1.34(3)
Cl(1)	-O(1)	1.421(16)	Cl(1)	-O(2)	1.433(16)
Cl(1)	-O(3)	1.416(16)	Cl(1)	-O(4)	1.401(14)
Cs(1)	-Cs(2)	1.43(3)	Cs(1)	-H(1sx)	1.096(19)
Cs(2)	-Ns(1)	1.09(3)			

TABLE 5 Bond angles ($^{\circ}$) for $[\text{ZnL}^1][\text{ClO}_4]_2 \cdot 2\text{CH}_3\text{CN}$

N(2a) -Zn -N(1)	77.4(5)	N(2b) -Zn -N(1)	72.7(4)
N(2b) -Zn -N(2a)	148.9(5)	C(1a) -N(1) -Zn	118(1)
C(1b) -N(1) -Zn	121.0(9)	C(1b) -N(1) -C(1a)	119(1)
C(11b)-C(12) -C(11a)	121(2)	C(1a) -C(11a)-C(2)	117(1)
C(11a)-C(1a) -N(1)	123(2)	C(2a) -C(1a) -N(1)	113(1)
C(2a) -C(1a) -C(11a)	123(1)	N(2a) -C(2a) -C(1a)	118(1)
H(2a) -C(2a) -C(1a)	125(2)	H(2a) -C(2a) -N(2a)	114(1)
C(2a) -N(2a) -Zn	113(1)	C(3a) -N(2a) -Zn	127.6(9)
C(3a) -N(2a) -C(2a)	119(1)	N(2a) -Zn -N(2a)	95.1(7)
C(31a)-C(3a) -N(2a)	122(1)	C(4a) -C(3a) -N(2a)	118(1)
C(4a) -C(3a) -C(31a)	120(1)	C(32a)-C(31a)-C(3a)	120(1)
C(42a)-C(32a)-C(31a)	120(1)	C(41a)-C(42a)-C(32a)	120(1)
C(4a) -C(41a)-C(42a)	120(1)	C(41a)-C(4a) -C(3a)	120(1)
O(1a) -C(4a) -C(3a)	116(1)	O(1a) -C(4a) -C(41a)	124(1)
C(5a) -O(1a) -C(4a)	117(1)	C(6a) -C(5a) -O(1a)	107(1)
H(5a1)-C(5a) -O(1a)	116(2)	H(5a1)-C(5a) -C(6a)	108(1)
C(61a)-C(6a) -C(5a)	118(1)	C(62a)-C(61a)-C(6a)	122(2)
C(1b) -C(11b)-C(2)	120(2)	C(11b)-C(1b) -N(1)	120(1)
C(2b) -C(1b) -N(1)	114(1)	C(2b) -C(1b) -C(11b)	125(1)
N(2b) -C(2b) -C(1b)	117(1)	H(2b) -C(2b) -C(1b)	108(1)
H(2b) -C(2b) -N(2b)	135(1)	C(2b) -N(2b) -Zn	113(1)
C(3b) -N(2b) -Zn	128.0(9)	C(3b) -N(2b) -C(2b)	118(1)
N(2b) -Zn -N(2b)	89.0(6)	C(31b)-C(3b) -N(2b)	120.9(9)
C(4b) -C(3b) -N(2b)	119(1)	C(4b) -C(3b) -C(31b)	120.0(8)
C(32b)-C(31b)-C(3b)	120.0(9)	C(42b)-C(32b)-C(31b)	120(1)
C(41b)-C(42b)-C(32b)	120.0(8)	C(4b) -C(41b)-C(42b)	120.0(9)
C(41b)-C(4b) -C(3b)	120(1)	O(1b) -C(4b) -C(3b)	120.4(9)
O(1b) -C(4b) -C(41b)	119.5(9)	C(5b) -O(1b) -C(4b)	115(1)
C(6b) -C(5b) -O(1b)	114(1)	C(61b)-C(6b) -C(5b)	122(2)
C(62b)-C(61b)-C(6b)	123(2)	O(2) -Cl(1) -O(1)	109.3(9)
O(3) -Cl(1) -O(1)	109.4(9)	O(3) -Cl(1) -O(2)	108.2(9)
O(4) -Cl(1) -O(1)	109.2(9)	O(4) -Cl(1) -O(2)	110.6(9)
O(4) -Cl(1) -O(3)	110.0(9)	H(1sx)-Cs(1) -Cs(2)	122(2)
Ns(1) -Cs(2) -Cs(1)	176(3)		

TABLE 6 Intermolecular distances (\AA) for $[\text{ZnL}^1][\text{ClO}_4]_2 \cdot 2\text{CH}_3\text{CN}$

atom1	atom2	dist	S	a	b	c
O(1a) ... N(1)		3.28	-2	0.0	0.0	1.0
N(2b) ... N(1)		2.93	-2	0.0	0.0	1.0
C(3b) ... N(1)		3.21	-2	0.0	0.0	1.0
Ns(1) ... H(12)		2.91	-2	1.0	0.0	1.0
Ns(1) ... H(11a)		2.82	-2	1.0	0.0	1.0
C(3b) ... C(1a)		3.40	-2	0.0	0.0	1.0
C(4b) ... C(1a)		3.45	-2	0.0	0.0	1.0
C(4b) ... C(2a)		3.49	-2	0.0	0.0	1.0
O(1b) ... C(2a)		3.10	-2	0.0	0.0	1.0
H(41b) ... C(2a)		3.07	2	-0.5	0.5	-1.0
N(2a) ... N(2a)		3.16	-2	0.0	0.0	1.0
N(2b) ... N(2a)		3.36	-2	0.0	0.0	1.0
O(1b) ... N(2a)		3.07	-2	0.0	0.0	1.0
Ns(1) ... H(32a)		2.82	-2	0.5	-0.5	1.0
Ns(1) ... H(42a)		2.97	-2	0.5	-0.5	1.0
O(1b) ... O(1a)		2.93	-2	0.0	0.0	1.0
C(5b) ... O(1a)		3.04	-2	0.0	0.0	1.0
H(5b2) ... O(1a)		2.79	-2	0.0	0.0	1.0
C(6b) ... O(1a)		3.04	-2	0.0	0.0	1.0
C(5b) ... C(5a)		2.98	-2	0.0	0.0	1.0
H(5b2) ... C(5a)		2.59	-2	0.0	0.0	1.0
C(6b) ... C(5a)		2.56	-2	0.0	0.0	1.0
H(1sx) ... H(5a2)		2.59	-2	0.0	0.0	1.0
C(2b) ... C(6a)		3.38	-2	0.0	0.0	1.0
O(1b) ... C(6a)		3.27	-2	0.0	0.0	1.0
C(5b) ... C(6a)		2.49	-2	0.0	0.0	1.0
H(5b2) ... C(6a)		2.61	-2	0.0	0.0	1.0
C(6b) ... C(6a)		1.40	-2	0.0	0.0	1.0
C(61b) ... C(6a)		2.38	-2	0.0	0.0	1.0
C(62b) ... C(6a)		2.76	-2	0.0	0.0	1.0
C(1b) ... C(61a)		3.44	-2	0.0	0.0	1.0
C(2b) ... C(61a)		3.47	-2	0.0	0.0	1.0
C(6b) ... C(61a)		2.40	-2	0.0	0.0	1.0
C(61b) ... C(61a)		2.70	-2	0.0	0.0	1.0
C(62b) ... C(61a)		2.34	-2	0.0	0.0	1.0
Cs(1) ... H(61a)		3.00	-2	0.0	0.0	1.0

TABLE 6 Intermolecular distances (Å) for $[\text{ZnL}^1][\text{ClO}_4]_2 \cdot 2\text{CH}_3\text{CN}$ continued.

atom1	atom2	dist	S	a	b	c
Cs(2) ...H(61a)		2.87	-2	0.0	0.0	1.0
C(6b) ...C(62a)		2.79	-2	0.0	0.0	1.0
C(61b)...C(62a)		2.35	-2	0.0	0.0	1.0
C(62b)...C(62a)		1.36	-2	0.0	0.0	1.0
H(62b)...C(62a)		2.11	-2	0.0	0.0	1.0
H(2b) ...C(62a)		2.95	-2	0.0	0.0	1.0
Cl(1) ...C(11b)		3.84	-2	0.5	0.5	1.0
O(1) ...C(11b)		3.42	-2	0.5	0.5	1.0
Cl(1) ...H(11b)		3.03	-2	0.5	0.5	1.0
O(1) ...H(11b)		2.43	-2	0.5	0.5	1.0
N(2b) ...C(1b)		3.41	-2	0.0	0.0	1.0
C(31b)...C(1b)		3.43	-2	0.0	0.0	1.0
O(3) ...C(2b)		3.03	-2	0.5	0.5	1.0
N(2b) ...N(2b)		3.33	-2	0.0	0.0	1.0
H(62b)...C(31b)		3.04	-1	0.0	0.0	0.0
O(3) ...C(31b)		3.37	1	0.5	0.5	0.0
H(62b)...C(32b)		2.94	-1	0.0	0.0	0.0
Cl(1) ...H(31b)		3.31	1	0.5	0.5	0.0
O(3) ...H(31b)		2.36	1	0.5	0.5	0.0
O(3) ...H(31b)		2.72	-2	0.5	0.5	1.0
O(4) ...H(32b)		2.83	1	0.5	0.5	0.0
O(1b) ...H(41b)		2.69	-1	-0.5	0.5	0.0
H(5a1)...C(5b)		2.97	-2	0.0	0.0	1.0
O(2) ...H(5b1)		2.57	2	0.5	0.5	0.0
H(5a1)...H(5b2)		2.26	-2	0.0	0.0	1.0
H(5a1)...C(6b)		2.85	-2	0.0	0.0	1.0
Cl(1) ...H(61b)		3.13	2	0.5	0.5	0.0
O(1) ...H(61b)		2.59	2	0.5	0.5	0.0
O(2) ...H(61b)		2.90	2	0.5	0.5	0.0
H(62a)...C(62b)		2.14	-2	0.0	0.0	1.0
Hs(1y)...Cl(1)		3.11	-2	1.0	0.0	1.0
H(2b) ...Cl(1)		3.13	-2	0.5	-0.5	1.0
H(2b) ...O(1)		2.58	-2	0.5	-0.5	1.0
Cs(1) ...O(2)		3.25	-2	1.0	0.0	1.0
Hs(1y)...O(2)		2.35	-2	1.0	0.0	1.0
Cs(2) ...O(2)		3.31	-2	1.0	0.0	1.0

TABLE 6 Intermolecular distances (Å) for $[\text{ZnL}^1][\text{ClO}_4]_2 \cdot 2\text{CH}_3\text{CN}$ continued.

atom1	atom2	dist	S	a	b	c
O(3)	...O(3)	2.96	-2	1.0	0.0	1.0
Hs(1y)	...O(3)	2.76	-2	1.0	0.0	1.0
H(2b)	...O(3)	2.59	-2	0.5	-0.5	1.0
H(5a1)	...Ns(1)	2.81	2	-0.5	0.5	0.0

Symmetry Transformations:

The second atom is related to the first atom, at (x,y,z), by the symmetry operation S with (a,b,c) added to the (x',y',z') of S
Where S = 1 x, y, z

TABLE 7 Intramolecular distances (Å) for $[\text{ZnL}^1][\text{ClO}_4]_2 \cdot 2\text{CH}_3\text{CN}$

C(11a)...Zn	4.21	C(1a) ...Zn	2.88
C(2a) ...Zn	2.90	C(3a) ...Zn	3.19
C(4a) ...Zn	3.65	O(1a) ...Zn	3.24
C(11b)...Zn	4.24	C(1b) ...Zn	2.96
C(2b) ...Zn	3.08	C(3b) ...Zn	3.45
C(4b) ...Zn	4.07	O(1b) ...Zn	3.90
C(12) ...N(1)	2.73	C(11a)...N(1)	2.38
C(2a) ...N(1)	2.34	N(2a) ...N(1)	2.60
C(11b)...N(1)	2.37	C(2b) ...N(1)	2.40
N(2b) ...N(1)	2.62	H(11a)...C(12)	2.13
C(1a) ...C(12)	2.35	H(11b)...C(12)	2.14
C(1b) ...C(12)	2.36	C(11a)...H(12)	2.12
C(11b)...H(12)	2.12	C(2a) ...C(11a)	2.53
C(11b)...C(11a)	2.38	C(1b) ...C(11a)	2.74
O(2) ...C(11a)	3.02	H(2a) ...C(11a)	2.94
C(1a) ...H(11a)	2.17	C(2a) ...H(11a)	2.82
O(2) ...H(11a)	2.28	N(2a) ...C(1a)	2.38
C(11b)...C(1a)	2.70	C(1b) ...C(1a)	2.31
H(2a) ...C(1a)	2.29	C(3a) ...C(2a)	2.33
C(31a)...C(2a)	2.93	C(4a) ...C(2a)	3.45
H(31a)...C(2a)	2.78	Cl(1) ...C(2a)	3.63
O(2) ...C(2a)	3.31	O(4) ...C(2a)	3.35
C(31a)...N(2a)	2.44	C(4a) ...N(2a)	2.40
H(31a)...N(2a)	2.69	O(1a) ...N(2a)	2.67
H(2a) ...N(2a)	2.00	C(32a)...C(3a)	2.42
C(42a)...C(3a)	2.79	C(41a)...C(3a)	2.42
H(31a)...C(3a)	2.15	O(1a) ...C(3a)	2.36
H(2a) ...C(3a)	2.44	C(42a)...C(31a)	2.42
C(41a)...C(31a)	2.79	C(4a) ...C(31a)	2.42
H(32a)...C(31a)	2.15	O(1) ...C(31a)	3.31
H(2a) ...C(31a)	2.56	C(41a)...C(32a)	2.42
C(4a) ...C(32a)	2.79	H(31a)...C(32a)	2.15
H(42a)...C(32a)	2.15	C(4a) ...C(42a)	2.42
H(32a)...C(42a)	2.15	H(41a)...C(42a)	2.15
H(42a)...C(41a)	2.15	O(1a) ...C(41a)	2.44
C(5a) ...C(41a)	2.84	H(5a2)...C(41a)	2.86
H(5a1)...C(41a)	2.70	H(41a)...C(4a)	2.15
C(5a) ...C(4a)	2.42	H(5a2)...C(4a)	2.77

TABLE 7 Intramolecular distances (Å) for $[\text{ZnL}^1][\text{ClO}_4]_2 \cdot 2\text{CH}_3\text{CN}$ continued.

H(5a1)...C(4a)	2.66	Cl(1) ...H(31a)	3.03
O(1) ...H(31a)	2.59	O(4) ...H(31a)	2.45
H(2a) ...H(31a)	2.22	O(1a) ...H(41a)	2.70
C(5a) ...H(41a)	2.52	H(5a1)...H(41a)	2.21
H(5a2)...O(1a)	2.04	C(6a) ...O(1a)	2.38
H(5a1)...O(1a)	2.15	C(61a)...C(5a)	2.49
H(61a)...C(5a)	2.67	C(6a) ...H(5a2)	2.21
C(61a)...H(5a2)	2.67	H(5a1)...H(5a2)	1.68
H(61a)...C(6a)	2.15	C(62a)...C(6a)	2.43
H(5a1)...C(6a)	2.10	H(62a)...C(61a)	2.11
C(62a)...H(61a)	2.12	C(2b) ...C(11b)	2.54
H(2b) ...C(11b)	2.63	C(1b) ...H(11b)	2.12
C(2b) ...H(11b)	2.77	H(2b) ...H(11b)	2.41
N(2b) ...C(1b)	2.33	H(2b) ...C(1b)	2.12
C(3b) ...C(2b)	2.30	C(31b)...C(2b)	3.03
C(4b) ...C(2b)	3.34	H(31b)...C(2b)	2.97
C(6b) ...C(2b)	3.33	C(61b)...C(2b)	3.37
C(62b)...C(2b)	3.48	C(31b)...N(2b)	2.46
C(4b) ...N(2b)	2.44	H(31b)...N(2b)	2.69
O(1b) ...N(2b)	2.78	C(6b) ...N(2b)	3.34
H(2b) ...N(2b)	2.18	C(32b)...C(3b)	2.42
C(42b)...C(3b)	2.79	C(41b)...C(3b)	2.42
H(31b)...C(3b)	2.15	O(1b) ...C(3b)	2.40
C(5b) ...C(3b)	3.33	C(6b) ...C(3b)	3.43
H(2b) ...C(3b)	2.76	C(42b)...C(31b)	2.42
C(41b)...C(31b)	2.79	C(4b) ...C(31b)	2.42
H(32b)...C(31b)	2.15	C(41b)...C(32b)	2.42
C(4b) ...C(32b)	2.79	H(31b)...C(32b)	2.15
H(42b)...C(32b)	2.15	C(4b) ...C(42b)	2.42
H(32b)...C(42b)	2.15	H(41b)...C(42b)	2.15
H(42b)...C(41b)	2.15	O(1b) ...C(41b)	2.38
C(5b) ...C(41b)	3.15	H(5b1)...C(41b)	2.85
H(41b)...C(4b)	2.15	C(5b) ...C(4b)	2.38
H(5b1)...C(4b)	2.57	C(6b) ...C(4b)	3.03
C(61b)...C(4b)	3.38	O(1b) ...H(41b)	2.62
H(5b1)...O(1b)	2.07	H(5b2)...O(1b)	2.07
C(6b) ...O(1b)	2.47	C(61b)...O(1b)	3.34
C(61b)...C(5b)	2.49	H(61b)...C(5b)	2.68

TABLE 7 Intramolecular distances (Å) for $[\text{ZnL}^1][\text{ClO}_4]_2 \cdot 2\text{CH}_3\text{CN}$ continued.

C(6b) ...H(5b1)	2.08	C(61b)...H(5b1)	2.59
C(6b) ...H(5b2)	2.08	H(61b)...C(6b)	2.11
C(62b)...C(6b)	2.39	H(62b)...C(61b)	2.07
H(2b) ...C(61b)	2.91	C(62b)...H(61b)	2.09
H(2b) ...C(62b)	2.71	Cs(1) ...Cl(1)	3.77
Hs(1z)...Cl(1)	3.05	H(2a) ...Cl(1)	2.74
O(2) ...O(1)	2.33	O(3) ...O(1)	2.32
O(4) ...O(1)	2.30	H(2a) ...O(1)	2.60
O(3) ...O(2)	2.31	O(4) ...O(2)	2.33
Hs(1z)...O(2)	2.56	H(2a) ...O(2)	2.60
O(4) ...O(3)	2.31	Hs(1z)...O(4)	2.81
H(2a) ...O(4)	2.72	Ns(1) ...Cs(1)	2.52
Cs(2) ...Hs(1y)	2.03	Ns(1) ...Hs(1y)	3.01
H(1sx)...Hs(1y)	1.74	Cs(2) ...Hs(1z)	2.03
H(1sx)...Hs(1z)	1.72	H(1sx)...Cs(2)	2.21

Appendix II

TABLE 1 Fractional atomic coordinates and thermal parameters (\AA^2)
for $[\text{NiL}^{\text{I}}][\text{ClO}_4]_2 \cdot 2\text{CH}_3\text{CN}$

Atom	x	y	z	U_{iso} or U_{eq}
Ni	0.00000	0.22673(10)	0.25000	0.0295(10)
Cl(1)	0.3515(2)	0.4283(2)	0.3095(1)	0.053(2)
O(1)	0.3205(5)	0.4599(4)	0.3651(4)	0.078(6)
O(2)	0.3833(6)	0.3570(4)	0.3283(4)	0.077(6)
O(3)	0.4264(6)	0.4694(4)	0.2959(5)	0.097(7)
O(4)	0.2749(5)	0.4269(5)	0.2505(4)	0.090(7)
Cs(1)	0.3965(8)	0.3156(8)	0.1623(6)	0.082(10)
Cs(2)	0.4336(10)	0.2471(9)	0.1483(7)	0.068(10)
Ns(1)	0.4617(9)	0.1940(7)	0.1355(7)	0.103(11)
N(1)	0.1312(5)	0.2067(4)	0.2437(3)	0.027(2)
C(12)	0.3087(7)	0.1545(5)	0.2657(5)	0.039(3)
C(11a)	0.2917(6)	0.2116(5)	0.3032(5)	0.039(3)
C(1a)	0.2001(6)	0.2386(5)	0.2907(4)	0.032(2)
C(2a)	0.1684(6)	0.2988(5)	0.3256(5)	0.038(2)
N(2a)	0.0768(5)	0.3065(4)	0.3176(4)	0.032(2)
C(31a)	0.0814(7)	0.4365(6)	0.3287(5)	0.056(3)
C(32a)	0.0515(8)	0.5008(7)	0.3546(6)	0.068(3)
C(42a)	-0.0141(7)	0.4963(7)	0.3927(6)	0.062(3)
C(41a)	-0.0503(7)	0.4320(6)	0.4062(5)	0.053(3)
C(4a)	-0.0218(6)	0.3678(5)	0.3816(5)	0.039(3)
C(3a)	0.0467(7)	0.3710(5)	0.3431(5)	0.042(3)
O(1a)	-0.0536(4)	0.3012(3)	0.3924(3)	0.043(2)
C(5a)	-0.1014(7)	0.2947(5)	0.4470(5)	0.052(3)
C(6a)	-0.1032(7)	0.2178(5)	0.4656(5)	0.043(3)
C(61a)	-0.1880(7)	0.1802(6)	0.4545(5)	0.054(3)
C(62a)	-0.1922(7)	0.1076(6)	0.4721(6)	0.058(3)
C(11b)	0.2366(6)	0.1225(5)	0.2165(5)	0.038(3)
C(1b)	0.1469(6)	0.1512(5)	0.2079(4)	0.033(2)
C(2b)	0.0610(6)	0.1219(5)	0.1610(5)	0.035(2)
N(2b)	-0.0169(5)	0.1480(4)	0.1683(3)	0.028(2)
C(31b)	-0.1409(6)	0.0574(5)	0.1455(5)	0.040(3)
C(32b)	-0.2275(7)	0.0321(6)	0.1070(5)	0.050(3)
C(42b)	-0.2728(7)	0.0695(6)	0.0485(5)	0.051(3)

TABLE 1 Fractional atomic coordinates and thermal parameters (\AA^2)
for $[\text{NiL}^1][\text{ClO}_4]_2 \cdot 2\text{CH}_3\text{CN}$ continued

Atom	x	y	z	U_{iso} or U_{eq}
C(41b)	-0.2358(7)	0.1308(5)	0.0285(5)	0.046(3)
C(4b)	-0.1491(6)	0.1562(5)	0.0666(5)	0.034(2)
C(3b)	-0.1026(6)	0.1185(5)	0.1252(4)	0.030(2)
O(1b)	-0.1128(4)	0.2203(3)	0.0499(3)	0.042(2)
C(5b)	-0.0750(7)	0.2162(6)	-0.0102(5)	0.049(3)
C(6b)	0.0202(7)	0.1808(5)	0.0039(5)	0.042(3)
C(61b)	0.0248(8)	0.1090(6)	-0.0147(5)	0.055(3)
C(62b)	0.1096(8)	0.0705(6)	-0.0030(6)	0.064(3)

TABLE 2 Fractional atomic coordinates for the hydrogen atoms for
 $[\text{NiL}^1][\text{ClO}_4]_2 \cdot 2\text{CH}_3\text{CN}$

Atom	x	y	z
H(2)	0.3793	0.1339	0.2737
H(11a)	0.3469	0.2354	0.3426
H(2a)	0.2176	0.3356	0.3570
H(31a)	0.1315	0.4382	0.2973
H(32a)	0.0789	0.5524	0.3443
H(42a)	-0.0377	0.5449	0.4127
H(41a)	-0.1019	0.4305	0.4364
H(5a1)	-0.0642	0.3250	0.4911
H(5a2)	-0.1722	0.3150	0.4300
H(61a)	-0.2522	0.2082	0.4310
H(11b)	0.2486	0.0771	0.1862
H(2b)	0.0638	0.0814	0.1230
H(31b)	-0.1040	0.0295	0.1912
H(32b)	-0.2584	-0.0158	0.1226
H(42b)	-0.3391	0.0499	0.0179
H(41b)	-0.2729	0.1598	-0.0165
H(5b1)	-0.1229	0.1858	-0.0495
H(5b2)	-0.0686	0.2701	-0.0283
H(61b)	-0.0399	0.0818	-0.0385
Hs(1x)	0.4051	0.3235	0.2166
Hs(1y)	0.3228	0.3176	0.1369
Hs(1z)	0.4335	0.3573	0.1424

TABLE 3 Anisotropic thermal parameters (\AA^2) for $[\text{NiL}^1][\text{ClO}_4]_2 \cdot 2\text{CH}_3\text{CN}$

Atom	U_{11}	U_{22}	U_{33}	U_{23}	U_{13}	U_{12}
N1	0.019(1)	0.044(1)	0.026(1)	0.000	0.004(1)	0.000
Cl(1)	0.050(2)	0.059(2)	0.050(2)	0.005(2)	0.012(2)	-0.005(2)
O(1)	0.072(5)	0.095(7)	0.067(6)	-0.021(5)	0.024(5)	0.006(5)
O(2)	0.095(6)	0.045(5)	0.091(7)	0.010(5)	0.011(5)	0.004(5)
O(3)	0.087(6)	0.079(6)	0.126(8)	0.011(6)	0.050(6)	-0.020(5)
O(4)	0.064(6)	0.151(9)	0.056(5)	0.003(6)	-0.009(5)	0.004(6)
Cs(1)	0.065(9)	0.122(13)	0.060(9)	-0.013(9)	0.020(7)	-0.005(9)
Cs(2)	0.053(9)	0.085(13)	0.067(9)	0.013(10)	0.013(7)	-0.012(8)
Ns(1)	0.099(10)	0.091(10)	0.119(12)	0.020(10)	0.019(8)	0.005(9)

TABLE 4 Bond lengths (Å) for $[\text{NiL}^1][\text{ClO}_4]_2 \cdot 2\text{CH}_3\text{CN}$

N1	-N(1)	1.996(7)	N1	-N(2a)	2.138(7)
N1	-N(2b)	2.168(7)	N(1)	-C(1a)	1.342(10)
N(1)	-C(1b)	1.311(10)	C(12)	-C(11a)	1.360(12)
C(12)	-C(11b)	1.395(12)	C(11a)	-C(1a)	1.400(12)
C(1a)	-C(2a)	1.456(12)	C(2a)	-N(2a)	1.323(10)
N(2a)	-C(3a)	1.417(11)	C(31a)	-C(32a)	1.417(14)
C(31a)	-C(3a)	1.379(13)	C(32a)	-C(42a)	1.370(14)
C(42a)	-C(41a)	1.364(14)	C(41a)	-C(4a)	1.394(13)
C(4a)	-C(3a)	1.411(12)	C(4a)	-O(1a)	1.361(10)
O(1a)	-C(5a)	1.445(11)	C(5a)	-C(6a)	1.480(13)
C(6a)	-C(61a)	1.398(13)	C(61a)	-C(62a)	1.402(14)
C(11b)	-C(1b)	1.393(12)	C(1b)	-C(2b)	1.482(12)
C(2b)	-N(2b)	1.284(10)	N(2b)	-C(3b)	1.450(10)
C(31b)	-C(32b)	1.399(12)	C(31b)	-C(3b)	1.372(12)
C(32b)	-C(42b)	1.389(13)	C(42b)	-C(41b)	1.364(13)
C(41b)	-C(4b)	1.399(12)	C(4b)	-C(3b)	1.398(12)
C(4b)	-O(1b)	1.381(10)	O(1b)	-C(5b)	1.448(11)
C(5b)	-C(6b)	1.507(13)	C(6b)	-C(61b)	1.393(13)
C(61b)	-C(62b)	1.407(14)	Cl(1)	-O(1)	1.429(8)
Cl(1)	-O(2)	1.427(8)	Cl(1)	-O(3)	1.420(8)
Cl(1)	-O(4)	1.422(8)	Cs(1)	-Cs(2)	1.440(17)
Cs(2)	-Ns(1)	1.124(16)			

TABLE 5 Bond angles ($^{\circ}$) for $[\text{NiL}^1][\text{ClO}_4]_2 \cdot 2\text{CH}_3\text{CN}$

N(2a) -Ni	-N(1)	78.6(3)	N(2b) -Ni	-N(1)	76.2(3)
N(2b) -Ni	-N(2a)	153.5(3)	C(1a) -N(1) -Ni		116.6(6)
C(1b) -N(1) -Ni		118.8(6)	C(1b) -N(1) -C(1a)		122.1(8)
C(11b) -C(12) -C(11a)		121.1(9)	C(1a) -C(11a) -C(12)		118.6(9)
C(11a) -C(1a) -N(1)		119.6(8)	C(2a) -C(1a) -N(1)		113.8(8)
C(2a) -C(1a) -C(11a)		126.6(9)	N(2a) -C(2a) -C(1a)		117.4(8)
C(2a) -N(2a) -Ni		111.4(6)	C(3a) -N(2a) -Ni		131.0(6)
C(3a) -N(2a) -C(2a)		116.4(8)	N(2a) -Ni -N(2a)		92.1(4)
C(3a) -C(31a) -C(32a)		120(1)	C(42a) -C(32a) -C(31a)		118(1)
C(41a) -C(42a) -C(32a)		122(1)	C(4a) -C(41a) -C(42a)		121(1)
C(3a) -C(4a) -C(41a)		118(1)	O(1a) -C(4a) -C(41a)		125.5(9)
O(1a) -C(4a) -C(3a)		116.3(9)	C(31a) -C(3a) -N(2a)		120.6(9)
C(4a) -C(3a) -N(2a)		119.3(9)	C(4a) -C(3a) -C(31a)		120(1)
C(5a) -O(1a) -C(4a)		116.5(7)	C(6a) -C(5a) -O(1a)		108.3(8)
C(61a) -C(6a) -C(5a)		120.8(9)	C(62a) -C(61a) -C(6a)		122(1)
C(1b) -C(11b) -C(12)		117.1(9)	C(11b) -C(1b) -N(1)		121.5(8)
C(2b) -C(1b) -N(1)		113.8(8)	C(2b) -C(1b) -C(11b)		124.7(8)
N(2b) -C(2b) -C(1b)		115.6(8)	C(2b) -N(2b) -Ni		113.7(6)
C(3b) -N(2b) -Ni		129.1(5)	C(3b) -N(2b) -C(2b)		117.1(7)
N(2b) -Ni -N(2b)		95.0(4)	C(3b) -C(31b) -C(32b)		119.9(9)
C(42b) -C(32b) -C(31b)		119(1)	C(41b) -C(42b) -C(32b)		122(1)
C(4b) -C(41b) -C(42b)		120(1)	C(3b) -C(4b) -C(41b)		118.9(9)
O(1b) -C(4b) -C(41b)		120.8(8)	O(1b) -C(4b) -C(3b)		120.1(8)
C(31b) -C(3b) -N(2b)		119.7(8)	C(4b) -C(3b) -N(2b)		119.1(8)
C(4b) -C(3b) -C(31b)		120.9(8)	C(5b) -O(1b) -C(4b)		113.9(7)
C(6b) -C(5b) -O(1b)		113.2(8)	C(61b) -C(6b) -C(5b)		118.1(9)
C(62b) -C(61b) -C(6b)		123(1)	O(2) -Cl(1) -O(1)		108.8(5)
O(3) -Cl(1) -O(1)		109.7(5)	O(3) -Cl(1) -O(2)		109.4(5)
O(4) -Cl(1) -O(1)		108.8(5)	O(4) -Cl(1) -O(2)		110.2(6)
O(4) -Cl(1) -O(3)		109.9(6)	Ns(1) -Cs(2) -Cs(1)		178(2)

TABLE 6 Intermolecular distances (/Å) for $[\text{NiL}^1][\text{ClO}_4]_2 \cdot 2\text{CH}_3\text{CN}$

atom1	atom2	dist	S	a	b	c
O(1a) ... N(1)		3.22	-2	0.0	0.0	1.0
N(2b) ... N(1)		2.93	-2	0.0	0.0	1.0
C(3b) ... N(1)		3.21	-2	0.0	0.0	1.0
Ns(1) ... H(2)		2.82	-2	1.0	0.0	1.0
Ns(1) ... H(11a)		2.84	-2	1.0	0.0	1.0
C(5b) ... H(11a)		3.04	2	-0.5	0.5	-1.0
N(2b) ... C(1a)		3.44	-2	0.0	0.0	1.0
C(4b) ... C(1a)		3.49	-2	0.0	0.0	1.0
C(3b) ... C(1a)		3.33	-2	0.0	0.0	1.0
C(4b) ... C(2a)		3.48	-2	0.0	0.0	1.0
O(1b) ... C(2a)		3.17	-2	0.0	0.0	1.0
N(2a) ... N(2a)		3.08	-2	0.0	0.0	1.0
N(2b) ... N(2a)		3.11	-2	0.0	0.0	1.0
O(1b) ... N(2a)		3.04	-2	0.0	0.0	1.0
C(31a) ... C(31a)		3.47	-2	0.0	0.0	1.0
Ns(1) ... H(32a)		2.75	-2	0.5	-0.5	1.0
H(32b) ... C(41a)		2.89	-2	-0.5	-0.5	1.0
N(2b) ... O(1a)		3.36	-2	0.0	0.0	1.0
O(1b) ... O(1a)		2.86	-2	0.0	0.0	1.0
C(5b) ... O(1a)		3.08	-2	0.0	0.0	1.0
H(5b2) ... O(1a)		2.94	-2	0.0	0.0	1.0
C(6b) ... O(1a)		3.02	-2	0.0	0.0	1.0
C(5b) ... C(5a)		2.97	-2	0.0	0.0	1.0
H(5b2) ... C(5a)		2.67	-2	0.0	0.0	1.0
C(6b) ... C(5a)		2.51	-2	0.0	0.0	1.0
C(5b) ... H(5a1)		2.84	-2	0.0	0.0	1.0
C(6b) ... H(5a1)		2.76	-2	0.0	0.0	1.0
Ns(1) ... H(5a1)		2.86	2	0.5	0.5	-1.0
C(2b) ... C(6a)		3.29	-2	0.0	0.0	1.0
O(1b) ... C(6a)		3.26	-2	0.0	0.0	1.0
C(5b) ... C(6a)		2.55	-2	0.0	0.0	1.0
H(5b2) ... C(6a)		2.71	-2	0.0	0.0	1.0
C(6b) ... C(6a)		1.40	-2	0.0	0.0	1.0
C(61b) ... C(6a)		2.42	-2	0.0	0.0	1.0
C(62b) ... C(6a)		2.85	-2	0.0	0.0	1.0
C(2b) ... C(61a)		3.48	-2	0.0	0.0	1.0

TABLE 6 Intermolecular distances (/Å) for $[\text{NiL}^1][\text{ClO}_4]_2 \cdot 2\text{CH}_3\text{CN}$ continued

atom1	atom2	dist	S	a	b	c
C(6b) ...C(61a)	2.40	-2	0.0	0.0	1.0	
C(61b)...C(61a)	2.75	-2	0.0	0.0	1.0	
C(62b)...C(61a)	2.43	-2	0.0	0.0	1.0	
Cs(2) ...H(61a)	2.84	-2	0.0	0.0	1.0	
H(2b) ...C(62a)	3.03	-2	0.0	0.0	1.0	
C(6b) ...C(62a)	2.81	-2	0.0	0.0	1.0	
C(61b)...C(62a)	2.40	-2	0.0	0.0	1.0	
C(62b)...C(62a)	1.40	-2	0.0	0.0	1.0	
Cl(1) ...C(11b)	3.83	-2	0.5	0.5	1.0	
Cl(1) ...H(11b)	3.15	-2	0.5	0.5	1.0	
O(1) ...H(11b)	2.52	-2	0.5	0.5	1.0	
C(31b)...C(1b)	3.44	-2	0.0	0.0	1.0	
Cl(1) ...C(2b)	3.82	-2	0.5	0.5	1.0	
O(3) ...C(2b)	2.96	-2	0.5	0.5	1.0	
Cl(1) ...H(2b)	3.27	-2	0.5	0.5	1.0	
O(1) ...H(2b)	2.80	-2	0.5	0.5	1.0	
O(3) ...H(2b)	2.63	-2	0.5	0.5	1.0	
N(2b) ...N(2b)	3.20	-2	0.0	0.0	1.0	
O(3) ...C(31b)	3.37	1	0.5	0.5	0.0	
Cl(1) ...H(31b)	3.22	1	0.5	0.5	0.0	
O(3) ...H(31b)	2.33	1	0.5	0.5	0.0	
O(3) ...H(31b)	2.79	-2	0.5	0.5	1.0	
O(4) ...H(32b)	2.71	1	0.5	0.5	0.0	
O(1b) ...H(41b)	2.77	-1	-0.5	0.5	0.0	
O(2) ...H(5b1)	2.60	2	0.5	0.5	0.0	
Hs(1z)...C(61b)	2.85	-1	0.5	0.5	0.0	
O(2) ...C(61b)	3.39	2	0.5	0.5	0.0	
Cl(1) ...H(61b)	3.09	2	0.5	0.5	0.0	
O(1) ...H(61b)	2.57	2	0.5	0.5	0.0	
O(2) ...H(61b)	2.87	2	0.5	0.5	0.0	
Hs(1z)...C(62b)	3.03	-1	0.5	0.5	0.0	

TABLE 6 Intermolecular distances (/Å) for $[\text{NiL}^1][\text{ClO}_4]_2 \cdot 2\text{CH}_3\text{CN}$ continued

atom1	atom2	dist	S	a	b	c
O(1)	...C(62b)	3.40	-2	0.5	0.5	1.0
Hs(1z)	...Cl(1)	3.34	-2	1.0	0.0	1.0
Cs(1)	...O(2)	3.28	-2	1.0	0.0	1.0
Hs(1z)	...O(2)	2.61	-2	1.0	0.0	1.0
Cs(2)	...O(2)	3.32	-2	1.0	0.0	1.0
O(3)	...O(3)	3.16	-2	1.0	0.0	1.0
Hs(1z)	...O(3)	2.98	-2	1.0	0.0	1.0

Symmetry Transformations:

The second atom is related to the first atom, at (x,y,z), by the symmetry operation S with (a,b,c) added to the (x',y',z') of S
Where S = 1 x, y, z

TABLE 7 Intramolecular distances (Å) for $[\text{NiL}^1][\text{ClO}_4]_2 \cdot 2\text{CH}_3\text{CN}$

C(11a)...Ni	4.16	C(1a) ...Ni	2.86
C(2a) ...Ni	2.90	C(4a) ...Ni	3.79
C(3a) ...Ni	3.25	O(1a) ...Ni	3.44
C(11b)...Ni	4.17	C(1b) ...Ni	2.87
C(2b) ...Ni	2.93	C(31b)...Ni	4.06
C(4b) ...Ni	4.02	C(3b) ...Ni	3.28
O(1b) ...Ni	3.96	C(12) ...N(1)	2.71
C(11a)...N(1)	2.37	C(2a) ...N(1)	2.35
N(2a) ...N(1)	2.62	C(11b)...N(1)	2.36
C(2b) ...N(1)	2.34	N(2b) ...N(1)	2.57
H(11a)...C(12)	2.13	C(1a)...C(12)	2.37
H(11b)...C(12)	2.17	C(1b)...C(12)	2.38
C(11a)...H(2)	2.11	C(11b)...H(2)	2.14
C(2a) ...C(11a)	2.55	H(2a) ...C(11a)	2.87
C(11b)...C(11a)	2.40	C(1b) ...C(11a)	2.73
O(2) ...C(11a)	3.01	C(1a) ...H(11a)	2.15
C(2a) ...H(11a)	2.82	O(2) ...H(11a)	2.36
H(2a) ...C(1a)	2.22	N(2a) ...C(1a)	2.38
C(11b)...C(1a)	2.75	C(1b) ...C(1a)	2.32
O(2) ...C(1a)	3.41	C(31a)...C(2a)	2.87
H(31a)...C(2a)	2.68	C(4a) ...C(2a)	3.50
C(3a) ...C(2a)	2.33	Cl(1) ...C(2a)	3.68
O(2) ...C(2a)	3.32	O(4) ...C(2a)	3.40
N(2a) ...H(2a)	2.10	C(31a)...H(2a)	2.70
C(3a) ...H(2a)	2.54	Cl(1) ...H(2a)	2.94
O(1) ...H(2a)	2.75	O(2) ...H(2a)	2.66
C(31a)...N(2a)	2.43	H(31a)...N(2a)	2.64
C(4a) ...N(2a)	2.44	O(1a) ...N(2a)	2.71
H(32a)...C(31a)	2.18	C(42a)...C(31a)	2.39
C(41a)...C(31a)	2.76	C(4a) ...C(31a)	2.42
C(32a)...H(31a)	2.17	C(3a) ...H(31a)	2.13
Cl(1) ...H(31a)	3.18	O(1) ...H(31a)	2.81
O(4) ...H(31a)	2.51	H(42a)...C(32a)	2.12
C(41a)...C(32a)	2.39	C(4a) ...C(32a)	2.80
C(3a) ...C(32a)	2.43	C(42a)...H(32a)	2.13
H(41a)...C(42a)	2.12	C(4a) ...C(42a)	2.40
C(3a) ...C(42a)	2.77	C(41a)...H(42a)	2.11
C(3a) ...C(41a)	2.41	O(1a) ...C(41a)	2.45

TABLE 7 Intramolecular distances (Å) for $[\text{NiL}^1][\text{ClO}_4]_2 \cdot 2\text{CH}_3\text{CN}$ continued

C(5a) ... C(41a)	2.84	H(5a1) ... C(41a)	2.66
H(5a2) ... C(41a)	2.93	C(4a) ... H(41a)	2.14
O(1a) ... H(41a)	2.72	C(5a) ... H(41a)	2.54
C(5a) ... C(4a)	2.39	H(5a1) ... C(4a)	2.55
H(5a2) ... C(4a)	2.80	O(1a) ... C(3a)	2.35
H(5a1) ... O(1a)	2.07	H(5a2) ... O(1a)	2.08
C(6a) ... O(1a)	2.37	C(61a) ... C(5a)	2.50
H(61a) ... C(5a)	2.69	C(6a) ... H(5a1)	2.10
C(6a) ... H(5a2)	2.11	C(61a) ... H(5a2)	2.58
H(61a) ... C(6a)	2.14	C(62a) ... C(6a)	2.45
C(62a) ... H(61a)	2.15	C(2b) ... C(11b)	2.55
H(2b) ... C(11b)	2.87	C(1b) ... H(11b)	2.15
C(2b) ... H(11b)	2.80	H(2b) ... C(1b)	2.25
N(2b) ... C(1b)	2.34	C(31b) ... C(2b)	3.14
C(4b) ... C(2b)	3.27	C(3b) ... C(2b)	2.33
C(6b) ... C(2b)	3.26	C(61b) ... C(2b)	3.45
N(2b) ... H(2b)	2.07	C(3b) ... H(2b)	2.55
C(6b) ... H(2b)	2.97	C(61b) ... H(2b)	2.73
C(62b) ... H(2b)	2.78	C(31b) ... N(2b)	2.44
H(31b) ... N(2b)	2.64	C(4b) ... N(2b)	2.46
O(1b) ... N(2b)	2.80	H(32b) ... C(31b)	2.16
C(42b) ... C(31b)	2.40	C(41b) ... C(31b)	2.78
C(4b) ... C(31b)	2.41	C(32b) ... H(31b)	2.16
C(3b) ... H(31b)	2.12	H(42b) ... C(32b)	2.14
C(41b) ... C(32b)	2.40	C(4b) ... C(32b)	2.79
C(3b) ... C(32b)	2.40	C(42b) ... H(32b)	2.15
H(41b) ... C(42b)	2.13	C(4b) ... C(42b)	2.39
C(3b) ... C(42b)	2.75	C(41b) ... H(42b)	2.11
C(3b) ... C(41b)	2.41	O(1b) ... C(41b)	2.42
C(5b) ... C(41b)	3.10	H(5b1) ... C(41b)	2.74
C(4b) ... H(41b)	2.15	O(1b) ... H(41b)	2.65
C(5b) ... H(41b)	3.06	C(5b) ... C(4b)	2.37
H(5b1) ... C(4b)	2.52	C(6b) ... C(4b)	3.08
C(61b) ... C(4b)	3.46	O(1b) ... C(3b)	2.41
C(5b) ... C(3b)	3.38	H(5b1) ... O(1b)	2.07
H(5b2) ... O(1b)	2.06	C(6b) ... O(1b)	2.47
C(61b) ... O(1b)	3.37	C(61b) ... C(5b)	2.49
H(61b) ... C(5b)	2.64	C(6b) ... H(5b1)	2.12

TABLE 7 Intramolecular distances (Å) for $[\text{NiL}^1][\text{ClO}_4]_2 \cdot 2\text{CH}_3\text{CN}$ continued

C(61b)...H(5b1)	2.55	C(6b) ...H(5b2)	2.11
H(61b)...C(6b)	2.13	C(62b)...C(6b)	2.46
C(62b)...H(61b)	2.15	Cs(1) ...Cl(1)	3.81
Hs(1x)...Cl(1)	2.94	O(2) ...O(1)	2.32
O(3) ...O(1)	2.33	O(4) ...O(1)	2.32
O(3) ...O(2)	2.32	O(4) ...O(2)	2.34
Hs(1x)...O(2)	2.42	O(4) ...O(3)	2.33
Hs(1x)...O(4)	2.91	Ns(1) ...Cs(1)	2.56
Cs(2) ...Hs(1x)	2.09	Cs(2) ...Hs(1y)	2.06
Cs(2) ...Hs(1z)	2.06		

THE BRITISH LIBRARY
BRITISH THESIS SERVICE

TITLE SYNTHESIS, CHARACTERISATION AND STABILITY OF SOME N-DONOR
LIGANDS AND THEIR METAL COMPLEXES

AUTHOR **Ian Jonathan Scowen**

DEGREE

AWARDING BODY University of North London 1993.
DATE

THESIS
NUMBER

THIS THESIS HAS BEEN MICROFILMED EXACTLY AS RECEIVED

The quality of this reproduction is dependent upon the quality of the original thesis submitted for microfilming. Every effort has been made to ensure the highest quality of reproduction.

Some pages may have indistinct print, especially if the original papers were poorly produced or if the awarding body sent an inferior copy.

If pages are missing, please contact the awarding body which granted the degree.

Previously copyrighted materials (journal articles, published texts, etc.) are not filmed.

This copy of the thesis has been supplied on condition that anyone who consults it is understood to recognise that its copyright rests with its author and that no information derived from it may be published without the author's prior written consent.

Reproduction of this thesis, other than as permitted under the United Kingdom Copyright Designs and Patents Act 1988, or under specific agreement with the copyright holder, is prohibited.

1	2	3	4	5	6	REDUCTION X	12
cms						CAMERA	12.
						No. of pages	

DX

175943